Efnisyfirlit viðaukaheftis

VIÐAUKI I

CONSULTING ENGINEERS
VATNASKIL

Coda Terminal

Assessment of impacts on groundwater resources

Prepared for Carbfix hf.

Report no. 24.01

March 2024

Vatnaskil ehf.
Síðumúli 28
108 Reykjavík
Iceland

Tel. +354-512-2121
vatnaskil@vatnaskil.is
www.vatnaskil.is

Report no:	Published:	Number of pages:	Distribution:
24.01	March 2024	61	Open ☒ Closed ☐

Report title:
Coda Terminal. Assessment of impacts on groundwater resources

Authors:
Eric M. Myer, Andri Arnaldsson, Jean-Claude Berthet, Hrólfur Ásmundsson, Sveinn Óli Pálmarsson

Project manager:
Sveinn Óli Pálmarsson

Abstract:
Vatnaskil has designed and utilized a numerical groundwater model of the Straumsvík watershed to simulate the proposed production and injection from the Coda Terminal and predict potential impacts on the groundwater system. The current operational design strategy calls for an operational build-up in four phases beginning in 2027 and reaching a maximum production/injection rate of roughly 3000 kg/s in 2032. Impacts on the groundwater system were assessed, with a focus on changes within the shallow freshwater aquifer that could affect environmentally sensitive areas in the vicinity of the Coda Terminal wellfield. The fate and transport of CO_2 from the injection wells was outside of the defined scope of the assessment.

According to the model, the drawdown due to production is relatively small due to favorable hydro-geological conditions in the freshwater aquifer and the pressure support provided by injection. Increased pressure due to injection is substantial and causes a rise in groundwater levels. Changes in groundwater levels are not likely to significantly affect the natural-state regional groundwater flow (direction and magnitude) nor have significant environmental impacts.

Changes to groundwater salinity and temperature at the top of the freshwater aquifer (above -20 m a.s.l.) are relatively small and therefore are not likely to cause significant environmental impacts. Changes to groundwater salinity and temperature below -20 m a.s.l. are relatively large, however they do not significantly impact environmentally sensitive areas.

The planned production/injection at the Coda Terminal is not likely to negatively affect current ground-water producers in the area, although a slight increase in salinity and temperature are predicted at the Rio Tinto production wells. Drought conditions are not likely to have a significant influence on the impacts of production/injection from the Coda Terminal.

It is recommended that continued hydrogeological research focus on filling gaps in the current conceptual model, especially with respect to the morphology of the fresh/saline interface and the degree of hydrologic connection between the shallow freshwater aquifer and the deeper sections of the groundwater system. Due to the scale and magnitude of the proposed production/injection at the Coda Terminal, a robust groundwater and surface water monitoring program is needed to register the current state of the groundwater system (pre-operational) and to detect potential changes to the system once the first operational stages begin. Parallel updates to the groundwater model as new research and monitoring data become available may provide further support in lowering uncertainties and revising the initial impact assessment.

Client:	Client representative:
Carbfix hf.	Heiða Aðalsteinsdóttir

Keywords:
Straumsvík, groundwater, carbon sequestration, CO_2, coastal aquifer, saline intrusion

Table of Contents

List of Figures

List of Tables

Íslenskur útdráttur

Vegna mats á umhverfisáhrifum uppbyggingar og reksturs Coda Terminal við Straumsvík í Hafnarfirði óskaði Carbfix hf. eftir því að Vatnaskil meti hugsanleg áhrif af rekstri Coda Terminal á grunnvatnskerfið. Reksturinn felur í sér upptöku af u.þ.b. 3000 kg/s af grunnvatni og niðurdælingu á því vatni dýpra í grunnvatnskerfið eftir blöndun með koltvísýringi. Í því skyni var hannað þrívítt reiknilíkan af grunnvatnskerfinu á vatnasviði Straumsvíkur. Líkaninu var síðan beitt til að meta áhrif af fyrirhugaðri vatnstöku og niðurdælingu á vegum Coda Terminal á grunnvatnskerfið.

Sérstaklega var horft til viðkvæmra svæða sem gætu orðið fyrir áhrifum vegna breytinga í grunnvatnskerfinu (mynd 1). Má þar nefna strandtjarnir við Straumsvík sem Náttúrufræðistofnun Íslands leggur sérstaka áherslu á vegna einstaks vistkerfis. Inn í strandtjarnirnar rennur ferskt grunnvatn sem leiðir af sér mjög lága seltu í tjörnunum þrátt fyrir nálægð þeirra við strandlengjuna (Ingólfsson, 1998). Stærstar þessara strandtjarna eru Brunntjörn, Þorbjarnarstaðatjarnir (einnig þekktir sem Brunntjörnin), Gerðistjarnir og Óttarsstaðatjarnir. Nokkur stöðuvötn og tjarnir inn til landsins (Ástjörn, Hvaleyrarvatn og Urriðavatn), sem og núverandi vatnsból á vegum Rio Tinto (í Straumsvík) og Vatnsveitu Hafnarfjarðar (í Kaldárseli) voru einnig skoðuð sérstaklega.

Vatnajarðfræði vatnasviðs Straumsvíkur

Fyrirliggjandi vatnajarðfræðilegum upplýsingum frá fyrri rannsóknum á svæðinu var safnað saman ásamt nýjum gögnum sem Carbfix og ÍSOR söfnuðu í tengslum við uppbyggingu Coda Terminal, þ.m.t. með borun nýrra rannsóknarhola. Nýju gögnin voru notuð til að uppfæra hugmyndalíkan Vatnaskila af suðvesturlandi, sérstaklega m.t.t. dýpri hluta grunnvatnskerfisins (~100-1000 m dýpi) þar sem gögn hafa hingað til verið tiltölulega stöpul og slitrótt. Uppfærðu hugmyndalíkani er lýst ítarlega í kafla 3.3. Þrátt fyrir markverða bætingu hugmyndalíkansins, eru enn eyður í gagnasettunum og óvissuþættir til staðar, sérstaklega fyrir dýpri hluta grunnvatnskerfisins (t.d. vatnajarðfræðilegir eiginleikar berglaga, hversu langt lek berglög í tengslum við vatnsæðar teygja sig, lega og halli blandlagsins þar sem ferskt og salt vatn mætast o.fl.).

Líkangerð

Rennslislíkan Vatnaskila af Suðvesturlandi var haft til grundvallar líkanvinnunni fyrir Coda Terminal. Líkanið hefur verið í þróun í yfir 40 ár og er uppfært reglulega fyrir Samtök sveitarfélaga á höfuðborgarsvæðinu (SSH) og HS Orku (Vatnaskil, 2022a og 2023). Rennslislíkanið samanstendur af tveimur samþættum vatnafræðilegum líkönum, yfirborðsrennslislíkani og grunnvatnslíkani, sem hvort um sig líkir eftir mismunandi þáttum vatnafræðilegrar hringrásar. Yfirborðsrennslislíkanið reiknar magn vatns sem síast í gegnum ómettað jarðrakasvæði og niður að grunnvatnsborði. Grunnvatnslíkanið líkir eftir grunnvatnsrennsli um vatnsmettað svæði. Grunnvatnslíkanið er tvívíddarlíkan sem líkir eftir grunnvatnsrennsli í efstu ~100 m grunnvatnskerfisins.

Til þess að gera grein fyrir jarðsjó undir ferskvatnsleiðaranum á strandsvæðinu sem og dýpri hluta grunnvatnskerfisins þar sem koltvísýrðu vatni frá Coda Terminal verður dælt niður var líkanið dýpkað niður á 1100 m u.s. og uppfært í þrívítt líkan með lagskiptingu sem byggir á tiltækum jarðfræðiupplýsingum. iTOUGH2 líkanhugbúnaðurinn var notaður fyrir þrívíddarlíkanið þar sem hann býður m.a. upp á sveigjanleika í gegnum ýmsar ástandsjöfnur (e. equation of state, EOS) til að líkja eftir flæði vökva með breytilegum eðlismassa þar sem tekið er tillit til áhrifa uppleystra efna, t.d. salts og gasa, þ.m.t. andrúmslofts.

Niðurstöður úr grunnvatnslíkani Suðvesturlands voru notaðar til að afmarka, skilgreina og úthluta viðeigandi jaðarskilyrðum fyrir þrívíddarlíkanið, þar sem yfirborðs- og grunnvatnsskil umhverfis Straumsvík voru að fullu tekin inn (mynd 11). Að lokinni uppfærslu grunnvatnslíkansins var gerð ítarleg úttekt á nýja þrívíddarlíkaninu til að tryggja að viðunandi mynd af vatnasviði Straumsvíkur hefði náðst. Nauðsynlegt var að stilla og fínstilla inntaksbreytur til að útbúa grunntilfelli sem líkir á fullnægjandi hátt eftir náttúrulegum aðstæðum í grunnvatnskerfinu.

Mat á áhrifum starfseminnar

Grunnvatnslíkaninu var beitt til að líkja eftir fyrirhugaðri vatnstöku og niðurdælingu fyrir Coda Terminal og meta hugsanleg áhrif á grunnvatnskerfið, m.a. breytingar á seltu og hitastigi grunnvatns, sem og breytingar á grunnvatnsstöðu. Afdrif og flutningur koltvísýrings frá niðurdælingarholunum var metið sérstaklega hjá Carbfix og var því utan mats Vatnaskila.

Rekstrartilfelli

Hönnun vinnslusvæðisins sem Carbfix lagði til er sýnd á mynd 18 og samanstendur af 10 borteigum sem dreift er yfir u.þ.b. 5,5 km^2 svæði. Lóðréttar vinnsluholur frá borteigum 1-7 munu ná niður á u.þ.b. 50 m dýpi þar sem markmiðið er að vinna úr grunna ferskvatnsleiðaranum. Lóðréttar vinnsluholur frá borteigum 8-10 munu hins vegar teygja sig dýpra (>100 m) og er markmiðið þar að vinna jarðsjó neðan við blandlagið (skil fersk- og saltvatns). Niðurdælingarholur verða stefnuboraðar út frá borteigunum og ná þær niður á 300-800 m dýpi. Rekstrarhönnun Coda Terminal gerir ráð fyrir uppbyggingu í fjórum áföngum (fösum) eins og lýst er í töflu 1. Fyrsti áfanginn hefst árið 2027 með rekstri þriggja borteiga sem skila 665 kg/s af ferskvatni og dæla niður 688 kg/s af kolsýrðu vatni. Fleiri borteigar verða teknir í gagnið í síðari áföngum, sem lýkur með 4. áfanga þar sem allir 10 borteigarnir eru í notkun og unnin verða 2923 kg/s og dælt niður 3018 kg/s. Líkanið var keyrt yfir 30 ára rekstrartímabil, frá 2027 til 2057.

Niðurstöður líkansins voru greindar og bornar saman við grunntilfellið (núverandi ástand, áður en kemur til grunnvatnstöku og niðurdælingar vegna Coda Terminal) til að meta breytingar frá núverandi ástandi grunnvatns. Áhrif voru metin fyrir hvern hinna fjögurra fyrirhuguðu rekstrarfasa til að greina framvindu áhrifa með tíma og aukinni vinnslu og niðurdælingu. Greindar voru breytingar á grunnvatns-kerfinu og niðurstöðurnar m.a. dregnar fram í láréttu plani á mismunandi dýpi og þremur þversniðum í gegnum borteigana (myndir 20-40). Helstu niðurstöður eru einnig dregnar saman í töflu 2.

Hæð grunnvatnsborðs

Samkvæmt líkanreikningum verður niðurdráttur grunnvatnsborðs vegna starfsemi Coda Terminal mestur innan vinnslusvæðis stöðvarinnar, og reiknast rúmlega 20 cm við vinnsluholurnar að loknum fjórða fasa (mynd 23). Niðurdráttur reiknast allt að 7 cm við vinnsluholur Rio Tinto að loknum fjórða fasa samanborið við núverandi ástand. Reiknaður niðurdráttur við vinnsluholur Rio Tinto er talinn ólíklegur til að valda neikvæðum áhrifum á vinnslugetu þeirra, en þó fer það eftir núverandi vinnslu-fyrirkomulagi og ástandi vinnsluholanna. Við Brunntjörn, Þorbjarnarstaðatjarnir og Gerðistjarnir reiknast 2-4 cm niðurdráttur að loknum fjórða fasa, borið saman við núverandi ástand. Nokkur óvissa er gagnvart reiknuðum niðurdrætti við tjarnirnar vegna stöðu og nákvæmni líkansins á þessu stigi, en niðurstöður benda þó til þess að niðurdráttur sé mögulegur við þær.

Hækkun grunnvatnsborðs reiknast við Ástjörn (allt að 30 cm), Hvaleyrarvatn (allt að 40 cm) og Urriðavatn (allt að 20 cm) vegna þrýstiáhrifa frá niðurdælingu. Talið er að öll þrjú vötnin hafi einhverja tengingu við grunnvatn og því er mögulegt að hækkun grunnvatnsborðs geti leitt til aukins innrennslis (lindarennslis) í þau. Útrennsli úr vötnunum stjórnast með náttúrulegu yfirfalli sem gerir það að verkum

að breytingar á vatnsstöðu vatnanna takmarkast við hámarksvatnshæð yfirfallanna. Ólíklegt má því telja að reiknuð hækkun grunnvatnsborðs valdi verulegum áhrifum á vatnsstöðu í vötnunum þótt gegnumrennsli í þeim gæti aukist. Ástæða er engu að síður til þess að fylgjast með vötnunum og grunnvatnshæð í nágrenni þeirra á uppbyggingartíma Coda Terminal.

Selta grunnvatns

Líkansniðurstöður sýna einnig að mesta seltubreyting vegna vinnslu og niðurdælingar Coda Terminal reiknast neðan við u.þ.b. 50 m undir meðalsjó og niður á um 600 m dýpi. Breytingar ofar eru minni en valda þó einhverri seltuaukningu við grunnvatnsborðið, t.a.m. allt að 0,4 g/kg aukningu við Straumsvíkurtjarnirnar og allt að 0,5 g/kg aukningu við vinnsluholur Rio Tinto. Hafa ber þó í huga að á 20 m dýpi reiknast seltubreyting nærri 1 g/kg, á 30 m dýpi nærri 5 g/kg og á 50 m dýpi nærri 20 g/kg (mynd 33). Fullsaltur sjór er u.þ.b. 35 g/kg við Íslandsstrendur. Til viðmiðunar, gerir reglugerð um neysluvatn ráð fyrir hámarksstyrk seltu í neysluvatni sem 0,4 g/kg. Óvíst er því hvort framangreind seltuaukning geti valdið neikvæðum áhrifum á tjarnirnar, en ef gert er ráð fyrir að þær séu fullferskar í dag, þá mun 0,4 g/kg aukning ekki breyta þeirri flokkun innan ramma neysluvatnsreglugerðar. Ef miðað er hins vegar við reiknaða seltubreytingu aðeins neðar er möguleiki á að frávik geti orðið frá þessari flokkun. Einnig er óvíst hvort seltuaukning af þessari stærðargráðu geti valdið neikvæðum áhrifum á notkun vinnsluvatns Rio Tinto. Niðurstöður benda til þess að með fyrirliggjandi vinnslufyrirkomulagi sem gert er ráð fyrir í Coda Terminal gætu orðið vægar seltubreytingar í efri hluta ferskvatnsgeymisins, sem gæti því að óbreyttu takmarkað vinnslu á fullfersku vatni hjá öðrum hugsanlegum vinnsluaðilum á afmörkuðum svæðum vestan og austan við vinnslusvæði Coda Terminal.

Hitastig grunnvatns

Líkansniðurstöður sýna sömuleiðis að mesta hitabreyting vegna vinnslu og niðurdælingar Coda Terminal reiknast í dýpri hluta grunnvatnskerfisins, þar sem hitinn er náttúrulega hærri. Hitastig niðurdælingarvatnsins er áætlaður lægri en 10 °C. Breytingar í efri hluta ferskvatnsgeymisins eru minni en valda þó lítillegri hitaaukningu, t.a.m. allt að 1 °C hækkun grunnvatns við Straumsvíkurtjarnirnar og allt að 1,3 °C hækkun við vinnsluholur Rio Tinto. Óvíst er hvort hitaaukning á þessari stærðargráðu geti valdið neikvæðum áhrifum á tjarnirnar, en ástæða væri til að mæla hitastig tjarnanna fyrst um sinn við vöktun uppbyggingarinnar til að kortleggja náttúrulegan breytileika í þeim. Einnig er óvíst hvort hitastigsaukningin geti valdið neikvæðum áhrifum á notkun vinnsluvatns Rio Tinto.

Aðrennslissvæði

Líkaninu var beitt til að meta aðrennslissvæði vinnsluholanna (mynd 40). Aðrennslissvæðið nær til suðausturs, allt upp að grunnvatnsskilunum. Lögun og umfang svæðisins endurspeglar stefnu svæðisbundinna grunnvatnsrennslisleiða þar sem það er fremur þröngt við vinnslusvæðið en víkkar verulega innan Krýsuvíkursprungusveimsins til suðausturs þar sem grunnvatnsrennsli eykst í meginsprungustefnuna (NE-SV).

Þurrkatíð og afstaða niðurdælingar gagnvart blandlagi

Grunnvatnslíkaninu var beitt til að greina hvort áhrif vegna starfsemi Coda Terminal væru með öðrum hætti og jafnvel verri við lága grunnvatnsstöðu (þ.e. í þurrkatíð) samanborið við meðalgrunnvatnsstöðu eins og gert var ráð fyrir í grunntilfellinu. Niðurstaðan af þeirri greiningu var að mjög lítill munur reyndist af reiknuðum áhrifum við þessar mismunandi grunnvatnsaðstæður.

Líkaninu var einnig beitt til að meta næmni staðsetningar niðurdælingar m.t.t. blandlagsins (skilflöt fersk- og saltvatns). Fræðilegt tilfelli var skilgreint þannig að vinnsla og niðurdæling eiga sér stað

einungis í fersku grunnvatni suðaustan við blandlagið. Niðurstöðurnar sýna að töluverð næmni er fyrir því hvar niðurdæling fer fram innan fyrirhugaðs vinnslusvæðis og má ætla að áhrif minnki töluvert ef niðurdæling fer fram suðaustast á svæðinu og er þá dælt niður í ferskt vatn í stað ísalts og salts vatns þegar nær dregur ströndu.

Stjórn vatnamála

Líkansniðurstöður voru skoðaðar heildrænt m.t.t. Vatnaáætlunar Íslands 2022-2027. Á heildina litið eru áætluð áhrif frá vinnslu og niðurdælingar vegna Coda Terminal á bæði eðliseiginleika og efnafræðileg gæði grunnvatnshlotsins í Straumsvíkurstraumi talin lítil. Ekki er gert ráð fyrir að þau hafi áhrif á umhverfismarkmið grunnvatnshlotsins.

Rannsóknir og vöktun

Mælt er með því að áframhaldandi og auknar vatnajarðfræðilegar rannsóknir verði stundaðar með það að markmiði að fylla upp í eyður í núverandi hugmyndalíkani, sérstaklega m.t.t. legu og lögunar skilflatar milli fersk- og saltvatns (blandlagsins) og hversu mikil vatnafræðileg tengsl séu á milli grunna ferskvatnsleiðarans og dýpri hluta grunnvatnskerfisins. Samkvæmt niðurstöðum líkansins gegna þessir tveir þættir hugmyndalíkansins meginhlutverki við mat á hversu mikil áhrif munu verða á ferskvatnsleiðarann með tilkomu Coda Terminal.

Vegna umfangs fyrirhugaðrar vinnslu og niðurdælingar í tengslum við rekstur Coda Terminal þarf yfirgripsmikla áætlun fyrir vöktun á breytingum á grunnvatni og yfirborðsvatni til að meta betur og skrá núverandi ástand grunnvatnskerfisins (fyrir rekstur) og til að greina hugsanlegar breytingar á kerfinu eftir að fyrstu rekstraráfangarnir hefjast. Með því að uppfæra grunnvatnslíkanið eftir því sem nýjar rannsóknir og vöktunargögn verða aðgengileg verður enn frekar unnt að draga úr óvissu og endurmeta áhrif vegna starfsemi Coda Terminal.

1. Introduction

Carbfix hf. is currently in the design and planning phase of the Coda Terminal project, a carbon sequestration facility located at Straumsvík in SW Iceland. Design specifications of the Coda Terminal require approximately 3000 kg/s of freshwater which will be extracted from the local groundwater aquifer through a network of production wells. The produced water will undergo a carbonation process within Coda Terminal facilities and then be re-injected into deeper sections of the groundwater system where sequestration will take place.

In order to fulfill requirements within the EIA process, Carbfix has requested that Vatnaskil assess potential impacts from the planned groundwater production and injection at the Coda Terminal on the local groundwater system. For that purpose, a three-dimensional numerical model of the groundwater system within the Straumsvík watershed was designed based on Vatnaskil's regional watershed model of southwest Iceland. The model was then utilized to simulate the proposed production and injection from the Coda Terminal and predict potential impacts on the groundwater system. The following report documents the modelling work performed with an emphasis on interpretation of simulation results with respect to potential environmental impacts.

2. Geographical setting

Straumsvík is a coastal inlet at the eastern edge of the Hafnarfjörður municipality on the north side of the Reykjanes peninsula. Environmentally sensitive areas which could potentially be affected by changes to the local groundwater system were identified and are shown on Figure 1. Protected areas (green) are defined by the Environment Agency of Iceland (Umhverfisstofnun). Proposed protection areas (orange) are outlined in the Hafnarfjörður municipal master plan (Aðalskipulag Hafnarfjarðar 2013-2025) and within these areas are several sites registered as natural heritage sites by the Icelandic Institute of Natural History (Náttúrufræðistofnun Íslands).

In their description of the natural heritage sites in the Straumsvík area, the Icelandic Institute of Natural History places special emphasis on the unique ecosystems found within the intertidal zone and in coastal ponds. These coastal ponds are fed by fresh groundwater flow, resulting in very low saline water despite their proximity to the coastline (Ingólfsson, 1998). The largest of these coastal ponds are Brunntjörn, Þorbjarnarstaðatjarnir (also known as Brunntjörnin), Gerðistjarnir and Óttarsstaðatjarnir. They are highlighted on Figure 1 as well as several inland lakes and ponds (Ástjörn, Hvaleyrarvatn and Urriðavatn) which also have some degree of hydrologic connection to the local groundwater system.

Existing freshwater production wellfields are also shown on Figure 1. The Rio Tinto aluminum smelter in Straumsvík produces approximately 300 L/s of freshwater from seven wells just south of Reykjanesbraut. The Hafnarfjörður municipal water supply wellfield is located roughly 8 km to the southeast at Kaldársel. Annual production from the wellfield is roughly 190 L/s.

A rough outline of the extent of the Coda Terminal wellfield area is shown on Figure 1. The area extends from the highway (Reykjanesbraut) roughly 4 km inland towards the southwest and covers an area of approximately 5.5 km^2. Research commissioned by Carbfix, and initial groundwater modelling performed by Vatnaskil during the planning phase was used by Carbfix as input into the wellfield design.

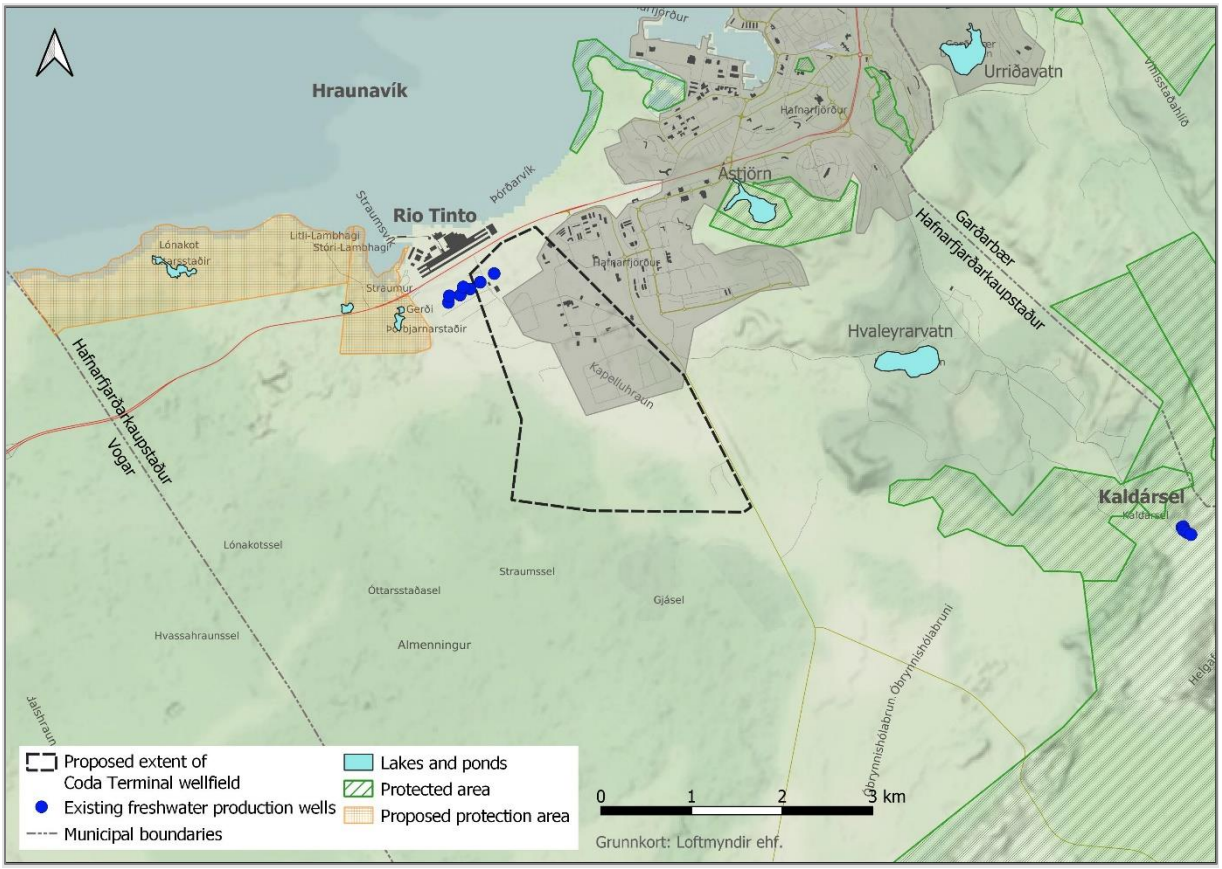

Figure 1. Overview of environmentally sensitive areas in the Straumsvík area and rough extent of Coda Terminal wellfield area.

3. Hydrogeology of Straumsvík watershed

An understanding of the main geological and hydrological features of the regional watershed encompassing Straumsvík is necessary in order to develop a comprehensive conceptual model of the groundwater system. Hydrogeological information is available from previous research in the area, the most noteworthy being a comprehensive study performed by Freysteinn Sigurðsson (Orkustofnun, 1976). Data collected from wells within the watershed are also available, including stratigraphical analyses and measured time-series of groundwater levels. The majority of this data has already been incorporated into Vatnaskil's extensive model development (both conceptual and numerical) of SW Iceland over the past 40 years. The main focus of this modelling to date has been on the shallow section of the groundwater system (upper ~100 m).

For the purpose of this study, it was necessary to collect and analyze hydrogeological information from deeper sections of the groundwater system (down to ~1000 m) in order to update the existing conceptual model of the Straumsvík watershed. Available data from previous studies were used, but the most valuable data was collected in the past two years by Carbfix and ÍSOR during the planning and design phase of the Coda Terminal. This recent research produced the first direct hydrogeological samples/measurements from the deeper sections of the groundwater system at Straumsvík. Research on the deep groundwater system at Straumsvík is, however, still considered in the early phases, and more research is needed to fill in remaining data gaps, reduce uncertainties and strengthen the conceptual model. A general overview of the current version of the conceptual model, highlighting the main hydrogeological features of the Straumsvík area, is provided below.

3.1. Geological setting

Iceland lies on the Mid-Atlantic Ridge, a divergent tectonic plate boundary separating the North American continental plate to the west and the Eurasian continental plate to the east. The plate boundary dissects Iceland, creating an active volcanic zone along its path. The Reykjanes peninsula is a segmented section of the Mid-Atlantic Ridge consisting of several volcanic systems which are defined by areas of concentrated fissure swarms with NE-SW striking eruptive fissures and normal faults (Jenness and Clifton, 2009). The Straumsvík area is located on the northern edge of the peninsula just west of the Krýsuvík fissure swarm (Figure 2).

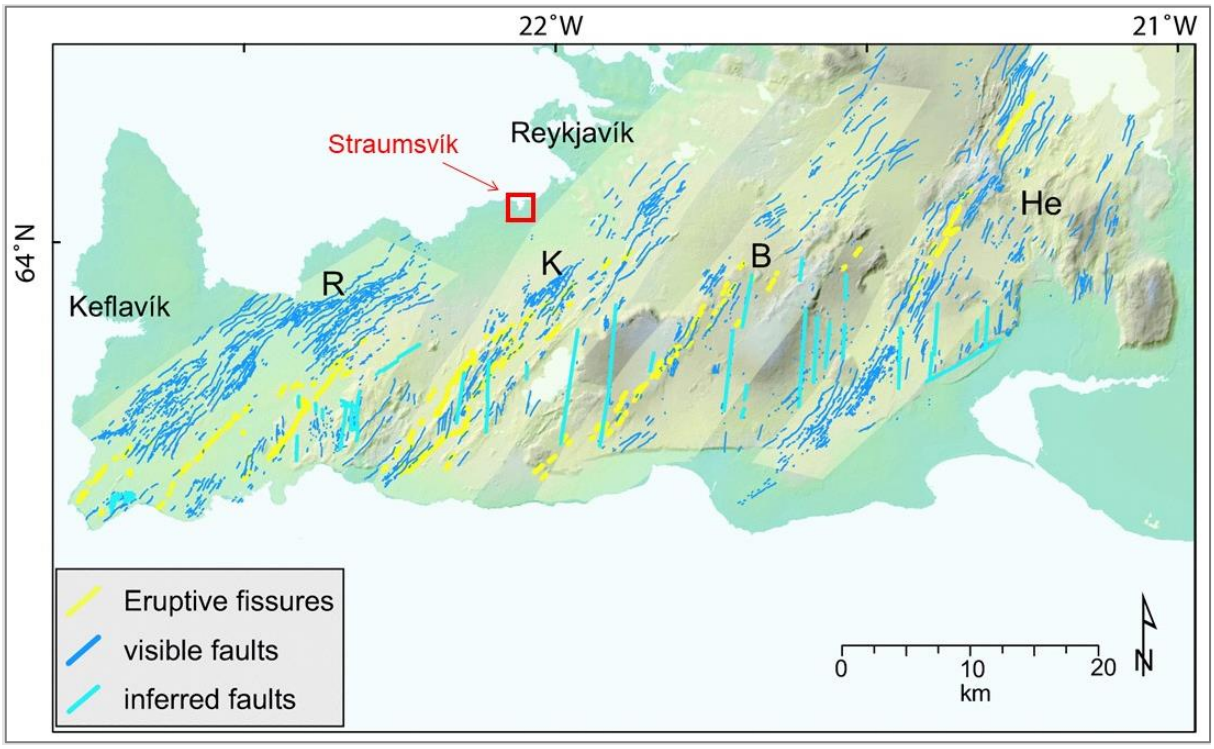

Figure 2. Map of Reykjanes peninsula showing main tectonic features (modified from Jenness and Clifton, 2009). Fissure swarms from Sæmundsson (1978) shown as lighter shaded areas R (Reykjanes), K (Krýsuvík), B (Brennisteinsfjöll) and He (Hengill).

The surface geology in the Straumsvík watershed can be classified roughly into three main rock types. Low elevations in the coastal area around Straumsvík are dominated by post-glacial lava flows, the youngest being Kapelluhraun from the year 1151 (Jóhannesson and Einarsson, 1998). Older inter-glacial lava flows (grágrýti) outcrop to east of Straumsvík in the vicinity of Ástjörn and Hvaleyrarvatn at elevations above roughly 30 m a.s.l. The NE-SW trending mountainous ridges in the higher elevations south of Straumsvík (e.g., Undirhlíðar) consist of hyaloclastic formations (móberg) which formed during sub-glacial eruptions. A surface geology map of the Straumsvík area (Sæmundsson et al., 2016) is shown on Figure 3. All three main rock types are basaltic, however their rock properties vary significantly. Due to the fresh, porous nature of the post-glacial lava formations, their permeability is very high, as much as 2-3 orders of magnitude higher than the grágrýti and hyaloclastite formations (Tómasson and Tómasson, 1966). Enhanced (secondary) permeability due to fracturing is significant in the Straumsvík watershed, especially within the Krýsuvík fissure swarm (Figure 2).

Until recently, the local stratigraphy below 100 m depth in the coastal area around Straumsvík was unknown. Although many wells had been drilled in the area, none extended to depths greater than 100 m. Deeper wells drilled in connection with geothermal investigations do exist within the Straumsvík watershed, however, they are located further inland. Well KS-02 is 986 m deep and is located roughly 9 km southeast of Straumsvík at Kaldársel (Figure 1). Kaldársel lies roughly at the surface boundary between the hyaloclastite ridges within the Krýsuvík fissure swarm and the coastal lowlands to the west. Stratigraphic analysis from the well shows that below the post-glacial lava formations at the surface, alternating layers of inter-glacial lava flows and hyaloclastites are the dominant formations with intermittent sedimentary layers (Orkustofnun, 1977). Geothermal alteration is evident in the formations below roughly 400 m depth. Further west in the highlands at Trölladyngja, well TR-01 (2307 m deep) shows a similar stratigraphy of alternating lava flows and hyaloclastites (Orkustofnun, 2002). However, geothermal alteration is evident throughout the entire depth range of the well, indicating a higher temperature environment in the area.

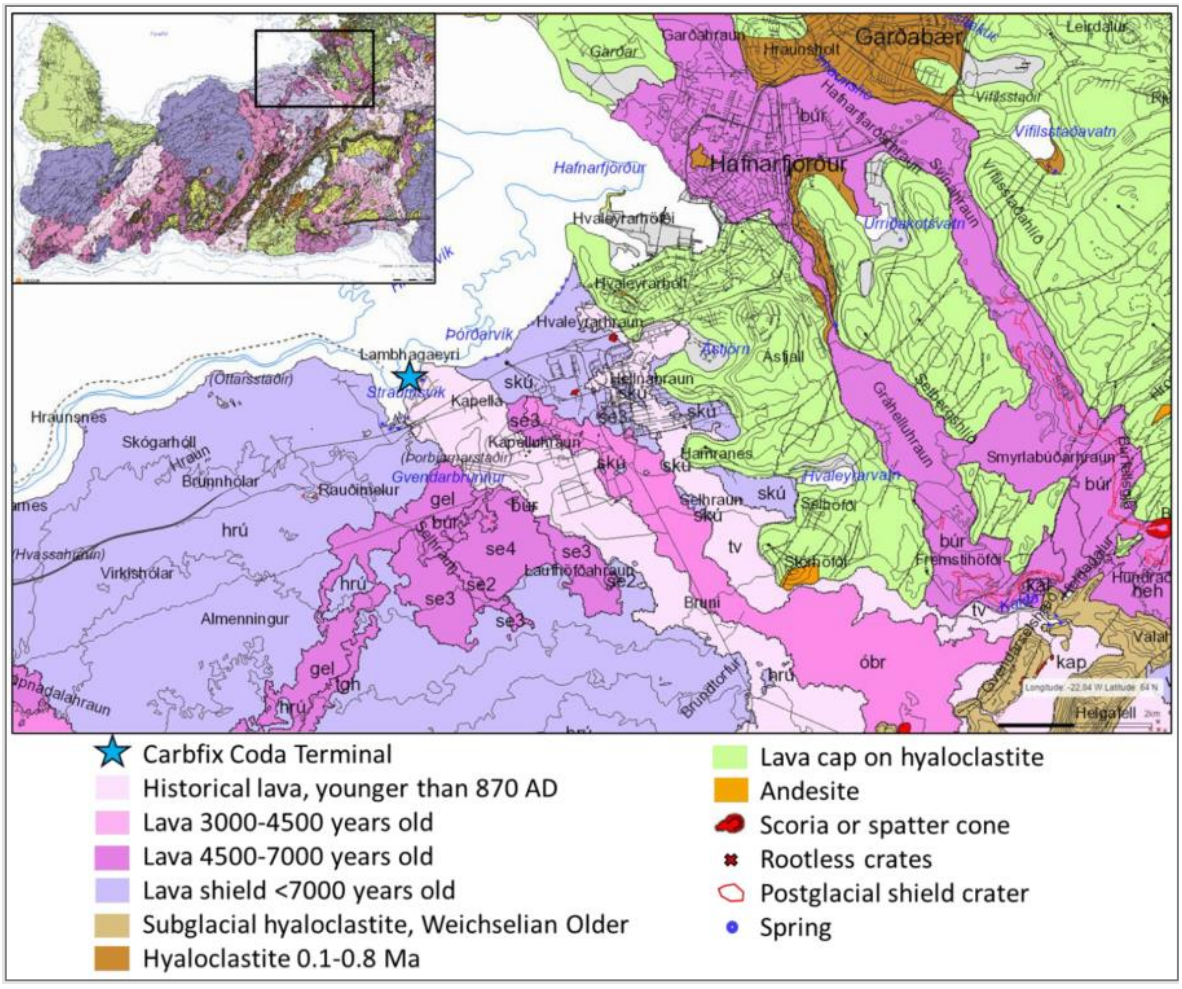

Figure 3. Surface geology map of the Straumsvík area (taken from ÍSOR, 2021). Post-glacial lavas are shown in shades of pink and purple, inter-glacial lavas (grágrýti) in light green and hyaloclastites (móberg) in light brown.

3.2. Recent research

In order to obtain information on the hydrogeology in the coastal area at Straumsvík, Carbfix commissioned the drilling of several wells (locations shown on Figure 4). Their first research well, CSI-01, was completed in the autumn of 2022 (ÍSOR, 2023b). It was drilled to a depth of 982 m with casing extending from the surface to 328 m depth. ÍSOR performed a detailed lithological analysis of the well cuttings (ÍSOR, 2023a) which revealed that post-glacial lava flows extend from the surface down to 68 m depth. Below those surface layers lies a 54 m thick layer of grágrýti, the same formation that outcrops at the surface in the area immediately east of Straumsvík. Underlying the grágrýti is an 8 m thick sedimentary rock, possibly a tillite formed by an advancing glacier. The depth range of 122-710 m is dominated by a series of alternating glassy basalt, breccia and lava flows, indicating that lava flowed into the ocean at this location. The bottom of the well, from 710-982 m depth, is a rather uniform series of lava flows.

A second research well, CSM-01, was commissioned by Carbfix in the summer of 2023 in an effort to obtain hydrogeological data further inland and widen the scope of their research area (ÍSOR, 2024a). The well is located approximately 1.4 km southeast of well CSI-01 (Figure 4) and was drilled to a depth of 618 m. Lithological analysis of the well cuttings by ÍSOR show a similar stratigraphic sequence in the upper 120 m as is found in well CSI-01. However, below this depth there was significantly less glassy basalt and breccias observed in well CSM-01 compared to well CSI-01, indicating a difference in paleoenvironmental conditions between the wells at the time the rocks were formed.

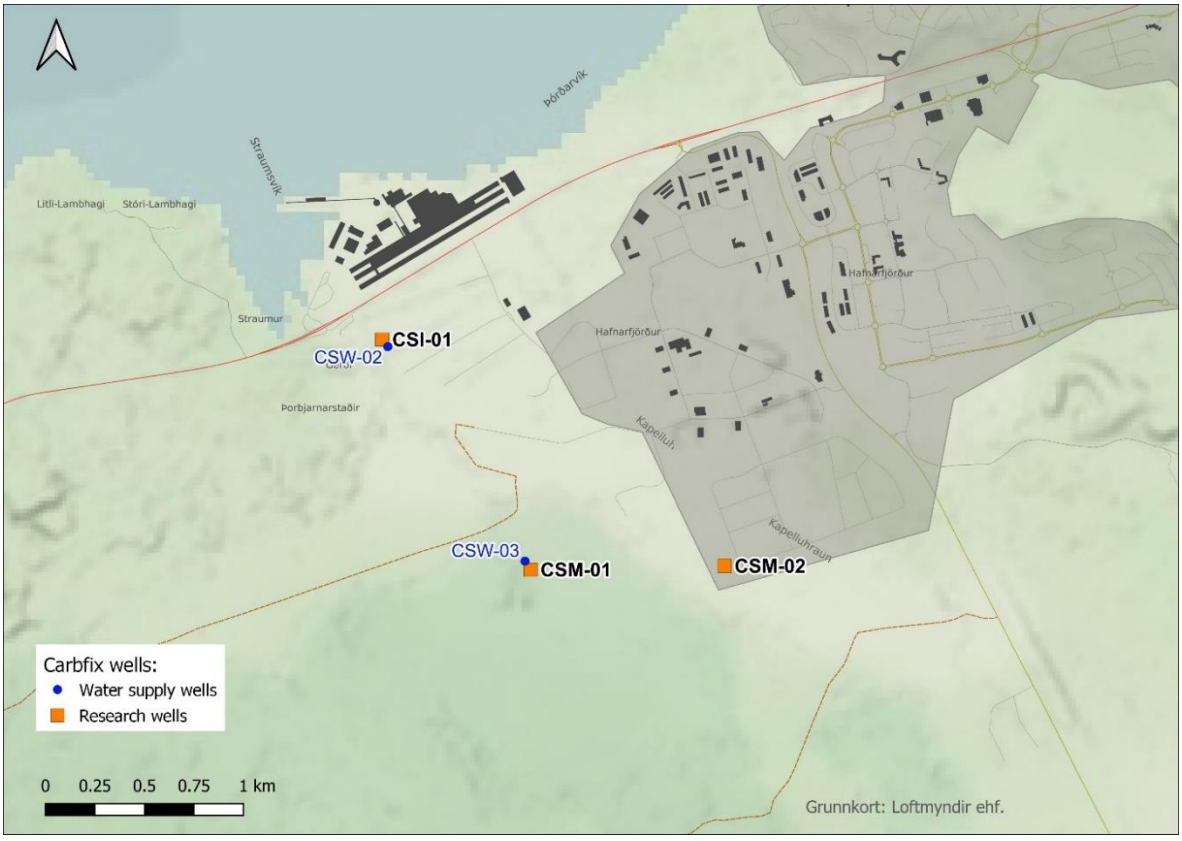

Figure 4. Location of Carbfix wells from which hydrogeological data was collected.

Drilling of a third research well, CSM-02, roughly 1 km east of well CSM-01, is currently underway (Figure 4). Current plans are to drill to a similar depth as CSM-01, with the goal of providing further information for understanding of the local hydrogeology. Initial information from the upper 200 m of the well indicates a similar lithological sequence as observed in well CSM-01.

With the stratigraphic information gathered from the new Carbfix exploration wells, ÍSOR updated their existing geological model of the greater Reykjavík area which is built on extensive data from the Reykjavík low-temperature geothermal fields to the NE. The model characterizes the stratigraphy down to a depth of 2 km and provides geological information on the main individual lithological units (ÍSOR, 2023d). Two cross sections from the geological model are shown on Figure 5. A paleoenvironmental shift is clearly evident in the upper 1000 m along the WNW-ESE section. The eastern edge of the section is dominated by hyaloclastite formations indicating a sub-glacial eruptive environment, whereas the western part of the section is dominated by glassy basalt formations indicating a coastal, sub-aqueous depositional environment.

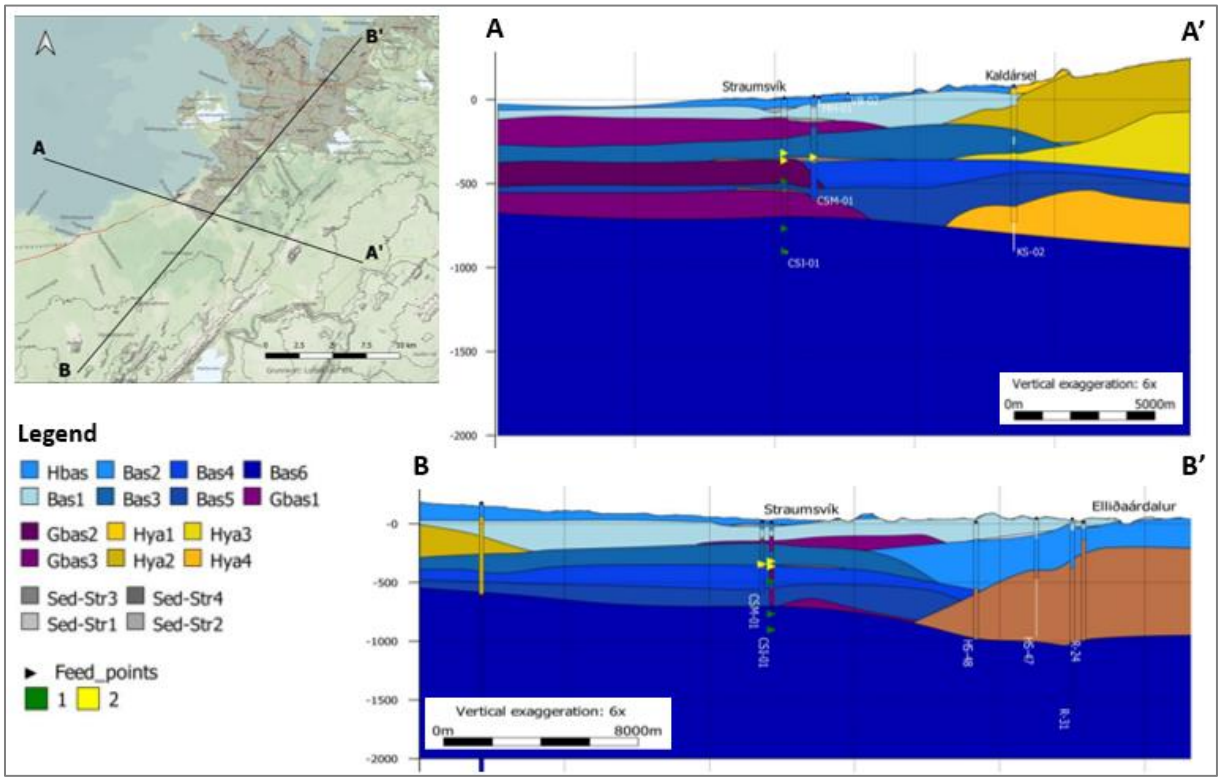

Figure 5. Geological stratigraphy in the Straumsvík area. Cross sections are taken from ÍSOR's geological model (ÍSOR, 2023d) with basaltic lava flows represented with shades of blue, sedimentary layers with grey, hyaloclastites with yellow and brown and glassy basalts with purple. Locations of feed zones are indicated with yellow (main feed zones) and green (minor feed zones) arrows.

A comprehensive set of measurements and tests were carried out by ÍSOR in wells CSI-01 and CSM-01, including geophysical logging, Televiewer analysis, salinity and temperature profiles and injectivity testing. Analysis of this new data by ÍSOR (2023a, b, c, d, e; 2024a, b) provided valuable information on key characteristics of the groundwater system in the Straumsvík area. These analyses included identification of feed zones in both wells, which provided important information on the relative permeability of penetrated rock formations and in turn, where injection fluid is most likely to enter the groundwater system. Injectivity tests indicate that the majority of feed zones in both wells lie within a

depth range of roughly 320-370 m b.s.l., with the most productive feed zones at 364 m b.s.l. in CSI-01 and 338 m b.s.l. in CSM-01 (ÍSOR, 2024b). The tests suggest limited permeability below this depth range in both wells, however temperature profiles in CSI-01 indicate the presence of minor feed zones down to roughly 509 m b.s.l. Calculated injectivity index in well CSI-01 (5 L/s/bar) was considerably lower than in CSM-01 (25 L/s/bar) suggesting higher permeability formations in well CSM-01 (ÍSOR, 2024b). Although no fractures are visible at the surface in the immediate Straumsvík area, Televiewer analysis confirmed that they are present in the subsurface formations and predominantly strike in the NE-SW direction (ÍSOR, 2023c). According to ÍSOR, the data indicate that feed zones in wells CSI-01 and CSM-01 are more likely controlled by lithological boundaries rather than by fractures. The main feed zones in both exploration wells (depths indicated on Figure 5) appear to coincide roughly with lithological boundaries in the vicinity of a 10-30 m thick sedimentary layer („Sed-Str3“ formation defined by ÍSOR).

Temperature and electrical conductivity logs recorded in wells CSI-01 and CSM-01 after drilling support the conclusions drawn from the injectivity tests regarding location and productivity of feed zones. They also provide valuable information on variability in groundwater characteristics at different depth ranges within the groundwater system. Figure 6 compares temperature and electrical conductivity logs measured shortly after drilling of each well (dashed lines) with the most recently measured logs (solid lines). The temperature logs show that well CSI-01 was cooled during drilling and has heated up significantly since then. The most recent log from November 2023 indicates that a relatively stable temperature of approximately 80 °C has been reached at the bottom of the well. Both wells CSI-01 and CSM-01 show a similar temperature gradient of around 80 °C/km which corresponds to the expected regional gradient in the area (ÍSOR, 2023d).

Electrical conductivity logs typically provide valuable information on groundwater salinity and can help identify the interface between the shallow freshwater aquifer and the underlying saline aquifer. Due to technical issues, reliable measurements of electrical conductivity could not be performed in well CSI-01 during drilling. The two electrical conductivity logs shown on Figure 6 for well CSI-01 were performed after drilling, meaning that measurements above 318 m b.s.l. are within the well casing and therefore do not reflect natural conditions. However, a rough estimation of the depth to the fresh/saline interface was made by interpretation of water samples taken during drilling. These water samples show a sharp increase in electrical conductivity at approximately 100-110 m b.s.l. indicating that the top of the fresh/saline interface is most likely within this depth range at well CSI-01 (Figure 6). The electrical conductivity logs from well CSM-01 provide strong evidence for the depth to the fresh/saline interface. Measurements show a sharp rise in electrical conductivity at approximately 350 m b.s.l. which is below the bottom of the well casing (200 m b.s.l.). The top of the fresh/saline interface, therefore, lies at approximately 350 m b.s.l. at well CSM-01. Both wells CSI-01 and CSM-01 show an increase in conductivity below ~350 m a.s.l. after drilling, indicating that drilling fluids likely caused a decrease in salinity below this depth and that the salinity is still recovering back to natural conditions. The most recent electrical conductivity logs in both wells show a decrease in conductivity with increased depth below ~350 m b.s.l. It is not known for certain whether this behavior represents the natural conditions or if it is caused by disturbance from drilling and testing of the wells. Continued well logging is necessary in order to confirm the natural-state conditions at the wells.

ÍSOR also performed profile measurements in well KS-02 at Kaldársel at the beginning of 2023. The results confirmed older measurements from the well, showing that freshwater extends from the surface all the way to the bottom of the well (986 m depth). Temperature in the well is < 6 °C down to a depth of 800 m, below which it steadily increases up to roughly 18 °C at the bottom of the well.

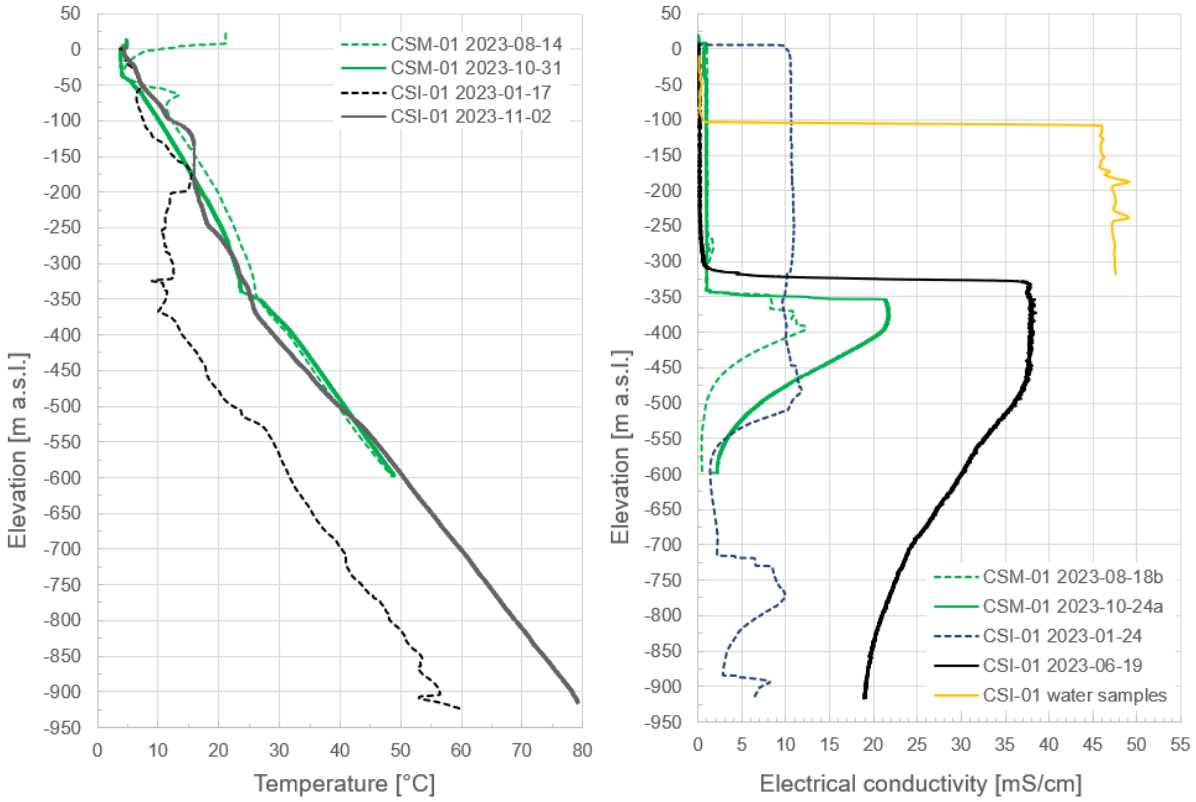

Figure 6. Measured temperature (left) and electrical conductivity (right) logs taken in wells CSI-01 and CSM-01. Electrical conductivity of water samples taken from well CSI-01 during drilling are also shown.

ÍSOR performed four TEM (micro-TEM) survey campaigns in the Straumsvík area between October 2022 and April 2023 in an effort to gain a better understanding of saline intrusion in the coastal region (ÍSOR, 2023e). Limitations on the TEM technique, including disturbances caused by electromagnetic noise (e.g., power lines) prevent an accurate mapping of the fresh/saline interface. However, the survey results can be useful in gaining an understanding of general patterns in the interface. Survey locations are shown on Figure 7. Analysis performed by ÍSOR indicate that the top of the interface increases in depth along the cross section "STVcross" from < 25 m b.s.l. at the coastline to roughly 50 m b.s.l. at a distance of roughly 2 - 2.5 km inland (Figure 8). Further inland beyond approximately 2.5 km, no interface was detected along the cross section, indicating that it lies very deep or does not exist. However, soundings to the east of the "STVcross" cross section show a different behavior of the interface. Sounding STV-20, located next to exploration well CSI-01, indicates an interface level of about 120 m b.s.l. which corresponds roughly to the level (100-110 m b.s.l.) estimated from water samples taken from CSI-01 during drilling (shown on Figure 6). Well CSM-01 lies roughly 1.4 km from well CSI-01 on a line roughly parallel to cross section "STVcross". As explained above and shown on Figure 6, electrical conductivity logs show that the interface lies at approximately 350 m b.s.l. at CSM-01. Therefore, the data indicate that a shift occurs in the fresh/saline interface within a relatively short distance from cross section "STVcross" towards the east, with a significant deepening of the top of the interface. It should be stressed that a high level of uncertainty is associated with interpretation of TEM soundings. ÍSOR suggests that additional TEM surveys positioned at strategic locations are needed to gain a clearer understanding of the behavior of the fresh/saline interface at Straumsvík.

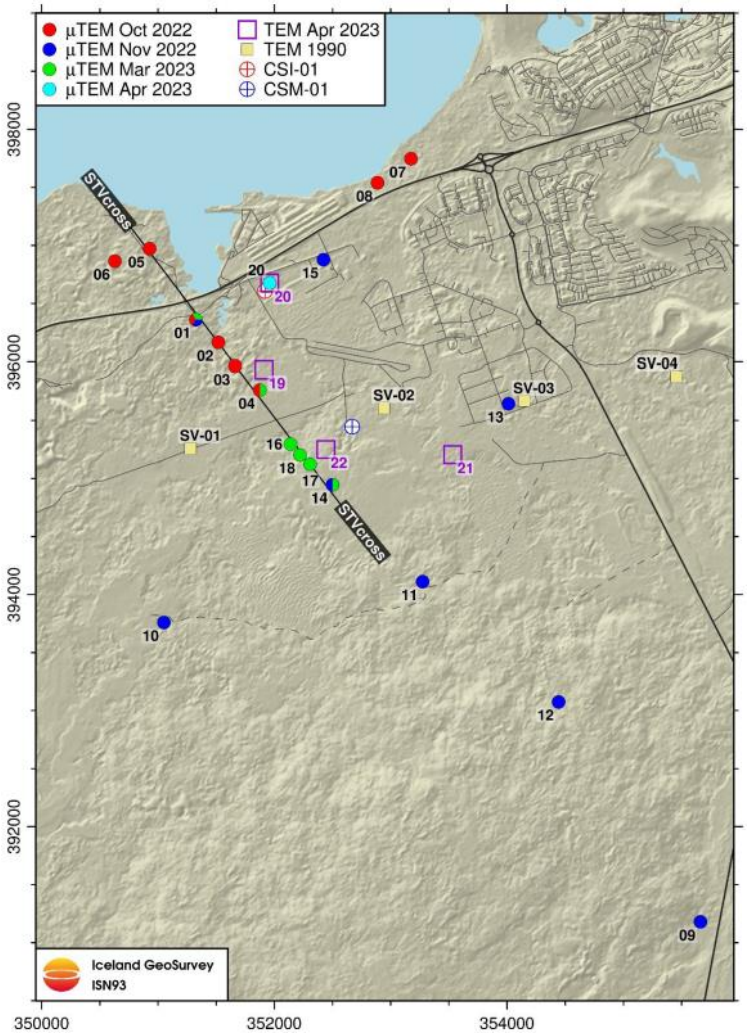

Figure 7. Location of TEM soundings performed by ÍSOR (map taken from ÍSOR, 2023e).

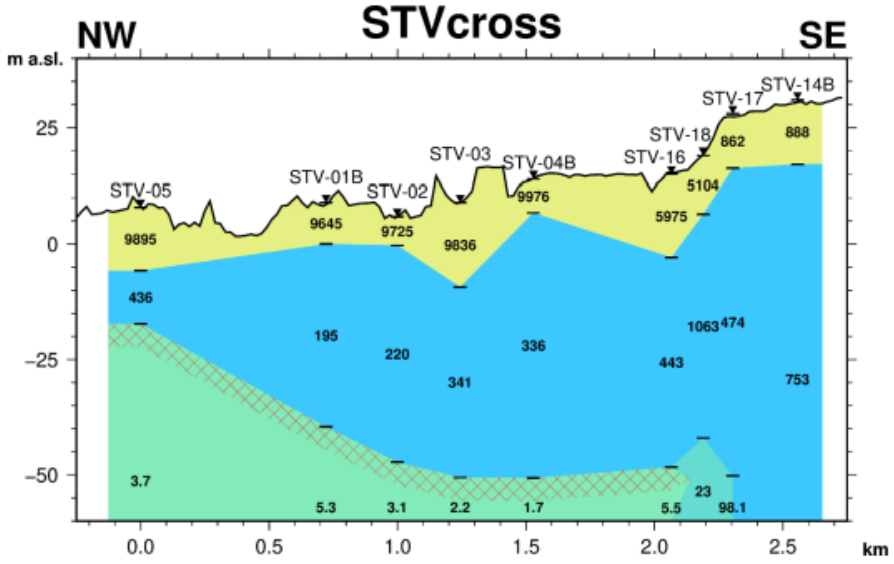

Figure 8. Cross section „STVcross“ (location shown on Figure 7) taken from ÍSOR (2023e) showing interpretation of TEM measurements. Yellow and blue areas reflect rocks above saline water, and the green area represents saline water. The red mesh represents the top of the fresh/saline interface.

3.3. Conceptual model of groundwater system

A shallow groundwater aquifer exists within the post-glacial lava formations in the coastal region surrounding Straumsvík. The lava formations are roughly 40-70 m thick (Orkustofnun, 1976) and are conducive to groundwater flow due to their high permeability. In addition to favorable geological conditions, the hydrology of the Straumsvík watershed is also favorable for supporting a productive groundwater aquifer. The watershed receives a relatively high amount of precipitation which provides significant recharge to the groundwater system. Annual precipitation is around 1 m/year in the Straumsvík area and increases with elevation up to over 3 m/year at the groundwater divide in the Bláfjöll mountain range (Icelandic Meteorological Office, 2007). Due to the fresh, permeable nature of the surface geology, surface runoff is minimal and the majority of the precipitation infiltrates into the groundwater system.

Observations in shallow wells in the vicinity of the Rio Tinto aluminum smelter, including measurements from shallow Carbfix wells CSW-02 and CSW-03 (locations shown on Figure 4), show a clear tidal influence on the groundwater aquifer, as the water table fluctuates with the ocean tides (Tómasson and Tómasson, 1966). These tidal effects are greatest at the coastline and gradually dissipate with increased distance inland. Semidiurnal fluctuations in groundwater levels due to tidal effects are roughly two meters near the coastline at Straumsvík (ÍSOR, 2010), 65 cm at Carbfix well CSW-02 (500 m inland) and less than 10 cm at Carbfix well CSW-03 (1.7 km inland). Tidal effects are also observed in the freshwater coastal ponds in the area (Ingólfsson, 1998). Despite this tidal influence on water levels, the water itself at the water table and in the coastal ponds is fresh and not affected by saline intrusion. This is attributed to the strong groundwater flow in the shallow aquifer. However, intrusion of saline water from the ocean inland does occur below the freshwater. The groundwater system in the coastal zone is therefore divided into two salinity zones, a shallow zone of freshwater flowing seaward and an underlying saline zone which extends inland. The density difference between the fresh and saline water causes the lighter freshwater to flow on top of the denser saline water. A dynamic pressure equilibrium exists between the freshwater and the underlying saline water. Pressure changes induced by external forces (e.g., variable infiltration, tidal fluctuations and production) disrupt the equilibrium and create a mixing zone at the interface between the two zones with a range of salinity between fresh and fully saline (brackish water).

A hydrogeological map of the Straumsvík area (Hjartarson et al., 1992) is shown on Figure 9. Dark green shaded areas on the map are classified as having very permeable, anisotropic rock. These areas indicate the most productive sections of the shallow groundwater aquifer within the post-glacial lavas. Areas classified as having permeable and semipermeable rock correspond to less productive sections of the aquifer within lower permeability geological formations such as grágrýti and hyaloclastites.

Beside the new data collected in Carbfix wells CSI-01 and CSM-01 and well KS-02 in Kaldársel (Chapter 3.2), few definitive measurements of depth to the fresh/saline interface exist in the Straumsvík area. Electrical conductivity measurements in well HH-02 at Hvaleyri and well VL-08 at Vatnsleysuvík indicate that the top of the mixing zone lies at a depth of roughly 30 m b.s.l. (Figure 10). Both wells are within 150 m from the shoreline. This data along with interpretation of TEM surveys by ÍSOR (Chapter 3.2) provide a very limited picture of the regional characteristics of the fresh/saline interface. As explained in Chapter 3.2 above, available data seem to suggest a distinct change in character of the interface in the vicinity of Straumsvík (just west of wells CSI-01 and CSM-01). It has been suggested by ÍSOR (2023f) that this change in character at Straumsvík corresponds to a shift from a mountain-dominated hydrogeological setting with high groundwater gradients towards the southeast (i.e. Bláfjöll) to a low-

lying coastal-dominated hydrogeological setting with low groundwater gradients towards the southwest (i.e., Reykjanes peninsula).

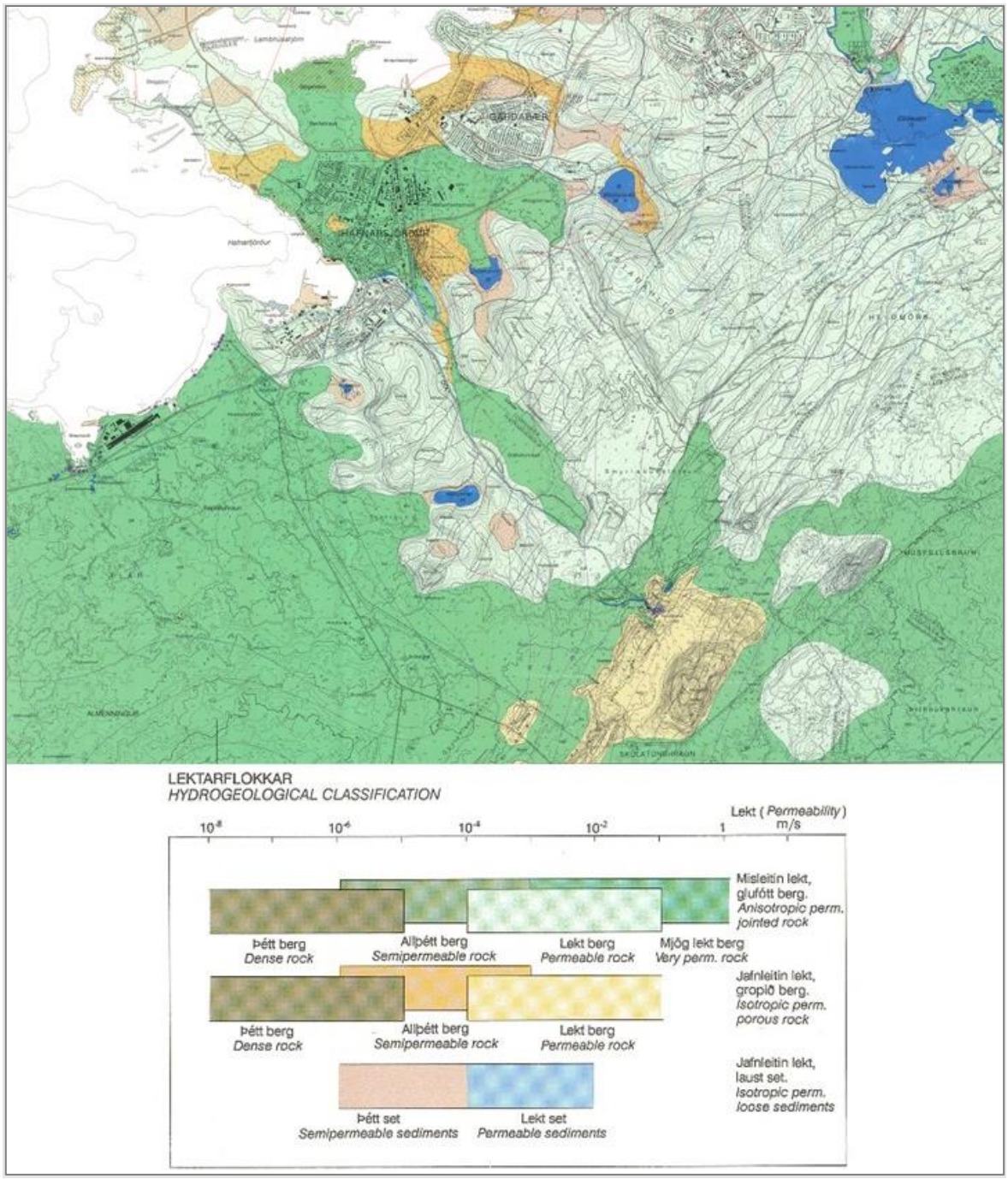

Figure 9. Hydrogeological map of the Straumsvík area (Hjartarson et al., 1992).

A relatively good distribution of groundwater level measurements is available within the Straumsvík watershed, allowing for a reasonably accurate general characterization of the groundwater surface and regional groundwater gradients (Figure 10). The groundwater divide forming the upper limit of the Straumsvík watershed extends from Kleifarvatn towards the northeast through the higher elevations of the Brennisteinsfjöll and Bláfjöll mountain ranges. Regional groundwater flow direction is from the

divide towards the coastline to the northwest, with the strongest flow concentrated within highly permeable post-glacial lava formations (Figure 10). Estimates of groundwater flow from the shallow aquifer have been made from observations of spring flow in intertidal zones in the area. Groundwater outflow into the ocean at Straumsvík has been estimated at roughly 8-10 m^3/s, making it the second largest coastal groundwater outflow area in Iceland behind only Lón in Kelduhverfi in NE Iceland (Sigurðsson, 1998). In Vatnsleysuvík bay to the west of Straumsvík, groundwater outflow at the coastline is estimated at roughly 7 m^3/s (Orkustofnun, 1976).

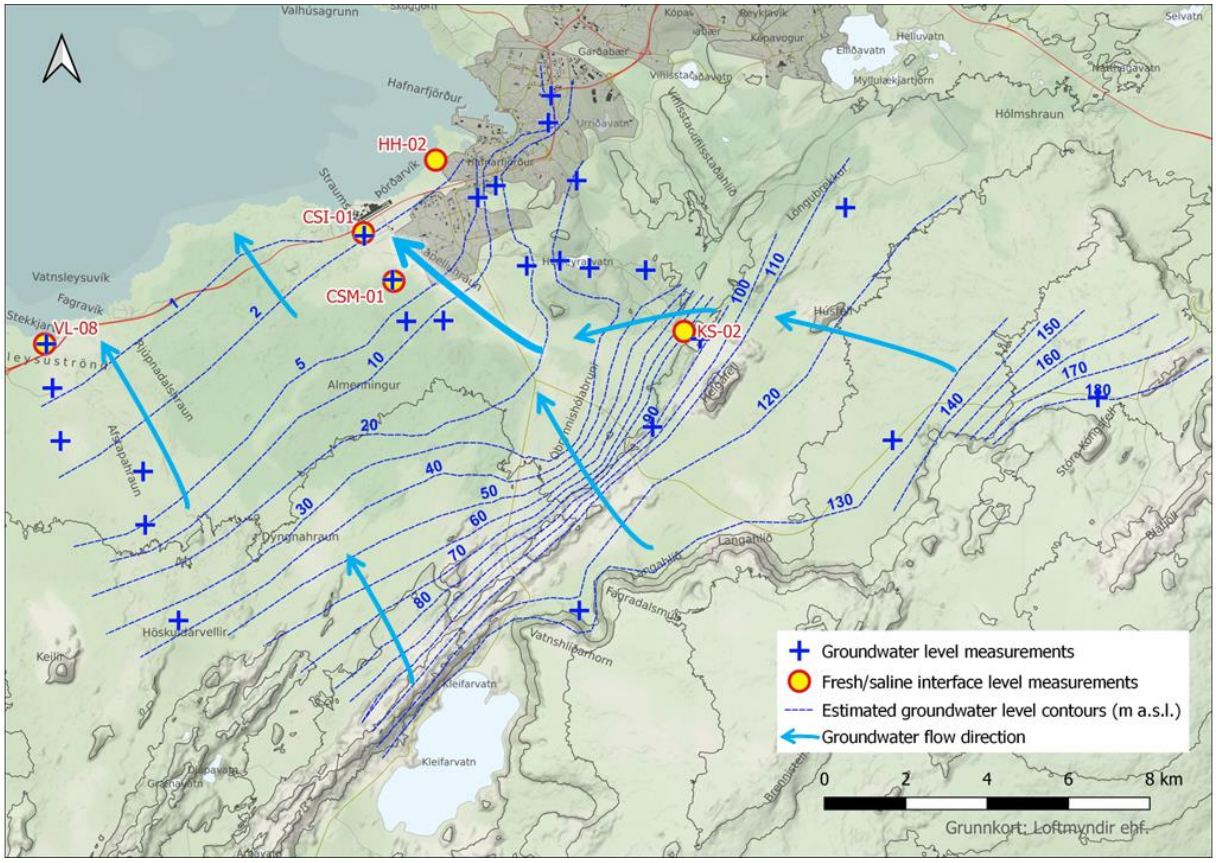

Figure 10. Measurement locations of groundwater level and fresh/saline interface level, estimated groundwater level contours and main groundwater flow paths.

4. Numerical model

A numerical modelling approach is required to assess the potential impacts from the planned production and injection at the Coda Terminal on the local groundwater system. Vatnaskil's existing regional watershed model of southwest Iceland was used as a foundation for the modelling work. However, due to the spatial and temporal scales of the project, an update to the watershed model was necessary to properly simulate the planned stages of production and injection at the Coda Terminal and assess their impacts.

4.1. Model update

Vatnaskil's regional watershed model of southwest Iceland covers the entire Reykjanes peninsula as well as the Capital area (Reykjavík and surrounding municipalities) and extends eastward to Ölfusá and

northward to Hvalfjörður. The model has been in development for over 40 years and is updated on a regular basis for the Association of municipalities in the Capital area (SSH) and HS Orka (Vatnaskil, 2022a and 2023). The watershed model consists of two integrated hydrological models, a surface-runoff model and a groundwater model, each one simulating a different aspect of the hydrological cycle. The surface-runoff model utilizes a variety of meteorological input (e.g., precipitation, temperature, humidity) produced by regional weather models and solves energy exchange equations to calculate snowmelt and surface runoff. The model takes into account land-use and soil-type characteristics and calculates the amount of water that infiltrates through the unsaturated zone and down to the groundwater table. The groundwater model receives infiltration input from the surface-runoff model, takes into account geological conditions, and simulates groundwater flow through the saturated zone. The groundwater model is a 2D model which simulates the shallow freshwater aquifer within the upper ~100 m of the groundwater system.

In order to account for the saline aquifer in the coastal region around Straumsvík as well as the deeper sections of the groundwater system at target injection depths, the model was extended down to a depth of 1100 m b.s.l. and upgraded to 3D with layering based on available geological information. The iTOUGH2 modelling software was utilized for the 3D model as it provides flexibility through various EOS (equation of state) modules for simulating the flow of variable density liquid under variable background conditions. Calculated infiltration from the surface-runoff model was applied as input at the top boundary of the updated groundwater model. Results from the regional groundwater model were used to delineate and assign appropriate boundary conditions for the 3D model, incorporating completely the surface and groundwater watersheds surrounding Straumsvík (Figure 11). Furthermore, the model was extended roughly 17 km out into the ocean in order to incorporate the saline aquifer below the seabed and therefore adequately model the intrusion of saline groundwater below the coastline towards the southeast. Measurements of ocean bathymetry were used to define the seabed in the model.

The updated geological model from ÍSOR (Figure 5) was used as a guideline for assigning rock types to model elements (Figure 12). Hydrogeological parameters (e.g., permeability, porosity, anisotropy) were assigned to each rock type based on published values from research and testing performed in the local Straumsvík area and other similar geological settings in Iceland (Hjartarson et al., 1992; Orkustofnun, 1976; Orkustofnun, 1977; Tómasson and Tómasson, 1966). Additionally, ÍSOR provided relative permeability values for the rock types within their geological model (ÍSOR, 2023d), and these were also used as a guideline during model construction. In general, permeability and porosity decrease with depth, especially below 400 m in the Straumsvík area where geothermal alteration becomes more prevalent, filling void spaces in rocks and hindering the flow of groundwater. Anisotropic conditions were applied to model elements within the main fissure swarms (Figure 2) in order to simulate preferred groundwater pathways due to fracturing.

As explained above in Chapter 3.2, the main feed zones identified in both exploration wells are within a depth range of 320-370 m b.s.l. and according to ÍSOR (2023d) they most likely coincide with lithological boundaries. In order to represent this enhanced permeability zone in the numerical model, vertical grid resolution was increased around this depth range and a unique rock type was defined with hydrogeological parameters corresponding to a productive water-bearing formation. The sedimentary unit was also represented in the model with a unique rock type with relatively low permeability as expected by ÍSOR (2023d).

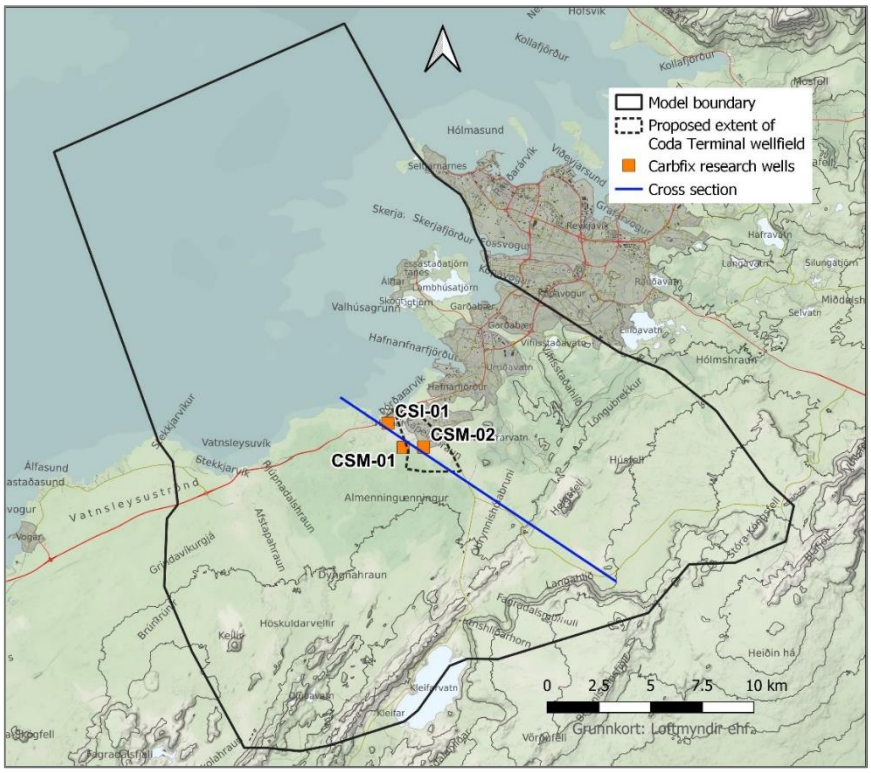

Figure 11. Outer boundaries of the 3D Straumsvík groundwater model.

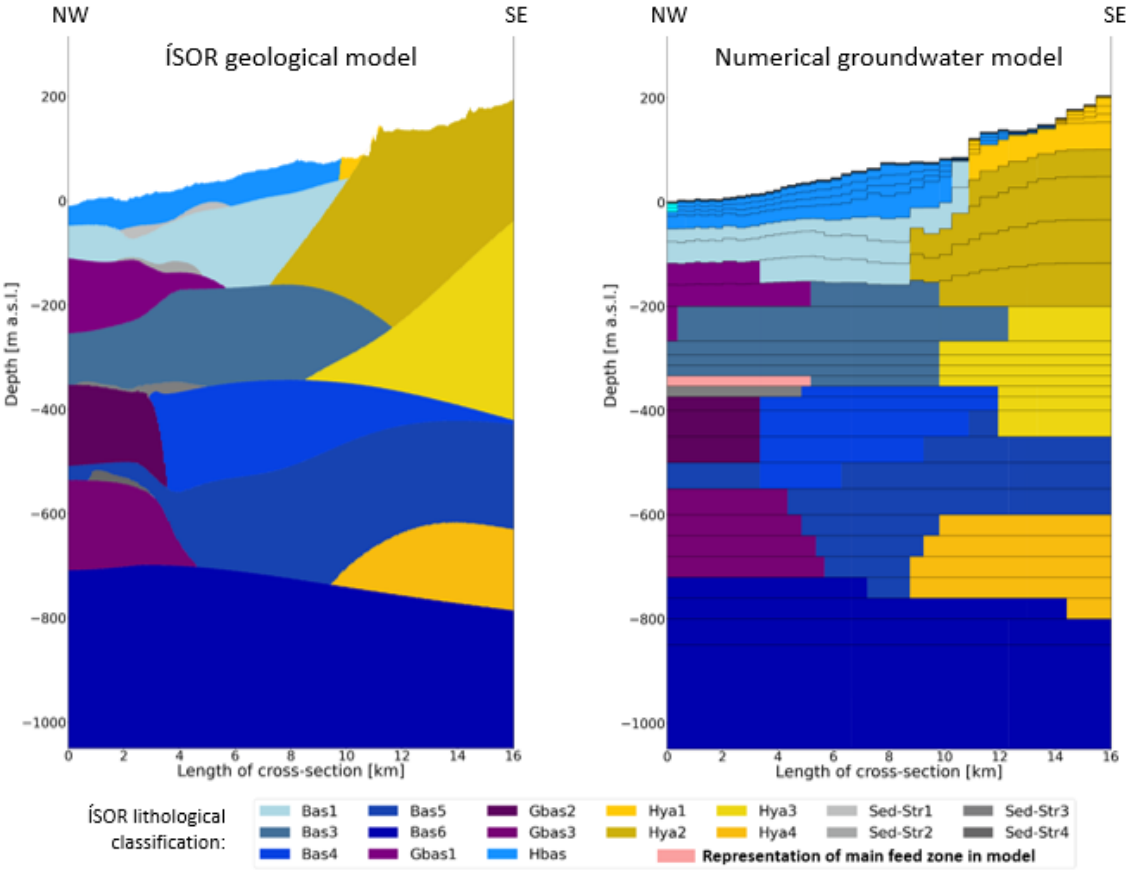

Figure 12. Representation of geological layering along NW-SE cross section (shown on Figure 11) in the ÍSOR geological model (left) and the numerical groundwater model (right).

4.2. Baseline model

After updating the groundwater model, a thorough assessment of the new 3D model was made to ensure that an acceptable representation of the Straumsvík watershed had been achieved. Adjustments and fine-tuning of input parameters were needed to produce a baseline model which adequately simulates the natural-state conditions in the groundwater system. In the context of this assessment, the term natural-state is used to describe the current conditions in the groundwater system prior to commencement of the Coda Terminal. These current conditions include existing groundwater production (e.g., at Rio Tinto and Kaldársel) which in reality have already altered the true natural state of the groundwater system (albeit to a relatively minor extent).

Simulated groundwater level contours and groundwater flow paths in the shallow freshwater aquifer are shown on Figure 13. Comparison with estimated groundwater levels contours based on measurements (Figure 10) shows that the baseline model is able to reproduces the large-scale regional groundwater table morphology and regional groundwater flow patterns. A cross section along the main regional groundwater flow path from Bláfjöll down to Straumsvík shows that the model simulates the measured slope of the groundwater table relatively well (Figure 14).

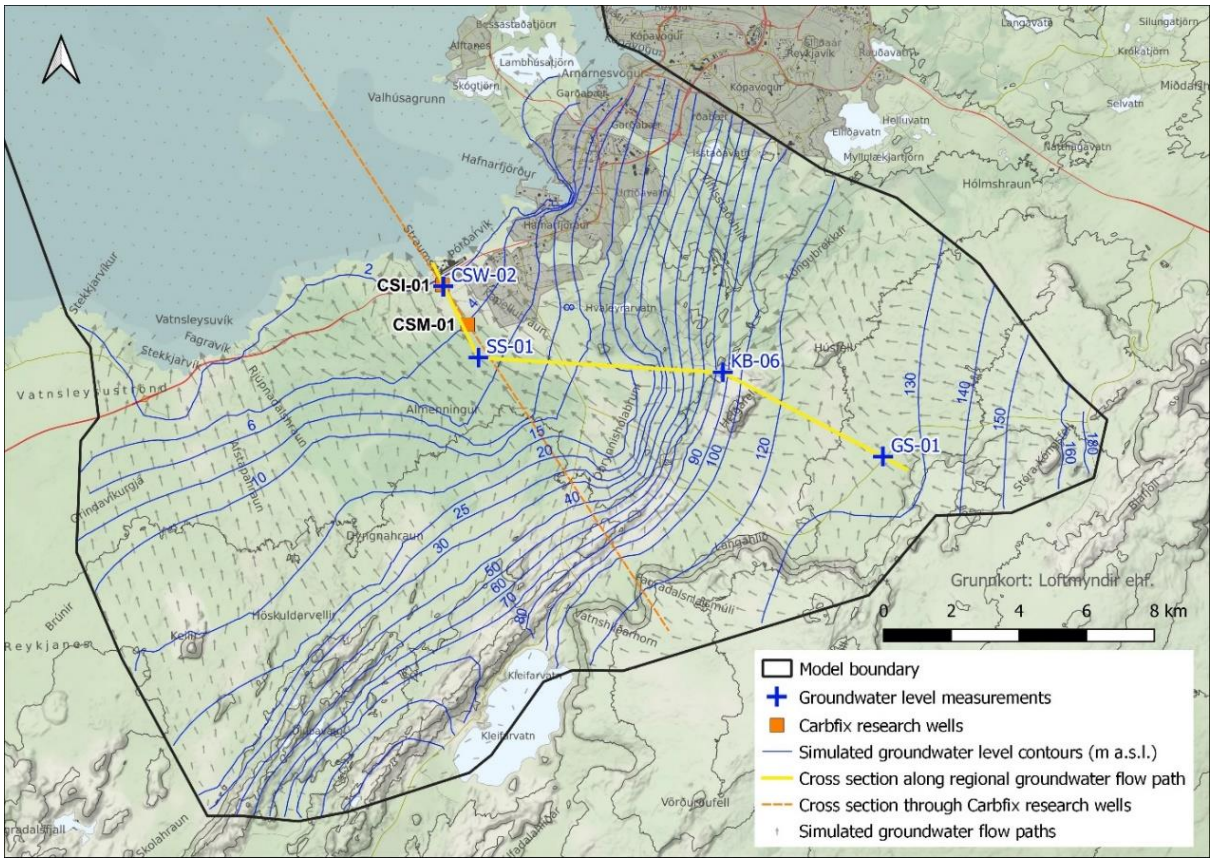

Figure 13. Simulated groundwater level contours and flow paths in the shallow freshwater aquifer. Measured and simulated groundwater levels along the yellow cross section are plotted on Figure 14. Simulated temperature and salinity along the orange cross section are shown in Figure 16.

Simulated groundwater temperature and salinity profiles in Carbfix wells CSI-01 and CSM-01 and well KS-02 in Kaldársel are shown on Figure 15. The model performs well in reproducing the measured temperature gradients in both Carbfix wells. The simulated temperature in well CSM-01 compares very

well with measurements, however the model slightly underestimates the temperature in well CSI-01 by roughly 2-5 °C. Comparison of measured and simulated temperature in well KS-02 shows that the model slightly overestimates the temperature in the well, particularly between 450-850 m b.s.l.

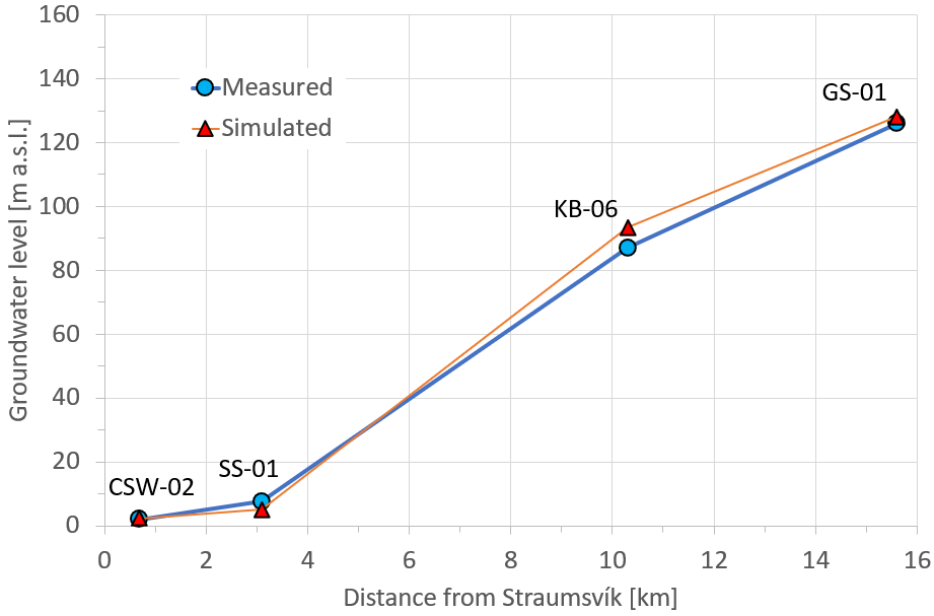

Figure 14. Cross section (location shown on Figure 13) along the regional groundwater flow direction from Bláfjöll to Straumsvík showing measured and simulated groundwater levels.

As discussed in Chapter 3.2 above, a variety of technical issues during drilling and disturbances to the natural-state conditions during well testing have resulted in uncertainties in the electrical conductivity measurements in both Carbfix wells. This makes interpretation of the measurements difficult and limits their applicability in model validation. However, together with the TEM analysis (described in Chapter 3.2), an initial estimation of the fresh/saline interface could be formulated and used as a rough guideline for the baseline model. This initial estimation positions the top of the fresh/saline interface at a depth of approximately 100 m b.s.l. in well CSI-01 and 350 m b.s.l. in well CSM-01 (estimated interface levels shown as dashed lines on Figure 15). As Figure 15 shows, the baseline model simulates an increase in salinity in well CSI-01 at approximately 100 m b.s.l. which corresponds to measurements, however, full salinity is not reached until around 230 m b.s.l. in the well. The simulated salinity in well CSM-01 begins to increase at roughly 150 m b.s.l. and reaches full salinity at 350 m b.s.l. which corresponds to the depth at which full salinity is measured in the well. In both wells, the model simulates a mixing zone at the fresh/saline interface which is thicker than interpretation of available measurements suggest. This overestimation of the thickness of the mixing zone is potentially due to limitations on numerical spatial resolution in the model. The model simulates a slight decrease in salinity below about 800 m b.s.l. in well CSM-01. This type of salinity inversion is observed in measurements from both wells, but as stated in Chapter 3.2 above, it is uncertain whether this behavior is natural or if it is caused by disturbance from drilling and/or testing of the wells. Continued well logging is necessary in order to confirm the natural-state conditions. The model simulates freshwater extending all the way down to the bottom of the well KS-02 (roughly 900 m b.s.l.) which agrees with measured data.

Simulated natural-state groundwater temperature and salinity from the baseline model are shown along a NE-SW cross section through wells CSI-01 and CSM-01 on Figure 16. The highest temperatures occur within a 7 km wide zone under the Carbfix wells and extending northwest. The temperature gradient within this zone is roughly 80-90 °C/km as confirmed by measurements in the Carbfix wells. The temperature gradient declines significantly towards the southeast as fractures within the Krýsuvík fissure swarm presumably allow the downflow of colder groundwater from the shallow aquifer (ÍSOR, 2023d). The temperature gradient also decreases towards the northwest end of the cross section, presumably due to increased distance from the active volcanic zone.

The salinity cross section on Figure 16 shows how saline groundwater from the northwest (under the ocean) intrudes landward towards the southeast and extends below the Straumsvík area. Saline intrusion reaches its maximum landward extent (roughly 4 km inland from the coastline at Straumsvík) at around 600 m b.s.l. Below that depth, saline intrusion decreases slightly down to 1000 m b.s.l. Simulated natural-state groundwater salinity is shown in plan-view at four depth intervals within the groundwater system on Figure 17. At -20 m a.s.l., saline intrusion occurs everywhere along the coastline except at the coastal inlet at Straumsvík where freshwater discharges into the ocean. As the figure shows, saline intrusion extends further inland with increased depth down to -525 m a.s.l. The fresh/saline interface trends in the NE-SW direction across the Straumsvík area.

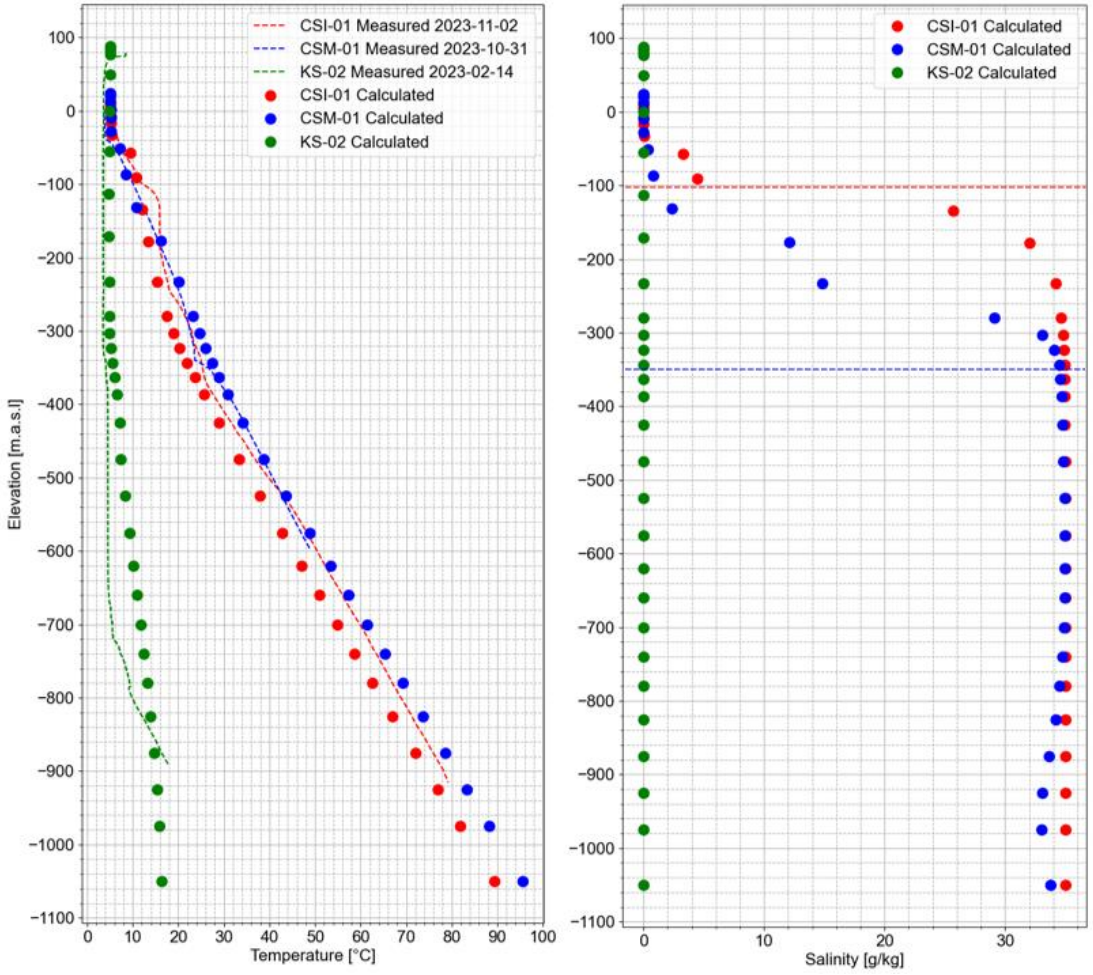

Figure 15. Simulated temperature (left) and salinity (right) profiles in Carbfix wells CSI-01 and CSM-01 and well KS-02 in Kaldársel. Dashed lines on salinity plot indicate estimated fresh/saline interface level in wells CSI-01 (red) and CSM-01 (blue).

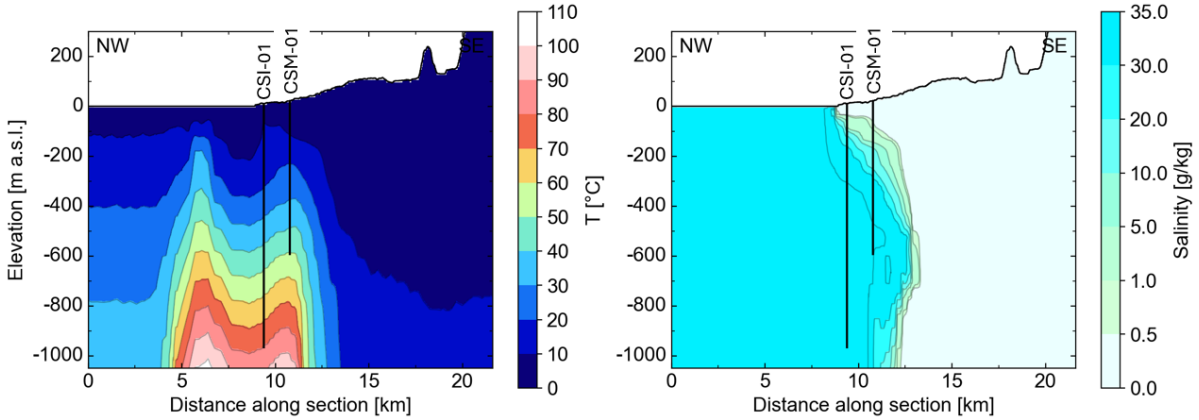

Figure 16. Cross section (location shown on Figure 13) through Carbfix research wells CSI-01 and CSM-01 showing simulated natural-state groundwater temperature (left) and salinity (right).

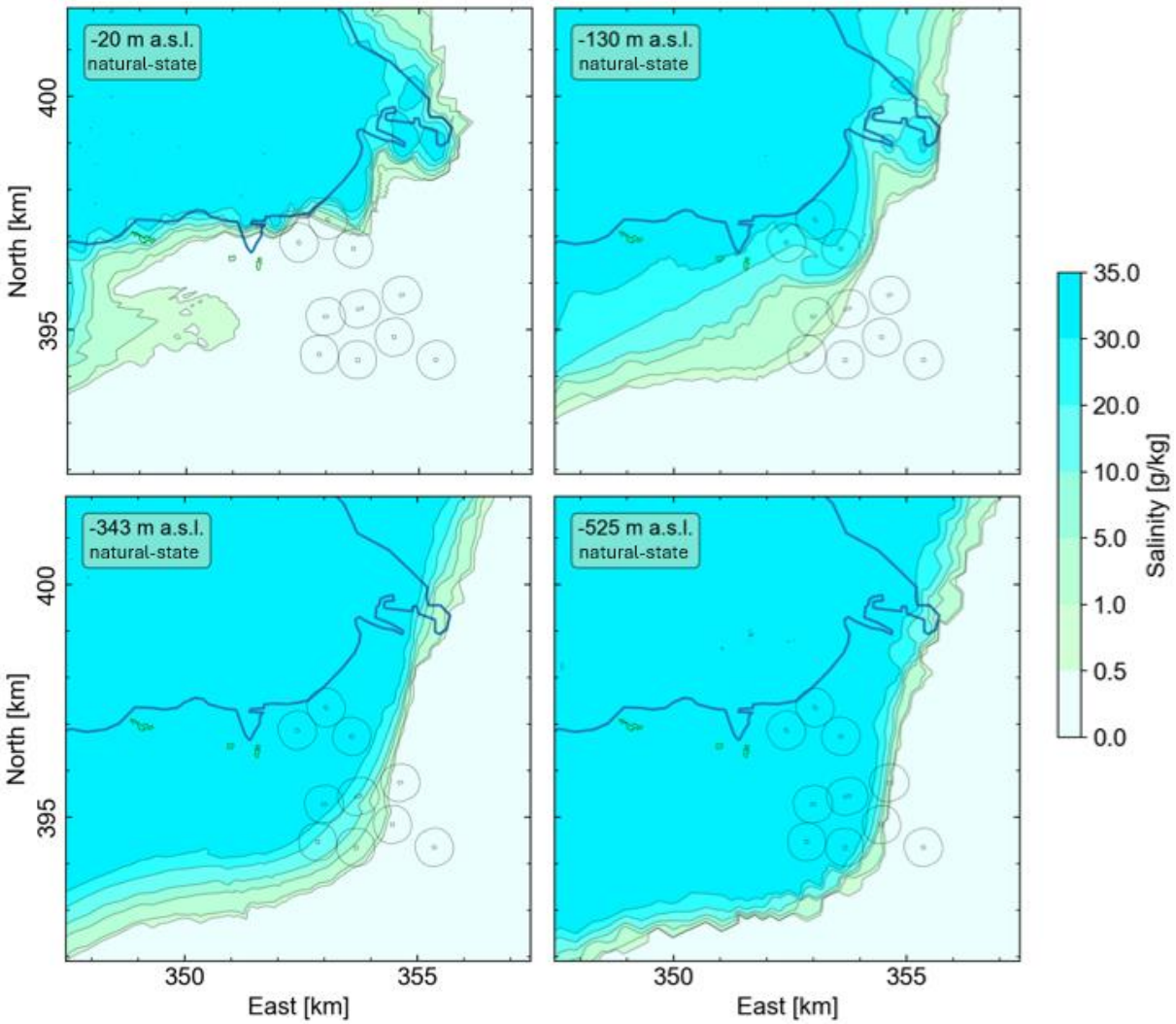

Figure 17. Simulated natural-state groundwater salinity at four depth intervals within the groundwater system.

Overall, the baseline model simulates the main characteristics of the natural-state conditions in the groundwater system within the Straumsvík watershed, producing an adequate representation of the conceptual model and the geological and hydrological data that it is built upon. It should be stressed, however, that research on the groundwater system is still in early stages, especially with respect to natural-state conditions below 100 m b.s.l. This is especially true for the fresh/saline interface, as recent data collected by ÍSOR in the Straumsvík area (Chapter 3.2) indicate a complex interface morphology. Gaining a clear picture of this morphology and an understanding of the factors controlling it should be a focus of future research. Therefore, due to limited data, a relatively high degree of uncertainty still remains regarding the natural-state conditions in the deeper groundwater system at Straumsvík. This uncertainty must be taken into account when interpreting the modelling results presented below in Chapter 5. Additional research is needed in the Straumsvík area in order to more thoroughly characterize the groundwater system, eliminate as many uncertainties as possible and increase the predictive capabilities of the model.

5. Impact assessment

The groundwater model was used to simulate the proposed production/injection at the Coda Terminal and assess potential impacts on the local groundwater system. Carbfix provided Vatnaskil with a list of specific impacts to be assessed, with a focus on changes within the shallow freshwater aquifer that could affect the environmentally sensitive areas shown in Figure 1. These impacts included changes in the salinity and temperature of groundwater and changes in groundwater level. The capture zone of the production wells within the shallow freshwater aquifer was also estimated. Additionally, effects of the proposed injection on natural-state conditions within the deeper groundwater system were examined. The fate and transport of CO_2 from the injection wells was modelled separately by Carbfix and was therefore outside of the defined scope of Vatnaskil's assessment.

5.1. Operational scenario

Carbfix supplied Vatnaskil with design parameters for the wellfield and planned production/injection rates for incremental operational stages of the facility. The wellfield design proposed by Carbfix is shown on Figure 18 and consists of 10 well pads (numbered from 1 to 10) distributed over an area of roughly 5.5 km^2. Vertical production wells from well pads 1-7 will extend from the well pads to depths of roughly 50 m with the aim of producing from the shallow freshwater aquifer. Vertical production wells from well pads 8-10 will extend deeper (>100 m) with the aim of producing saline water from below the fresh/saline interface. Injection wells will be drilled directionally from the well pads, remaining within a 400 m radius from the well pads (injection radius shown on Figure 18). Current design parameters assume that injection wells would be drilled to depths of between 300-800 m. However, it is likely that the performance of the first injection wells drilled (largely based on injectivity rates) will play a role in determining the depths of subsequent injection wells.

The operational design strategy for the Coda Terminal calls for an operational build-up in four phases as outlined in Table 1. The first phase commences in 2027 with the operation of 3 well pads (numbered 1-3 on Figure 18) producing 665 kg/s of freshwater and injecting 688 kg/s of carbonized water. Additional well pads are brought online with subsequent operational phases, culminating in the final phase (Phase 4) in which all 10 well pads are in operation, producing 2923 kg/s and injecting 3018 kg/s. Carbfix assumes that by the time Phase 4 is implemented in 2032, they will possess the technology to utilize saline water in the carbonation process. Therefore, well pads 8-10 will produce and inject saline water instead of fresh water.

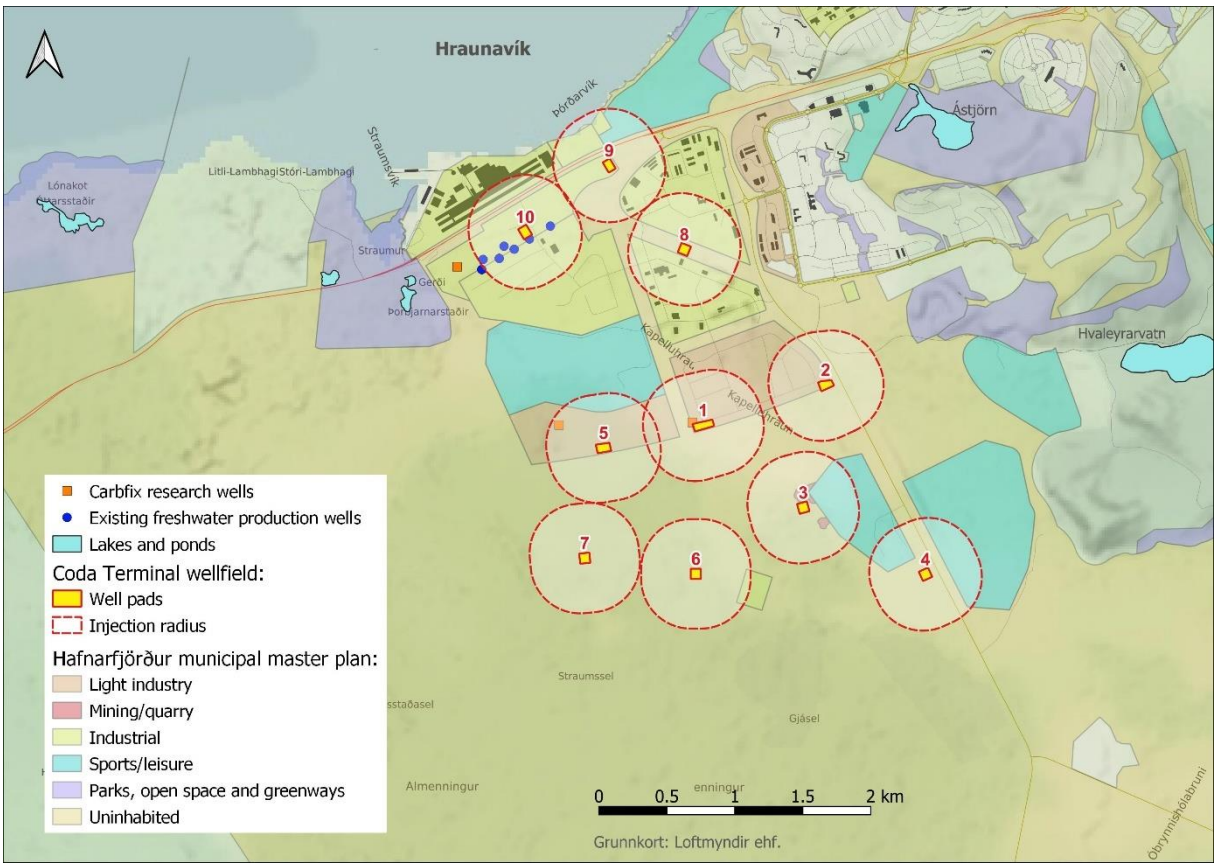

Figure 18. Location of proposed Coda Terminal production/injection well pads.

Table 1. Operational design strategy for the Coda Terminal.

Operational phase	Start date	Well pads in use	Production		Injection	
			Per well pad [kg/s/pad]	Total [kg/s]	Per well pad [kg/s/pad]	Total [kg/s]
Phase 1	2027 Q4	#1-3	221.8	665	229.2	688
Phase 2	2029 Q2	#1-6	221.8	1331	229.2	1375
Phase 3	2030 Q4	#1-7	285.2	1996	294.7	2063
Phase 4	2032 Q2	#1-10	292.3	2923	301.8	3018

The model was run for a 30-year operational period, from 2027 to 2057, with operational phase 4 operating for approximately 25 years. Several modelling assumptions were made in defining run parameters for the operational scenario. Based on the feed zone analysis by ÍSOR (Chapter 3.2), it was assumed that the majority of the injection fluid (80%) will enter the groundwater system within the main feed zone depth range (320-370 m b.s.l.), with the remaining injection fluid (20%) entering minor

feed zones between approximately 375-550 m b.s.l. The injection water was assumed to be 8 °C as specified by Carbfix design parameters.

5.2. Results

Model results from the operational scenario were analyzed and compared with the baseline model in order to assess changes from the natural-state groundwater conditions caused by the proposed production/injection from the Coda Terminal. Impacts were assessed for each of the four planned operational phases in order to analyze the progression of impacts with time and increased production/injection rates. Simulated changes to groundwater system were analyzed, and the results were plotted in plan-view at three depth intervals and along three cross sections through the wellfield (Figure 19).

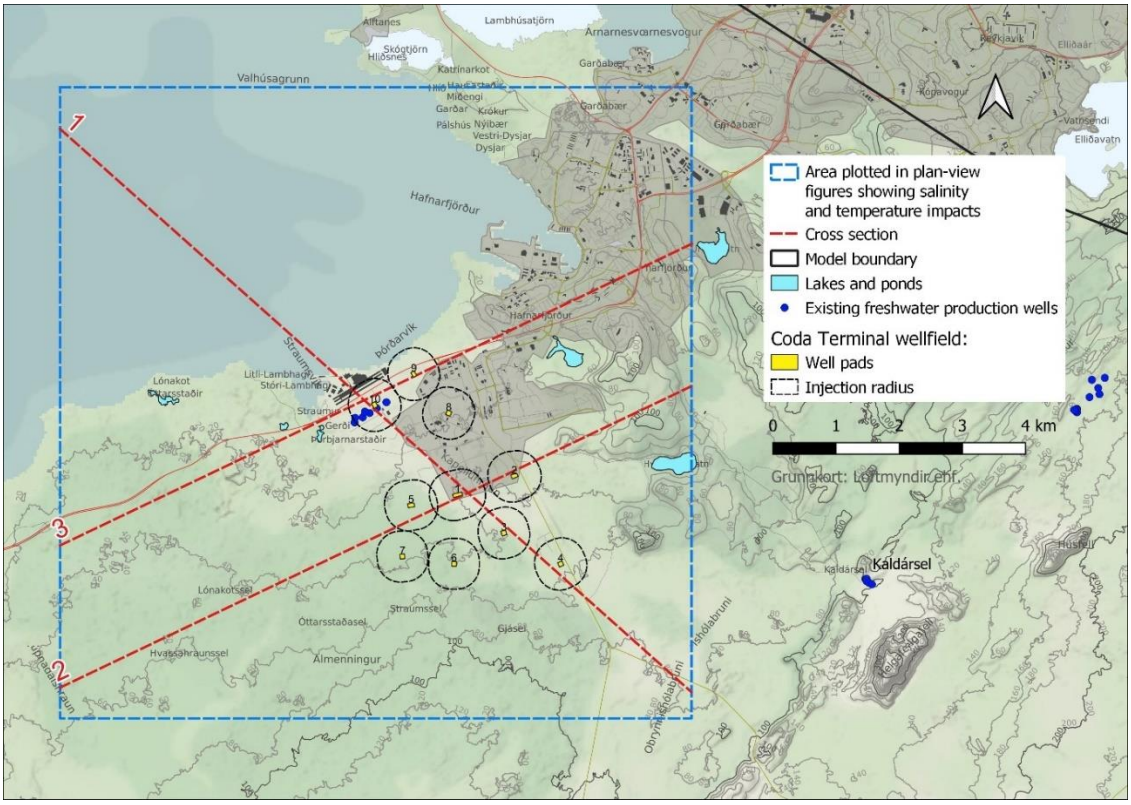

Figure 19. Extent of plan-view figures and location of cross sections used for displaying simulated impacts on the groundwater system.

5.2.1. Groundwater levels

Simulated changes to the groundwater table are shown on Figure 20 - Figure 23. The model calculates a decrease in groundwater levels (drawdown) due to production from the Coda Terminal wellfield. The drawdown forms a cone of depression in the groundwater table centered within the wellfield which increases in size with increased production. Maximum drawdown increases from just over 10 cm during operational phase 1 to approximately 20 cm during operational phase 4. The model predicts a maximum drawdown of around 5-7 cm at the nearby Rio Tinto freshwater production wells and between 0-4 cm at the Straumsvík coastal ponds. As calculated values of drawdown approach small values (less than 5 cm) at the outer edges of the main cone of depression, their degree of uncertainty

increases due to numerical limitations of the model in its current development state. Therefore, calculated drawdown less than 5 cm should be interpreted as a possibility that drawdown could occur.

It is clear that drawdown due to production is counter-balanced by the injection. Injection induces a pressure increase in the deeper sections of the groundwater system, which is transmitted upward towards the surface. It provides pressure support to the shallow freshwater aquifer, reducing the amount of drawdown that would otherwise occur if there was no injection. Pressure increase due to injection can be clearly seen on Figure 24 - Figure 26 along cross sections 1-3. Maximum calculated pressure increase occurs at the injection depths and dissipates outward in all directions. A pressure decrease is calculated at the production depth under well pads 8-10 (-130 m a.s.l.) due to production from those wells. Calculated pressure decrease is significantly lower at the production depth under well pads 1-7 (-20 m a.s.l.) due to significant differences in rock permeability between the production depths.

The model was run without injection (only production) in order to analyze the calculated effect of pressure support on drawdown. Results from the test run showed that a maximum drawdown of roughly 1.2 m was predicted by the model within the wellfield during operational phase 4. This is approximately 1 m more drawdown than the model predicts with injection included, confirming that pressure support does have a significant effect on limiting drawdown according to the model.

This increased pressure caused by injection is evident to the northeast and southwest of the wellfield where the model predicts an increase in groundwater levels (Figure 20 - Figure 23). To the northeast of the wellfield in the Hafnarfjörður area, the model predicts a maximum increase in groundwater levels of just over 10 cm during operational phase 1, increasing up to approximately 40 cm during operational phase 4. To the southwest of the wellfield, the model predicts an increase in groundwater levels of just over 30 cm during operational phase 1, increasing up to roughly 1.2 meters during operational phase 4.

The shape and extent of the areas with calculated groundwater level changes are controlled by the hydrological and geological conditions in the groundwater system. As shown on Figure 23, the cone of depression due to drawdown extends outward from the wellfield in the NW-SE direction, parallel to the groundwater flow direction in the shallow groundwater aquifer. This behavior is typical of production from highly permeable aquifers. The areas with a calculated increase in groundwater levels are located on either side of the cone of depression and are aligned in the NE-SW direction. As discussed above, increased groundwater levels are caused by the transfer of injection-induced pressure upward towards the surface. The vertical transfer of pressure is focused along this NE-SW zone due to preferred vertical pressure pathways which are most likely caused by a combination of several hydrogeological factors. These could include 1) enhanced vertical permeability due to fracturing associated with the Krýsuvík fissure swarm, 2) alignment with the relatively high permeability transition zone in the geological stratigraphy between glassy basalt formations to the NW and hyaloclastite formations to the SE (see discussion in Chapter 3.2) and 3) correspondence with the landward (freshwater) side of the fresh/saline interface.

The design parameters of the Coda Terminal call for 100% re-injection of the extracted groundwater. Water is therefore not lost from the groundwater system; it is rather transferred from the shallow sections of the system to the deeper sections. As shown in Table 1, there is actually a slightly higher mass of injected water compared to the amount extracted due to the addition of CO_2 to the water. Therefore, the planned production and injection will produce a net positive mass balance in the groundwater system as a whole. The degree of vertical hydrologic connection between the shallow and deep systems will determine to what extent the pressure decrease (due to production) and the

pressure increase (due to injection) will counter-balance each other. As the results of the operational scenario show, the model predicts a significant degree of vertical hydrologic connection. However, there is still a relatively large amount of uncertainty on whether this is the case in reality. No large-scale field testing has been performed to verify the degree of vertical hydrologic connection, and the main parameters controlling it (e.g., vertical permeability of geological formations between the production and injection depths, horizontal extent of injection feed zones) have a high degree of uncertainty. Therefore, the results presented here should be viewed as initial estimations subject to updating after experience is gained from the first large-scale pilot testing of production/injection.

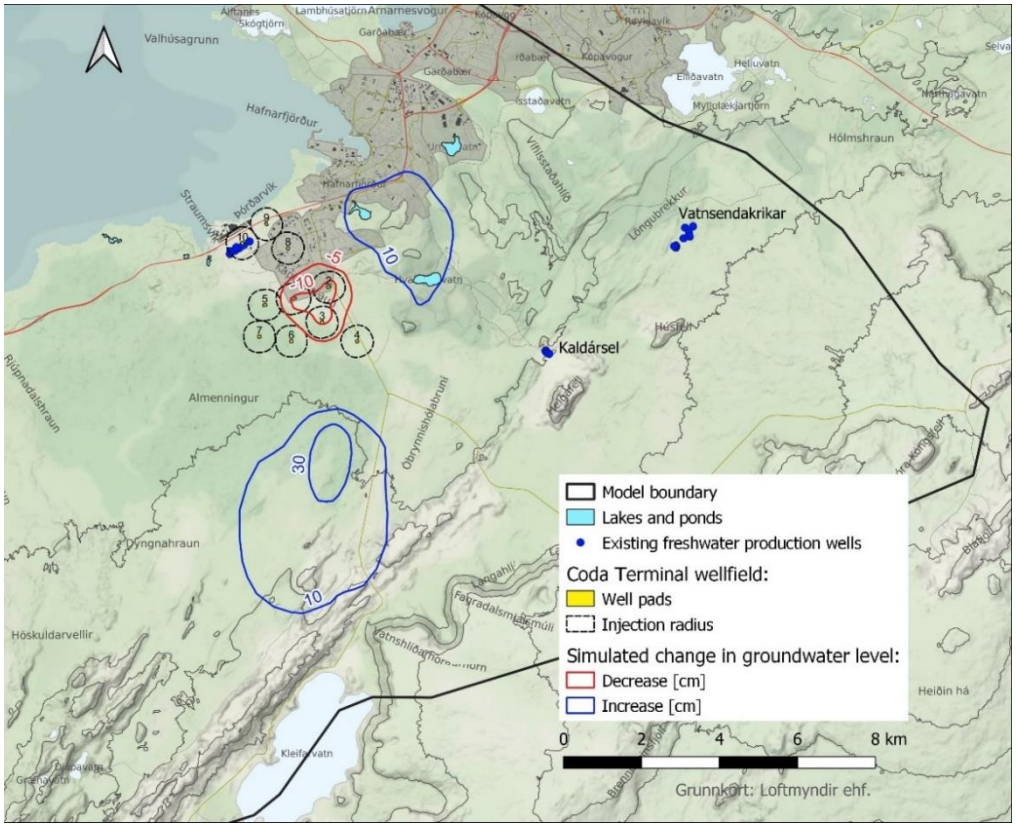

Figure 20. Simulated changes to the groundwater table during operational phase 1.

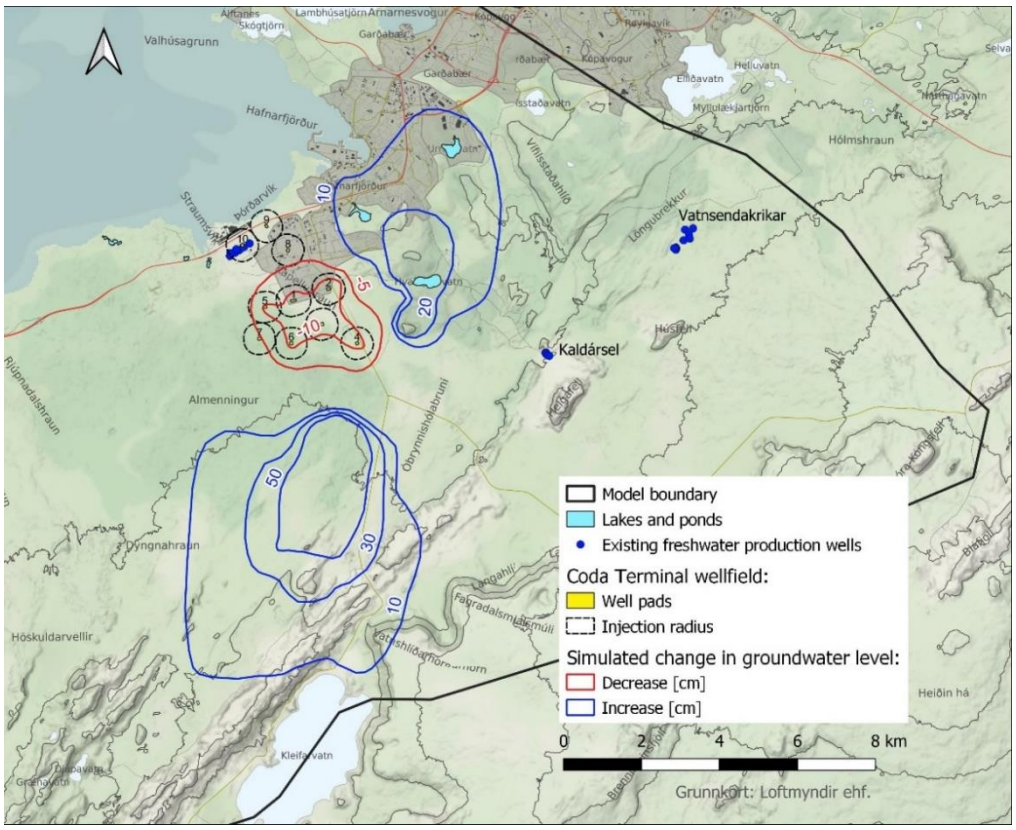

Figure 21. Simulated changes to the groundwater table during operational phase 2.

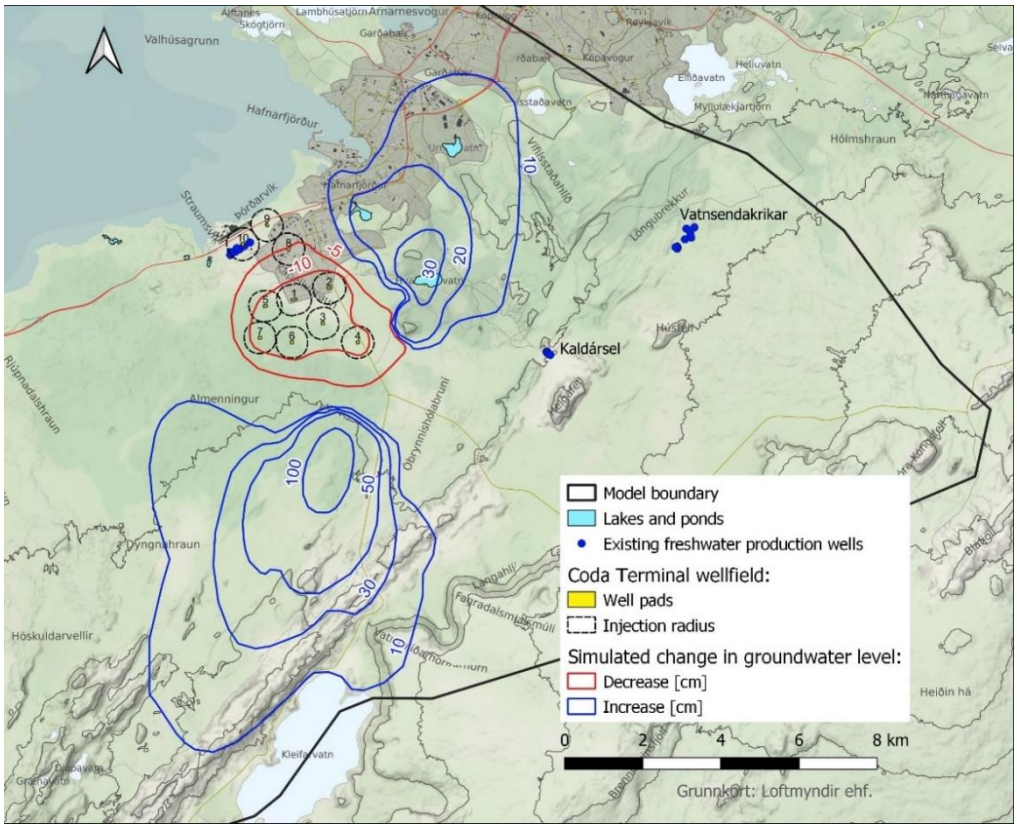

Figure 22. Simulated changes to the groundwater table during operational phase 3.

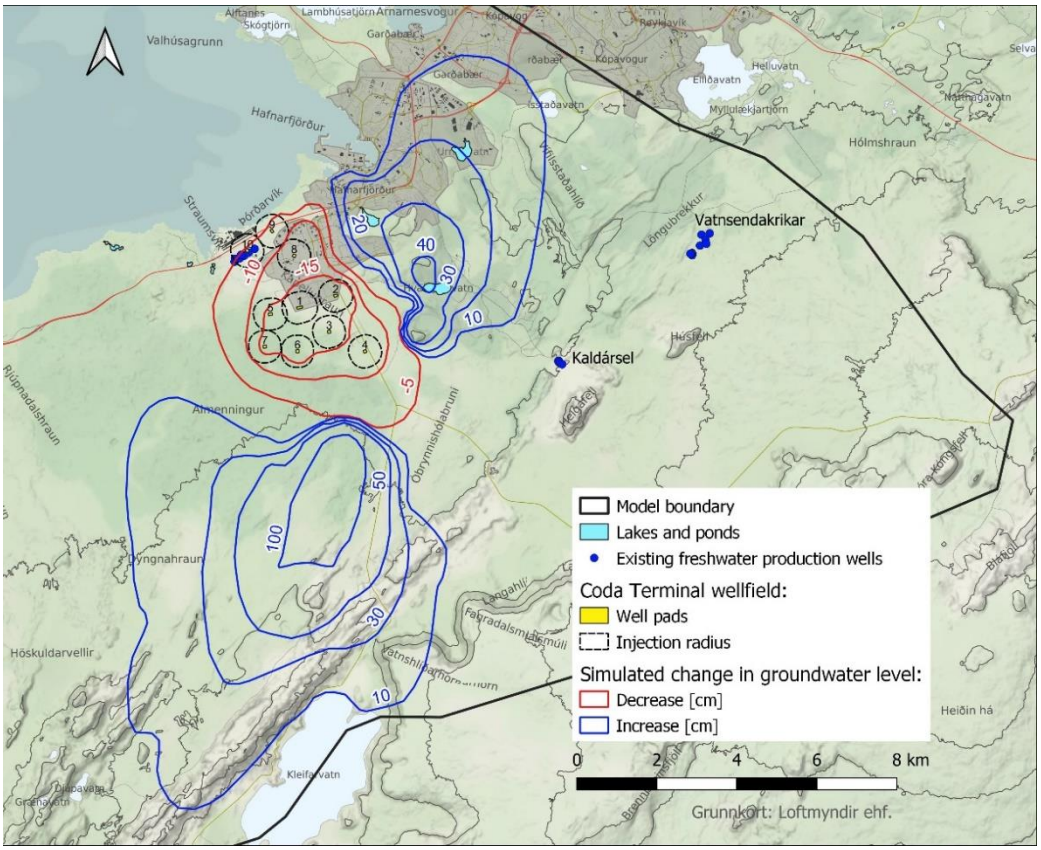

Figure 23. Simulated changes to the groundwater table during operational phase 4.

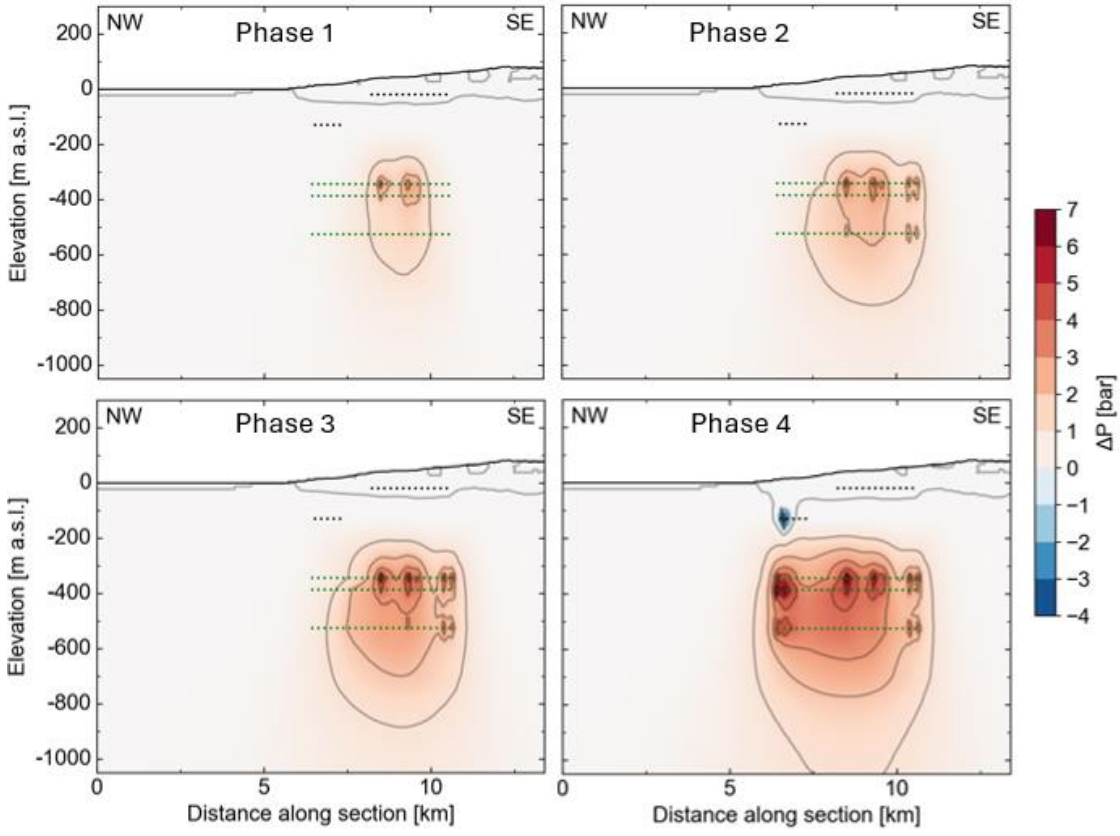

Figure 24. Simulated changes to groundwater pressure along NW-SE cross section 1.

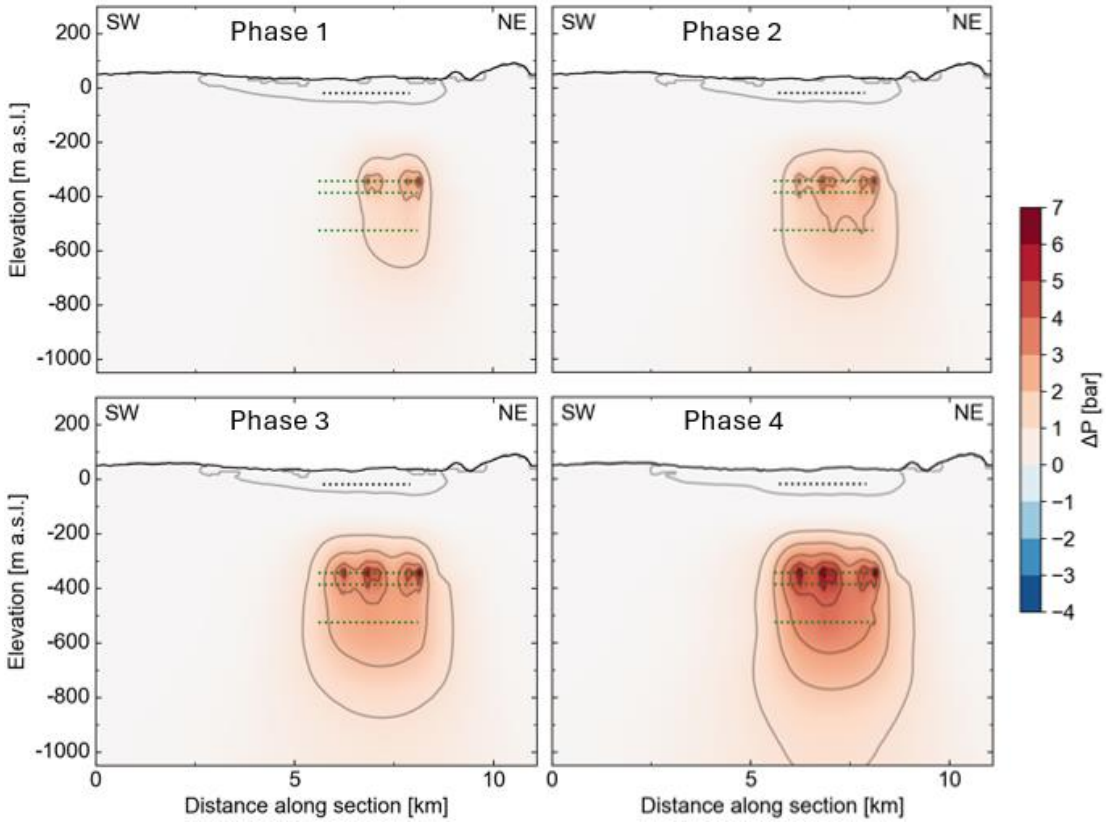

Figure 25. Simulated changes to groundwater pressure along SW-NE cross section 2.

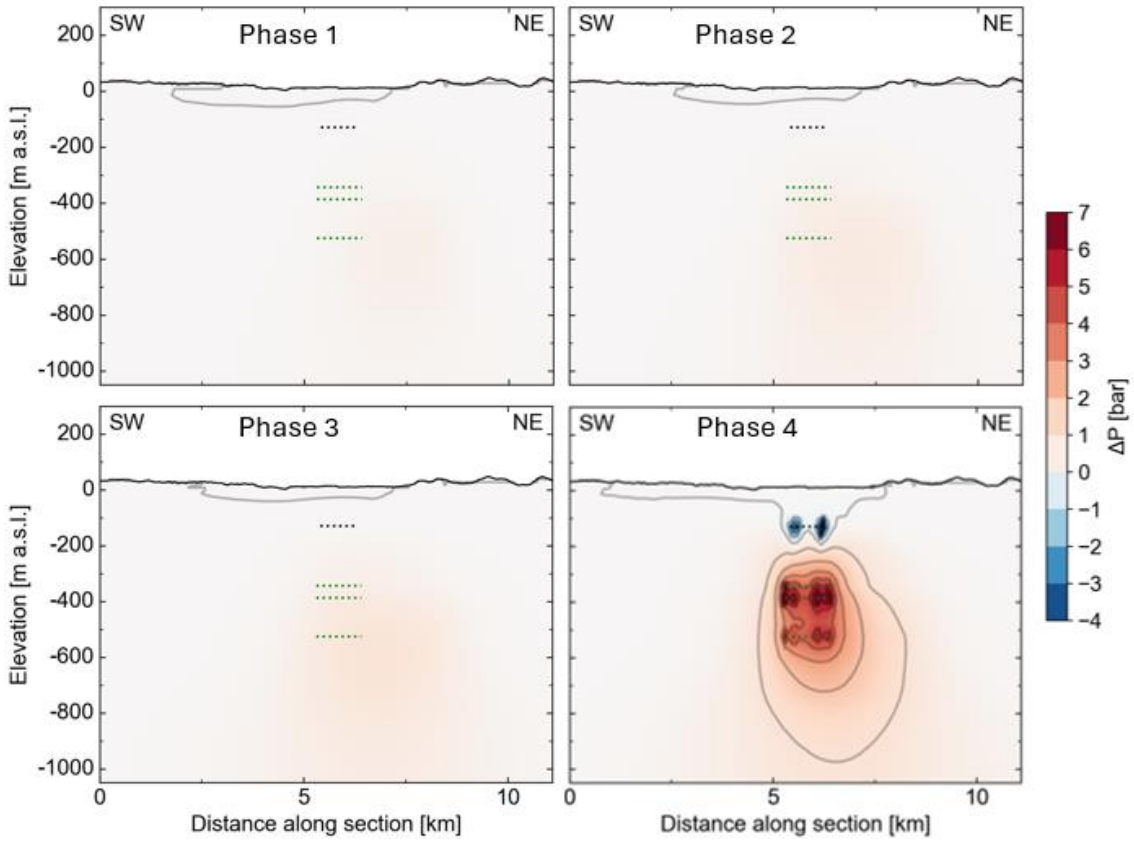

Figure 26. Simulated changes to groundwater pressure along SW-NE cross section 3.

5.2.2. Groundwater salinity

Simulated changes to groundwater salinity were analyzed, and the results were plotted in plan-view at three depth intervals within the groundwater system and along three cross sections through the wellfield (Figure 19).

Figure 27 shows simulated salinity changes at 0 m a.s.l. which is near the top of the freshwater aquifer in the coastal area at Straumsvík and is within the depth range at which groundwater is entering the coastal ponds at Straumsvík and the Rio Tinto production wells. The model calculates salinity changes in a relatively localized area along the coastline to the northeast of well pads 8 and 9. Both an increase and decrease in salinity are predicted (less than 5 g/kg), and the area affected by the salinity change increases with each successive operational stage. Predicted salinity changes are less than 0.5 g/kg at the coastal ponds at Straumsvík and the Rio Tinto production wells (which are located in the vicinity of well pad 10, see Figure 19).

Figure 28 shows simulated salinity changes at -20 m a.s.l. which is deeper in the freshwater aquifer and within the depth range at which well pads 1-7 are producing water. The model calculates salinity changes in the same area as at 0 m a.s.l. to the northeast of well pads 8 and 9, but also within well pad 10 and in a large area west of the wellfield. There is more overall area affected by salinity change than at 0 m a.s.l. due to closer proximity to the fresh/saline interface (which is being altered by the effects of production/injection), however maximum changes remain within 5 g/kg.

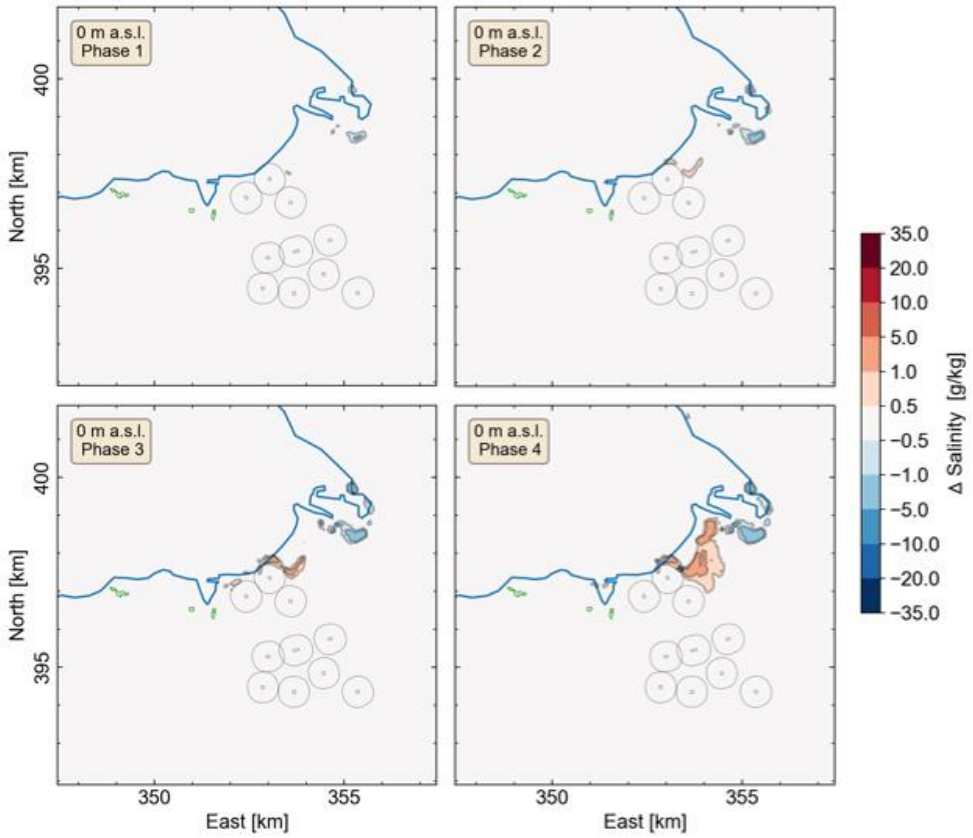

Figure 27. Simulated changes to groundwater salinity at 0 m a.s.l. in the freshwater aquifer.

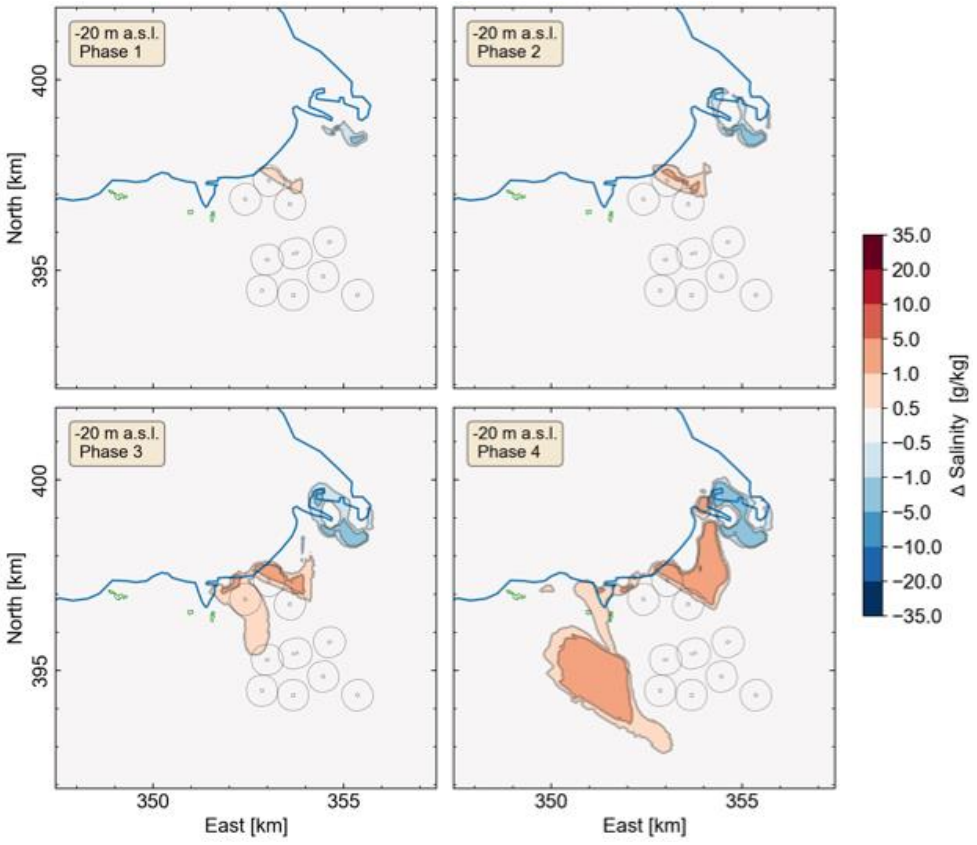

Figure 28. Simulated changes to groundwater salinity at -20 m a.s.l. in the freshwater aquifer.

Figure 29 shows simulated salinity changes at -350 m a.s.l. which is within the depth range at which the majority of the injection water is entering the groundwater system. Predicted salinity changes at this depth are much greater and more widespread than at the shallower depths shown above, indicating that injection has more impact on groundwater salinity than production. The area affected by salinity changes lies within a roughly 1-5 km band cutting across the wellfield from northeast to southwest. This band corresponds roughly to the lateral extent of the mixing zone at the fresh/saline interface at this depth, with saline water on the northwest side of the band, and fresh water on the southeast side (refer to Figure 17). A predicted decrease in salinity, with a maximum decrease exceeding 20 g/kg in operational phase 4, is centered roughly around well pad 5 at the west side of the wellfield. This salinity decrease is caused by the injection wells forcing injected fresh water into areas (within and below the mixing zone) with brackish and saline natural-state conditions. A predicted increase in salinity, with a maximum increase exceeding 20 g/kg in operational phase 4, extends out in both directions from the area with decreased salinity. The salinity increase is due to displacement of brackish and saline water from within and below the mixing zone upward into areas with fresher natural-state conditions within and above the mixing zone. This displacement of water is caused by injection-induced pressure increase around the injection depths.

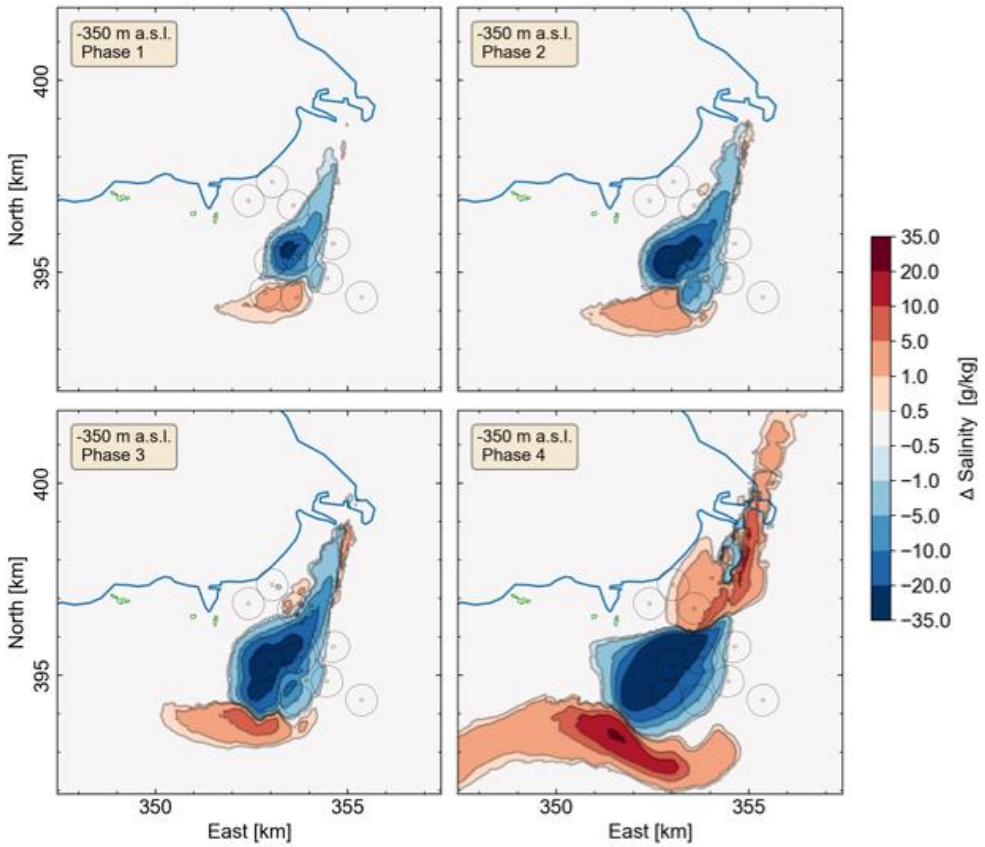

Figure 29. Simulated changes to groundwater salinity at -350 m a.s.l. at the main injection depth.

The simulated changes in groundwater salinity are shown along three cross sections (locations shown on Figure 19) on Figure 30 - Figure 32. The depth and lateral extent of the production and injection wells are shown with black and green dotted lines respectively. Cross section 1 (Figure 30) illustrates well how the predicted salinity changes occur within a band corresponding to the mixing zone which slopes from NW to SE (refer to salinity cross section in Figure 16). The predicted salinity decrease is focused mainly around the injection depth range (320-550 m b.s.l.) while the predicted salinity increase occurs above and below the injection area.

Cross section 2 (Figure 31) also shows how the predicted salinity decrease is focused mainly around the injection depth range, but also how the injection-induced pressure increase causes an increase in salinity in an area extending southwest from the wellfield.

Predicted salinity changes displayed on cross section 3 (Figure 32) show a different overall character than in the other cross sections due to its location. Cross section 3 is parallel to the coastline and extends through well pads 9 and 10, both of which are producing and injecting saline water (unlike well pads 1-7). The effects of deeper production (> 100 m depth) and injection of saline water can be seen clearly on the cross section for operational phase 4 (well pads 8-10 begin operating in phase 4). A small area of decreased salinity is predicted just above the production wells which produce from roughly 130 m b.s.l. This salinity decrease is caused by the production wells pulling fresher water down from within and above the overlying mixing zone. Unlike the effects of fresh injection from well pads 1-7 (Figure 29 and Figure 30), the injection of saline water at well pads 8-10 cause very little salinity change in the immediate vicinity of the injection zone since the natural-state conditions at those

depths are saline. An increase in salinity is predicted, however, to the southwest and northeast of the wellfield in this area, most likely due to displacement of water caused by injection-induced pressure.

The coastal ponds at Straumsvík are located just southwest of well pad 10 on cross section 3. As mentioned above, predicted salinity changes at the coastal ponds (elevation roughly 0 m a.s.l.) are relatively minor (less than 0.5 g/kg). However, as shown on Figure 32, a significant salinity increase is predicted at relatively shallow depths below the ponds. This is highlighted on Figure 33 which shows a close-up view of the upper 200 meters of the groundwater system. As the figure shows, a salinity increase of nearly 1 g/kg is calculated at a depth of roughly 20 m below the ponds, an increase of between 1-5 g/kg at about 30 m depth and an increase of 10-20 g/kg at 50 m depth. The vertical extent of salinity changes towards the surface is dependent on several factors, including vertical permeability values and pressure effects from injection, both of which have a relatively high degree of uncertainty associated with them. Therefore, there is a possibility that salinity changes at the coastal ponds could be greater than predicted in the current version of the model. This emphasizes the need for monitoring salinity and temperature in the coastal ponds as well as in the groundwater in their vicinity.

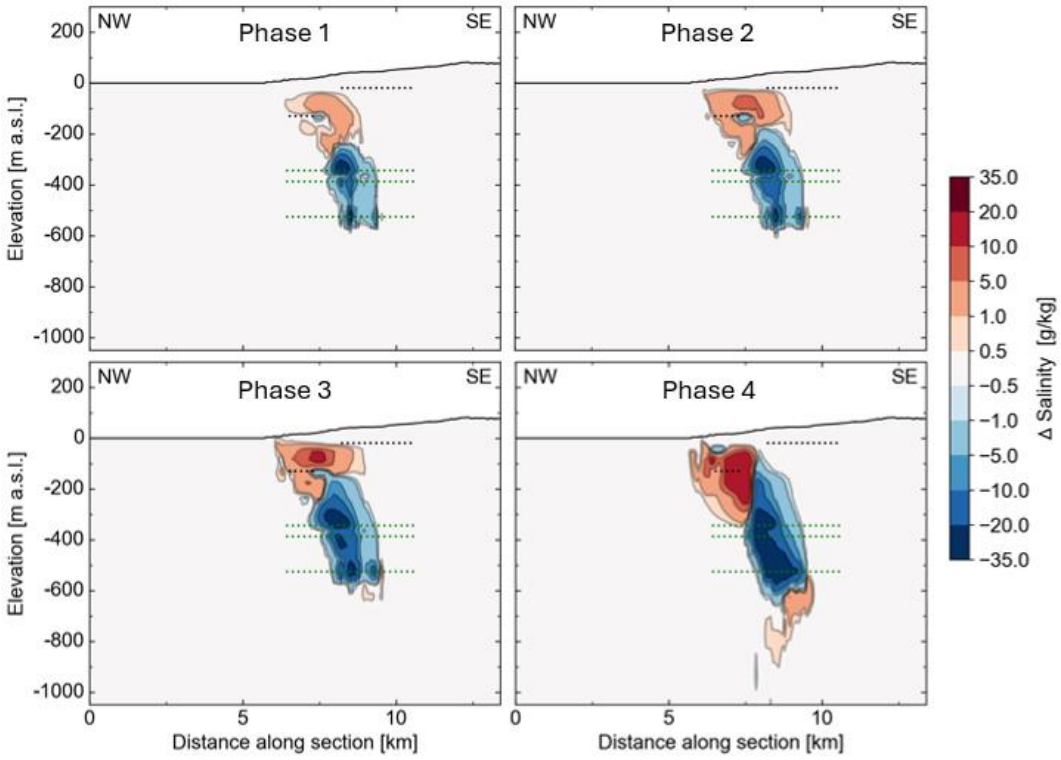

Figure 30. Simulated changes to groundwater salinity along NW-SE cross section 1.

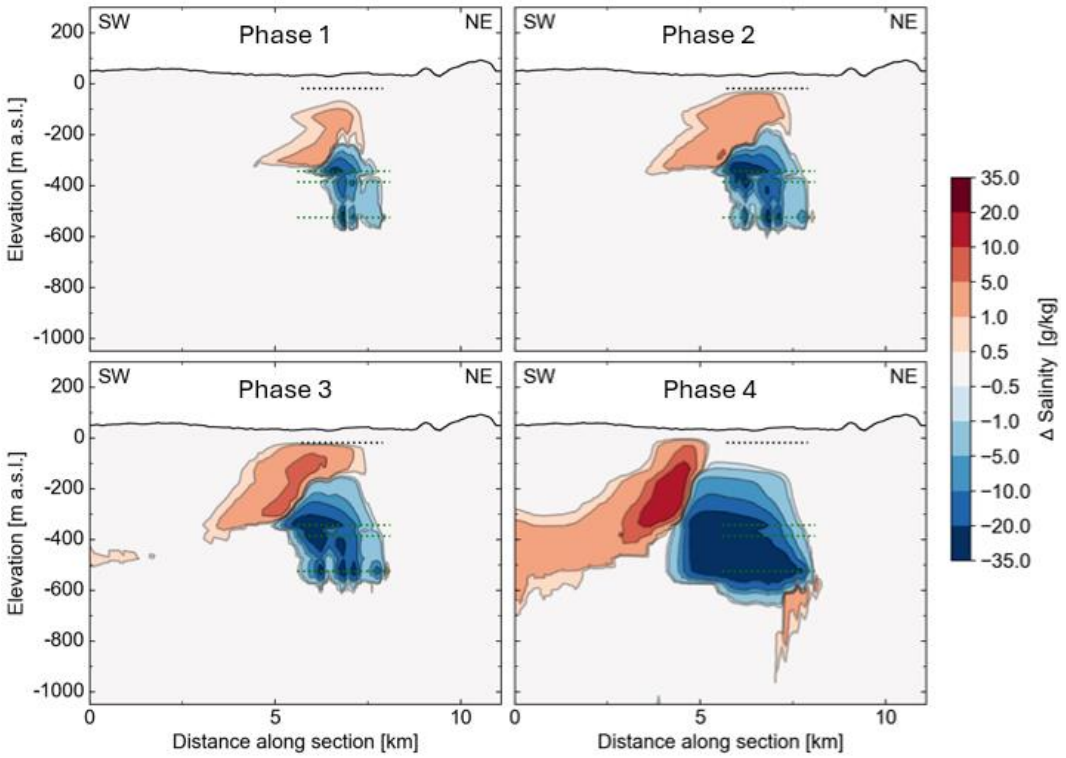

Figure 31. Simulated changes to groundwater salinity along SW-NE cross section 2.

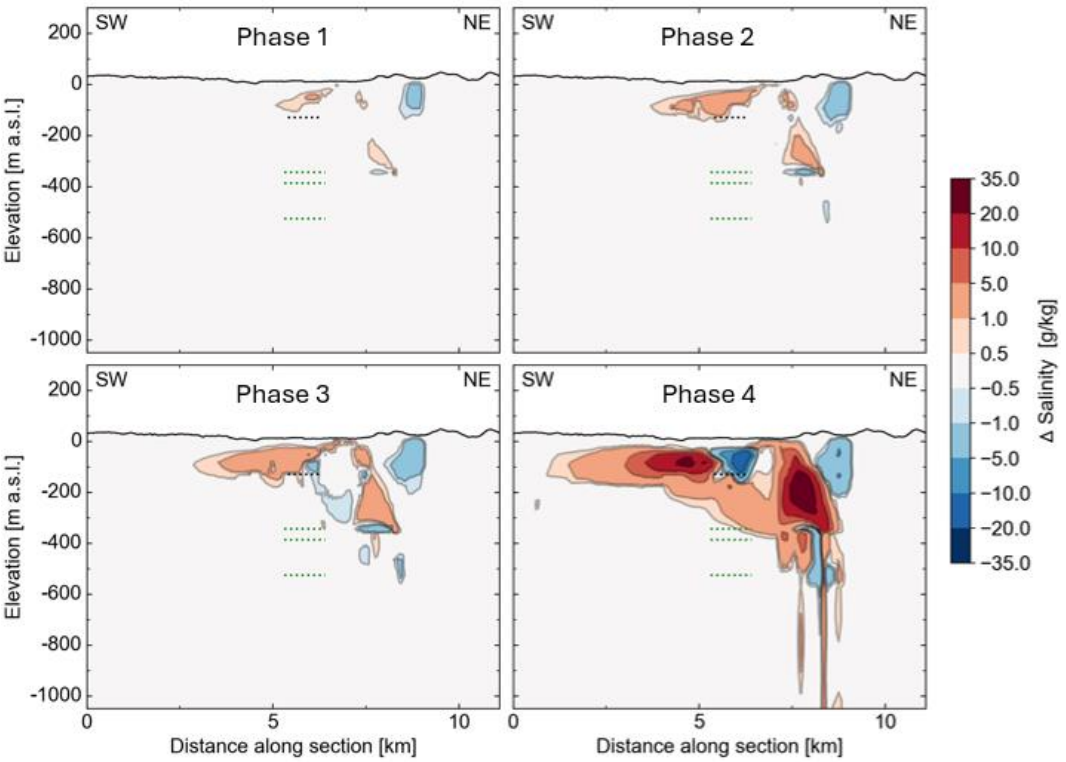

Figure 32. Simulated changes to groundwater salinity along SW-NE cross section 3.

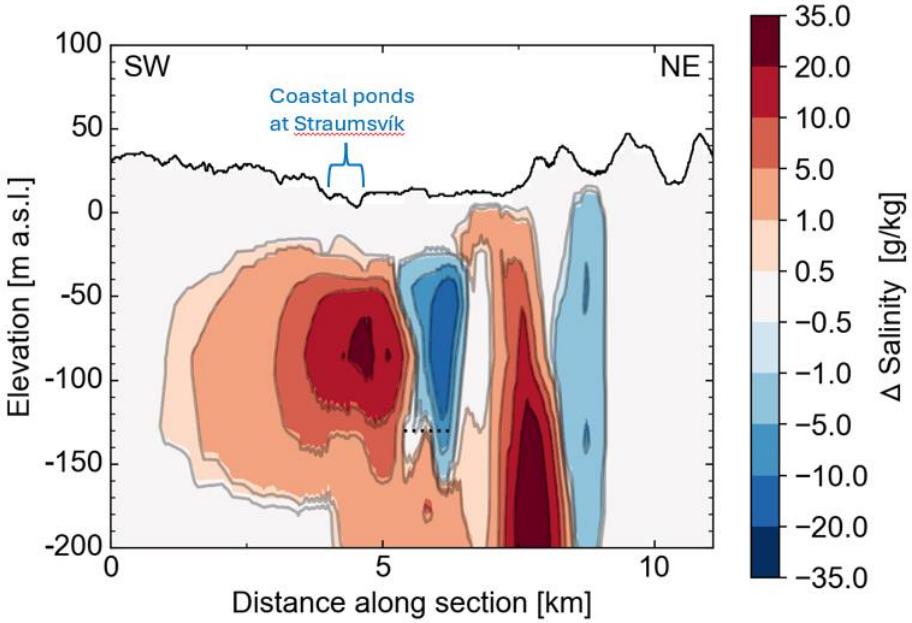

Figure 33. Simulated changes to groundwater salinity in the upper 200 m of the groundwater system along SW-NE cross section 3 (Phase 4).

5.2.3. Groundwater temperature

Simulated changes to groundwater temperature were analyzed, and the results plotted in plan-view at three depth intervals within the groundwater system and along three cross sections through the wellfield (Figure 19).

Figure 34 shows simulated temperature changes at 0 m a.s.l. which is near the top of the freshwater aquifer in the coastal area at Straumsvík and is within the depth range at which groundwater is entering the coastal ponds at Straumsvík and the Rio Tinto production wells. At this depth, the model calculates very minimal temperature changes (< 1 °C) during the first three operational phases, and only a minor temperature increase (1-2.5 °C) in phase 4 at small, isolated areas just west of the wellfield. Predicted temperature changes are < 1 °C at all the coastal ponds at Straumsvík except for the two easternmost ponds, Þorbjarnarstaðartjarnir (Brunntjörnin) and Gerðistjarnir, where the model predicts a temperature increase of roughly 1 °C.

Figure 35 shows simulated temperature changes at -20 m a.s.l. which is deeper in the freshwater aquifer and within the depth range at which well pads 1-7 are producing water. Similar to 0 m a.s.l., the model calculates very minimal temperature changes (< 1 °C) during the first three operational phases at -20 m a.s.l. During phase 4, the model predicts a temperature increase of up to 5 °C along the western boundary of the wellfield. There is more overall area affected by temperature change than at 0 m a.s.l. due to closer proximity to the fresh/saline interface, which is being altered by the effects of production/injection.

Figure 36 shows simulated temperature changes at -350 m a.s.l. which is within the depth range at which the majority of the injection water is entering the groundwater system. Predicted temperature changes at this depth are much greater and more widespread than at the shallower depths shown above, indicating that injection has more impact on groundwater temperature than production. The model results show clearly how the injection of 8 °C water cools the warmer natural-state groundwater at this depth. Model results show very localized cooling effects within each well pad radius as well pads

come online with each successive operational phase. Cooling effects extend slightly outside the wellfield during operational phase 4, and an increase in temperature is also predicted to the northeast and southwest of the wellfield, corresponding to the simulated salinity increase (see Phase 4 on Figure 29).

The simulated changes in groundwater temperature are shown along three cross sections (locations shown on Figure 19) on Figure 37 - Figure 39. The depth and lateral extent of the production and injection wells are shown with black and green dotted lines respectively. Cross section 1 (Figure 37) illustrates well how the predicted cooling occurs in the immediate vicinity of the injection wells. The model predicts an increase in temperature between the production and injection depths, most likely due to displaced water from below.

Cross section 2 (Figure 38) also shows how the predicted cooling is focused mainly around the injection depth range, but also how the injection-induced pressure increase causes an increase in temperature in an area above and extending southwest from the wellfield.

Predicted temperature changes displayed on cross section 3 (Figure 39) show minimal (< 1 °C) temperature changes during operational phases 1-3, as there is no production or injection along the cross section during these phases. Well pads 8-10 come online in phase 4 as can be seen from the cross section. As with the other well pads (1-7), injection causes localized cooling focused mainly around the injection depth range, with an increase in temperature above and adjacent to the cooling zone caused by displaced water from below.

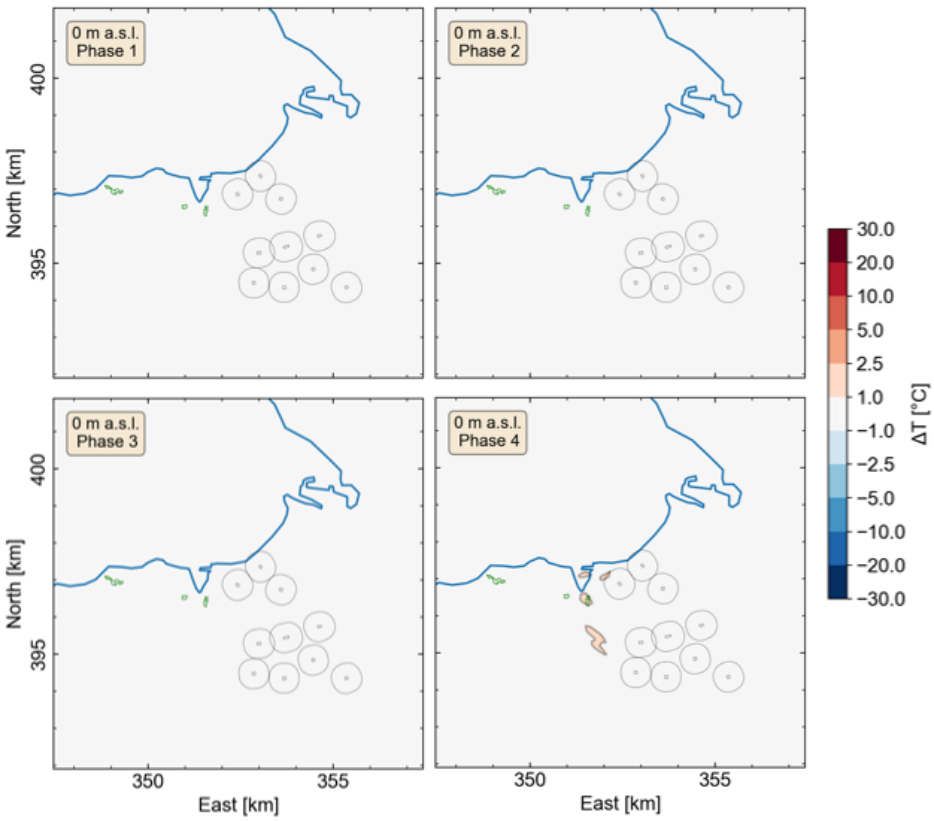

Figure 34. Simulated changes to groundwater temperature at 0 m a.s.l. in the freshwater aquifer.

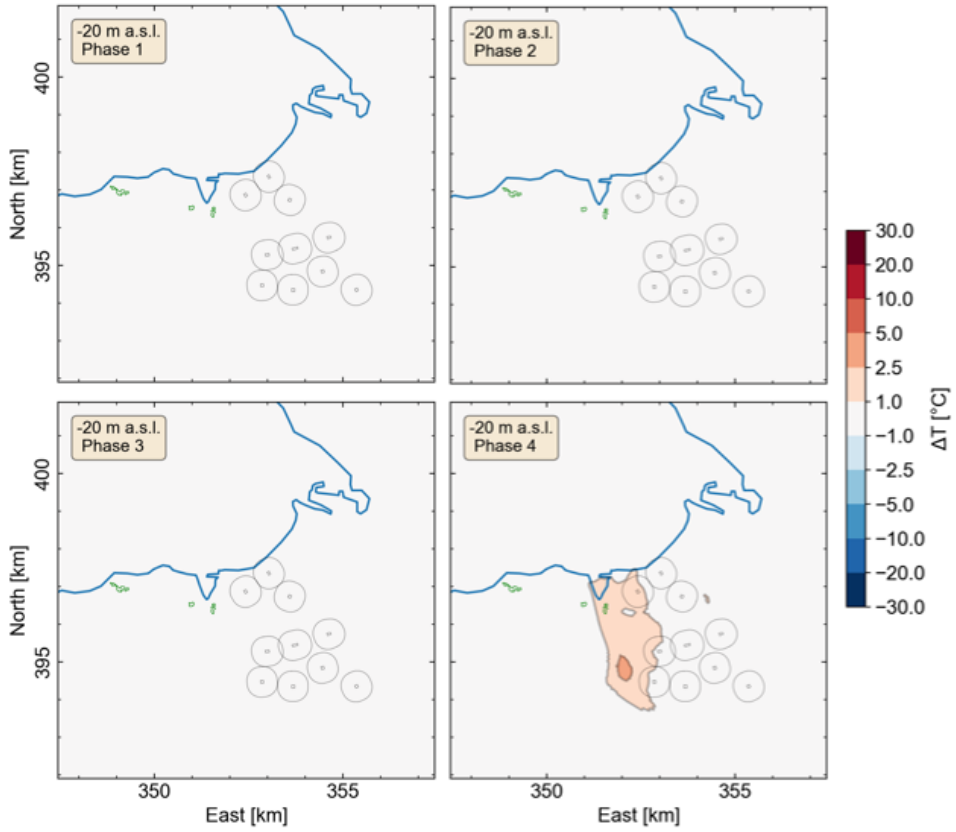

Figure 35. Simulated changes to groundwater temperature at -20 m a.s.l. in the freshwater aquifer.

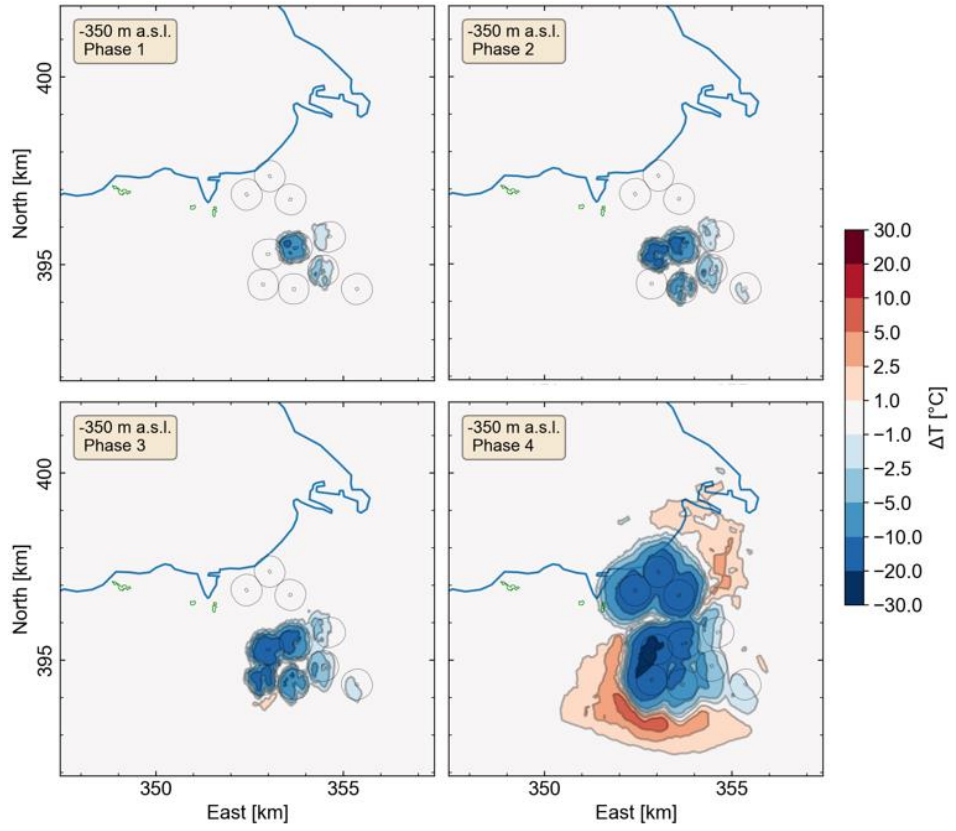

Figure 36. Simulated changes to groundwater temperature at -350 m a.s.l. at the main injection depth.

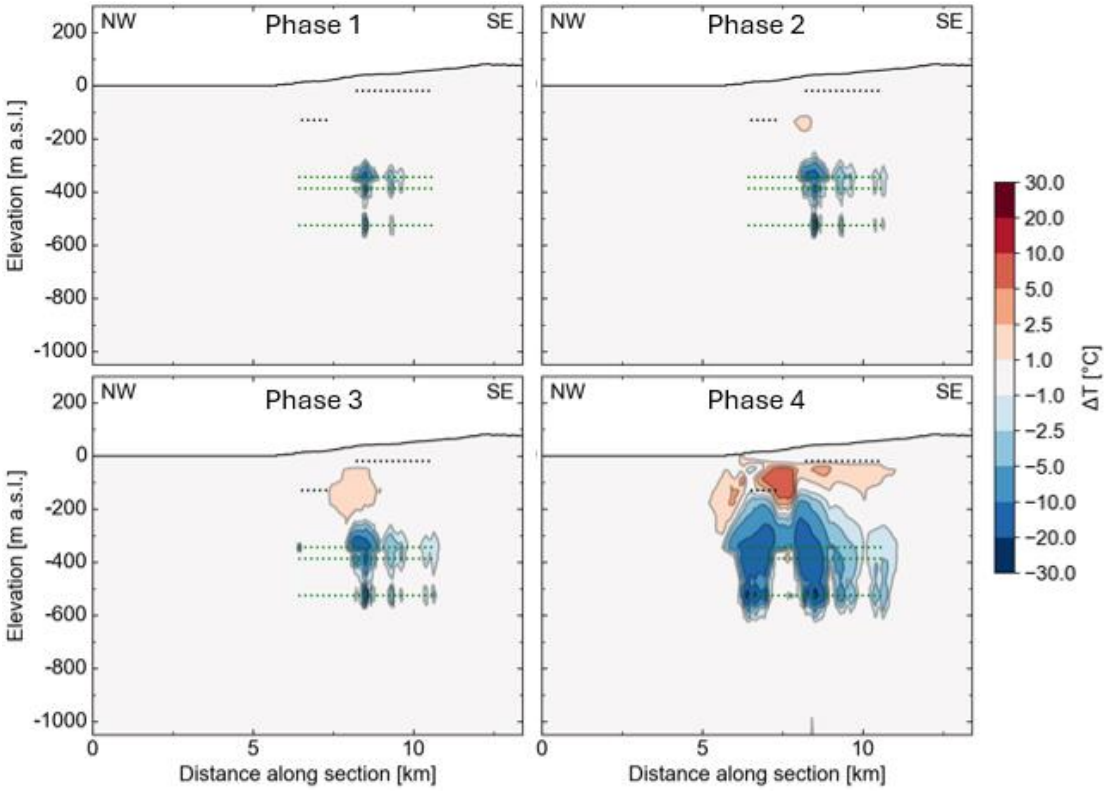

Figure 37. Simulated changes to groundwater temperature along NW-SE cross section 1.

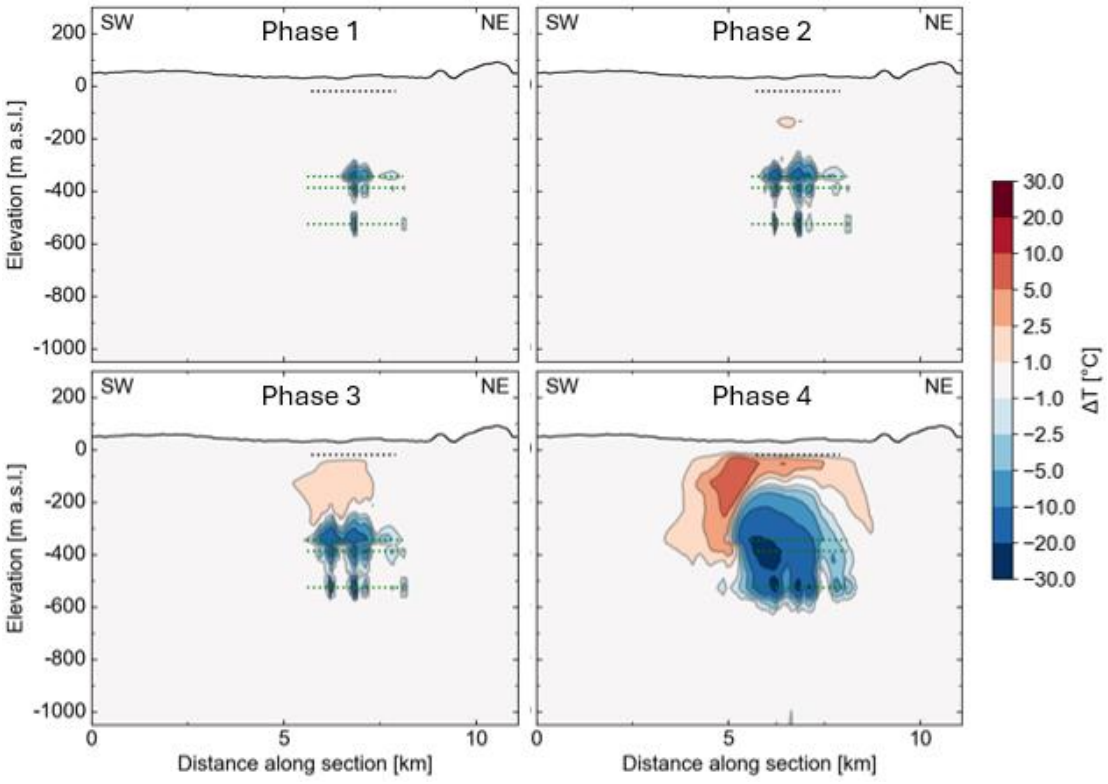

Figure 38. Simulated changes to groundwater temperature along SW-NE cross section 2.

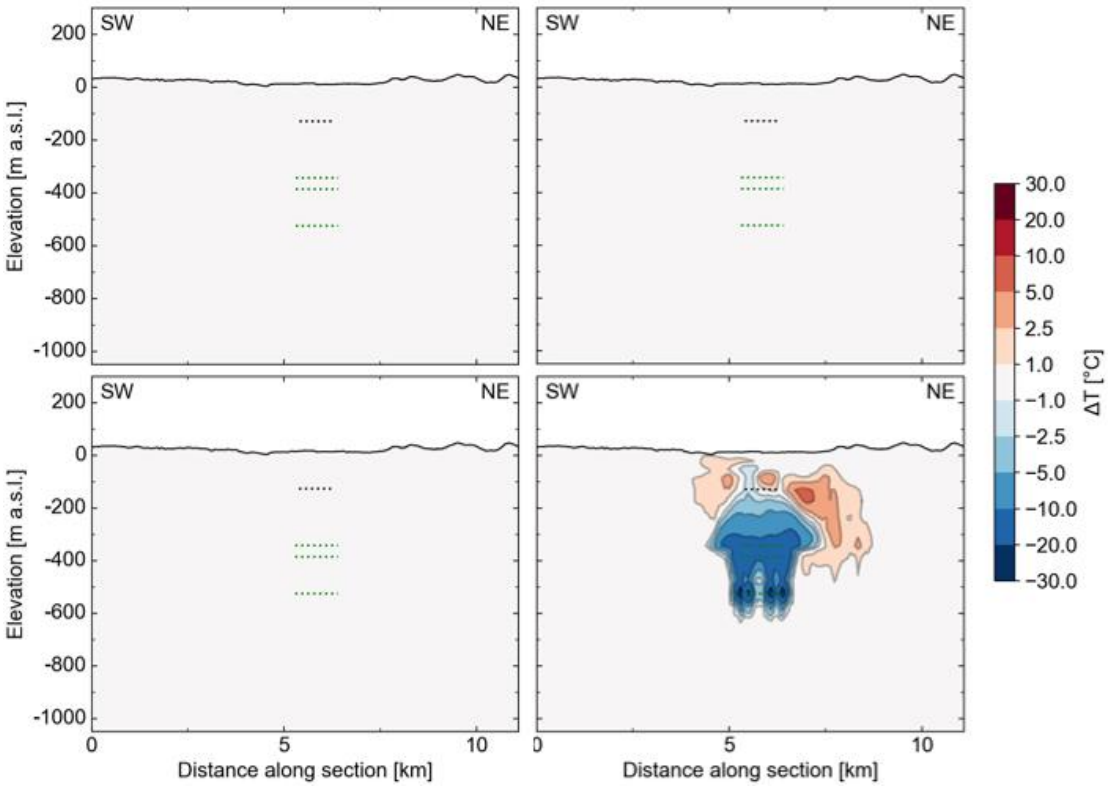

Figure 39. Simulated changes to groundwater temperature along SW-NE cross section 3.

5.2.4. Capture zone

The model was used to estimate the capture zone of the Coda Terminal production wells. Capture zones extend upgradient from production wells and indicate the region of the groundwater system that contributes water to the wells. The results are shown in Figure 40. The capture zone extends towards the southeast up to the model boundary at the groundwater divide. The shape and extent of the capture zone reflects the direction of the regional groundwater flow paths (Figure 10). The capture zone is rather narrow near the wellfield but widens sharply within the Krýsuvík fissure swarm to the southeast where groundwater flow is enhanced in the main fracture direction (NE-SW).

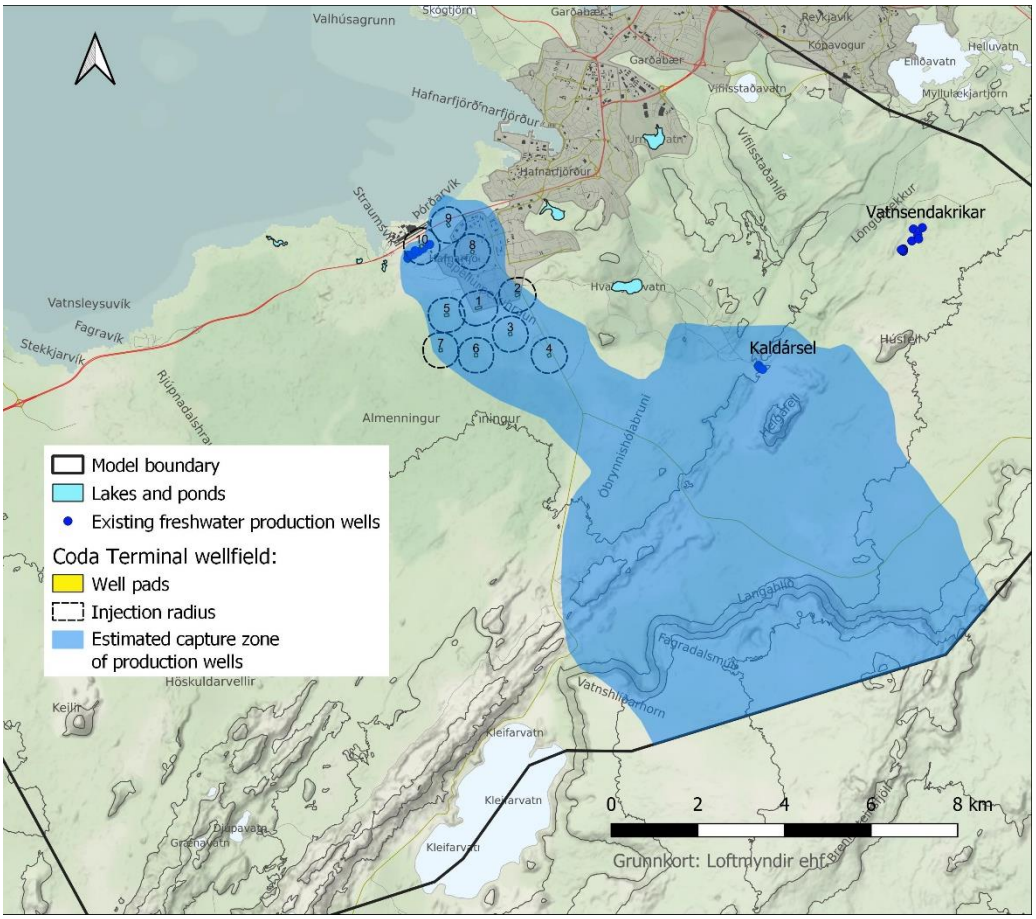

Figure 40. Estimated capture zones of the Coda Terminal production wells.

5.3. Summary

A summary of the main results of the impact assessment with regards to changes in groundwater levels, salinity and temperature are provided in Table 2.

The model predicts a maximum drawdown of 7 cm at the nearby Rio Tinto freshwater production wells and between 0-4 cm at the Straumsvík coastal ponds. As stated previously, calculated drawdown values less than 5 cm have an increased degree of uncertainty and should therefore not be overinterpreted. Nevertheless, they do indicate a possibility of drawdown near the ponds. A maximum drawdown of 7 cm at the Rio Tinto production wells is considered relatively low and unlikely to have significant effects on their production capacity, although this should be monitored during pilot testing of production/injection.

An increase in groundwater levels of as much as 40 cm is predicted to the northeast of the wellfield. Previous research indicates that Ástjörn, Hvaleyrarvatn and Urriðavatn all have some degree of hydrological connection with the groundwater system (Orkustofnun, 2001). Therefore, it is possible that the predicted increase in groundwater level at the lakes may lead to increased inflow (spring flow) into them. However, local geological conditions control outflow/leakage from the lakes and act as a natural buffer such that increased inflow will result in increased outflow (Orkustofnun, 2001). This limits both the maximum water level in the lakes as well as the amount of fluctuation in water levels. Therefore, it is considered unlikely that the predicted increase in the groundwater level in the vicinity of the lakes will have a significant effect on the water level in them. Nevertheless, it is recommended

to monitor lake levels and surrounding groundwater levels during the construction and operation of the Coda Terminal. This monitoring is already underway at Ástjörn and Hvaleyrarvatn. It is not known whether monitoring is currently being performed at Urriðavatn.

A maximum increase in groundwater levels of roughly 1.2 meters is predicted to the southwest of the wellfield. Although this is a significant change, it is unlikely to have any direct environmental impact due to the depth of the groundwater table. According to the groundwater model, the average depth from the land surface down to the groundwater table is around 100 m in this area.

Although considerable increases in groundwater levels are predicted in the areas mentioned above, they are considered unlikely to have a significant effect on the regional groundwater flow patterns, as they occur in regions where the natural-state groundwater gradients are relatively high (Figure 13). It is important to note, however, that there is still a relatively large amount of uncertainty regarding the degree of vertical hydrologic connection in the groundwater system. Therefore, the groundwater level changes predicted by the model should be viewed as initial estimations subject to updating after experience is gained from pilot testing of production/injection. No changes in groundwater level are predicted at the existing production wells at Kaldársel.

Table 2. Predicted groundwater impacts of the operational scenario.

Environmentally sensitive area	**Groundwater level change [cm]**	**Salinity change [g/kg]**		**Temperature change [°C]**	
	Maximum	**Maximum**	**Mean**	**Maximum**	**Mean**
Óttarstaðar-tjarnir	0	+0.3	<+0.1	<+0.1	<+0.1
Brunntjörn	-2	+0.4	+0.2	+0.3	+0.1
Þorbjarnarstaðar-tjarnir (Brunntjörnin)	-4	+0.4	+0.2	+1.0	+0.4
Gerðistjarnir	-4	+0.3	+0.2	+1.0	+0.4
Rio Tinto production wells	-7	+0.5	+0.3	+1.3	+0.8
Ástjörn	+30	0	0	0	0
Hvaleyrarvatn	+40	0	0	0	0
Urriðavatn	+20	0	0	0	0
Production wells at Kaldársel	0	0	0	0	0

Maximum predicted salinity changes are < 0.4 g/kg at the coastal ponds at Straumsvík. According to Icelandic drinking water standards, the maximum salinity limit for drinking water is 0.4 g/kg. Therefore, this amount of salinity increase in the freshwater ponds will not affect their water quality classification

(i.e., the water will remain fresh). Maximum predicted salinity changes are 0.5 g/kg at the Rio Tinto production wells. It is uncertain whether this amount of salinity change would affect their utilization of the produced water. No salinity changes are predicted at Ástjörn, Hvaleyrarvatn, Urriðavatn nor the existing production wells at Kaldársel.

Maximum predicted groundwater temperature changes are as much as +1 °C at the coastal ponds at Straumsvík. It is assumed that there are natural-state fluctuations in the water temperature in the ponds, and the degree of those fluctuations will likely determine to some extent what type of environmental impacts, if any, the predicted groundwater temperature increase could have on the ponds. Maximum predicted temperature changes are +1.3 °C at the Rio Tinto production wells. It is uncertain whether this amount of temperature increase would affect their utilization of the produced water. No temperature changes are predicted at Ástjörn, Hvaleyrarvatn, Urriðavatn nor the existing production wells at Kaldársel.

It is important to understand the general behavior of the groundwater system (i.e., its response to the production/injection) when assessing potential environmental impacts. The pressure increase induced by injection is a key factor in this behavior, as it clearly plays a major role in causing changes in the groundwater system. This injection-induced pressure increase provides significant pressure support to the shallow freshwater aquifer, reducing drawdown due to production and causing a rise in groundwater levels. The injection-induced pressure increase also has a significant effect on groundwater salinity and temperature, mostly in the deeper sections of the groundwater system, but also extending up into the shallow freshwater aquifer to some extent. The model calculates relatively minor changes in the top section of the freshwater aquifer where environmentally sensitive areas are located (e.g., where groundwater is entering the coastal ponds and Rio Tinto production wells). However, calculated changes to salinity and temperature are greater in the lower sections of the freshwater aquifer as can be seen on the cross section figures in Chapter 5.2.2 and Chapter 5.2.3. As explained in detail earlier, the scale and magnitude of the injection-induced pressure increase is largely determined by the degree of vertical hydrologic connection in the groundwater system, which is controlled by several parameters which have a high degree of uncertainty. The vertical extent within which groundwater salinity and temperature are affected significantly is therefore subject to a degree of uncertainty, which needs to be addressed with future work. Additional research and field testing is necessary to verify the degree of vertical hydrologic connection in the system. Also, a robust monitoring program is needed in and around environmentally sensitive areas to determine baseline conditions and track potential changes during operational phases.

5.4. Drought conditions

Groundwater levels fluctuate naturally due to variability in infiltration caused by short- and long-term meteorological conditions. The magnitude and severity of impacts from groundwater production and injection can be affected by the state of the groundwater system. Typically, a shallow groundwater aquifer is considered more sensitive to impacts from production when regional groundwater levels are low (e.g., during extended drought periods).

The model was used to simulate drought conditions in order to estimate the effects of low groundwater levels on the impacts of the Coda Terminal. An analysis of historical groundwater levels was performed to determine appropriate infiltration rates to specify in the new drought scenario. One of the longest measured groundwater level time-series in southwest Iceland is in well I (formerly vhm189) in Heiðmörk. The well contains over 50 years of continuous measurements (Figure 41). The lowest recorded groundwater levels in the well occurred in consecutive years, 2010 and 2011, during

an extended period of below average precipitation for the area. A 3-year average infiltration rate was calculated using the 2-year extended drought period and the year leading up to it (2009). This 3-year infiltration rate is roughly 12% less than the 50-year average rate which was used in the original operational scenario (defined in Chapter 5.1). The 3-year average infiltration rate representing drought conditions and low groundwater levels was utilized to re-run the operational scenario.

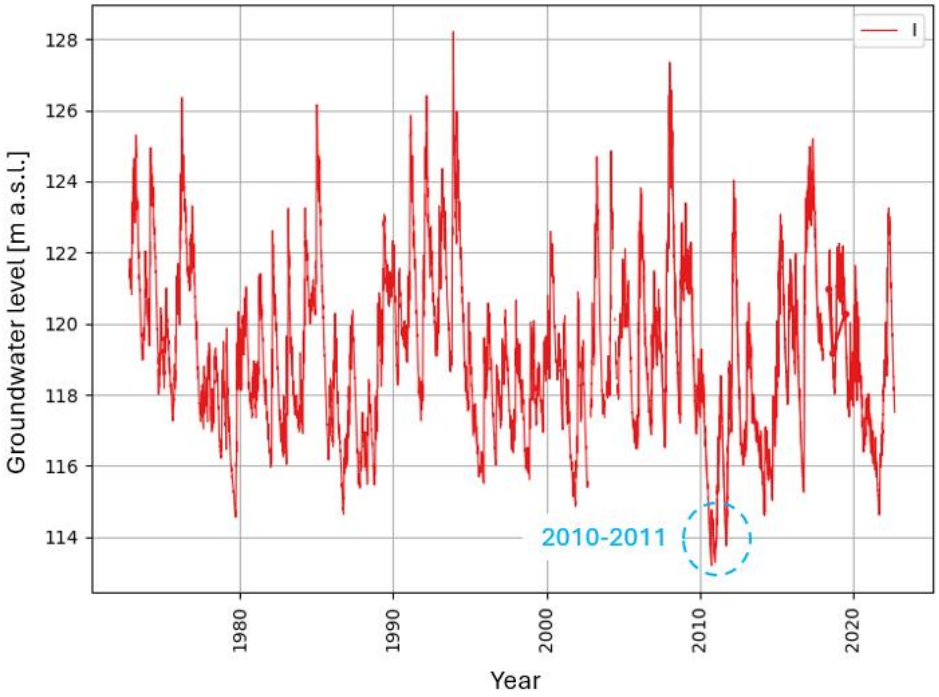

Figure 41. Measured groundwater levels in well I (vhm189) in Heiðmörk.

Model results from the drought scenario were analyzed and compared with the original operational scenario. Comparison of the model results showed relatively minor differences between the scenarios, indicating that drought conditions do not have a significant influence on changes in the groundwater system due to production/injection from the Coda Terminal.

An example is shown on Figure 42, which compares model results for simulated salinity change at 0 m a.s.l. during operational phase 4. The figure shows the same maximum salinity changes and only a slight increase in the area affected by those changes in the drought scenario.

Comparison of temperature changes at -20 m a.s.l. during operational phase 4 is shown on Figure 43. As with salinity, there is no difference in the maximum changes, however the area affected by temperature changes is slightly larger in the drought scenario.

Analysis of groundwater level changes and capture/advection zones show only slight variations between the original operational scenario and the drought scenario, supporting the conclusion that drought conditions do not significantly increase impacts on the groundwater system due to production/injection from the Coda Terminal.

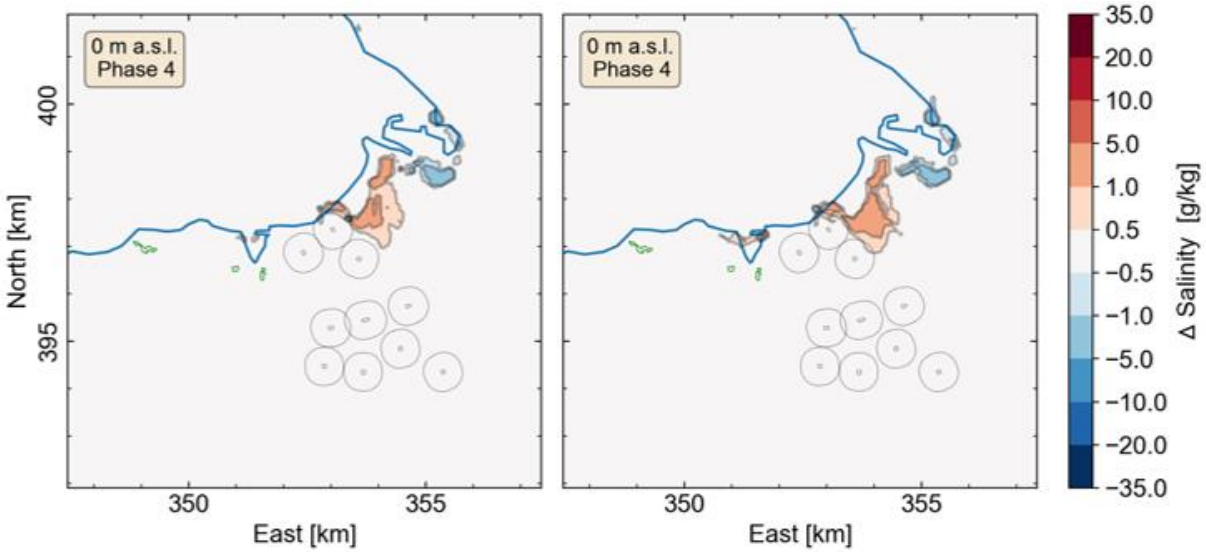

Figure 42. Simulated changes to groundwater salinity at 0 m a.s.l. in the freshwater aquifer from original operational scenario (left) and drought scenario (right).

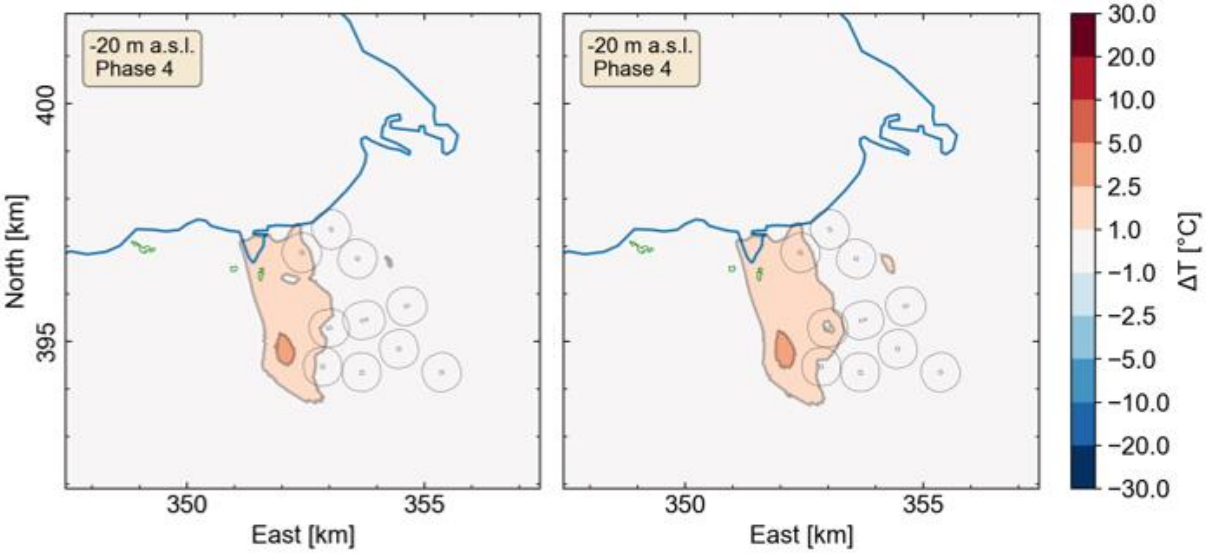

Figure 43. Simulated changes to groundwater salinity at -20 m a.s.l. in the freshwater aquifer from original operational scenario (left) and drought scenario (right).

Although changes to the groundwater system are not drastic due to the simulated drought conditions, there are slight changes to the impacts predicted at the environmentally sensitive areas as shown in Table 3. Compared to the operational scenario, the model predicts a slightly higher increase in salinity and temperature at Þorbjarnarstaðartjarnir (Brunntjörnin), Gerðistjarnir and the Rio Tinto production wells for the drought scenario.

Table 3. Predicted groundwater impacts of the drought scenario.

Environmentally sensitive area	Groundwater level change [cm]	Salinity change [g/kg]		Temperature change [°C]	
	Maximum	Maximum	Mean	Maximum	Mean
Óttarstaðar-tjarnir	0	+0.2	<+0.1	<+0.1	<+0.1
Brunntjörn	-2	+0.4	+0.2	+0.3	+0.1
Þorbjarnarstaðar-tjarnir (Brunntjörnin)	-4	+0.5	+0.2	+1.2	+0.4
Gerðistjarnir	-4	+0.4	+0.2	+1.1	+0.4
Rio Tinto production wells	-7	+0.7	+0.5	+1.5	+0.9
Ástjörn	+30	0	0	0	0
Hvaleyrarvatn	+40	0	0	0	0
Urriðavatn	+20	0	0	0	0
Production wells at Kaldársel	0	0	0	0	0

5.5. Sensitivity scenario

Although research commissioned by Carbfix (through borehole drilling/sampling and TEM/micro-TEM surveys) provided valuable information on the morphology of the fresh/saline interface (Chapter 3.2 and 3.3), a comprehensive understanding of the interface has still not been achieved. There remains uncertainty on the depth to the interface, especially below well pads 1-7. The current groundwater model simulates the position of the interface at roughly -100 m a.s.l. to -600 m a.s.l. below well pads 1-7 (Figure 17). This results in the vast majority of the defined injection at well pads 1-7 occurring within or below the interface (i.e., in brackish and saline groundwater) in the operational scenario. Only well pad 4, which is furthest to the southeast, is injecting into completely fresh groundwater according to the current baseline model.

Previous modelling work performed by Vatnaskil during early design stages of the Coda Terminal indicated that the location of the wellfield in relation to the fresh/saline interface was an important factor controlling the degree of impacts predicted by the model. Initial modelling results suggested that impacts on the salinity and temperature of the shallow freshwater aquifer were less when injection was focused in the freshwater sections of the groundwater system as opposed to the saline sections. As described in Chapter 4.2, the model overestimates the groundwater salinity between roughly -100 and -350 m a.s.l. at Carbfix well CSM-01, which is close to well pad 5. It is possible, therefore, that the model also overestimates the groundwater salinity below other well pads to the southeast of well pad 5 (i.e., well pads 1, 2, 3, 6 and 7). If this is indeed the case, then it is possible that

the impacts on the salinity and temperature of the shallow freshwater aquifer predicted in the operational scenario (Chapter 5.2) are overly pessimistic.

In order to investigate this possibility and assess the sensitivity of the location of injection with respect to the fresh/saline interface, a hypothetical production/injection scenario (scenario WP-4) was evaluated. The scenario was defined such that production and injection occur only at well pad 4 (no other well pads were active). This ensured that injection occurs only into fresh groundwater to the southeast of the fresh/saline interface (as the current Carbfix design plans call for at well pads 1-7). It should be stressed that scenario WP-4 is only a hypothetical scenario. In reality, it is not feasible to concentrate all production/injection at only one well pad. The purpose of scenario WP-4 was to account for uncertainties in the location of the fresh/saline interface below the Carbfix wellfield and to give an indication of the degree of impacts in the freshwater aquifer if the Carbfix design plans are fulfilled. Figure 44 shows a comparison of calculated groundwater salinity at the main injection depth (-343 m a.s.l.) between the operational scenario and scenario WP-4. With a majority of the injection occurring within or below the fresh/saline interface at well pads 1-7 (operational scenario), a major alteration to the morphology of the interface is predicted by the model at this depth. Calculated salinity for scenario WP-4, however, is similar to the baseline (natural-state) conditions simulated by the model (Figure 17), indicating that scenario WP-4 causes minimal disruption to the natural groundwater conditions at this depth.

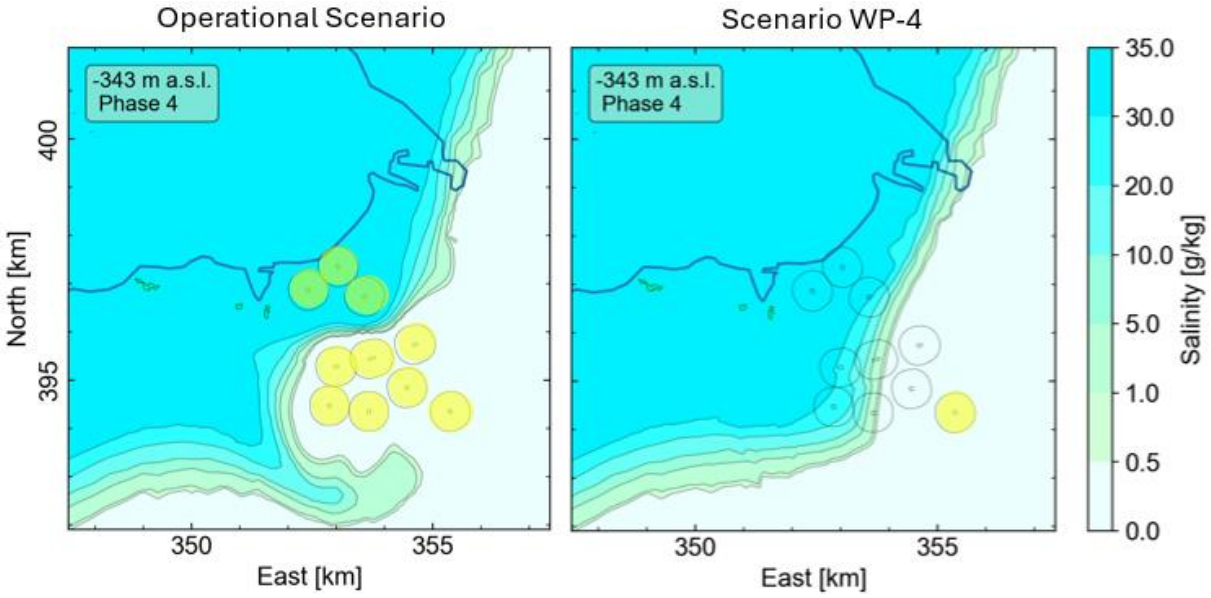

Figure 44. Simulated groundwater salinity at -343 m a.s.l. for the operational scenario (left) and scenario WP-4 (right). Active well pads for each scenario are highlighted in yellow.

The impacts of scenario WP-4 on groundwater salinity and temperature can be seen on Figure 45, which shows the calculated change in salinity and temperature along NW-SE cross section 1. Comparison with the operational Scenario shows that scenario WP-4 causes significantly less overall impact on groundwater salinity and temperature, especially within the upper 100 m at the Rio Tinto wellfield (and nearby coastal ponds).

In summary, results from the hypothetical scenario WP-4 indicate that the background conditions at the injection depths play a key role in the salinity and temperature effects predicted by the model.

Injecting freshwater into fresh background conditions causes less impact on the natural state of the groundwater system than injecting freshwater into saline background conditions. Therefore, if the baseline model overestimates the extent of saline intrusion inland (as available measurements indicate), then the impacts on groundwater salinity and temperature predicted in the operational scenario (Chapter 5.2) are most likely conservative. This highlights the importance of further research to map with more certainty the fresh-saline interface in the vicinity of the proposed Coda Terminal wellfield. Furthermore, the results of the hypothetical scenario provides a foundation for potential mitigation measures in the final design of the wellfield.

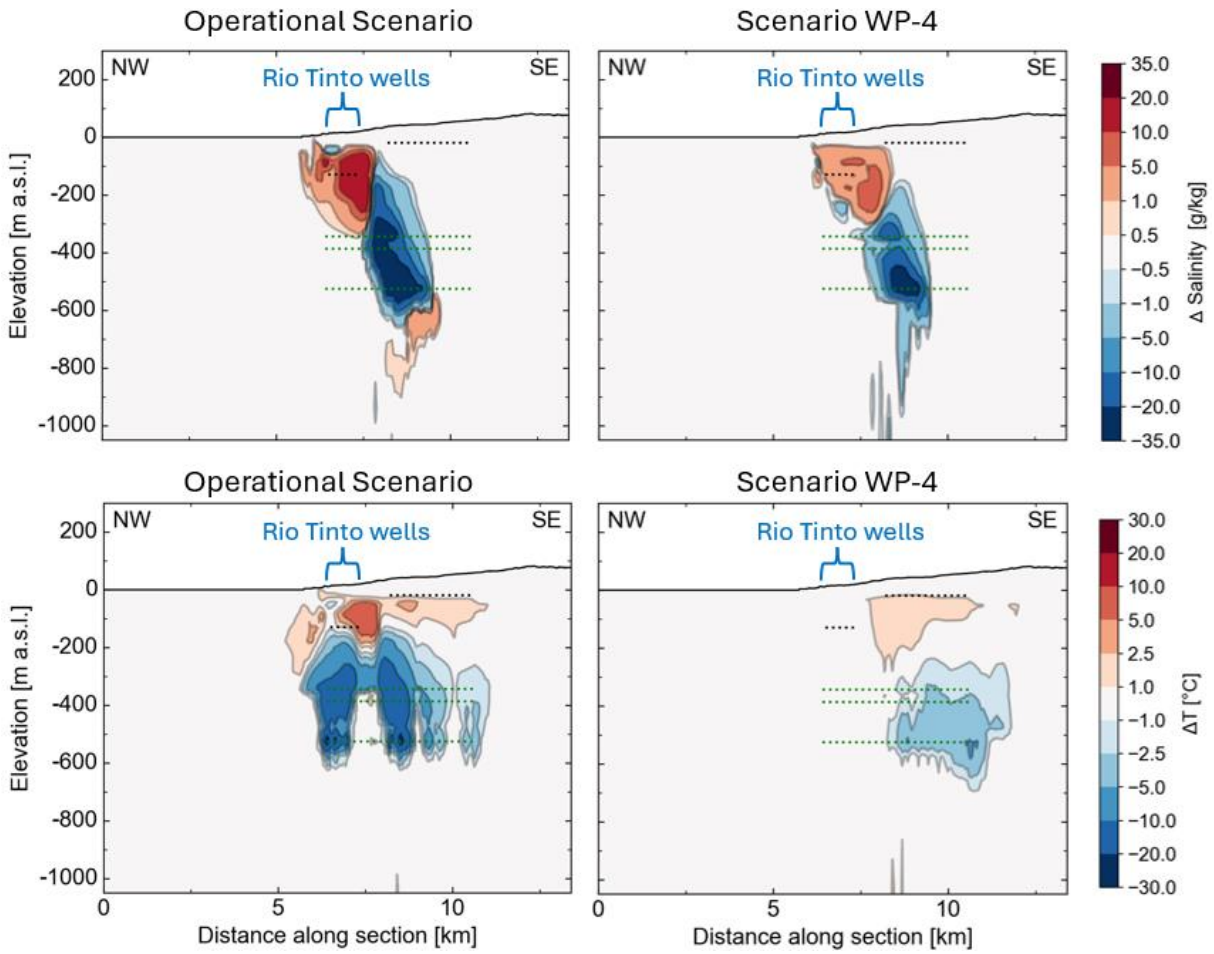

Figure 45. Simulated changes to groundwater salinity along NW-SE cross section 1 for the operational scenario (upper left) and scenario WP-4 (upper right). Simulated changes to groundwater temperature along NW-SE cross section 1 for the operational scenario (lower left) and scenario WP-4 (lower right).

6. Water Framework Directive

The planned Coda Terminal is located within the Straumsvíkurstraumur groundwater body (grunnvatnshlot) as shown on (Figure 46). The total area of the defined groundwater body is 332,1 km^2. The environmental goals of this groundwater body are to ensure good quantity and quality of water. Risks are not defined. Adjacent groundwater bodies are also within the influence area of the Coda Terminal as predicted by the groundwater model, in particular Kleifarvatn no. 104-264-G to the south and Stór-Reykjavík no. 104-261-2-G to the northeast. The assessment below focuses on

Straumsvíkurstraumur as the primary groundwater body impacted by the planned Coda Terminal operations, but also applies to the adjacent groundwater bodies.

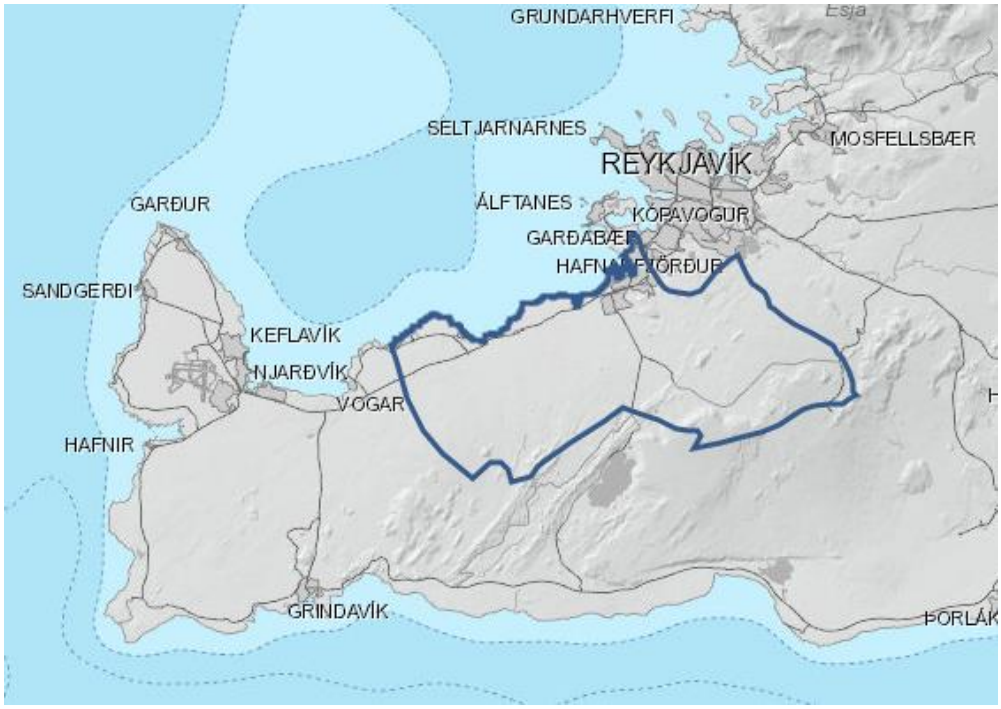

Figure 46. Location Straumsvíkurstraumur, no. 104-265-G. From vatnavefsjá (vatnavefsja.vedur.is).

According to the Icelandic Water Plan (Vatnaáætlun Íslands) 2022-2027, the following two classification elements should be assessed when determining impacts on a groundwater body:

1) Physical quantity

   Groundwater levels are defined in regulation no. 535/2011 as a measure of how much impact, direct or indirect, water abstraction has on the physical quantity of groundwater bodies. Groundwater levels are assessed to ensure that the height of the groundwater table must be such that the average water withdrawal per year in the long term does not exceed the available groundwater resource. Quantitative status is classified as either good or poor.

2) Chemical quality

   When determining the chemical quality of groundwater bodies, both electrical conductivity and concentration of pollutants should be assessed. Electrical conductivity values should not indicate the intrusion of saline water into the groundwater body, and the concentration of pollutants shall not exceed environmental limits. Qualitative status is classified as either good or poor.

The current assessment focuses on the area within the numerical groundwater model which covers only a part of the Straumsvíkurstraumur groundwater body but extends into other adjacent groundwater bodies, as mentioned above. It is assumed that any impacts imposed by the Coda Terminal production/injection on the groundwater body will not extend beyond the model boundaries. This is in agreement with the model results presented above. The main physical and chemical characteristics of the groundwater body within the model boundaries are described in Chapters 2 and

3 above, and the current state of the groundwater body is represented by the baseline model presented in Chapter 4.2.

6.1. Impacts on physical quantity

Estimated groundwater outflow into the ocean at Straumsvík from the shallow freshwater aquifer is estimated at roughly 8-10 m^3/s. The total planned production at the Coda Terminal is approximately 3 m^3/s, with roughly 2 m^3/s being produced from the freshwater aquifer and roughly 1 m^3/s being produced from the underlying saline aquifer from well pads 8-10 (Table 1). Results from the operational scenario (Chapter 5.2) show that the planned production/injection causes relatively little drawdown of the groundwater table. Both the extent and magnitude of estimated drawdown are small relative to the overall size of the groundwater body and natural groundwater fluctuations within it. This is due to several factors, one being the high permeability of the recent lava formations in which the freshwater aquifer lies. The other factor is the substantial amount of pressure support induced by the injection, which counterbalances the drawdown from production. Injection induces a pressure increase in the deeper sections of the groundwater system, which is transmitted upward towards the surface. It provides pressure support to the shallow freshwater aquifer, reducing the amount of drawdown that would otherwise occur if there was no injection. Since 100% of the produced water will be injected back into the groundwater body, there is essentially no net withdrawal from the groundwater body as a whole. Groundwater is merely moved from the shallow section of the groundwater system (upper ~200 m) to the deeper sections (> 300 m b.s.l.). Therefore, the planned production/injection at the Coda Terminal is considered unlikely to have measurable effects on the amount of groundwater outflow into the ocean at Straumsvík.

Results from the operational scenario (Chapter 5.2) show that very little drawdown is predicted at the coastal ponds at Straumsvík, indicating that groundwater flow into the ponds is unlikely to be impacted by the production/injection from the Coda Terminal. Additionally, no impacts on groundwater levels are predicted at the closest drinking water protection area at Kaldársel. An increase in groundwater levels is predicted at lakes east of the wellfield (Ástjörn, Hvaleyrarvatn and Urriðavatn) which could potentially result in increased groundwater inflow but is unlikely to have a significant effect on the lake levels.

Overall, estimated impacts from production/injection at the Coda Terminal on the physical quantity of the Straumsvíkurstraumur groundwater body are considered minimal and are not expected to affect the environmental objectives of the groundwater body. Predicted changes to the groundwater table (Chapter 5.2.1) are not likely to change natural-state groundwater flow paths nor the quantity of groundwater.

6.2. Impacts on chemical quality

Potential groundwater pollution associated with the construction and operation of the Coda Terminal was not within the scope of the current assessment, and therefore cannot be commented on here. Saline intrusion, however, was considered as part of the assessment. Results from the operational scenario (Chapter 5.2) show that the planned production/injection will affect groundwater salinity. Significant changes to groundwater salinity are predicted in the deeper sections of the groundwater system, however predicted salinity changes are relatively minor at the top of the freshwater aquifer where environmentally sensitive areas are located. Maximum predicted salinity changes are < 0.4 g/kg at the coastal ponds at Straumsvík. According to Icelandic drinking water standards, the maximum salinity limit for drinking water is 0.4 g/kg. This amount of salinity increase in the freshwater ponds will

not affect their water quality classification (i.e., the water will remain fresh). Maximum predicted salinity changes are 0.5 g/kg at the Rio Tinto production wells. It is uncertain whether this amount of salinity change would affect their utilization of the produced water. No salinity changes are predicted at Ástjörn, Hvaleyrarvatn, Urriðavatn nor the existing production wells at Kaldársel.

Overall, estimated impacts from production/injection at the Coda Terminal on the chemical quality (with regard to salinity) of the Straumsvíkurstraumur groundwater body are considered minor and are not expected to affect the environmental objectives of the groundwater body.

7. Conclusions

The Straumsvík watershed is characterized by a set of relatively complex hydrogeological conditions. Hydrogeological research in the coastal region at Straumsvík is still in the early stages, especially investigations focused on the deeper sections of the groundwater system (> 100 m), as only two deep wells (CSI-01 and CSM-01) have been completed to date. Therefore, significant gaps remain in the conceptual model of the local groundwater system, creating uncertainties which impose limitations on numerical modelling efforts. Despite these limitations, the model can still provide an initial estimate of potential environmental impacts from the proposed production and injection of the Coda Terminal. The following main conclusions can be drawn from the modelling results:

- The drawdown due to production is relatively small due to the hydrogeological conditions in the freshwater aquifer (e.g., high permeability and high groundwater flow) and the pressure support provided by injection.
- A rise in groundwater levels is predicted due to pressure support provided by injection. Increased pressure due to injection is substantial due to the hydrogeological conditions in the deeper sections of the groundwater system (e.g., low permeability and low groundwater flow).
- Changes in groundwater levels are not likely to significantly affect the natural-state regional groundwater flow (direction and magnitude).
- Changes to groundwater salinity and temperature at the top of the freshwater aquifer (above -20 m a.s.l.) are relatively small and therefore are not likely to cause significant environmental impacts.
- Changes to groundwater salinity and temperature below -20 m a.s.l. are relatively large, however they do not significantly impact environmentally sensitive areas.
- The planned production/injection at the Coda Terminal is not likely to negatively affect current groundwater producers in the area, although a slight increase in salinity and temperature are predicted at the Rio Tinto production wells.
- Drought conditions are not likely to have a significant influence on the impacts of production/injection from the Coda Terminal.
- Although predicted changes to groundwater levels, salinity and temperature at the top of the freshwater aquifer are relatively small, it is not possible to rule out the possibility of some environmental impacts. Model limitations and lack of available data on the degree of sensitivity of potentially affected natural (coastal ponds and inland lakes) and industrial (Rio Tinto's groundwater utilization) systems result in uncertainties in the model results. Therefore, groundwater monitoring in the vicinity of environmentally sensitive areas (outlined in Chapter 2) is recommended.

It is recommended that continued hydrogeological research focus on filling gaps in the current conceptual model, especially with respect to the morphology of the fresh/saline interface and the degree of hydrologic connection between the shallow freshwater aquifer and the deeper sections of the groundwater system. According to the model results, these two aspects of the conceptual model play a significant role in determining the degree of impacts on the freshwater aquifer.

Carbfix is currently in the process of drilling their third research well, CSM-02, which is located next to well pad 1. It is assumed that a robust set of measurements and testing will be performed in the well, providing valuable new hydrogeological information. Additional TEM surveys in the coastal area at Straumsvík are suggested in order to gain a clearer understanding of the morphology of the fresh/saline interface at Straumsvík. Carbfix plans on conducting pilot tests of production and injection, which should provide the first direct measurements of impacts on the groundwater system as well as an indication of the vertical hydrologic connection in the groundwater system.

Due to the scale and magnitude of the proposed production/injection at the Coda Terminal, a robust groundwater and surface water monitoring program is needed to register the current state of the groundwater system (pre-operational) and to detect potential changes to the system once the first operational stages begin. Parallel updates to the groundwater model as new research and monitoring data become available may provide further support in lowering uncertainties and revising the initial impact assessment.

References

Hafnarfjörður, 2014. **Aðalskipulag Hafnarfjarðar 2013-2025**. Apríl 2014.

Hjartarson, Á., Gunnlaugsson, E., Sigurðsson, F., Jónsson, J. and Saemundsson, K., 1992. **Vatnafarskort, Elliðavatn 1613 III SV, 1:25.000**. Landmælingar Íslands, Orkustofnun, Hafnarfjarðarbær, Garðarbær, Kópavogsbær, Seltjarnarnesbær og Reykjavík.

Icelandic Meteorological Office, 2007. **Precipitation in Iceland (1971-2000)**. In collaboration with Hydrological Service, National Energy Authority, Institute of Earth Sciences, University of Iceland. October, 2007.

Ingólfsson, Agnar, 1998. **Lífríki í tjörnum við Straumsvík**. Náttúrufræðingurinn 67 (3-4). bls. 255-262.

ÍSOR, 2010. **Undirgöng við Straumsvík. Sjávarföll og sveiflur grunnvatnsborðs**. Unnið fyrir Vegagerðina. ÍSOR-2010/044. Október 2010.

ÍSOR, 2021. **Straumsvík - Holustaðsetning**. Unnið fyrir Carbfix. ÍSOR-2021/034. September 2021.

ÍSOR, 2023a. **Straumsvík – a short lithology overview**. Unnið fyrir Carbfix. Minnisblað. 18.01.2023. M.Á.S.

ÍSOR, 2023b. **Straumsvík – Well CSI-01. Drilling of Well CSI-01 from Surface down to 982 m**. Prepared for Carbfix. ÍSOR-2023/006. March 2023.

ÍSOR, 2023c. **Televiewer Logs from Well CSI-01 in Straumsvík**. Prepared for Carbfix. ÍSOR-2023/034. October 2023.

ÍSOR, 2023d. **Baseline Geology and Three-Dimensional Geological Model of the Straumsvík Area. Prepared for Carbfix's Coda Terminal Project for the Environmental Impact Assessment**. Prepared for Carbfix. ÍSOR-2023/018. December 2023.

ÍSOR, 2023e. **Saline Groundwater Exploration near Straumsvík using TEM. October 2022 to April 2023**. Prepared for Carbfix. ÍSOR-2023/050. December 2023.

ÍSOR, 2024a. **Straumsvík – Well CSM-01. Drilling of Well CSM-01 from Surface down to 618 m**. Prepared for Carbfix. ÍSOR-2024/002. January 2024.

ÍSOR, 2024b. **Wells CSM-01 and CSI-01. Injection Test and Spinner**. Prepared for Carbfix. Short report ÍSOR-24003. January 2024.

Jenness, M.H. and Clifton, A.E, 2009. **Controls on the geometry of a Holocene crater row: a field study from SW Iceland**. Bulletin of Volcanology, (71) 7, 715-728.

Jóhannesson, H. and Einarsson,S., 1998. **Hraun í nágrenni Straumsvíkur**. Náttúrufræðingurinn, (67) 171-177.

Mannvit, 2023. **Niðurdaeling CO_2 til geymslu í jörðu á Hellisheiði. Umhverfismatsskýrsla**. Unnið fyrir Carbfix hf. Janúar 2023.

Orkustofnun, 1976. **Straumsvíkursvæði. Skýrsla um vatnafræðilega frumkönnun**. Unnið fyrir Íslenska álfélagið h.f. Straumsvík. OS JKD 7603. Marz 1976.

Orkustofnun, 1977. **Höfuðborgarsvæði. Jarðhitarannsóknir 1965-1973**. OSJHD 7703. Febrúar 1977.

Orkustofnun, 2001. **Náttúrufar á vatnasvæðum í landi Hafnarfjarðar. Umhverfisúttekt**. Unnið fyrir Hafnarfjarðarbæ af Náttúrufræðistofnun Íslands, Náttúrufræðistofu Kópavogs og Orkustofnun. OS-2001/064. Desember 2001.

Orkustofnun, 2002. **Trölladyngja – Hola TR-01. Áfangaskýrsla um borun og rannsóknir**. Unnið fyrir Jarðlind ehf. OS-2002/053. Nóvember 2002.

Sigurðsson, F., 1998. **Grunnvatnið í Straumsvík**. Náttúrufræðingurinn, (67) 179-188.

Sæmundsson, K., 1978. **Fissure swarms and central volcanoes of the neovolcanic zones of Iceland**. Geol J Spec Issue 10:415–432.

Sæmundsson, K., Sigurgeirsson, M. Á., Hjartarson, Á, Kaldal, I., Kristinsson, S. G. and Víkingsson, S., 2016. **Jarðfraeðikort af Suðvesturlandi, 1:100.000**. (2. útgáfa). Reykjavík: Íslenskar orkurannsóknir.

Tómasson, H. and Tómasson, J., 1966. **Geological report on the aluminium plant site and Straumsvík**. Performed for the Icelandic Aluminium Company Ltd. December 1966.

Vatnaskil, 2022a. **Reykjanesskagi. Vatnafarslíkan. Endurskoðun líkans og uppfærsla fyrir árin 2020-2021.** Unnið fyrir HS Orku. Skýrsla 22.07. Júlí 2022.

Vatnaskil, 2023. **Höfuðborgarsvæði. Árleg endurskoðun rennslislíkans. Framgangur endurskoðunar 2023.** Unnið fyrir Samtök sveitarfélaga á höfuðborgarsvæðinu. Skýrsla 23.08. Desember 2023.

VIÐAUKI II

Specialist report:

Impact Assessment of the Injection of CO_2 on the storage complex for the Coda Terminal

---

Three Dimensional Models of the Reservoir Response to the Proposed CO_2 Injection and Mineral Storage Operations at the Coda Terminal

---

Report prepared by:
Kjartan Marteinsson
Thomas Ratouis
Benjamin Smith

Reservoir Engineering
Carbfix

May 16, 2024

Contents

Figures

Tables

Útdráttur

Coda Terminal er móttöku- og geymslustöð fyrir koldíoxíð (CO_2) sem fyrirhugað er að reisa í Straumsvík. Við full afköst er áætlað að stöðin muni geta tekið við allt að 3 Mt af CO_2 á ári sem leyst verður í vatni og dælt í geymslugeymi en þannig er leysnibindingu náð strax við niðurdælingu. CO_2-hlaðni niðurdælingarvökvinn hvarfast svo við basaltberg geymslugeymisins og leysir úr málma sem ganga í efnasamband við CO_2 og mynda steindir. Þannig bindist CO_2 varanlega í berggrunninum.

Geymslugeymirinn samanstendur af hraunlagasyrpum frá hlýskeiðum, móbergi og glerjuðu basalti. Bergfræðileg einkenni og steindasamsetning bergsins sýna að um basalt er að ræða sem ríkt er af frumsteindum á borð við plagíóklas, pýroxen og í minna mæli ólivín. Lághitaummyndunarsteindir á borð við smektít og zeólíta eru til staðar neðan 400 m u.s. Engin skýr merki eru um sprungur eða misgengi á Straumsvíkursvæðinu, hvorki á yfirborði né í borholugögnum. Lekt í efstu 1000 m jarðlagastaflans er að mestu bundin við jarðlagamót milli hraunlaga og er lárétt lekt ríkjandi á svæðinu. Ádælingarpróf í rannsóknarborholum Carbfix CSI-01 og CSM-01 sýna að mesta lekt á svæðinu er á milli 300-400 m u.s. dýpi og benda borholugögn til þess að lektin tengist jarðlagamótum. Báðar holurnar sýna litla lekt neðan 500 m u.s.. Inn til landsins er vökvinn í geymslugeyminum ferskt grunnvatn en nær ströndinni er einnig jarðsjó að finna. Þar sem jarðsjór er til staðar er ísalt blandlag milli ferskvatns og jarðsjávar. Hitamælingar í CSI-01 og CSM-01 benda til þess að hitastigull í geymslugeyminum sé á bilinu 80-90°C/km.

Gögn um jarðfræðilegar aðstæður á svæðinu voru notuð til að þróa jarðfræði- og hugmyndalíkan fyrir geymslugeyminn. Þessi líkön voru svo notuð sem grunnur að reiknilíkani fyrir geymslugeyminn. Reiknilíkanið var látið herma náttúrulegt ástand geymslugeymisins með tilliti til þrýstings, hita, seltu, flæðis, CO_2-innihalds og eðlisþyngdar vökvans. Þegar niðurstöður hermana eru bornar saman við fyrirliggjandi gögn af svæðinu sýnir það að reiknilíkanið hermir náttúrulegt ástand svæðisins á fullnægjandi hátt og því var hægt að nota niðurstöður þess til að herma ýmsar sviðsmyndir fyrir niðurdælingu og vatnstöku á svæðinu.

Hermanir voru framkvæmdar til að áætla 1) hámarksdreifingu CO_2 í geymslugeyminum, 2) stöðugleika leysnibindingar CO_2 í geymslugeyminum og 3) dreifingu eðlisþyngdar vökva á svæðinu. Reiknilíkön voru látin herma kerfið í 30 ár sem er fyrirhugaður líftíma Coda Terminal og var hermd niðurdæling á CO_2 á svæðinu aukinn í fjórum þrepum upp í 3 Mt í samræmi við þrepaskiptingu verkefnisins. Einnig voru reiknilíkönin látin herma stöðu kerfisins í 100 ár eftir að niðurdælingu vegna verkefnisins er hætt á svæðinu. Reiknilíkönin voru ekki látin herma áhrif efnahvarfa, s.s. steinnrenningu CO_2, á dreifingu CO_2 og sýna þau því áætlaða hámarksdreifingu CO_2 á svæðinu byggt á þeim forsendum þ.e.a.s. að ekkert CO_2 steinrennist. Reiknilíkanið sem er notað til grundvallar fyrir líkönin hermir varmafræðilega eiginleika H_2O-CO_2-NaCl vökva, þar á meðal eðlisþyngd hans og leysni CO_2 í honum. Reiknilíkanið hermir aðstreymis- og sveimisflæði H_2O-CO_2-NaCl vökva í margvíðum, misleitum kerfum.

Niðurstöður reiknilíkana fyrir hámarksdreifingu CO_2 í geymslugeyminum bendir til að allt niðurdælt CO_2 haldist bundið innan geymslusvæðisins á líftíma verkefnisins og að ekkert CO_2 nær upp í efri lög grunnvatnskerfisins ($<$ 100 m u.s). Hætta á CO_2-leka vegna flæðis eða afgösunar á uppleystu CO_2 er talin hverfandi og þar af leiðandi er ekki talið að niðurdælingin muni hafa áhrif á sýrustig grunnvatns á svæðinu. Niðurstöður reiknilíkana sýna að hitastig í geymslugeyminu nærri niðurdælingarholum lækkar vegna niðurdælingarinnar. Þrýstingur gæti aukist um allt að 25 bör í geymslugeyminum á 300 - 1000 m u.s. dýpi vegna niðurdælingar vatns. Litlar þrýstingsbreytingar verða í efri lögum grunnvatns á svæðinu og líkön sýna að þrýstingsaukning í geymslugeymi hefur ekki í för með sér að CO_2 berist í efri lög grunnvatns á svæðinu. Líkanareikningar benda til þess að þrýstingsbreytingar gangi að mestu til baka eftir

100 ár en breytingar á hita eru mun hægari vegna takmarkaðs náttúrulegs hitaflæðis á svæðinu.

Niðurstöður hermana sýna að niðurdæling hefur áhrif á seltumagn í geymslugeyminum en mestu breytingar á seltumagni munu eiga sér stað í fjórða áfanga verkefnisins. Aðeins minniháttar seltubreytingar sjást í efri lögum grunnvatnskerfisins á svæðinu (< 100 m u.s). Þá benda hermanir til þess að selta breytist í átt að náttúrulegu ástandi en óvíst er hversu langan tíma sú breyting tekur. Niðurstöður reiknilíkana sýna að geymslugeymirinn í Straumsvík er fýsilegur kostur fyrir niðurdælingu á CO_2 leystu í vatni á stórum skala (Mt). Hermanir sýna einnig að umhverfisáhrif á geymslugeyminn, geymslusvæðið og nærliggjandi umhverfi eru takmörkuð.

Niðurstöður hermana vegna verkefnisins eru háðar ýmsum óvissum s.s. vegna óvissu í stærð jarðfræðilegrar misleitni á svæðinu, óvissu í mæligögnum, óvissu í túlkun og framreikningi mæligagna sem og óvissu vegna tölulegra nálgana í reiknilíkönunum. Þeir óvissuþættir sem taldir eru hafa hvað mest áhrif á reiknilíkönin af svæðinu eru dýpi og þykkt blandlags milli ferskvatns og jarðsjós sem og stærðargráða vatnafræðilega tengsla, s.s. vatnsleiðni, milli geymslugeymis og yfirborðs. Nauðsynlegt er að safna frekari gögnum af svæðinu til að minnka óvissu á þessum þáttum en það munu auka áræðanleika og forspárgetu líkana af svæðinu. Niðurstöður reiknilíkananna ætti að nýtast við áhættumatsgerð og aðstoða við að taka upplýstar ákvarðanir við mat á umhverfisáhrifum.

Abstract

The Coda Terminal is a mineral storage project located at Straumsvík in the Southwest of Iceland which, at full capacity, will receive and store up to 3 $MtCO_2$ per year via mineral trapping. Mineral storage of CO_2 involves the injection of dissolved CO_2 into a mafic reservoir and relies on immediate solubility trapping of CO_2 followed by rapid in-situ mineralization of CO_2 via interaction with the host rock. The storage reservoir for the Coda Terminal is composed of a succession of interglacial lava flows, hyaloclastites, and/or glassy basalts. The lithology and mineralogy are consistent with basaltic rocks rich in primary minerals including plagioclase, pyroxene, and to a lesser extent olivine. Small amounts of alteration minerals such as smectites and zeolites are also present in the subsurface below -400 m a.s.l. No clear evidence of faults or fissures has been found in the Straumsvik area although it is close to known SW-NE fissure swarms. The permeability in the upper 1000 m of the subsurface is controlled by lithological contacts between lava flows and is characterized by an anisotropic permeability field, in which the horizontal permeability is dominant. Injectivity tests in wells indicate that most of the permeability in the storage reservoir is between -300 m a.s.l. and - 450 m a.s.l., and is linked to lithological contacts. The storage reservoir fluid ranges from fresh groundwater, inland of the site, to saline water closer to the shore. The saline and fresh water in the area is separated by a thin layer of brackish water known as the saltwater-freshwater interface. The temperature within the storage reservoir is between 20 to 90°C.

A geological model (Helgadóttir et al., 2023) and a conceptual model of the storage complex were developed. These models were used to construct a natural state, or baseline, model of the reservoir. The natural state model simulates the reservoir conditions, e.g. temperature, salinity, CO_2 content, and natural fluid flow prior to anthropogenic activity in the area. The results of the natural state simulations were found to reproduce the available field data in the area satisfactorily. Following the development of the natural state model, a forecast reservoir model was created which simulated CO_2 injection into the subsurface over a duration of 30 years. The forecast model also simulated a 100 year post closure period after 30 years of CO_2 injection. The forecast reservoir model was used to simulate the behavior of the injected CO_2 and to predict where it will interact with geologic structures and rocks in the reservoir. The forecast model uses a conservative transport numerical scheme, i.e. no chemical interactions between the rock and fluid were considered. This means that no CO_2 mineralization is simulated. The numerical framework used, however, simulates the thermodynamics and thermophysical properties of H_2O–NaCl–CO_2 mixtures, which includes simulating the density and mutual solubility of CO_2 and H_2O in gas and brine phases. The framework provides capabilities for modeling advective and diffusive flow and transport of H_2O–NaCl–CO_2 mixtures in multidimensional heterogeneous systems. The results of the forecast model show that after 30 years of continuous injection, the CO_2 remains dissolved within the storage complex without exsolving. The simulation results indicate that the storage reservoir is a good candidate for large-scale injection of dissolved CO_2 and that environmental impacts on the storage reservoir, storage complex, and neighboring formation are limited. These results are valid for a scenario in which no CO_2 mineralization occurs, therefore it represents a **maximum theoretical impact of the operations**.

There are multiple uncertainties in the models and their results. These include uncertainties in the geological heterogeneity, the data collection, the data interpretation and extrapolation, the physical processes included in the simulations, as well the numerical approximations in the models. Additional data from the Straumsvík area needs to be collected, in order to further characterize the storage reservoir and storage complex. Currently, the key uncertainties in models that need to be further explored include the location of the saltwater-freshwater

interface and the connectivity between the storage reservoir and the overlying formation. More data on these factors, as well as others, will aid in reducing the uncertainties and increasing the predictive capabilities of the reservoir models. At present the simulation results should be treated as risk assessment tools that can be used to make informed decisions during an environmental impact assessment.

1 Íslensk samantekt

1.1 Inngangur

Coda Terminal er móttöku- og geymslustöð fyrir koldíoxíð (CO_2) sem ráðgert er að reisa í Straumsvík á Suðvesturlandi. Yfirlit yfir staðsetningu verkefnisins má sjá á mynd 1.1. Við full afköst mun stöðin geta tekið við allt að 3 Mt af CO_2 á ári sem leyst verður í vatni og dælt í geymslugeymi. Áætlað er að Coda verkefnið muni þurfa allt að 3 m^3/s af vatni fyrir slíka niðurdælingu. Gert er ráð fyrir að nota aðeins ferskvatn í fyrstu áföngum verkefnisins, en við full afköst er gert ráð fyrir að niðurdælt vatn verði 2/3 ferskvatn og 1/3 jarðsjór. Ráðgert er að þetta vatn verð tekið úr grunnvatni á Straumsvíkursvæðinu með sérstöku vatnstökuholum. Þar til gerðar niðurdælingarholur verða síðan notaðar til að dæla vatni og uppleystu CO_2 niður í geymslugeyminn. Gert er ráð fyrir að þessar niðurdælingar- og vatnstökuholur verði staðsettar á tíu mismunandi borpöllum sem verða staðsettir nærri Straumsvík. Til að meta áhrif niðurdælingar og vatnstöku á vatn neðanjarðar við Straumsvík og nærliggjandi svæðum útbjó Carbfix nokkur líkön af geymslugeyminum, framkvæmdarsvæðinu öllu sem og af nálægum svæðum.

Geymslugeymirinn er sá hluti vatnsgeymisins á svæðinu sem tekur við og geymir niðurdælt CO_2. Í Straumsvík er geymslugeymirinn skilgreindur sem sá hluti vatnsgeymisins milli 300 m u.s. til 1200 m u.s.. Fyrir ofan geymslgeyminn eru efri lög grunnvatnsins, frá yfirborði niður í 100 m u.s., ásamt hinu eiginlega grunnvatnskerfi, sem er að finna milli 100 m u.s. til 300 m u.s.. Neðan geymslugeymisins er svo að finna botn jarðmyndunnar á svæðinu.

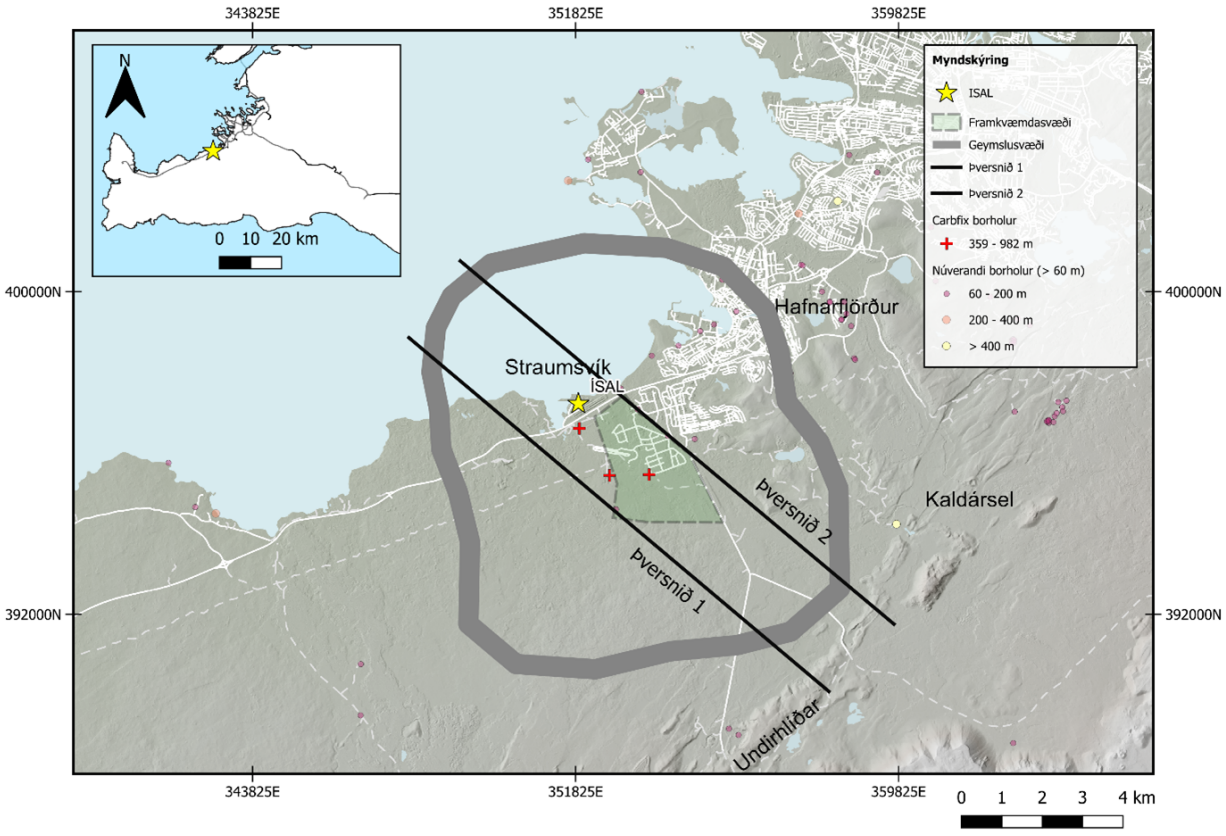

Figure 1.1: Kort af fyrirhuguðu framkvæmdasvæði (grænt svæði), og geymslusvæði (dökkgrá útlína) Coda Terminal. Núverandi rannsóknarborholur Carbfix eru táknaðar með rauðum krossum. Gul stjarna sýnir staðsetningu álvers Rio Tinto/ÍSAL.

1.2 Jarðlagabinding í Coda Terminal verkefninu

Kolefnisföngunar og -geymslu verkefni, líkt og Coda terminal, snúast um að reyna tryggja varanlega geymslu CO_2 neðanjarðar. Slík verkefni nota almennt fjórar mismunandi aðferðir til að tryggja varanlega geymslu CO_2, en þær eru:

- **Stemmingsbinding** - CO_2 er geymt fyrir neðan þakberg sem kemur í veg fyrir að CO_2 rísi upp á yfirborðið.
- **Hárpípubinding** - Hárpípukraftur sogar inn, einangrar og festir CO_2 í holrýmunum í berginu.
- **Leysnibinding** - CO_2 er leyst upp í vatninu sem er neðanjarðar og við það helst CO_2 í einum fasa og rís ekki upp á yfirborðið.
- **Steindabinding** - CO_2 steinrennist í karbónat steindir.

Carbfix aðferðin notar leysni- og steindabindingu til að tryggja varanlega geymslu CO_2 en aðferðin hermir eftir náttúrulegum ferlum. Carbfix tæknin hraðar þessum ferlum og tryggir þannig að CO_2 steinnrennis neðanjarðar á nokkrum árum, í stað þúsunda ára. Í Carbfix aðferðinni er CO_2 uppleyst í vatni dælt niður í geymslugeymi með hagstæðri berg- og efnasametningu. Þessi niðurdælingarvökvi er mjög súr og leysir upp hluta bergsins í geymslugeyminum. Við það lækkar sýrustig vökvans og ýmsar katjónir losna úr berginu sem blandast við vökvann. Þetta leiðir til þess að bróðurpartur CO_2 í vökvanum fer að mynda karbónat steindir í geymslugeyminum. Carbfix tæknin tryggir einnig leysnibindingu CO_2 strax við niðurdælingu og því þarf ekki þakberg til að viðhalda geymslu CO_2 neðanjarðar, og sker Carbfix tæknin því sig frá öðrum kolefnisföngunar og -geymslu verkefnum sem þurfa slíkt þakberg. Slík leysnibinding minnkar einnig mikið líkurnar á því að niðurdælt CO_2 flæði upp á yfirborðið. Carbfix tæknin hefur verið mikið rannsökuð en um 100 vísindagreinar hafa verið birtar um tæknina í samstarfi við um 30 mismunandi háskóla og rannsóknarstofnanir.

1.3 Eiginleikar framkvæmdarsvæðisins

Fyrirhugað framkvæmdarsvæði Coda Terminal er í Straumsvík, suðvestur af Hafnafirði. Mikið grunnvatnsflæði er til staðar á svæðinu, sem lýsir sér í því að gríðarlegt magn af ferskvatni streymir út til sjávar hjá Straumsvík. Ásamt þessu mikla ferskvatnsflæði er einnig að finna jarðsjó undir a.m.k. hluta svæðisins sem streymir neðanjarðar inn frá sjónum. Þessi atriði munu hafa mikil áhrif á hugsanlega niðurdælingu og geymslu CO_2 á svæðinu og því er mikilvægt að kanna og skilgreina svæðið m.t.t. jarðlaga, vatnafræði eiginleika, jarðefnafræðilegra eiginleika og annarra eiginleika á svæðinu. Niðurdæling vökva á svæðinu getur haft áhrif á náttúrulegt flæði vatns neðanjarðar ásamt því að valda efnafræðilegum breytingum á fyrirliggjandi vökva og bergi sem er að finna á svæðinu. Einnig geta náttúrulegar aðstæður á svæðinu hjálpað við að bera kennslu á möguleg áhættu og erfiðleika sem gætu skapast þegar niðurdæling CO_2 hefst á svæðinu. Í þessum undirkafla er farið í gegnum þau gögn sem til eru af svæðinu til að gefa mynd af náttúrulegu ástandi og eiginleikum svæðisins. Þessi gögn eru meðal annars fenginn frá rannsóknum Carbfix á svæðinu sem fólst meðal annars í borun rannsóknaborholna CSI-01, CSM-01 og CMS-02, sem og frá eldri rannsóknum á svæðinu.

Skipta má jarðlögum í Straumsvík í fjóra megin flokka, hraunlagasyrpum frá hlýskeiðum, grágrýti, glerjað basalt og móberg. Hraunlagasyrpur frá hlýskeiðum eru yngstu jarðlögin á svæðinu og eru tengd eldgosum austan og suðaustan af svæðinu. Talið er að meirihluta grunnvatnsflæði á svæðinu fari í gegnum þessi hraunlög. Slík hraun hafa fundist í rannsóknarborholum

Carbfix, CSI-01, CSM-01 og CSM-02 og á yfirborði við Kaldársel og Trölladyngju. Grágrýti á svæðinu er upprunið úr eldgosum sem áttu sér stað á hlýskeiðum þar sem hraun streymdi frá hálendinu og niður til sjávar. Ummerki um slík hraun er að finna í flest öllum borholum á svæðinu og í nágrenni þess. Glerjað basalt á svæðinu er talið hafa myndast þegar hraun ofan af landi komst í snertingu við sjó við ströndina. Slík jarðlög hafa aðeins sést nærri ströndinni í tveim Carbfix borholum á svæðinu, CSI-01 og CSM-01. Móberg er að finna inn til lands, bæði nærri Trölladyngju sem og hjá Kaldárseli og verður til við eldgos undir jökli. Allir fjórir jarðlagaflokkarnir eru basalthraun og eru þau öll rík af frumsteindum á borð við plagíóklas, pýroxen og í minna mæli ólivín. Lághitaummyndunarsteindir á borð við smektít og zeólíta eru til staðar neðan 400 m u.s.. Ásamt þessum fjórum jarðlagaflokkum hefur set fundist í borholum á svæðinu en þær tengjast hlétímabilum milli eldgosa á svæðinu. Talið er að jarðlög á svæðinu henti vel til steinrenningar CO_2 vegna efnasamsetningu þeirra.

Engin skýr ummerki eru um sprungur eða misgengi á Straumsvíkursvæðinu, hvorki á yfirborði né í borholugögnum. Lekt í efstu 1000 m jarðlagastaflans er að mestu bundin við jarðlagamót milli hraunlaga og er lárétt lekt ríkjandi á svæðinu. Ádælingarpróf í rannsóknarborholum Carbfix CSI-01 og CSM-01 sýna mestu lekt á 300 m u.s. til 450 m u.s. dýpi og benda borholugögn til þess að hún tengist jarðlagamótum. Ádælingarpróf hafa sýnt að hola CSI-01 hefur niðurdælingarstuðull upp á 5 (L/s)/bar og CSM-01 25 (L/s)/bar.

Hiti og þrýstingur hefur verið mældur nokkrum holum á svæðinu, en mælingar fyrir holur CSI-01, CSM-01 og KS-02 má sjá á myndum 1.2, 1.3 og 1.4. Mælingar sýna að hiti í CSI-01 og CSM-01 eru um 50°C við 600 m, og hafa báðar holurnar 80°C/km til 90°C/km hitastigull. Dýpsta holan við Kaldársel, KS-02, sýnir fastan hitaferill, 5°C, niður í 750 m. Holan hitnar neðan þessa dýpis, og nær 15°C við holubotn. Þetta gefur til kynna að hiti neðanjarðar lækkar inn til lands. Túlkaðir ferlar á myndunum sýna áætlaðan berghitaferill nærri holunum. Allir holur á svæðinu sýna stöðuþrýsting, sem gefur til kynna að vökvinn neðanjarðar sé í þrýstingssambandi við yfirborðið undir öllu svæðinu.

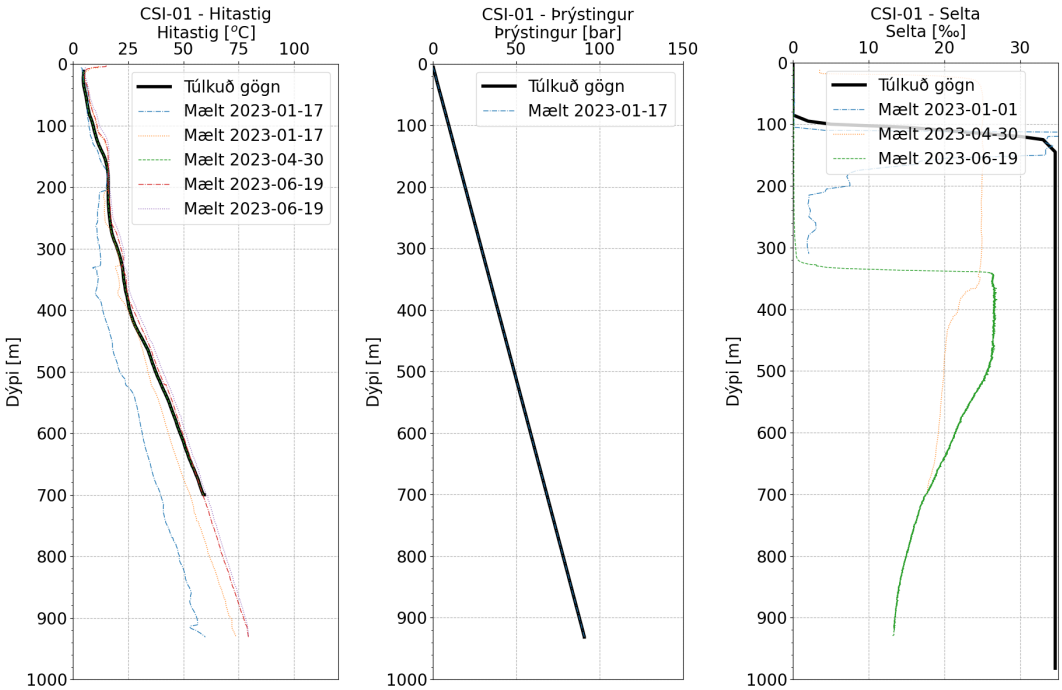

(a) (b) (c)

Figure 1.2: Mældur hiti (a), þrýstingur (b), og selta (c) í holu CSI-01, ásamt áætluðum ferli fyrir geyminn sjálfan.

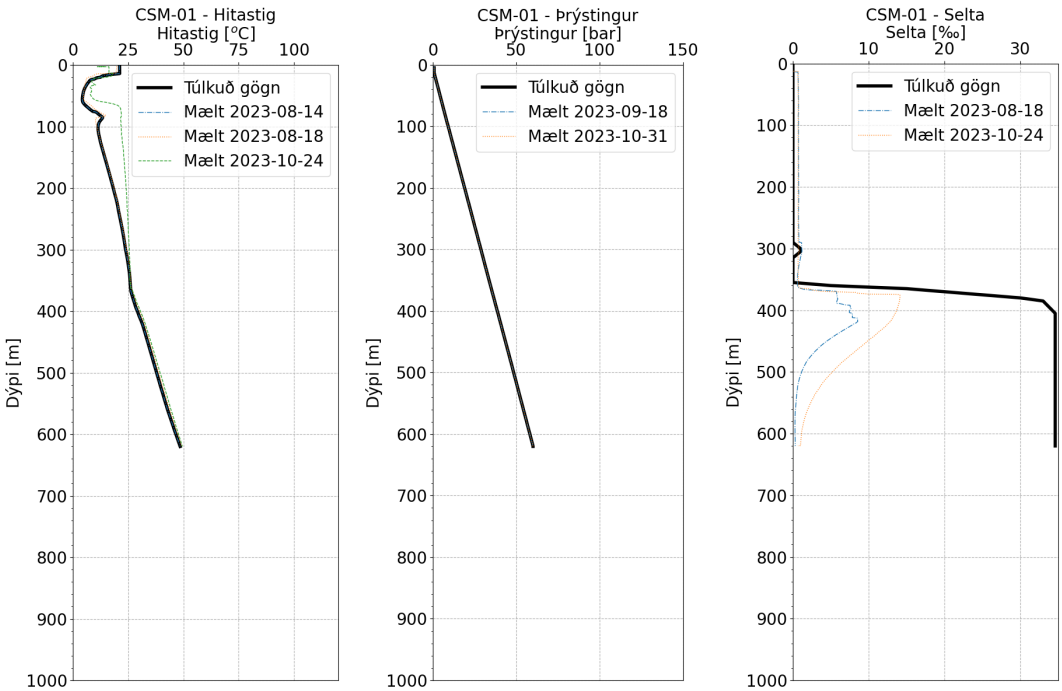

(a) (b) (c)

Figure 1.3: Mældur hiti (a), þrýstingur (b), og selta (c) í holu CSM-01, ásamt áætluðum ferli fyrir geyminn sjálfan.

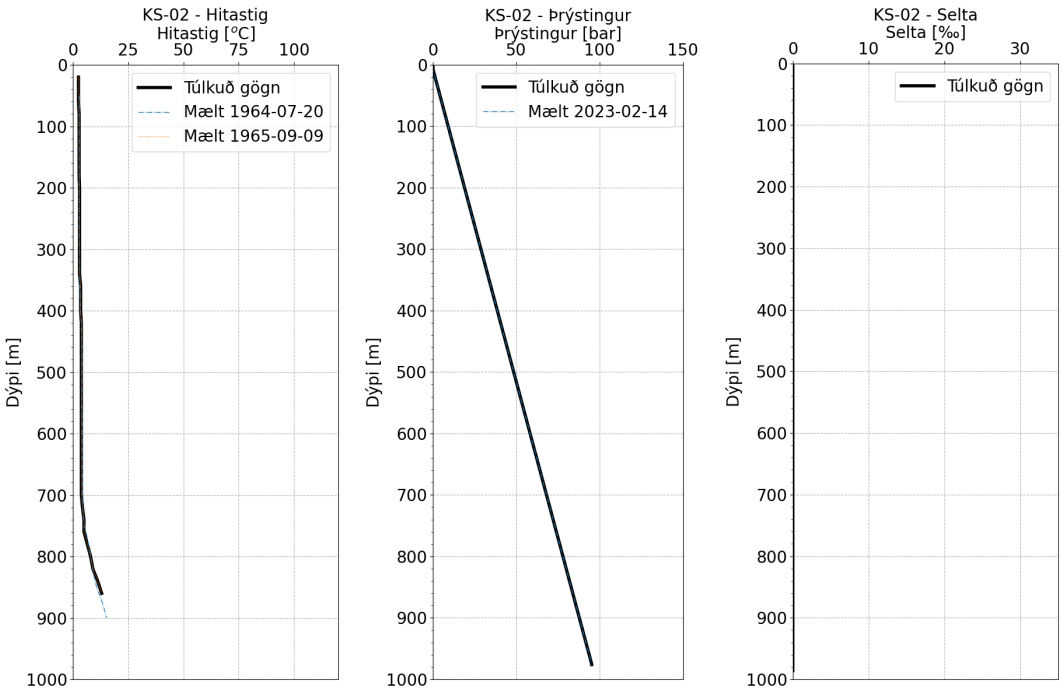

(a) (b) (c)

Figure 1.4: Mældur hiti (a), þrýstingur (b), og selta (c) í holu KS-02, ásamt áætluðum ferli fyrir geyminn sjálfan.

Grunnvatnskerfið á Straumsvíkursvæðinu er flókið, en svæðið er á mörkum strandumhverfis sem er ráðandi á Reykjanesskaga og meginlandsumhverfis sem er ríkjandi í Reykjavík. Gropin og lek jarðlög við ströndina hjá Straumsvík leyfa sjó að streyma inn á land neðanjarðar. Við þetta myndist lagskipting á vökvanum neðanjarðar þar sem eðlisléttara ferskvatnið flýtur ofan á eðlisþyngri jarðsjónum og myndar ferskvatnslinsu. Ferskvatnslinsan og jarðsjórinn er aðskilin af ísöltu blandlagi sem getur verið allt frá 1 m þykkt upp 100 m þykkt. Skipta má vatni í Straumsvík í þrjá flokka eftir seltustigi (Selta sjávar er í kringum 34 - 35 ‰):

- Ferskt vatn (< 0.5 ‰ af seltu).
- Ísalt vatn (0.5 – 30 ‰ af seltu).
- Jarðsjór (> 30 ‰ af seltu).

Magn seltu neðanjarðar nærri Straumsvík kemur til með að hafa mikil áhrif á niðurdælingu Carbfix þar sem eðlisþyngd vatns breytist mjög með seltu. Magn seltu hefur áhrif á leysnibindingu CO_2 neðanjarðar, sem tryggir það að CO_2 haldist uppleyst, og þarf því að velja staðsetningu og dýpi niðurdælingar með tilliti til hennar. Einnig hefur aðeins verið sýnt fram á steinnrenning CO_2 í sjó á rannsóknarskala en Carbfix stendur nú að rannsóknarverkefni í Helguvík til að sýna fram á steinnrenningu í sjó á stærri skala.

Til að kortleggja dreifingu seltu neðanjarðar var notast við tvær aðferðir, mælingar á rafleiðni í borholum og mælingum á viðnámi á yfirborði. Leiðnimælingar í CSI-01 sýna að staðsetning blandlagsins milli ferskvatnslinsu og jarðsjós er í kringum 100 m u.s. nærri þeirri holu. Í CSM-01 sýna leiðnimælingar að blandlagið þar sé á um 350 m u.s. dýpi. Í báðum holunum virðist þykkt ísalts blandlagsins vera í kringum 20 m. Túlkuð gögn á myndum 1.2, 1.3 og 1.4 sýna áætlaða seltu nærri hverri holu, en gert er ráð fyrir að jarðsjó sé að finna neðan ísalts lags í öllum holum sem sést ekki mælingum vegna holuáhrifa. Viðnámsmælingar á yfirborði sýna að þykkt ferskvatnslinsunnar eykst með fjarlægð frá ströndinni og sýndu mælingarnar enga seltu lengra en 2 km frá ströndinni.

Tekin voru vatnssýni úr holu CSI-01 og efnasamsetning vatnsins greint. Efnagreininginn sýndi að aðeins 0.01 - 0.02 g/kg af CO_2 er til staðar í vatninu, sem er hverfandi miðað við áætlaðan styrk CO_2, 30 g/kg, í niðurdælingarvökva Carbfix. Efnagreininginn sýndi einnig selta vatns úr CSI-01 er um 24.5 ‰, sem er töluvert lægra en selta sjávar. Mögulegt er að vatnssýnið úr CSI-01 sé blanda af ferskvatni og jarðsjó úr mismunandi dýpum í holunni og að selta í fyrirhuguðum geymslugeymi nærri CSI-01 sé í raun nærri full söltum sjó. Sýnið úr CSI-01 sýnir einnig að styrkur klór, sem og natríum, í vatninu sé töluvert hærri en styrkur annarra efna í sýninu. Þar sem styrkur klór fylgir almennt seltumagni í vökva má gera ráð fyrir að selta sé ráðandi fyrir eðlisþyngd vökva á svæðinu.

1.4 Hugmyndalíkan af Straumsvík

Gögn frá Straumsvík og nágrenni voru notuð til að útbúa hugmyndalíkan af fyrirhuguðu framkvæmdarsvæði, en líkanið sést á mynd 1.5. Slíkt líkan gefur einfaldaða mynd af jarðfræðilegum, vatnafræðilegum og eðlisfræðilegum eiginleikum svæðisins, sem er grundvöllur þess að skilja hegðun geymslugeymisins betur. Þetta hugmyndalíkan inniheldur áætlað flæði grunnvatns á svæðinu þ.á.m. flæði og mót ferskvatns og jarðsjós á svæðinu. Vert er þó að benda á að þetta hugmyndalíkan er takmarkað við gögn úr tveim rannsóknarborholum Carbfix og yfirborðsmælingum á svæðinu. Nauðsynlegt er að safna frekari gagna af svæðinu og uppfæra hugmyndalíkanið í samræmi við þau gögn.

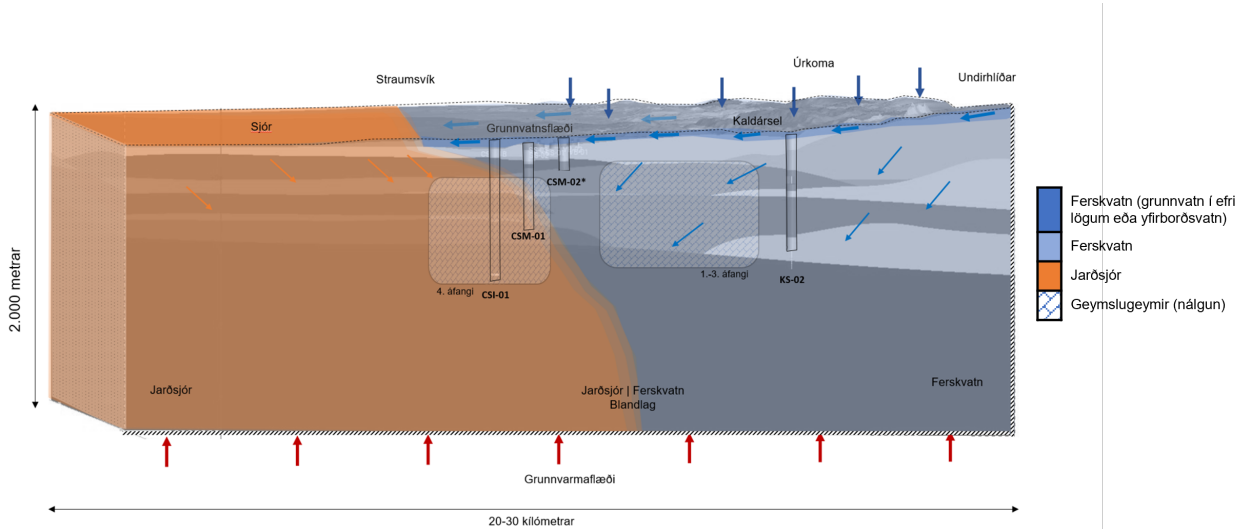

Figure 1.5: Hugmyndalíkan af fyrirhuguðu framkvæmdasvæði Coda Terminal. Myndin sýnir skil milli ferskvatns (bláir litir) og jarðsjávar (brúnir litir) ásamt flæði frá landi til sjávar. Borholur á svæðinu eru merktar inn á myndina ásamt fyrirhugaðri áfangaskiptingu verkefnisins.

1.5 Líkangerð og hermun

Hugmyndalíkanið var nota til að útbúa reiknilíkan af fyrirhuguðum geymslugeymi Coda Terminal, til að herma fyrirhugaða niðurdælingu á svæðinu. Slíkt reiknilíkan þarf að geta hermt þrjár lykilstærðir með ásættanlegri nákvæmni. Þær lykilstærðir eru hámarksdreifing CO_2 í geyminum vegna niðurdælingar Carbfix, eðlisþyngd vökva í geymslugeyminum og stöðuleika CO_2-leysnibindingar í geymslugeyminum. Hámarksdreifing CO_2 í geyminum er nauðsynlegt að meta til að áætla hvort geymslugeymirinn getur haldið utan um niðurdælt CO_2 og til að meta áhættuna á CO_2 leka úr geymslugeyminum. Vitneskja um dreifingu CO_2 neðanjarðar hjálpar einnig við hönnun vöktunaráætlunnar fyrir svæðið. Eðlisþyngd vökvans í geymslugeyminn er mikilvægt að vita svo hægt sé að taka ákvarðanir um dýpi niðurdælingar á svæðinu og með því tryggja að niðurdælt CO_2 leiti frekar dýpra niður í geyminn frekar en upp á yfirborðið. Slíkt hjálpar að tryggja örugga leysnibindingu CO_2 í geymslugeyminum. Loks er nauðsynlegt að ganga úr skugga um að niðurdælt CO_2 haldist í leysnibindingu og að ekki myndist gasbólur af CO_2 sem leita upp á yfirborðið. Reiknilíkanið byggir á gögnum sem safnað hefur verið um svæðið, m.a. poruhluti, lekt, þrýstingur, hitastig og selta.

Reiknilíkanið var útbúið í TOUGHREACT herminum sem er byggður á TOUGH2 herminum. Hermirinn hermir þrívítt flæði vökva í gropnum og lekum jarðlögum. TOUGHREACT getur hermt flæði massa, sem og hita, í slíkum jarðlögum, og getur einnig hermt efnahvörf milli vökva og bergs. TOUGH2 og TOUGHREACT hafa verið notuð til að útbúa reiknilíkön fyrir t.d. grunnvatns-, jarðhita- og kolefnisgeymsluverkefni bæði hérlendis og erlendis. Sem dæmi má nefna að TOUGHREACT hefur verið notað til að herma niðurdælingu CO_2 neðanjarðar á Íslandi í öðrum verkefnum Carbfix. Notast var við ECO2N ástandsjöfnuna, en hún getur hermt áhrif seltu og CO_2 á massa- og hitaflæði vatns neðanjarðar. Í reiknilíkaninu fyrir Coda Terminal voru efnahvörf s.s. steinnrenning CO_2, ekki hermd, og spáir því líkanið fyrir hámarksdreifingu niðurdælts CO_2 um svæðið.

Tvö mismunandi reiknilíkön voru gerð fyrir verkefni, eitt sem hermir náttúrulegt ástand svæðisins (kafli 1.6) og annað sem spáir fyrir um áhrif niðurdælingar CO_2 á geymslugeyminn (kafli 1.7). Seinni reiknilíkanið er byggt á niðurstöðum úr líkaninu sem lýsir náttúrulegu ástandi. Reiknilíkönin voru látin ná yfir svæði sem samsvarar rúmlega 576 km^2 og ná þau yfir gjörvallan geymslugeyminn ásamt mögulegu vöktunarsvæði fyrir niðurdælinguna sem og nægjanlega stórt svæði til að ganga úr skugga um að líkanniðurstöður verði ekki fyrir jaðaráhrifum, þ.e.a.s. að stærð þrýstingurbreytinga á niðurdælingarsvæðinu ráðist ekki af eiginleikum jaðra líkansins. Svæðinu var skipt upp í misstóra líkanakubba þar sem minnstu líkanakubbana er að finna við fyrirhuguð niðurdælingarsvæði. Líkönin ná frá grunnvatnsborði niður í 3000 m u.s. og er líkönunum skipt upp í 50 misstór lóðrétt lög sem eru á milli 10 til 250 m að þykkt. Undir sjónum markast efri útmörk líkananna við áætlað dýpi sjávarbotns. Við neðri jaðar líkansins var sett inn fast flæði hita inn í líkanið, til að herma eftir færslu hita frá iðrum jarðar.

Til að herma eiginleika mismunandi jarðlagamyndanna á svæðinu var hver líkanakubbur setur í ákveðin jarðlagaflokk. Slíkir flokkar segja til um t.d. poruluta, lekt og eðlisþyngd bergs í hverjum kubb. Jarðlagaflokkarnir sem skilgreindir voru í líkönunum voru hraunlagasyrpur frá hlýskeiðum, grágrýti, glerjað basalt, móberg, setlög og botn jarðmyndunnar. Jarðfræðilíkan af svæðinu, sjá mynd 1.6, var notað til að skipa líkanskubba í jarðlagaflokka. Fyrir spálíkanið var bætt við flokki fyrir jarðlagamót við æðar í borholum, til geta hermt betur flæðið sem sést í rannsóknarborholum á svæðinu. Lekt og poruhluti fyrir mismunandi jarðlagaflokka má sjá í töflu 1.1. Gert er ráð fyrir að lekt og poruhluti grágrýtis og sets breytist með dýpi þeirra, því hafa þeir jarðlagaflokkar gildisbil fyrir þær breytur.

Table 1.1: Lekt og poruhluti fyrir jarðlagaflokka.

	Poruhluti (%)	Lekt [md] Lárétt	Lóðrétt
Hraun frá hlýskeiðum	20	200,000	400
Grágrýti	10	250 - 2.5	50 – 0.5
Glerjað basalt	10 – 15	500	100
Móberg	10	10	2
Setlög	10 – 20	500 - 250	100 – 50
Botn jarðmyndunnar	5	1	0.2
Jarðlagamót	15	2000	800

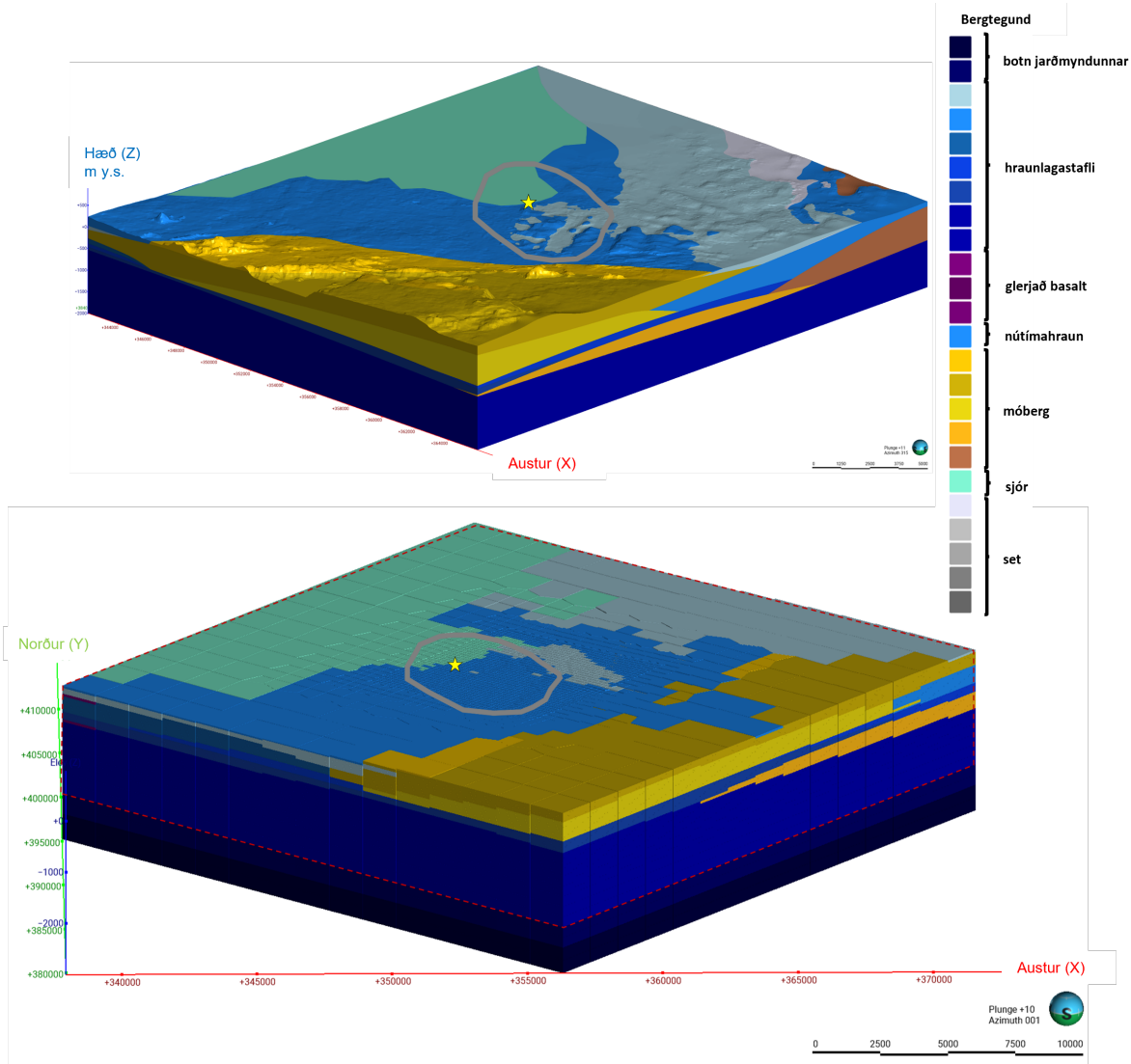

Figure 1.6: Jarðmyndanir í jarðfræði- (efri mynd) og reiknilíkönum (neðri mynd). Geymslugeymir neðanjarðar (grár fláki á yfirborði) og staðsetning Rio Tinto/ÍSAL (gul stjarna) við Straumsvík eru merkt inn á myndirnar.

1.6 Náttúrulegt ástand

Til að meta áhrif niðurdælingar og vatnstöku Carbfix við Straumsvík var nauðsynlegt að fá yfirlit yfir náttúrulegt ástand svæðisins, þ.e.a.s. hvernig flæði á svæðinu er talið vera í dag. Til að gera það var notast við reiknilíkan fyrir náttúrulegt ástand. Slíkt reiknilíkan þarf að geta hermt eftir náttúrulegu vatnsflæði á svæðinu bæði fyrir ferskvatn og jarðsjó, ásamt því að geta hermt dreifingu hitastigs og seltu í geymslugeyminum. Til að þess er reiknilíkanið látið herma svæðið í nokkur hundruð milljón ár, eða í nægjanlegan tíma fyrir stöðugt ástand að myndast á svæðinu. Til að ganga úr skugga um að reiknilíkanið lýsi raunverulegu ástandi á svæðinu er það kvarðað við gögn af svæðinu, þ.e.a.s. athugað er hversu vel niðurstöðum reiknilíkansins og raungögnunum koma saman. Niðurstöður hermana fyrir náttúrulegt ástand geymslugeymisins m.t.t. þrýstings, hita og seltu má sjá á mynd 1.7.

Líkanið sýnir að geymslugeymirinn er í þrýstingssambandi við yfirborð og að hiti er á bilinu 20 - 100 °C, sem er í samræmi við niðurstöður úr rannsóknarholum. Reiknilíkanið sýnir mikið grunnvatnsrennsli nálægt yfirborði sem kemur innan úr landi og flæðir í átt til sjávar og að innflæði jarðsjávar í dýpri vatnslög er aðeins nálægt ströndinni, fyrst og fremst vestan Straumsvíkur. Innflæði sjávar nær ekki lengra en 1–2 km inn í land, fyrst og fremst við og austan Straumsvíkur, sjá mynd 1.8. Gögn af svæðinu sýna að líkanið virðist hermir náttúrulegt ástand svæðisins á fullnægjandi hátt. Því má nota niðurstöður þess til að spá fyrir um áhrif niðurdælingar og vatnstöku á geymslugeyminn.

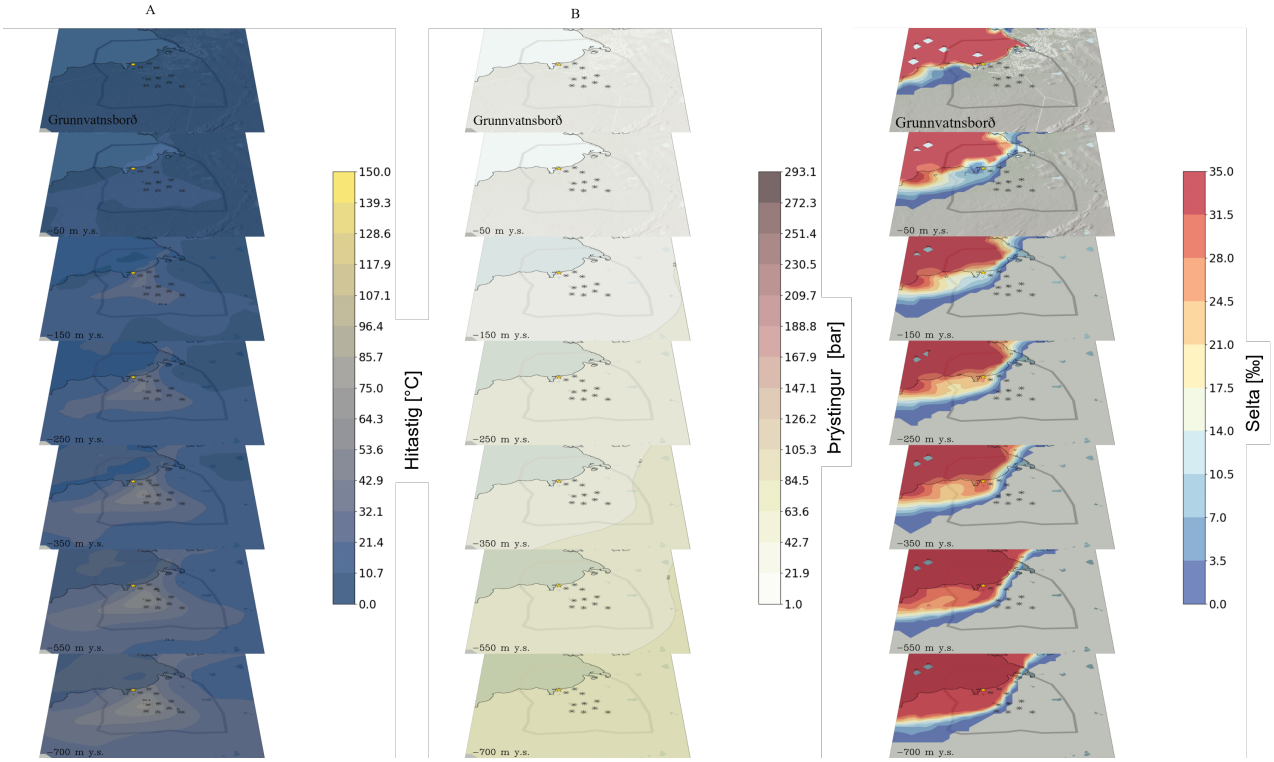

Figure 1.7: Áætlað náttúrlegt ástand hitastigs (til vinstri), þrýstings, og seltu (til hægri) með dýpi í geymslusvæðinu og efri lögum grunnvatns á svæðinu samkvæmt reiknilíkani. Myndi til vinstri sýnir að hiti er hærri í fyrirhuguðum geymslugeymi miðað svæðin í kring. Mynd til hægri sýnir að þrýstingur eykst með dýpi og inn til landsins. Myndin sýnir innflæði sjávar nálægt og vestur af Straumsvík. Jarðsjó er ekki að finna inn til landsins og í austurátt. Stjörnur tákna fyrirhugaða borteiga.

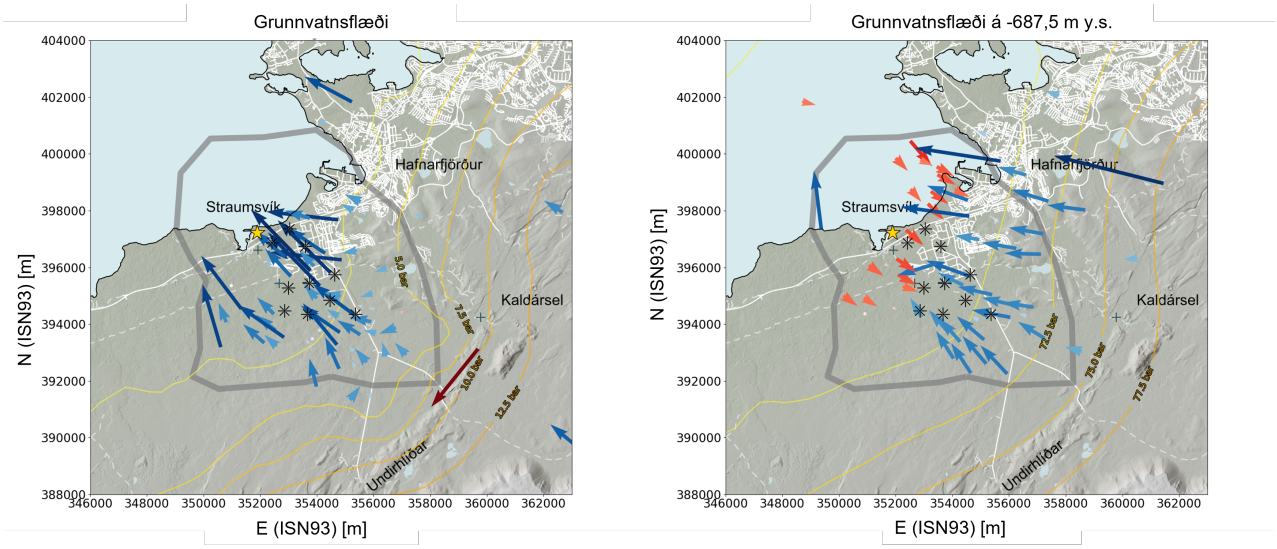

Figure 1.8: Áætlað grunnvatnsrennsli við vatnsborð (0 - 100 m u.s.) (vinstri) og rennsli í geymslugeymi á -687,5 m y.s. (hægri) samkvæmt reiknilíkani. Lengd og litur örva sýna magn flæðis, þ.e. lengri og dekkri örvar tákna meira flæði. Bláar örvar sýna flæði með ríkjandi grunnvatnsstraumi, þ.e.a.s. frá landi til sjávar. Rauðar örvar sýna flæði á móti þessum straumi. Stjörnur tákna fyrirhugaða borteiga. Gul stjarna sýnir staðsetningu álvers Rio Tinto/ÍSAL.

Þversnið af áætlaðri seltudreifingu á svæðinu er að finna á mynd 1.9. Þversniðið sýnir að í grennd þeirra svæða þar sem fyrirhugað er að dæla niður CO_2 með ferskvatni er ferskvatn nú þegar í geymslugeyminum samkvæmt líkaninu. Einnig sýnir reiknilíkanið að jarðsjór og ísalt vatn eru í þeim hluta geymslugeymisins sem notaður verður í fjórða áfanga framkvæmdarinnar þar sem stendur til að dæla niður CO_2 með jarðsjó. Geymslugeymirinn virðist því hafa hagstæða eðlisþyngdardreifingu fyrir leysnibindingu og steinrenningu CO_2 miðað við áformaða niðurdælingu.

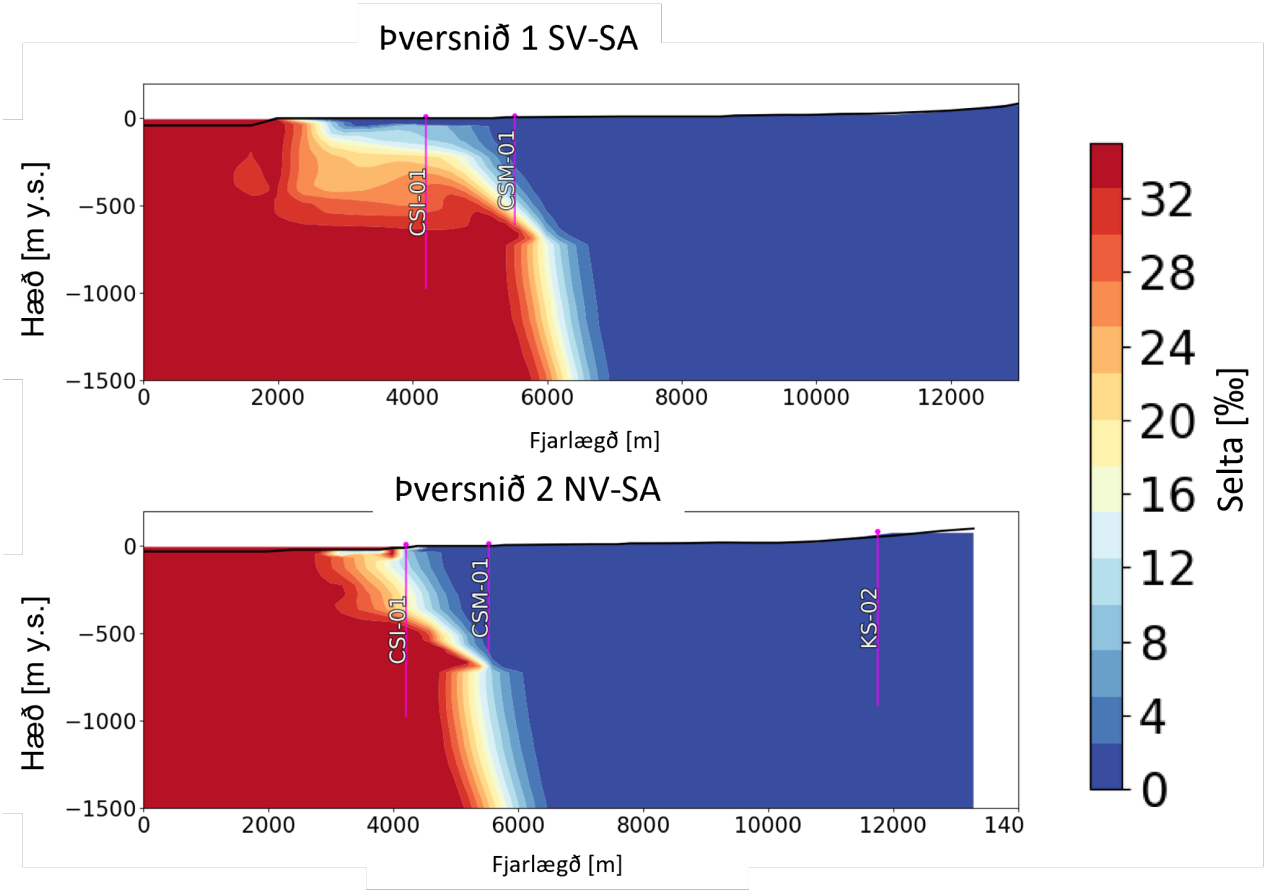

Figure 1.9: Þverskurður af seltudreifingu geymslugeymis samkvæmt reiknilíkani. Myndin sýnir að ferskvatnslinsa þykknar eftir því sem innar dregur í land og að jarðsjó og ísalt vatn er að finna hjá rannsóknarholum Carbfix, CSI-01 og CSM-01.

1.7 Áhrif niðurdælingar og vatnstöku Carbfix

Þróað var reiknilíkan fyrir geymslugeyminn til að spá fyrir um áhrif vatnstöku og niðurdælingu CO_2 við Straumsvík. Hermanir í þessu reiknilíkani voru gerðar til að áætla 1) hámarksdreifingu CO_2 í geymslugeyminum, 2) stöðugleika CO_2-leysnibindingar í geymslugeyminum og 3) dreifingu eðlisþyngdar vökva á svæðinu. Hermt var CO_2 niðurdælingu yfir 30 ára tímabil og einnig var hermt 100 ára lokunartímabil fyrir svæðið eftir að niðurdælingu er hætt. Áform erum um að byggja niðurdælingu CO_2, sem og vatnstöku, á svæðinu í fjórum þrepum, 700 ktCO_2/ári 2027, 1400 ktCO_2/ári 2029, 2100 ktCO_2/ári 2030 og loks 3000 ktCO_2/ári við full afköst 2032. Þessi áætlun er tekin inn í reiknilíkanið. Áætlað er að nota ferskvatn til niðurdælingar í fyrstu þrem áföngum verkefnisins en að nota bæði jarðsjór og ferskvatn í fjórða áfanga verkefnisins. Áætlað er að nýta tíu borpalla þar sem hver borpallur mun hafa allt að átta niðurdælingarholur og allt að fjórar vatnstökuholur. Gert er ráð fyrir að niðurdælingarholur verða 800 til 1000 m djúpar en vatnstökuholur verði grynnri eða í kringum 50 m djúpar.

Reiknilíkanið gerir ráð fyrir því að allt niðurdælt CO_2 komi inn í geymslugeyminn uppleyst í vatni. Í reiknilíkaninu er öll niðurdæling í föstu vatns og CO_2 hlutfalli, 30/1 fyrir niðurdælingu með fersku vatni og 32.5/1 fyrir niðurdælingu með jarðsjó. Einnig gerir líkanið ráð fyrir að niðurdælt sé 8°C heitum vökva við 40 kg/s í hverri niðurdælingarholu. Líkanið hermir ekki efnahvörf á milli bergs og vökvans og hermir því einungis flæði CO_2 neðanjarðar. Niðurstöður spálíkansins sýna því hámarksdreifingu CO_2 í geymslugeyminum miða við að engin steinrenning CO_2 eigi sér stað.

Niðurstöður reiknilíkans sýna að geymslugeymirinn í Straumsvík er fýsilegur kostur fyrir niðurdælingu á CO_2 leystu í vatni á stórum skala (Mt). Hermanir sýna einnig að umhverfisáhrif á geymslugeyminn, geymslusvæðið og nærliggjandi umhverfi eru takmörkuð. Niðurstöður reiknilíkans fyrir hámarksdreifingu CO_2 í geymslugeyminum benda til að allt niðurdælt CO_2 haldist innan geymslusvæðisins á meðan líftíma verkefnisins stendur og að ekkert CO_2 nær upp í efri lög grunnvatnskerfisins (< 100 m u.s.) eins og sjá má á myndum 1.10, 1.11 og 1.12. Leysnibinding CO_2 er mæld sem mismunur á milli þrýstings í geymslugeymi og afgösunnar þrýstings CO_2 í geymslugeyminum. Þar af leiðandi telst hætta vegna leka og/eða afgösunar á CO2 óveruleg á líftíma verkefnisins.

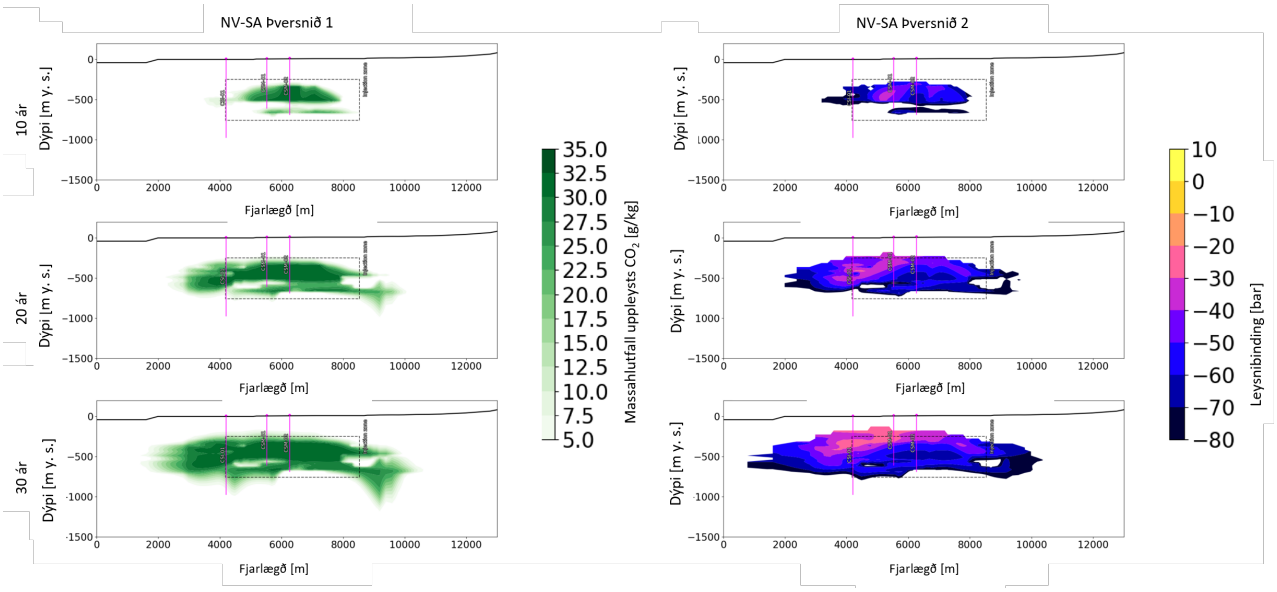

Figure 1.10: NV-SA þversnið sem sýnir magn CO_2 (vinstri) og leysnibindingu CO_2 (hægri) eftir 10 ár (efsta mynd), 20 ár (mynd fyrir miðju) og 30 ár (neðsta mynd) af starfsemi í Coda Terminal ef gert er ráð fyrir að ekkert CO_2 steinrennist. Mynd til vinstri sýnir að ekkert CO_2 berst upp í efri lög grunnvatns á svæðinu. Mynd til hægri sýnir að CO_2 er uppleyst á svæðinu, þ.e.a.s. þrýstingur á svæðinu er nægjanlegur til að ekkert CO_2 er í gasfasa. Legu þversniða má sjá á mynd 1.1.

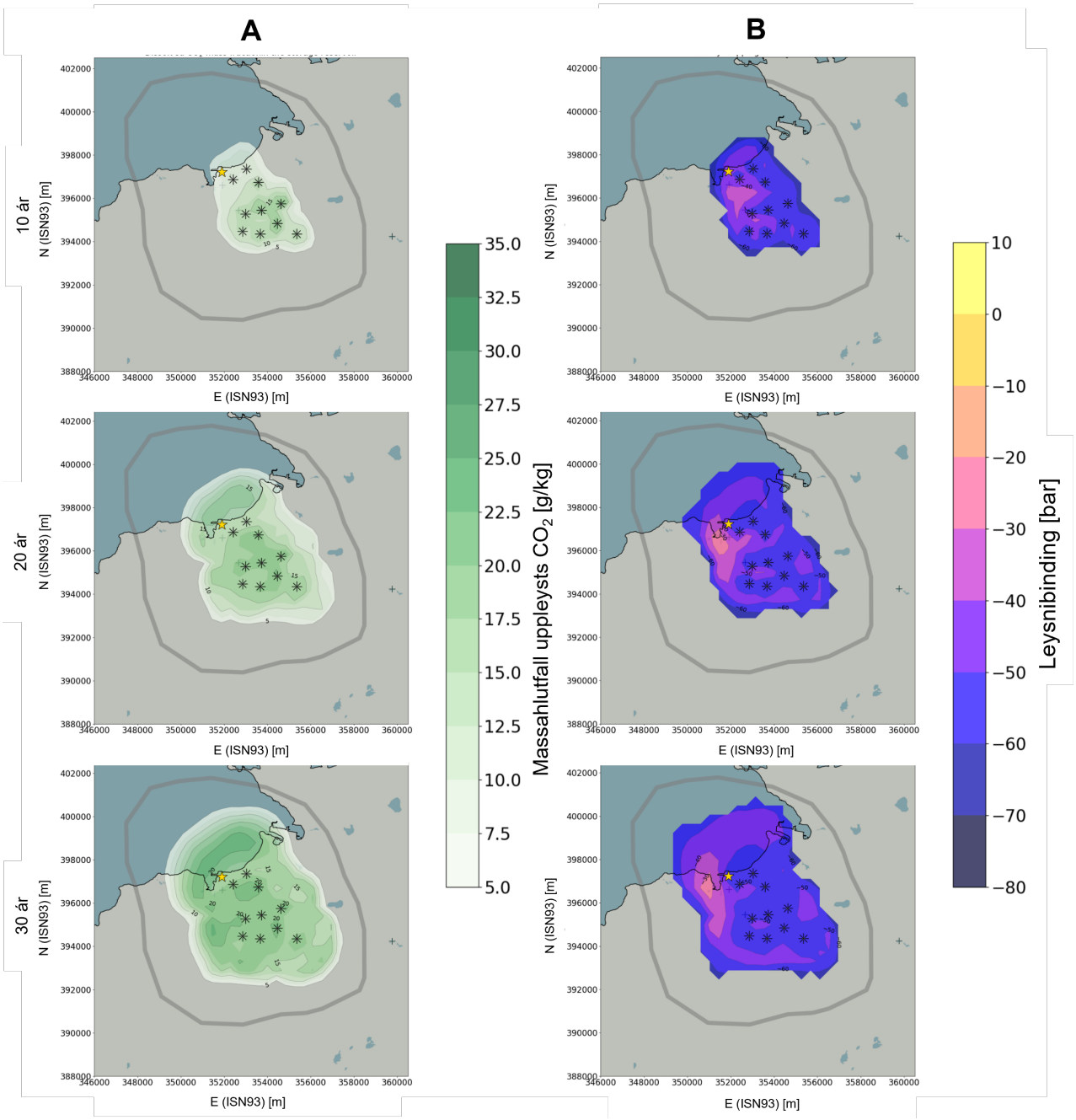

Figure 1.11: Áætluð hámarksdreifing uppleysts CO_2 (A) ásamt leysnibindingu (B) í geymslugeyminum (300 - 1200 m u.s.) eftir niðurdælingu í 10 ár (efsta mynd), 20 ár (mynd fyrir miðju) og 30 ár (neðsta mynd) ef gert er ráð fyrir að ekkert CO_2 steinrennist. Mynd A sýnir að allt niðurdælt CO_2 helst innan geymslusvæðis yfir 30 ára lífstíma verkefnisins. Mynd B sýnir að CO_2 helst uppleyst í vatni alls staðar í geymslugeyminum. Stjörnur tákna fyrirhugaða borteiga. Gul stjarna sýnir staðsetningu álvers Rio Tinto/ÍSAL.

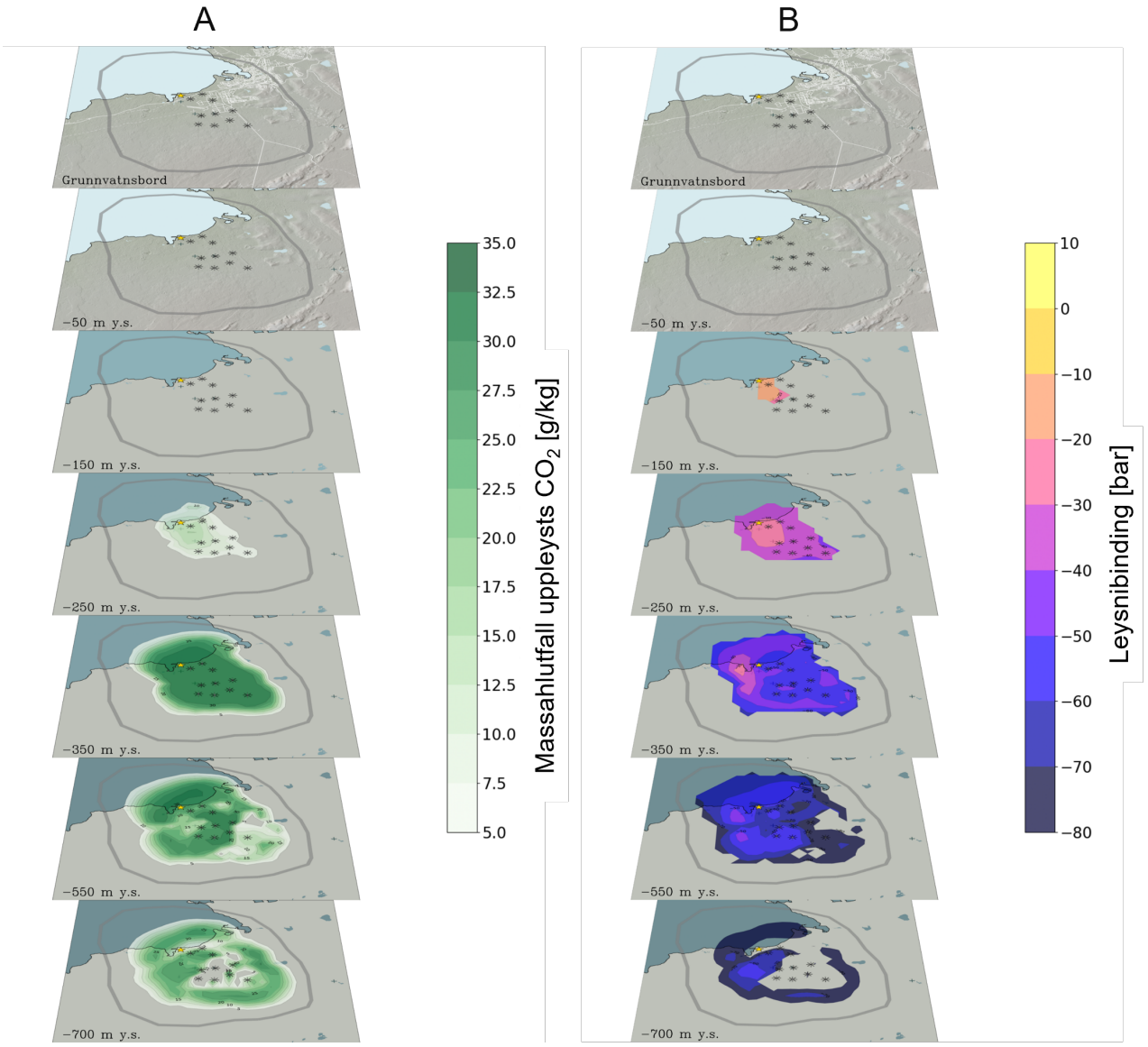

Figure 1.12: Áætluð dreifing uppleysts CO_2 (A) ásamt leysnibindingu (B) með dýpi á geymslusvæðinu og efri lögum grunnvatns á svæðinu eftir 30 ár af niðurdælingu ef gert er ráð fyrir að ekkert CO_2 steinrennist. Mynd A sýnir að allt niðurdælt CO_2 helst innan geymslusvæðis yfir 30 ára lífstíma verkefnisins. Einnig er ekkert CO_2 í efri lögum grunnvatnsins. Mynd B sýnir að CO_2 helst uppleyst í vatni alls staðar í geymslugeyminum. Stjörnur tákna fyrirhugaða borteiga. Gul stjarna sýnir staðsetningu álvers Rio Tinto/ÍSAL.

Niðurstöður reiknilíkana sýna að framkvæmdin hefur óveruleg áhrif á hitastig á svæðinu, sjá mynd 1.13. Þrýstingur gæti aukist um allt að 25 bör í geymslugeyminum á 300 til 1000 m u.s. dýpi vegna niðurdælingar vatns. Litlar þrýstingsbreytingar verða í efri lögum grunnvatns á svæðinu og líkön sýna að þrýstingsaukning í geymslugeymi hefur ekki í för með sér að CO_2 berist í efri lög grunnvatns á svæðinu. Niðurstöður reiknilíkana sýna að framkvæmdin hefur áhrif á seltumagn í geymslugeyminum, en aðeins minniháttar seltubreytingar sjást í efri lögum grunnvatnskerfisins á svæðinu, eins og sýnt er á mynd 1.14.

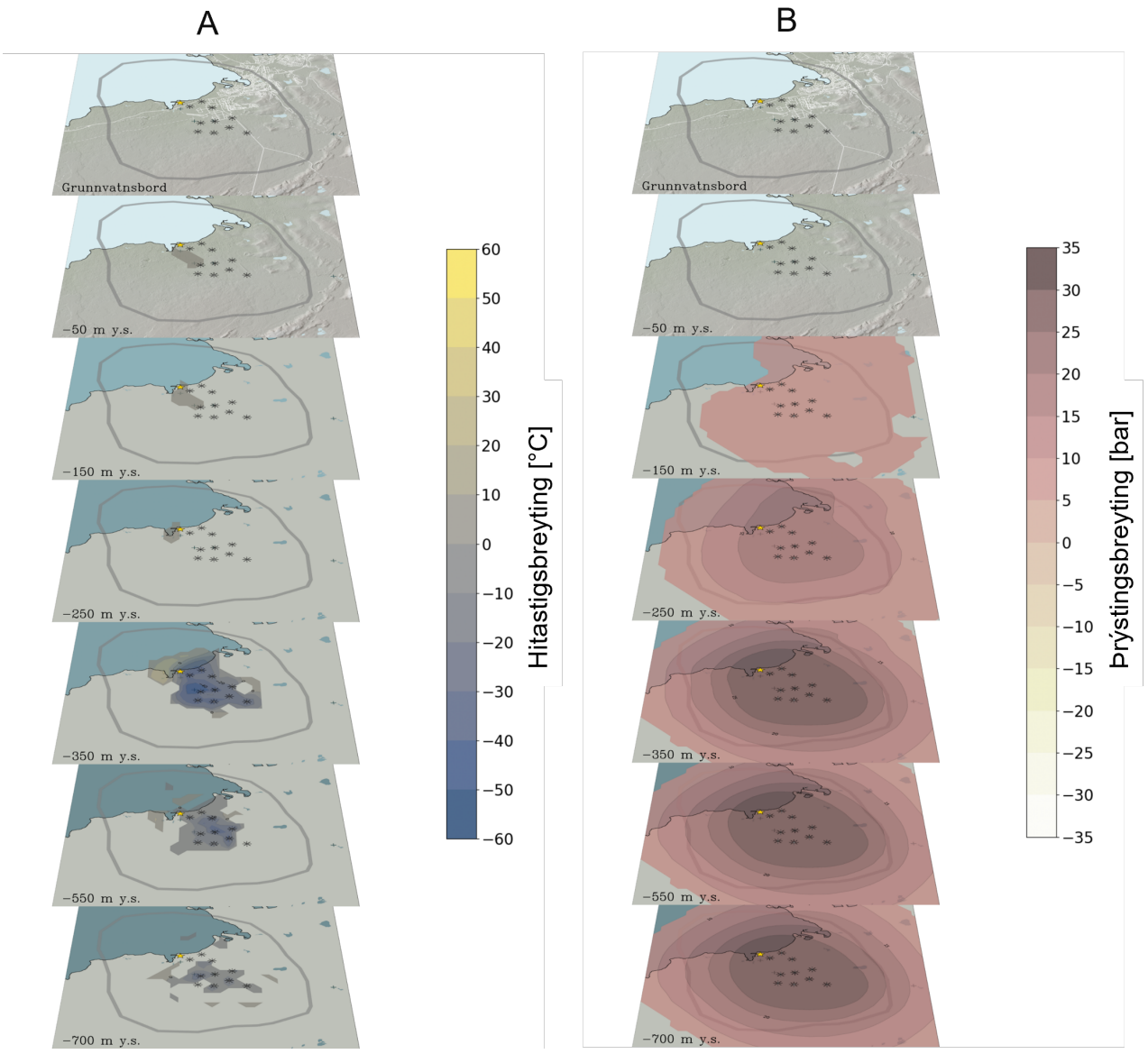

Figure 1.13: Áætluð breyting á hitastigi (A) og þrýstingi (B) með dýpi á geymslusvæðinu og efri lögum grunnvatns á svæðinu miðað við náttúrulegt ástand eftir 30 ár af niðurdælingu. Mynd A sýnir að staðbundin kæling á sér stað í kringum niðurdælingarholur í geymslusvæðinu. Einnig er minniháttar (< 5°C) kæling í efri lögum grunnvatns suðaustur af Straumsvík. Mynd B sýnir 25 bara þrýstingsaukningu í geymslugeyminum. Enginn þrýstingsaukning kemur fram í efri lögum grunnvatnsins. Stjörnur tákna fyrirhugaða borteiga. Gul stjarna sýnir staðsetningu álvers Rio Tinto/ÍSAL.

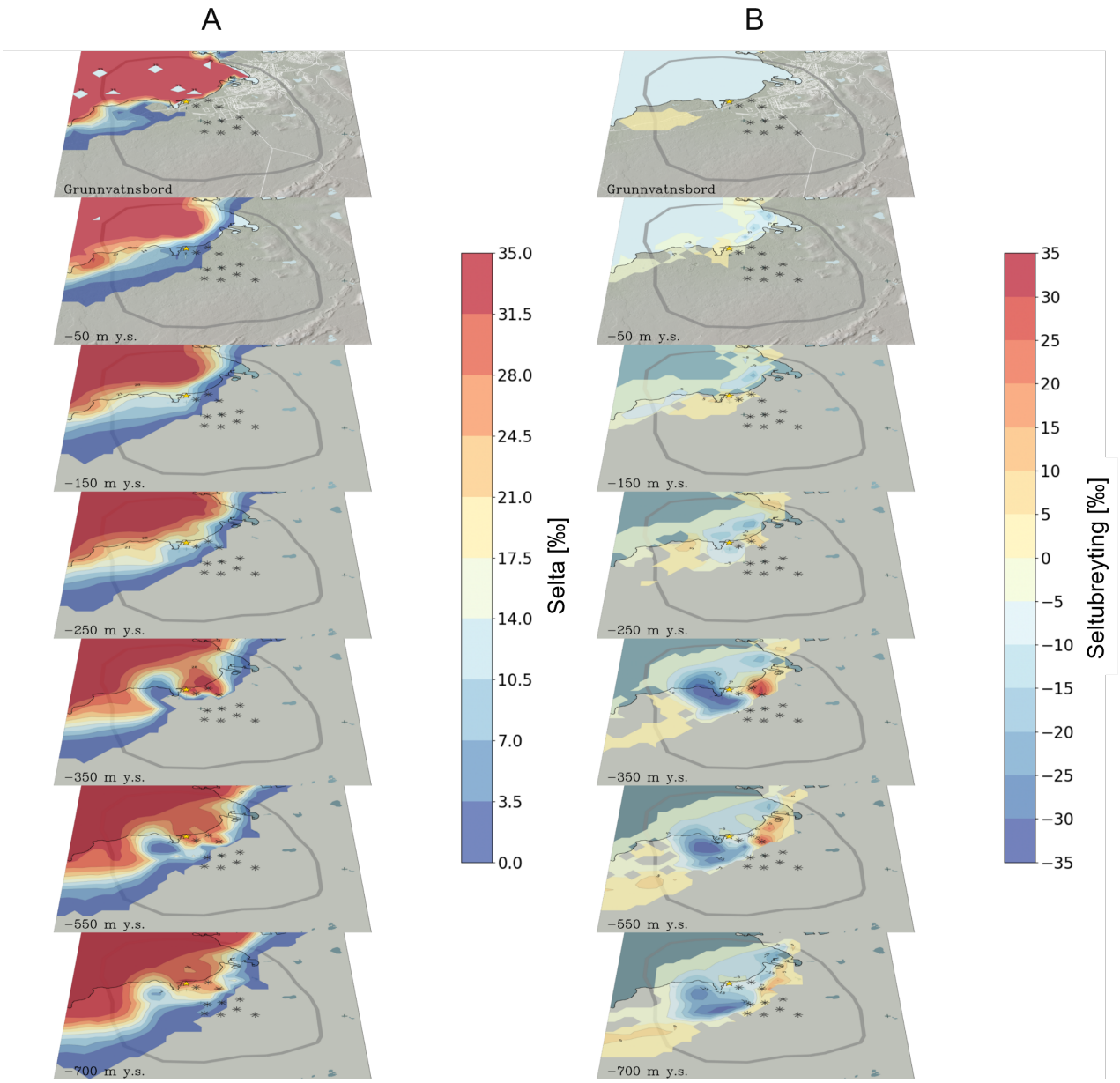

Figure 1.14: Áætluð breyting á seltu (A) og seltudreifingu (B) á geymslusvæðinu og í efri lögum grunnvatns á svæðinu eftir 30 ár af niðurdælingu. Myndirnar sýna að selta minnkar til vestur af niðurdælingarholum og eykst til austurs. Takmarkaðar seltubreytingar eru til staðar á yfirborði. Stjörnur tákna fyrirhugaða borteiga. Gul stjarna sýnir staðsetningu álvers Rio Tinto/ÍSAL.

Reiknilíkanið var einnig látið spá fyrir stöðu kerfisins í 100 ár eftir að niðurdæling er hætt á svæðinu. Spárnar sýndu að svæðið stefnir í átt að langtíma stöðuleika, sjá mynd 1.15. Lengd þess tíma mun fara eftir náttúrulegu vatns- og varmaflæði á svæðinu, en óvissa ríkir um nákvæm gildi þess. Líkanareikningar benda til þess að þrýstingsbreytingar vegna niðurdælingar Carbfix gangi að mestu til baka eftir 100 ár en breytingar á hita eru munu taka lengri tíma til að ganga til baka vegna takmarkaðs náttúrulegs hitaflæðis á svæðinu. Þá bendir reiknilíkanið til þess að selta breytist einnig í átt að náttúrulegu ástandi en að því verði ekki náð 100 árum eftir að niðurdælingu er hætt. Reiknilíkanið sýndi einnig að flæði vatns með leystu CO_2 á svæðinu minnkar en heldur samt sem áður áfram að dreifast lárétt og niður á við frá niðurdælingarholum. Samhliða þessu þynnist styrkur CO_2 í vatninu. Vert er að taka fram að gögn um niðurdælingu CO_2 í basalt sýna að CO_2 steinrennur hratt og því má leiða að því líkur að meirihluti uppleysts CO_2 í geymslugeymi muni steinrennast og að styrkur CO_2 leystu í vatni verði mun lægri en niðurstöður líkanreikninga.

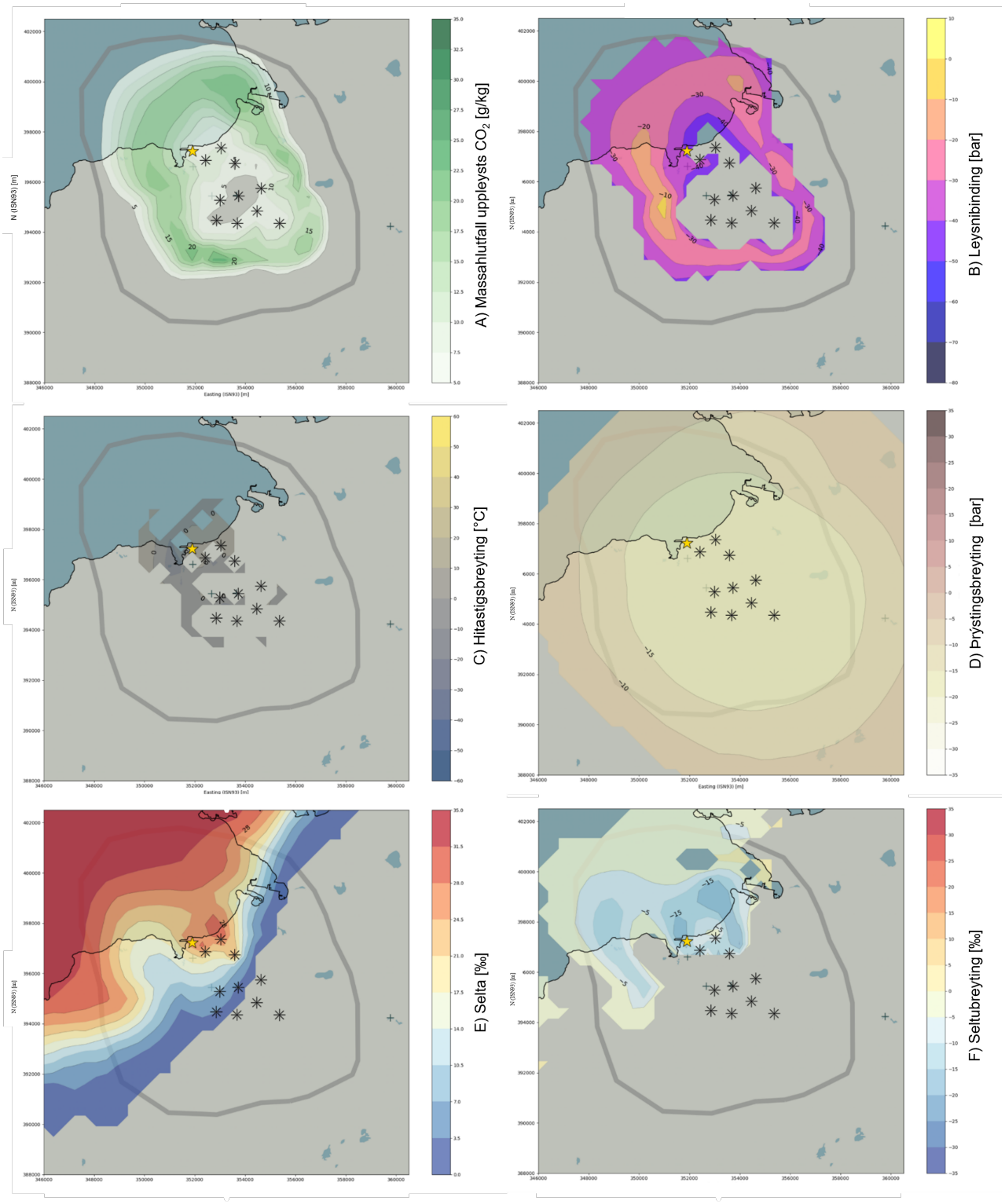

Figure 1.15: (A) Meðaldreifing CO_2-hlaðins vökva, (B) leysnibinding CO_2, (C) hitabreyting, (D) þrýstingsbreyting, (E) meðalseltu og (F) seltubreyting í geymslugeyminum 100 árum eftir að niðurdælingu Carbfix á svæðinu er hætt, ef gert er ráð fyrir að ekkert CO_2 steinrennist. Breytingar eru sýndar nálægt niðurdælingardýpi í geymslugeyminum og miða við stöðu kerfisins rétt eftir stöðvun niðurdælingar. Myndir A og B sýna að CO_2 helst innan geymslugeymis, og helst uppleyst í vatni, 100 árum eftir að niðurdælingu er hætt. Myndir C, D, E og F sýna að þrýstingur, hiti og selta á svæðinu stefnir í átt að náttúrulegu ástandi eftir að niðurdælingu er hætt. Stjörnur sýna fyrirhugaða borteiga. Gul stjarna sýnir staðsetningu álvers Rio Tinto/ÍSAL.

1.8 Rýmd geymslugeymis Coda Terminal

Hægt er að meta heildarrýmd geymslugeymisins m.t.t. steinrenningar CO_2 út frá áætluðu rúmmáli poruhluta jarðlaga á áhrifasvæði niðurdælingarinnar. Gróft mat á geymslugetu geymslugeymis er reiknað á þann hátt að steinrenning CO_2 með myndun kalsíts ($CaCO_3$) fylli í allt að 10% af þeim porum sem eru til staðar í jarðlögum geymslugeymis. Fyrirhugaður geymslugeymir í Straumsvík nær yfir svæði sem er u.þ.b. 99 km^2 að flatarmáli og nær yfir dýptarbil sem samsvarar um 900 m. Reikningar sýna að miðað við þessar forsendur væri hægt að steinrenna allt að 1.100 milljón tonn (Mt) af CO_2 í geymslugeyminum. Miðað við þessar forsendur myndi Coda Terminal nýta minna en 1% af geymslugetu geymslugeymisins á líftíma verkefnisins.

Efnagreiningar og önnur jarðfræðigögn voru notuð til að gera efnavarmafræðilega útreikninga fyrir niðurdælingu á CO2 leystu í vatni í basaltberggrunninn í Straumsvík. Niðurstöður staðfesta mikla bindigetu berggrunnsins í Straumsvík og sýna fram á að allt að 100% af því CO_2 sem dælt er niður steinrenni sem kalsít ($CaCO_3$).

1.9 Niðurstöður

Helstu niðurstöður líkana á geymslugeyminum eru eftirfarandi:

- Reiknilíkan hermir ásættanlega náttúrulegt ástand svæðisins.
- Reiknilíkanið sýnir mikið grunnvatnsrennsli nálægt yfirborði, innan úr landi í átt til sjávar. Innrennsli jarðsjós er aðeins nálægt ströndinni og fyrst og fremst vestan Straumsvíkur og nær ekki lengra en 1-2 km inn í land.
- Þar sem fyrirhugað er að dæla niður CO_2 með ferskvatni sýnir líkanið að ferskvatn er þegar til staðar í geymslugeyminum. Jarðsjór og ísalt vatn eru á móti til staðar í þeim hluta geymslugeymisins sem notaður verður í fjórða áfanga verkefnisins þar sem stendur til að dæla niður CO_2 með jarðsjó.
- Umhverfisáhrif á geymslugeyminn, geymslusvæðið og nærliggjandi umhverfi vegna niðurdælingar CO_2 í geymslugeymi í Straumsvík eru óveruleg. Niðurstöður reiknilíkana fyrir hámarksdreifingu CO_2 í geymslugeyminum benda til að allt niðurdælt CO_2 haldist innan geymslusvæðisins yfir 30 ára líftíma verkefnisins og í a.m.k. 100 ár eftir að niðurdælingu á svæðinu er hætt.
- Niðurstöður reiknilíkans sýna að hætta vegna leka og/eða afgösunar á CO_2 í geymslugeyminum er óveruleg.
- Litlar þrýstingsbreytingar verða í efri lögum grunnvatns á svæðinu og líkön sýna að þrýstingsaukning í geymslugeymi, sem getur verið allt að 25 bör, hefur ekki í för með sér að CO_2 berist í efri lög grunnvatns á svæðinu. Þrýstingsaukning á svæðinu gengur að mestu leyti til baka eftir að niðurdælingu er hætt á svæðinu.
- Niðurdæling CO_2 hefur áhrif á seltumagn í geymslugeyminum en aðeins minniháttar seltubreytingar sjást í efri lögum grunnvatnskerfisins á svæðinu. Hermanir sýna að selta breytist í átt að náttúrulegu ástandi eftir að niðurdælingu er hætt. Hins vegar ríkir óvissa um hversu lengi það muni taka seltu að ná aftur náttúrulegri stöðu.
- Hermanir sýna að fræðilega væri hægt að steinrenna allt að 1.100 milljón tonn (Mt) af CO_2 í geymslugeyminum. Það er miðað við að kalsít ($CaCO_3$) vegna steinrenningar CO_2 gæti fyllt allt að 10% af poruhluta jarðlaga í geymslugeyminum.

- Miðað við þessar forsendur myndi Coda Terminal nýta minna en 1% poruhluta í jarðlögum geymslugeymisins vegna steinrenningar CO_2 á líftíma verkefnisins og allt bendir til að það bindist varanlega eftir að því líkur.

- Reiknilíkön sýna að breytingar á þrýstingi, hita og seltu á svæðinu vegna áhrifa af niðurdælingu framkvæmdaraðila stefna í átt að náttúrulegu ástandi svæðisins en þó óvíst er hversu langan tíma það tekur.

Niðurstöður reiknilíkana byggja á þeim gögnum sem til eru af svæðinu og því er óvissa innbyggð í þær. Hægt er að vega upp á móti þessari óvissu með eftirfarandi aðgerðum:

- Minnkun óvissu á lykilstærðum í geymslugeyminum með frekari rannsóknum. Samhliða því ættu líkön af svæðinu uppfærð með nýjustu upplýsingum eftir því sem þau berast til að minnka óvissu á niðurstöðum hermana sem og til að betrumbæta áhættumat af geymslugeyminum vegna verkefnisins. Einnig ættu efnahvörf, s.s. steinrenning CO_2, að vera hermd samhliða flæði í líkönum af svæðinu, sem mun enn frekar minnka óvissu á niðurstöðum hermana. Slíkar upplýsingar auk uppfærðum líkönum ættu að nýtast til að stýra niðurdælingu á svæðinu. Einnig ætti að vera farið í næmnisgreiningu og óvissugreiningu á líkönum til að afmarka betur hvar helstu óvissupunktar í hermunum liggja.

- Nákvæm vöktunaráætlun fyrir geymslusvæðið og nágrenni ætti að vera útbúinn, þar sem meðal annars ætti að fylgjast með breytingum á þrýstingi, hitastigi, seltu og leysni CO_2. Slík vöktun nýtist til að sannreyna niðurstöður líkana af svæðinu og hjálpa þannig við uppfærslur þeirra.

- Byggja upp niðurdælingu í jöfnum skrefum með góðu millibili. Þannig mun gefast tími til að safna gögnum og meta viðbrögð geymslugeymisins við niðurdælingu ásamt því að uppfæra líkön áður en næstu áfangar hefjast. Með því móti er hægt að nýta reynsluna af hermunum fyrri áfanga inn í þá seinni.

2 Introduction

The Coda Terminal is a mineral storage project located at Straumsvík in Southwest Iceland, which will include a CO_2 offloading depot and a CO_2 injection site. At full scale the terminal aims to receive and store, via permanent in-situ carbon mineralization, up to 3 Mt of CO_2 per year. For injection of CO_2 into the subsurface, the Coda Terminal, as currently designed, will require 3 m^3/s of water (freshwater initially and approximately 2/3 freshwater and 1/3 saline water at full capacity). The water will be extracted from the local groundwater aquifer through a network of production wells. This produced water will then be used to dissolve the CO_2. The CO_2-charged water will be re-injected deeper into the storage reservoir, via a network of injection wells. The wells, both for injection and production, will be situated on ten distinct well pads. As part of the Environmental Impact Assessment (EIA) for the Coda terminal, Carbfix developed a series of models of the storage reservoir, storage complex, and neighboring formations. These models were used to assess the potential impacts from the planned injection and production on the area near Straumsvík.

The **storage reservoir** is defined as the subsurface reservoir or hydraulic unit that receives and stores the injected CO_2. In Straumsvík, the storage reservoir consists of a succession of basalt lava flows interlaid by hyaloclastic and glassy basalt sequences (Chapter 4). It is overlain by the shallow groundwater system, defined as the top of the water table down to -100 m a.s.l., the groundwater system, between -100 m a.s.l. to - 300 m a.s.l.. It is underlain, below - 1200 m a.s.l., by the basement (Figure 2.1).

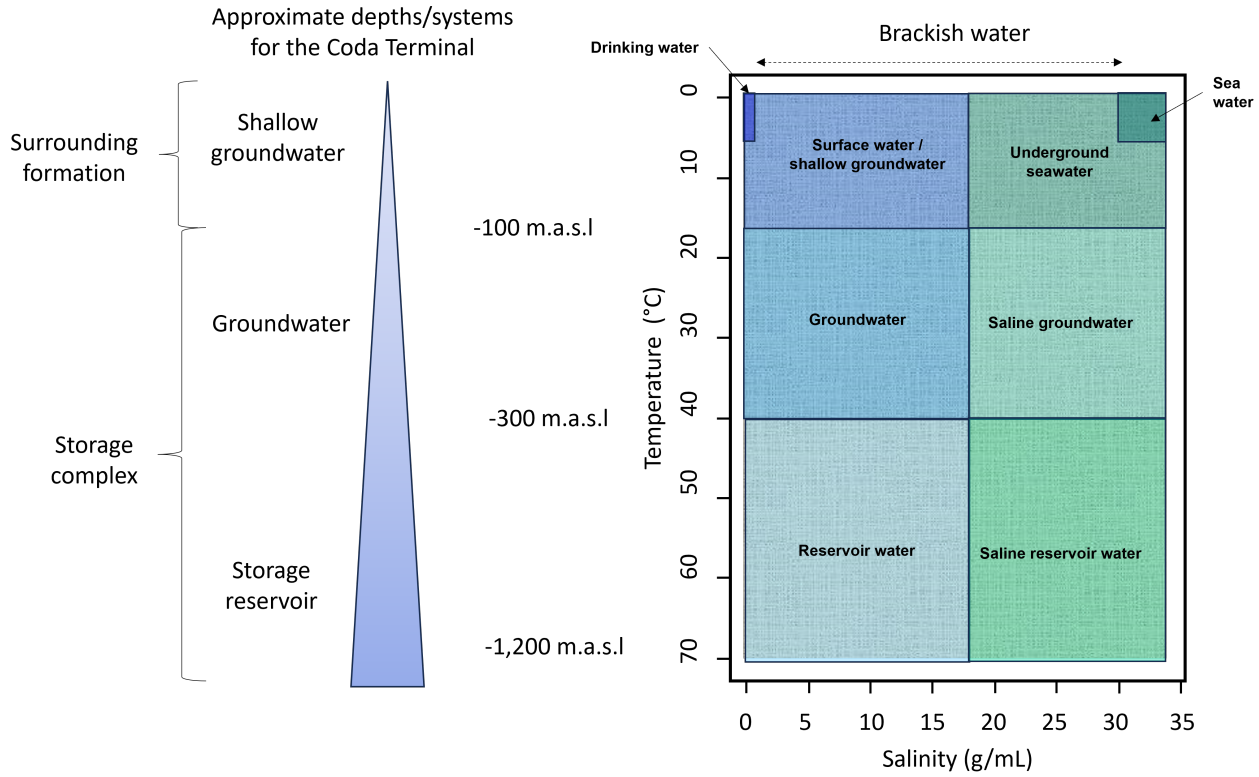

Figure 2.1: Subsurface water systems, including the shallow groundwater, groundwater, and storage reservoir. Adapted from Stefánsdóttir et al., 2020.

The **storage site** is comprised of:

- The storage reservoir, from -300 m a.s.l. down to - 1200 m a.s.l.
- The injection and monitoring wells, from the well heads down to the well bottoms.
- The surface facilities, including the control valve and well head instruments.

The **storage complex** refers to the storage site and the surrounding geological domain. These surrounding formations, including secondary containment formations, can have an effect on the overall storage integrity and security. The storage complex consists of:

- The storage site.
- The groundwater system, including geological formations, above the storage reservoir, from - 100 m a.s.l. down to -300 m a.s.l.
- The geological formations below the storage reservoir, down to -3000 m a.s.l.
- Any water supply wells, as well as other existing wells that penetrate the groundwater system, from the well heads down to the well bottoms.

The **monitoring area** consists of:

- The storage complex.
- The shallow groundwater system, from the surface down to -100 m a.s.l., including the geological layers.
- Any surface water features.
- The neighbouring geological formations.
- Any water supply wells, as well as other existing wells that penetrate the shallow groundwater system, from the well heads down to the well bottoms.

Mineral storage of CO_2 does not rely on a caprock, or a geologic seal, to contain the CO_2. This is because the CO_2 is not in a free gaseous state, which is buoyant and highly mobile, but rather dissolved in water. Mineral storage instead relies on the confining pressure provided by the overlaying groundwater to keep CO_2 in solution prior to mineralization. As a consequence, to fully encapsulate the hydrodynamic system, any models of mineral storage must include the entire saturated zone from the top of the water table, which provides the hydrostatic pressure in the storage reservoir down to geological basement formations, where permeability is low and fluid movement is limited.

The models developed to estimate the impact of the CO_2 injection, for the EIA, consist of three-dimensional field-scale models representing the injection of dissolved CO_2 at the storage site. The modeling work was done in two successive steps. First, a natural state model of the storage complex prior to injection was created(Chapter 7). This natural state model was then used to create a forecast model to simulate the flow of injected CO_2 underground using physical reservoir processes (Chapter 6). The models were developed according to best practices in the geothermal industry (Nugraha et al., 2022) and in the CCS industry (2009/31/EC, 2009, Carbfix Methodology, 2022, DNV-RP-J203, 2021). While the storage complex and neighboring formations were included in the reservoir models, this work focuses primarily on the properties

and response of the storage reservoir to the CO_2 injection. The impact on the shallow ground- and surface water (including protected ponds, lakes, etc.) has been assessed by Vatnaskil in a separate specialist report (Myer et al., 2024).

The natural state model (Chapter 7) describes the reservoir prior to anthropogenic activity and represents a baseline scenario for the site. The model inputs include, among others, the surface of the water table, bathymetry of the ocean, subsurface fluid chemistry, basal heat flux, and geology. The geology in the natural state model was based on the three-dimensional geological model developed for the Coda Terminal detailed in Helgadóttir et al., 2023. The natural state model is used to constrain the initial condition of the reservoir and to identify the main physical and thermodynamic controls in the reservoir. It also provides initial conditions for the storage reservoir, such as pressure, temperature, and fluid saturation distributions, prior to injection/production, for the forecast model. Specifically, the natural state model focused on:

- The distribution of saline fluid in the subsurface at the storage site.
- The subsurface heat and mass flux at the site.
- The natural groundwater flow and recharge system.

The forecast reservoir transport model (Chapter 8) was used to simulate the behavior of CO_2 injected into the subsurface, and estimate the storage reservoirs response to the injection. Such simulations help to determine the efficiency of the trapping mechanisms at the site and to identify potential risks. The forecast model focused on:

- Defining the extent of the storage site by estimating the maximum migration of dissolved CO_2 and its evolution with time.
- Predicting the expected efficiency of CO_2 trapping in the storage reservoir, by estimating the bubble point pressure of CO_2 and comparing it against reservoir pressure, temperature, and salinity.
- Assessing the impact of the injection on the storage reservoir, and its surrounding environments, in terms of changes to salinity, temperature, and pressure.
- Assessing whether favorable conditions for in situ carbon mineralization prevail within the storage reservoir.
- Providing a preliminary estimate of the maximum storage capacity of the storage reservoir.

3 Mineral Storage Operation at the Coda Terminal

Carbon capture and storage (CCS) projects consist of the capture and permanent sequestration of CO_2 in the subsurface, in order to fight climate change. To ensure the permanency of this storage, CCS relies on four main CO_2-trapping mechanisms (Snæbjörnsdóttir et al., 2020), shown in Figure 3.1. Each of these mechanisms work to decrease the mobility of CO_2 in the subsurface, and range from highly mobile free phase CO_2 to immobile mineralized CO_2:

- **Structural trapping** - CO_2 is stored below a caprock or sealing formation (as in supercritical or traditional CCS).
- **Residual (or Capillary) trapping** - CO_2 gets trapped in pores by capillary effects.
- **Solubility trapping** - CO_2 is dissolved in subsurface water, so it is less buoyant and mobile.
- **Mineral trapping** - CO_2 gets mineralized due to carbonate mineral precipitation.

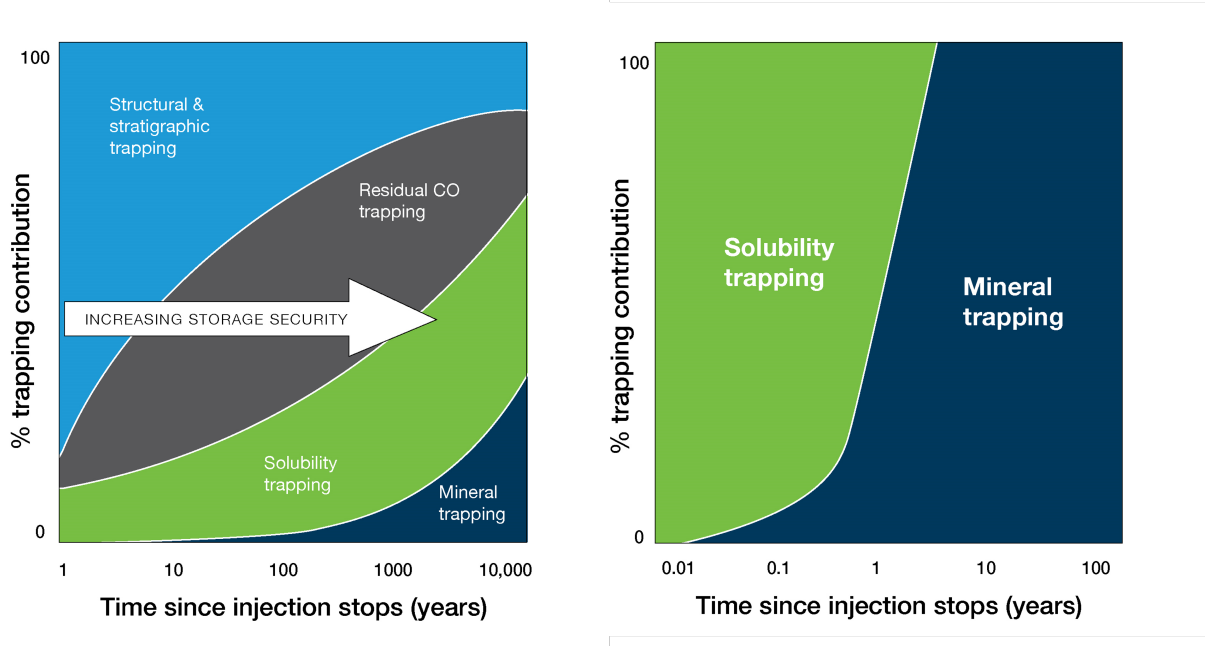

Figure 3.1: Comparison of CO_2-trapping mechanisms for supercritical (left) and dissolved CO_2 injections (right). The contribution of trapping mechanisms gradually changes over time for both conventional and mineral storage. In mineralization storage, immediate solubility trapping occurs. Over a month-year time scale the CO_2 is mineralized, leading to storage security on geologic time scales via permanent mineralization. Taken from Snæbjörnsdóttir et al., 2020.

The Carbfix method relies on the last two trapping mechanisms in a way that imitates natural processes, namely the silicate weathering cycle, which regulate the Earth's climate on geologic timescales. These natural processes are accelerated through the application of the Carbfix technology to permanently trap and mineralize CO_2 in the subsurface within a timescales of years (Gunnarsson et al., 2018; Matter et al., 2016; Pogge von Strandmann et al., 2019). The Carbfix technology promotes mineral carbonation via dissolution of CO_2 into water prior to, or during, CO_2 injection. Since the injected CO_2-charged fluid is acidic, it is

strongly under-saturated with respect to the primary and secondary minerals of the reservoir rocks (Clark et al., 2018). This promotes the dissolution of the rocks, which releases cations (Ca_2^+, Mg_2^+, Fe_2^+) into the reservoir fluid, and gradually increase its pH and alkalinity. Subsequently, this leads to precipitation of carbonate minerals which mineralizes the bulk of the injected CO_2 (Pogge von Strandmann et al., 2019). This method of CO_2 storage reduces significantly the risk of leakage since the CO_2 is not present as a highly buoyant and mobile free gas phase. Under favorable conditions, mineral trapping can occur in just a few months, or years, after CO_2 injection. This effectively reduces the possibility of CO_2 leakage and ensures the security, permanence, and sustainability of the CO_2 storage. This method significantly differentiates the Carbfix technology from other CCS projects, that inject highly mobile and buoyant supercritical CO_2. Injection of supercritical CO_2 requires a seal, or caprock, in the storage reservoir, in order to achieve structural trapping of CO_2. This difference has led to high public acceptance of mineral storage projects that use the Carbfix method. The Carbfix storage process has been studied extensively, in collaboration with over 30 universities and research institutes, since the founding of the Carbfix research project in 2007. About 100 scientific papers (carbfix.com/scientific-papers) have also been published on the Carbfix method. Studies on the Carbfix method have also been summarized in the Annual reports of Reykjavík Energy, the parent company of Carbfix.

Carbfix conducted the first pilot injections of carbon dioxide (CO_2) and mixtures of CO_2 and hydrogen sulfide (H_2S) in 2012, when gas charged injection was performed into the basaltic subsurface formations at the Þrengsli site in southwest Iceland (Snæbjörnsdóttir et al., 2017). The site, Carbfix1, was located in the Hellisheiði Geothermal Field. Rapid mineralization of the injected gases was confirmed via geochemical sampling (Matter et al., 2016, Pogge von Strandmann et al., 2019, Snæbjörnsdóttir et al., 2017), geochemical modeling (Snæbjörnsdóttir et al., 2018), as well as reservoir scale transport modeling (Aradóttir et al., 2012). The results proved the suitability of basalts for mineral storage of CO_2 (Matter et al., 2016), resulting in the upscaling of the project in 2014 with capture of CO_2 and H_2S from the Hellisheiði Geothermal Power Plant and injection into a hotter geothermal reservoir at the Carbfix2 injection site (Gunnarsson et al., 2018, Sigfússon et al., 2018). The injection of CO_2 and H_2S has been an integral part of the operations at the power plant since 2014, with over 80 kt of CO_2 injected to date. The operation has been scaled up step-wise since commissioning and, at current rates, about 12 kt of CO_2 and about 6 kt of H_2S are injected annually in Hellisheiði (Sigfússon et al., 2018).

Experiments with DAC (Direct air capture) of CO_2 combined with its injection into the subsurface for mineral storage started in 2017, in partnership with the Swiss company Climeworks. In September 2021 a demonstration plant, Orca, was commissioned in the Geothermal Park west of the Hellisheiði Power Plant. The plant's capturing capacity is up to 4 kt/y of CO_2. The captured CO_2 is injected into a storage reservoir located between the groundwater system and the deep geothermal system at Hellisheiði, at around 500 m depth. As a part of Orca project the Carbfix methodology was also certified following ISO standard ISO 14064-2.

In 2023, project Seastone, funded by Eurostars and the Technology Development Fund, was commissioned at the Helguvik site on the Reykjanes Peninsula. It is the first full cycle CO_2 capture project, with cross-border transportation of CO_2 and permanent mineralization storage. It is also the first project which utilizes the Carbfix method with saline water. A proof of concept for the mineralization of CO_2 in saline water was demonstrated through laboratory and modeling work. These studies strongly indicated the feasibility of CO_2 mineralization using saline water (Marieni et al., 2021, Voigt et al., 2021). The aim of the Seastone project is thus to demonstrate the validity of incorporating saline water into the Carbfix method by perform-

ing in-situ pilot injection of dissolved CO_2 into saline water. This approach will significantly extend the applicability of the Carbfix method, particularly in coastal areas and regions where fresh water is scarce. Additionally, the full life cycle approach of the project, i.e. capturing and transporting CO_2 from mainland Europe to Iceland, is a proof of concept that will be implemented at scale at the Carbfix Coda Terminal.

4 Site Characterization

The Straumsvík area, which hosts the Coda Terminal project, is located southwest of the town of Hafnarfjörður. Hafnarfjörður is located in the southwest of Iceland, and is the southernmost town of the greater Reykjavik capital area (Figure 4.1). Straumsvík can be literally translated to "Stream cove", which alludes to the large groundwater flow in the area which flows out into the bay. The hydrology of the site is complex, with a freshwater component which is amplified by the strong groundwater flow and a saline component due to saltwater intrusions from the coast. The characterization of the storage reservoir in terms of the distribution of saline water, hydrological properties, and the dynamic equilibrium between fluids of different densities is critical to the development of a mineral storage project in the area. A robust understanding of the subsurface processes involved is necessary in order to accurately estimate the effects of large scale CO_2 injection on the storage reservoir and its surroundings.

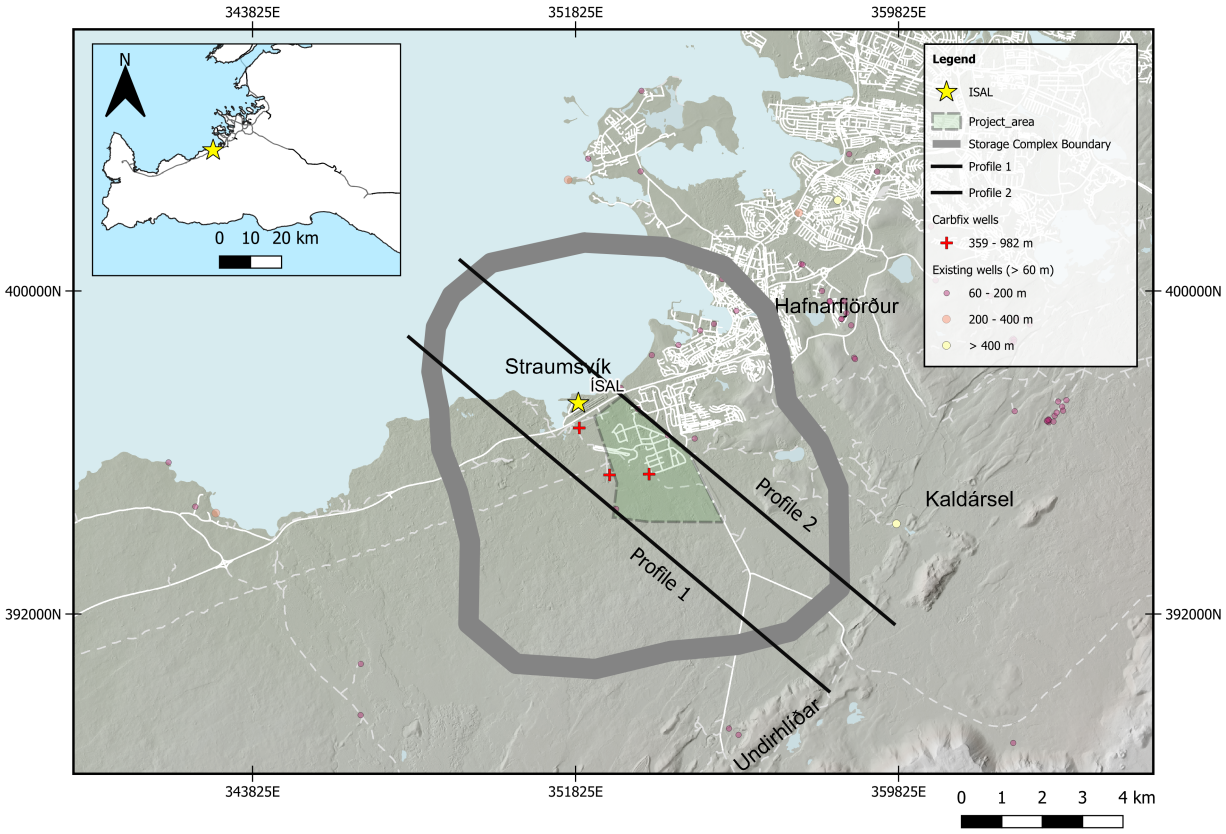

Figure 4.1: An overview of the Coda Terminal and storage complex.

A site characterization includes determining the lithology, hydrogeology, geochemistry, and other relevant physical attributes of the site. The properties of subsurface geological formations, as well as in-situ conditions, will impact carbon mineralization. Injection of water and CO_2 into the subsurface can cause migration of flow paths, changes in flow velocities, dilution, and mixing of, resident fluid with injected fluid, heat transfer, CO_2 solubility, and the feasibility of mineral storage at the site. The site characterization further provides the necessary data and information to assess the site's suitability for long-term CO_2 storage. It also helps to identify potential risks and challenges that may arise during the storage process, which includes potential leakage pathways and adverse environmental impacts. Furthermore, it aids in the design of monitoring programs that ensure the safety and effectiveness of the CO_2 storage.

Three main aspects relevant to fluid flow and fluid-rock interactions, and thus the potential CO_2 mineralization of the site, have been identified and are considered in this chapter, namely:

1. Lithology and mineralogy.
2. Structures and permeability controls.
3. In-situ pressure, temperature, and salinity distribution.

In order to study these three aspects, data acquisition and data review for the characterization of the Coda Terminal storage site was done. This data includes:

- Geological information, including stratigraphical analyses and data on hydrogeological characteristics from previous research in the area (F. Sigurðsson, 1976).
- Downhole measurements, such as temperature and salinity from existing wells.
- Stratigraphical information on wells in Kaldársel (KS-02) and Trölladyngja (TR-wells) (Table 4.1).
- Recent research at the site, from newly drilled wells CSI-01 and CSM-01, along preliminary information from the drilling of well CSM-02.

A detailed report on the geology and development of a three-dimensional geological model of the site is using the collected data is detailed in Helgadóttir et al., 2023. Recent research at the site includes a comprehensive set of measurements and tests that were carried out in wells CSI-01 and CSM-01 in order to characterize the storage reservoir. These included:

- Drill cutting analysis.
- Geophysical logging.
- Injectivity tests.
- Televiewer measurements.
- Spinner measurements.
- Pressure and temperature measurements.
- Salinity profile measurements.

In addition to research at these wells, surface geophysical campaigns were also conducted to help estimate the distribution of saline water in the subsurface. Details on the wells and surface measurements are given in Vilhjálmsson et al., 2023 and Jónsson, 2024.

Table 4.1: Summary of the main wells located in the area of interest. Drilling depth, surface geology, dominant stratigraphical sequence, alteration, and presence of saline water in indicated. Data from other wells was also used in the site characterization. *Final depth not reached.

Wellname	Depth (m)	Location	Surface geology	Stratigraphical sequence	Alteration	Saline-fresh water interface (m)
CSI-01	982	Northwestern part of the injection site	Post glacial lava formation	Alternating layers of inter-glacial lava flows and glassy basalts with intermittent sedimentary layers	Minor zeolites	100
CSM-01	618	Central western part of the injection site	Post glacial lava formation	Alternating layers of inter-glacial lava flows with one glassy basalt formation and intermittent sedimentary layers		360
CSM-02	220*	Central part of the injection site	Post glacial lava formation	Alternating layers of inter-glacial lava flows and intermittent sedimentary layers		NA (fully fresh)
KS-02	986	Kaldársel located southeast of the injection site	Post glacial lava formation	Alternating layers of inter-glacial lava flows and hyaloclastites with intermittent sedimentary layers	Minor zeolites below 400m	NA (fully fresh)
TR-01	2307	Trölladyngja located southwest of the injection site		Alternating layers of inter-glacial lava flows and hyaloclastites	High temperature alteration	NA (fully fresh)

4.1 Lithology and mineralogy

4.1.1 Stratigraphical sequence

The lithology at the Straumsvík site can be classified into four main rock types. Low elevations in the coastal area around Straumsvík are dominated by post-glacial, or Holocene, lava flows (Figure 4.2). Older inter-glacial lava flows (grágrýti) outcrop to the East of Straumsvík. Close to the shore, glassy basalts are present which formed when lava flows reach the sea. NE-SW trending ridges in the higher elevations south of Straumsvík, e.g. Undirhlíðar, consist of hyaloclastic formations which formed during sub-glacial eruptions.

Stratigraphical analyses of the well cuttings were conducted and a detailed lithology of the wells was produced. From this, a simplified lithology for all the wells was established, and four main types of geological formations representing lithological units of similar properties and characteristics were defined (Helgadóttir et al., 2023):

- **Holocene basaltic lava flows**, related to post-glacial volcanic eruptions to the East and Southeast of the area. They are mostly fine to medium-grained basalt. The Holocene basalt lavas have been identified in wells CSI-01, CSM-01, and CSM-02. Holocene lavas are also found at the surface at Kaldársel (KS-02) and Trölladyngja (TR-wells).

- **Interglacial lava flows**, related to the interglacial periods where lavas erupted in the highlands and flowed to the lowlands. Their thickness can vary between a few meters to several hundreds of meters. They usually correspond to medium to coarse grained basaltic lithologies. They have been identified in wells CSI-01, CSM-01, and CSM-02 and in wells in Kaldársel, Trölladyngja, and the capital area.

- **Glassy basalt formations** resulting from the interaction of basalt lavas with water. From Straumsvík towards Kaldársel in the Southeast, the glassy basalt is presumed to be related to a coastal environment where lavas flowed into the sea and cooled quickly (quenched). These rocks are therefore very glassy (foreset breccia or glassy basalt). They have been identified in wells CSI-01 and CSM-01 but are absent from the other wells located further inland (KS-02).

- **Hyaloclastite formations** resulting from sub-glacial volcanic activity. This geological formation groups two sub-lithologies from the lithology logs, namely basaltic breccia and basaltic tuff. Hyaloclastite formations are found inland, at both Kaldársel and Trölladyngja.

- **Sediments** related to hiatuses in volcanic activities and formation of sediments in lacustrine or oceanic depositional systems. These formations may include sandstone, mudstone, or tuff-rich sediments, with or without shells.

The lithology shows that the storage reservoir, between -300 and -1200 m a.s.l., is expected to be composed of a succession of interglacial lava flows, hyaloclastites, and glassy basalts

All four main rock types in the area are basaltic, however their rock properties vary significantly. Due to the fresh and porous nature of the Holocene lava formations, their permeability is very high, as much as two to three orders of magnitude higher than the other lithological formations (H. Tómasson and Tómasson, 1966). The majority of the shallow groundwater flow is expected in the top Holocene lavas.

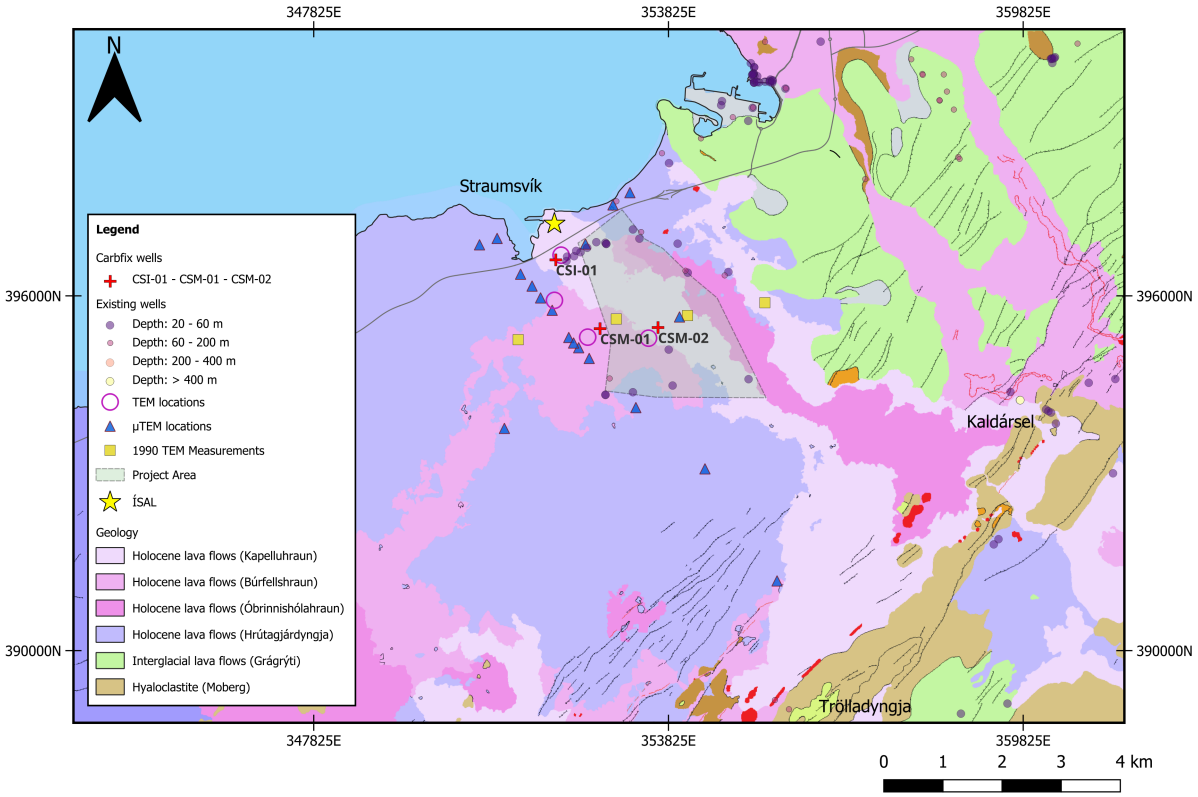

Figure 4.2: Surface geology at Straumsvik. Pink and purple areas represent Holocene lavas, green areas the interglacial lava flows, and brown areas the hyaloclastic ridges. Adapted from "Geological map of Southwest Iceland 1:100 000", 2016.

4.1.2 Primary and alteration mineralogy

The bulk chemical composition and mineralogy of rock samples collected from CSI-01 and CSM-01 were obtained using X-Ray fluorescence (XRF) and X-Ray diffraction (XRD) analyses (Galeczka, 2023b). The results of these analyses are shown in Tables 4.2 and 4.3. The results show that the samples contain approximately 8 wt.% MgO, 10 wt.% CaO, and 12 wt.% Fe_2O_3 (total Fe). These are elements that can be mobilized for the mineralization process. The composition is very similar to the composition of mid-ocean ridge basalts and Stapafell basaltic glass used in studies of CO_2-water-basalt reactions (Galeczka, 2023b). The samples have a mineralogical composition dominated by the primary minerals plagioclase 40 wt.%, pyroxene 35 wt.%, and olivine 6.2 wt.%.

Table 4.2: XRF analysis of the major elements in rock samples collected from CSI-01. The depth of the samples is indicated in the sample name.

Sample	Na2O %	MgO %	Al2O3 %	SiO2 %	P2O5 %	SO3 %	K2O %	CaO %	TiO2 %	Mn2O3 %	Fe2O3 %	BaO %	LOI %
CSI-0I∼330	1.67	11.39	11.42	44.00	0.17	<0.01	0.17	11.25	2.28	0.28	15.08	0.03	1.1
CSI-01∼338	1.66	8.96	14.47	45.19	0.15	0.03	0.18	10.96	1.24	0.20	10.65	0.02	5.3
CSI-01∼378	1.84	9.28	14.76	45.97	0.10	<0.01	0.15	11.62	1.08	0.20	10.61	0.02	2.9
CSI-01∼496	1.78	8.56	14.65	47.50	0.14	<0.01	0.11	12.00	1.32	0.22	11.63	0.03	1.5
CSI-01∼580	1.92	9.32	14.62	45.34	0.12	0.02	0.13	11.24	1.20	0.20	10.83	0.04	4.6
CSI-01∼654	2.05	9.12	13.92	44.31	0.21	0.01	0.18	9.98	1.82	0.23	12.37	0.02	5.5
CSI-01∼784	1.94	8.46	13.94	44.06	0.21	0.02	0.18	10.59	1.76	0.22	12.21	0.01	5.7
CSI-01∼810	2.10	8.83	14.00	44.64	0.19	0.02	0.16	11.01	1.72	0.22	12.11	<0.01	4.3
CSI-01∼924	0.90	4.86	11.38	45.08	0.52	0.06	0.75	7.50	2.21	0.24	13.18	0.03	12.3
CSI-01∼980	1.92	6.24	13.28	45.11	0.30	0.17	0.35	10.16	2.09	0.24	12.72	0.01	6.7

Table 4.3: XRD analysis of the mineralogy in rock samples collected from CSI-01. The depth of the samples is indicated in the sample name.

Sample	Smectite	Quartz	Plagioclase	Pyroxene	Olivine	Analcime	Zeolite	Calcite	Magnesite	Hematite	Total
CSI-01∼330	TR	1.5	37.4	42.5	14.4	0.0	0.0	0.0	1.6	2.6	100
CSI-01∼338	8.4	1.5	42.6	40.2	2.9	0.0	4.4	0.0	0.0	0.0	100
CSI-01∼378	1.8	0.7	45.1	40.1	6.6	TR	4.7	0.0	0.0	1.1	100
CSI-01∼496	1.4	1.2	50.9	39.5	3.5	0.0	0.0	0.0	0.6	2.9	100
CSI-01∼580	2.3	0.4	42.4	36.5	9.9	2.0	6.6	0.0	0.0	0.0	100
CSI-01∼654	8.8	0.8	42.5	31.5	9.7	2.2	4.5	0.0	0.0	0.0	100
CSI-01∼784	4.8	0.6	41.0	34.1	7.2	2.3	9.6	0.0	0.4	0.0	100
CSI-01∼810	5.6	0.7	41.2	35.4	7.8	1.8	7.0	0.0	0.5	0.0	100
CSI-01∼924	50.1	1.1	21.7	13.8	0.0	0.0	10.1	3.2	0.0	0.0	100
CSI-01∼980	15.7	0.5	38.6	36.8	0.0	3.2	4.5	0.0	0.6	0.0	100

Over time, primary minerals tend to alter into secondary minerals in the presence of water. The formation of these alteration minerals is usually dependent on the temperature, permeability, pressure, fluid composition, rock composition, and duration of hydrothermal activity (Lagat, 2009). As the fluid flows through the rock, it alters the composition of the rocks by adding, removing, or redistributing chemical components. This alteration can, therefore, influence the release rate of cations and their availability for in situ mineralization. In addition, studies on Icelandic bedrock show that porosity and permeability generally decrease with progressive alteration, gradual burial, and/or increasing rock age since these processes result in the pore space being filled with secondary minerals (Neuhoff et al., 1999, Ó. Sigurðsson and Stefánsson, 1994).

The alteration state in the formations in Straumsvík is minor, as indicated by the presence of smectites and zeolites in samples below 400 m. The sequence of the alteration minerals

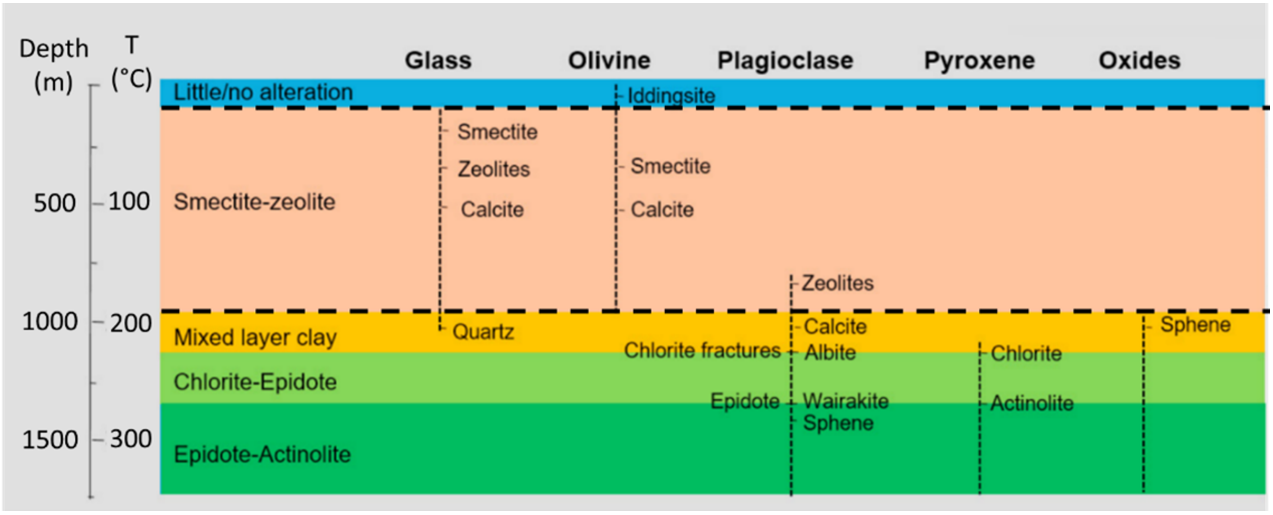

Figure 4.3: The alteration zones and the breakdown of the primary phases. Adapted from Snæbjörnsdóttir et al., 2018.

indicates a progressive increase in temperature with depth, with the smectite-zeolite alteration zone down to 800 — 1000 m depth, as can be seen from Figure 4.3 (Franzson et al., 2008, Kristmannsdóttir and Tómasson, 1978, and Snæbjörnsdóttir et al., 2018). In terms of the bedrock, the geochemical characteristics at Straumsvík are similar to other pilots, demonstrations, and storage sites in Iceland, e.g. Hellisheiði, Þrengsli, and Nesjavellir (Matter et al., 2016, Gunnarsdóttir et al., 2021). The majority of the reservoir consists of young and reactive basalts, which are favorable for CO_2 mineralization. Based on the composition of the reservoir a high CO_2 mineralization potential exists within the storage reservoir (Galeczka, 2023b). Previous studies, in similar basaltic reservoirs, show that mineralization is expected to occur within years from injection (Matter et al., 2016).

4.2 Structures and permeability controls

4.2.1 Hydrogeology and permeability control

Results and interpretations from televiewer logs suggest that NNE-SSW/NE-SW trending faults are present in wells CSI-01 and CSM-01. There are also indications of minor N-S trending faults in both wells and ENE-WSW and WNW-ESE trends in CSM-01 (Helgadóttir et al., 2023). However, from analysis of the televiewer data, it is not clear whether these fractures are tectonic faults or represents cooling fractures. Analysis of the feedzones in wells CSI-01 and CSM-01 showed that while some may be linked to fractured areas, the main feedzones were correlated to horizontal lithological boundaries or permeable rock formations. Therefore, it is more likely that control of flow in the region is linked to lithological boundaries between basaltic lavas, and to permeable, primarily glassy basalts, rather than faults (Helgadóttir et al., 2023). This is in agreement with studies on high-temperature areas in Iceland where aquifers are, in the majority, linked to lithological boundaries down to 800 – 900 m (Franzson, 1988, Gunnarsdóttir et al., 2021).

4.2.2 Well testing

Step rate injection tests were performed in wells CSI-01 and CSM-01 after drilling, along with pressure, temperature, and spinner (PTS) measurements, to determine the hydraulic properties of the wells (Jónsson, 2024). They were also used to identify possible feed zones in the wells. A list of estimated feed zones in wells CSI-01, CSM-01, and KS-02 is given in Table 4.4. In addition to PTS measurements, other downhole measurements were done in the wells, such as caliper, neutron-neutron (NN), and conductivity logs. These were compared with the lithology profiles from the wells. The findings from these measurements are summarized in Jónsson, 2024 and Helgadóttir et al., 2023.

Table 4.4: List of loss zones and their relative size, in wells CSI-01, CSM-01, and KS-02. The well logs that indicate the loss zones are also listed. Data taken from Jónsson, 2024, Sigurgeirsson et al., 2023, Sigurgeirsson et al., 2024, and J. Tómasson et al., 1977.

Well	Depth [m]	Relative size	Observed in
CSI-01	342	Medium	Spinner, temperature, conductivity, lithology, loss of circulation fluid
	365	Small	Spinner, temperature, conductivity, lithology
	375 – 400	Medium/large	Spinner, caliper, loss of circulation fluid
	400 – 520	Small	Temperature, conductivity, loss of circulation fluid
	780	Small	Loss of circulation fluid
	915	Small	Loss of circulation fluid
CSM-01	341	Small	Spinner, temperature, caliper, lithology
	348	Medium	Spinner, temperature, caliper, lithology
	360	Large	Spinner, temperature, caliper, loss of circulation fluid
	375	Small	Temperature, conductivity, caliper, NN, lithology
KS-02	80	NA	Loss of circulation fluid
	105	NA	Loss of circulation fluid
	225	NA	Loss of circulation fluid
	255	NA	Loss of circulation fluid
	396	NA	Loss of circulation fluid
	462	NA	Loss of circulation fluid
	580	NA	Loss of circulation fluid
	750	NA	Loss of circulation fluid
	778	NA	Loss of circulation fluid
	800	NA	Loss of circulation fluid

Spinner logs in well CSI-01 show loss zones at 342 m, 365 m, and 375 m depth. There are also loss zones in an interval from 375 m, down to roughly 400 m visible for the higher injection rates. Most of the water flowed out at about 375 m. Anomalies in the spinner curves were also correlated to anomalies in the temperature profiles and other logs from the well. However, temperature logs show that there is a small amount of water, undetectable by the spinner, flowing below the loss zone at 375 m, down to about 520 m. It can be argued that there is minor seepage of water down to about 840 m. The entire permeable part of the well is within a saline water system, which is consistent with the results of downhole conductivity measurements (Jónsson, 2024).

Spinner logs in well CSM-01 show loss zones at 341 m, 348 m, and 360 m depth. Most of the water flows out of the wellbore at a depth of about 360 m. The spinner data are correlated with anomalies in the temperature profiles and other logs from the well. However, the temperature profiles also show that there is a small amount of water, undetectable by the spinner, flowing below the loss zone at 360 m, down to about 376 m depth. The permeable part of the well is thought to be within the freshwater system, although the permeable part at 375 m seems to be in a brackish water layer (Jónsson, 2024).

CSI-01 has an estimated injectivity index of about 5 (L/s)/bar and CSM-01 has an estimated injectivity index of about 25 (L/s)/bar, shown in figure 4.4 (Jónsson, 2024).

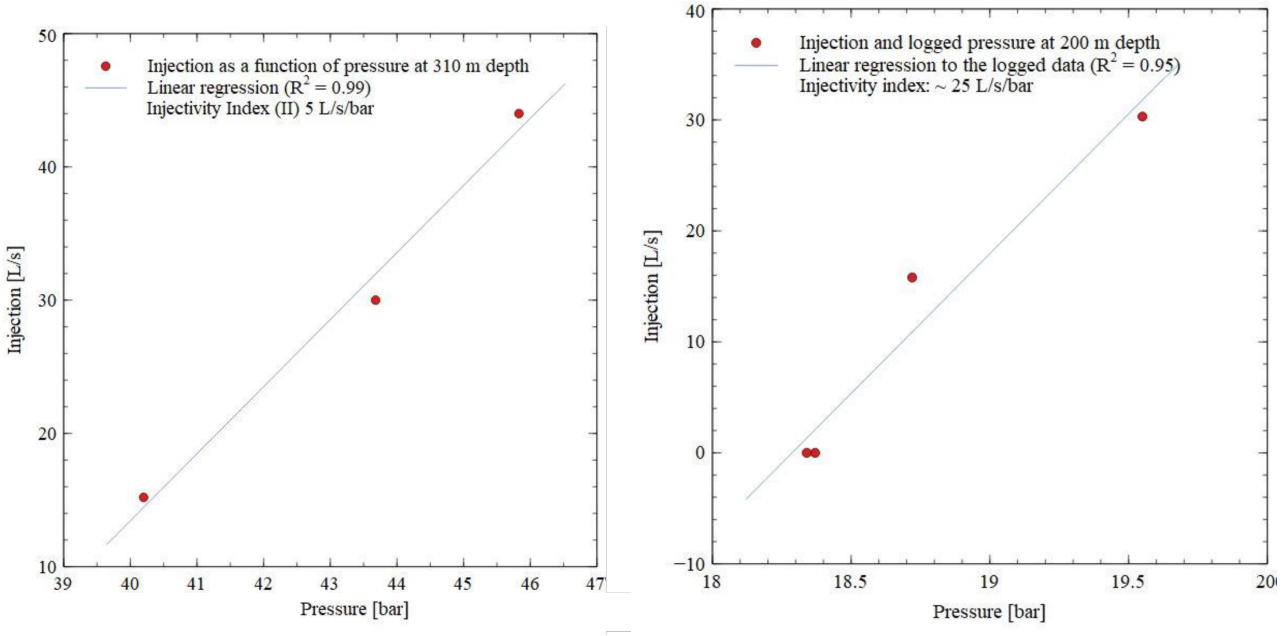

(a) (b)

Figure 4.4: Injection rates versus the pressure during step rate injection tests in CSI-01 (a) and CSM-01 (b). The injectivity indexes of the wells are derived from a linear regression line through the datapoints. Adapted from Jónsson, 2024.

4.3 Heat and mass distribution

Downhole pressure and temperature logs were taken in wells CSI-01 and CSM-01 during, and after, drilling. Fluid samples were also collected from the wells at different times. These measurements provide valuable information on the conditions and properties of the subsurface fluids with depths. However, it should be noted that the measurements may be influenced by drilling activities, which usually involve injection of large volumes of cold, fresh, water into the well during drilling. The values from these measurements may, therefore, not represent baseline conditions in the reservoir.

Downhole temperature measurements can be used to determine the temperature gradient in an area and can indicate the existence of feedzones in a well. Temperature measurements were taken regularly in both CSI-01 and CSM-01, and are shown in Figures 4.5 and 4.6. The newest temperature measurements are thought to be the closest to the natural state of the reservoir around the well and are marked as interpreted data in the figures. The well log shows that both CSI-01 and CSM-01 reach temperatures of around 50 °C at 600 m depth. Furthermore, CSM-01 reaches a bottom temperature of 80°C at around 900 m depth. Both wells exhibit the same temperature gradient, which is estimated to be around 80 – 90°C/km (Helgadóttir et al., 2023). This temperature gradient is expected to dominate within the entire storage reservoir. Both wells show a clear change in the temperature profiles at around 350 m depth, which indicates the presence of feedzones near those depths. This is in agreement with the results of the spinner test detailed in the previous chapter. Temperature well logs were also taken in KS-02, and are shown in Figure 4.7. The measurements show that KS-02 has a constant temperature of around 5°C from the surface down to 750 m. This is thought to be due to the large amount of cold freshwater near Kaldársel, which cools down the reservoir (J. Tómasson et al., 1977). The temperature in the well increases after 750 m, and the well has a bottom temperature of 15 °C at 900 m. Below 750 this corresponds to a temperature gradient of around 65°C/km. This indicates that cold groundwater is present much deeper at Kaldársel compared to the proposed injection site.

Downhole pressure logs show the pressure gradient at the site and provide insight into the structure of the system. Pressure well logs were taken in wells CSI-01 and CSM-01. Both wells show a hydrostatic gradient from the surface of the water table down to the bottom of the well. This means that, down to at least a 1000 m depth, the storage reservoir is in pressure contact with the surface. This suggests that no significant aquitards are present in the storage reservoir. The logs also show no evidence of the presence of a convective regime, like the ones found in geothermal systems. The newest pressure measurements are thought to be the closest to the natural state of the reservoir around the wells and are marked as interpreted data in the figures.

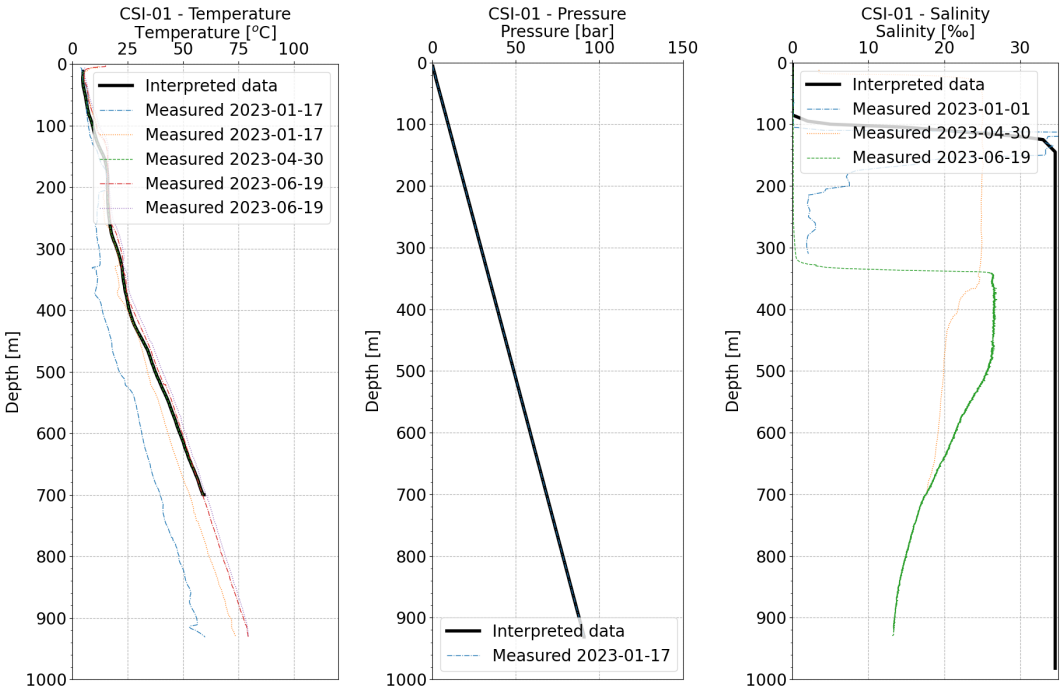

(a) (b) (c)

Figure 4.5: Downhole temperature (a), pressure (b), and salinity (c) measurements from well CSI-01.

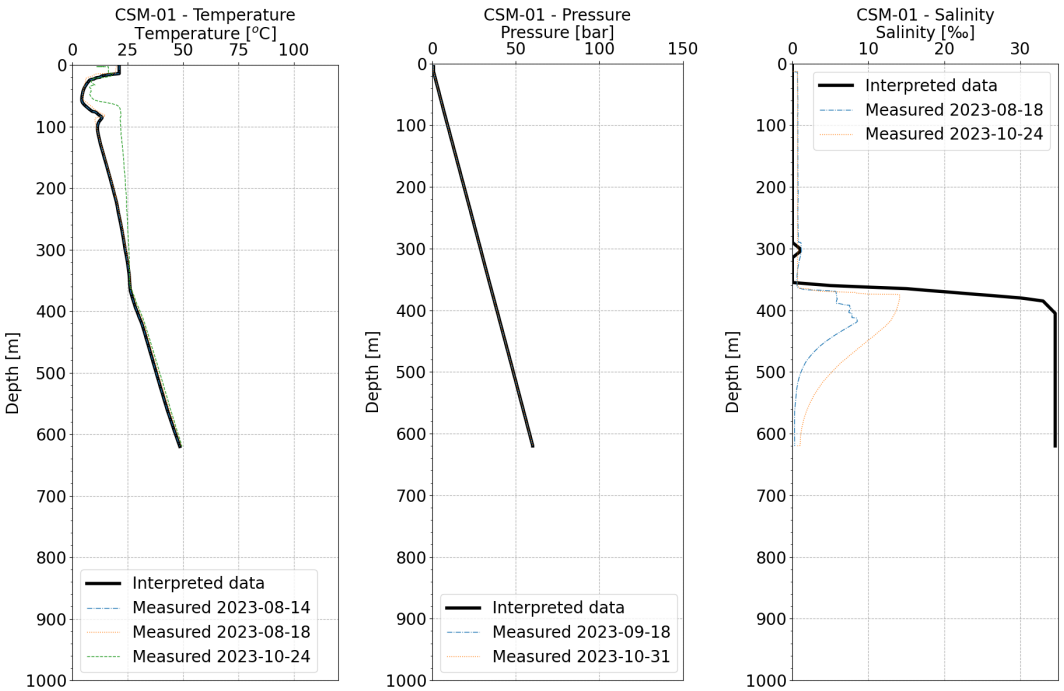

(a) (b) (c)

Figure 4.6: Downhole temperature (a), pressure (b), and salinity (c) measurements from well CSM-01.

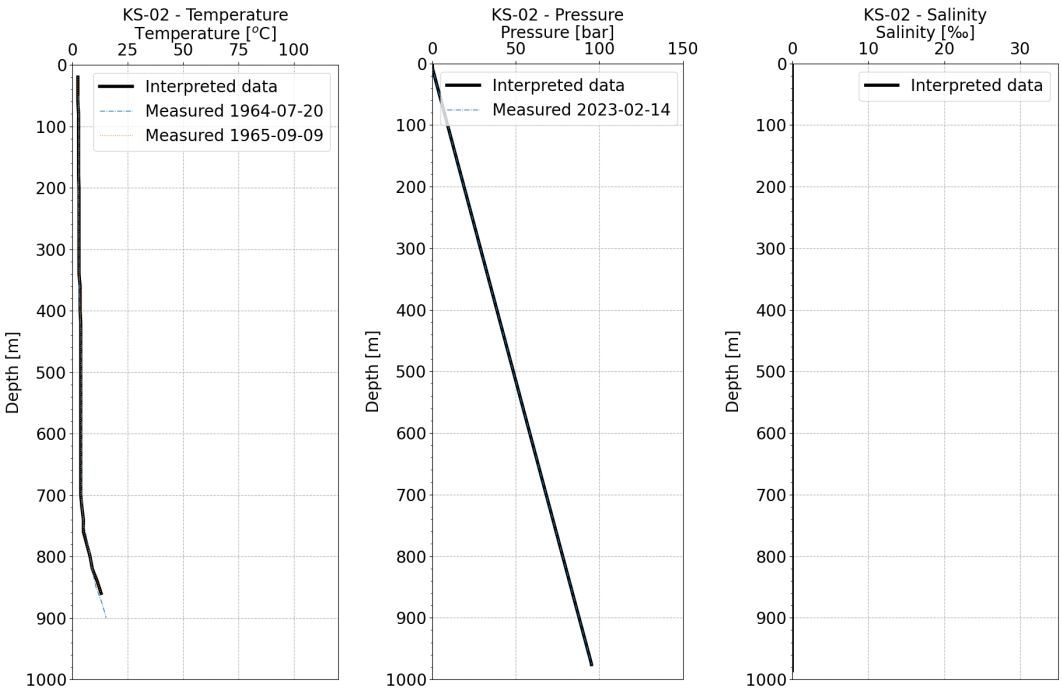

(a) (b) (c)

Figure 4.7: Downhole temperature (a), pressure (b), and salinity (c) measurements from KS-02.

4.4 Saline intrusion and the saltwater-freshwater interface

In coastal regions, like Straumsvík, the presence of permeable and porous rock formations near the coast can cause intrusion of saline water (seawater) into the otherwise fresh groundwater. Since salinity increases the density of water, the presence of these intrusions forms a layered structure in the groundwater aquifer. This structure is characterized by the lighter fresh water floating on top of the denser saline water, forming a freshwater lens. In Iceland, a good example of such saline intrusions is found in the Reykjanes Peninsula, where there is a layer of fully saline water overlain by a lens of freshwater under the entire peninsula. In Reykjanes the depth down to the saline water varies and, in general, it increases with distance from the coast (F. Sigurðsson, 1985).
The saline and fresh water layers are often separated by a mixing layer, a layer of brackish water known as the saltwater-freshwater interface. The salinity in the interface layer increases with depth, with the salinity changing from more-or-less fresh water at the top, to saline water at the bottom. The interface layer is the result of dispersion by the natural flow of saline water, as well as the effects of tides and recharge on the system. The thickness of the saltwater-freshwater layer can be anywhere from less than 1 m up to more than 100 m (Todd and Mays, 2005). In Reykjanes, this interface layer is relatively thin near the coast, usually on the order of a few tens of meters. Salinity in the water in the subsurface can roughly be divided into three groups:

- Fresh water (< 0.5 ‰ salinity).
- Brackish water (0.5 – 30 ‰ salinity), corresponding to the saltwater-freshwater interface.
- Saline water (> 30 ‰ salinity).

** Note that the salinity of seawater is in general around 34 - 35 ‰.*

The mapping of saline intrusion near Straumsvík is central to the site characterization efforts and the associated modelling activities. This is due to several factors:

- Saline water has a density of 1024 kg/m^3 at 20°C and is denser than freshwater, which has a density of 998 kg/m^3 at 20°C. This leads to a delicate pressure-density balance in the subsurface that influences subsurface flow regimes.
- The density difference between saline, brackish, and fresh water may also impact the target areas and depth of the storage reservoir for in-situ mineralization.
- Injection into saline water has been demonstrated in the lab and there is currently a pilot project for such injection in progress. However, this type of injection has not been conducted at scale and further field demonstration may be required.

To facilitate the mapping of salinity in the subsurface two methods were used; electrical conductivity well logging and surface resistivity, or TEM, measurements.
Electrical conductivity logs provide valuable information on the salinity of the subsurface fluid and can help identify the depth of the saltwater-freshwater interface. Water samples collected from CSI-01 show a sharp increase in electrical conductivity at approximately -100 m a.s.l. The electrical conductivity logs from well CSM-01, Figure 4.6, show a similar sharp rise in electrical conductivity at approximately -350 m a.s.l. Note that electrical conductivity logs are not accurate inside well casings, so well logs in CSI-01, which is cased down to around 320 m, are not useful in locating the depth of the interface. This indicates that the depth of the saltwater-freshwater interface is around -100 m a.s.l. in CSI-01 and -350 m a.s.l. in CSM-01. The thickness of the interface in both locations is estimated to be around 20 m. Electrical

conductivity logs in both CSI-01 and CSM-01 show a gradual increase in salinity below the interface depth with time. The measurements also show a decrease in conductivity with depth in the bottom sections of the wells. The working assumption is that this behavior is due to disturbance from drilling and injection testing in the wells, which involves pumping a large amount of fresh water into the wells. Therefore, it is likely that the well has not yet reached equilibrium with the natural state of the surrounding reservoir after these tests. The interpreted data curves for salinity for both CSI-01 (Figure 4.5) and CSM-01 (Figure 4.6) show the currently estimated natural state near both wells. Continued well logging in both CSI-01 and CSM-01 is necessary to confirm the natural state conditions near the wells. Electrical conductivity measurements were also conducted in well KS-02 at Kaldársel in 2023. These showed that fresh water extends from the surface down to the bottom of the well, at 986 m. This is consistent with older measurements and shows that salinity disappears at a certain distance from the coast. Resistivity measurements, namely μTEM and TEM soundings, were conducted in the Straumsvík area in 2022 and 2023 (Vilhjálmsson et al., 2023). Such geophysical methods are well suited for the purpose of mapping saline intrusions in the subsurface as they can detect subsurface resistivity variations, especially where resistivity decreases with depth. This is expected in reservoirs where dry rocks are underlain with rocks saturated with fresh water and saline water. This can help map the thickness of the fresh water lens in the subsurface from the coast inland. The bulk of the soundings were located along a NW-SE trending cross-section, inland from the Straumsvík inlet, see Figure 4.8. A shallow brackish water layer, thought to be the saltwater-freshwater interface, was traced from the coast along this cross-section. The depth down to the interface in the cross-section increases gradually inland until it terminates abruptly less than 2 km away from the inlet.

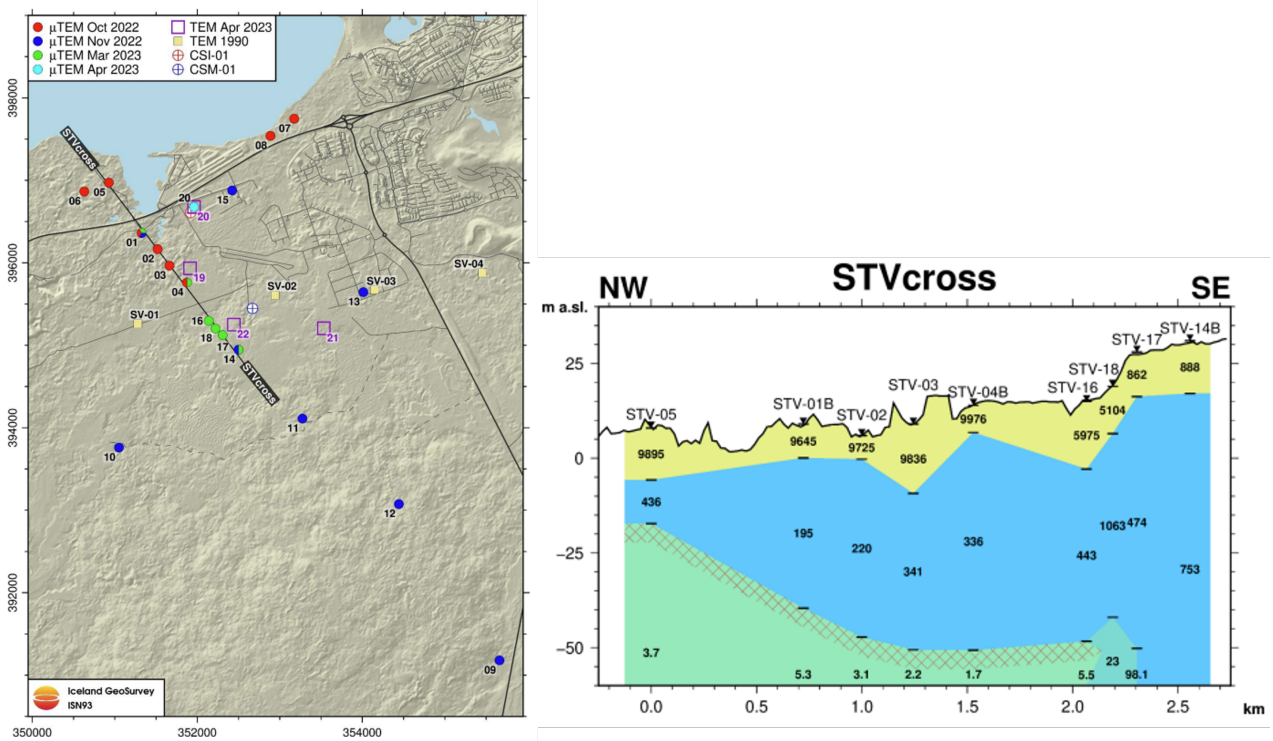

Figure 4.8: Overview of TEM and μTEM sounding locations near Straumsvík (left). Resistivity layers in a cross section STVcross (right). The yellow shading represents the unsaturated zone (above the water table), the blue shading represents freshwater, and the green shading shows saline water (right). From Vilhjálmsson et al., 2023.

4.5 Reservoir fluid chemistry

The make-up of the fluid in the proposed storage reservoir has been studied as part of the characterization of the Straumsvík site (Galeczka, 2023b). The fresh water reservoir fluid was based on the chemical composition of the drinking water in Hafnafjörður. The saline water reservoir fluid was based on water samples from well CSI-01. The estimated reservoir chemical composition is shown in Table 4.5, along with the composition of seawater near Reykjanes. The ambient mass fraction of CO_2 in the reservoir fluid seems to around 10 – 20 mg/L, or around 0.01 – 0.02 g/kg, which is negligible compared to the estimated injected mass fraction of 3 – 4 g/kg. The estimated salinity of the saline reservoir is around 24.5 ‰, which is quite low compared to the salinity of seawater, which is around 34 – 35 ‰. However, it should be noted that the saline water chemistry is estimated from samples gathered during discharge testing of CSI-01. It is therefore possible that the water sampled was a composite of fresh water and saline water, and that the true salinity at depth will be closer to 34 ‰. Newer measurements of water from the well show an increasing Cl concentration in the well with time (Galeczka, 2023a). Thus, it might be more accurate to say that the saline water in the reservoir will have a salinity in the range 24.5 – 35 ‰. Finally, the chemistry shows that the Cl content, and to a lesser extent the Na content, is quite a bit higher than other components in the saline water sample. Therefore, since Cl is directly related to salinity of water, we expect that the evolution in water density with chemical composition in the reservoir will be controlled by salinity.

Table 4.5: Estimated fluid chemistry of fresh and saline reservoir water in Straumsvík, along with fluid chemistry of seawater near Reykjanes. Adapted from Galeczka, 2023b.

	Fresh water - Reservoir	**Saline water - Reservoir**	**Seawater**
Temperature [°C]	3.10	15.00	-
pH/°C	8.98/22.2	8.36/20.0	8.15/23.1
SiO_2 [mg/L]	15.20	6.22	0.7
B [mg/L]	< 0.01	1.04	4.17
Na [mg/L]	10.4	6860	10560
K [mg/L]	0.641	84.90	380
Ca [mg/L]	5.33	2200	377
Mg [mg/L]	1.8	222	1230
Al [mg/L]	0.00148	0.01	0.001
Fe [mg/L]	< 0.0004	0.18	0.002
CO_2 [mg/L]	20.7	10.4	100
Cl [mg/L]	8.54	14202	18800
SO_4 [mg/L]	2.88	1629	2550
F [mg/L]	< 0.2	< 0.2	0.81
Salinity [‰]	0.02	25.7	34.0

5 Conceptual Model of the Storage Complex

The data and information obtained from the site characterization were used to create a qualitative conceptual model of the storage site. This model provides a simplified representation of the site's geological, hydrological, and physical attributes, and serves as a basis for understanding the behavior of the storage reservoir.

The groundwater regime in the Reykjanes Peninsula is a characteristic coastal environment in which seawater is present at a relatively shallow depth over the entire peninsula (F. Sigurðsson, 1985). The saltwater-freshwater interface is primarily controlled by salinity gradients between the seawater intrusion from the coast and the groundwater influx from the watershed, which leads to the establishment of an overlying fresh water lens. The Straumsvík site is located in a transition area between a coastal environment, as seen on the Reykjanes Peninsula, and a more continental environment, as seen in Reykjavík proper. As such, the area has a complex subsurface regime in which there is a sharp boundary between saline and fresh water, with only fresh water present at depth inland, as evidenced by measurements in deep wells in Kaldársel and TEM measurements. This may be further influenced by a very large flow of cold, fresh, water recharge or influx from the Southeast. The additional pressure support provided by this cold, fresh, water recharge influences the density balance in the subsurface and prevents the saltwater intrusion from reaching far inland. The morphology of the saltwater-freshwater interface may also be impacted locally by lithological units. The lithological and structural impact on this interface and distribution of saline water at depth will however be further investigated as new data is collected and analyzed.

The surface geology in the greater Straumsvík area consists of postglacial lavas, interglacial lava flows (grágrýti), and hyaloclastite mountains (móberg) further south and southeast towards the Krýsuvík fissure swarm. No evidence of faults or fissures on the surface has been found in the Straumsvik area (Helgadóttir et al., 2023). The stratigraphy of Straumsvík in the upper 1000 m of the subsurface is characterized by an anisotropic permeability field where the horizontal permeability dominates the system. Injectivity tests in wells CSI-01 and CSM-02 indicate that most of the permeable layers in the storage reservoir are found at depths between -300 m a.s.l. and -450 m a.s.l., and correspond to locations of lithological contacts (Jónsson, 2024).

Using data collected at the site (Chapter 4), a preliminary conceptual model of the Straumsvík area was constructed and can be seen in Figure 5.1. This model encompasses the fluid behavior in the area, including the balance between saline and fresh groundwater. It is important to note that our current understanding of the area is limited to information from only two wells, along with resistivity measurements performed in the area. While this provides us with some valuable insights, it significantly restricts the scope of the analysis. Therefore, to enhance the accuracy and reliability of our subsurface understanding, the collection of additional data is essential. Doing so will not only refine our existing model but also provide a more robust and comprehensive understanding of the subsurface structure and fluid behavior.

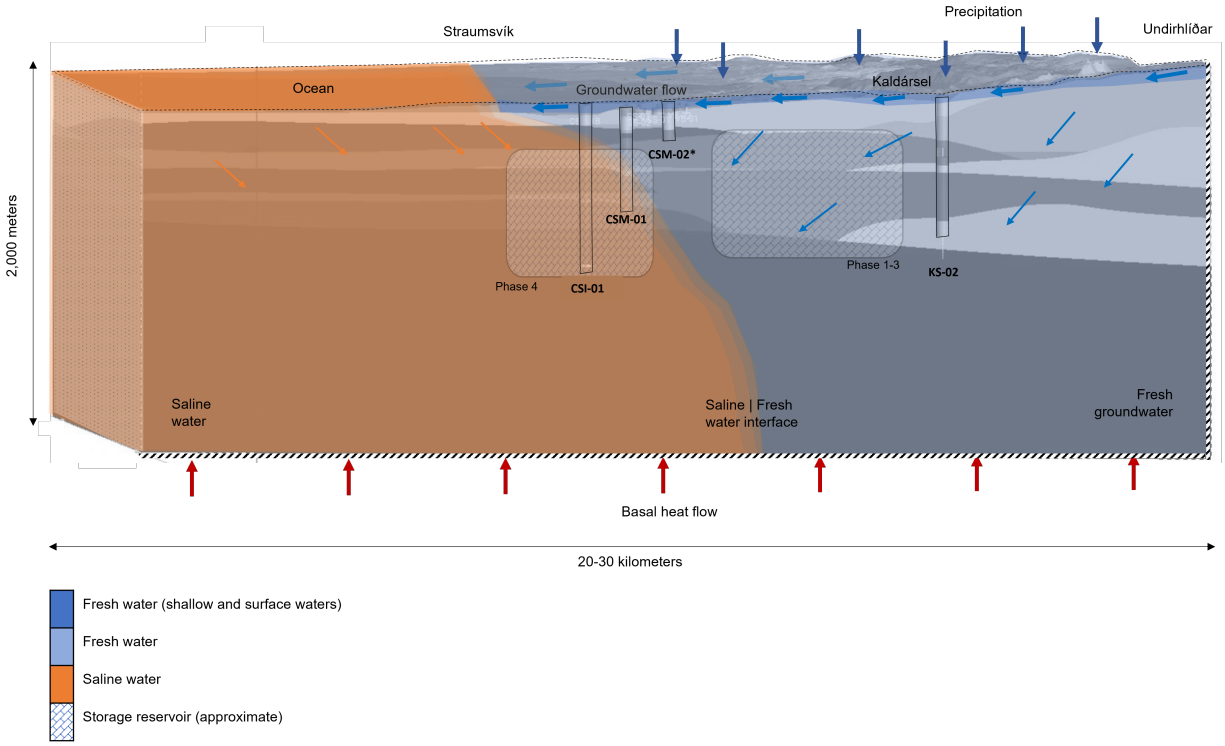

Figure 5.1: Conceptual model - schematic three-dimensional diagram highlighting the freshwater-seawater interface and the flow between wells CSI-01 and CSM-01 in Straumsvík and well KS-02 in Kaldársel (adapted from Helgadóttir et al., 2023).

6 Numerical Formulation and Approach

The conceptual model is further refined and quantified to develop a numerical reservoir model. This model is a mathematical representation of the storage reservoir that can be used to simulate the injection and storage of CO_2. The focus of the numerical model was to accurately simulate three key factors in the storage reservoir and the surrounding subsurface. The first of these is the estimation of the maximum extent of CO_2 migration in the reservoir due to Carbfix's injection. This information is key in judging whether or not the storage reservoir can contain the injected CO_2, without leakage, and to estimate if carbon mineralization is feasible in the storage reservoir. The estimated extent of CO_2 migration also helps in setting up effective monitoring plans in the area, so any adverse environmental impact will be found quickly. The second factor is the density of the resident reservoir water in the storage reservoir. Since Carbfix aims to use solubility trapping to ensure the containment of CO_2 prior to mineralization, it is important to have good estimates of the water density in the reservoir to judge if the injected CO_2 charge water will sink or rise to the surface. The final factor is estimating the bubble point pressure of CO_2 in the reservoir, to ensure that there is no danger of the injected dissolved CO_2 exsolving in the storage reservoir and rising to the surface as gas. In order to simulate these three key factors the numerical reservoir model incorporates detailed data on the reservoir's porosity, permeability, pressure, temperature, salinity, and other properties.

6.1 Material and method

The numerical simulations are carried out with TOUGHREACT, a parallel simulator for three-dimensional non-isothermal multiphase reactive transport in porous and fractured rock (Sonnenthal et al., 2021). TOUGHREACT is based on the non-isothermal multi-component fluid and heat flow simulator TOUGH2 (Pruess, 1991), and adds reactive transport into the framework of TOUGH2. It has been used to simulate many geological, environmental, and subsurface engineering problems, including geological carbon sequestration, subsurface nuclear waste emplacement, geothermal reservoir management, contaminant transport, and groundwater quality. It has also been used in the past in Iceland to estimate the effects of CO_2 injection into basaltic reservoirs (Aradóttir et al., 2012, Ratouis et al., 2022, Liu et al., 2019, Gunnarsdóttir et al., 2021).

Currently, the reaction processes are not fully integrated in the reservoir models. The transport models developed represent a non-reactive transport numerical scheme of the CO_2-charged fluid through the reservoir and hence, predict the maximum potential impact that the injection may have in the system for a theoretical scenario in which no mineralization occurs.

The governing equations solved by TOUGH2 and TOUGHREACT describe the conservation of mass and energy in the system. The change in mass/energy in a given subdomain V_n resulting from fluxes across enclosing surface A_n is represented as

$$\frac{d}{dt}\int_{Vn} M^K dV_n = \int_{An} F^K * dA_n + \int_{Vn} q^K dV_n \tag{1}$$

where M^K represents the mass or energy per unit volume of the component K, $F^K * dA_n$ is the flux of component K through surface A_n and q^K denotes mass flow into/out of sinks and sources. Equation 1 expresses that the rate of change of fluid mass in V_n is equal to the net inflow across the surface of V_n plus net gain from external fluid sources and sinks. Advective

flux is defined for each component K as

$$F^K|_{adv} = \sum_\beta X_\beta^k F_\beta \tag{2}$$

with individual phase flux is given by Darcy's law

$$F_\beta = \rho_\beta u_\beta = -K \frac{K_{r_\beta} \rho_\beta}{\mu_\beta} (\bigtriangledown P_\beta - \rho_\beta g) \tag{3}$$

where F_β is the flux of phase β, ρ_β is the density of phase β, u_β is the Darcy velocity in phase β, K is the absolute permeability, $K_{r\beta}$ is the relative permeability of phase β, μ_β is the dynamic viscosity of phase β, P_β is the sum of the pressure of a reference phase and the capillary pressure and g is the vector of gravitational acceleration. Transport is controlled by advection, and dispersion was not included in this modeling work. Molecular diffusion was included in the modeling framework because while the transport is dominated by the high advection velocities within the fracture network at the injection site, matrix diffusion may be an important process in retarding the movement of solutes and attenuating their concentrations (Walter, 1982). Diffusive flux f is written as being proportional to the gradient in the concentration of the diffusing component (Fick's law) as

$$f = -d \bigtriangledown C \tag{4}$$

where d is the effective diffusivity, which in general will depend on the properties of the diffusing component, the pore fluid, and the porous medium and C the concentration. Heat transfer is controlled conduction and convection as

$$F^{NK+1} = -\lambda \bigtriangledown T + \sum_\beta h_\beta F_\beta \tag{5}$$

where λ is the thermal conductivity, T is the temperature and h_β is the specific enthalpy in phase β. Description of thermodynamic conditions assumes local equilibrium of all phases. TOUGH uses an integral finite difference (IFD) method for space discretization, and first-order fully implicit time differencing. The resulting strongly coupled, nonlinear algebraic equations are solved simultaneously using Newton-Raphson iterations for each time step. Time steps are automatically adjusted during a simulation run, based on the convergence rate of the iteration process. The IFD method avoids any reference to a global system of coordinates and is applicable to regular or irregular discretization in one, two, and three dimensions. The IFD method also makes it possible to implement double- and multiple-porosity methods for fractured media.

6.2 Reservoir modelling workflow

Reservoir modeling plays an important role in the reservoir management of the mineral storage operations at the Coda Terminal. It provides tools to predict and optimize the long-term management of the injection of dissolved CO_2 and contributes to the safe application of the Carbfix carbon storage method. Comparison between the observed and modeled behavior of the subsurface CO_2 transport and mineralization is an integral part of the verification process during conformance monitoring of the site. The ability to model the fate of the injected CO_2 as well as to quantify the amount of CO_2 that can be mineralized also increases the overall confidence in the effective permanent storage of CO_2.

Two successive reservoir models were developed, the first model was used to simulate the natural state of the reservoir. This is followed by the second model, which was used to forecast the effects of injection of CO_2 in the storage reservoir. In the following sections, the model assumptions, characteristics, and results for both models are presented. The natural state model results provide the initial conditions (temperature, pressure, salinity, and dissolved CO_2 distribution as well as heat and mass flow) for the forecast model. The modeling workflow developed consists of:

1. A **conceptual model** of the system, describing the main physical processes (Chapter 5).

2. A **numerical grid** of the system. The grid used is irregular with different levels of refinement, ranging from large blocks at the outskirts of the model to smaller blocks at the injection site(s) (Figure 6.1). This configuration decreases the computational cost of the simulation while preserving a high level of detail in the area of interest. The multi-scale heterogeneity in the reservoir can be represented by assigning individual model blocks with a specific permeability and porosity values. The different levels of refinement in the grid enables the model to include the individual structural features such as faults, which allows for the modeling of discrete flow paths for the fluid. Local refinement of the grid is carried out by performing a Delaunay triangulation of the transition zone in which blocks of intermediate sizes are created (Croucher and O´Sullivan, 2013). The connections are usually not orthogonal and may introduce mass balance errors in the IFD solution. This is addressed by optimizing the connection angle block geometry using a non-linear least squares optimization formulation at the transition zone between blocks.

3. The **Geological representation** and **permeability field** as described in the geological model (Chapter 4 and Helgadóttir et al., 2023) is represented in the numerical model by defining a rock-type for each geological unit, which populates the three-dimensional array of blocks of the numerical grid of the system (Figures 6.2 and 6.4). The rock-type parameters represent the properties of each geological unit. Distinct hydro-geological parameters (permeability, porosity, density, conductivity, etc.) are then assigned to each rock-type to represent the characteristics of each unit (Table 6.2).

4. **Equation of State** (EoS) provides the thermodynamic and thermophysical properties of the considered fluid mixture. For the present work, we use ECO2N (Pan et al., 2014), which considers the fluid in the subsurface as a mixture of H_2O, NaCl, and CO_2. This allows us to represent both the influence of salinity and of CO_2 on the reservoir. ECO2N reproduces fluid properties of H_2O - NaCl - CO_2 mixtures within experimental errors for reservoir fluid between 10 °C to 300 °C in temperature, with less than 600 bar in pressure, and with salinity up to halite saturation. This includes estimating density, viscosity, and specific enthalpy of fluid phases as functions of temperature, pressure, and mass composition, as well as estimating the partitioning of mass components among the different phases.

5. **Boundary conditions** that represent heat and mass influx and outflow into the system, which control the regional heat and mass distribution.

6. **Natural state simulations** were performed and provide a baseline for the state of the storage complex prior operations of the Coda Terminal.

7. **Forecast simulations** were performed to assess the reservoir response to injection and determine the migration and fate of the injected fluids.

– **Initial conditions** for the forecast models are extracted from the natural state model. The forecast model covers the same area but the grid for the forecast model is coarser than the grid developed for the natural state in this study (Table 6.1). The values were interpolated onto the finer grid using a spatial three-dimensional Delaunay triangulation.

– **Injection/Production** scenario are defined and provided.

– **Simulation time** is set for the duration of operation, closure, and post-closure of the site.

Table 6.1: Natural state and forecast models specifications

	Natural State	**Forecast**
Grid extent		
Number of grid blocks	100,777	195,456
Level of refinements	4	5
Top surface	Water level	Water level
Side boundary conditions	Open towards the ocean Closed inland	Open towards the ocean Closed inland
Influx	Basal heat	Basal heat, pure water, CO_2, and brine
Outflux	None	Water production from CSW wells
Simulation time	320 million years	30 years operation, 1 years post closure, and 100 years post closure

6.3 Grid structure

The three-dimensional model covers an area of 576 km^2 (24 km × 24 km) and is large enough to encompass the geological storage reservoir and monitoring areas (Figure 6.1), as well as to ensure any changes due to the simulated production/injection in the field are not influenced by boundary conditions. The grid used is irregular and has different levels of refinement between the natural state and the forecast model:

- The grid for the natural state contains four levels of refinement from 1.6 km by 1.6 km at the outskirts of the model to 200m by 200m in the storage complex.
- The grid for forecast simulations is further refined to 100 m by 100 m at the injection site(s).

This configuration decreases the computational cost of the simulation while preserving a high level of detail in the geological storage reservoir.

The model is made up of 50 layers ranging from -125 to -3000 m a.s.l. and with thicknesses between 10 to 250 m. A minimum thickness of 10 m was assigned to layers close to sea level, to better model the effects of the coastal boundary on the fluid flow between the groundwater and the sea. The vertical refinement of the grid was also finer in the estimated depth range of the proposed storage reservoir, between –300 and -700 m a.s.l. The top of the model was set to follow the top of the water table on land (provided by Myer et al., 2024), and the bathymetry of the oceanic floor offshore.

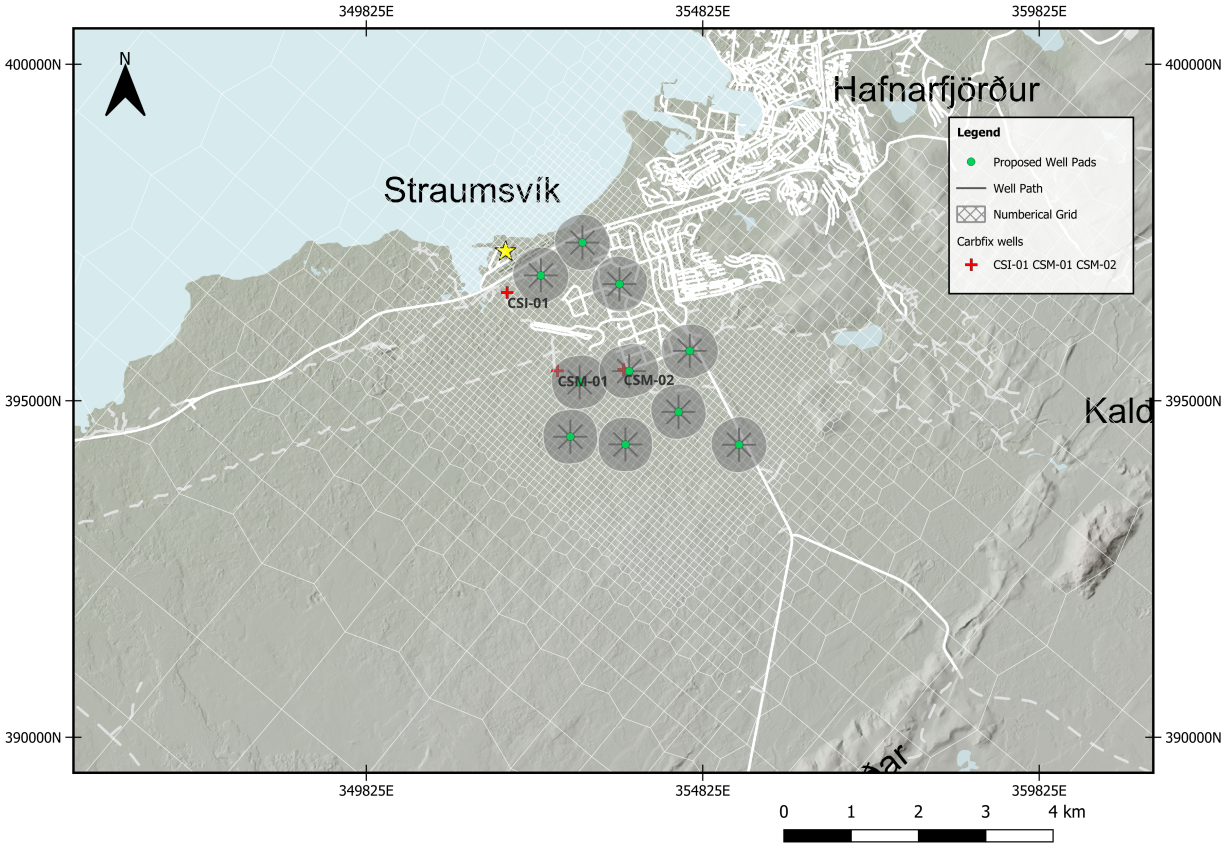

Figure 6.1: Numerical grid used in the reservoir models. The figure is centered on the main area of interest around Straumsvík and shows the sequential grid refinements around the proposed storage reservoir.

6.4 Geology and permeability field

The multi-scale heterogeneity in the reservoir is represented by assigning individual blocks with a corresponding rock-type (Figures 6.2, 6.3, and 6.4). The distribution of these rock-types is based on the geological model described in Chapter 4. The rock-type parameters represent the properties of each geological unit, namely the porosity, permeability, density, specific heat, and liquid-heat conductivity. The geological units considered are the Holocene lavas, basalt lava flows, hyaloclastites, glassy basalts, sediments, and the crystalline basement. All rock-types have a density of 2600 kg/m^3, a specific heat of 900 kJ/kgK, and liquid-saturated heat conductivity of 1.5 W/mK. The porosity and permeability of rock-types were based on site estimates (F. Sigurðsson, 1985, Helgadóttir et al., 2023) and the natural state calibration, detailed in the Chapter 7. The estimated values are provided in Table 6.2. Contact zones between lithological units in the storage reservoir were also treated as a distinct rock-type. These contact zones are where the largest feed zones in the groundwater and storage reservoir are expected to be found. For the basaltic lava flows, it was assumed that the permeability of the lavas decreased with depth, as a function of age and alteration, with the relatively fresh lava at the top of the model having the highest permeability. The sediments were given porosity and permeability of neighboring rock-types since insufficient data exists on their extent to constrain their properties.

Table 6.2: Permeability and porosity ranges for the rock-types defined in the model.

	Porosity	Permeability [md]	
	(%)	Horizontal	Vertical
Holocene Lavas	20	200,000	400
Basaltic Lava Flows	10	250 - 2.5	50 – 0.5
Glassy Basalts	10 – 15	500	100
Hyaloclastite	10	10	2
Sediment	10 – 20	500 - 250	100 – 50
Basaltic Basement	5	1	0.2
Lithological Contact Zones	15	2000	800

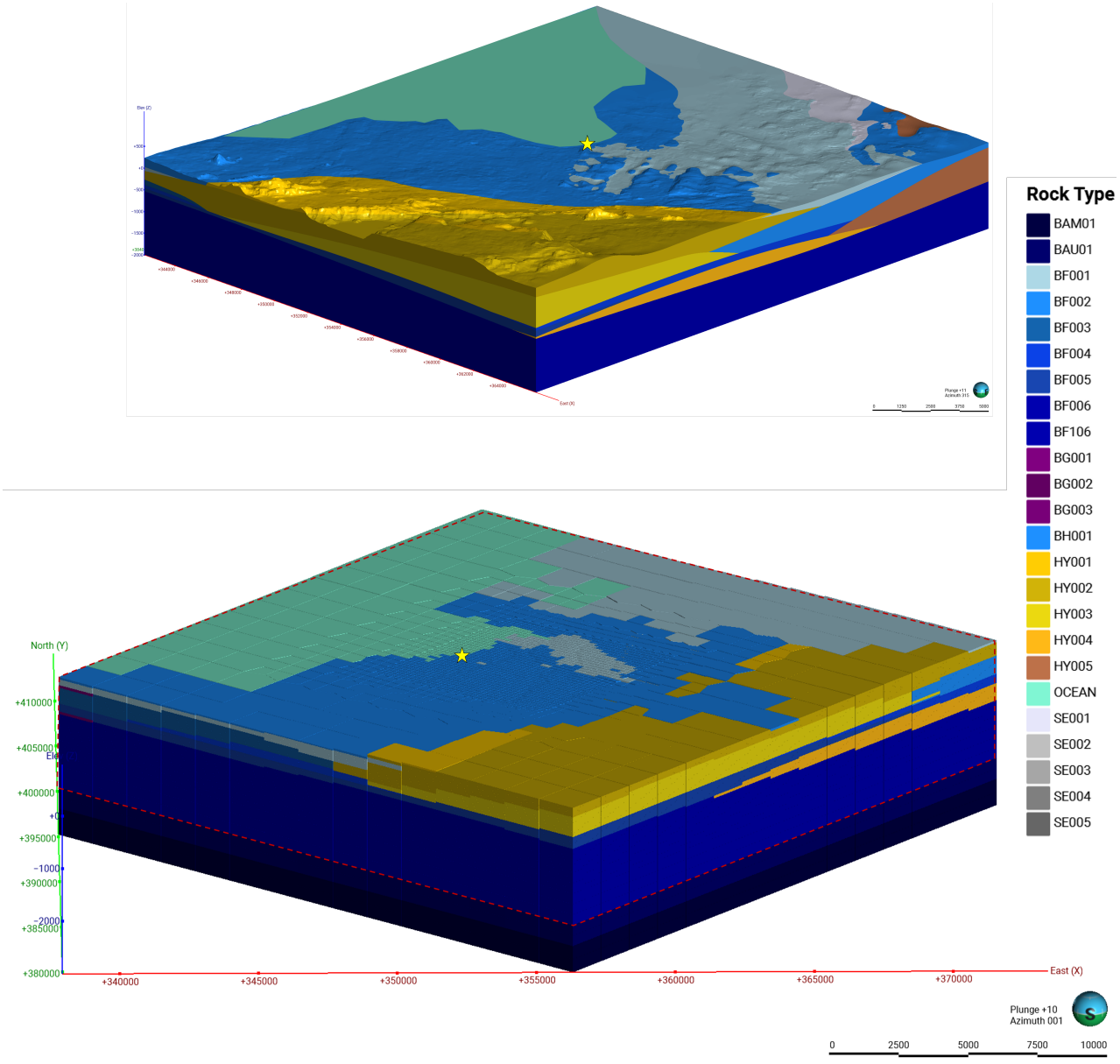

Figure 6.2: Rock-type distribution in the 3D geological model (top) and in the numerical model grid (bottom). The rock-type assignment was based on the 3D geological model of the area (Helgadóttir et al., 2023). The storage complex is shown by a grey polygon and the dashed red lines represent the extent of the geological model.

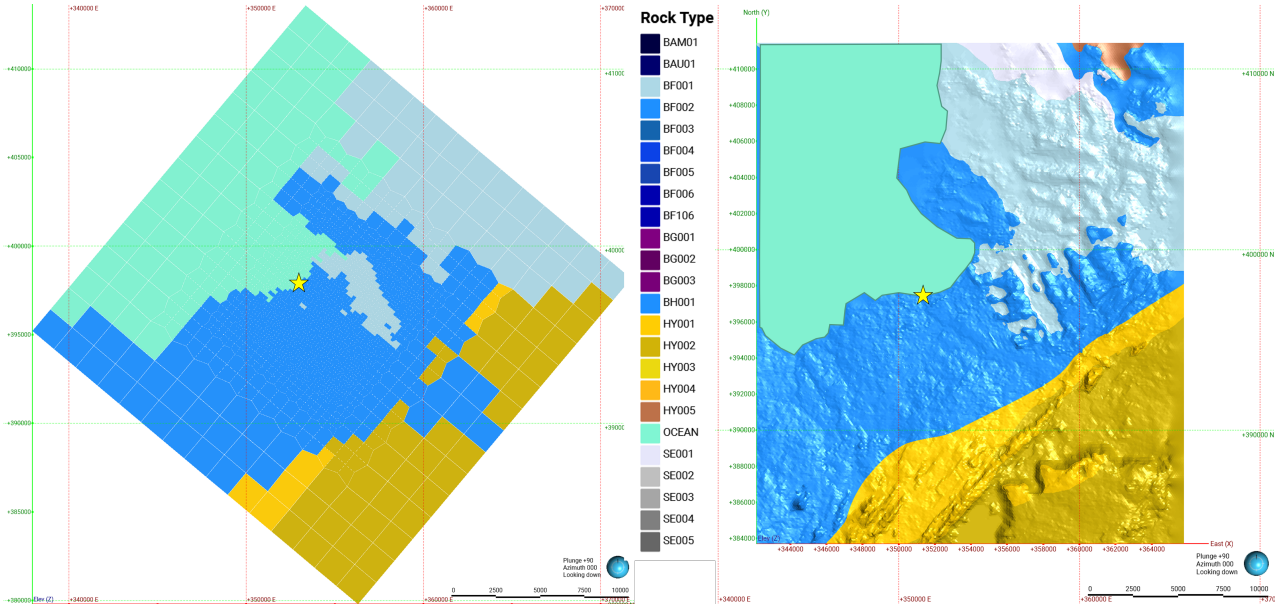

Figure 6.3: Surface rock-type distribution in the model grid. The storage complex is shown by a grey polygon. From Helgadóttir et al., 2023.

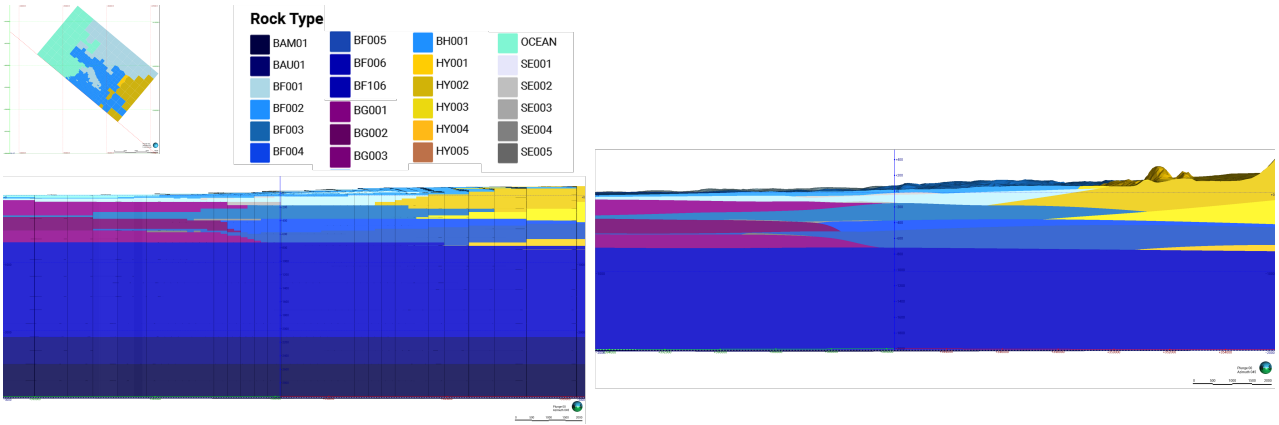

Figure 6.4: Rock-type distribution in the model grid following a WNW-ESE cross section. From Helgadóttir et al., 2023.

6.5 Equation of State - ECO2N

The numerical framework includes a fluid property module, the equation of state. The equation of state used for the simulations is the 2nd version of the ECO2N module, which was designed for simulating geological sequestration of CO_2 in saline and geothermal aquifers. ECO2N includes a comprehensive description of the thermodynamic and thermophysical properties of the H_2O - NaCl - CO_2 system for temperatures between 3.5°C to 300°C, pressure up to 600 bar, and salinity up to halite saturation. The equation of state has been found to reproduce the thermodynamic and thermophysical properties of these systems to within experimental errors (Pan et al., 2014).

Three key properties that control flow and heat in subsurface reservoirs are density, viscosity, and specific enthalpy. For multi-component systems, like H_2O - NaCl - CO_2 fluid mixtures, the solubility of the additional components in water is also a key factor in accurate reservoir modeling. For the density of the H_2O - NaCl - CO_2 fluid, the density of brine (H_2O - NaCl) and the density of pure CO_2 are considered separately. Thus, the fluid density is estimated by

$$\frac{1}{\rho_{\mathrm{aq}}(T,P)} = \frac{1 - X_{CO_2}}{\rho_b(T,P)} + \frac{X_{CO_2}}{\rho_{CO_2}(T,P)} \tag{6}$$

where T is the temperature, P is the pressure, ρ_{aq}, ρ_{b} and $\rho_{\mathrm{CO_2}}$ are the density of the fluid, brine, and pure CO_2 respectively, and $X_{\mathrm{CO_2}}$ is the mass fraction of CO_2 in the fluid. The brine density is calculated using the properties of pure water (Committee, 1967) with corrections added to account for salinity (Haas, 1976, Andersen et al., 1992, Battistelli et al., 1997). The aqueous density of pure CO_2 is calculated using

$$\rho_{CO_2} = \frac{M_{CO_2}}{37.51 + -9.585 * 10^{-2} T + 8.740e-4 * T^2 + -5.044e-7 T^3} * 10^3 \tag{7}$$

where $M_{\mathrm{CO_2}}$ is the molecular weight of CO_2. This equation is based on the correlations of the molar volume of CO_2 at infinite dilution (Garcia, 2001), since dissolved CO_2 is always considered diluted at reservoir conditions.

The viscosity of the reservoir fluid is assumed to be the viscosity of brine at the same temperature and pressure (Phillips et al., 1981), and any effects of CO_2 concentration on the fluid viscosity are ignored.

The specific enthalpy is calculated in a similar way to the density, by considering brine and CO_2 separately, i.e.

$$h_{aq}(T,P) = (1 - X_{CO_2}) h_{\mathrm{b}}(T,P) + X3(h_{\mathrm{CO_2,g}}(T,P) + h_{\mathrm{dis,g}}(T,P)) \tag{8}$$

where h_{b} and $h_{\mathrm{CO_2,g}}$ are the specific enthalpies of brine and gaseous CO_2, and $h_{\mathrm{dis,g}}$ is the enthalpy of dissolution of CO_2. These specific enthalpies of CO_2 and NaCl are estimated from the correlations of Altunin (Altunin, 1975) and Lorenz (Lorenz et al., 2000), and the enthalpy of dissolution of CO_2 is estimated from equations by Himmelblau (Himmelblau, 1959).

The solubility of CO_2, or the phase transition from dissolved CO_2 to pure gas, is based on correlations by Spycher and Pruess (Spycher and Pruess, 2005, Spycher and Pruess, 2010). The solubility of NaCl, or the phase transition from dissolved NaCl to solid halite (Chou, 1987).

6.6 Boundary conditions

A Dirichlet boundary condition is applied to the top boundary of the grid, which allows fluid to flow in and out of the system. The pressure, temperature, and salinity of the top blocks are fixed

and represent the groundwater table and the ocean. As such, the open boundary conditions on land were set to fresh water (no salinity) at a temperature of 8°C and an atmospheric pressure of 1 bar. Under the ocean, the boundary conditions were set to saline water (35 ‰ salinity) with a temperature of 8°C and at a hydrostatic pressure resulting from the mass of the overlaying seawater (based on the bathymetry) as follows:

$$P_{\text{boundary}} = \rho g h_{\text{sea}} \tag{9}$$

where ρ is the density of seawater at 8°C, g is the acceleration due to gravity, and h_{sea} the height of the seawater column.

Since the side boundaries located in the SE part are assumed to be sufficiently far from the injection as to not cause boundary effects they were set as closed, i.e., no heat or mass can come into or go out of the system through those blocks. The side boundaries located in the NW part of the model, including all the blocks under the ocean, are open boundary conditions that allow water to flow in or out of the model. These are used to represent the recharge from the ocean into the system.

The bottom layer of the model was a closed mass boundary, with a constant conductive heat-flow of 60 mW/m^2. This model boundary represents the natural temperature gradient at the site (Chapter 4).

7 Natural State Model (Baseline Model)

In order to assess the effects of Carbfix's proposed injection and production on the storage reservoir and groundwater at the site; it is first necessary to establish a baseline for the region. To estimate such a baseline we used a numerical model (Chapter 6) to simulate the state of the system prior to anthropogenic activity in the area. This baseline model is generally referred to as a natural state model of the system. It simulates the natural state of reservoir fluid in the area, including reproducing the expected regional groundwater flow patterns and temperature distributions in the watershed. This includes simulating the coastal component of the Straumsvík site and thus the distribution of salt, or salinity, in the subsurface. A natural state model can provide insights into the flow and subsurface processes at work in a reservoir and increases our understanding of the storage reservoir. Also, once a natural state model has been created it becomes possible to use it to quantify the effects of Carbfix's injection/production on the region.

Using the numerical approach, detailed in Chapter 6, as a base for the natural state model, a simulation of the region was run until the model reached a steady state. The initial conditions of the model were set to follow a hydrostatic gradient, with the reservoir starting at a cold isothermal temperature, with an underlying heat flux of 60 mW/m^2 over the entire region. Since the simulated steady state can take a larger time span to achieve compared to a natural steady state, this generally means simulating the system for several hundred million years. This simulated steady state was then compared with the available field data collected as part of the site characterization, detailed in Chapter 4. The parameters of the numerical model were adjusted to improve the fit between simulated and measured values. This included changing permeability, porosity, and heat flow in the model. These steps were then repeated until a numerical model was created that was judged to adequately reproduce the field data. The results detailed in the following chapters represent the conditions simulated for the baseline, or natural state, of the system.

7.1 Subsurface temperature, pressure, and salinity distribution

Simulated distributions of temperature, pressure, and salinity in the numerical model were compared to measurements. For the temperature it has been estimated that the thermal gradient in Straumsvík is around 80 – 90°C/km (Helgadóttir et al., 2023). Further inland, near the freshwater wells in Kaldársel, the temperature is almost a constant 5°C down to 800 m, as can be seen from measurements in well KS-02 (Figure 4.7). This means that the temperature should decrease with distance from the coast. Known geothermal areas exist both to the South (Trölladyngja) and Northeast (Reykjavík) of Straumsvík. However, these are thought to not significantly influence the temperature distribution near Straumsvík (F. Sigurðsson, 1976) and are not explicitly modeled.

A comparison between the estimated temperature in three wells, CSI-01, CSM-01, and KS-02, and the natural state model is shown in Figure 7.1. We can see that the model simulates the temperature differences between the wells close to Straumsvík, namely CSI-01 and CSM-01, and the Kaldársel cold water well KS-02. The temperature gradient in CSM-01 is around the expected value of 80°C/km. However, the gradient in CSI-01 is only 60°C/km, and the temperature at depth in that region is underestimated by the model. For both CSI-01 and CSM-02, the simulated temperature near 300 m is around 20 – 30 °C higher than the measured temperature. This is due to a heat up-flow in the model near those wells, which we will discuss in detail later. In the case of KS-02, the temperature is also 15 – 20°C hotter than expected.

This difference can be explained in part by the choice of a higher surface temperature in the model compared to measured values. The surface water temperature in the model was set to be 8°C, which is higher than the value of 2.5°C measured in KS-02. This value was chosen to be within the temperature range for the equation of state ECO2N, which is accurate down to 3.5°C (Pan et al., 2014). A decision was thus to set the surface temperature slightly higher than the value indicated by measurements since a 5°C discrepancy is less relevant at the depth of the storage reservoir, where the temperature is thought to be up to 100°C. This was judged to be an acceptable compromise to avoid computational issues arising from hitting the minimum temperature of 3.5°C.

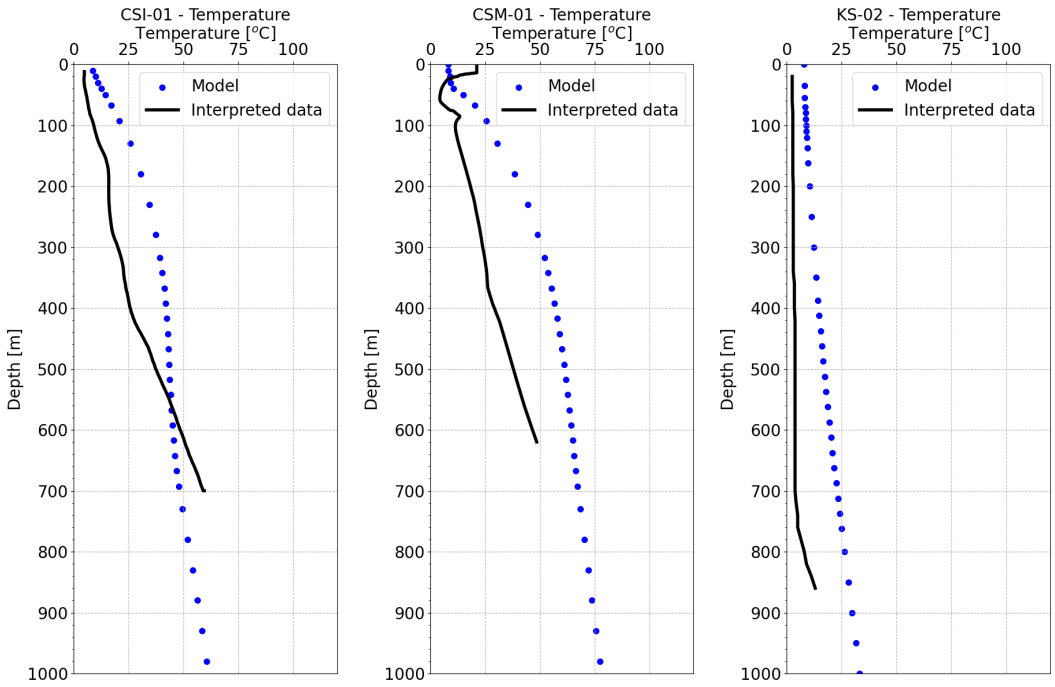

Figure 7.1: Comparison between measured and simulated temperature values for three wells. Two of the wells, CSI-01 (a) and CSM-01 (b), are near Straumsvík, while KS-02 (c) is in Kaldársel. The interpreted data curves are based on several different temperature measurements in the wells.

The simulated distribution of temperature in the natural state model is shown in Figures 7.5 and 7.2. We see that, in general, the temperature increases with depth over the entire region. However, there is a zone of higher temperature centered near Straumsvík, which stretches to the Southwest. This zone of higher relative temperature helps explain the large temperature difference between the wells close to the coast of Straumsvík and the wells further inland, near Kaldársel. This temperature structure is also responsible for the misfit, between the measured and simulated temperature values, at 300 m in CSI-01 and CSM-01, seen in Figure 7.1. The temperature increase is, in part, explained by the influence of the saltwater-freshwater interface between the freshwater and saline water found at the same location. The interface drives heat from depth up towards the surface. The location of this interface near Straumsvík remains uncertain, and it is expected that as more data is gathered on the salinity distribution around Straumsvík, as well as temperature, the location of this temperature structure will be better constrained.

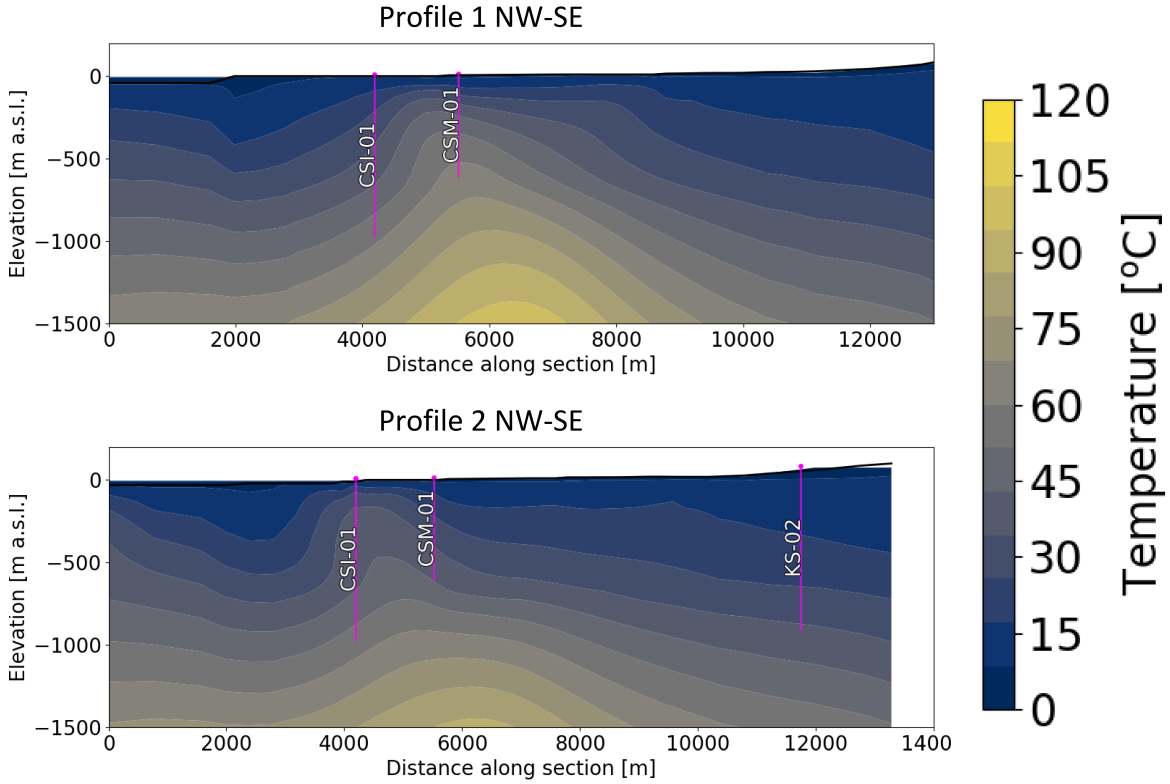

Figure 7.2: Two NW-SE cross sections of the model area, showing the temperature distribution in the natural state. The aerial extents of the cross-sections are shown in Figure 4.1.

The measured pressure in three wells in the region can be seen in Figure 7.3. The reservoir exhibits a hydrostatic pressure curve down to 1000 m. This is consistent with the conceptual model detailed in Chapter 5, i.e. that we assume that there are no explicit aquitards in the reservoir. This means that fluid in the subsurface remains in pressure contact with the surface over the entire model area. This hydrostatic regime can also be seen in Figures 7.5 and 7.4. From the figures it can also be seen that the pressure increases inland. Since the surface of the model was chosen to align with the water level surface, this simply means that the water level rises with distance from the coast. This fits with water level data from the area (Myer et al., 2024).

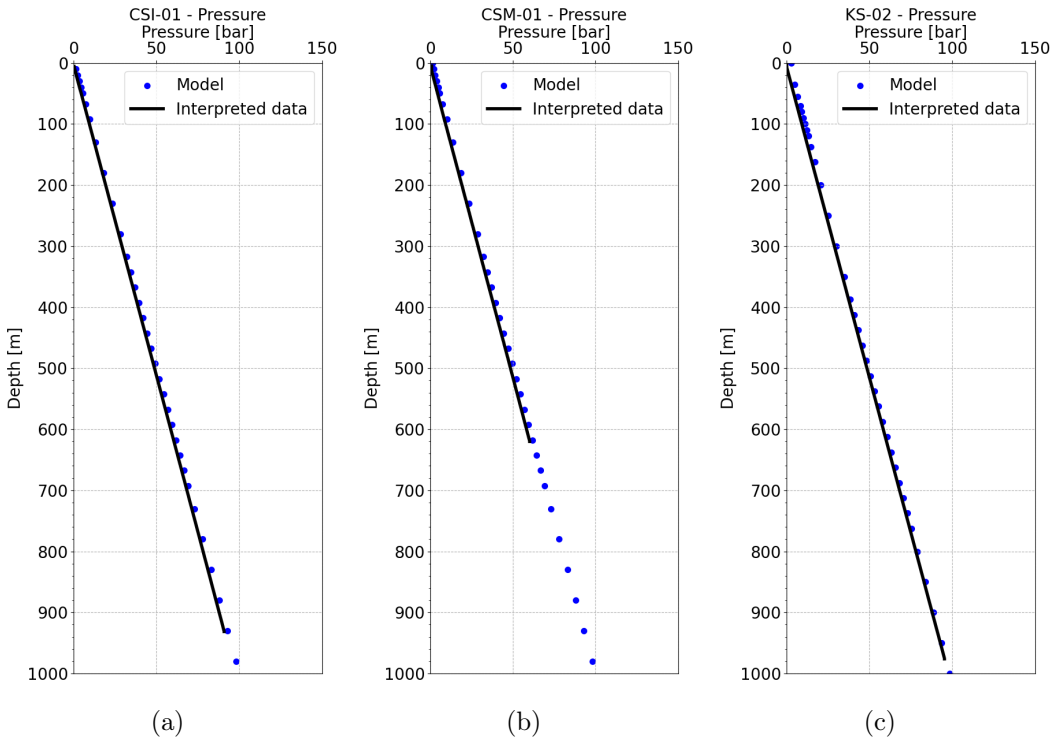

Figure 7.3: Comparison between measured and modelled pressure for three wells. Two of the wells, CSI-01 (a) and CSM-01 (b), are near Straumsvík, while KS-02 (c) is in Kaldársel.

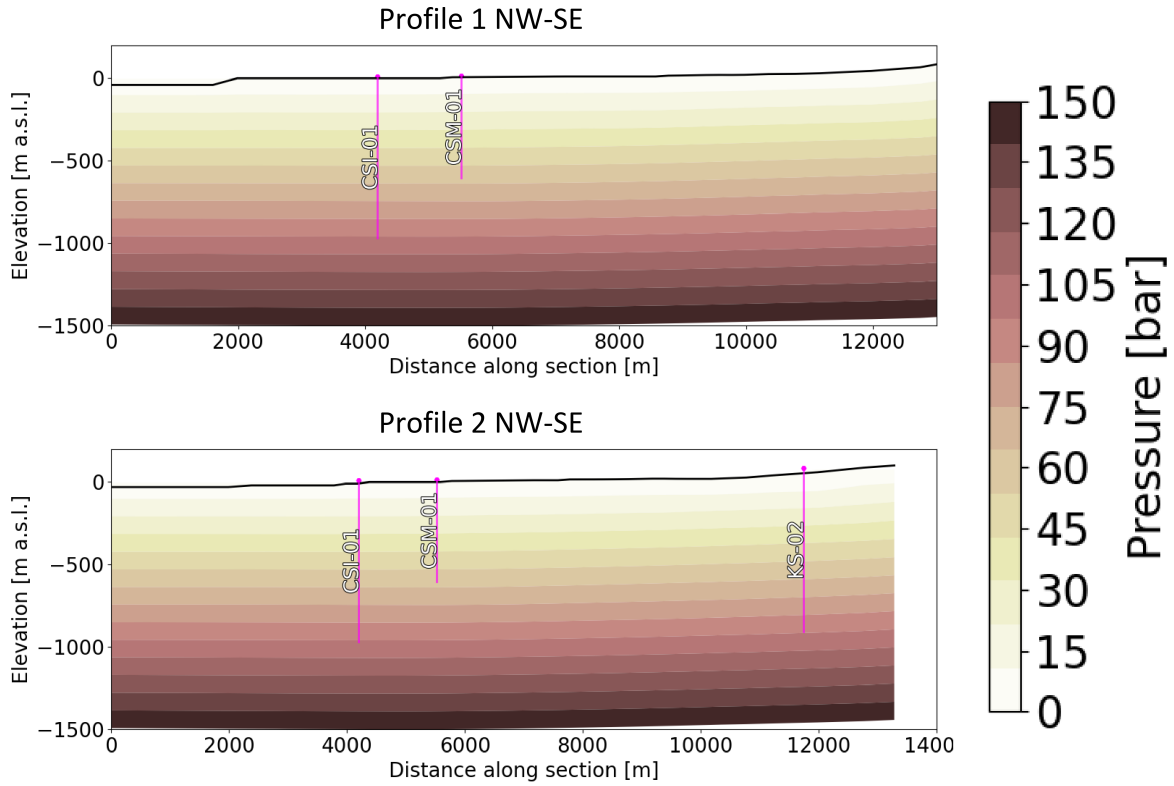

Figure 7.4: Two NW-SE cross sections of the model area, showing the pressure distribution in the natural state. The aerial extents of the cross-sections are shown in Figure 4.1.

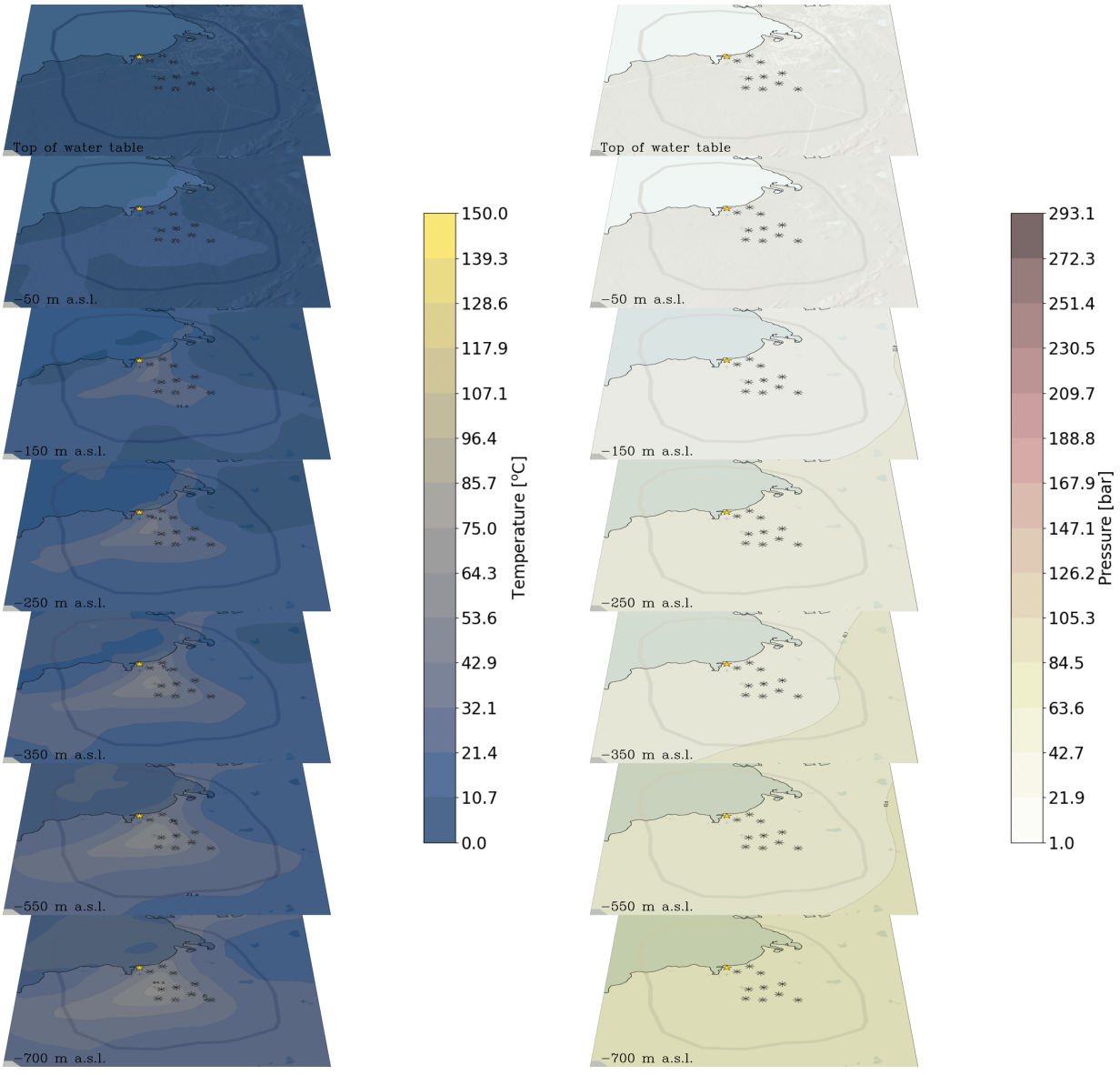

(a) (b)

Figure 7.5: Distribution of temperature (a) and pressure (b) in the natural state model at several different depths.

The correlation between the distribution of salinity in the natural model and measured data can be seen in Figure 7.6. Note that the interpreted data shown has been constructed from measurements performed in the wells, see Chapter 4. The measurements show that the thickness of the freshwater lens increases with distance from the shore, and there is no saline water near Kaldársel. The natural state model simulates this behaviour in all three wells. For both CSI-01 and CSM-01 the depth of the measured saltwater-freshwater interface corresponds to the depth in the model where salinity is greater than 5‰. However, for both CSI-01 and CSM-01 the simulated saltwater-freshwater interface layer is too thick. This is evident in that salinity starts increasing at a very shallow depth, where there should only be fresh water, and doesn't reach full salinity until a depth greater than one expected by the measured data. This is explained, in part, by the choice of grid for the model.

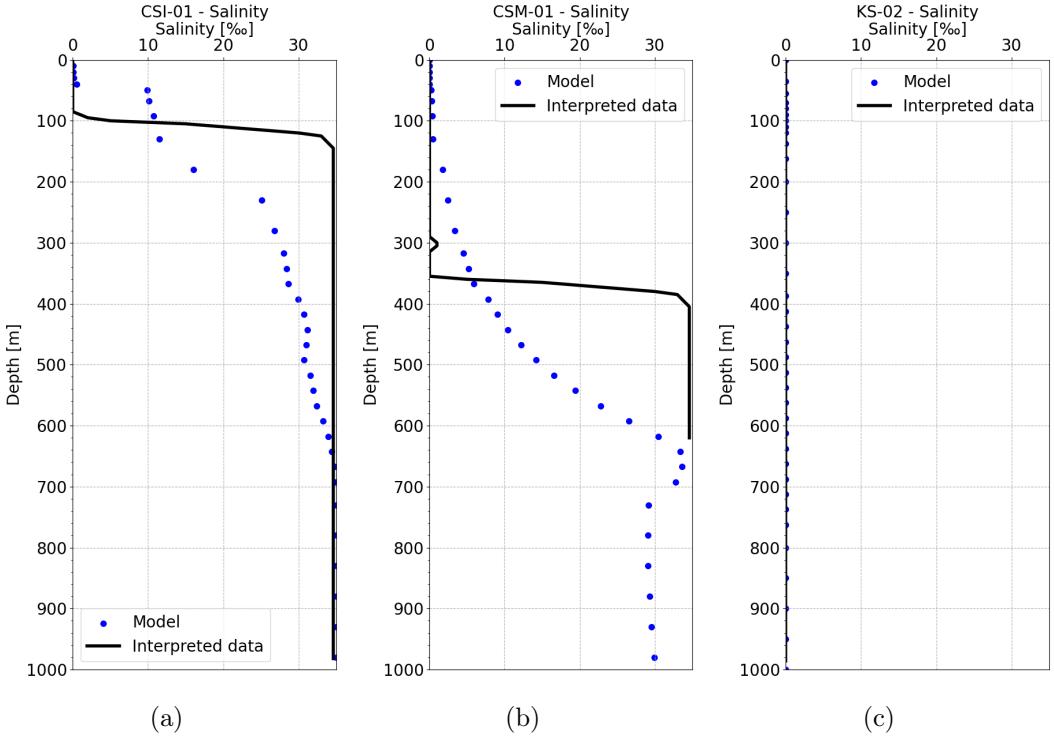

Figure 7.6: Comparison between measured and modelled salinity for three wells. Two of the wells, CSI-01 (a) and CSM-01 (b), are near Straumsvík, while KS-02 (c) is in Kaldársel. The interpreted data curves are based on several different salinity measurements in the wells.

Errors arising from numerical approximations in non-linear solute transport equation can behave like additional dispersion when treating solute transport, a phenomena known as numerical dispersion. This is an important consideration when simulating coastal regions with saltwater intrusions since these models depend on the simulation of the solute transport of salt in water. The shape and thickness of the saltwater-freshwater interface is heavily dependent on dispersion. Numerical dispersion leads to under- and overestimation of the simulated amount of salinity on both sides of the interface, effectively "smoothing" out the sharp boundary between fresh and saline water. The effects of numerical dispersion in a model are dependent on the size of the longitudinal dispersivity in the system. In general the longitudinal dispersivity for coastal reservoirs, especially for vertical flow, is on the order of meters. This means that, in order to minimize the effects of numerical dispersion in such systems, the thickness of model blocks should at most be a 1 – 10 m. (Oude Essink, 2001). Since the purpose of the current

model is to simulate the effects on CO_2 injection into the storage reservoir, which reaches down to -1200 m a.s.l., the choice was made to extend the reservoir down into the theoretical, relatively impermeable, basement formations in the region. This was done in order to eliminate the possibility of any CO_2 charged water flow being influenced by the bottom boundary. This means that in order to be able to simulate the system in acceptable computational time the thickness of the layers in the top of the reservoir had to be larger than 10 m. This results in increased uncertainty in the simulation of the saltwater-freshwater interface due to numerical dispersion, as can be clearly seen in Figures 7.6. However, the need to accurately simulate the effects of CO_2 injection was deemed important enough to sacrifice model fidelity in regards to the saltwater-freshwater interface.

The distribution of salinity in the reservoir can be seen in Figures 7.7 and 7.8. From the figures we can see that fully saline water intrudes further inland as we go deeper into the subsurface. At the surface we see that the groundwater around the Straumsvík bay is not saline water, even under the ocean. This can be explained by the high outflow in the area, and fits with observed behaviour in the region (Friðleifsson, 1989). We also see that the saline intrusion inland is more pronounced to the west and south-west, with only minimum saline intrusion visible towards Reykjavik. This is consistent with the theory that Straumsvík is situated at the transition between a coastal regime, which dominates on the Reykjanes peninsula, and a more continental regime, such as the one found near Reykjavík (Vilhjálmsson et al., 2023). A steep decline in salinity a few kilometres inland can also be seen from the figures. This steep decline is consistent with the results of the TEM/μTEM measurement campaign, which showed that the thickness of the freshwater lens increased very rapidly near CSM-01. The natural state model adequately simulates the salinity distribution in Straumsvík compared to available data.

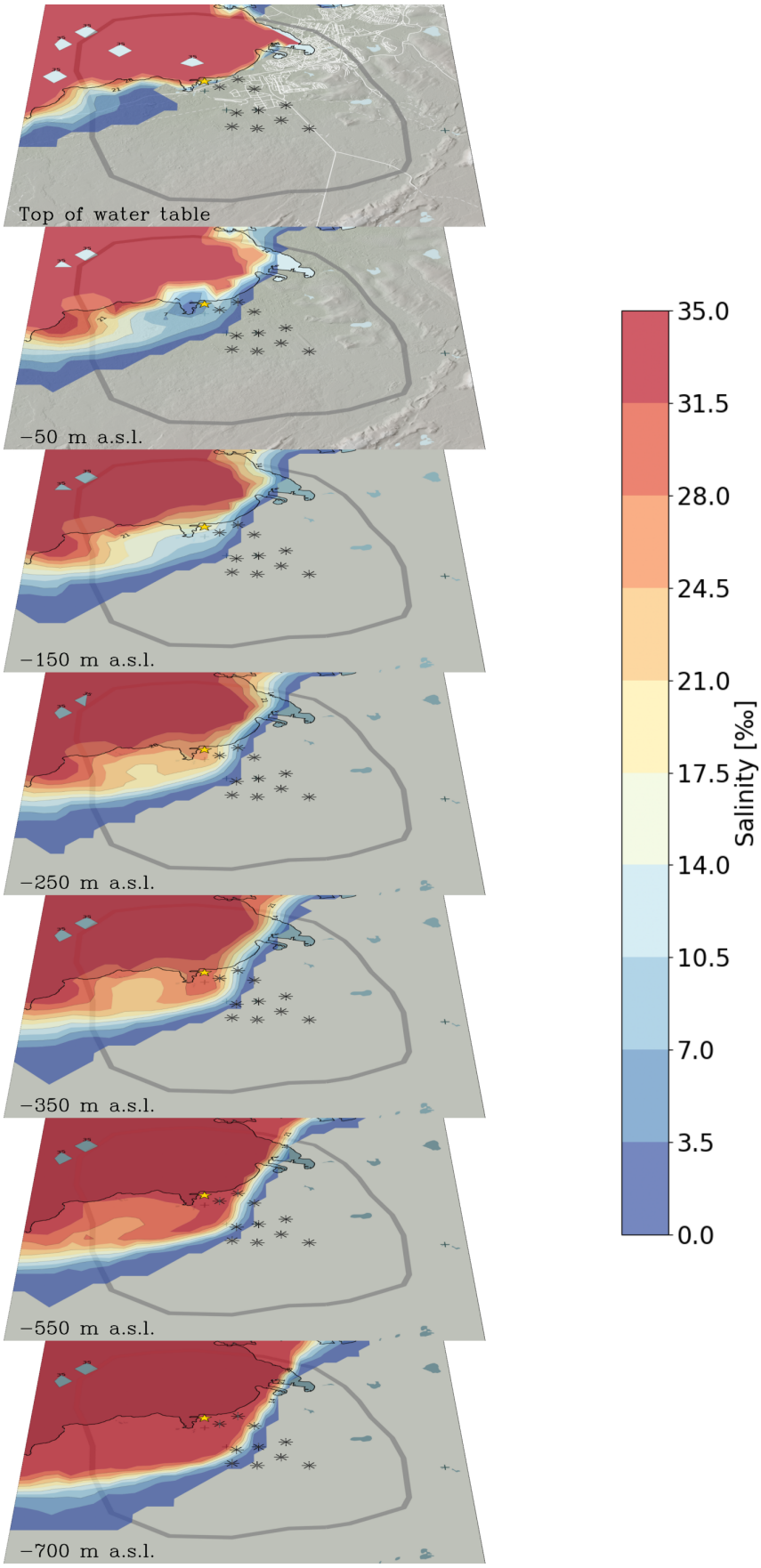

Figure 7.7: Distribution of salinity in the natural state model at several different depths. Uncolored areas represent freshwater (no salinity present).

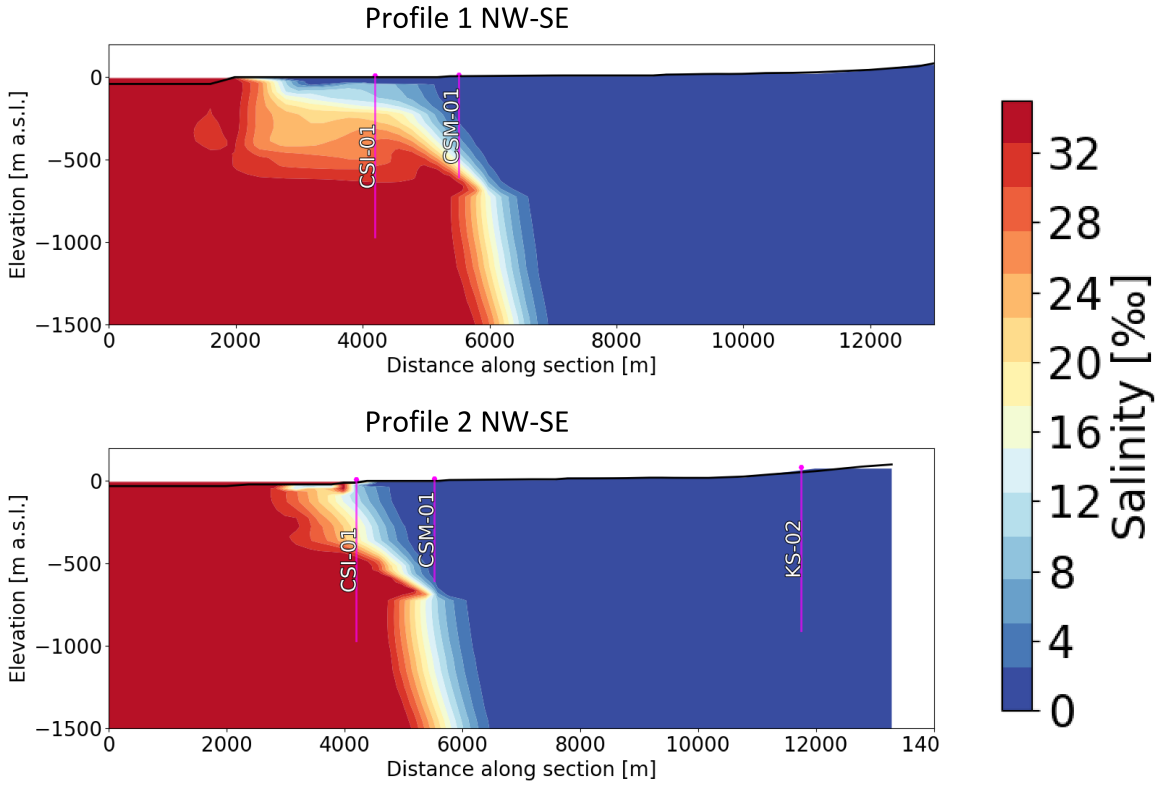

Figure 7.8: Two NW-SE cross sections of the model area, showing the salinity distribution in the natural state. The aerial extents of the cross-sections are shown in Figure 4.1.

7.2 Local and regional mass flow

It has been estimated that the outflow in Straumsvík is the second largest freshwater outflow in Iceland (F. Sigurðsson, 1998). The total outflow of freshwater into Straumsvík alone has been estimated to be around $5 - 10$ m^3/s near the surface, with freshwater outflow decreasing, but still remaining high, along the coast to the east and west. One of the goals of the natural state model is to recreate this flow regime and to estimate the size and direction of the flow in the subsurface. Figure 7.9 shows an outline of the flow at the surface of the natural state model, in the shallow groundwater flow in the region. We see that the largest part of the flow goes through the area of interest around the proposed well pad sites, and flows out into the sea near Straumsvík. This is consistent with estimates that the flow of fresh water in the area tends to follow the Holocene lava, see e.g. F. Sigurðsson, 1976.

Figure 7.10 shows the flow in the storage reservoir. Unlike in the shallow groundwater, the flow is more spread out in the region. Flow can be seen coming in from the sea, which drives the saline intrusion in the area. Note that the flow in the storage reservoir is slower than in the groundwater.

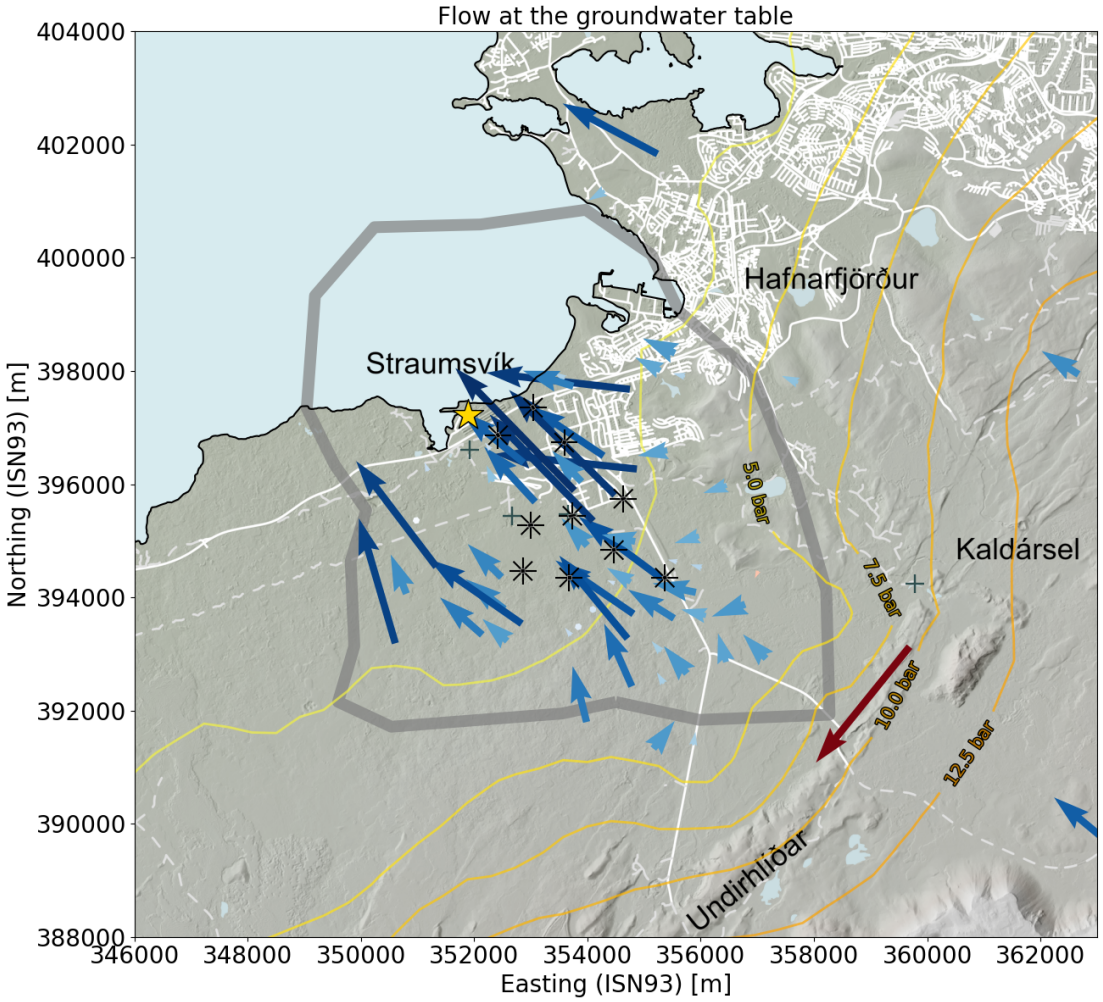

Figure 7.9: Schematic of the estimated surface fresh water flow in the natural state model. Arrows are scaled relative to other flows at the same depth, with longer, and brighter, arrows denoting larger flows. Blue arrows show flow along the prevailing groundwater current direction, from land towards the sea. Red arrows show flow against this current.

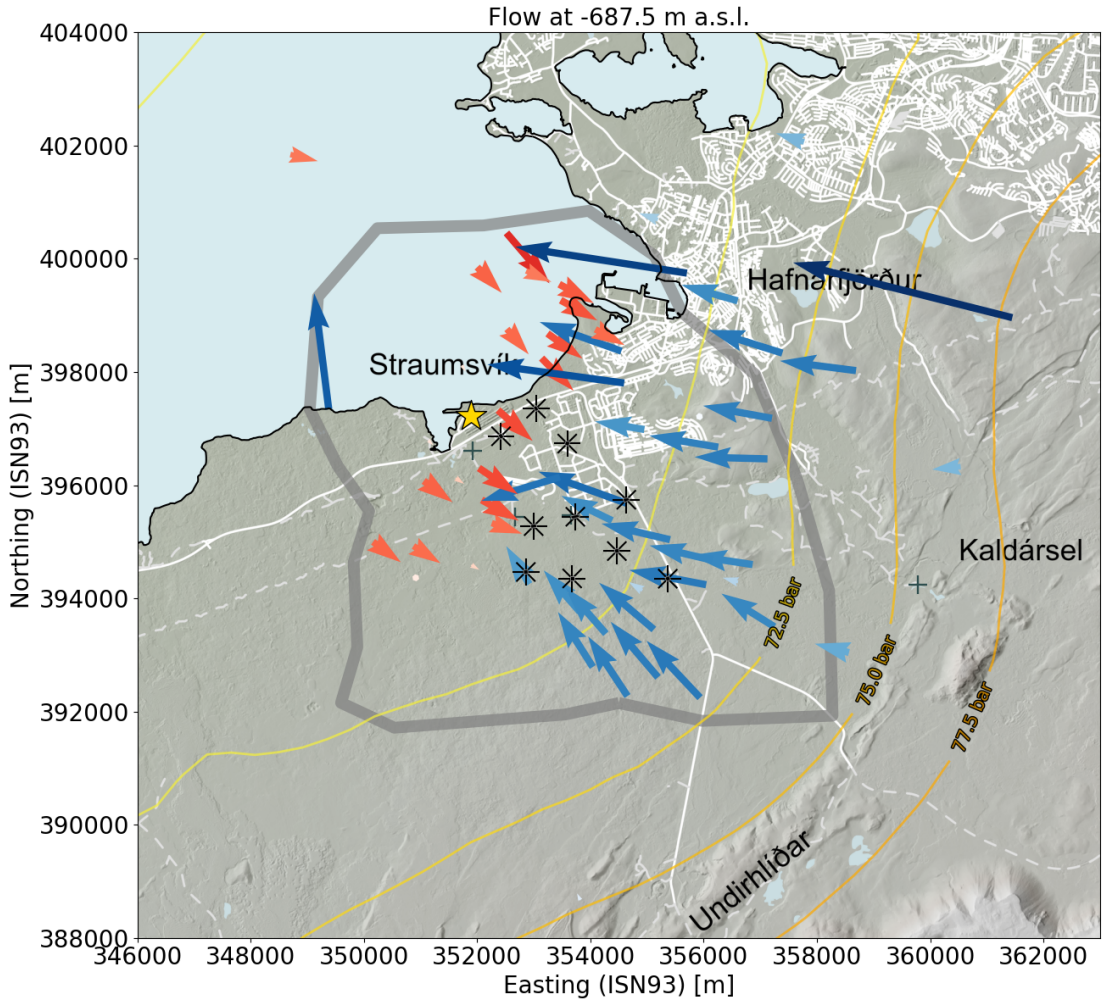

Figure 7.10: Schematic of the estimated storage reservoir fluid flow in the natural state model. Arrows are scaled relative to other flows at the same depth, with longer, and darker, arrows denoting larger flows. Blue arrows show flow along the prevailing groundwater current direction, from land towards the sea. Red arrows show flow against this current.

7.3 Density of water, CO_2, and salinity

Density plays a key role in CO_2 sequestration in the form of solubility trapping. Since CO_2 charged water is denser, and thus heavier, than water without dissolved CO_2, it tends to sink when injected into a reservoir. In fresh water reservoirs, the density of the resident water is mainly controlled by temperature and pressure. In coastal regions like Straumsvík, however, the presence of salinity has a large impact on the density of the reservoir water. As discussed in Chapter 4, saline water is much denser than fresh water at the same temperature and pressure, and thus will generally underlie fresh water in coastal aquifers. This means that injection sites must be carefully chosen, with respect to temperature, pressure and salinity. A series of one-block models were created, using TOUGHREACT and ECO2N, in order to estimate the densities in the storage reservoir and the injected water at different temperature, pressure, salinity and CO_2 content.

For the Coda terminal project the plan is to inject dissolved CO_2 into the fresh water part of the storage reservoir in the first three phases, and only inject into the saline water part of the reservoir in the last phase. The injection depth of the dissolved CO_2 into the storage reservoir is expected to be between -300 and -600 m a.s.l. Measurements in the Straumsvík area, along with the natural state model, show that the reservoir there is at a temperature of around 20 – 50°C. At this temperature range the fresh water storage reservoir has an estimated fluid density of 992 – 1000 kg/m^3, while the saline water storage reservoir has an estimated fluid density of 1012 – 1024 kg/m^3 (Figure 7.11). The distribution of salinity in the natural state model (Figure 7.7) shows that at those depths only three well pads are inside the saline water part of the reservoir. One of those pads is on the edge of the saltwater-freshwater interface, with a salinity content of less than 2.5 ‰. At this salinity the resident storage reservoir water has the same density range as the fresh water.

Figure 7.11 also shows the expected change in water density with the inclusion of dissolved CO_2. The estimated density change of the CO_2 charged water that will be injected compared to the fluid in the fresh water storage reservoir is around 4.8 – 5.0 kg/m^3. For the injection into the saline water storage reservoir this density change is 4.4 – 4.6 kg/m^3. The density change due to dissolved CO_2 at reservoir temperatures is between 5.6 – 6.6 kg/m^3 for the fresh water, and between 5.2 – 6.2 kg/m^2 in saline water. So the injected water is denser than the resident water in the storage reservoir at all temperatures. Thus, in the absence of pressure differential with density as the controlling factor in reservoir flow, solubility trapping will be achieved, even after the injected water has been heated up to reservoir temperatures.

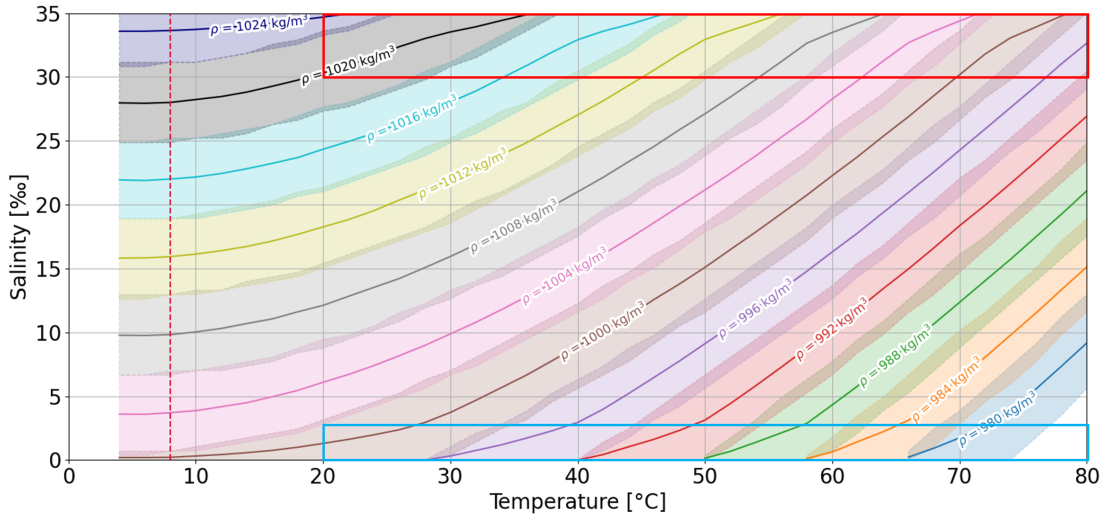

(a)

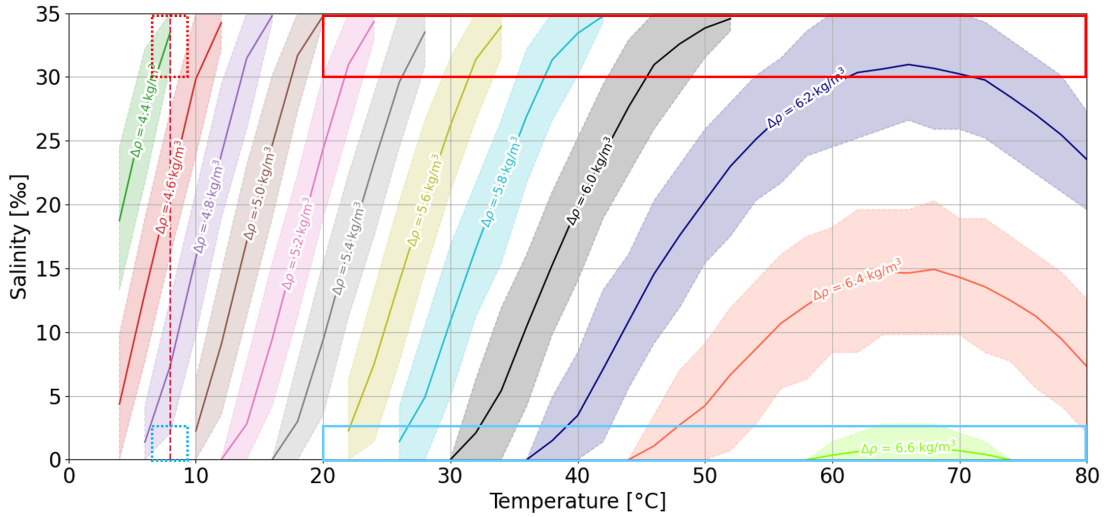

(b)

Figure 7.11: The evolution of water density with salinity and temperature (a) with no CO_2 present and (b) change at 3% CO_2 content. The shaded areas show the temperature and salinity ranges where the water has the specific density (change) values for all pressures (where water is still liquid). Only areas for the specified density values are shown, other density values will lie between these curves. The red line shows the estimated injection temperature of 8°C. The blue box shows the expected range of the fresh water storage reservoir, while the red box shows the range for the saline water storage reservoir. The dotted blue line box shows the expected range of fresh water injection and the dotted red line box shows the expected range of saline water injection

7.4 Summary

The natural state model manages to simulate the state of the reservoir to an adequate degree of certainty. This baseline should therefore allow for an estimation of the effects of CO_2 injection on the region. It should be stressed that while there exist many measurements of the shallow groundwater in the region, only a limited number of wells reach down into the depth of the proposed storage reservoir. The reservoir data from the site was determined from two research wells drilled by Carbfix and the exploration well KS-02. While Carbfix has performed several TEM and μTEM measurements to try to supplement the data from wells in the area, the distribution of salinity and the thickness of fresh water lens in the region remains uncertain. The upper groundwater, or freshwater, part of the system is thus fairly well constrained at the site, while the sparseness of data for the deeper parts of the reservoir serves to increase the uncertainty of the calibration of the deeper parts of the natural state model. However, we expect that this uncertainty will decrease with time, as more deep wells are drilled in the area.

8 Impact Assessment

In order to assess the impact of the injection on the subsurface near Straumsvík a forecast reservoir model was developed using the numerical model described in Chapter 6. Using the results of the natural state model detailed in Chapter 7 as initial conditions, this forecast model was run with CO_2 injection over a duration of 30 years. After this 30 years of injection/production, a 100 year post-closure period was also simulated at the site.

8.1 Operational scenarios

The injection scenario for the Coda terminal project consists of four successive scale-up phases, starting from 700 kt of CO_2 per year in 2027 up to 3 Mt of CO_2 per year in 2032 (Figure 8.1). An 18 month period between scale-up steps has been assumed. The target storage reservoir for phases one through three is a fresh water reservoir located to the southeast of the Straumsvík harbour. The fourth phase targets a saline water reservoir and saline water, rather than fresh water, will be used as the injection fluid in this phase (Figure 8.2). The scale-up strategy, injected CO_2 mass, and water requirements for the phases are summarised in table 8.1. During the closure of the site, injection of water with no CO_2 added to the stream is planned for one year. The flowrate represents 10 % of the water injected annually during phase 4 and is used to provide a pressure gradient for the CO_2 injected prior to the start of the closure period, and to support the mixing and transport of this CO_2 into the storage reservoir. This also serves to mitigate the risk of accumulation of CO_2 in the immediate vicinity of the injection wells.

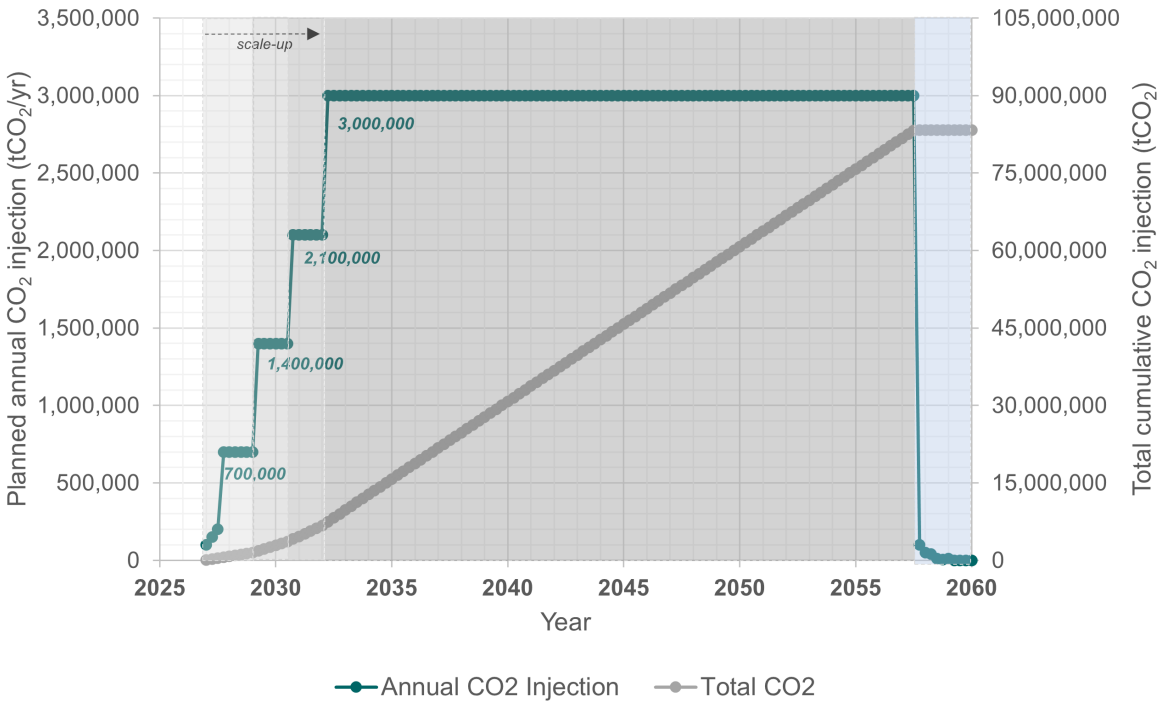

Figure 8.1: Planned CO_2 injection strategy for the Coda Terminal project.

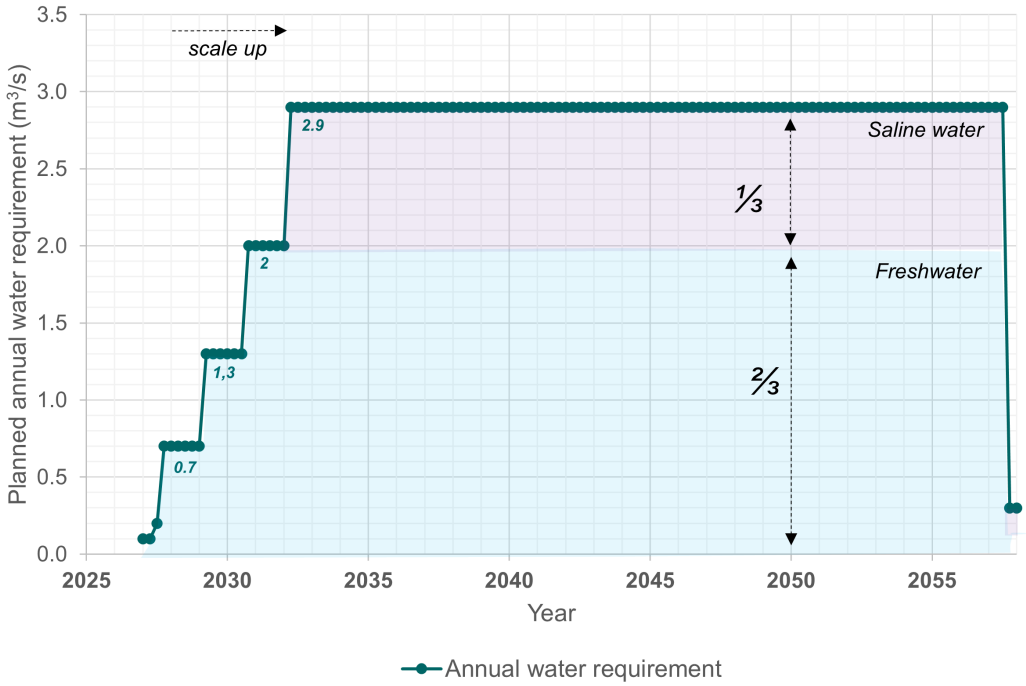

Figure 8.2: Water Requirements for the CO_2 injection for the Coda terminal project.

Table 8.1: The scale-up strategy for the Coda Terminal

	Start Date	Injection Capacity		Water Requirement		Number of
		$ktCO_2/yr$	$kgCO_2/s$	m^3/yr	l/s	Pads in Use
Phase 1	2027	700	22	21,000,000	670	3
Phase 2	2029	1,400	44	42,000,000	1,350	6
Phase 3	2030	2,100	67	63,000,000	2,000	7
Phase 4	2032	3,000	95	92,250,000	2,900	10

8.1.1 Injection and production wells

A series of injection and production wells are planned in Straumsvík as a part of the Coda Terminal, as well as multiple monitoring wells. The injection wells will handle the injection of the CO_2 and water into the storage reservoir, using water from production wells. Both injection and production wells will be situated at ten different well pad locations, with a fixed number of injection and production wells planned at each well pad. The placement of the well pads is shown in Figure 8.3. The plan for the injection wells in the area is as follows:

- Up to eight injection wells per well pad, with:
  - Phase 1: up to 24 injection wells from three well pads
  - Phase 2: up to 48 injection wells from six well pads
  - Phase 3: up to 56 injection wells from seven well pads
  - Phase 4: up to 80 injection wells from ten well pads

Wells are expected to be drilled down to 800 – 1000 m and cased down to 250 – 350 m, or to the depth of proposed the storage reservoir. The injection wells are expected to be directionally drilled away from the well pads, as can be seen in Figure 8.3.

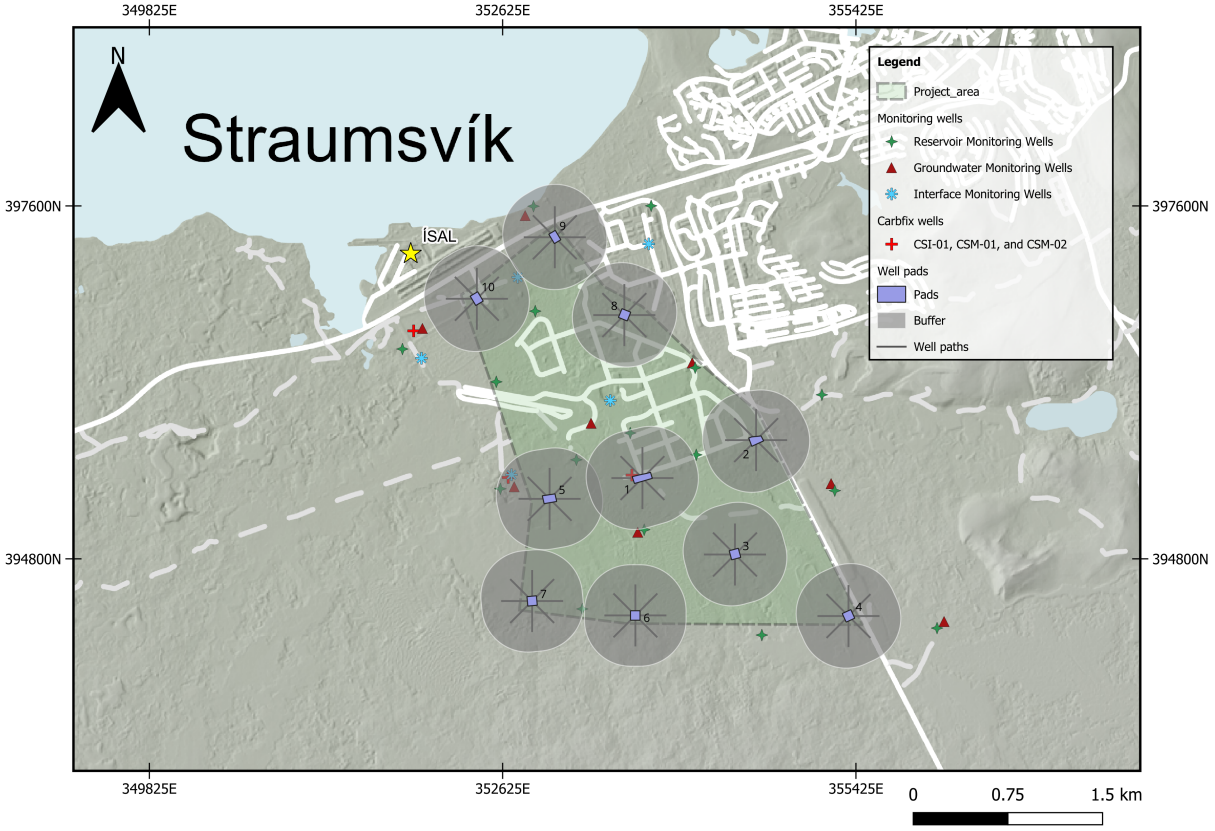

Figure 8.3: The Coda terminal storage complex. Proposed well pads and the surface footprint is shown.

Water production in the project is planned to be from the shallow groundwater for phases one to three. This water production will provide the required water for the injection process, in which CO_2 is dissolved in the extracted water during injection. It is estimated that up to

Table 8.2: Modelled feedzones for future injection (CSI) and production (CSW) wells in Straumsvík.

Wells	Feedzones depth [m a.s.l.]	Contribution
CSI wells	-350, -400, -600	60%, 25%, 15%
CSW wells	-5, -15	50%, 50%

four water production wells per well pad will be needed in order to satisfy the water need of the CO_2 injection. The production wells are expected to be less than 50 m deep, with a very shallow casing. The water will consist of fresh water at a temperature of approximately 5 °C, and during phase three up to 2,000 l/s will be extracted from the production wells (Figure 8.2). During phase four, for wellpads eight, nine, and ten, the injection scenario assumes that saline water will be used as the fluid carrier for the CO_2. The water production wells in those well pads will therefore target shallow saline groundwater. Approximately 900 l/s of saline water will be used once the project is at full capacity, alongside 2,000 l/s of fresh water. The produced saline water represents a third of the total amount of water required for the project, thereby reducing the fresh water requirement of the project significantly. The possibility of using water from the storage reservoir compared to using water from the shallow groundwater is discussed at the end of the chapter.

8.1.2 Model assumptions

Simplifying assumptions were made in the forecast model when simulating the proposed injection/production in the Straumsvík area. One such assumption is that the injected CO_2 will be fully dissolved prior to entry into the reservoir. Dissolution of CO_2 can occur either on the surface or in the wellbore. When it is dissolved in the wellbore gaseous CO_2 is pumped into the well alongside water, where it mixes and dissolves into the water. In both cases, i.e. dissolution at the surface or in the wellbore, the CO_2 exiting out of the wellbore should be in a fully dissolved state. A constant water/CO_2 ratio was set for all injections, with the ratio for saline water injection being slightly higher than for fresh water due to the slightly lower solubility of CO_2 in saline water. The ratios used were 30/1 for fresh water and 32.5/1 for saline water. In all cases an injection temperature of 8 °C was assumed.

Using the results of well testing in CSI-01 and CSM-01, detailed in Chapter 4, a conservative estimate of 50 kt of CO_2 per year per well was selected. This is approximately equivalent to an overall injection rate of 40 kg/s. This constant injection rate was assumed in the model for all injection wells over the entire duration of the project. Note that this represents a conservative value since testing in both wells showed they have an injectivity sufficient to support injection in excess of 70 kg/s. All simulated injection wells were assumed to have three feed-zones based on data from CSI-01 and CSM-01, which was detailed in Chapter 4. The modeled feed-zones for the injection wells and the distribution of injection fluid into each feed-zone is shown in table 8.2. All production and injection wells in the area were simulated in the forecast model as mass generators, with each well coming online following the scale-up strategy in table 8.1.

8.2 Simulation results

8.2.1 Key reservoir performance indicators

The Carbfix storage method involves injection of dissolved CO_2 into a subsurface storage reservoir. The dissolution of the CO_2 into water can take place either at the surface or in the injection

wellbore. The CO_2 is fully dissolved in the fluid prior to entering the reservoir to ensure that free phase CO_2 is not present and that the CO_2 migrates in a water-dissolved state through the storage reservoir. Furthermore, this allows the CO_2-charged water to interact immediately with the host rock in the storage reservoir. In the reservoir, the dissolved CO_2 lowers the pH of the reservoir fluid and promotes the release of divalent metal ions. This release of metal ions gradually increases pH and alkalinity in the reservoir fluid and, under the right conditions, allows the released ions to combine with the injected CO_2 to form stable carbonate minerals. These processes, along with the dilution of the CO_2-charged fluid in the storage reservoir fluid, reduce the bubble point pressure of CO_2 in the fluid and further contain the CO_2 in the storage site.

The bubble point pressure is the pressure at which bubbles of dissolved gas, in our case CO_2, can start forming in the fluid. It is a function of dissolved CO_2 content, temperature, and fluid chemistry (e.g. salinity and alkalinity):

$$P_{BubblePoint} = f(X_{CO_2}, T, X_{NaCl}) \tag{10}$$

where f is the Peng-Robinson equation of state for the solubility of gases and X_{CO_2}, T and X_{NaCl} are the mass fraction of CO_2, temperature and salinity in the subsurface respectively.

To ensure that no highly mobile free phase CO_2 is present in the storage reservoir during and after the operations at the Coda Terminal, the CO_2-charged fluid must be injected deep enough in the storage reservoir to ensure that the ambient reservoir pressure, P, in the injection area is substantially higher than the bubble point pressure of the fluid, $P_{BubblePoint}$. The difference between these two values represented as an indicator of solubility trapping in the reservoir, i.e.

$$\text{Solubility Trapping} = P_{BubblePoint} - P \tag{11}$$

Effective solubility trapping of CO_2 in the storage reservoir is therefore achieved when

$$\text{Solubility Trapping} < 0 \tag{12}$$

The reservoir model simulates non-reactive transport of the injected CO_2-charged fluid through the reservoir (Chapter 6) and focuses on CO_2 migration and fluid phase changes. It thus predicts the potential impact that dissolved CO_2 injection can have on the system, for a theoretical scenario where no other water-rock interactions (including basalt dissolution, alkalinity increase, or CO_2 mineralization) occur. This is a conservative scenario in terms of CO_2 containment, as water-rock-CO_2 reactions further lower the pressure required to keep the CO_2 dissolved in the reservoir fluid.

To predict the behavior of the injected CO_2, the reservoir response, and the efficiency of the trapping mechanism the following metrics are used:

- The CO_2 mass fraction (kg_{CO_2}/kg_{H_2O}), which show the migration and maximum extent of the dissolved CO_2 in the storage reservoir. This also shows the mixing and dilution of the injected CO_2 in the storage complex.
- The effectiveness of the solubility trapping in the reservoir, as described by the difference between the calculated bubble point pressure of CO_2 and estimated reservoir pressure (Equation 11). The reservoir pressure should be at least 5 bars higher than the bubble point pressure to ensure solubility trapping.
- The temperature, pressure, and salinity changes due to the CO_2 injection in the storage reservoir, including potential hydraulic interference between wells.

These metrics reflect the effectiveness and permanency of the proposed injection in Straumsvík.

8.2.2 Impact on the storage reservoir during scale up

The simulation results show that at the end of the scaleup, the extent of the dissolved CO_2 lies in the vicinity of wellpads one through seven (Figure 8.4). The results show that the average concentration in the storage reservoir reaches a maximum of 30 g/kg in the vicinity of the well pads. Bubble point pressure of CO_2 and reservoir conditions comply with solubility trapping requirements, and the solubility metric (Equation 11) is below -35 bar, indicating an extremely low risk of degassing. At the end of the scale-up phases, a limited amount of cooling is predicted around wellpads one, two, and three (Figure 8.5). An increase in reservoir pressure is forecast and appears in concentric circles around the active wellpads. A minor decrease in salinity is expected reflecting minor mixing of the injected freshwater in existing brackish water (Figure 8.6).

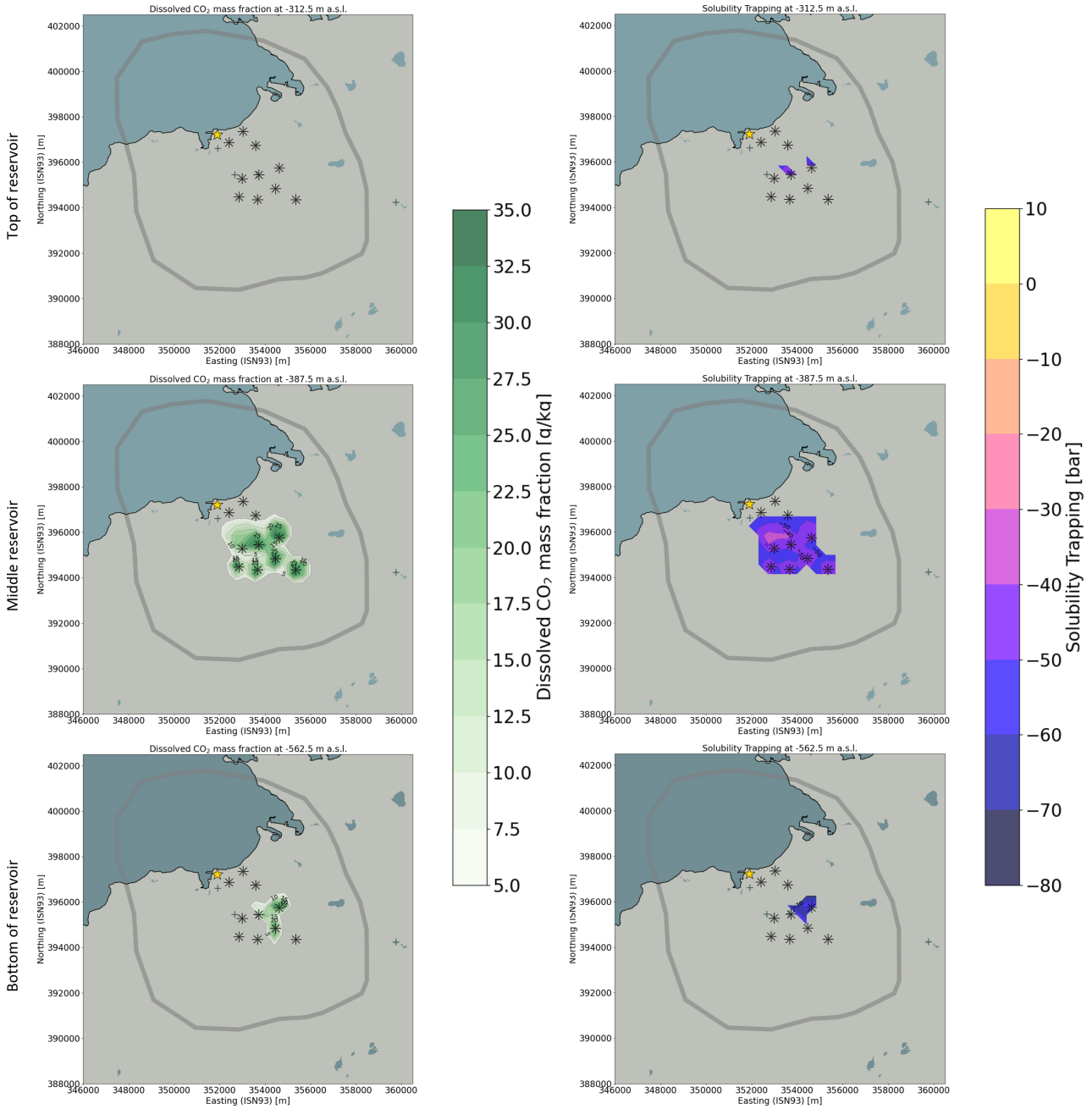

Figure 8.4: Aqueous CO_2 migration (left) and solubility trapping (right) within the storage reservoir at the end of the scale up. The results are shown 5 years after the start of injection.

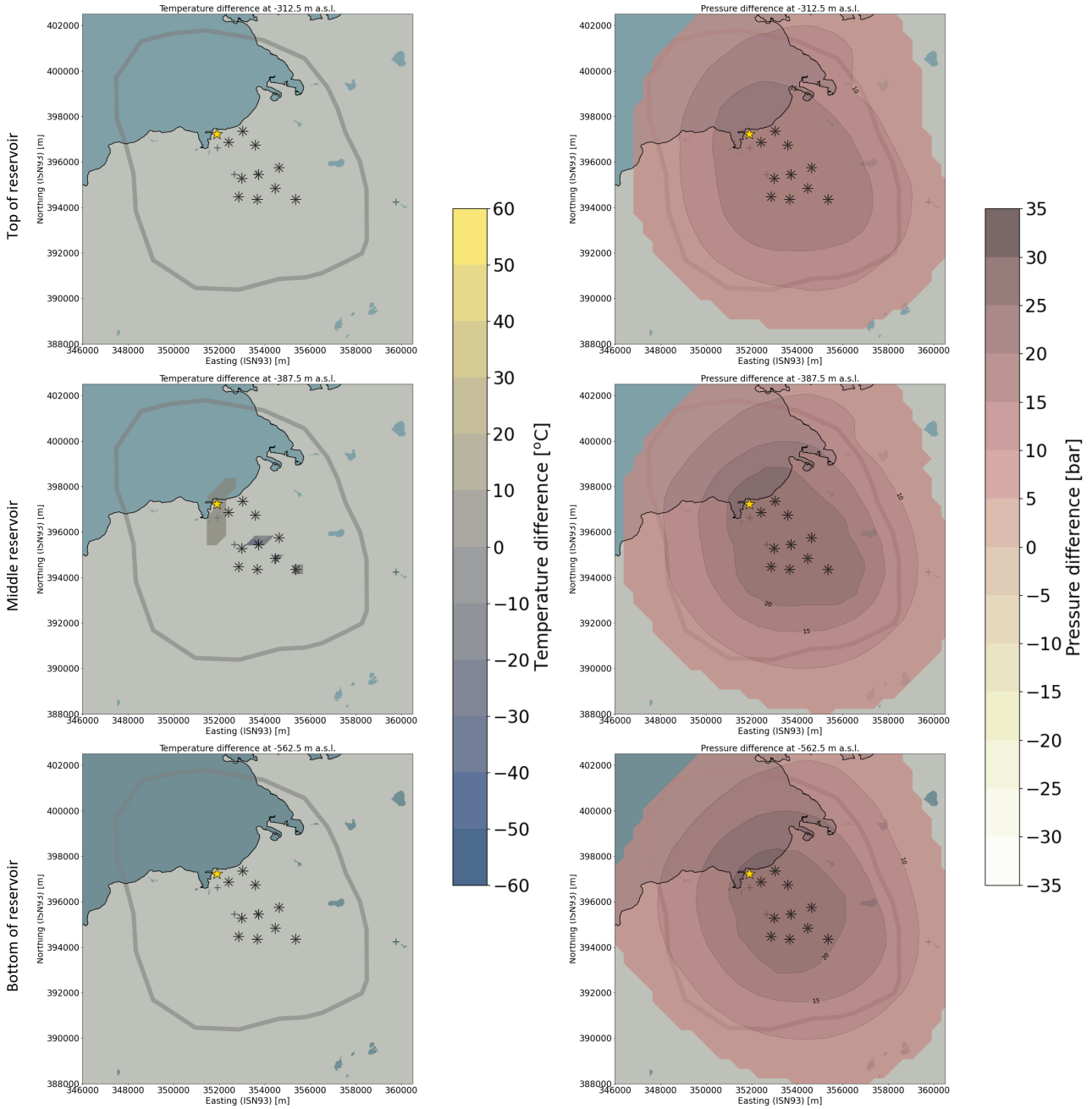

Figure 8.5: Change in temperature (left) and pressure (right) within the storage reservoir at the end of the scale up. The results are shown 5 years after the start of injection.

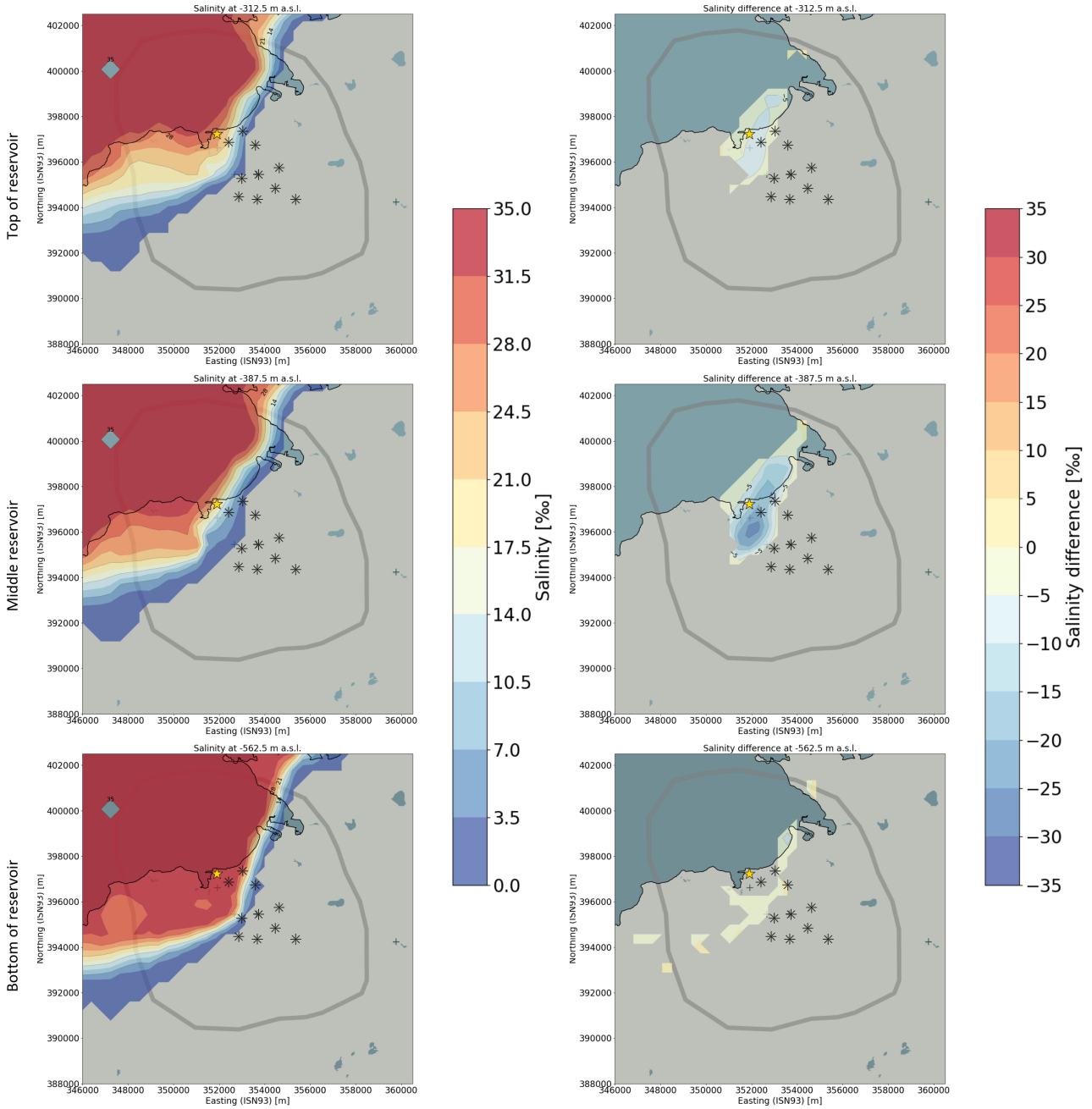

Figure 8.6: Salinity (left) and salinity difference (right) within the storage reservoir at the end of the scale up. The results are shown 5 years after the start of injection.

8.2.3 Impact on the storage reservoir at the end of the operations

The values presented in this chapter, including dissolved CO_2, temperature, pressure and salinity differences, represent the average values of the parameters in the storage reservoir, which lies between -300 and -1200 m a.s.l depth. For the solubility trapping the maximum values for the storage reservoir are presented. These results show the effects of the migration of CO_2 without mineralization and thus denote the maximum theoretical perturbation that injection of dissolved CO_2 could have on the region.

The simulation results show that after 30 years of continuous operations the extent of the dissolved CO_2 lies within the estimated extent of the storage complex (Figure 8.7). The results also show that the average concentration in the storage reservoir ranges from approximately 30 g/kg in the vicinity of the well pads down to < 5 g/kg two to three km away from the well pads. This indicates a gradual mixing or dilution of the injected CO_2-charged fluid with the resident reservoir fluid. The dissolved CO_2 extends radially from the injection well pads, with a slight bias towards the north and west. Simulation results also show that the dissolved CO_2 is expected to migrate to the north of Straumsvík, with the dissolved CO_2 residing several hundreds of meters below the bottom of the sea floor (Figure 8.10). The CO_2 in the storage reservoir remains in solution via solubility trapping everywhere within the storage reservoir as seen from Figure 8.8. Solubility trapping conditions remain largely below -20 bar in the storage reservoir highlighting that the model predicts no phase change and that dissolved CO_2 remains in solution at all times.

Finally Figures 8.9 and 8.10 show the evolution of the CO_2 migration and the solubility trapping in storage reservoir after 10, 20, and 30 years of injection. The simulation shows that the injected CO_2 preferentially flows laterally and the portion of the injected CO_2 that sinks deeper into the subsurface increases with time. A small portion rises above the injection well casing depth (indicated by a black dashed box in the Figure) due to the pressure increase in the storage reservoir in the vicinity of the injection wells. However, no CO_2 reaches the shallow groundwater. In addition, the solubility trapping is satisfied at all depths during the operational lifetime of the project.

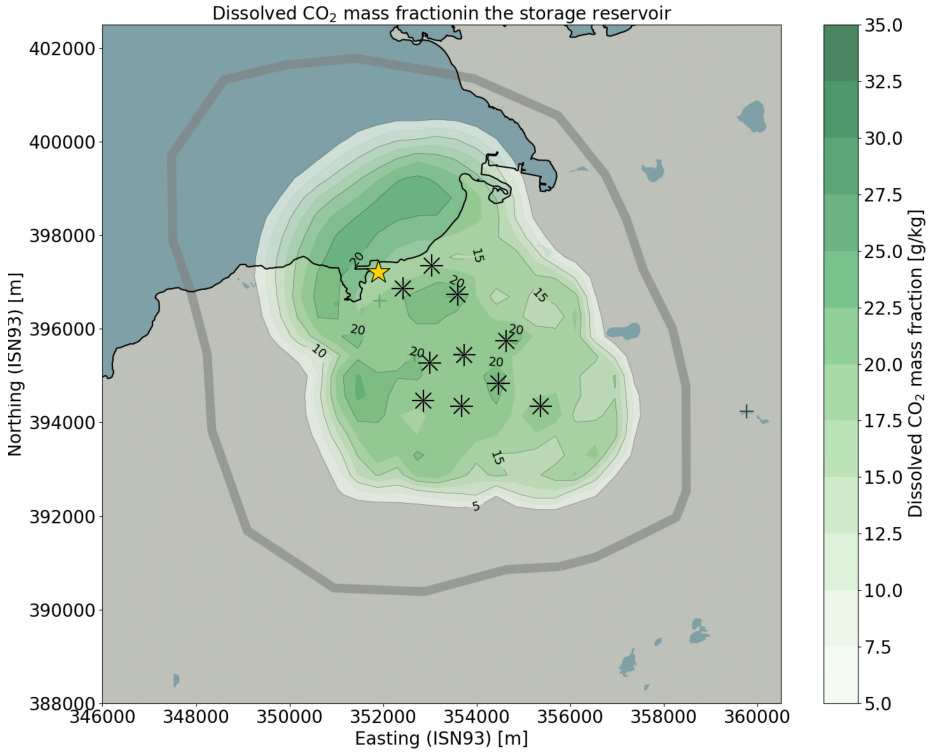

Figure 8.7: Average aqueous CO_2 migration in the storage reservoir after 30 years of injection. The grey line represents the boundary of the storage complex.

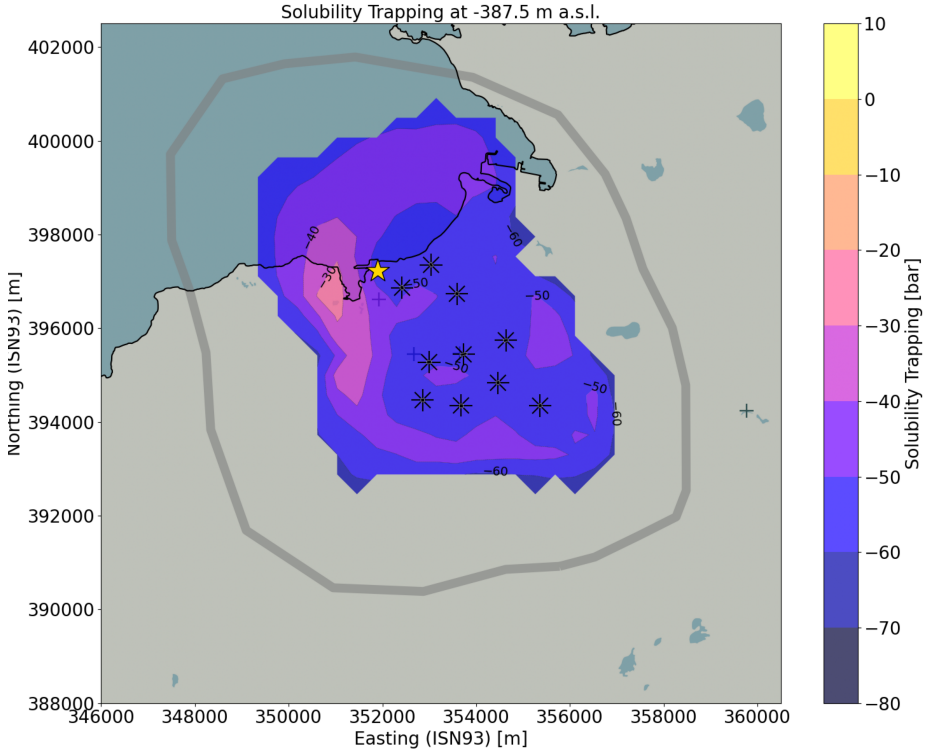

Figure 8.8: Maximum solubility trapping in the storage reservoir after 30 years of injection.

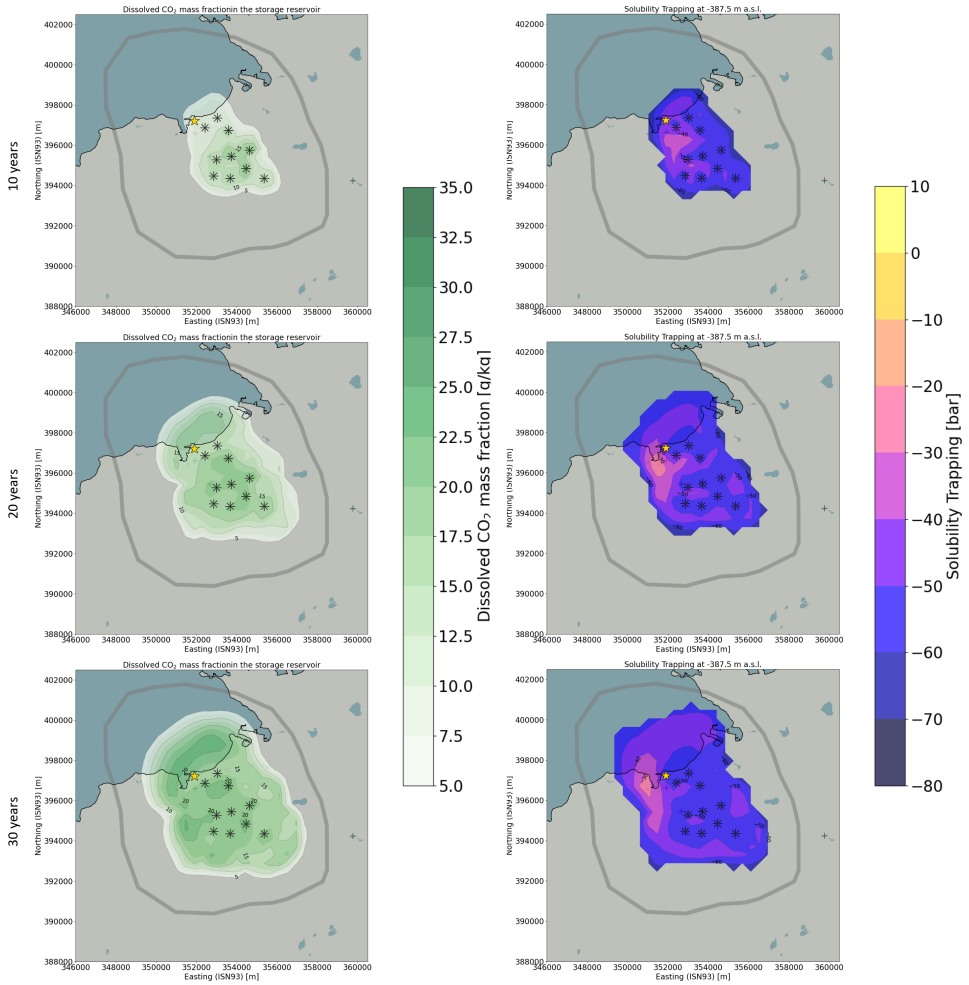

Figure 8.9: Average aqueous CO_2 migration and maximum solubility trapping in the storage reservoir after 10, 20, and 30 years of injection.

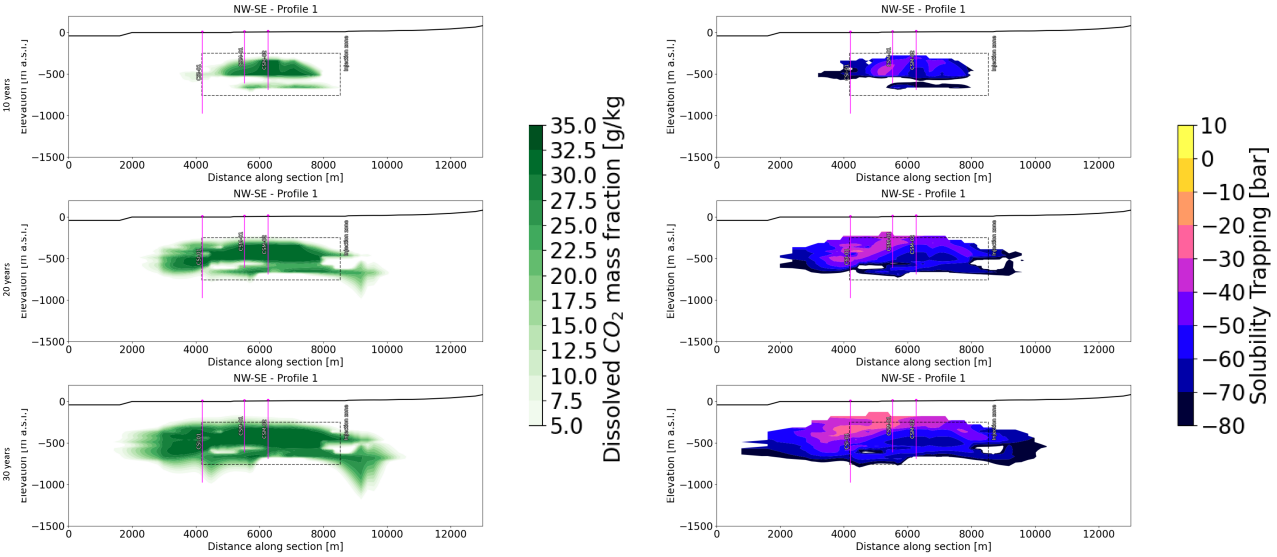

Figure 8.10: Cross-section of aqueous CO_2 migration and solubility trapping after 10, 20, and 30 years of injection.

The effect on the temperature and pressure in the reservoir is shown in Figures 8.11 and 8.12. The Figures show the average change of these two properties in the storage reservoir after 30 years of injection. There is a very minor temperature change in the storage reservoir, less than 20°C, fairly close to the injection wells. This is unsurprising, since the injected water, at 8°C, is much colder than 20 - 50°C temperature of the resident water in the storage reservoir. In contrast to the small temperature change, the pressure difference from the baseline has been estimated to be over 25 bar close to the injection wells. However, the model shows that this pressure increase does not translate into CO_2 injected water flowing up into the shallow groundwater. There is also no increase in pressure in the shallow groundwater. The cross-section of the temperature and pressure changes in the storage reservoir, Figure 8.14, further shows that the temperature decrease in the reservoir is largely localized near the injection wells and increases with time as more cold water is injected into the subsurface.

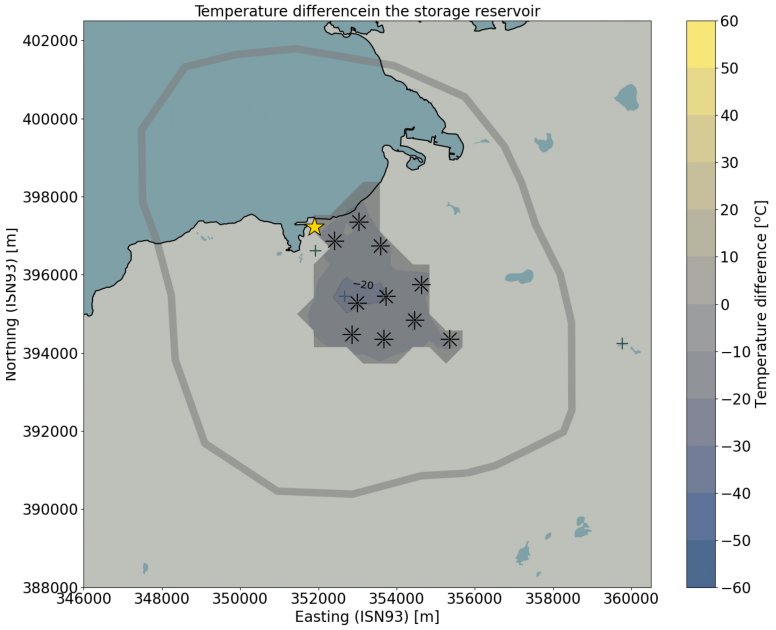

Figure 8.11: Average change in temperature in the storage reservoir after 30 years of injection.

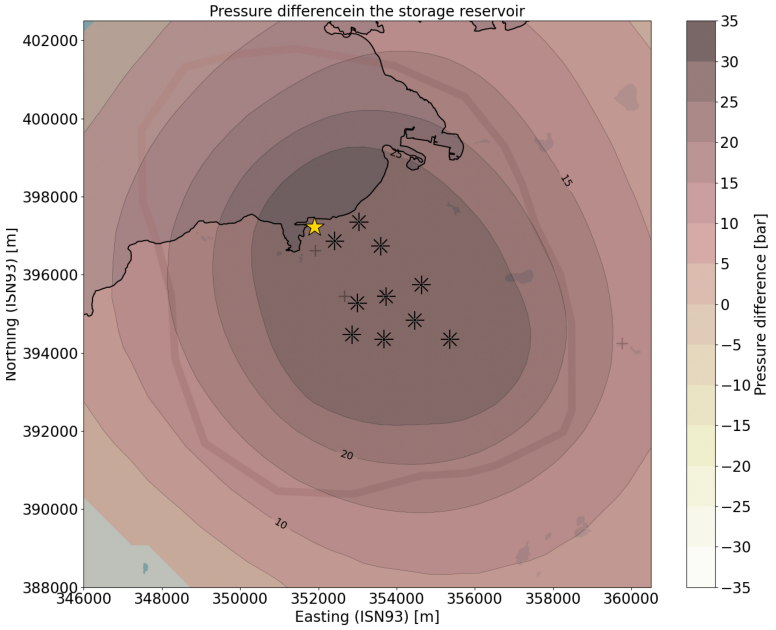

Figure 8.12: Average change in pressure in the storage reservoir after 30 years of injection.

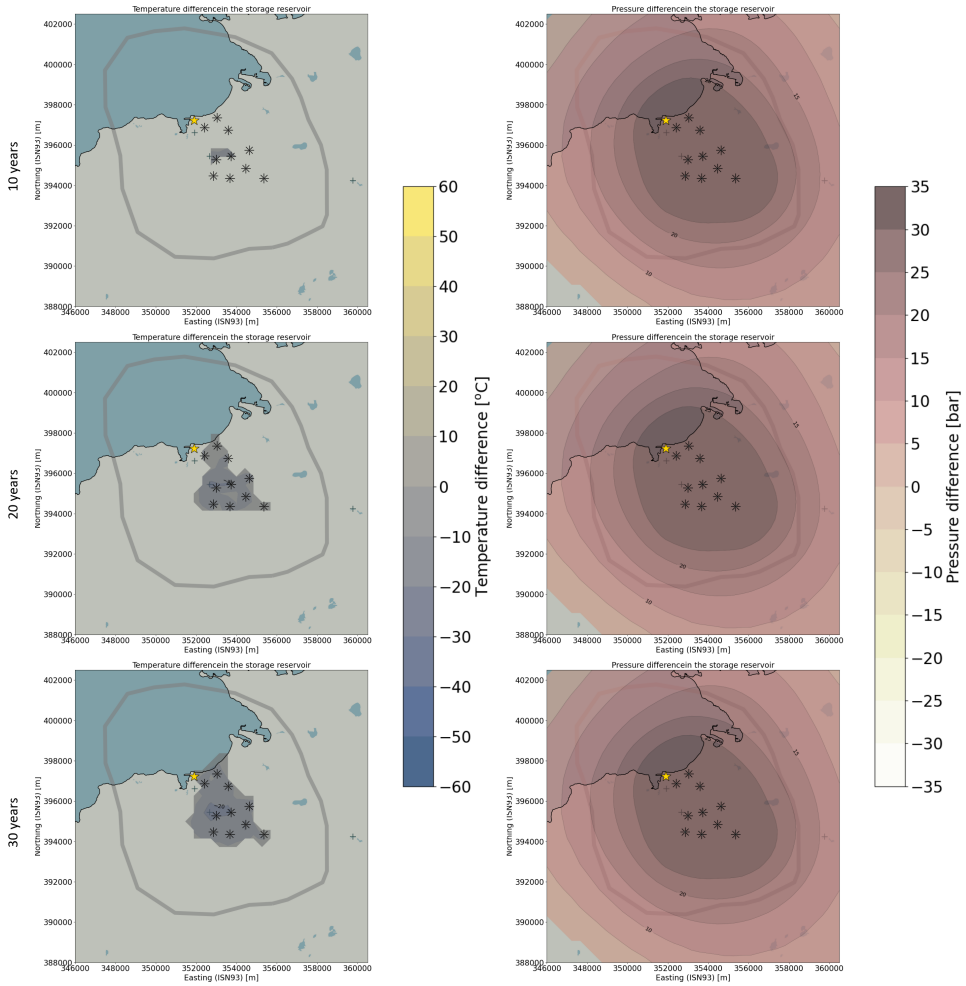

Figure 8.13: Change in temperature and pressure after 10, 20, and 30 years of injection

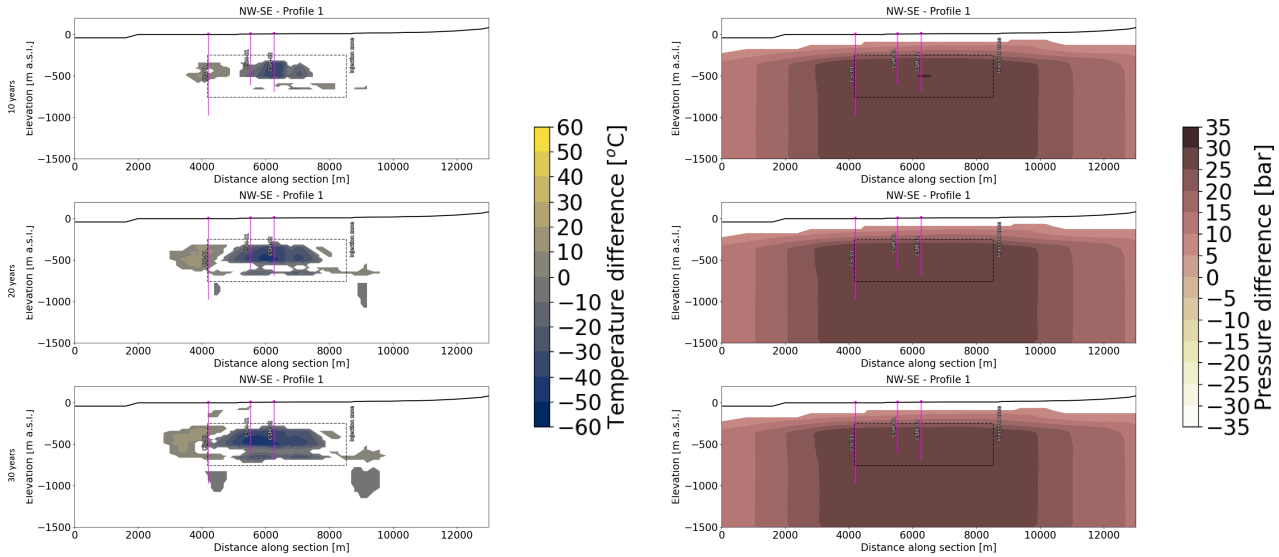

Figure 8.14: Cross-section of temperature and pressure changes in the storage reservoir after 10, 20, and 30 years of injection.

The average salinity difference in Figure 8.15 shows that after 30 years the salinity in the storage reservoir has increased near the coast east of the well pads eight, nine, and ten. This indicates that saline water has migrated eastward into an area of the reservoir that originally contained less salinity. Directly west of these three well pads, on the other hand, the opposite trend is observed. The salinity of the reservoir fluid in this area decreases by a similar order of magnitude as the salinity increases to the east. This salinity migration is the result of saline water injection into the saline storage reservoir. This injection pushes the saline water into areas of fresh or brackish water. The symmetry in the salinity differences between the East and West is also related to the SW-NE transition from a coastal environment to a more continental environment, as discussed in Chapter 4. This means that the baseline reservoir fluid is more saline in the west and less saline in the east, which is reflected in the salinity changes. It should be noted, that despite this change in salinity, and therefore density, in the saline storage reservoir, no change in the solubility trapping of CO_2 was observed in those areas, as demonstrated in Figure 8.8. The evolution of salinity changes can be seen in Figures 8.16 and 8.17. They show the decrease in salinity in the storage reservoir to the west of well pads eight, nine and ten. We see that there is some minor increase in salinity at the surface, which should be closely monitored. It should be noted that since the model overestimates the thickness of the brackish saltwater-freshwater interface (see Chapter 7), the salinity increase is likely overestimated.

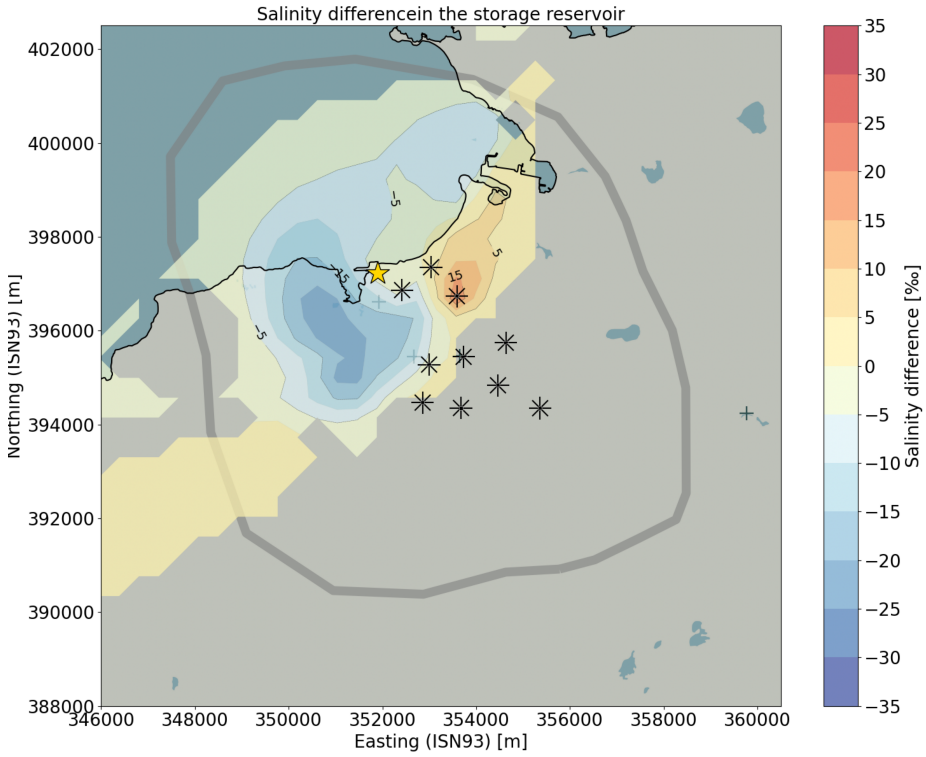

Figure 8.15: Average change in salinity in the storage reservoir after 30 years of injection.

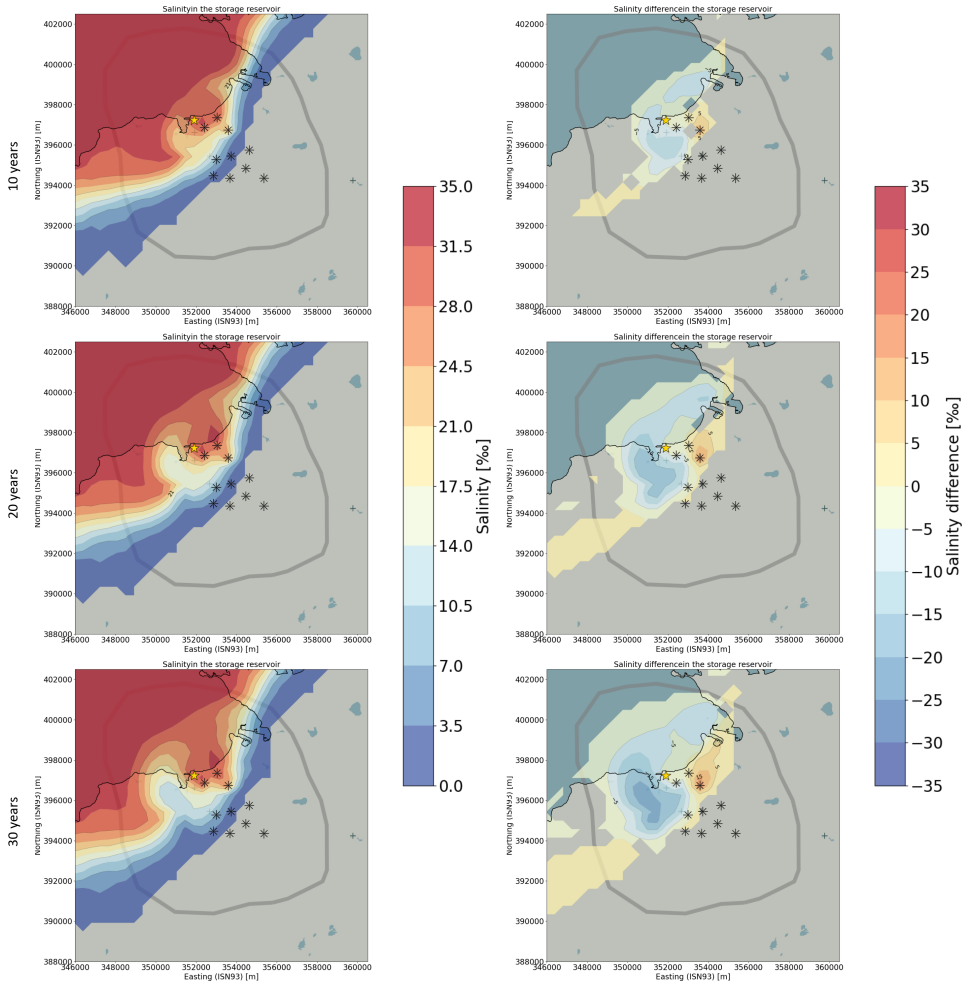

Figure 8.16: The average salinity and change in average salinity in the storage reservoir after 10, 20, and 30 years of injection.

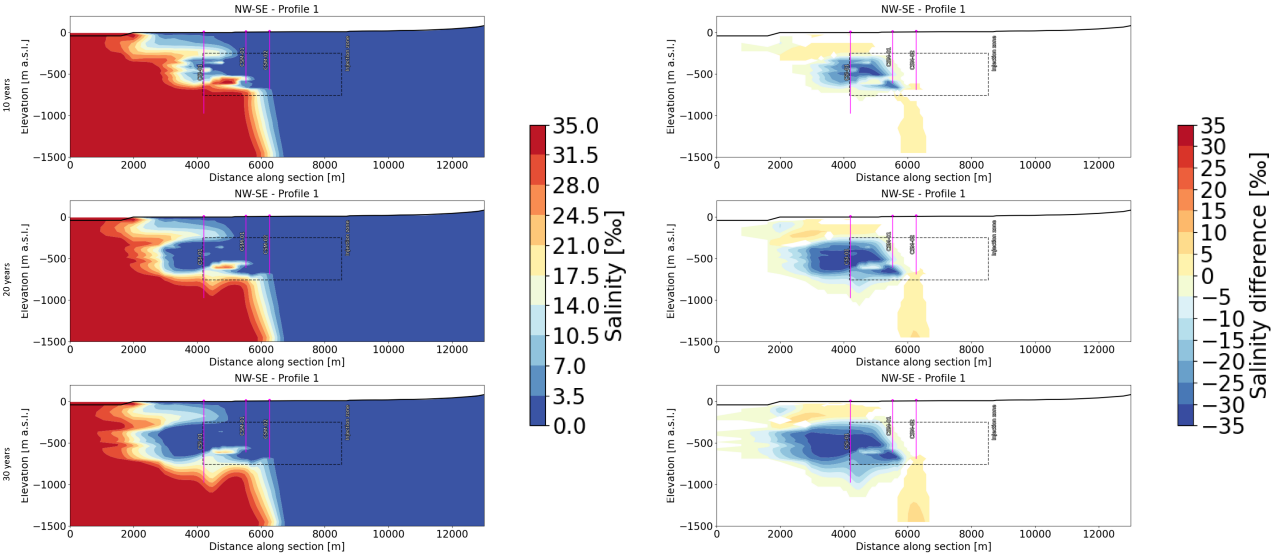

Figure 8.17: Cross-section of salinity and salinity change in the storage reservoir after 10, 20, and 30 years of injection.

8.2.4 Impact of the operations on the storage complex and surrounding formations

The forecast model results above, in, and below the storage complex after 30 years of injection are shown and represent the potential impact on the storage complex. Figure 8.18 shows that no CO_2 enters the shallow groundwater system and thus CO_2 containment is fully achieved. It further shows that a portion of CO_2 sinks within the storage reservoir due to density differences, as was expected (Chapter 7). Figure 8.19 shows that the temperature impact outside of the storage reservoir is minimal. The pressure impact is however much more present and overall a pressure increase in the subsurface is visible. This is not expected to represent an adverse impact of the region as, on the contrary, this could provide pressure support for water extraction from the shallow groundwater in the area. Figure 8.20 shows that an increase in salinity above the storage reservoir is possible. This change must be monitored, and Carbfix has proposed drilling several monitoring wells in the area to explicitly monitor salinity changes. In layers below the storage reservoir, a small decrease in salinity is noted.

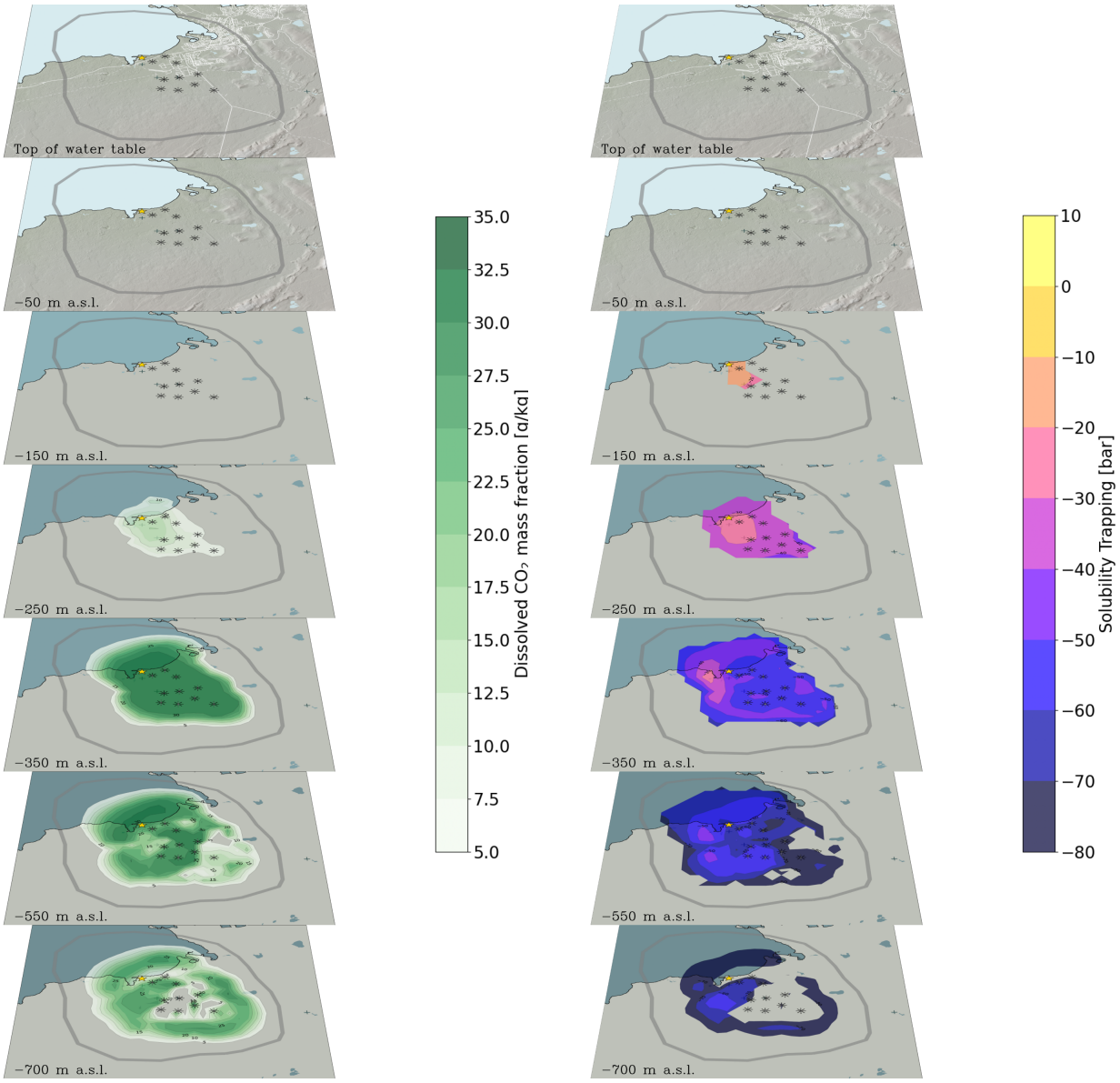

(a) (b)

Figure 8.18: Aqueous CO_2 migration (a) and solubility trapping (b) at different depths in the subsurface at the end of operations.

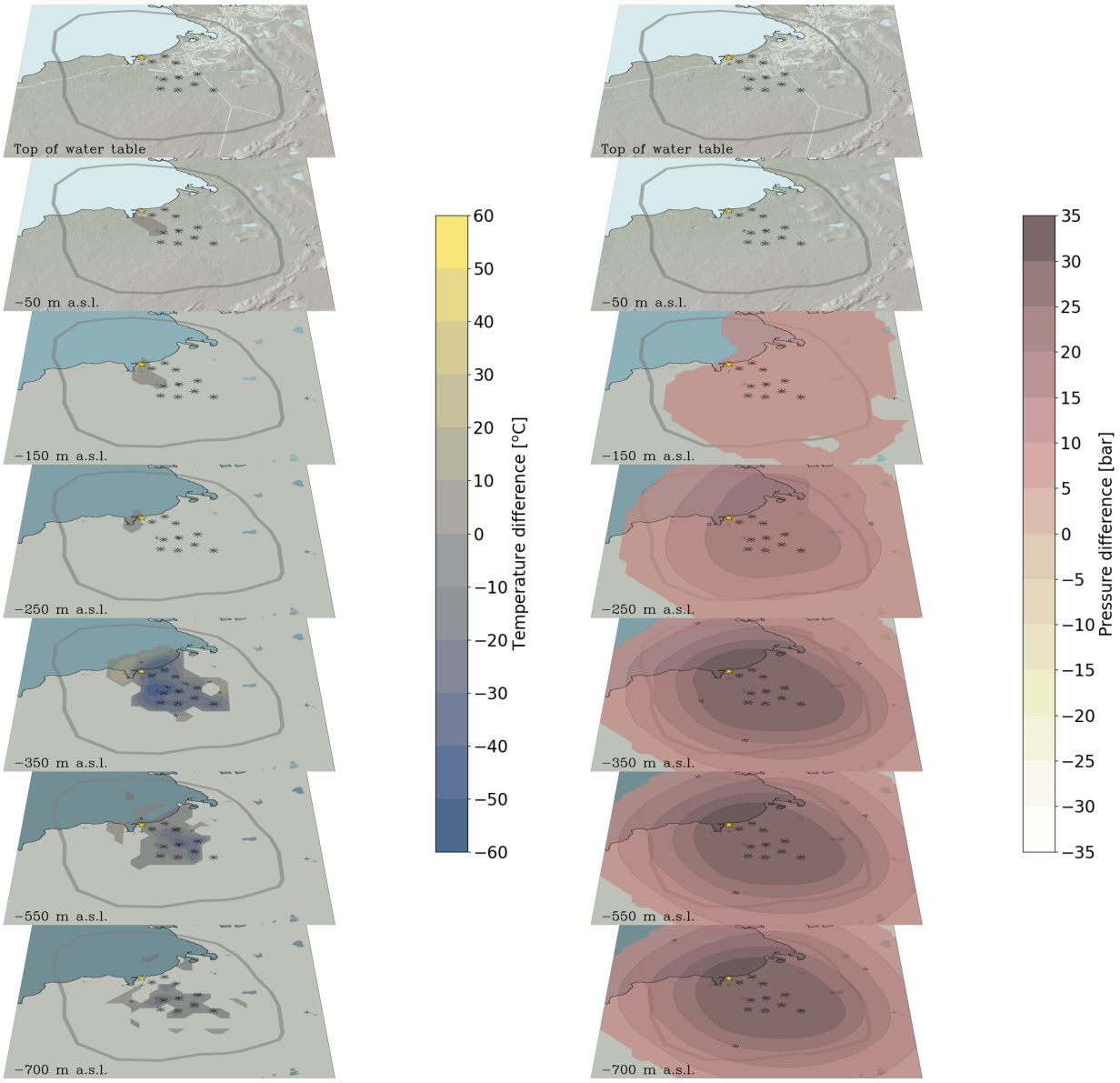

(a) (b)

Figure 8.19: Change in temperature (a) and pressure (b) at different depths in the subsurface at the end of operations.

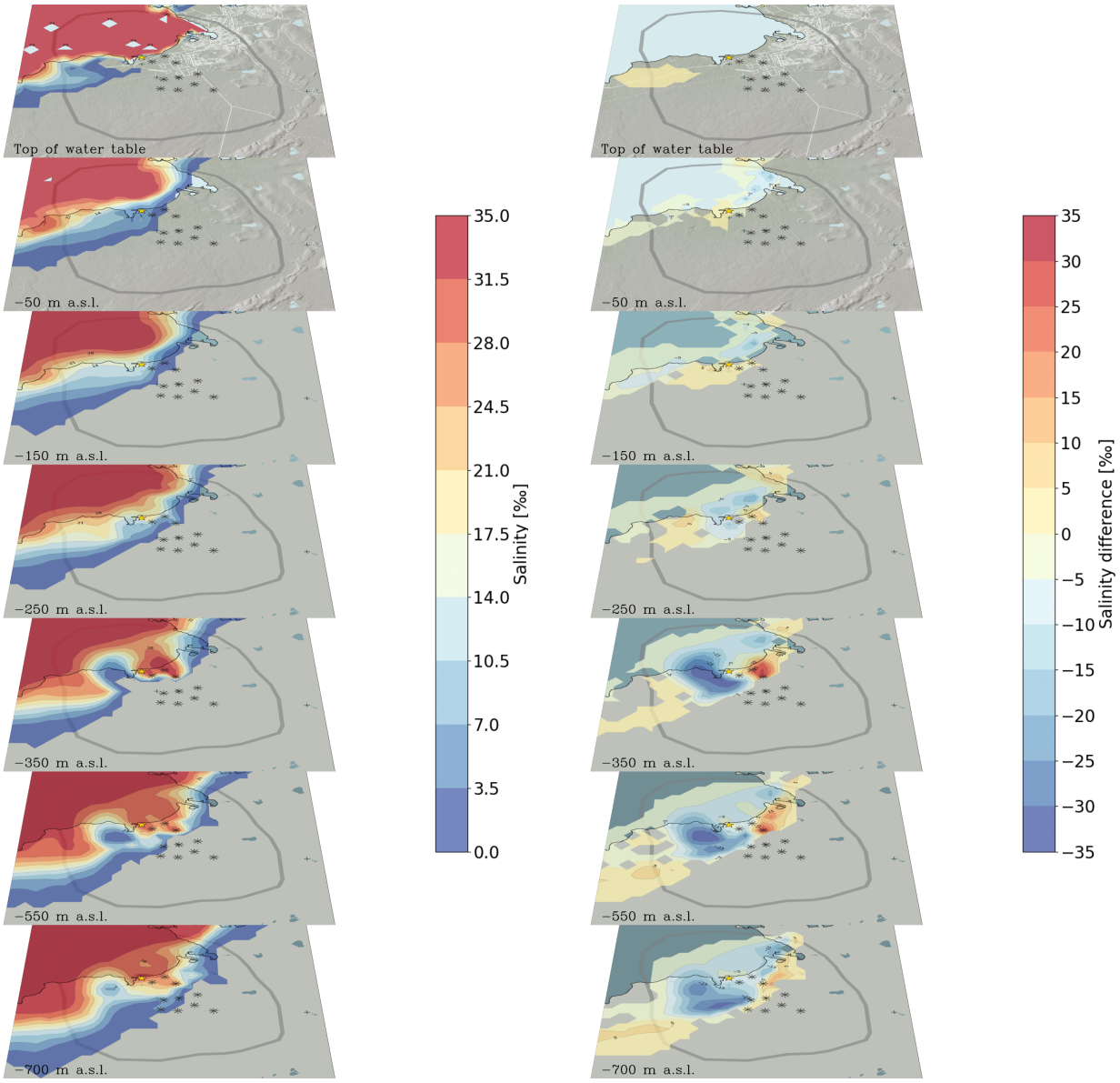

(a) (b)

Figure 8.20: Salinity (a) and change in salinity (b) at different depths in the subsurface at the end of operations.

8.2.5 Impact of the operations on the storage complex post closure

As in the previous section, and unless otherwise noted, the values presented here represent the average values of the parameters in the storage reservoir, which lies at depths between -300 and -1200 m a.s.l.

The forecast model was also used to check the status of the site 100 years after closure of operations at the Coda Terminal during which all injection and production of fluid are stopped. The model shows that the region trends toward long-term stability (Figure 8.21). CO_2 continues to migrate downward and outward from the injection site but at a much slower rate. The injected CO_2 also gets more diluted with the resident fluid increases with time. It should be noted that since the numerical scheme does not include chemical reactions between the water and rock, the mass fraction of CO_2 in the system will be further lower than is shown in the results as the majority of the CO_2 in the subsurface will mineralize over time (Galeczka, 2023b) In addition, even in the scenario in which no fluid-rock interaction is considered CO_2 remains fully dissolved. After 100 years simulation results show that temperatures in the storage reservoir are trending toward baseline values but changes occur at a low rate due to small heat recharge. Pressure changes, however, occur much faster and reservoir pressure equilibriates rapidly. After 100 years, salinity changes are also trending toward baseline values but similar to temperature, baseline values are not reached. Both temperature and salinity impact are reversible but the time frame may be longer than 100 years. This will be heavily impacted by the natural recharge (heat and flow) of the system over a long timescale which is currently uncertain.

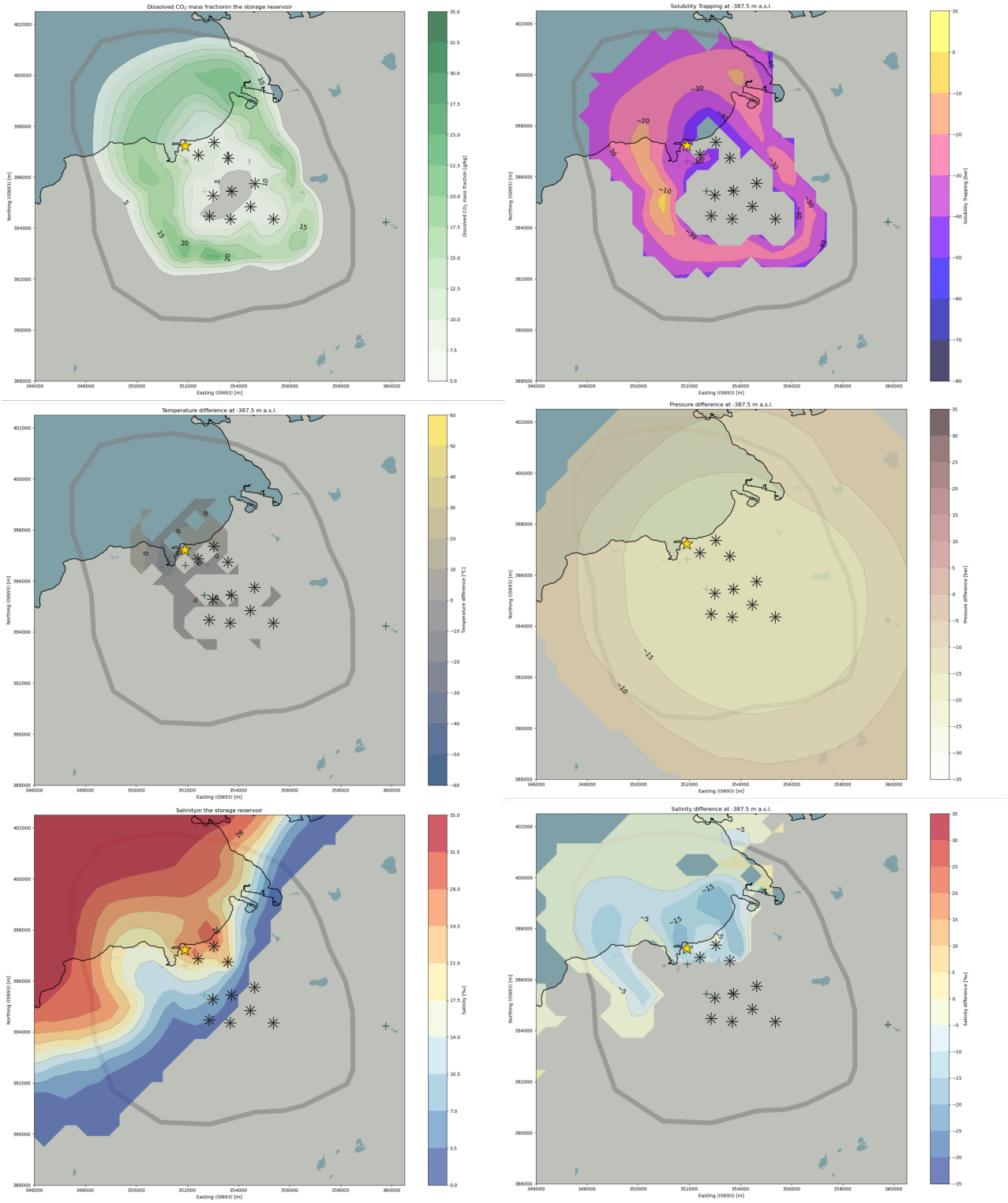

Figure 8.21: Average aqueous CO_2 migration and maximum solubility trapping (top), change in temperature and pressure (middle), and salinity and change in salinity (bottom) in the storage reservoir at 100 years.

8.2.6 Environmental impact of the operations

8.2.6.1 CO_2 migration and solubility trapping

The forecast model shows that solubility trapping of CO_2 is maintained over the entire subsurface for the duration of injection at the site, and for at least 100 years after end of injection operations. During that time CO_2 also remains in solution. No CO_2 bubbles form in the reservoir, so there is no risk of gaseous CO_2 rising to the surface. The solubility trapping mechanism is therefore effective at confining CO_2 in a dissolved state, which will promote in-situ mineralization of CO_2 in the storage reservoir. The simulations show that the migration of CO_2 is limited to the storage complex during operation and post-closure. No dissolved CO_2 flows outside of the lateral and vertical boundary of the storage complex. In addition, CO_2 does not, at any depth, enter the Kaldársel water protection zone, one of the main areas of concern in the region. The simulation also shows that the injected CO_2 does not migrate up to the shallow groundwater, or the surface, and should therefore not enter protected surface features, like the coastal ponds. Simulations show that the injection of CO_2 into the subsurface does not impact other users of the shallow groundwater resource in Straumsvík.

Negligible risk of CO_2 leakage via migration, or degassing, of dissolved CO_2 is expected. As a result, no impact on the acidity of the groundwater and shallow groundwater systems is expected. This should however be verified through monitoring of the groundwater and shallow groundwater.

8.2.6.2 Temperature and pressure impact

Temperature change is expected near the injection sites, where cooling is expected due to the injection of cold fluid into the reservoir. The temperature impact, however, is very localized, with a maximum decrease of 50°C near the injection wells, and is contained within the storage reservoir. A widespread rise in reservoir pressure (up to 25 bar within the storage reservoir) is modeled during the operation phase as a result of the proposed injection. This pressure impact extends outside of the storage complex at reservoir depths and extends up to - 150 m a.s.l. However, the pressure increase is not seen within the shallow groundwater (within a 1 bar uncertainty), and does not result in CO_2 migration up into the shallow groundwater. While both temperature and pressure impacts are reversible and trend toward natural state values during post-closure, pressure equilibriates rapidly whereas the temperature recovery occurs more slowly.

As there are no other planned usages for the subsurface resource a reservoir depths, the temperature and pressure impacts are not of significant concern.

Due to the lack of significant drawdown in the shallow groundwater system and surface constraints of the current configuration of the injection system (water produced from the wellpads) the feasibility of using water from the storage reservoir, rather than from the shallow groundwater, was not considered as it requires wells located away from the wellpads. However, the possibility of extracting water from the storage reservoir rather than the shallow groundwater system, and thereby reducing the pressure increase in the storage reservoir, remains under consideration. This would reduce the area impacted by the pressure increase in the storage reservoir. It does, however, require changes to the injection parameters due to differences in fluid chemistry and temperature between water from the storage reservoir and the shallow groundwater.

8.2.6.3 Salinity change and impact on the saltwater-freshwater interface

Changes in salinity in the storage reservoir are expected. The largest of these changes are mainly linked with the injection of saline water from well pads eight, nine, and ten during phase four. The injection of mass into the saline storage reservoir at the injection site displaces the resident reservoir fluid and may increase salinity in areas with brackish and fresh water. Minor changes in salinity may also occur at shallower depths in the shallow groundwater system. A robust monitoring program including sampling of monitoring wells and surface water should be implemented before operation to evaluate natural fluctuation in salinity (if any) and during operation to monitor changes to the fluid salinity.

The impact on salinity on the subsurface (groundwater systems and storage reservoir) is reversible the timescale of this change to natural state is uncertain.

9 Storage Capacity at the Coda Terminal

Storage capacity at the Coda Terminal is primarily controlled by the availability of divalent metal cations (Ca^2+, Mg^2+, Fe^2+), with porosity, permeability, partial pressure of CO_2, and temperature also playing a part in the overall success of mineralization (Snæbjörnsdóttir et al., 2014). Volumetric methods have been developed to estimate the storage potential of CO_2 mineralization storage reservoirs based on injection strategies, lithological assumptions, and physical constraints of carbon mineralization (Gislason et al., 2009, Goldberg et al., 2008, Snæbjörnsdóttir et al., 2014). These methods form a basis for the storage capacity estimate, or the storage capacity model, for the Coda Terminal site.

9.1 Static storage capacity

The geological model of the Straumsvík area (Helgadóttir et al., 2023) was used as the base model for the storage potential, with the physical boundaries of the storage area defined by the reservoir extent and depth of injection. Storage capacity estimates for the modelled area are confined to the bounds of the storage reservoir shown in Figure 4.1. The polygon shows the maximum possible extent of the migration of the CO_2 after 30 years of injection plus a buffer area to incorporate the uncertainty of modelling. This polygon represents the aerial boundary of the storage complex and serves as the basis for the static storage capacity estimates. The minimum depth for injection of CO_2 using the Carbfix method is dictated by the bubble point pressure of CO_2 in the water during injection. The CO_2 must be fully dissolved at the injection depth prior to entering the reservoir and the reservoir pressure at the injection site must be sufficient to prevent CO_2 bubbles from forming. Under the planned injection strategy the ideal depth of injection in the Coda Terminal is below -300 m a.s.l., at which depth there is enough reservoir pressure to ensure solubility trapping and eliminate the risk of the CO_2 degassing (Snæbjörnsdóttir et al., 2014). This minimum injection depth serves as the upper boundary for the storage capacity model. Any porous volume between this depth and the surface is excluded from the calculations. In addition the bottom boundary of the storage reservoir is defined as the maximum migration depth of CO_2 at the end of operations. This has been estimated by reservoir models to be around -1200 m a.s.l. It should also be noted, however, that temperature may also play a part in determining the bottom boundary of the storage reservoir.

Carbon mineralization has been demonstrated at ambient temperatures (around 35°C) at Hellisheiði during pilot injections at Carbfix1 in 2012 (Matter et al., 2016) and temperatures of greater than 250°C at the Carbfix2 site (Clark et al., 2020). Increased temperature has been shown to enhance the dissolution and release of cations from glassy basalt, increasing the overall mineralization rate. The thermodynamic stability of carbonates is limited at temperatures $>$ 300°C but can vary in natural conditions. At the Coda Terminal the temperature gradient is 80 – 90 °C/km and the temperature remains largely within the thermal stability range of calcite and thus should not play a big part in the storage capacity at the site.

9.2 Theoretical CO_2 storage capacity of the Coda Terminal

The CO_2 storage potential via mineralization is estimated by calculating the pore volume available in the subsurface, and assuming that a fixed proportion of this pore volume is available for carbonate mineralization. The static storage capacity of the storage reservoir is calculated using the theoretical volumetric estimate of the storage reservoir and the approaches described by Gislason et al., 2009 and Goldberg et al., 2008. Using the estimated aerial extent of the

storage complex, of around 99 km^2 (Figure 4.1), and the estimated vertical extent of the storage reservoir, 900 m (from -300 down to -1200 m a.sl.), the storage capacity has been estimated at:

- 1,100 Mt CO_2, assuming that 10% of the available pore space is filled with calcite (Gislason et al., 2009). This represents the lower bound of the storage capacity.
- 10,600 Mt CO_2 assuming that 100% of the available pore volume is filled with calcite (Goldberg et al., 2008). This represents the higher bound of the storage capacity.

It is estimated that after 30 years of operation around 90 Mt of CO_2 will be injected into the storage reservoir. Considering the minimum storage capacity estimate of 1,100 Mt CO_2, and assuming all injected CO_2 will be mineralized, around 8.1 % of the total storage capacity of the site will be utilized. Considering the upper storage capacity estimates of 10,600 Mt CO_2, 0.8 % of the total storage capacity of the site will be utilized. At the planned injection capacity of 3 Mt CO_2/year, the above results indicate that it would take anywhere from approximately 360 to approximately 3,500 years to exhaust the storage capacity of the reservoir.

10 Summary

In this report reservoir models, developed by Carbfix, of the proposed storage reservoir of the Coda Terminal project in Straumsvík were detailed. The simulation results presented in this report provide estimates of the potential environmental impacts associated with the proposed production and injection of the project. In particular, these models were created to assess three key parameters, 1) the maximum migration of CO_2 in the subsurface assuming no mineralization of CO_2 takes place, 2) the efficiency of the CO_2 solubility trapping mechanism in the storage reservoir, and 3) the impact on the storage complex and surrounding formations in terms of pressure, temperature, salinity, and CO_2. A conceptual model of the region was created based on data collected for the characterization of the proposed injection site. This data included a three-dimensional geological model of the region, results of measurements and tests in several wells, and surface resistivity measurements of the area. The region around Straumsvík has a complex hydrological structure, including natural saline intrusion into the groundwater from the coast and a very high fresh groundwater flow in the shallow subsurface towards the coast. From the conceptual model, a numerical reservoir model of the subsurface in the area of interest was developed to represent the storage reservoir and the main physical processes of the hydrogeological system, from the top of the water table down to a depth of three kilometers. This numerical reservoir model was calibrated to the natural state of the region using field data collected in, and near, the proposed project site. This natural state model was then used as a baseline for the simulation of a forecast model based on the planned CO_2 injection into the proposed storage reservoir. This forecast model incorporated currently planned scale-up and well designs for injection and production, as well as proposed well pad sites for the Coda Terminal project.

10.1 Results

The natural state model replicates the processes identified in the conceptual model and serves as a good baseline for any injection forecast. The model reproduces the available field data including natural groundwater flows, downhole pressure, temperature, and salinity measurements. The model results show a large shallow groundwater flow at the surface from inland

towards the sea and an inversion at reservoir depths where mass flows from under the sea inland. This leads to a portion of the targeted storage reservoir, in the area closest to the shore, having saline or brackish reservoir fluid. The natural state model shows that the proposed storage reservoir has a favorable density distribution for mineral storage and solubility trapping of CO_2. The main results of the natural state model are:

- The natural state model shows a large groundwater flow at the surface, from inland towards the sea.
- The natural state model shows the presence of saline intrusions in the subsurface close to the coast, primarily next to, and to the west of, Straumsvík.
- The natural state model shows that the saline intrusions disappear one to two kilometers inland.
- The natural state model shows that the proposed storage reservoir has a temperature gradient of 80 to 90°C/km.
- The natural state model shows that the fluid in the storage reservoir is in pressure contact with the surface, as seen by the hydrostatic pressure profiles.
- The natural state model shows that the storage reservoir, at the depth and the location of the proposed fresh water injection well pads, have fresh water.
- The natural state model shows that the storage reservoir, at the depth and the location of the proposed saline water injection well pads, has saline or brackish water.

The results of the forecast model, with no geochemical water-rock interactions simulated, i.e. no CO_2 mineralization, show that the proposed storage reservoir is a good candidate for large-scale injection of dissolved CO_2. The model results suggest that the environmental impact on the storage reservoir, storage complex, and neighboring formation is limited. The migration of CO_2 is fully confined to the lateral and vertical boundaries of the storage complex during operation and post-closure. No CO_2 enters neighboring formations or the shallow groundwater system. CO_2 remains fully dissolved and CO_2 trapping is fully maintained via solubility trapping during operation and post-closure. The risk of leakage or degassing is not expected to be significant.

Assuming full dissolution of gaseous CO_2 during injection, no CO_2 reaches the shallow groundwater and no impact on the chemistry of the shallow groundwater is expected. Furthermore, the proposed operation does not impact the temperature and has a limited impact on the salinity of the shallow groundwater system.

Considering the minimum storage capacity estimate of 1,100 Mt CO_2, and assuming all injected CO_2 will be mineralized, around 8.1 % of the total storage capacity of the site will be utilized. Considering the upper storage capacity estimates of 10,600 Mt CO_2, 0.8 % of the total storage capacity of the site will be utilized. At the planned injection capacity of 3 Mt CO_2/year, the above results indicate that it would take anywhere from approximately 360 to approximately 3,500 years to exhaust the storage capacity of the reservoir.

The main results of the forecast models are:

- After 30 years of injection the dissolved CO_2 remains within the lateral and vertical boundary of the storage complex.
- After 30 years of injection the dissolved CO_2 reaches, at most, a distance of 2–3 km from the injection wells.

- The injected CO_2-charged fluid mixes with the reservoir water and gets diluted, as it flows in the storage reservoir.
- The CO_2 will flow mainly laterally in the storage reservoir, with a portion of the CO_2 sinking deeper into the subsurface.
- After 30 years of injection no CO_2 migrates into the shallow groundwater.
- After 30 years of injection the CO_2 migrates under the ocean off the coast of Straumsvík, several hundred meters below the seafloor.
- After 30 years of injection the CO_2 remains in solution via solubility trapping everywhere in the subsurface.
- The temperature of the reservoir will decrease by 50 °C or less close to the injection wells.
- The pressure might increase by an average of 25 bars near the injection wells. However, this does not translate into CO_2 injected water flowing into the shallow groundwater. There is also no increase in pressure in the shallow groundwater.
- The distribution of salinity will be impacted by the proposed injection, with local increases/decreases in salinity.
- The salinity will increase in the storage complex east of Straumsvík, and decrease to the west.
- Once injection has stopped the reservoir stabilizes rapidly and trends toward long term stability.

It should be noted that above the storage reservoir and below the shallow groundwater system the bubble point pressure of CO_2 falls within 20 bars of the reservoir pressure during operation and 10 bars during post closure. Additional work should be conducted to better constrain temperatures and salinity distribution in that part of the storage reservoir, to reduce uncertainty in the model to better constrain reservoir pressure and bubble point pressure.

The preliminary modeling results highlight that the storage reservoir is a good candidate for large-scale injection of dissolved CO_2. The environmental impacts of such an injection on the storage reservoir, storage complex, and neighboring formation are limited, even for a scenario where no CO_2 mineralization takes place; i.e. solubility trapping is the main CO_2 trapping mechanism. Further work is required to reduce uncertainties in the simulation and better constrain the model (see below).

10.2 Mitigation measures

The report's findings, based on modeling studies, underscore that the anticipated environmental effects of the Coda Terminal on the storage reservoir, storage complex, and adjacent formation are minimal. However, it's important to note that these model outcomes inherently carry uncertainties. Therefore, they should be integrated into a comprehensive risk evaluation of the subsurface.

Reservoir models are instrumental in combining our current understanding of the system with mathematical representations of governing equations and physical processes. These models offer predictions of how the reservoir might react to injection. Given that these models are built on incomplete data, their results should be viewed as potential scenarios for the system, aiding

in the establishment of precautionary measures. Furthermore, as we acquire new data and develop new tools, it's crucial to regularly update these model results. Mitigation measures to prevent, reduce, or control adverse environmental effects of a project for the Coda Terminal include:

- **Uncertainty reduction** via continued site characterization and updates to the modeling framework and risk assessment. Collecting more data on subsurface properties will enhance the design of safe injection operations.
- **Implementation of a robust monitoring system** in the project and surrounding area. Regular data collection allows for real-time tracking of changes in pressure, temperature, salinity, and dissolved CO_2 and helps identify any deviations from expected values. This data can effectively manage risks and initiate timely mitigation measures if necessary.
- A **gradual scale-up injection strategy** to adapt the injection strategy and reservoir management based on observed storage performance.

10.2.1 Uncertainty reduction

Uncertainties can arise from various sources and are highlighted in the list below:

- **Geological heterogeneity**: The complexity and variability of geological formations can lead to significant uncertainties in volumetric estimation and fluid flow behavior within the reservoir.
- **Hydrogeologial and geochemical reservoir properties**: The data gathered during site characterization can be uncertain due to limitations in sampling techniques and the hidden nature of the subsurface. The interpretation and extrapolation of collected data can further introduce uncertainties, especially when data only covers part of the reservoir interval.
- **Physical processes**: The physical processes that are either simulated or not simulated in the models can contribute to uncertainty. This includes factors like petrophysical complexity, matrix-fracture interaction, and geochemical reactions.
- **Numerical approximations**: Numerical approximations made within the models can also introduce uncertainty.

These uncertainties can influence decisions related to the subsurface, from assessing the impact on the subsurface to designing reservoir development plans and well placement. While uncertainties are inherent in any subsurface system due to their complex and dynamic nature, they can be effectively managed through comprehensive site characterization and advanced modeling techniques.

Two significant factors that determine the extent and magnitude of dissolved CO_2 injection-induced effects are the density of the resident reservoir fluid and the hydrogeologic characteristics of the storage reservoir.

Simulations suggest that mapping the reservoir density, which is correlated with salinity, is crucial for containing CO_2. This will also affect the chosen injection strategy and the properties of the selected injection fluid.

The maximum migration extent of the injection fluid and the extent of its mixing with the reservoir fluid is sensitive to hydrological properties including the magnitude and distribution

of porosity, permeability, and permeable pathways in the reservoir. Therefore, it's necessary to characterize in detail the formations intersected by the wells through well logging and dynamic testing. This includes injection tests of individual wells, inter-well characteristic testing through interference, and tracer tests.

Alongside this data collection, it is recommended to update the modeling approach to reduce uncertainties. This could involve incorporating new site-collected data, quantifying the uncertainty of simulation results, and including reactive transport modeling. The current approach simulates the thermodynamics and thermophysical properties of H_2O–NaCl–CO_2 mixtures. While the framework can model the advective and diffusive flow and transport of H_2O–NaCl–CO_2 mixtures it does not include water-rock interactions and mineralization processes. Additionally, while a deterministic approach was chosen here, a stochastic approach that incorporates randomness and uncertainty may be relevant to further quantify uncertainty.

Therefore, it's recommended to collect further data from the site to better constrain the distribution of saline water in the storage reservoir. This includes understanding the morphology of the saline-freshwater interface and the hydrogeological properties of the storage complex, such as permeability, porosity, and preferential migration flow paths. It's also recommended to execute updates to the modeling framework. A summary of the recommendations for future data acquisition is presented below

The uncertainty on the **geological heterogeneity** of geological formations and **subsurface distribution** of the reservoir fluid can be addressed by:

1. **Electromagnetic characterization** of the saltwater-freshwater interface.
2. **Drilling** of additional wells.
3. **Downhole logging** of the conductivity in existing and additional wells.
4. **Stratigraphical analysis** of additional wells to determine the disposition of rock formations and inter-well interpolation.

The uncertainty on the **Hydrogeologial and geochemical reservoir properties** of geological formations can be addressed by:

1. **Hydrogeological properties** of the rock formation.
   - **Downhole logging** of additional wells to characterize porosity.
   - **Televiewer** of additional wells to characterize porosity.
   - **Downhole temperature and pressure** measurement in additional wells to determine feedzone depths.
   - **Injectivity test** and spinner to identify feedzones and constrain the injectivity potential of the site.
2. **Storage reservoir properties** and inter-well characteristics.
   - **Interference test** between wells to characterize porosity.
   - **Tracer tests** between wells to characterize flow paths in the storage reservoir.
   - **Conductivity logging** in new and existing wells to further constrain the distribution of salinity in the storage reservoir.
   - **Temperature and pressure logging** in new wells.

3. **Rate of in situ mineralization** in the targeted rock formations.
    - **Dissolution experiments** on well cuttings to confirm under a controlled environment representing the conditions at the site the dissolution rate.
    - **Pilot CO_2 injection** into proposed storage reservoir to validate in-situ mineralization at the site.

The **numerical framework** developed in this report will be subject to:

1. **Regular updates** to include the latest data and revisions done on the environmental risk assessment of the operation on the subsurface. This include data from the monitoring plan as part of conformance monitoring.
2. **Uncertainty quantification** to assess the impact of uncertain parameters.
3. **Sensitivity Analysis** to help prioritize data collection efforts.
4. **Scenario Testing** to evaluate system behavior.
5. **Reactive transport numerical scheme** to simulate water-rock interactions and evaluate system behavior. Mineral storage relies on the interaction between rock formations rich in divalent metal cations and dissolved CO_2. Calcium, magnesium, and iron present in the rock formations can combine with dissolved CO_2 to form carbonate minerals such as calcite ($CaCO_3$), dolomite ($CaMg(CO_3)_2$), magnetite ($MgCO_3$), siderite ($FeCO_3$), and Ca-Mg and Mg-Fe carbonate solid solutions (Snæbjörnsdóttir et al., 2014). The stratigraphy at the Coda Terminal is dominated by basaltic lavas and glassy hyaloclastites with abundant cation exchange capacity, thus the storage capacity estimation method assumes favorable rock composition to supply cations and mineralize carbon (Galeczka, 2023b). However, to further constraints, the reservoir behavior and response to injection, water-rock interaction including dissolution and precipitation should be implemented. It is also necessary to carry out these steps in order to monitor compliance and to compare the results of the model to the data obtained from the field.

10.2.2 Monitoring of the subsurface

The simulation results discussed in this report are based on the assumption that CO_2 is fully dissolved prior to or during injection. Therefore, these results are applicable only if no buoyant gaseous CO_2 is injected into the storage reservoir. Consequently, the monitoring plan necessitates instruments capable of measuring the temperature, pressure, salinity of the injected fluid, and the concentration and purity of the CO_2 stream. These measurements will be used to calculate the bubble point pressure of CO_2 and confirm that full dissolution of CO_2 in the injection fluid is achieved.

The current monitoring plan at the Coda Terminal involves regular monitoring of subsurface conditions in the storage reservoir using monitoring wells, in the storage complex using interface wells, and in the shallow groundwater using groundwater monitoring wells. This is complemented by regular water level measurements and sampling of surface water and/or gas flux measurements at the injection site. The collected data will be compared against forecast models to identify any deviations from expected values and initiate timely mitigation measures if required.

In addition, the extent of dissolved CO_2 and its migration suggests that the current placement of monitoring wells shown in Figure 8.3 is adequate. However, simulation results indicate

that additional monitoring wells further away from the well pads should be drilled to track the migration of the CO2. This is necessary to verify modeling results, confirm the efficiency of the storage process, and ensure the safety of the water protection area.

10.2.3 Gradual scale-up injection strategy

The Coda Terminal project aims to mitigate greenhouse gas emissions by sequestering CO_2 in a subsurface storage reservoir at the Straumsvík site. As part of the risk management strategy, a gradual scale-up approach will be employed during the injection phase. Key details include:

- **Project Timeline**: The project is scheduled to commence in 3 years (2027). During this period, Carbfix's efforts will focus on implementing uncertainty reduction measures outlined in the project plan.
- **Gradual Scale-Up**: To minimize risks associated with large-scale injection, the project will follow an 18-month scale-up cycle. This phased approach allows for continuous monitoring, assessment, and informed decision-making. By incrementally increasing injection volumes, Carbfix can closely evaluate reservoir behavior, pressure dynamics, and potential environmental impacts and make informed decisions on injection and management of the storage reservoir.

The gradual scale-up not only ensures operational safety but also allows for the adjustment of injection and reservoir management strategies based on real-time data. Monitoring protocols will track subsurface conditions, fluid migration, and any adverse effects on local ecosystems. Additionally, contingency plans will be in place to address unforeseen challenges.

Bibliography

References

2009/31/EC, C. D. (2009, April 23). CCS directive. https://eur-lex.europa.eu/eli/dir/2009/31/oj/eng

Altunin, V. V. (1975). *Thermophysical properties of carbon dioxide*. Publishing House of Standards.

Andersen, G., Probst, A., Murray, L., & Butler, S. (1992). An accurate PVT model for geothermal fluids as represented by h2o-NaCl-CO2 mixtures. *Proceedings 17th Workshop on Geothermal Reservoir Engineering*.

Aradóttir, E., Sonnenthal, E., Björnsson, G., & Jónsson, H. (2012). Multidimensional reactive transport modeling of CO2 mineral sequestration in basalts at the hellisheidi geothermal field, iceland. *International Journal of Greenhouse Gas Control*, *9*, 24–40. https://doi.org/10.1016/j.ijggc.2012.02.006

Battistelli, A., Calore, C., & Pruess, K. (1997). The simulator TOUGH2/EWASG for modeling geothermal reservoirs with brines and non-condensible gas. *Geothermics*, *26*(4), 437–464.

Carbfix Methodology, C. (2022, June 15). *Carbfix methodology*.

Chou, I.-M. (1987). Phase relations in the system NaCl-KCl-h2o. III: Solubilities of halite in vapor-saturated liquids above 445°c and redetermination of phase equilibrium properties in the system NaCl-h2o to 1000°c and 1500 bars. *Geochimica et Cosmochimica Acta*, *51*(7), 1965–1975. https://doi.org/10.1016/0016-7037(87)90185-2

Clark, D. E., Gunnarsson, I., Aradóttir, E. S., Þ. Arnarson, M., Þorgeirsson, Þ. A., Sigurðardóttir, S. S., Sigfússon, B., Snæbjörnsdóttir, S. Ó., Oelkers, E. H., & Gíslason, S. R. (2018). The chemistry and potential reactivity of the CO2-h2s charged injected waters at the basaltic CarbFix2 site, iceland. *Energy Procedia*, *146*, 121–128. https://doi.org/10.1016/j.egypro.2018.07.016

Clark, D. E., Oelkers, E. H., Gunnarsson, I., Sigfússon, B., Snæbjörnsdóttir, S. Ó., Aradóttir, E. S., & Gíslason, S. R. (2020). CarbFix2: CO2 and h2s mineralization during 3.5 years of continuous injection into basaltic rocks at more than 250 °c. *Geochimica et Cosmochimica Acta*, *279*, 45–66. https://doi.org/10.1016/j.gca.2020.03.039

Committee, I. F. (1967). A formulation of the thermodynamic properties of ordinary water substance.

Croucher, A. E., & O´Sullivan, M. J. (2013). Approaches to local grid refinement in TOUGH2 models. *New Zealand*.

DNV-RP-J203. (2021, September). *DNV report* (Geological storage of carbon dioxide No. DNV-RP-J203).

Franzson, H. (1988). Nesjavellir: Permeability in geothermal reservoir OS-88046/JHD-09.

Franzson, H., Zierenberg, R., & Schiffman, P. (2008). Chemical transport in geothermal systems in iceland: Evidence from hydrothermal alteration. *Journal of Volcanology and Geothermal Research*, *173*(3), 217–229. https://doi.org/10.1016/j.jvolgeores.2008.01.027

Friðleifsson, G. Ó. (1989, January). *Athugun á sjótökumöguleikum fyrir sædýrasafnið* (GÓF-89-01). National Energy Authority.

Galeczka, I. (2023a). *Deliverable d1.3: Report on geochemical sampling*. The Coda Terminal. Iceland.

Galeczka, I. (2023b, June). *Geochemical model of the coda injection reservoir* (for Carbfix No. ÍSOR-2023/017). Iceland GeoSurvey. Iceland.

Garcia, J. E. (2001, October 10). *Density of aqueous solutions of CO2* (Lawrence Berkeley National Laboratory Report No. LBNL-49023). Lawrence Berkeley National Laboratory. https://doi.org/10.2172/790022

Geological map of southwest iceland 1:100 000 (2nd ed.). (2016).

Gislason, S. R., Wolff-Boenisch, D., Stefansson, A., Oelkers, E. H., Gunnlaugsson, E., Sigurdardottir, H., Sigfusson, B., Broecker, W. S., Matter, J. M., Stute, M., Axelsson, G., & Fridriksson, T. (2009). Mineral sequestration of carbon dioxide in basalt: A pre-injection overview of the CarbFix project. *International Journal of Greenhouse Gas Control*, *4*(3), 537–545. https://doi.org/10.1016/j.ijggc.2009.11.013

Goldberg, D. S., Takahashi, T., & Slagle, A. L. (2008). Carbon dioxide sequestration in deep-sea basalt. *Proceedings of the National Academy of Sciences*, *105*(29), 9920–9925. https://doi.org/10.1073/pnas.0804397105

Gunnarsdóttir, S. H., Akın, S., Weisenberger, T. B., Clark, D., Galeczka, I. M., Helgadóttir, H. M., Marteinsson, K., Þorgilsson, G., Akın, T., Baser, A., Erol, S., Kucuk, S., Saracoglu, O., Trumpy, E., Montegrossi, G., Batini, F., Bonini, M., Brogi, A., Bicocchi, G., … Seidel, T. (2021, January). *Report on integrated geological and reservoir models and injection modelling* (Demo-sites geological and technical characterization No. 818169-GECO). Geothermal Emission Control. Iceland.

Gunnarsson, I., Aradóttir, E. S., Oelkers, E. H., Clark, D. E., Arnarson, M. Þ., Sigfússon, B., Snæbjörnsdóttir, S. Ó., Matter, J. M., Stute, M., Júlíusson, B. M., & Gíslason, S. R. (2018). The rapid and cost-effective capture and subsurface mineral storage of carbon and sulfur at the CarbFix2 site. *International Journal of Greenhouse Gas Control*, *79*, 117–126. https://doi.org/10.1016/j.ijggc.2018.08.014

Haas, J. L. J. (1976). *Physical properties of the coexisting phases and thermochemical properties of the h_2o component in boiling NaCl solutions* (Geological Survey Bulletin No. 1421-A). https://doi.org/10.3133/b1421A

Helgadóttir, H. M., Sigurgeirsson, M. Á., Gunnarsdóttir, S. H., & Einarsson, G. M. (2023). Baseline geology and three dimensional geological model of the straumsvík area. *ÍSOR-2023/018*.

Himmelblau, D. M. (1959). Partial molal heats and entropies og solution for gases dissolved in water from the freezing point to near the critical point. *J. Phys. Chem.*, *63*(11).

Jónsson, J. E. (2024). *Wells CSM-01 and CSI-01. injection test and spinner.* (ÍSOR-24003). Iceland GeoSurvey.

Kristmannsdóttir, H., & Tómasson, J. (1978). Zeolite zones in geothermal areas in iceland. natural zeolites: Occurrence, properties, and use. *Pergamon Press, Elmsford, New York*. https://www.semanticscholar.org/paper/Zeolite-zones-in-geothermal-areas-in-Iceland-Kristmannsdo%CC%81ttir/569241d101d3b853237744d34609afcc7d5ab6dd

Lagat, J. (2009). Hydrothermal alteration mineralogy in geothermal fields with case examples from olkaria domes geothermal field, kenya. *Short Course IV on Exploration for Geothermal Resources*, 24. https://orkustofnun.is/gogn/unu-gtp-sc/UNU-GTP-SC-11-02.pdf

Liu, D., Agarwal, R., Li, Y., & Yang, S. (2019). Reactive transport modeling of mineral carbonation in unaltered and altered basalts during CO2 sequestration. *International Journal of Greenhouse Gas Control*, *85*, 109–120. https://doi.org/10.1016/j.ijggc.2019.04.006

Lorenz, S., Maric, D., & Rirschl, C. (2000). *Eine analytische funktion zur bestimmung der enthalpie wässriger NaCl lösungen* (Draft report). Institut für Sicherheitstechnologie.

Marieni, C., Voigt, M., Clark, D. E., Gíslason, S. R., & Oelkers, E. H. (2021). Mineralization potential of water-dissolved CO2 and h2s injected into basalts as function of temper-

ature: Freshwater versus seawater. *International Journal of Greenhouse Gas Control*, *109*, 103357. https://doi.org/10.1016/j.ijggc.2021.103357

Matter, J. M., Stute, M., Snæbjörnsdottir, S. Ó., Oelkers, E. H., Gislason, S. R., Aradottir, E. S., Sigfusson, B., Gunnarsson, I., Sigurdardottir, H., Gunnlaugsson, E., Axelsson, G., Alfredsson, H. A., Wolff-Boenisch, D., Mesfin, K., Taya, D. F. d. l. R., Hall, J., Dideriksen, K., & Broecker, W. S. (2016). Rapid carbon mineralization for permanent disposal of anthropogenic carbon dioxide emissions. *Science*, *352*(6291), 1312–1314. https://doi.org/10.1126/science.aad8132

Myer, E. M., Arnaldsson, A., Berthet, J.-C., & Pálmarsson, S. Ó. (2024, February). *Coda terminal: Assessment of impacts on groundwater resources* (No. 24.xx). Vatnaskil.

Neuhoff, P. S., Friðriksson, Þ., Arnórsson, S., & Bird, D. K. (1999). Porosity evolution and mineral paragenesis during low-grade metamorphism of basaltic lavas at teigarhorn, eastern iceland. *American Journal of Science*, *299*(6), 467–501. https://doi.org/10.2475/ajs.299.6.467

Nugraha, R., O'Sullivan, J., O'Sullivan, M., & Abdurachman, F. (2022). Geothermal modelling: Industry standard practices.

Oude Essink, G. (2001, March 1). *Density dependent groundwater flow: Salt water intrusion*.

Pan, L., Spycher, N., Doughty, C., & Pruess, K. (2014, December). *ECO2n v. 2.0: A new TOUGH2 fluid property module for mixtures of water, NaCl, and CO_2* (LBNL–6930E, 1170605). https://doi.org/10.2172/1170605

Phillips, S. L., Igbene, A., Fair, J. A., Ozbek, H., & Tavana, M. (1981). *A technical databook for geothermal energy utilization* (Lawrence Berkeley Laboratory Report No. LBL-12810). Lawrence Berkeley Laboratory.

Pogge von Strandmann, P. A. E., Burton, K. W., Snæbjörnsdóttir, S. O., Sigfússon, B., Aradóttir, E. S., Gunnarsson, I., Alfredsson, H. A., Mesfin, K. G., Oelkers, E. H., & Gislason, S. R. (2019). Rapid CO2 mineralisation into calcite at the CarbFix storage site quantified using calcium isotopes [Number: 1 Publisher: Nature Publishing Group]. *Nature Communications*, *10*(1), 1983. https://doi.org/10.1038/s41467-019-10003-8

Pruess, K. (1991, May). *TOUGH2: A general-purpose numerical simulator for multiphase fluid and heat flow* (User guide. No. LBL-29400, 5212064). Lawrence Berkeley National Laboratory. California, USA. https://doi.org/10.2172/5212064

Ratouis, T. M., Snæbjörnsdóttir, S. Ó., Voigt, M. J., Sigfússon, B., Gunnarsson, G., Aradóttir, E. S., & Hjörleifsdóttir, V. (2022). Carbfix 2: A transport model of long-term CO2 and h2s injection into basaltic rocks at hellisheidi, SW-iceland. *International Journal of Greenhouse Gas Control*, *114*, 103586. https://doi.org/10.1016/j.ijggc.2022.103586

Sigfússon, B., Arnarson, M. Þ., Snæbjörnsdóttir, S. Ó., Karlsdóttir, M. R., Aradóttir, E. S., & Gunnarsson, I. (2018). Reducing emissions of carbon dioxide and hydrogen sulphide at hellisheidi power plant in 2014-2017 and the role of CarbFix in achieving the 2040 iceland climate goals. *Energy Procedia*, *146*, 135–145. https://doi.org/10.1016/j.egypro.2018.07.018

Sigurðsson, F. (1976, March). *Straumsvíkursvæði: Skýrsla um vatnafræðilega frumkönnun* (OS-JKD-7603). National Energy Authority.

Sigurðsson, F. (1985). Hydrogeology and groundwater on the reykjanes peninsula. *Jökull*, *36*(1), 11–29.

Sigurðsson, F. (1998). Grunnvatnið í straumsvík. *Náttúrufræðingurinn*, *67*(3). https://timarit.is/page/4258631#page/n20/mode/2up

Sigurðsson, Ó., & Stefánsson, V. (1994). *Forðafræðistuðlar – mælingar á bergsýnum (reservoir properties – sample measurements)* (Report OS-94049/JHD-28 B). Reykjavík: Orkustofnun.

Sigurgeirsson, M. Á., Jónsson, J. E., & Ingólfsson, H. (2023, March). *Straumsvík - well CSI-01: Drilling of well CSI-01 from surface down to 982 m* (ÍSOR-2023/006). Iceland GeoSurvey.

Sigurgeirsson, M. Á., Jónsson, J. E., Ingólfsson, H., Kaldal, G. S., & Gunnarsdóttir, S. H. (2024, January). *Straumsvík - well CSM-01: Drilling of well CSM-01 from surface down to 618 m* (ÍSOR-2024/002). Iceland GeoSurvey.

Snæbjörnsdóttir, S. Ó., Oelkers, E. H., Mesfin, K., Aradóttir, E. S., Dideriksen, K., Gunnarsson, I., Gunnlaugsson, E., Matter, J. M., Stute, M., & Gislason, S. R. (2017). The chemistry and saturation states of subsurface fluids during the in situ mineralisation of CO2 and h2s at the CarbFix site in SW-iceland. *International Journal of Greenhouse Gas Control*, *58*, 87–102. https://doi.org/10.1016/j.ijggc.2017.01.007

Snæbjörnsdóttir, S. Ó., Sigfússon, B., Marieni, C., Goldberg, D., Gislason, S. R., & Oelkers, E. H. (2020). Carbon dioxide storage through mineral carbonation. *Nature Reviews Earth & Environment*, *1*(2), 90–102. https://doi.org/10.1038/s43017-019-0011-8

Snæbjörnsdóttir, S. Ó., Tómasdóttir, S., Sigfússon, B., Aradóttir, E. S., Gunnarsson, G., Niemi, A., Basirat, F., Dessirier, B., Gislason, S. R., Oelkers, E. H., & Franzson, H. (2018). The geology and hydrology of the CarbFix2 site, SW-iceland. *Energy Procedia*, *146*, 146–157. https://doi.org/10.1016/j.egypro.2018.07.019

Snæbjörnsdóttir, S. Ó., Wiese, F., Fridriksson, T., Ármansson, H., Einarsson, G. M., & Gislason, S. R. (2014). CO2 storage potential of basaltic rocks in iceland and the oceanic ridges. *Energy Procedia*, *63*, 4585–4600. https://doi.org/10.1016/j.egypro.2014.11.491

Sonnenthal, E., Spycher, N., Xu, T., & Zheng, L. (2021). TOUGHREACT v4.13-OMP & TReactMech v1.0.

Spycher, N., & Pruess, K. (2005). CO2-h2o mixtures in the geological sequestration of CO2. II. partitioning in chloride brines at 12–100°c and up to 600 bar. *Geochimica et Cosmochimica Acta*, *69*(13), 3309–3320. https://doi.org/10.1016/j.gca.2005.01.015

Spycher, N., & Pruess, K. (2010). A phase-partitioning model for CO2–brine mixtures at elevated temperatures and pressures: Application to CO2-enhanced geothermal systems. *Transport in Porous Media*, *82*(1), 173–196. https://doi.org/10.1007/s11242-009-9425-y

Stefánsdóttir, G., Egilson, D., & Þorláksdóttir, S. B. (2020, April). *Eiginleiki grunnvatnshlota undir efnaálagi* (VÍ 2020-002). Icelandic Met Office.

Todd, D., & Mays, L. W. (2005). *Groundwater hydrology* (Third Edition). John Wiley & Sons, Ltd.

Tómasson, H., & Tómasson, J. (1966, December). Geological report on the aluminium plant site at straumsvík.

Tómasson, J., Thorsteinsson, Þ., Kristmannsdóttir, H., & Friðleifsson, I. B. (1977, February). *Höfuðborgarsvæði: Jarðhitarannsóknir 1965 - 1973* (OS-JHD-7703). National Energy Authority.

Vilhjálmsson, A. M., Klausen, K. Ó., Karlsdóttir, K. Á., & Gunnarsdóttir, S. H. (2023). *Saline groundwater exploration near straumsvík using TEM: October 2022 to april 2023* (ÍSOR-2023/50). Iceland GeoSurvey.

Voigt, M., Marieni, C., Baldermann, A., Galeczka, I. M., Wolff-Boenisch, D., Oelkers, E. H., & Gislason, S. R. (2021). An experimental study of basalt–seawater–CO_2 interaction at 130 °c. *Geochimica et Cosmochimica Acta*, *308*, 21–41. https://doi.org/10.1016/j.gca.2021.05.056

Walter, G. R. (1982). Theoretical and experimental determination of matrix diffusion and related solute transport properties of fractured tuffs from the nevada test site. *Los Alamos National Laboratory*, 137.

VIÐAUKI III

ÍSOR
ÍSLENSKAR ORKURANNSÓKNIR
ICELAND GEOSURVEY

Geochemical Model of the Coda Injection Reservoir

Iwona Galeczka

Prepared for Carbfix

ÍSOR-2023/017 June 2023

ICELAND GEOSURVEY
Kópavogur: Urðarhvarf 8, 203 Kóp., Iceland - Tel.: 528 1500
Akureyri: Rangárvellir, P.O. Box 30, 602 Akureyri, Iceland - Tel.: 528 1500
isor@isor.is - www.isor.is

ÍSOR
ICELAND GEOSURVEY

Key page

Report no.	Date	Distribution
ÍSOR-2023/017	June 2023	☒ Open ☐ Closed

Report name / Main and subheadings	Number of copies
Geochemical Model of the Coda Injection Reservoir	1
	Number of pages: 34
Authors: Iwona Galeczka	Project manager: Sveinborg H. Gunnarsdóttir
Classification of report	Project no.: 23-0003

Prepared for
Carbfix

Cooperators

Abstract

The reaction path models were carried out to assess the potential of CO_2 mineralization in the Coda reservoir in Straumsvík. In these models, basalt was dissolved in the CO_2 charged water and secondary minerals were allowed to precipitate at local equilibrium. The resulting water chemical compositions and secondary mineralogies predicted by the models during the CO_2 injection water-host rock interaction are similar to what has previously been observed during basalt weathering and its low temperature alteration. Mixing of the CO_2 injection water and the reservoir water does not affect the overall chemical and mineralogical trends and mineralization efficiencies. The results of the simulations confirm high CO_2 mineralization potential with up to 100% of the injected CO_2 mineralized as calcite. However, due to limited capabilities of the reaction path models and incomplete input data, the spatial and temporal evolution of this process is, however, unknown.

Key words

CO_2 mineralization, Coda Terminal reservoir, reaction path modelling, Straumsvík, Carbfix methodology

Project manager's signature
Sveinborg H. Gunnarsdóttir

Reviewed by
Deirdre Clark

Table of contents

List of tables

List of figures

Ágrip

Í þessari skýrslu er greint frá hermireikningum sem gerðir voru fyrir Coda-verkefnið. Hermireikningar voru gerðir til að spá fyrir um efnahvörf milli CO_2-hlaðna niðurdælingarvökvans og basaltberggrunnsins í geymslugeymi Coda-verkefnisins til að meta fýsileika svæðisins í Straumsvík fyrir steinrenningu CO_2. Hermt var eftir leysingu basaltbergs í niðurdælingarvatninu og efnasamsetning vatnsins og bergs eftir efnahvörf var reiknuð. Í líkangerðinni var notast við efnagreiningar á fersku vatni úr grunnvatnsstraumi í Straumsvík sem áætlað er að leysa CO_2 í og vatni sem er í geymslugeyminum sem safnað var úr rannsóknarborholum ásamt efnagreiningum á bergsýnum úr geymslugeyminum.

Notast var við heildarefnagreiningu á svarfi af 378 m dýpi úr niðurdælingarholu CSI-01 sem boruð var í Straumsvík. Gerð var XRF-greining (*X*-ray fluoroscene) og niðurstöðurnar bornar saman við efnagreiningar á basaltgleri úr Stapafelli á Reykjanesi sem notast hefur verið við í fyrri hermunum á samspili basalts og CO_2 leystu í vatni hér á landi. Niðurstöður á efnagreiningum sýna að bergið í Straumsvík er sambærilegt basalti með efnasamsetninguna $Si_{1.0}Ti_{0.018}Al_{0.378}Fe_{0.174}Mg_{0.301}Ca_{0.271}Na_{0.078}K_{0.004}O_{3.420}$, með steindasamsetninguna 46,1% plagíóklas, 38,9% pýroxen, og 6,9% ólivín. Smektít og zeólítar greindust jafnframt í litlu magni.

Þær síðsteindir sem notast var við í hermireikningunum voru valdar út frá rannsóknum á lághitaummyndun basalts; aðallega leirsteindir, kísilsteindir (kaolinít og kalsedón), kalsít, zeólítar, og járnhýdroxíð.

Vatnssýni úr vatnstökuholum úr Straumsvík voru notuð fyrir hermanir á niðurdælingarvökvanum. Þá voru tvenns konar vökvasýni notuð til að endurspegla geymslugeyminn, annars vegar jarðsjór úr holu CSI-01, sem safnað var við dæluprófun úr holunni, og hinsvegar ferskvatn úr vatnsbóli Hafnarfjarðar. Leiðni í vatnssýni úr vatnstökuholunni í Straumsvík mældist um 100 µS/cm, pH 9,3, basavirkni mældist 0,47 meq/kg og styrkur Cl um 10 mg/L. Leiðni sem mæld var í sýni af jarðsjó úr holu CSI-01 mældist um 40.000 µS/cm, Cl styrkur um 14.200 mg/L, og basavirkni um 0,27 meq/kg. Líkanareikningar fyrir geymslugeymi með jarðsjó voru gerðir við 21°C, sem er það hitastig sem mælt var í holu CSI-01. Líkanreikningar fyrir geymslugeymi með ferskvatni voru gerðir við 4–14°C vegna óvissu um hitastig. Hitastig hafði lítil áhrif á niðurstöður líkanreikninga, enda ekki notast við hvarfhraða við útreikningana.

Notast var við PHREEQC 3.3.12 forritið (Parkhurst og Apello, 2013) og efnavarmafræðilega gagnagrunninn *carbfix.dat* (Voigt o.fl., 2018). Niðurstöðurnar voru svo bornar saman við annars vegar náttúruleg kerfi, þar sem steinrenning CO_2 á sér stað, og hins vegar við fyrri rannsóknir á steinrenningu CO_2 í basalti. Þessi samanburður var gerður til að gefa frekari innsýn í þau ferli sem eiga sér stað við niðurdælingu á CO_2 í geymslugeyminn.

Öfugt við forðafræðilíkön, þar sem reikningar fara fram í tíma og rúmi, gefa efnavarmafræðilegir hermireikningar innsýn í helstu efnaferli milli vatns og bergs sem geta átt sér stað. Þau eru minna viðkvæm fyrir óvissu sem tengist vökvaflæði (poruhluta og lekt) innan geymslugeymisins og henta því betur þegar gögn um slíka eiginleika eru takmörkuð.

Hermireikningarnir voru gerðir til að varpa ljósi á: 1) breytingar á efnasamsetningu niðurdælingarvökvans m.t.t. til leysingar bergs (framvinda efnahvarfa); 2) samsetningu steindafylkis m.t.t. leysingar bergs (eðli og umfang síðsteinda); 3) skilvirkni steindabindingar CO_2 m.t.t mismunandi blöndunar niðurdælingarvökvans og vökvans sem fyrir er í geymslugeyminum (magn uppleysts bergs og magn þess CO_2 sem steinrennur í hermireikningum).

Nokkur líkön efnahvarfa voru hermd í skrefum til að varpa ljósi á framvindu efnahvarfa milli vökvans og bergsins í geymslugeyminum (mynd 1). Í hverju skrefi var fyrirfram ákveðið magn af bergi leyst í vökvanum og í kjölfarið var ákveðnum síðsteindum leyft að falla út. Til að skoða mismunandi sviðsmyndir fyrir niðurdælingu CO_2 í geymslugeymi Coda voru eftirfarandi hermireikningar gerðir:

1) Leysing bergs úr geymslugeymi í niðurdælingarvökvanum.
2) Leysing bergs í mismunandi blöndum af niðurdælingarvökva og vatni sem fyrir er í mynduninni (vatn úr geymslugeymi).
3) Blöndun niðurdælingarvökvans við vatn úr geymslugeymi samhliða leysingu bergs í geymslugeyminum.
4) Blöndun niðurdælingarvökvans við vatn úr geymslugeymi án efnahvarfa.

Í fyrsta líkaninu voru 4 mól/kgw (mól sem magn bergs á hvert kíló af vatni) af bergi leyst upp í niðurdælingarvökvanum í 20 jöfnum skrefum. Framvinda efnahvarfa er skilgreind sem magn bergs sem leyst er í 1 kg af vatni. Niðurstöður sýna að pH hækkar smám saman með auknu magni bergs sem leysist í niðurdælingarvökvanum, úr 3,4 í 11,8 við 21°C, sem er í samræmi við efri mörk pH-gildis í grunnvatnskerfum í basalti (gagnagrunnur ÍSOR). Samhliða lækkar styrkur CO_2 úr um 42.000 ppm í 4 ppm vegna útfellingar kalsíts. Í þessu líkani var kalsít eina karbónatsteindin sem leyft var að falla út, í samræmi við náttúrulegar hliðstæður, en kalsít er langalgengasta karbónatsteindin í grunnvatnskerfum í basalti. Allt CO_2 í niðurdælingarvökvanum var steinrunnið þegar 3,4 mól/kgw af bergi hafði verið leyst í niðurdælingarvökvanum. Fyrstu síðsteindir til að myndast við leysingu bergs í hermireikningunum eru kalsedón, kalsít, leirsteindir (Fe- og Mg-saponít og Na-beidellít) auk hematíts sem var notað sem ígildi járnsteinda í líkaninu. Eftir því sem leysingu bergs vindur fram í hermireikningum og pH hækkar falla út gibbsít og zeólítar (analsím og kabasít). Þessi steindafylki eru í samræmi við lághitaummyndun í basalti.

Í öðru líkaninu var blöndun niðurdælingarvökvans við það vatn úr geymslugeymi hermd og í kjölfarið voru 4 mól/kgw af bergi leyst í mismunandi blöndum. Blöndun var hermd fimm sinnum og voru mismunandi hlutföll hermd hverju sinni milli CO_2-hlaðna niðurdælingarvökvans annars vegar og vatns úr geymslugeymi hinsvegar. Eftirfarandi hlutföll voru hermd: 0,1/0,9, 0,3/0,7, 0,5/0,5, 0,7/0,3, 0,9/0,1. Hermireikningar voru gerðir bæði fyrir blöndun við jarðsjó og ferskvatn. Niðurstöður eru sambærilegar og fyrir líkan 1. Blöndun niðurdælingarvökvans við vökvann sem fyrir er í mynduninni breytir nokkuð magni síðsteinda sem myndast við leysingu bergsins og aukin blöndun verður til þess að minna af bergi þarf til að steinrenna CO_2 úr niðurdælingarvökvanum. Niðurstöður sýna sambærilega samsetningu steindafylkja sem falla út og í fyrsta líkani og ennfremur var lítill munur á milli líkans þegar vatn í geymslugeymi var ferskvatn eða jarðsjór. Niðurstöður benda til þess að efnasamsetning vökvans í geymslugeyminum hafi lítil áhrif við steinrenningu eftir að nægilegt magn af bergi hefur verið leyst upp.

Í þriðja líkaninu var vatni úr geymslugeyminum blandað smátt og smátt við CO_2-hlaðna niðurdælingarvökvann. Í fyrsta skrefinu var 0,01 mól/kgw af bergi leyst í niðurdælingarvökvanum og í kjölfarið blandað við vatn úr geymslugeymi í hlutföllunum 0,9/0,1. Í öðru skrefi var 0,05 mól/kgw af bergi leyst í blöndunni úr fyrsta skrefi og í kjölfarið blandað við vatn úr geymslugeymi í hlutföllunum 0,9/0,1. Seinna skrefið var endurtekið þar til 2 mól/kgw af bergi höfðu verið leyst og vökvinn var yfir >90% vatn úr geymslugeymi. Minna berg var leyst í fyrsta

þrepi til að fá betri sýn á fyrstu efnahvörfin sem verða við niðurdælingu CO_2. Tilraunir þar sem CO_2 er hvarfað við basalt sýna að hröðustu breytingarnar eru í upphafi. Blöndun niðurdælingarvökvans við vatn úr geymslugeymi gerist svo smám saman en óvíst er hvernig hlutfall vatns úr geymslugeyminum eykst eftir því sem fjarlægð frá niðurdælingarholu eykst. Það má þó gera ráð fyrir að pH-gildi niðurdælingarvökvans muni hækka vegna blöndunar við vatn úr geymslugeymi og vegna leysingar á basaltbergi. Þessi pH-hækkun mun hægja á uppleysingu bergs og því var aðeins 2 mól/kgw leyft að leysast í vökvanum í líkaninu. Niðurstöður líkanareikninga fyrir þriðja líkanið, þar sem blöndun og uppleysing bergs gerist smám saman, eru í samræmi við líkan 1 og líkan 2. Líkt og í fyrri líkanareikningum fellur allt CO_2 út í formi karbónatsteinda en í þessum útreikningum gerast efnahvörfin fyrr en í líkani 1. Niðurstöður benda til að blöndun niðurdælingarvökvans við vökvann sem fyrir er í geymslugeyminum hækki pH-gildi vökvans vegna lægri styrks CO_2 við blöndunina. Þessi hækkun verður til þess að steindir hafa aukna tilhneigingu til að myndast. Þessi blöndun verður jafnframt til þess að hlutþrýstingur CO_2 í vökvanum lækkar sem minnkar líkur á því að CO_2 geti afgasast úr vökvanum og lekið til yfirborðs, og eykur því öryggi leysnibindingar CO_2 í geymslugeyminum. Útfelling zeólíta eykst umtalsvert við lok hermireikninga þegar nánast allt berg er uppleyst, nánast allt CO_2 fallið út sem karbónatsteindir, og pH-gildi vökvans hefur hækkað. Þetta er í samræmi við niðurstöður leysnitilrauna þar sem basalt er leyst í CO_2-hlöðnu vatni og í samræmi við náttúrulegar hliðstæður. Þetta bendir jafnframt til þess að myndun zeólíta, sem eru rúmmálsfrekar steindir, muni ekki taka pláss í porum í berggrunninum í námunda við niðurdælingarholur, og munu því ekki hafa umtalsverð áhrif á niðurdælingargetu.

Tilgangur fjórða líkansins, n, er að meta hvort hætta sé á því að kalsít falli út í niðurdælingarholum eða í næsta nágrenni þeirra og hafi þar með áhrif á niðurdælingargetu. CO_2-hlöðnu niðurdælingarvatni var blandað við jarðsjó í mismunandi hlutföllum og var ekkert berg látið leysast í hermununum. Niðurstöður sýna að engin hætta er á útfellingu kalsíts (kalsít er undirmettað) við blöndun niðurdælingarvökvans og vatns í geymslugeyminum án efnahvarfa við berg geymslugeymisins.

Helstu áskoranir hermireikninga fyrir niðurdælingu á CO_2-leystu í vatni í basalt tengjast takmarkaðri þekkingu á efnavarmafræðilegum eiginleikum steinda og myndlausra fasa sem berggrunnurinn samanstendur af, og takmörkuðum gögnum um hvarfhraða. Lágur hvarfhraði veldur því að yfirmettun einstakra steinda í vökvanum verður ekki endilega til þess að steindin fellur út, sér í lagi við lágt hitastig. Þá er óvissa tengd yfirborðseiginleikum steinda, t.d. myndun minna hvarfgjarnra útfellinga á yfirborði, sem hefur áhrif á leysingu bergs og útfellingu síðsteinda sem takmarka getu líkanareikninga til að herma að fullu slík kerfi.

Efnivarmafræðilegir hermireikningar gefa einfalda mynd af þeim ferlum og efnahvörfum sem eiga sér stað, bæði í náttúrulegum kerfum og manngerðum kerfum (e. engineered systems), og geta því ekki gefið nákvæma mynd af skilvirkni steindabindingar. Líkanareikningar af slíkum toga gefa hinsvegar góða mynd af þeim efnahvörfum sem gera má ráð fyrir að eigi sér stað við niðurdælingu CO_2 í basalt í Straumsvík. Þau gefa jafnframt mynd af því hvaða síðsteindir geta myndast og haft áhrif á steinrenningu CO_2 í geymslugeyminum. Hermireikningar geta nýst á margan hátt og hafa ekki aðeins verið notaðir í tengslum við rannsóknir á steinrenningu CO_2 heldur jafnframt til að rannsaka náttúruleg ferli á borð við samspil vatns og bergs í nágrenni eldvirkni, uppsprettur og efnageyma sem hafa áhrif á uppleyst efni í grunnvatni, og til að skoða ferli sem valda útfellingum og tæringu í kerfum. Jafnvel þótt

efnavarmafræðilegir líkanreikningar séu að mörgu leyti takmörkunum háðir eru þeir oft fyrsta rannsóknaraðferðin sem beitt er þegar takmörkuð gögn eru til staðar.

Niðurstöður hermireikninga sýna að geymslugeymir Coda í Straumsvík getur steinrunnið allt CO_2 sem dælt er niður. Eiginleikar bergsins eru svipaðir og basaltbergs þar sem hröð steinrenning CO_2 hefur verið staðfest. Þau steindafylki sem falla út og efnasamsetning vökvans eru sambærileg við það sem gerist í náttúrulegum kerfum vegna efnahvarfa vatns og basalts. Þá eru niðurstöður jafnframt sambærilegar við aðra hermireikninga sem gerðir hafa verið fyrir svipuð kerfi. Hermireikningarnir varpa ekki ljósi á hraða eða útbreiðslu efnahvarfa sem fjallað er um í þessari skýrslu.

Helstu niðurstöður þessarar skýrslu eru m.a. eftirfarandi:

1. Líkanreikningar staðfesta fýsileika berggrunnsins í Straumsvík til að steinrenna CO_2 og sýna steinrenningu allt að 100% þess CO_2 sem dælt er niður sem kalsít. Þróun steinrenningar í geymslugeymi í tíma og rúmi er hinsvegar óþekkt.
2. Efnasamsetning vatns og þeirra síðsteinda sem niðurstöður hermireikninga benda til að myndist við niðurdælingu CO_2 í geymslugeymi í Straumsvík eru í takt við það sem sést við lághitaummyndun basalts. Það staðfestir áreiðanleika líkanareikninga.
3. Niðurstöður líkanreikninga eru jafnframt í samræmi við fyrri líkanareikninga fyrir kerfi þar sem samspil CO_2, basalts og vatns á sér stað.
4. Blöndun CO_2-hlaðins niðurdælingarvatns og þess vatns sem fyrir er í geymslugeyminum hefur ekki áhrif á efnafræðiferli, helstu steindafylki og skilvirkni steindabindingar CO_2. Efnasamsetning vatns í geymslugeymi hefur heldur ekki teljandi áhrif.
5. Blöndun niðurdælingarvatnsins við vatn í geymslugeymi getur hinsvegar hjálpað til við steinrenningu CO_2 á þann hátt að hún á sér stað fyrr í ferlinu.
6. Efnasamsetning basaltsins í geymslugeyminum er sambærileg basalti sem notast hefur verið við í tilraunum á samspili CO_2, basalts og vatns. Þessar tilraunir hafa sýnt fram á mikla getu basaltsins til að steinrenna CO_2, sem aftur bendir til þess að basaltið sem geymslugeymirinn samanstendur af hafi sömu eiginleika.
7. Það er ekki talin hætta á útfellingum kalsíts í niðurdælingarholum eða í næsta nágrenni við þær sem geta haft áhrif á niðurdælingargetu.

Líkan 1: Leysing bergs úr geymslugeymi í niðurdælingarvökva

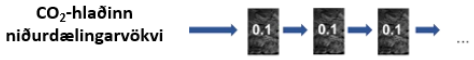

Líkan 2: Blöndun niðurdælingarvökva við vatn úr geymslugeymi og leysing bergs í þeim vökva í kjölfarið

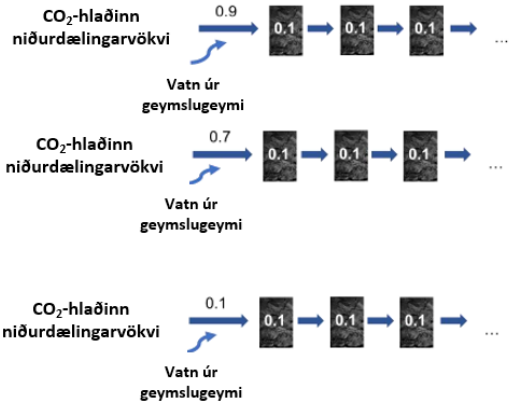

Líkan 3: Blöndun niðurdælingarvökva við vatn úr geymslugeymi ásamt leysingu bergs í þeim vökva í skrefum

Líkan 4: Blöndun niðurdælingarvökva við vatn úr geymslugeymi án leysingar bergs úr geymslugeymi

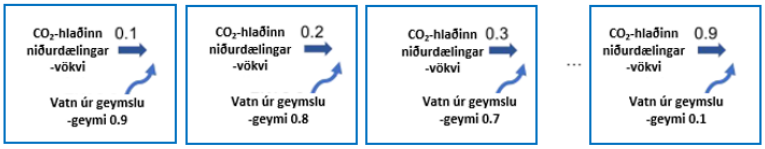

Mynd 1. *Þau fjögur líkön sem hermd voru til að varpa ljósi á efnahvörf milli basaltbergs, CO_2-hlaðna niðurdælingarvökvans og vatns sem fyrir er í myndunninni (vatn úr geymslugeymi).*

1 Introduction

The Carbfix methodology has been demonstrated to be a safe and cost-effective approach to reduce the carbon dioxide (CO_2) emission into the atmosphere. The 2012 pilot study proved that 95% of the CO_2 that was initially injected mineralized mainly as calcium carbonate (calcite, $CaCO_3$) in the shallow reservoir at 20-50°C in less than two years (Matter et al., 2016; Oelkers et al., 2019a; Oelkers et al., 2019b; Snæbjörnsdóttir et al., 2017). Additional H_2S that was injected together with CO_2 precipitated as pyrite in four months. The industrial application of the methodology through the CarbFix2 project started in June 2014 with capturing and injecting a portion of the Hellisheiði geothermal plant emissions into the basaltic subsurface at temperatures of about 260°C (Gunnarsson et al., 2018; Matter et al., 2016; Přikryl et al., 2018). Clark et al. (2020) calculated that 60% of injected CO_2 and over 85% of injected H_2S were mineralized within four months after the gas-charged waters were continuously injected into CarbFix2 site. Followed by its successful outcome, the Carbfix methodology has been a foundation for newly developing CO_2 mineralization projects such as Silverstone, CO_2-Seastone, and Coda Terminal. Once operational in 2026, the first phase of the Coda project assumes an annual injection of 500 kT of CO_2. The CO_2 will be dissolved in fresh water from water supply wells and injected into the storage reservoir. Initial site characterization indicates that at the injection target depth (350-800 m), the water chemical composition varies from seawater to freshwater depending on the location. Using seawater as a CO_2 medium for carbon mineralization has only been studied at laboratory scales (e.g., Voigt et al., 2021; Wolff-Boenisch and Galeczka, 2018) and through geochemical modelling (Marieni et al., 2021). These studies showed that calcite precipitates in CO_2-charged fresh and seawater and mixtures thereof. However, up to date, a field scale injection of freshwater dissolved CO_2 into a mixed seawater and freshwater reservoir does not exist. Therefore, the Coda project and its development is the first of its kind.

This study aims to model the possible chemical reactions between the CO_2-charged injection water (the CO_2 injection water) and basaltic subsurface within the Coda reservoir, ultimately assessing its CO_2 mineralization efficiency. Although similar studies have been performed earlier for the other CO_2 injection sites (CarbFix1, Snæbjörnsdóttir et al., 2018; CarbFix2, Marieni et al., 2021; GECO, Galeczka et al., 2022), here the *in situ* chemical compositions of water and rocks within the Coda storage aquifer are considered. In addition, these model calculations take into account mixing of the CO_2 injection water and the storage reservoir water. The results of the model calculations are also compared with natural analogues and previous studies on CO_2-basalt interaction, providing insight into the Coda carbon mineralization potential.

2 Methodology

2.1 Reaction path model

Geochemical modelling was carried out using the PHREEQC 3.3.12 geochemical code (Parkhurst and Apello, 2013) together with the *carbfix.dat* thermodynamic database (Voigt et al., 2018). As opposed to a reactive transport modeling where time and place of the reactions are predicted, the reaction path simulations provide insights into general trends in water-rock interaction. They are less susceptive to errors related to an unknown fluid flow (porosity, permeability) within the reservoir and are more suitable when only limited data on reservoir properties exist.

The reaction path calculations were performed to assess 1) the composition of the injection water as a function of the amount of dissolved host rock (reaction progress), 2) the secondary mineral assemblages as a function of the amount of dissolved basalt, and 3) the efficiency of CO_2 mineralization considering various mixing scenarios of the CO_2 injection water and the reservoir water (in the targeted storage reservoir). The system was divided into reactive steps to track the progress of the fluid-rock interaction within the host rock. In each reactive step a fixed quantity of rock was dissolved stoichiometrically in the inlet solution followed by precipitation of selected minerals. To account for different scenarios of water-rock interaction during the CO_2 injection into the aquifer, the following models were carried out (also depicted in Figure 1):

1. The host rock (Coda basalt) dissolution in the CO_2 injection water.
2. Mechanical mixing of the CO_2 injection water with the reservoir water followed by the host rock dissolution.
3. Gradual mixing of the CO_2 injection water and the reservoir water with simultaneous dissolution of the host rock.
4. Mechanical mixing with no host rock dissolution.

In the first model, 4 mol_r/kg_w (mol as mass of rock per kilogram of water) of the host rock was stoichiometrically dissolved in the CO_2 injection water in 20 steps. The resulting chemical composition of the reactive solution and the mass of secondary minerals is presented as a function of mass of the dissolved host rock. The reaction progress is defined as the mass of rock dissolved into 1 kg of water.

In the second model, mixing of the CO_2 injection water with the reservoir water was followed by the host rock dissolution. Mixing of both endmembers was simulated five times using different volume fractions, 0.1/0.9, 0.3/0.7, 0.5/0.5, 0.7/0.3, and 0.9/0.1 of CO_2 injection water and reservoir water, respectively. Each water mixture was then used for dissolution of 4 mol_r/kg_w of the host rock in 20 steps. The increasing fraction of the reservoir water in the final mixture simulates the increasing dilution of the CO_2 injection water with the reservoir water. The ratio of the reservoir water in the final mixture increases with increasing distance from the injection well. After mixing, the host rock is dissolved stoichiometrically as described above.

In the third model, the host rock dissolution and mixing of the CO_2 injection water with the reservoir water was simultaneous. In the first step of this model, 0.01 mol_r/kg_w of host rock was dissolved in the CO_2 injection water followed by its mixing with the reservoir water in proportion of 0.9/0.1. In the second step 0.05 mol_r/kg_w of the host rock was dissolved in the

resulting mixture from the first step and the subsequent solution was mixed with the reservoir water in proportion of 0.9/0.1. This calculation step was repeated until 2 mol_r/kg_w of basalt was dissolved and the final solution was composed of >90% reservoir water.

The smaller quantity of the dissolving rock in the first step compared to the second step was chosen to increase the resolution of the modelled chemical trends at the very initial stage of the reaction progress. As observed during water-basalt interaction experiments, the fastest changes in the chemical composition of the reactive outlet solutions are seen in the first hours into the experimental duration (e.g., Clark et al., 2019; Galeczka et al., 2013; Olsson et al., 2013; Wolff-Boenisch et al., 2004). It is anticipated that gradual mixing of the injection and the reservoir water is likely to happen in the subsurface, however, the exact ratios of both endmembers as a function of distance from the injection well are unknown at this stage (Snæbjörnsdóttir et al., 2018). It is expected that a gradual mixing of the CO_2 injection water with the reservoir water will additionally increase the pH of the injection water compared to the pH increase caused by only the dissolution of the host rock (Snæbjörnsdóttir et al., 2018). It is anticipated that this pH increase will slow down the kinetics of the host rock dissolution (e.g., Gislason and Oelkers, 2003). Therefore, only 2 mol_r/kg_w of host rock was allowed to dissolve in the gradual mix reaction path model.

Lastly, to assess whether there is a risk of calcite formation (calcite scaling) in the injection well as the mixture of CO_2 injection water and the saline reservoir water, an additional simulation was carried out where there was mechanical mixing at various mixing fractions of both endmembers. This mechanical mixing was not followed by dissolution of the host rock.

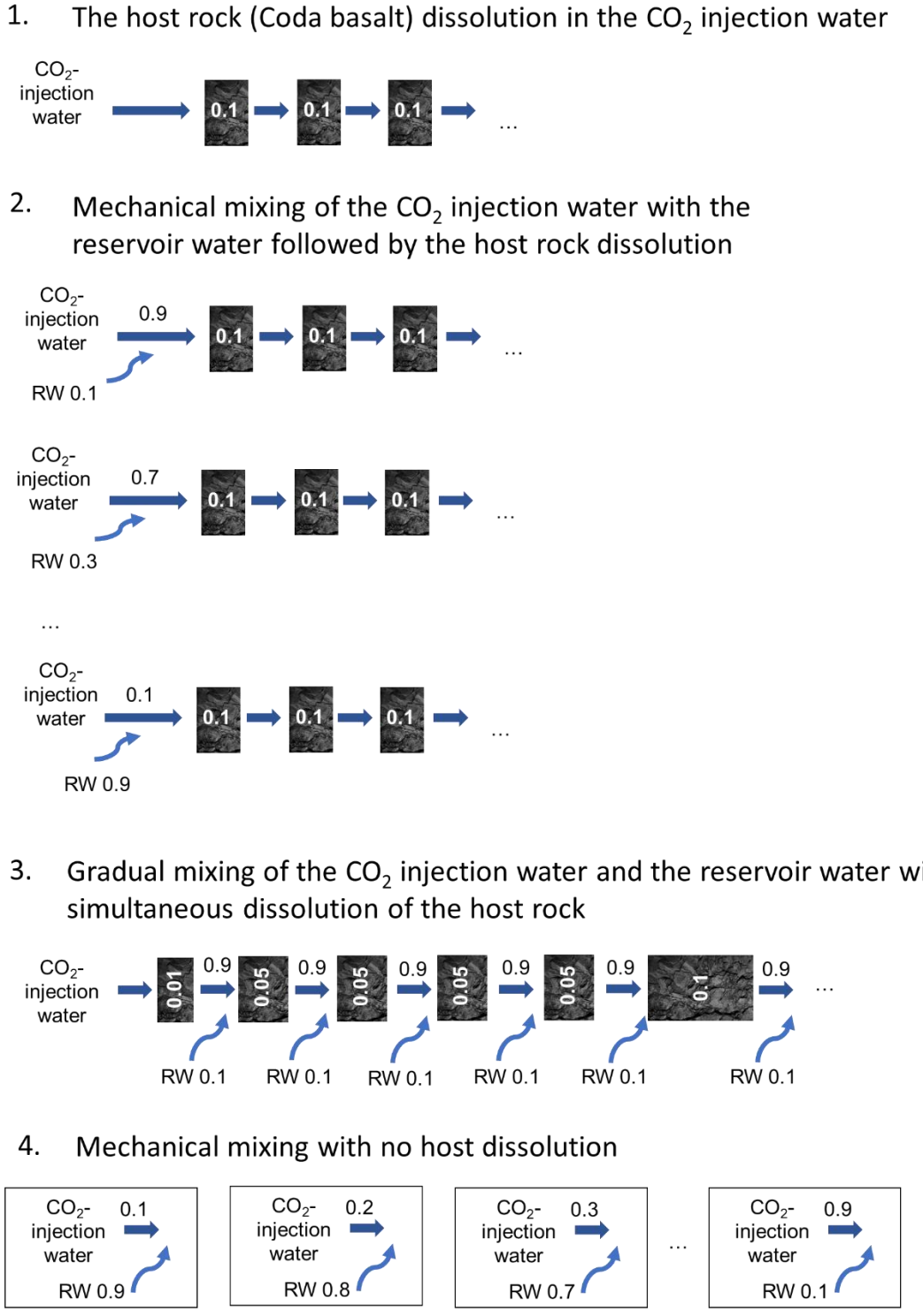

Figure 1. *Conceptual illustration of the scenarios used in the reaction path models simulating interaction between the CO_2 injection water and the host rock and its mixing with the reservoir water. The RW represents the reservoir water; its chemical characteristics is described further in the text. The numbers in the dark grey boxes represent the mol_r/kg_w of the host rock dissolved in the reactive solutions. The numbers next to the reactive solutions (CO_2 injection water, RW) represent the mixing fractions.*

2.2 Host rock composition and secondary mineral alteration

The main feed of the injection well (CSI-01) was identified at an approximate depth of 378 m. Therefore, the bulk chemical composition of basalt from this depth was used as the primary dissolving phase and represents the aquifer host rock (Coda basalt). The chemical composition of the host rock obtained by XRF analysis (X-ray fluorescence) is similar to the composition of mid-ocean ridge basalt (MORB) and Stapafell basaltic glass used in previous studies of CO_2-water-basalt interaction both in the experiments and in the modelling (Table 1; e.g., Clark et al., 2019; Galeczka et al., 2014b; Gislason and Oelkers, 2003; Stockmann et al., 2011; Wolff-Boenisch et al., 2011). The Coda basalt is consistent with $Si_{1.0}Ti_{0.018}Al_{0.378}Fe_{0.174}Mg_{0.301}Ca_{0.271}Na_{0.078}K_{0.004}O_{3.420}$ with the mineralogical composition dominated by plagioclase 46.1 wt.% pyroxene 38.9 wt.%, and olivine 6.9 wt.%. Minor amounts of smectite and zeolites were also found.

Table 1. *The results of the XRF chemical analysis of the Coda host rock used in the current reaction path models. The Stapafell basalt from Gislason and Oelkers (2003) is presented for a comparison.*

Element	Coda basalt	Stapafell basalt
		wt%
SiO_2	46.0	48.1
Al_2O_3	14.8	14.6
CaO	11.6	11.8
$Fe_2O_{3t}^*$	10.6	n.a.
Fe_2O_3	n.a.	1.11
FeO	n.a.	9.82
K_2O	0.15	0.29
MgO	9.28	9.08
MnO	0.20	0.19
Na_2O	1.84	1.97
TiO_2	1.08	1.56
Total	95.6	98.6

n.a. not analyzed; $Fe_2O_{3t}^*$- according to the Mossbauer measurement of the Coda basalt, Fe^{+2} accounts for 65% and Fe^{+3} for 35% of Fe_{tot} resulting in FeO and Fe_2O_3 equal to 6.24 and 3.71 wt%, respectively.

The secondary mineralogy used for the reaction path modelling (Table 2) was constrained based on the alteration mineralogy observed in low temperature basaltic formations. It consists mainly of clays, SiO_2 phases (kaolinite, chalcedony), calcite, zeolites, and Fe-oxy-hydroxides (Alfredsson et al., 2013; Gislason et al., 1996; Gysi and Stefánsson, 2012a; Kristmannsdóttir, 1979; Larsson et al., 2002; Stefánsson and Gíslason, 2001; Marieni et al., 2021). A list of minerals included in the calculations and their reactions are provided in Table 2. Similar to previous studies, secondary minerals were allowed to form at local equilibrium. This approach was taken rather than using an explicit account of mineral-fluid reaction rates due to 1) uncertainties in mineral-fluid interfacial surface area in the subsurface system and 2) the lack of mineral precipitation rate data (Oelkers et al., 2009). Two approaches in the formation of secondary minerals can be used. If secondary minerals are not allowed to dissolve after their precipitation, the models simulate reactions of the injected water front while travelling through the rock reservoir. This is most likely happening in active flow paths. If secondary minerals are allowed to dissolve after their precipitation, the models simulate

mineral replacement reactions that happen in parts of the reservoir where flow is limited such as closed pores.

Table 2. *Primary and secondary phases used in the reaction path modelling. The mineral dissolution reactions were taken from Voigt et al. (2018).*

Phases	Reaction
Host rock composition	$Si_{1.000}Ti_{0.018}Al_{0.378}Fe_{0.174}Mg_{0.301}Ca_{0.271}Na_{0.078}K_{0.004}O_{3.4205}$ + 2.769H^+ + 0.6515H_2O = 2H_2O + 0.378Al^{+3} + 0.271Ca^{+2} + 0.113Fe^{+2} + 0.061Fe^{+3} + 0.004K^+ + 0.301Mg^{+2} + 0.078Na^+ + SiO_2 + 0.018$Ti(OH)_4$
Silicate	
Chalcedony	$SiO_2 = SiO_2$
Carbonates	
Calcite	$CaCO_3 + H^+ = Ca^{+2} + HCO_3^-$
Clay minerals	
Kaolinite	$Al_2Si_2O_5(OH)_4 + 6H+ = 2Al^{+3} + 2SiO_2 + 5H_2O$
Beidellite-Ca	$Ca_{0.175}Al_{2.35}Si_{3.65}O_{10}(OH)_2 + 7.4H^+ = 0.175Ca^{+2} + 2.35Al^{+3} + 3.65SiO_2 + 4.7H_2O$
Beidellite-Fe	$Fe_{0.175}Al_{2.35}Si_{3.65}O_{10}(OH)_2 + 7.4H^+ = 0.175Fe^{+2} + 2.35Al^{+3} + 3.65SiO_2 + 4.7H_2O$
Beidellite-K	$K_{0.35}Al_{2.35}Si_{3.65}O_{10}(OH)_2 + 7.4H^+ = 0.35K^+ + 2.35Al^{+3} + 3.65SiO_2 + 4.7H_2O$
Beidellite-Mg	$Mg_{0.175}Al_{2.35}Si_{3.65}O_{10}(OH)_2 + 7.4H^+ = 0.175Mg^{+2} + 2.35Al^{+3} + 3.65SiO_2 + 4.7H_2O$
Saponite-Fe-Fe	$Fe_{3.175}Al_{0.35}Si_{3.65}O_{10}(OH)_2 + 7.4H^+ = 0.35Al^{+3} + 3.175Fe^{+2} + 3.65SiO_2 + 4.7H_2O$
Saponite-Mg-Mg	$Mg_{3.175}Al_{0.35}Si_{3.65}O_{10}(OH)_2 + 7.4H^+ = 0.35Al^{+3} + 3.175Mg^{+2} + 3.65SiO_2 + 4.7H_2O$
Saponite-Mg-K	$K_{0.35}Mg_3Al_{0.35}Si_{3.65}O_{10}(OH)_2 + 7.4H^+ = 0.35K^+ + 0.35Al^{+3} + 3Mg^{+2} + 3.65SiO_2 + 4.7H_2O$
Saponite-Mg-Fe	$Fe_{0.175}Mg_3Al_{0.35}Si_{3.65}O_{10}(OH)_2 + 7.4H^+ = 0.175Fe^{+2} + 0.35Al^{+3} + 3Mg^{+2} + 3.65SiO_2 + 4.7H_2O$
Saponite-Mg-Na	$Na_{0.35}Mg_3Al_{0.35}Si_{3.65}O_{10}(OH)_2 + 7.4H^+ = 0.35Al^{3+} + 0.35\ Na^+ + 3Mg^{2+} + 3.65SiO_2 + 4.7H_2O$
Zeolites	
Analcime	$Na_{0.96}Al_{0.96}Si_{2.04}O_6{:}H_2O + 3.84H^+ = 0.96Al^{+3} + 2.04SiO_2 + 0.96Na^+ + 2.92H_2O$
Laumontite	$CaAl_2Si_4O_{12}{:}4.5H_2O + 8H^+ = 2Al^{+3} + 4SiO_2 + Ca^{+2} + 8.5H_2O$
Mordenite-Ca	$Ca_{0.5}AlSi5O_{12}{:}4H_2O = Al(OH)_4^- + 0.5Ca^{+2} + 5SiO_2 + 2H_2O$
Chabazite-Ca	$CaAl_2Si_4O_{12}{:}6H_2O = 2Al(OH)_4^- + Ca^{+2} + 4SiO_2 + 2H_2O$
Chabazite-Na	$Na_2Al_2Si_4O_{12}{:}6H_2O = 2Al(OH)_4^- + 2Na^+ + 4SiO_2 + 2H_2O$
Other minerals	
Celadonite	$KMgAlSi_4O_{10}(OH)_2 + 6H^+ = Al^{+3} + K^+ + Mg^{+2} + 4H_2O + 4SiO_2$
Hematite	$Fe_2O_3 + 6H+ = 2Fe^{+3} + 3H_2O$

2.3 Reactive solutions

The reactive solutions used in the models are shown in Table 3. The CO_2 injection water consists of freshwater from the supply well (CSW-02) in Straumsvík. In the model the chemical composition of this water was modified by increasing its CO_2 concentration according to maximum CO_2 solubility at conditions relevant for the injection aquifer (M. Voigt, Carbfix, personal communication, 17.03.2023). Two types of reservoir waters were considered in the model due to possible variability in the chemical composition of water in the storage aquifer. The chemical composition of water discharged from the injection well (CSI-01) during the pumping tests represents the saline aquifer and it is referred to here as the saline reservoir, while the freshwater reservoir is represented by the chemical composition of the drinking water in Hafnarfjörður (Vatnsveita Hafnarfjarðar; Óskarsson, 2022). The reaction path models involving the CO_2 injection water and the saline reservoir were carried out at a temperature of 21°C, which is the temperature measured in the injection well. The temperature in the freshwater reservoir is less known, therefore the final temperature in models simulating

reactions with the freshwater reservoir were performed at temperatures of 4 to 14°C, depending on the mixing fractions between the CO_2 injection water and the freshwater. This temperature difference has little effect on the outcome of the models as the kinetics of dissolution and precipitation were not included in the models. For comparison the chemical composition of seawater collected in Reykjanes is also given in Table 4.

Table 3. *The chemical composition of waters that were used in the reaction path models. Concentrations are given in mg/L.*

	Freshwater[1]	Saline reservoir (CSI-01)	Freshwater reservoir[2]	Reykjanes seawater[3]
Temp. °C	4.20	15.00	3.10	-
pH/°C	9.3/4.2	8.36/20.0	8.98/22.2	8.15/23.1
SiO_2	14.70	6.22	15.20	0.7
B	<0.010	1.04	<0.01	4.17
Na	11.90	6860	10.4	10560
K	0.68	84.90	0.641	380
Ca	4.98	2220	5.33	377
Mg	1.88	212	1.8	1230
Al	0.02	0.01	0.00148	0.001
Fe	0.01	0.18	<0.0004	0.002
CO_2	21.10	10.40	20.7	100
Cl	10.12	14202	8.54	18800
SO_4	2.92	1629	2.88	2550
F	0.09	<0.2	<0.2	0.81

[1] *Freshwater from the supply well (CSW-02). Its chemical composition after increasing the CO_2 concentration to 0.9 mol/L represents the CO_2 injection water. The pH of this CO_2 charged water is calculated to be 3.4 at 21°C.*
[2] *Freshwater reservoir is represented by the chemical composition of the Hafnarfjörður drinking water.*
[3] *Seawater collected in Reykjanes according to the ÍSOR database.*

3 Results and discussion

3.1 Chemical characteristics of the water at the Coda injection site

The freshwater that was collected from the supply well in Straumsvík is dilute with a conductivity of about 100 µS/cm and Cl concentration of 10 mg/L. This water has a pH of 9.3 with a total alkalinity of 0.47 meq/kg. In contrast the saline aquifer water is concentrated with a conductivity of about 40,000 µS/cm, Cl concentration of about 14,200 mg/L, and alkalinity of 0.27 meq/kg. This water has not reached full salinity even after long term well testing (Table 3). The chemical compositions of both waters are similar to the chemical composition of water found in low temperature basaltic subsurface (Table 3; ÍSOR database). The relative mobility (the water/rock concentration ratio, normalized to Na) of cations in the freshwater and the saline aquifer shows typical surface and groundwater mobility with Al, Ti, Fe being the least mobile and Na, K, Ca, and Si the most mobile (Gislason et al., 1996). The freshwater is lighter compared to Reykjanes meteoric water (Figure 2; Pope et al., 2009) based on the oxygen and hydrogen isotopes. This difference suggests that these waters originate from different locations and is consistent with the study of Čypaitė (2015) that the Straumsvík freshwater is affected by groundwater coming from north, probably from Heiðmörk. The processes that control the isotopic signature of the current CSI-01 reservoir water are not fully understood.

However, it is likely that the reservoir water is a mixture of the Reykjanes seawater and the Reykjanes meteoric water.

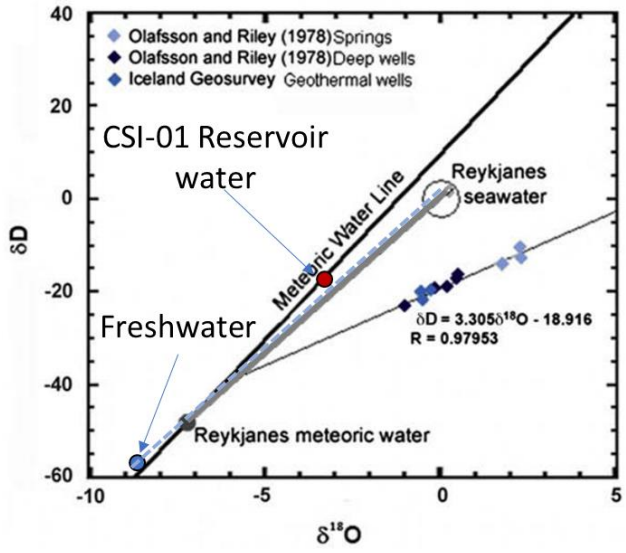

Figure 2. *The isotopic signature of the CSI-01 reservoir and the freshwater from the supply well in Straumsvík. Modified from Pope et al. (2009).*

3.2 Model 1 – The host rock dissolution in the CO_2 injection water

Similar to Alfredsson et al. (2013), in this model 4 mol_r/kg_w of basalt was dissolved in the CO_2 injection water. Although it is uncertain what percentage of the storage reservoir this mass of rock corresponds to, and therefore at what distance from the injection well it would fully dissolve, the resulting modelled concentrations are comparable to groundwaters and low temperature thermal waters in Iceland (e.g., ÍSOR database, Stefánsson et al., 2017). The agreement between the modelled and observed chemical compositions can serve as a theoretical validation of the model outputs. At the final stage of the reaction progress, the concentration of SiO_2 was about 60 ppm, Na 170 ppm, Ca 3 ppm, and Mg, K, and Fe < 1 ppm. The pH equaled to 11.8, which is in the upper range of pH values observed in basalt-hosted groundwater (ÍSOR database).

The results of the reaction path calculations show that with the increasing mass of the dissolved host rock, the pH of the reactive solution gradually increases from the initial pH of 3.4 to 11.8 at 21°C (Figure 3). At the same time the CO_2 concentration decreases from about 42,000 ppm to 4 ppm, coinciding with precipitating calcite (Figure 3). In this model only calcite was allowed to precipitate since it is the main carbonate mineral typically found in basaltic subsurface. The SiO_2 concentration is rather stable reflecting its release from the host rock and instantaneous consumption due to the formation of chalcedony, clays, and zeolites (Figure 4). The slight increase in dissolved SiO_2 at the end of the reaction progress was due to the dissolution of clays followed by the precipitation of zeolites. The concentrations of the other dissolved constituents increase and decrease at different stages of the reaction progress, consistent with the dissolution of the host rock and precipitation of secondary minerals. For example, the modelled Na concentration results from the dissolution of the host rock and its

consumption by clays (Na-beidellite) and zeolites (analcime) at the earlier and later stages of the reaction progress, respectively. Note that in this model the secondary minerals were allowed to dissolve, opposite to that of the Marieni et al. (2021) model. This modification resulted in a better fit of the modelled concentrations to the concentrations observed in low temperature groundwater in Iceland.

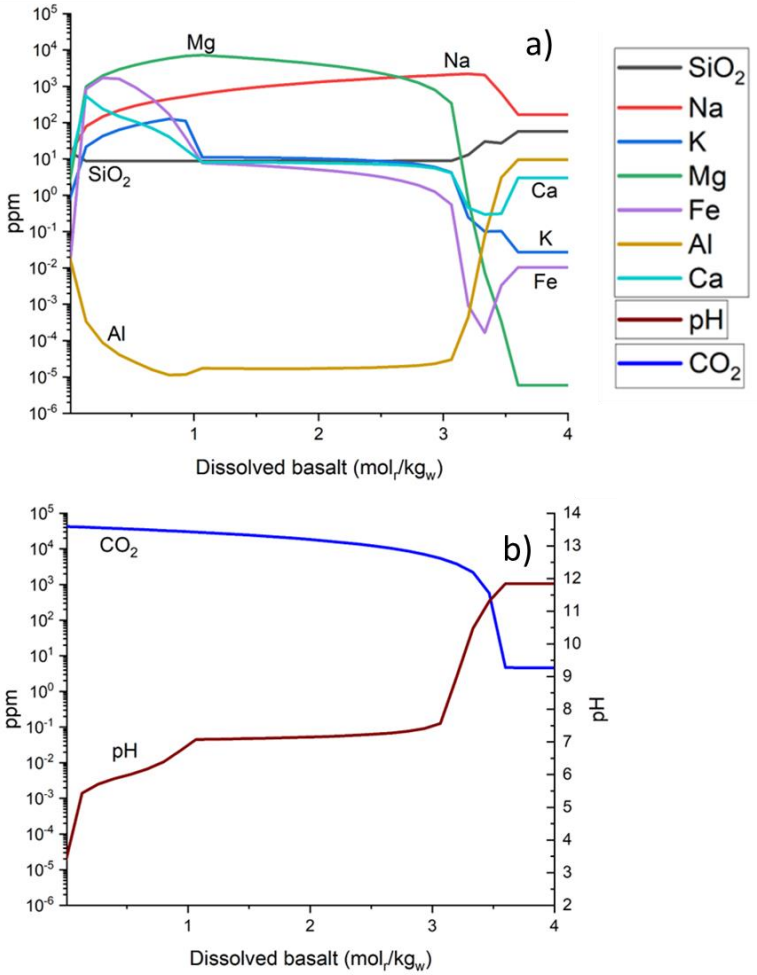

Figure 3. *The evolution of the chemical composition and pH of the CO_2 injection water as a function of reaction progress.*

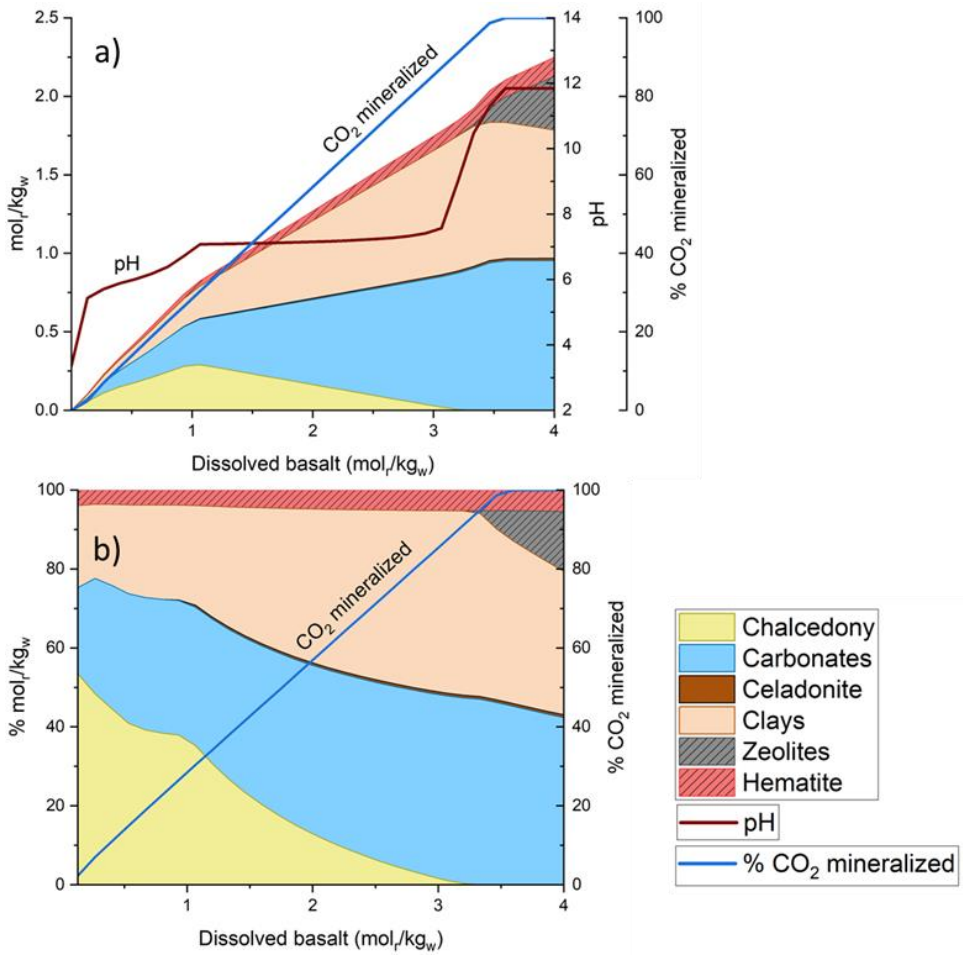

Figure 4. *The results of the reaction path modelling showing the secondary mineral assemblage (a) and mol% of the secondary minerals (b) as a function of reaction progress. The CO_2 mineralization efficiency (% of CO_2 mineralized) and the pH evolution is also shown.*

The first minerals to form as the host rock dissolves are chalcedony, calcite, clays (saponite Fe-Fe, saponite Mg-Mg, beidellite-Na), and hematite (Figure 4). Note that here hematite represents the Fe-containing phase since the reactive solution had too high dissolved Fe concentrations when other Fe-phases (e.g., Fe-hydroxide) were allowed to precipitate in the model. Later into the reaction progress, gibbsite and zeolites (analcime, chabazite-Ca) formed. Similar to the chemical composition, the resulting mineral assemblage is consistent with what has been observed in basaltic low temperature systems (e.g., Alfredsson et al., 2013; Stefánsson and Gíslason, 2001) and in the experiments on CO_2-water-basalt interaction (e.g., Gysi and Stefánsson, 2012a,b). Most calcite was predicted to form up to a pH 11.3 and CO_2 concentration of about 500 ppm ($fCO_2 = 2^{-7}$ atm, where f represents fugacity). With a further decrease in CO_2 concentration, only a small amount of calcite formed and most of the dissolved Ca was consumed by zeolites. This indicates that low concentrations of CO_2 (low fCO_2) might limit carbon mineralization, assuming a sufficient dissolution of a host rock and supply of divalent cations. This dissolution, however, is often considered a limiting factor for carbon mineralization due to the slow kinetics of basalt dissolution, especially at low temperature. As calculated by Marieni et al. (2021), basaltic glass dissolution proceeds at rates almost two orders of magnitude slower at 25°C compared to 260°C. As can be seen in Figure 3, all the initially

dissolved CO_2 in the CO_2 injection water was mineralized after dissolution of 3.5 mol_r/kg_w of the host rock. Similarly, substantial amount of basalt dissolution was needed for efficient CO_2 mineralization in models carried out by Alfredsson et al. (2013) and Marieni et al. (2021).

3.3 Model 2 – Mechanical mixing followed by the host rock dissolution

This simulation involved mixing of the CO_2 injection water and the reservoir water at various proportions as described in the method section. In the resulting mixture, 4 mol_r/kg_w of the host rock was dissolved stoichiometrically. In the first scenario, saline water represented the reservoir water. As can be seen in Figure 5, the general trends in secondary mineral assemblage are similar to the results of model 1 where the host rock was dissolved in the CO_2 injection water. Mixing of the CO_2 injection water with the saline reservoir water, however, changes slightly the amount of secondary minerals and the mol% of the minerals in the secondary alteration. At a mixing fraction of 0.1/0.9 of the CO_2 injection water and the saline water and after dissolution of 4 mol_r/kg_w of the host rock, 1.3 mol_r/kg_w of secondary minerals forms. In contrast, 1.6 mol_r/kg_w and 2.2 mol_r/kg_w of secondary minerals precipitate at mixing proportions of 0.5/0.5 and 0.9/0.1, respectively. As the proportion of the saline water in the mixture decreases, the contribution of calcite in the secondary mineral assemblage increases. Moreover, with the increasing proportion of the reservoir water, the mass of dissolved basalt to reach 100% CO_2 mineralization decreases. Although the mineralization efficiency reaches 100% in all the scenarios, it decreases further into the reaction progress. This is because calcite is allowed to dissolve in the simulation when the mixture is undersaturated with respect to this mineral. If calcite was not allowed to dissolve, the CO_2 mineralization efficiency would have remained at 100%. Note that mineralization efficiency is calculated using the CO_2 concentration after mixing with the reservoir water. The conditions at which the water-rock interaction takes place will determine whether precipitation and dissolution of the secondary minerals occurs. As mentioned before, in a closed system, with a finite supply of CO_2 (e.g., closed pore space), it is likely that calcite would be replaced by another mineral (e.g., Gislason et al., 1996). At the injected waterfront, where water moves away from the precipitated minerals – secondary minerals would probably not dissolve. It is most likely that both scenarios happen at the same time. Modeling of such complex scenarios is beyond the scope of this study.

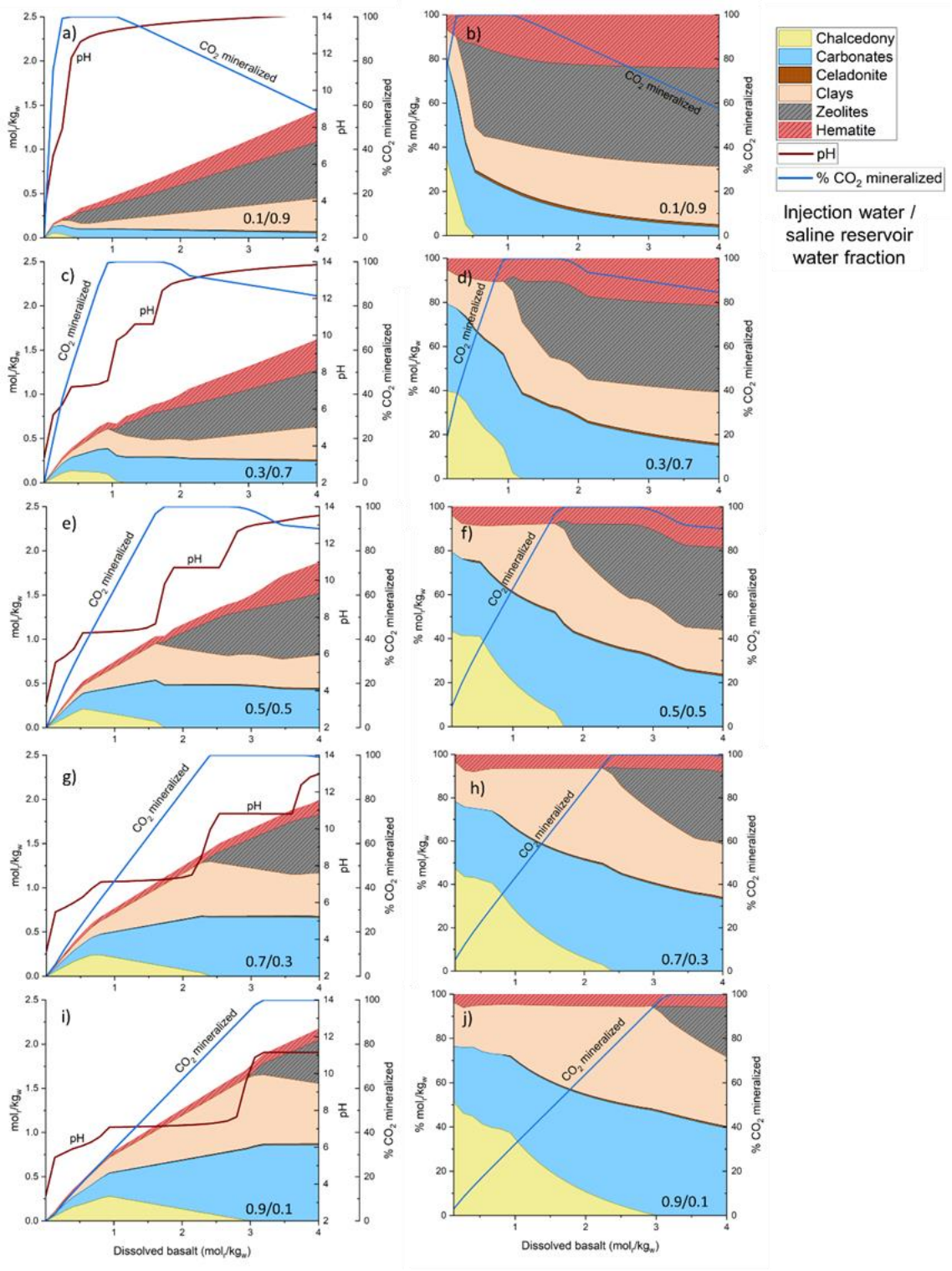

Figure 5. *The results of the reaction path model when the CO_2 injection water is mixed with the saline reservoir water at various fractions followed by dissolution of 4 mol_r/kg_w of the host rock. The mixing fraction shown on the plots indicate a fraction of the CO_2 injection water and the saline water, respectively. The CO_2 mineralization efficiency (% of CO_2 mineralized) and the pH evolution is also shown.*

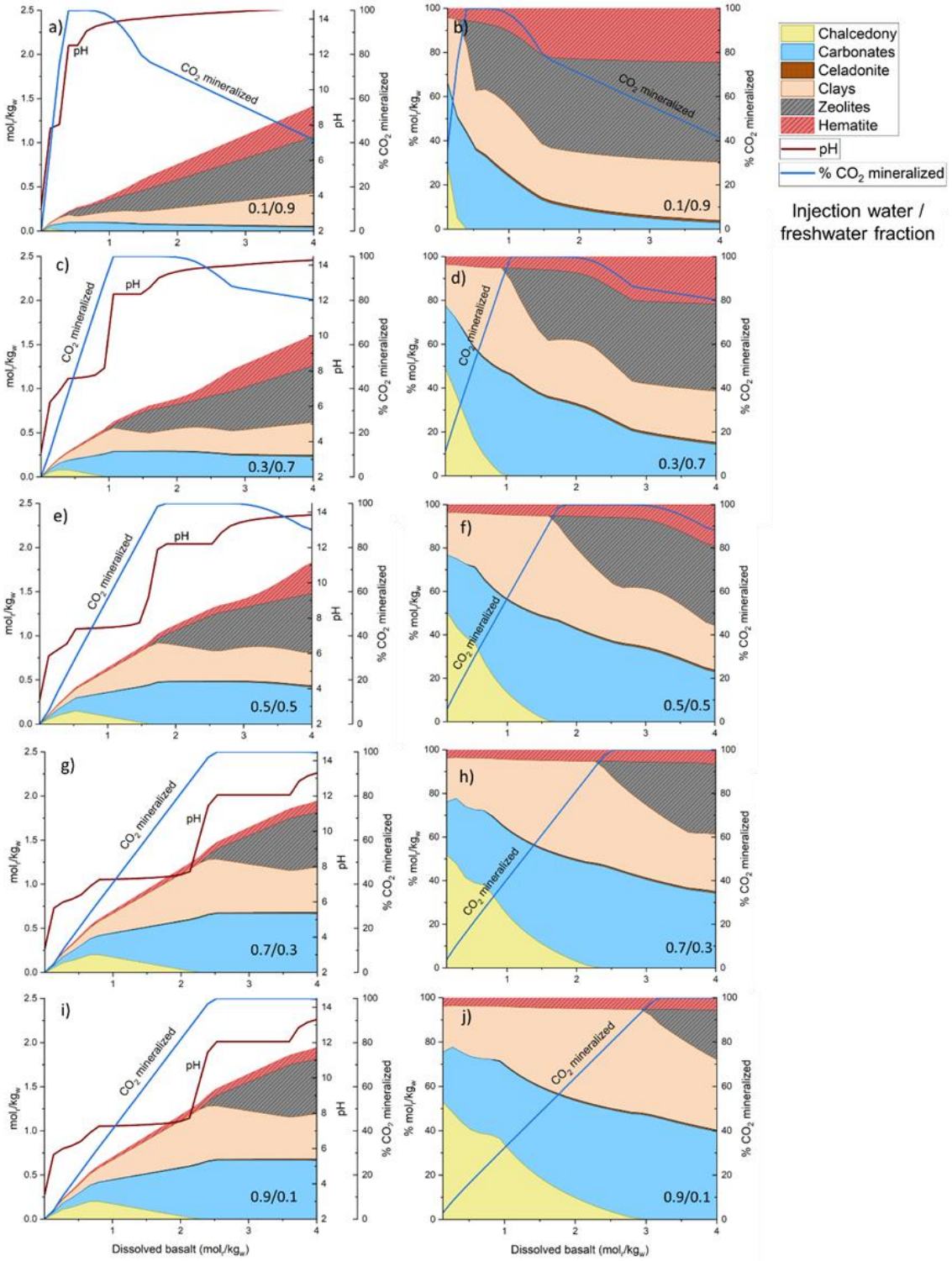

Figure 6. *The results of the reaction path model when the CO_2 injection water is mixed with the freshwater at various fractions followed by dissolution of 4 mol_r/kg_w of the host rock. The mixing fraction shown on the plots indicate a fraction of the CO_2 injection water and the freshwater, respectively. The CO_2 mineralization efficiency (% of CO_2 mineralized) and the pH evolution is also shown.*

The results of the simulation where the host rock dissolution is preceded by mixing the CO_2 injection water with the freshwater are shown in Figure 6. Similar mineral assemblages and mineral mol% contributions compared to previous model are predicted. The slight differences between both models (saline vs freshwater) are within the uncertainty of the model calculations. This indicates that the chemical composition of water in the storage reservoir plays a minor role in the mineralization process when sufficient amounts of host rock are dissolved. As shown previously, the ionic strength can affect basalt dissolution kinetics and carbon mineralization (Voigt et al., 2021; Wolff-Boenisch et al., 2011). Consequently, more substantial differences in secondary mineral assemblages as a function of the reaction progress compared to the model outcome might be observed during the CO_2 field injection depending on the salinity of the storage aquifer.

3.4 Model 3 – Gradual mixing of the CO_2 injection water and the reservoir water with simultaneous dissolution of the host rock

Results of the simulations where mixing of the CO_2 injection water and the reservoir water (saline and freshwater) is shown in Figure 7 and 8, respectively. Both models predict similar quantities and mineral assemblages compared to previous models. Similar mineralization efficiencies reaching 100% of the initial CO_2 dissolved in the injection water are predicted by the models. Note that this full mineralization is anticipated earlier in terms of the reaction progress compared to model 1 where the host rock was dissolved in the CO_2 injection water (Figure 4). This faster mineralization applies also to the models where dissolution of the host rock is followed by mixing the CO_2 injection water with the reservoir water (saline and freshwater; Figure 5 and 6). This indicates that mixing with the reservoir water dilutes the CO_2 concentration, which increases the pH of the reactive solution and therefore enhances the mineralization at the earlier stages of the reaction progress. This further decreases the pCO_2 in the reservoir water, making it less buoyant at the initial stage of the reaction progress resulting in reduced risk of CO_2 leakage, and consequently increasing the safety of the CO_2 injection. The early stage of reaction progress represents with close proximity to the CO_2 injection well. However, it is unknown what distance from the injection well a specific reaction progress stage corresponds to.

The mol% of zeolites increases substantially at the end of reaction progress after most of injected CO_2 is mineralized. This is in accord with field and experimental observations (e.g., Gysi and Stefánsson, 2012ab). This also indicates that formation of zeolites characterized by high molar volume will not consume pore space during the early stage of reaction progress, therefore their precipitation will have a limited effect on the injectivity in the vicinity of the CO_2 injection well.

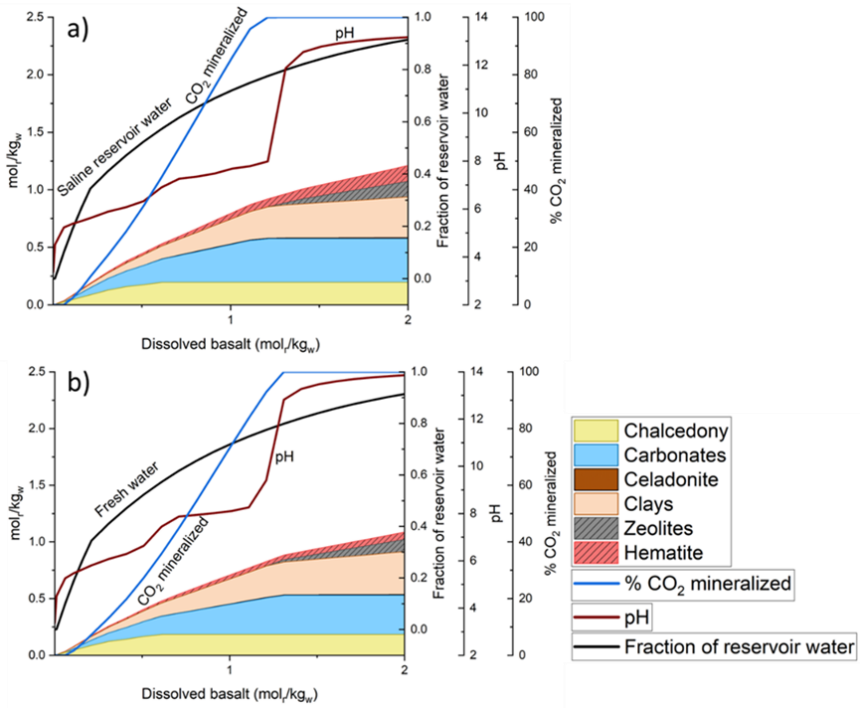

Figure 7. *Secondary mineral assemblages according to the results of the reaction path model simulating gradual mixing of the CO_2 injection water with the reservoir water and subsequent dissolution of 2 mol_r/kg_w of the host rock. The reservoir water is represented by the saline water (a) and the freshwater (b).*

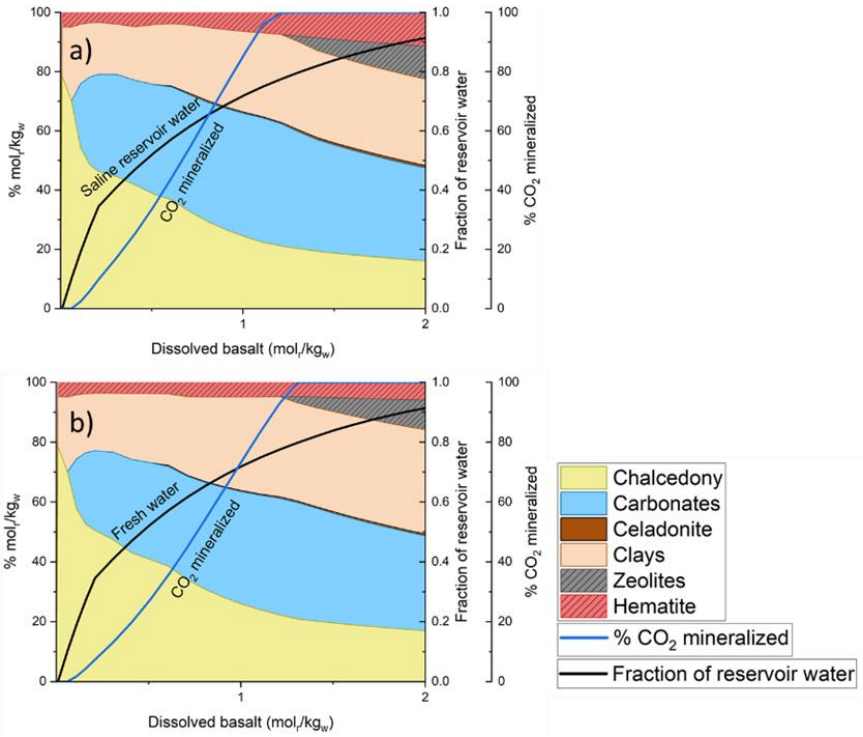

Figure 8. *Mol% of minerals in secondary assemblages according to the results of the reaction path models simulating gradual mixing of the CO_2 injection water with the reservoir water and subsequent dissolution of 2 mol_r/kg_w of the host rock. Reservoir water is represented by the saline water (a) and the freshwater (b).*

3.5 Model 4 - Mechanical mixing with no host rock dissolution

The calcite saturation index (SI) of the saline reservoir water is equal to 0.6 indicating a possibility of calcite precipitation as opposite to freshwater, which is slightly undersaturated with respect to calcite (-0.1). Calcite formation in geothermal surface installations has been observed when waters with distinct salinities/ionic strengths mix (e.g., Selfoss district heating; Galeczka et al., 2020; Ólafsson et al., 2005). Because the CO_2 injection water has more than two orders of magnitude lower ionic strength compared to the saline storage aquifer (1.8 vs 490 $mmol/kg_w$, respectively) the mechanical mixing of both endmembers was simulated to assess the risk of calcite formation in the injection well as the CO_2 injection water and the saline reservoir water mix. As can be seen in Figure 9, the final mixture of the CO_2 injection water and the saline water is supersaturated with respect to calcite only when the contribution of the latter is high, e.g., > 0.9999 volume fraction. This is because the CO_2 concentration in the CO_2 injection water is high and the pH low, resulting in water being highly undersaturated with respect to calcite. As the proportion of the CO_2 injection water increases in the mixture, the pH decreases rapidly to 5.6, 4.6, and 3.8 at CO_2 injection water fractions of 0.001, 0.01, and 0.1, respectively. With higher amounts of CO_2 injection water, the pH decreases but not as rapidly.

The results of this model show that there is no risk of calcite precipitation during mixing of the CO_2 injection water with the saline water without dissolution of the host rock. Moreover, without dissolution, considerable pH increase happens only when the contribution of the saline water in the final mixture is high, e.g., to rise the pH from 3.4 to 5.6, the fraction of the saline water would have to be > 0.999 in the final mixture. This indicates that instant dilution of the CO_2 injection water with the saline water that can take place inside/close to the injection well will most likely keep the pH low and enhance the host rock dissolution, and therefore the supply of divalent cations for carbon mineralization.

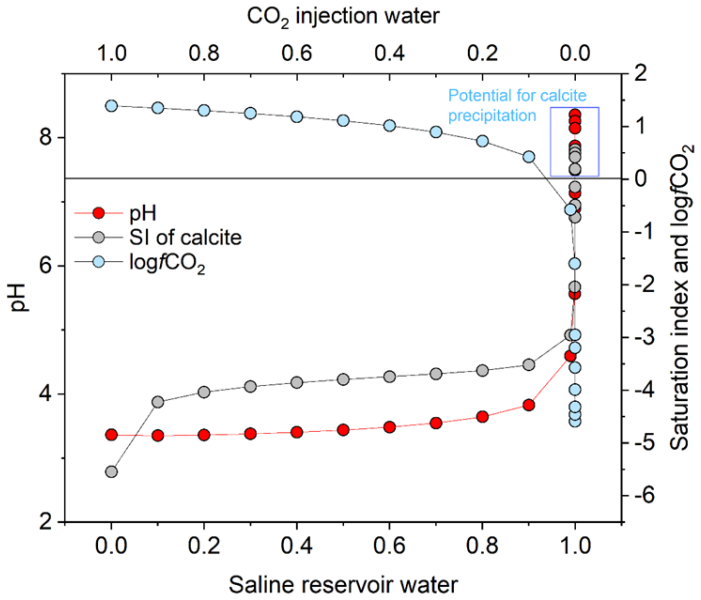

Figure 9. *The evolution of pH, logfCO₂ and Cl during mechanical mixing between the CO₂ injection water and the saline reservoir water. The numbers on the x-axis represent the mixing fractions of both endmembers.*

4 Concluding remarks

4.1 Limitations and capacities of the geochemical reaction path models

Poor understanding of the thermodynamic properties of minerals and amorphous phases that represent the host rock and limited availability of their kinetic data (e.g., Heřmanská et al., 2022; Oelkers et al., 2009) are the main challenges in modelling of the fate and consequences of CO_2 water injection into the subsurface. The secondary phases attaining local equilibrium with the fluid control to a large extent the mobility of dissolved constituents that are further affecting the dissolution of host rock (Gislason and Oelkers, 2003). The supersaturation of fluid with respect to a given mineral does not necessarily result in its immediate precipitation due to sluggish kinetics, especially at low temperatures (e.g., Saldi et al., 2009; Schott et al., 2012). In addition, the presence of passivating layers on the primary minerals slows mineral dissolution rates, and due to complexity of this process are not included in this geochemical modelling calculations (Daval et al., 2011). Furthermore, uncertainty related to mineral reactive surface areas that controls dissolution and precipitation limits successful prediction of the reaction progress (e.g., Navarre-Sitchler et al., 2013; White and Brantley, 2003; Zhu et al., 2006).

The geochemical simulation using reaction path modelling simplifies the processes and/or reactions that happen in natural or engineered systems, and they cannot be used for definite quantification of the mineralization efficiency. These models give, however, an idea of what can be expected during CO_2 injection into the basaltic subsurface in (Straumsvík) Iceland. They also identify competing secondary minerals formation that can impact the CO_2 mineralization in the injection aquifer. The applicability of these models is wide; they have not only been used in CO_2 mineralization studies (e.g. Alfredsson et al., 2013; Clark et al., 2019; Galeczka et al., 2014b; Gysi and Stefánsson, 2011; Marieni et al., 2021; Paukert et al., 2012; Přikryl et al., 2018), but also to investigate natural processes like water-rock interaction in the presence of volcanic products (Flaathen et al., 2009; Galeczka et al., 2014a; Kaasalainen and Stefánsson, 2012), sources and sinks of dissolved constituents in aquifers (Kleine et al., 2020), and assessment of engineering processes such as scaling and corrosion (Bozau et al., 2015; Li et al., 2020). Even though the limitations of reaction path models are substantial, they are often the first ones to be carried out when only limited field data on water flow and mixing properties in the storage reservoir exists.

4.2 The Coda storage reservoir

The results of the reaction path models of the Coda injection reservoir indicate that full mineralization of the injected CO_2 is possible (100% of the injected CO_2 precipitates as calcite). However, this modeling does not provide information about where and when in the reservoir this will happen. The reaction path models that were carried out for the Carbfix1 and CarbFix2 injection reservoirs (Snæbjörnsdóttir et al., 2018; Marieni et al., 2021) were validated against the chemical data acquired from the monitoring boreholes. The results of current models of the CO_2 injection at the Coda storage site cannot be validated due to the unavailability of such data. However, the general chemical trends and CO_2 mineralization efficiencies predicted by the current models are similar to previous CO_2-water-basalt interaction models, giving credibility to the outcome of these models.

The Coda host rock has similar characteristics to basaltic host rocks where formation of carbonate minerals as a result of CO_2 injection has been proven. In addition, the low temperature in the Coda storage reservoir is suitable for carbonate minerals formation. Marieni et al. (2021) showed that at lower temperatures CO_2 mineralizes more efficiently as there are fewer Ca-bearing non-carbonate minerals that compete for Ca. The slow reaction rates at these low temperatures should, however, be compensated for by longer flow paths or slower flow rates than at higher temperatures. The extent and direction of the flow paths in Coda reservoir is, however, unknown at the time of writing this report. At the CarbFix1 injection site, calcite started to form at a relatively low pH in accordance with the pH 'sweet spot' estimated to be 5.2-6.5 at 20-50°C (Snæbjörnsdóttir et al., 2018). Similarly, in Coda models, calcite is predicted to form at a relatively early stage of the reaction progress, limiting the risk of CO_2 leakage in the vicinity of the injection site. Moreover, mixing of the CO_2 injection water with the reservoir water will further accelerate (as a function of reaction progress) mineralization, assuming that the kinetics of the host rock dissolution and calcite precipitation will not be hindered. The relatively high initial CO_2 concentration in the CO_2 injection water (0.9 mol/L) is similar to the CarbFix1 pilot injection (0.8 mol/L) (Snæbjörnsdóttir et al., 2017). Such high CO_2 concentrations are beneficial as it delays the formation of zeolites and enhances the host rock dissolution. This has been observed at the CarbFix2 injection site where the CO_2 mineralization efficiency increased from 50% to 60% after increasing the initial concentration of CO_2 in the injection fluid from 31 mM to 51 mM (Clark et al., 2020).

5 Summary

Major conclusions of this study include:

1. The reaction path models confirm high CO_2 mineralization potential with up to 100% of the injected CO_2 mineralized as calcite. The spatial and temporal evolution of this process is, however, unknown.
2. The water chemical compositions and secondary mineralogies predicted during the CO_2 injection into the Coda reservoir are similar to what has previously been observed during basalt weathering and its low temperature alteration. This gives credibility to the outcomes of the current models.
3. Results of the reaction path models are also consistent with the previous geochemical models of CO_2-basalt-water interaction systems.
4. Mixing of the CO_2 injection water and the reservoir water does not affect the overall chemical and mineralogical trends and mineralization efficiencies. These trends are also independent of characteristics of the reservoir water (saline vs freshwater).
5. The mixing will, however, allow mineralization of the injected CO_2 at an earlier stage of reaction progress, limiting the risks associated with a CO_2 leakage in the vicinity of the injection well.
6. The chemical composition of the Coda basalt is similar to the chemical composition of rocks that were used during the CO_2-basalt-water interaction experiments. These experiments proved high CO_2 mineralization potential in such rocks indicating high potential for CO_2 mineralization in the Coda basalt.
7. There is a limited risk of calcite scaling when the CO_2 injection water will mix with the reservoir water within the injection well.

6 References

Alfredsson, H.A., Oelkers, E.H., Hardarsson, B.S., Franzson, H., Gunnlaugsson, E., and Gislason, S.R. (2013). The geology and water chemistry of the Hellisheidi, SW-Iceland carbon storage site. *International Journal of Greenhouse Gas Control 12*, 399-418.

Bozau, E., Häußler, S., and van Berk, W. (2015). Hydrogeochemical modelling of corrosion effects and barite scaling in deep geothermal wells of the North German Basin using PHREEQC and PHAST. *Geothermics 53*, 540-547.

Clark, D.E., Galeczka, I.M., Dideriksen, K., Voigt, M.J., Wolff-Boenisch, D., and Gislason, S.R. (2019). Experimental observations of CO_2-water-basaltic glass interaction in a large column reactor experiment at 50 °C. *International Journal of Greenhouse Gas Control 89*, 9-19.

Clark, D.E., Oelkers, E.H., Gunnarsson, I., Sigfússon, B., Snæbjörnsdóttir, S.Ó., Aradóttir, E.S., and Gíslason, S.R. (2020). CarbFix2: CO_2 and H_2S mineralization during 3.5 years of continuous injection into basaltic rocks at more than 250 °C. *Geochimica et Cosmochimica Acta 279*, 45-66.

Čypaitė, Vaiva (2015). *Determination of groundwater flow in SW Iceland with environmental tracers.* Master's thesis, Faculty of Earth Sciences, University of Iceland, pp. 76

Daval, D., Sissmann, O., Menguy, N., Saldi, G.D., Guyot, F., Martinez, I., Corvisier, J., Garcia, B., Machouk, I., Knauss, K.G., and Hellmann, R. (2011). Influence of amorphous silica layer formation on the dissolution rate of olivine at 90°C and elevated pCO_2. *Chemical Geology 284*, 193-209.

Flaathen, T.K., Gislason, S.R., Oelkers, E.H., and Sveinbjörnsdóttir, Á.E. (2009). Chemical evolution of the Mt. Hekla, Iceland, groundwaters: A natural analogue for CO_2 sequestration in basaltic rocks. *Applied Geochemistry 24*, 463-474.

Galeczka, I. M., Harðardóttir, V., and Haraldsson, S.Þ. (2020). The Metal Scavenging by Calcite Scaling Formed During Utilization of the Low Temperature Geothermal Waters. a Case Study in Selfoss Geothermal Area, Sw Iceland. In *Proceedings World Geothermal Congress 2020+1, Reykjavík, Iceland, April - October 2021.*

Galeczka, I., Oelkers, E.H., and Gislason, S.R. (2014a). The chemistry and element fluxes of the July 2011 Múlakvísl and Kaldakvísl glacial floods, Iceland. *Journal of Volcanology and Geothermal Research 273*, 41-57.

Galeczka, I., Wolff-Boenisch, D., and Gislason, S. (2013). Experimental Studies of Basalt-H_2O-CO_2 Interaction with a High Pressure Column Flow Reactor: The Mobility of Metals. *Energy Procedia 37*, 5823-5833.

Galeczka, I., Wolff-Boenisch, D., Oelkers, E.H., and Gislason, S.R. (2014b). An experimental study of basaltic glass–H_2O–CO_2 interaction at 22 and 50°C: Implications for subsurface storage of CO_2. *Geochimica et Cosmochimica Acta 126*, 123-145.

Galeczka, I.M., Stefánsson, A., Kleine, B.I., Gunnarsson-Robin, J., Snæbjörnsdóttir, S.Ó., Sigfússon, B., Gunnarsdóttir, S.H., Weisenberger, T.B., and Oelkers, E.H. (2022). A pre-injection assessment of CO_2 and H_2S mineralization reactions at the Nesjavellir (Iceland) geothermal storage site. *International Journal of Greenhouse Gas Control 115*, 103610.

Gislason, S.R., and Oelkers, E.H. (2003). Mechanism, rates, and consequences of basaltic glass dissolution: II. An experimental study of the dissolution rates of basaltic glass as a function of pH and temperature. *Geochimica et Cosmochimica Acta 67*, 3817-3832.

Gislason, S.R., Arnorsson, S., and Armannsson, H. (1996). Chemical weathering of basalt in Southwest Iceland; effects of runoff, age of rocks and vegetative/glacial cover. *American Journal of Science 296*, 837-907.

Gunnarsson, I., Aradóttir, E.S., Oelkers, E.H., Clark, D.E., Arnarson, M.Þ., Sigfússon, B., Snæbjörnsdóttir, S.Ó., Matter, J.M., Stute, M., Júlíusson, B.M., and Gíslason, S.R. (2018). The rapid and cost-effective capture and subsurface mineral storage of carbon and sulfur at the CarbFix2 site. *International Journal of Greenhouse Gas Control 79,* 117-126.

Gysi, A.P., and Stefánsson, A. (2011). CO_2–water–basalt interaction. Numerical simulation of low temperature CO_2 sequestration into basalts, *Geochimica et Cosmochimica Acta 75 (17)*, 4728-4751.

Gysi, A.P., and Stefánsson, A. (2012a). CO_2-water–basalt interaction. Low temperature experiments and implications for CO_2 sequestration into basalts. *Geochimica et Cosmochimica Acta 81*, 129-152.

Gysi, A.P., and Stefánsson, A. (2012b). Experiments and geochemical modeling of CO_2 sequestration during hydrothermal basalt alteration. *Chemical Geology 306-307*, 10-28.

Heřmanská, M., Voigt, M.J., Marieni, C., Declercq, J., and Oelkers, E.H. (2022). A comprehensive and internally consistent mineral dissolution rate database: Part I: Primary silicate minerals and glasses. *Chemical Geology 597*, 120807.

Kaasalainen, H., and Stefánsson, A. (2012). The chemistry of trace elements in surface geothermal waters and steam, Iceland. *Chemical Geology 330–331*, 60-85.

Kleine, B.I., Stefánsson, A., Kjartansdóttir, R., Prause, S., Weisenberger, T.B., Reynolds, H.I., Sveinbjörnsdóttir, Á.E., Jackson, M.D., and Gudmundsson, M.T. (2020). The Surtsey volcano geothermal system: An analogue for seawater-oceanic crust interaction with implications for the elemental budget of the oceanic crust. *Chemical Geology 550*, 119702.

Kristmannsdóttir, H. (1979). Alteration of Basaltic Rocks by Hydrothermal-Activity at 100-300 °C. Developm. Sed. 27, 359-367.

Larsson, D., Grönvold, K., Oskarsson, N., and Gunnlaugsson, E. (2002). Hydrothermal alteration of plagioclase and growth of secondary feldspar in the Hengill Volcanic Centre, SW Iceland. *Journal of Volcanology and Geothermal Research 114*, 275-290.

Li, Y., Pang, Z., and Galeczka, I.M. (2020). Quantitative assessment of calcite scaling of a high temperature geothermal well in the Kangding geothermal field of Eastern Himalayan Syntax. *Geothermics 87,* 101844.

Matter, J.M., Stute, M., Snæbjörnsdottir, S.Ó., Oelkers, E.H., Gislason, S.R., Aradottir, E.S., Sigfusson, B., Gunnarsson, I., Sigurdardottir, H., Gunnlaugsson, E., Axelsson, G., Alfredsson, H.A., Wolff-Boenisch, D., Mesfin, K., Taya, D.F.d.l.R., Hall, J., Dideriksen, K., and Broecker, W.S. (2016). Rapid carbon mineralization for permanent disposal of anthropogenic carbon dioxide emissions. *Science 352*, 1312-1314.

Marieni, C., Voigt, M., Clark, D.E., Gíslason, S.R., and Oelkers, E.H. (2021). Mineralization potential of water-dissolved CO_2 and H_2S injected into basalts as function of temperature: Freshwater versus Seawater. *International Journal of Greenhouse Gas Control 109*, 103357.

Navarre-Sitchler, A.K., Cole, D.R., Rother, G., Jin, L., Buss, H.L., and Brantley, S.L. (2013). Porosity and surface area evolution during weathering of two igneous rocks. *Geochimica et Cosmochimica Acta 109*, 400-413.

Oelkers, E.H., Bénézeth, P., and Pokrovski, G.S. (2009). Thermodynamic Databases for Water-Rock Interaction. *Reviews in Mineralogy and Geochemistry 70*, 1-46.

Oelkers, E.H., Butcher, R., Pogge von Strandmann, P.A.E., Schuessler, J.A., von Blanckenburg, F., Snæbjörnsdóttir, S.Ó., Mesfin, K., Aradóttir, E.S., Gunnarsson, I., Sigfússon, B., Gunnlaugsson, E., Matter, J.M., Stute, M., and Gislason, S.R. (2019a). Using stable Mg isotope signatures to assess the fate of magnesium during the *in situ* mineralisation of CO_2 and H_2S at the CarbFix site in SW-Iceland. *Geochimica et Cosmochimica Acta 245*, 542-555.

Oelkers, E.H., Pogge von Strandmann, P.A.E., and Mavromatis, V. (2019b). The rapid resetting of the Ca isotopic signatures of calcite at ambient temperature during its congruent dissolution, precipitation, and at equilibrium. *Chemical Geology 512*, 1-10.

Olsson, J., Stipp, S.L.S., Dalby, K.N., and Gislason, S.R. (2013). Rapid release of metal salts and nutrients from the 2011 Grímsvötn, Iceland volcanic ash. *Geochimica et Cosmochimica Acta 123*, 134-149.

Ólafsson, J., and Riley, J.P. (1978). Geochemical studies on the thermal brine from Reykjanes (Iceland). *Chemical Geology 21*, 219-237.

Ólafsson, M., Hauksdóttir, S., Thórhallsson, S., and Snorrason, Th. (2005). Calcite scaling at Selfossveitur Hitaveita, S-Iceland, when mixing waters of different chemical composition. In *Proceedings World Geothermal Congress. Antalya, Turkey, 24-29 April 2005.*

Óskarsson, F. (2022). *Efnasamsetning neysluvatns. Vatnsveita Hafnarfjarðar, Kópavogs og Mosfellsbæjar*. Prepared for Heilbrigðiseftirlit Garðabæjar, Hafnarfjarðar, Kópavogs, Mosfellsbæjar og Seltjarnarness. Iceland GeoSurvey, short report ÍSOR-22056.

Parkhurst, D.L. and Appelo, C.A.J. (2013). Description of Input and Examples for PHREEQC Version 3 - A Computer Program for Speciation, Batch-Reaction, One-Dimensional Transport, and Inverse Geochemical Calculations, in: *Survey*, U.S.G. (Ed.), Techniques and Methods, p. 497.

Paukert, A.N., Matter, J.M., Kelemen, P.B., Shock, E.L., and Havig, J.R. (2012). Reaction path modeling of enhanced in situ CO_2 mineralization for carbon sequestration in the peridotite of the Samail Ophiolite, Sultanate of Oman. *Chemical Geology 330–331*, 86-100.

Pope, E.C., Bird, D.K., Arnórsson, S., Fridriksson, T., Elders, W.A., and Fridleifsson, G.Ó. (2009). Isotopic constraints on ice age fluids in active geothermal systems: Reykjanes, Iceland. *Geochimica et Cosmochimica Acta 73*, 4468-4488.

Přikryl, J., Marieni, C., Gudbrandsson, S., Aradóttir, E.S., Gunnarsson, I., and Stefánsson, A. (2018). H2S sequestration process and sustainability in geothermal systems. *Geothermics 71*, 156-166.

Saldi, G.D., Jordan, G., Schott, J., and Oelkers, E.H. (2009). Magnesite growth rates as a function of temperature and saturation state. *Geochimica et Cosmochimica Acta 73*, 5646-5657.

Schott, J., Oelkers, E.H., Bénézeth, P., Goddéris, Y., and François, L. (2012). Can accurate kinetic laws be created to describe chemical weathering? *Comptes Rendus Geoscience 344*, 568-585.

Snæbjörnsdóttir, S.Ó., Oelkers, E.H., Mesfin, K., Aradóttir, E.S., Dideriksen, K., Gunnarsson, I., Gunnlaugsson, E., Matter, J.M., Stute, M., and Gislason, S.R. (2017. The chemistry and saturation states of subsurface fluids during the in situ mineralisation of CO_2 and H_2S at the CarbFix site in SW-Iceland. *International Journal of Greenhouse Gas Control 58*, 87-102.

Snæbjörnsdóttir, S.Ó., Gislason, S.R., Galeczka, I.M., and Oelkers, E.H. (2018). Reaction path modelling of in-situ mineralisation of CO_2 at the CarbFix site at Hellisheidi, SW-Iceland. *Geochimica et Cosmochimica Acta 220*, 348-366.

Stefánsson, A., and Gíslason, S.R. (2001). Chemical Weathering of Basalts, Southwest Iceland: Effect of Rock Crystallinity and Secondary Minerals on Chemical Fluxes to the Ocean. *American Journal of Science 301*, 513-556.

Stefánsson, A., Hilton, D.R., Sveinbjörnsdóttir, Á.E., Torssander, P., Heinemeier, J., Barnes, J.D., Ono, S., Halldórsson, S.A., Fiebig, J., and Arnórsson, S. (2017). Isotope systematics of Icelandic thermal fluids. *Journal of Volcanology and Geothermal Research 337*, 146-164.

Stockmann, G.J., Wolff-Boenisch, D., Gislason, S.R., and Oelkers, E.H. (2011). Do carbonate precipitates affect dissolution kinetics? 1: Basaltic glass. *Chemical Geology 284*, 306-316.

Voigt, M., Marieni, C., Baldermann, A., Galeczka, I.M., Wolff-Boenisch, D., Oelkers, E.H., and Gislason, S.R. (2021). An experimental study of basalt–seawater– CO_2 interaction at 130 °C. *Geochimica et Cosmochimica Acta 308*, 21-41.

Voigt, M., Marieni, C., Clark, D.E., Gíslason, S.R., and Oelkers, E.H. (2018). *Evaluation and refinement of thermodynamic databases for mineral carbonation*. Energy Procedia, 81-91.

White, A.F., and Brantley, S.L. (2003). The effect of time on the weathering of silicate minerals: why do weathering rates differ in the laboratory and field? *Chemical Geology 202*, 479-506.

Wolff-Boenisch, D., and Galeczka, I.M. (2018). Flow-through reactor experiments on basalt-(sea)water-CO_2 reactions at 90°C and neutral pH. What happens to the basalt pore space under post-injection conditions? *International Journal of Greenhouse Gas Control 68*, 176-190.

Wolff-Boenisch, D., Gislason, S.R., Oelkers, E.H., and Putnis, C.V. (2004). The dissolution rates of natural glasses as a function of their composition at pH 4 and 10.6, and temperatures from 25 to 74°C. *Geochimica et Cosmochimica Acta 68*, 4843-4858.

Wolff-Boenisch, D., Wenau, S., Gislason, S.R., and Oelkers, E.H. (2011). Dissolution of basalts and peridotite in seawater, in the presence of ligands, and CO_2: Implications for mineral sequestration of carbon dioxide. *Geochimica et Cosmochimica Acta 75*, 5510-5525.

Zhu, C., Veblen, D.R., Blum, A.E., and Chipera, S.J. (2006). Naturally weathered feldspar surfaces in the Navajo Sandstone aquifer, Black Mesa, Arizona: Electron microscopic characterization. *Geochimica et Cosmochimica Acta 70*, 4600-4616.

VIÐAUKI IV

ÍSOR
ÍSLENSKAR ORKURANNSÓKNIR
ICELAND GEOSURVEY

Seismic Assessment in the Greater Straumsvík Area

Prepared for the Environmental Impact Assessment of Carbfix's Coda Terminal Project

Egill Árni Guðnason
Þorbjörg Ágústsdóttir

Prepared for Carbfix

ÍSOR-2023/042

December 2023

ICELAND GEOSURVEY

Kópavogur: Urðarhvarf 8, 203 Kópavogur, Iceland - Tel.: 528 1500
Akureyri: Rangárvellir, P.O. Box 30, 602 Akureyri, Iceland - Tel.: 528 1500
isor@isor.is - www.isor.is

ÍSOR
ICELAND GEOSURVEY

Key page

Report no.	Date	Distribution
ÍSOR-2023/042	December 2023	☒ Open ☐ Closed

Report name / Main and subheadings	Number of copies
Seismic Assessment in the Greater Straumsvík Area. Prepared for the Environmental Impact Assessment of Carbfix's Coda Terminal Project.	1
	Number of pages: 40
Authors: Egill Árni Guðnason and Þorbjörg Ágústsdóttir	Project manager: Sveinborg H. Gunnarsdóttir
Classification of report	Project no.: 23-0003

Prepared for: Carbfix
Cooperators

Abstract

The Coda Terminal of Carbfix is a planned carbon transport and storage hub in the Straumsvík area, SW Iceland, where CO_2, dissolved in water, will be pumped into the basaltic bedrock through a network of shallow injection wells. Before the large-scale injection of dissolved CO_2 can be initiated, the Coda Terminal project will go through an environmental impact assessment (EIA).

In this report, results of a new seismic assessment in the greater Straumsvík area for the EIA are presented, taking into account new data on research drilling, initial injection tests and earthquake activity in the area.

The greater Straumsvík area seems to be tectonically inactive and seismically quiet, with permeability mostly related to lithological boundaries. Based on all available data, and the shallow nature of the injection operations, it is concluded that the probability of felt seismicity in Straumsvík is low. It is recommended that seismicity in Straumsvík is closely monitored prior to and during the injection operations, using the already installed local seismic network in the area. For the EIA, the probability and extent of possible earthquake activity in the area is evaluated, and a response plan to any potential activity is put forward in the form of a seismic traffic light system.

Key words	
Carbfix, Coda Terminal, ÍSOR, Straumsvík, Reykjanes Peninsula, earthquakes, seismicity, induced, environmental, assessment	Project manager's signature: Sveinborg H. Gunnarsdóttir Reviewed by: Steinunn Hauksdóttir

Table of contents

List of tables

List of figures

Ágrip

Coda Terminal er fyrirhuguð móttöku- og geymslustöð koldíoxíðs (CO_2) á Straumsvíkursvæðinu. Þar verður Carbfix-tækninni beitt til þess að binda CO_2 varanlega í jörðu með því að dæla uppleystu CO_2 í vatni niður í hentug jarðlög í gegnum net grunnra niðurdælingarholna. Áður en til framkvæmda kemur og niðurdæling hefst þarf Coda Terminal verkefnið að fara í mat á umhverfisáhrifum, m.a. mat á jarðskjálftahættu. Í þessari skýrslu eru kynntar niðurstöður frummats á jarðskjálftahættu á Straumsvíkursvæðinu.

Við vinnslu frummatsins er stuðst við eftirfarandi gögn og rannsóknir:

- Jarðfræði og jarðhnik (e. tectonics) svæðisins (sjá kafla 2).
- Ný gögn um rannsóknarboranir og fyrstu ádælingarpróf í Straumsvík (sjá kafla 2.1).
- Forkönnun á jarðskjálftahættu á svæðinu unnin af ÍSOR fyrir Carbfix í samræmi við reglur Orkustofnunar (eldri skýrsla ÍSOR).
- Greining á aðgengilegum jarðskjálftagögnum úr SIL-jarðskjálftamælanetinu frá árinu 1995 til dagsins í dag (sjá kafla 4.1.1).
- Greining á nýlegri gögnum úr jarðskjálftamælum CODA-jarðskjálftamælanetsins, ásamt gögnum úr nálægum jarðskjálftamælum úr REYKJANET og SIL-jarðskjálftamælanetunum (sjá kafla 4.1.2), nánar tiltekið frá árinu 2022 til dagsins í dag, m.a. á meðan rannsóknarboranir og ádælingarpróf stóðu yfir í Straumsvík.

Við mat á áhrifum framkvæmdarinnar á jarðskjálftavirkni er stuðst við eftirfarandi reglur:

- Reglur Orkustofnunar um viðbúnað og viðbrögð við jarðskjálftavá vegna losunar á vökva í jörðu um borholur, nr. OS-2016-R01-01.

Fyrirhugað framkvæmdasvæði Coda Terminal í Straumsvík er á norðanverðum Reykjaneskaga (sjá grænan reit á mynd 5). Reykjaneskaginn er náttúrulega virkt jarðskjálfta- og eldgosasvæði og samanstendur hann af sex eldstöðvakerfum sem raða sér skáhallt eftir honum í NA-SV stefnu (mynd 1). Tvö þeirra eru í nálægð við Straumsvík og framkvæmdasvæði Coda Terminal; annars vegar eldstöðvakerfið sem kennt er við Eldvörp-Svartsengi, en nyrsti hluti þess teygir sig í átt að Straumsvík vestur af framkvæmdasvæðinu, og hins vegar Krýsuvíkurkerfið, sem nær frá suðurströnd Reykjaneskagans og teygir sig til norðausturs og liggur því suðaustan við framkvæmdasvæðið.

Jarðskjálftavirkni á Reykjaneskaga er fyrst og fremst bundin við plötuskilin sem ganga í gegnum suðurhluta skagans (mynd 3). Í sögulegu samhengi hefur jarðskjálftavirkni í Straumsvík og nágrenni verið lítil sem engin ef skoðuð eru aðgengileg gögn frá annars vegar landsneti Veðurstofu Íslands (SIL) frá árinu 1995, og hins vegar CODA-jarðskjálftamælanetinu sem ÍSOR setti upp fyrir Carbfix vegna Coda Terminal verkefnisins í september 2022 (sjá mynd 2 af jarðskjálftamælanetum). Uppruna þeirra jarðskjálfta sem mælst hafa í grennd við Straumsvík má fyrst og fremst rekja til sprungusveims Krýsuvíkurkerfisins (mynd 5). Á framkvæmdasvæðinu eru engar sprungur kortlagðar á yfirborði, og m.v. öll fyrirliggjandi gögn virðist svæðið því tektóníska óvirkt, jafnvel í yfirstandandi umbrotahrinu jarðskjálfta og eldgosa á Reykjaneskaga sem hófst síðla árs 2019. Því er ljóst að framkvæmdasvæði Coda Terminal í Straumsvík er utan virkra sprungu- og jarðskjálftasvæða Reykjaneskagans.

Jarðskjálftar eru náttúruleg fyrirbæri og verða þegar spenna myndast í bergi og nær að lokum brotþolum þess. Í tímans rás hleðst upp spennuorka í berginu og þegar spennan nálgast brotþol bergsins þarf oft einungis lokahnykkinn til þess að bergið bresti í jarðskjálfta. Niðurdæling á vatni getur verið slíkur lokahnykkur og þannig orsakað það sem í daglegu tali eru kallaðir örvaðir jarðskjálftar (e. induced earthquakes) eins og dæmi eru um bæði hérlendis og erlendis. Það er þó háð ýmsum þáttum og jarðfræðilegum aðstæðum á hverjum stað fyrir sig, líkt og dýpi og magni niðurdælingar, lekt bergsins og spennuástandi jarðskorpunnar.

Almennt er ekki talið að grunn niðurdæling (< 1,5 km), líkt og áformuð er í Coda Terminal í Straumsvík, valdi örvaðri jarðskjálftavirkni sökum þess að jarðskorpan í efstu ~2 km á Íslandi er talin of veik til þess að brotna í jarðskjálftum. Dæmi þessu til staðfestingar eru um grunna niðurdælingu víðs vegar á Íslandi, bæði innan og utan virkra sprungu- og jarðskjálftasvæða, t.d. á Nesjavöllum, Þeistareykjum, í Geldinganesi og Hveragerði. Í mörgum þessara tilvika var fylgst náið með mögulegri örvaðri jarðskjálftavirkni með þéttum jarðskjálftamælanetum samhliða niðurdælingunni. Niðurstöður gefa einhlítt til kynna að lítil sem engin örvuð jarðskjálftavirkni hafi mælst í þessum tilvikum. Hins vegar sýna rannsóknir að örvuð jarðskjálftavirkni á Íslandi hefur fyrst og fremst átt sér stað þegar dælt hefur verið niður í djúpar borholur (> 1,5 km) á virkum háhita- og sprungusvæðum þar sem bergspenna er að jafnaði hærri en í efstu 1–2 km jarðskorpunnar, t.d. í Húsmúla á Hengilssvæðinu.

Carbfix hefur þegar hafið rannsóknarboranir á framkvæmdasvæðinu til þess að meta grunnástand svæðisins. Fyrstu niðurstöður benda til þess að lekt í borholum á svæðinu sé fyrst og fremst bundin við jarðlagamót, og virðist lektin aukast eftir því sem sunnar dregur. Engar vísbendingar eru um undirliggjandi jarðhitakerfi á Straumsvíkursvæðinu, og þær sprungur sem greinst hafa í borholum benda ekki til þess að hreyfing hafi orðið á þeim í gegnum tíðina, þ.e.a.s. að þær hafi hreyfst í jarðskjálfta. Í kjölfar rannsóknarborana í Straumsvík hófust borholumælingar og ádælingarpróf. Engin örvuð jarðskjálftavirkni hefur mælst á meðan ádælingarprófum stóð í borholum, né eftir að þeim lauk. Jarðskjálftagögn voru rýnd sérstaklega m.t.t. smáskjálftavirkni en aðeins var mögulegt að greina titring af völdum vatnspumpu sem notuð var við ádælingarprófin. Tekið skal þó fram að í fullum afköstum verður niðurdæling í hverja borholu Coda Terminal ívið meiri en í dæmigerðu ádælingarprófi, eða allt að 40 L/s fyrir hverja holu, og allt að 3.000 L/s samtals. Tekið er tillit til þessa við mat á áhrifum framkvæmdarinnar á mögulega örvaða jarðskjálftavirkni á Straumsvíkursvæðinu.

Niðurstaða frummatsins er að fyrirhuguð framkvæmd falli undir lið 2 í 4. gr. reglna um viðbúnað og viðbrögð við jarðskjálftavá vegna losunar á vökva í jörðu um borholur (OS-2016-R01-01), þ.e. að *hætta á finnanlegri skjálftavirkni sé* **óveruleg**. Áhrifin eru metin minniháttar með tilliti til umfangs framkvæmdasvæðisins og eru talin tímabundin og afturkræf. Ráðlagt er að fylgjast náið með jarðskjálftavirkni;

i) þegar boranir hefjast,
ii) þegar niðurdæling hefst,
iii) þegar magn niðurdælingar er aukið.

Sömuleiðis er ráðlagt að byggja upp geymslusvæðið og auka niðurdælingu í litlum skrefum og fylgjast með mögulegum landhæðarbreytingum á svæðinu. Áhrifasvæði með tilliti til upptaka jarðskjálfta er framkvæmdasvæði Coda Terminal, nánar tiltekið í og við borteiga þar sem niðurdæling fer fram, en ekki er gert ráð fyrir að örvuð jarðskjálftavirkni geti orðið í meira en 2 km fjarlægð frá niðurdælingarholum.

Í skýrslunni er sett fram viðbragðsáætlun vegna mögulegrar örvaðrar jarðskjálftavirkni í formi svokallaðs umferðarljósakerfis (e. Traffic Light System, TLS) (mynd 10). Kerfið er til þess fallið að takmarka hættu á örvaðri jarðskjálftavirkni og verður tekið í gagnið áður en niðurdæling Coda Terminal hefst en álíka kerfi hafa verið notuð bæði hérlendis og erlendis með góðum árangri.

Framkvæmdaraðili kemur til með að fylgjast vel með mögulegri jarðskjálftavirkni á Straumsvíkursvæðinu á meðan á uppbyggingarfasa verkefnisins stendur til þess að meta grunnástand framkvæmdasvæðisins áður en niðurdæling hefst. Til þess er stuðst við rauntímagögn úr CODA-jarðskjálftamælaneti Carbfix og ÍSOR í Straumsvík og nágrenni, auk rauntímagagna af nálægum jarðskjálftastöðvum úr landsneti Veðurstofu Íslands (SIL) og jarðskjálftamælaneti Tékknesku vísindaakademíunnar og ÍSOR á Reykjanesskaga.

1 Introduction

Coda Terminal is a planned carbon transport and storage hub in the industrial Straumsvík area, SW Iceland (https://www.carbfix.com/codaterminal). CO_2 will be captured at industrial sites in Northern Europe and shipped to the Terminal, where it will be uploaded into onshore tanks for temporary storage. The CO_2, dissolved in water, will be pumped into the basaltic bedrock in Straumsvík through a network of shallow injection wells, where it transforms rapidly into solid minerals through a natural, but accelerated, reaction. Before a large-scale injection of dissolved CO_2 can be initiated, the Coda Terminal project will go through an environmental impact assessment (EIA), which includes e.g., a seismic assessment.

During the preparation phase for the injection activities of the Coda Terminal project, an independent risk assessment of potential induced seismicity in Straumsvík was carried out (Kristjánsdóttir and Ágústsdóttir, 2020). The assessment concluded, based on existing data, that the probability of felt seismicity due to the proposed injection is low, especially due to the shallow nature of the injection operations. For the independent risk assessment, no information was available on either drilling or injection in the Straumsvík area.

In this report are presented results of a new seismic assessment in the greater Straumsvík area, for the EIA of the Coda Terminal project of Carbfix. New data is available on e.g., research drilling and initial injection tests in the area, as well as recent earthquake activity. The probability and extent of possible earthquake activity in the area is discussed and evaluated, and a response plan to any potential earthquake activity is discussed with regards to the results of recent research drillings.

2 Geological and tectonic setting

The Reykjanes Peninsula (RP) in SW Iceland is the onshore continuation of the Mid-Atlantic Ridge, which comes onshore at the SW tip of the Peninsula and extends from there as a 60 km long N70°E striking oblique rift, until it joins the Western Volcanic Zone and the South Iceland Seismic Zone at the Hengill Triple Junction in the east (Sigmundsson et al., 2020). As such, it is part of the divergent plate boundary of the North American and Eurasian plates. The RP oblique rift, or trans-tensional zone, is expressed by a 5-10 km wide seismic and volcanic zone, highly oblique with the spreading direction of N120°E in this region (Keiding et al., 2009; Sigmundsson et al., 2020; Sæmundsson et al., 2020). The extensional component of the rifting is accommodated by the intrusion of magma in NE-SW oriented dikes, oblique to the plate boundary, while the remaining strike-slip component of the rifting is accommodated by N-S oriented strike-slip faults, of which some are known to be capable of producing large earthquakes (Einarsson, 1991; Björnsson et al., 2020) (Fig. 1).

The divergence of the North American and Eurasian plates is expressed in six rift segments, arranged en-echelon on the RP, which accommodate the rifting. These rift segments, often referred to as either volcanic systems or fissure swarms, are areas with the highest density of i) eruptive fissures and ii) tectonic faults and fractures, and they are from west to east; Reykjanes, Eldvörp-Svartsengi, Fagradalsfjall, Krýsuvík, Brennisteinsfjöll and Hengill (Fig. 1). Their outlines or boundaries are rough estimates, drawn according to Sæmundsson and Sigurgeirsson (2013). The volcanic systems are centred on eruptive fissures producing lava flows during ice-free periods, and hyaloclastite during glacial periods. Faults and fractures

continue far beyond the eruptive sections of the volcanic systems, and apparently dikes continue at depth even farther (Sæmundsson et al., 2020) (Fig. 1).

The upper crustal structure of the RP consists of extrusive basaltic rocks, with a downward increasing alteration and a greater proportion of intrusive rocks at depth. The upper crust is roughly 4.5 km thick, while the lower crust, believed to consist of intrusive rocks down to Moho, extends down to roughly 15 km depth on the RP (Flóvenz, 1980; Weir et al., 2001). There are indications from petrological and geochemical analyses of basaltic lava flows from the 800-1240 AD Fires on the RP, that the Moho depth increases further to the east of the Brennisteinsfjöll volcanic system (Caracciolo et al., 2023).

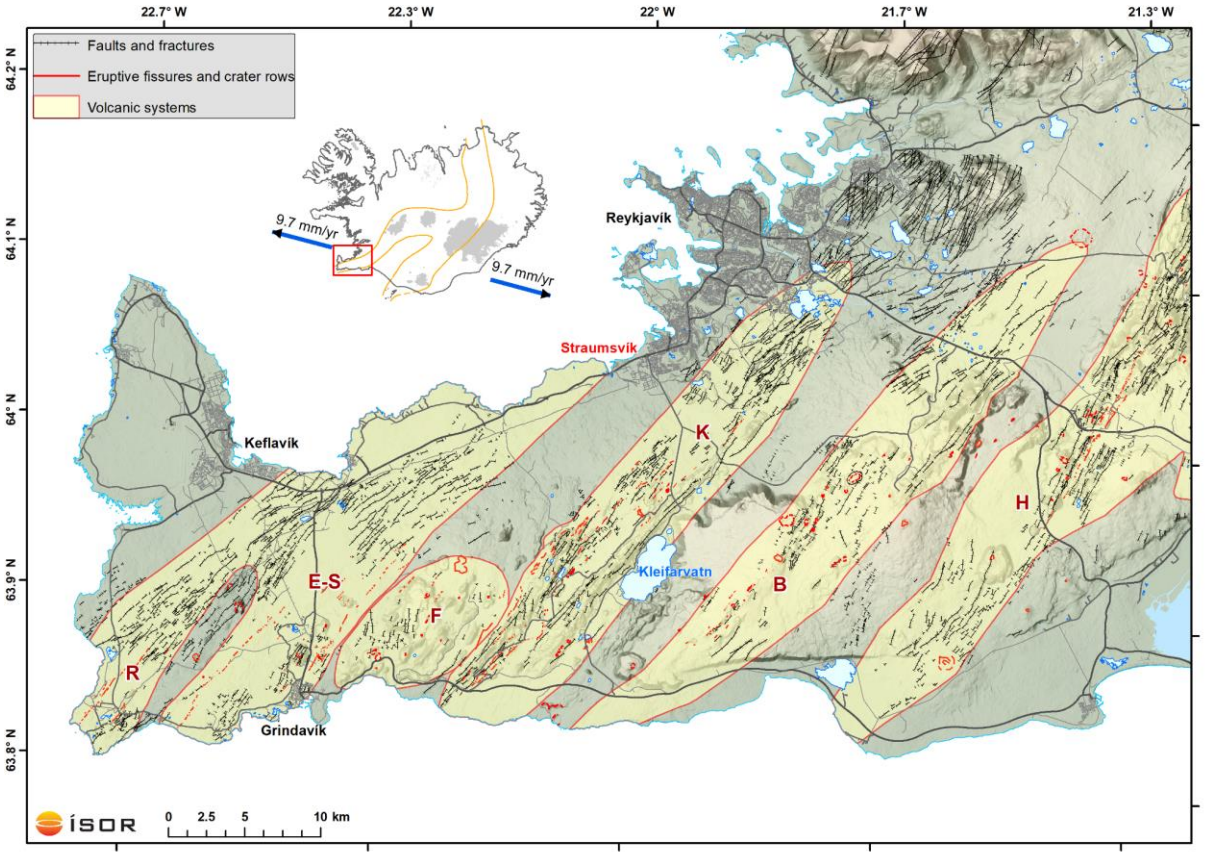

Figure 1. *A geological map of the Reykjanes Peninsula, SW Iceland. Black and red fault lines denote postglacial opening and eruptive fissures, respectively (Sæmundsson et al., 2016). The volcanic systems are shaded in light green, marked with a bold letter; R: Reykjanes, E-S: Eldvörp-Svartsengi, F: Fagradalsfjall, K: Krýsuvík, B: Brennisteinsfjöll, H: Hengill (Sæmundsson and Sigurgeirsson, 2013). Main roads are in black and main landmarks referenced in the text are shown on the map, with Straumsvík highlighted in red colour. The inset shows volcanic zones of Iceland (orange) with blue arrows indicating the plate spreading rate in Iceland (Sigmundsson et al., 2020). The red rectangle on the inset shows the location of the zoomed-in area. Digital elevation model used for all maps in this report is from the National Land Survey of Iceland.*

The active plate boundary of the RP is highlighted by earthquake epicentres, as further discussed in chapter 4 (Fig. 3). In Iceland, earthquakes usually terminate sharply at a certain depth, variable between different areas, defining the brittle-ductile transition of the crust. This transition is defined as the surface above which 95% of earthquakes occur, and based on both laboratory measurements and geothermal drilling, this transition is clearly temperature dependent. In basaltic rocks, the estimated temperature at the brittle-ductile transition is around 600°C (Ágústsson and Flóvenz, 2005; Violay et al., 2012; Bali et al., 2020). In general, the brittle-ductile transition beneath the RP is at roughly 6-8 km depth, doming up to roughly 3-5 km depth below the known high-temperature geothermal fields of Reykjanes, Svartsengi and Krýsuvík (Kristjánsdóttir, 2013; Blanck et al., 2020; Gudnason et al., 2021; Flóvenz et al., 2022).

2.1 The Straumsvík area

The Straumsvík area is located just west of the town of Hafnarfjörður, and the name refers to "current bay", as it is known for a large underground current of groundwater, entering the ocean at Straumsvík (Sigurðsson, 1986). Straumsvík is located north of and outside the rift segments, or volcanic systems, of the RP, and no faults or fractures have been mapped in the area, mainly because of young Holocene lava flows covering the surface (Helgadóttir et al., 2023b) (Figs. 1 and 2). However, mapped faults and fractures in the vicinity of Straumsvík are i) NE-SW striking ones that belong to the Krýsuvík volcanic system to the east, and ii) ENE-WSW striking ones that belong to the volcanic system of Eldvörp-Svartsengi to the southwest.

From late November 2022 to mid-January 2023, the first research well, CSI-01, was drilled down to 982 m depth in Straumsvík, in preparation for the Coda Terminal project (Sigurgeirsson et al., 2023a) (Fig. 2). The main feed points in well CSI-01 are observed at 330 and 375 m depth, while three minor feed points are observed at 500, 780 and 915 m depth (Sigurgeirsson et al., 2023a; Helgadóttir et al., 2023a). The second research well of the Coda Terminal project, CSM-01, intended for monitoring, was drilled down to 618 m depth from June to August 2023 (Sigurgeirsson et al., 2023b) (Fig. 2). The well is located further inland, roughly 1.3 km SE of well CSI-01. Similar to well CSI-01, the main feed point in well CSM-01 is observed at 360 m depth, while three minor feed points are observed a bit deeper, i.e., at 389, 404 and 412 m depth (Sigurgeirsson et al., 2023b).

The data collected during drilling of the two wells, on e.g., the subsurface stratigraphy, temperature and alteration, is essential for the characterization of the Straumsvík area, as there are no other deep wells in the area. In both wells, a lithological change, or boundary, is observed at a similar depth as all feed points. Acoustic Borehole Images (televiewer) from within well CSI-01 suggest that there is some evidence of ENE-WSW striking fractures that might belong to the Eldvörp-Svartsengi volcanic system, although the main fracture trends observed are the dominant NNE-SSW/NE-SW striking fractures typical for the volcanic systems on the RP, as well as the N-S striking transform, or strike-slip, faults (Helgadóttir et al., 2023a).

Importantly, the fractures or lineaments observed in the televiewer images of well CSI-01 do not give evidence of any movement, i.e., they do not look like proper tectonic faults capable of producing earthquakes (Helgadóttir et al., 2023b).

While there is a possibility that some fracture-controlled permeability may be present in the Straumsvík area, permeability is more likely related to lithological boundaries of some sort, as seen in wells CSI-01 and CSM-01. A greater chance of permeability related to faults and fractures is inland, e.g., within the Krýsuvík volcanic system. Permeability relation to the Eldvörp-Svartsengi system is not clear, as there does not seem to be a strong ENE-WSW trend in the observed fractures of well CSI-01, as previously mentioned.

Sæmundsson et al. (2020) suggest that the extent of the volcanic systems on the RP can be traced beyond the visible surface manifestations. The suggestion is based on low-temperature geothermal areas in the greater Reykjavík area, that are located beyond the extent of the volcanic systems, but in line with their strike. These areas, e.g., Laugarnes, Seltjarnarnes and Geldinganes, have high temperature gradients and have been utilised for geothermal exploitation for decades.

Whether the Eldvörp-Svartsengi volcanic system can be traced beyond its visible surface manifestations and into the Straumsvík area remains to be seen with further exploration drilling in the area. However, there is no indication or evidence of an underlying geothermal system in Straumsvík, as the temperature gradient in the static parts of wells CSI-01 and CSM-01 (below ~400 m) is ~80°C/km, i.e., only close to the expected regional temperature gradient in the area (Helgadóttir et al., 2023b). Alteration of the formation in both wells is minor, also indicating a low temperature environment. Maximum temperature measured in the wellbore at the bottom of the two wells, CSI-01 and CSM-01, was only 49°C and 74°C, respectively (Sigurgeirsson et al., 2023a, 2023b).

3 The seismic network and processing

The existing seismic network in the Straumsvík area consists of seismic stations from three different seismic networks; i.e., the CODA seismic network of Carbfix and ÍSOR, supplemented by continuous seismic data from nearby stations of long-time operating seismic networks on the RP, i.e., REYKJANET and SIL, further described in the following paragraphs (Fig. 2):

- The **CODA** seismic network of Carbfix and ÍSOR was installed in early September 2022, and currently consists of three short-period seismic stations (green triangles on Fig. 2). Eventually, the CODA network will consist of five seismic stations in total, but the two remaining stations will be installed once the research and development area for the Coda Terminal of Carbfix has been finalised and located in such a way as to minimise the inevitable azimuthal gap in the seismic network.
- The **REYKJANET** seismic network was deployed on the RP in 2013, funded by the Czech Academy of Science and supported by ÍSOR (Ágústsdóttir et al., 2022). The network consists of 17 broadband seismic stations deployed along the RP, roughly between the Svartsengi and Hengill high-temperature geothermal fields (orange triangles on Fig. 2). The maintenance of REYKJANET, data analysis and interpretation are currently done within the NASPMON project, and a mutual data sharing agreement between Carbfix and NASPMON sees NASPMON share continuous seismic data from the north easternmost stations of REYKJANET; STH, ASH, HRG and LHL, with the CODA seismic network (Fig. 2).

- The **SIL** seismic network has since 1993 served as the regional seismic network in Iceland, operated by the Icelandic Meteorological Office (IMO), with both short-period and broadband seismic stations distributed along the active plate boundary of Iceland (e.g., Jakobsdóttir, 2008). A data sharing agreement between Carbfix and the IMO sees the IMO share continuous seismic data from two seismic stations on the RP; KAS and KRI, with the CODA seismic network (blue triangles on Fig. 2).

Hereafter, the combined set of seismic stations is referred to as the 'extended CODA seismic network'. All stations of the extended seismic network in the greater Straumsvík area transmit data in real-time to ÍSOR, where the data is automatically processed using the SeisComP software (https://www.seiscomp.de). Results of the automatic processing and subsequent location of events are published on an external webpage (http://carbfix.isor.is/).

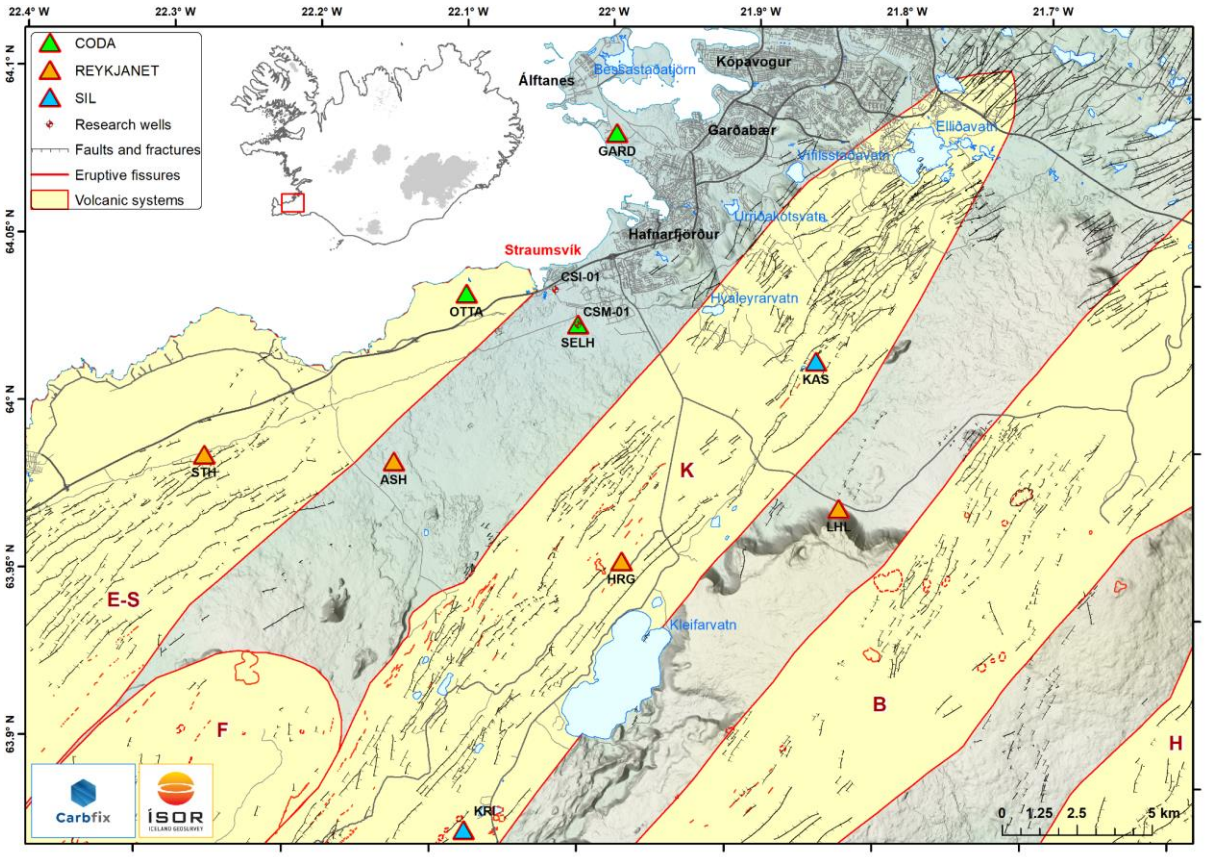

Figure 2. *The extended CODA seismic network in the greater Straumsvík area consists of seismic stations of the CODA, REYKJANET and SIL seismic networks, shown as green, orange and blue triangles, respectively. The two research wells of Carbfix and the Coda Terminal, CSI-01 and CSM-01, are shown with red crosses. For further references to the map, see Fig. 1.*

4 Seismicity

Historical descriptions on seismicity on the RP exist from annals dating back to the 18th century AD, e.g., reporting large magnitude events in 1929 on a 10 km long N-S oriented Hvalhnúkur fault within the Brennisteinsfjöll fissure swarm (Erlendsson and Einarsson, 1996) and in 1933 within the Fagradalsfjall fissure swarm (Halldórsson, unpublished manuscript from 2011 on historical earthquakes in Iceland). In the annals, seismicity is only reported from areas within the active plate boundary of the RP, i.e., not on the northern part of the Peninsula, e.g., in the greater Straumsvík area.

Microearthquake activity was first monitored on the RP during the summers of 1967 and 1968, when analogue seismographs were operated for a few days near the Reykjanes and Krýsuvík geothermal areas (Ward and Björnsson, 1971). In 1971 and 1972, a dense temporary network of 23 seismic stations was installed on the western part of the RP, providing accurate earthquake locations for the first time on the Peninsula, e.g., capturing an intense swarm of microearthquakes NNW of the Reykjanes high-temperature geothermal field in 1972 (Klein et al., 1973, 1977; Björnsson et al., 2020). In general, the period from 1967 to 1975 represents an active earthquake episode on the RP, with nine earthquake swarms illuminating a 50 km long segment of the oblique plate boundary, cutting across the volcanic systems (Björnsson et al., 2020).

Continuous recordings of seismicity on the RP exist since the deployment of the regional SIL seismic network in Iceland. The first development of the network started in 1989, and in 1997, all but one of the eight seismic stations of the SIL network on the RP were up and running (Ágústsson et al., 1998) (Fig. 3). Earthquake locations of the SIL network are publicly available since 1995, shown in Fig. 3.

The presently active seismic zone on the RP is narrow, less than 2 km wide in some parts of the Peninsula but up to 5-10 km wide in others and defines the plate boundary that enters Iceland near the tip of Reykjanes, as shown by the epicentres in Fig. 3. Seismic activity on the Peninsula is high and occurs episodically, with large earthquake swarms occurring every 20 to 40 years, separated by more quiet intervals (Björnsson et al., 2020). The seismicity is caused by deformation of a brittle crust above a deeper aseismic deformation zone (Einarsson, 1991).

Earthquakes on the RP are not located on any one particular fault, but small-scale structures and seismic lineations can be resolved within the seismic zone. On the western part of the Peninsula and the Reykjanes Ridge to the southwest, earthquake swarms are prominent and mainshock-aftershock sequences are rare (Einarsson, 1991; Keiding et al., 2009; Björnsson et al., 2020; Einarsson et al., 2020). Towards east, the mainshock-aftershock character of the activity increases gradually, while the central part of the Peninsula acts as a transition between the two. The largest earthquakes occur on N-S trending strike-slip faults with magnitudes up to M_L 6 (Einarsson et al., 2020; Fischer et al., 2022).

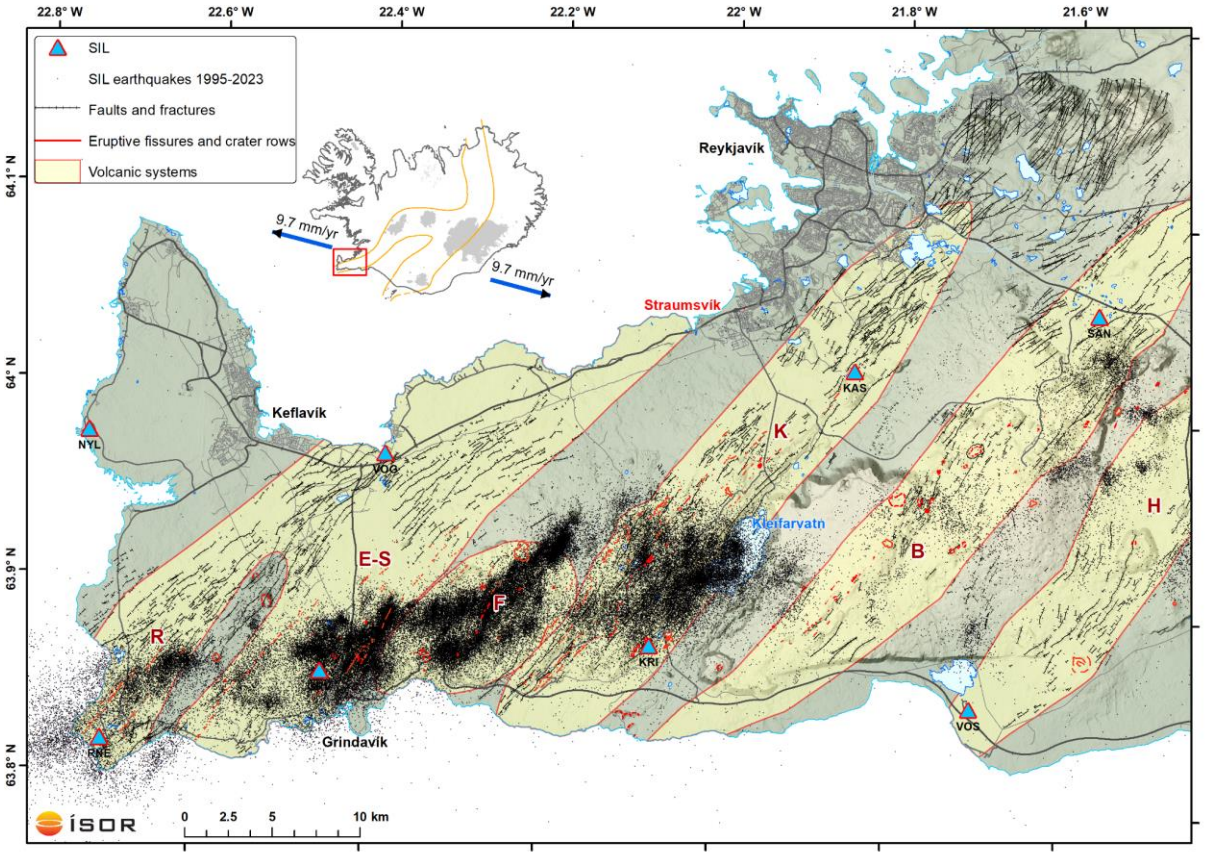

Figure 3. *Earthquake locations of the SIL seismic network on the Reykjanes Peninsula from 1995 to September 2023, shown as black dots. The seismic stations of the SIL network are shown as blue triangles. For further references to the map, see Fig. 1.*

As previously mentioned, the brittle-ductile transition beneath the RP is at roughly 6-8 km depth, doming up to roughly 3-5 km depth below the known high-temperature geothermal fields of Reykjanes, Svartsengi and Krýsuvík (Kristjánsdóttir, 2013; Blanck et al., 2020; Gudnason et al., 2021; Flóvenz et al., 2022). Importantly, seismicity within the uppermost crust of the Peninsula, i.e., the top 1-2 km, is only minor compared to the deeper part of the brittle crust down to 8 km, or around 10% of located earthquakes (Fig. 4). The shallowest activity is mostly confined to the Svartsengi high-temperature geothermal area and the Fagradalsfjall volcanic system, and mainly occurring after the current volcano-tectonic unrest started on the RP in late 2019 (Fig. A1 in Appendix A).

Seismic studies from several areas in Iceland, both within and outside the active plate boundary, indicate that, in general, the uppermost 1-2 km of the crust is too weak for brittle failure (e.g., Flóvenz et al., 2015; Ágústsdóttir et al., 2016; Guðnason et al., 2022; Fischer et al., 2022). Examples of the opposite, i.e., of seismicity within the uppermost 1-2 km, are in most cases confined to high-temperature geothermal areas, where there is continuous stress build-up and high natural background seismicity, further discussed in chapter 5. As previously mentioned, there is no indication or evidence of an underlying geothermal system in the Straumsvík area.

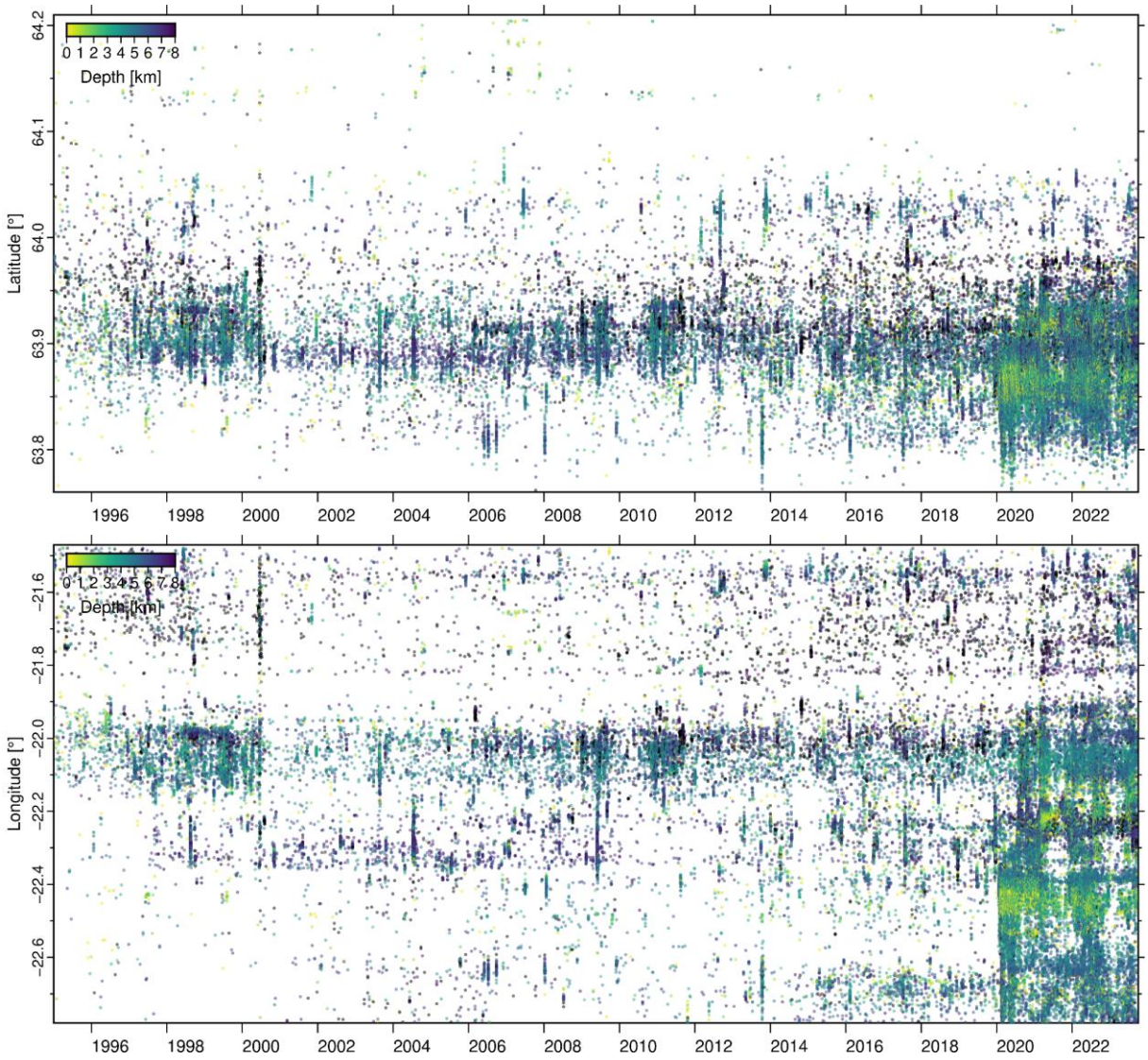

Figure 4. *Earthquake locations of the SIL seismic network on the Reykjanes Peninsula from 1995 to September 2023, shown as latitude (top) and longitude (bottom), as a function of time. Earthquakes are colour-coded according to depth (km), from surface down to 8 km. The data are the same as shown in Fig. 3, i.e., the same extent (latitude and longitude).*

4.1 Seismicity in the greater Straumsvík area

4.1.1 The SIL catalogue: 1995 to present

Since continuous recordings of seismicity on the RP started with the deployment of the SIL seismic network (data available since 1995), the greater Straumsvík area has been seismically quiet, even during times of intense volcano-tectonic unrest on the RP, affecting the nearby volcanic systems of Reykjanes, Eldvörp-Svartsengi, Fagradalsfjall and Krýsuvík (Figs. 5 and 6). Recorded events in the vicinity of Straumsvík are largely confined to the active plate boundary and the nearby volcanic systems, with an increase in activity since late 2019 (Fig. 6). During the current unrest, repeated inflation and deformation due to fluid and magma migration in three areas; i.e., in Svartsengi, Fagradalsfjall and Krýsuvík, has triggered intense seismicity along the whole active plate boundary, releasing previously accumulated tectonic

stress (e.g., Flóvenz et al., 2022; Fischer et al., 2022; Sigmundsson et al., 2022; Parks et al., 2023). To present, the greater Straumsvík area has been unaffected during these times, suggesting that the area is tectonically inactive. This is further discussed in chapter 5.

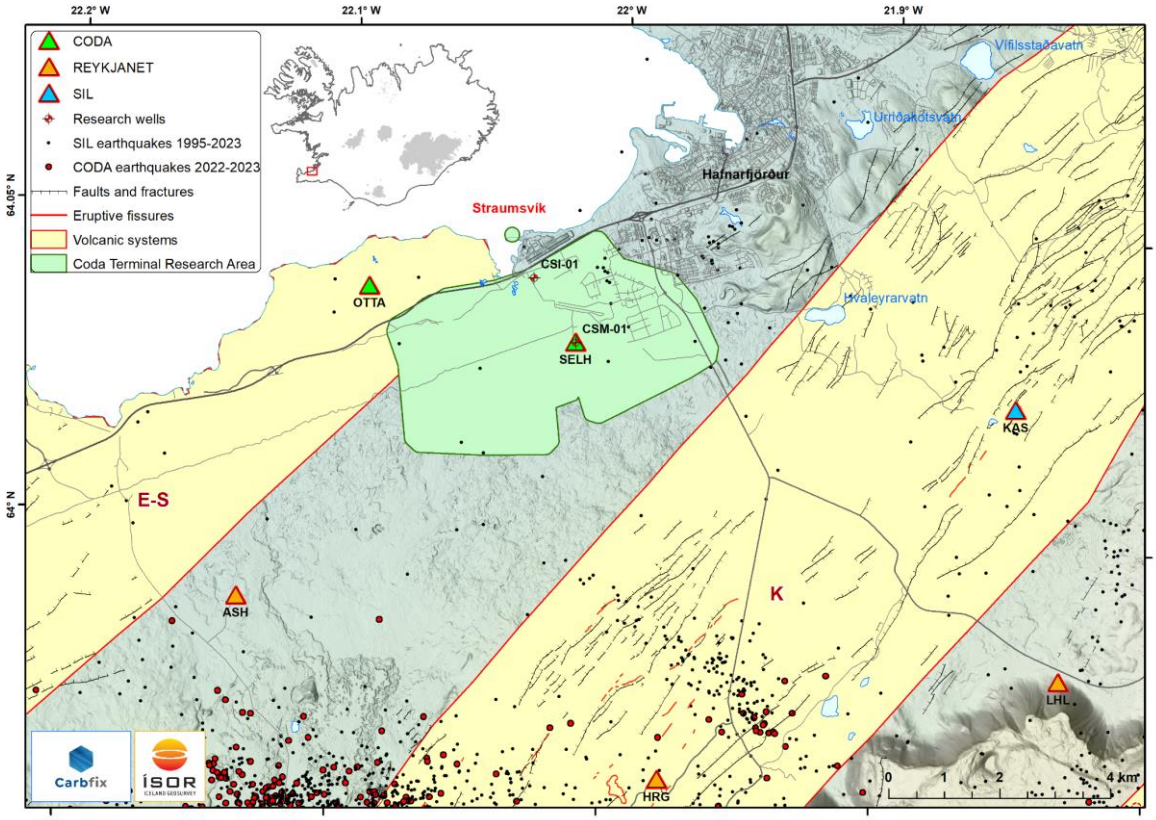

Figure 5. *Seismicity in the greater Straumsvík area, from 1995 to present day as recorded by the SIL seismic network (black dots), and from early September 2022 to late September 2023 as recorded by the extended CODA seismic network (red dots). The research area of the Coda Terminal is shown in green colour. For further references to the map, see Figs. 1 and 2.*

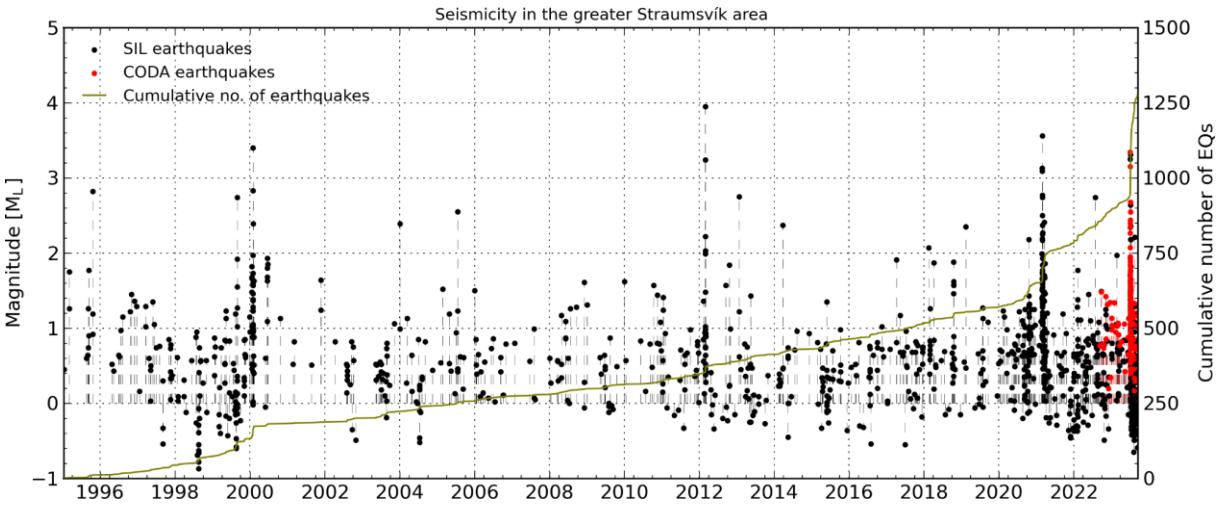

Figure 6. *Earthquake magnitudes (M_L) in the greater Straumsvík area, as recorded by the SIL (black) and extended CODA seismic networks (red), shown as a function of time. The cumulative number of earthquakes is shown with the olive-green line.*

Only a very few events are located within and to the east of the research area of the Coda Terminal in Straumsvík since 1995 (Fig. 5). Although confirmed or suspected mining activities are generally removed from the SIL catalogue, the distinction between a natural earthquake and an explosion can in some cases be difficult. This is especially difficult if the seismic network configuration is scattered, with large distances between seismic stations as in the regional SIL seismic network. As a result, there are some events related to explosions left in the SIL catalogue. The events in the SIL catalogue within and to the east of the research area are all suspected explosions for two reasons, i) they are all located near-surface, i.e., at very shallow depth (< 1 km), and ii) they are located in an area of heavy construction and mining.

4.1.2 The CODA catalogue: 2022 to present

Since the deployment of the seismic stations of the CODA seismic network in September 2022, seismicity has been thoroughly monitored in the greater Straumsvík area (Figs. 5 and 6). During this period, the first two research wells of the Coda Terminal have been drilled, and initial injection tests carried out.

As previously mentioned, drilling of the first research well, **CSI-01**, down to 982 m depth was finished mid-January 2023 (Sigurgeirsson et al., 2023a). After drilling, several well testing programs were applied. A three-step airlift test was performed on the 17th of January, after cold-water had been injected on the wellhead for 13 hours. During the airlift, injection started at 10 L/s and was increased to 25.8 L/s in three steps, with maximum wellhead pressure reaching 22 bar. The well response during the injection indicates that the permeability was stimulated during the airlift test.

The hydraulic stimulation of well CSI-01 was attempted from the 26th to the 29th of January, with a total of 60 hours of cold-water injection on the wellhead. The injection rate started at 30 L/s and was increased to 44.5 L/s in three steps. During the stimulation, the wellhead pressure remained constant at each step, indicating that the well was not stimulated. The maximum wellhead pressure reached 16.8 bar.

Drilling of the second research well, **CSM-01**, down to 618 m depth was finished in August 2023 (Sigurgeirsson et al., 2023b). An injection test was carried out in the well on the 31st of October, with a total of 5 hours of cold-water injection on the wellhead. The injection rate started at 16 L/s and was increased to 30 L/s in one step. During the injection, the water level in the wellbore never reached the wellhead, proving that well CSM-01 is considerably more permeable than well CSI-01. The estimated injectivity index of the two wells, ~5 L/bar/s compared to ~20 L/bar/s for CSI-01 and CSM-01, respectively, further indicates the higher permeability of well CSM-01.

In short, no seismicity has been recorded in the greater Straumsvík area, both during and after the drilling and initial injection tests in Straumsvík (Figs. 5 and 6), although the CODA catalogue has been thoroughly examined for any possible micro seismic events. For example, the seismic waveforms of the CODA seismic network stations were carefully inspected manually and automatically during and after the injection test in well CSM-01 on the 31st of October. The well is located very close to one of the stations, i.e., SELH (e.g., Fig. 5), and during the injection test, only vibration from the pumps used for the injection of water was detected in the corresponding waveform, with a noticeable increase in vibration once the injection rate was increased (Fig. B1 in Appendix B).

5 Discussion

When stresses yield a critical value, i.e., when the differential (deviatoric) stress in the Earth exceeds the rock strength, rock breaks or pre-existing faults are re-activated in an earthquake, in some cases generating pathways for fluid migration (Heidbach et al., 2023). Natural earthquake activity is in most cases caused by tectonic movements, stress changes due to surface deformation, or in some cases by geothermal processes. Changes in the natural stress field, e.g., by a pressure drop in a geothermal reservoir due to production or injection operations, can bring faults closer to rupture, and are a possible cause for induced seismicity.

Fluid induced seismicity is of concern because it poses a risk to safety, infrastructure and acceptance of both energy production and injection operations (e.g., Zang et al., 2014). It can either be caused directly by pore pressure changes due to injection or extraction of fluids, or by stress changes induced by either injection or extraction. Common mechanisms attributed to induced earthquakes are e.g., elevated pore pressure, poroelastic stress change, and fault loading through aseismic slip (e.g., Roth et al., 2023).

Historically, the greater Straumsvík area has been seismically quiet. Seismicity will be thoroughly monitored during the Coda Terminal project's lifetime with the on-site extended CODA seismic network set up for the Coda Terminal on the RP, in order to increase the detection level and location accuracy in Straumsvík. The area has already been monitored before and during the preparation phase of the Coda Terminal, where the first two wells have been drilled, and initial injection tests carried out. During these operations, no seismicity has been recorded. The storage site of the Coda Terminal will be developed incrementally, with each increment considering any possible induced seismicity due to previous phases. This approach furthermore minimises the risk for felt seismicity at the site.

5.1 Tectonic settings

The Straumsvík area is located north of and outside both the active plate boundary and the rift segments of the RP. No faults and fractures have been mapped in the area, mainly because of young Holocene lava flows covering the surface (Helgadóttir et al., 2023b). Geodetic measurements since the 1990s have shown stress and strain accumulation along the plate boundary, in agreement with plate motion models (Keiding et al., 2008; Sigmundsson et al., 2022). Plate motion across the RP, relative to a stable North-American plate, shows that velocities on the northern part of the Peninsula are low, with increasing eastward motion as one moves south across the plate boundary (Fig. 7) (Sigmundsson et al., 2020). This implies very little deformation in the greater Straumsvík area.

Periods of rifting and volcanism alternating with periods of earthquake episodes have occurred episodically on the RP for the last 4000 years, at intervals of ~800-1000 years, with most of the volcanic systems active, except Fagradalsfjall (Sæmundsson et al., 2020). The last eruption on the RP, within the Reykjanes volcanic system, culminated ~780 years ago, and the current volcano-tectonic unrest, starting in December 2019, seems to signal the beginning of the next active episode on the RP.

During the current unrest, accumulated stress and strain is being released during repeated dike intrusions and surface uplift within different volcanic systems on the RP. Using interferometric synthetic aperture radar (InSAR) applied to TerraSAR-X data collected over

2019–2021, Ducrocq et al. (2023) mapped fracture movements over the RP. Their study reveals extensive fracture movements mapped across most of the Peninsula and across an area much larger than seismic activity (~875 km² total), thus indicating significant aseismic fracture movements. Strikingly, 85% of the mapped fractures were previously undetected. However, the greater Straumsvík area was totally unaffected. Thus, it can be concluded from all available data, e.g., geological mapping, geodetic measurements and well data, that the greater Straumsvík area seems to be tectonically inactive. Therefore, the contemporary undisturbed stress state in Straumsvík is a key parameter for assessing the stability of the subsurface, and for quantifying whether stress changes induced by the proposed full-scale injection of the Coda Terminal will lead to a critical state.

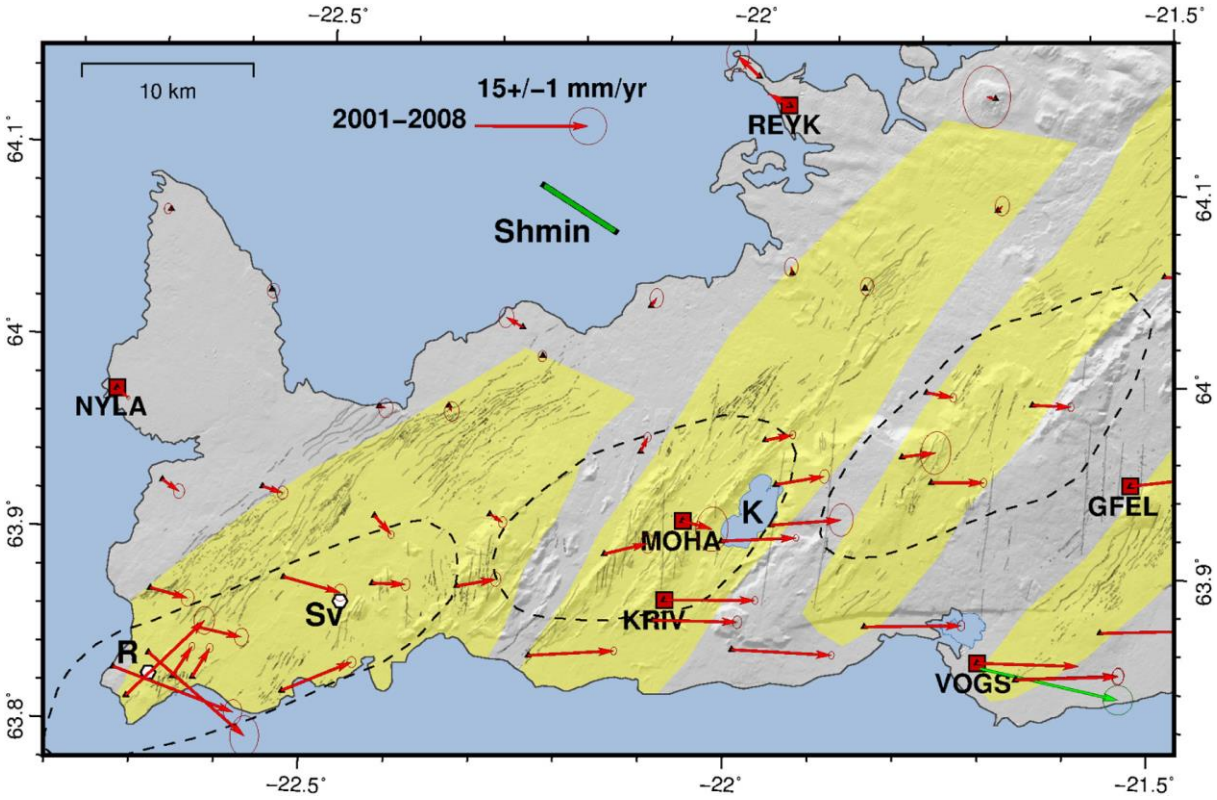

Figure 7. *Horizontal GPS velocities on the Reykjanes Peninsula during 2000-2008 (red arrows) (figure taken from Sigmundsson et al., 2020). Velocities are rotated to show motion of the Eurasian plate, relative to stable North-American plate. GPS stations are indicated with triangles (campaign stations) and red squares (continuous stations). The green bar shows the direction of the least compressive horizontal stress. For further references to the map, the reader is referred to Sigmundsson et al. (2020).*

Plate motion models indicate a locking depth of about 5-8 km on the RP, below which ductile deformation dominates and the tectonic plates slide freely, perturbed by earthquake and geothermal deformation (Sigmundsson et al., 2022). This locking depth is in good agreement with the brittle-ductile transition on the RP at roughly 6-8 km depth, determined from earthquake locations, doming up to roughly 3-5 km depth below the known high-temperature geothermal fields of Reykjanes, Svartsengi and Krýsuvík (Kristjánsdóttir, 2013; Blanck et al., 2020; Gudnason et al., 2021; Flóvenz et al., 2022).

Importantly, only minor seismicity is located within the uppermost 1-2 km of the RP, compared to the deeper part of the brittle crust down to 8 km. Seismic studies from several areas in Iceland confirm this indication that, in general, the uppermost 1-2 km of the crust is too weak for brittle failure (e.g., Flóvenz et al., 2015; Ágústsdóttir et al., 2016; Guðnason et al., 2022). This observation was further confirmed during the 2021 Fagradalsfjall dike intrusion, where weaker crust near the surface most likely contributed to very little seismicity observed within the uppermost 2 km of the crust, even as the depth of active magma emplacement progressively shallowed and magma eventually reached the surface (Fischer et al., 2022; Sigmundsson et al., 2022).

Examples of the opposite, i.e., of seismicity within the uppermost 1-2 km in Iceland, are in many cases confined to known high-temperature geothermal areas. These areas are generally associated with volcanism and fluid convection at the active plate boundary, and the heat source is hot or even molten magmatic intrusions, either dikes or sills, residing at shallow levels in the Earth's crust (Hersir et al., 2022). Near continuous stress buildup and stress change takes place within these geothermal systems due to e.g., tectonic movements, cooling and degassing of magmatic intrusions, cooling of rock, changes in fluid flow and fluid pressure within the geothermal system, and manmade effects like fluid extraction or injection associated with geothermal utilization. In some cases, the geothermal utilization leads to decompression boiling and steam cap formation at shallow depths (< 2 km) (e.g., Scott, 2020).

Examples of shallow seismicity confined to high-temperature geothermal areas are e.g., *Reykjanes* (Gudnason et al., 2021), *Svartsengi* (Flóvenz et al., 2022), *Hengill* (Jousset et al., 2011; Obermann et al., 2022), *Katla* (Einarsson and Brandsdóttir, 2000; Jónsdóttir et al., 2009), *Grímsvötn* (Klaasen et al., 2023) and *Krafla* (Schuler et al., 2016; Gudnason et al., 2021). Most of these areas are associated with high levels of natural background seismicity, and some with induced micro seismic activity. The continuous seismic activity opens up, and maintains open, fractures that are pathways for the circulating geothermal fluid. In Straumsvík, however, there is no indication of an underlying geothermal system.

5.2 Comparison to other areas

Shallow injection of fluid (< 1.5 km) has been conducted in several geothermal areas in Iceland, both within and outside the active plate boundaries, some nearby Straumsvík (Fig. 8). Most of these areas were monitored with dense local seismic networks during the injection operations, while only two areas, Hofstaðir and Eskifjörður, were only monitored with the regional SIL seismic network, and thus, the seismic sensitivity in these two areas is low. An overview of the individual shallow geothermal injection sites is given in the following paragraphs (Fig. 8) and summarised in Table 1.

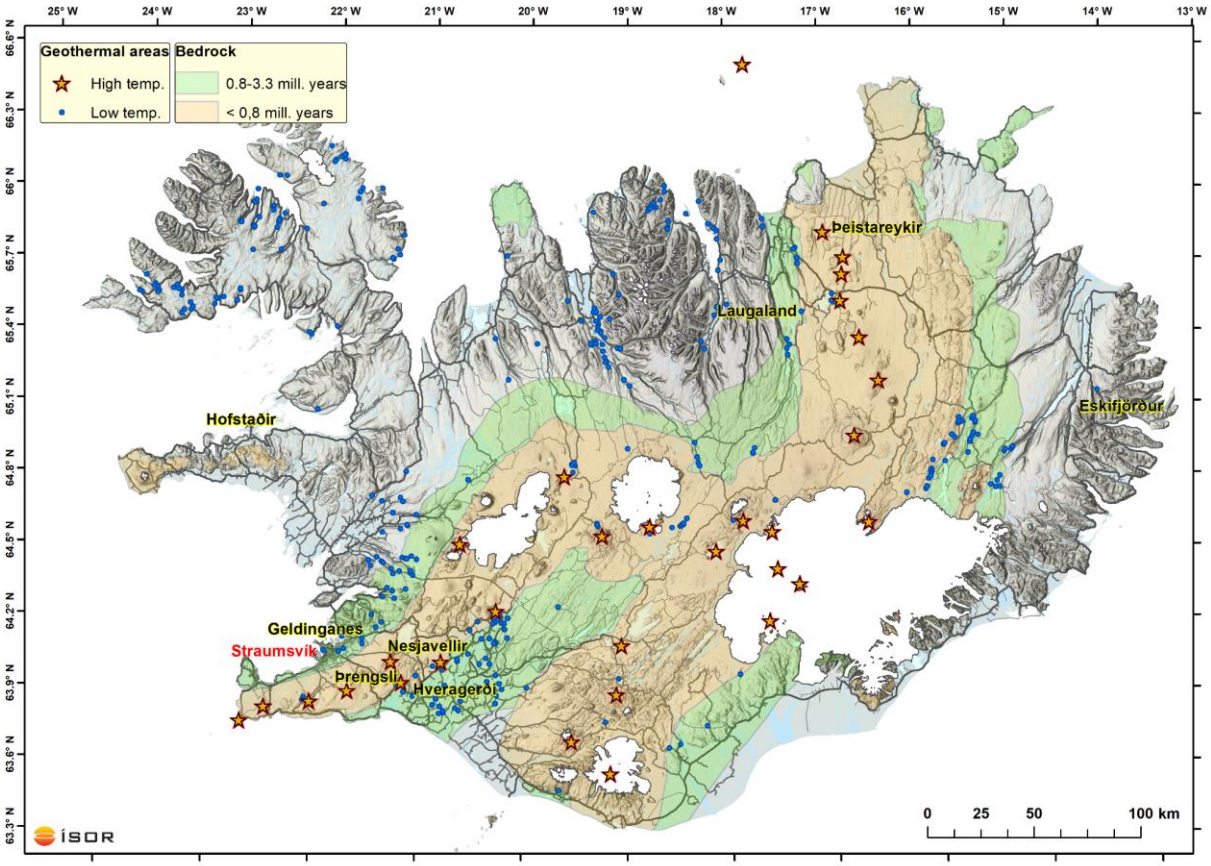

Figure 8. *A map of Iceland, showing the shallow injection areas of Geldinganes, Þrengsli, Nesjavellir, Hveragerði, Hofstaðir, Laugaland, Þeistareykir and Eskifjörður. The known geothermal areas of Iceland are either shown as red stars (high-temperature), or blue dots (low-temperature).*

i. **Þrengsli, SW-Iceland**: The Þrengsli area is on the western margin of the Hengill central volcano and high-temperature geothermal field, SW-Iceland, located at the triple junction of the Reykjanes Peninsula oblique rift zone, the Western Volcanic Zone and the South Iceland Seismic Zone. From late autumn 2016 until mid-2018, an injection experiment was conducted in four shallow wells in Þrengsli, ranging in depth from 800-2000 m, with the largest feed zones at ~420-760 m depth. The injection rate varied from 20 to 80 L/s, with the maximum injection rate applied at the initial stage of the experiment. The local seismic network of the geothermal operator in the Hengill area, Orka náttúrunnar, and ÍSOR, supplemented by nearby seismic stations of the regional SIL network, was up and running in the Hengill area during and after the two-year injection experiment. However, no microearthquakes were recorded (Guðnason et al., 2022).

ii. **Nesjavellir, SW-Iceland**: The high-temperature geothermal field of Nesjavellir is on the northern margin of the Hengill central volcano, SW-Iceland. The geothermal field has been utilised for hot water and electricity production since 1990, with an installed capacity of 120 MW_e and 300 MW_t at present. Shallow injection into eight wells in Nesjavellir, ranging in depth from 300-660 m, was started in 2002. The injection rate was increased in 2006, and again in 2016, and since 2016, the average injection rate has been ~450 L/s (Thomas Ratouis, Carbfix, personal communication, November 2023).

Seismicity in this area has been closely monitored since 2016, with the local seismic network in the Hengill area. However, no seismicity has been recorded at shallow depths in Nesjavellir that could be related to the shallow injection (Guðnason et al., 2022).

iii. **Hveragerði, SW-Iceland**: Hveragerði is located just east of the Hengill central volcano, SW-Iceland, on the westernmost part of the South Iceland Seismic Zone. Within the EU funded GECO project, a test injection of CO_2 dissolved in water was conducted into well HV-05 in Hveragerði from March to early May 2023. Well HV-05 was drilled to a depth of 1206 m in 1960, with feed zones at 246 m and 300 m depth (Steingrímsson, 1991; Jónsson et al., 2021). The maximum injection rate reached only ~10 L/s, with maximum wellhead pressure of ~14 bar. Seismicity was monitored both prior to, during and after the injection test with the local seismic network in the Hengill area, and three additional seismic stations installed in the vicinity of well HV-05, as part of the GECO project. However, no seismicity was recorded during this time period that could be related to the shallow injection (Guðnason and Ágústsdóttir, 2022; Gunnarsdóttir et al., 2023).

iv. **Geldinganes, SW-Iceland**: The undeveloped low-temperature geothermal field of Geldinganes is located within the city limits of Reykjavík, SW-Iceland. A high geothermal gradient of up to 450°C/km on Geldinganes triggered the drilling of the deviated well RV-43 in 2001, to a true vertical depth of 1550 m and a total measured depth of 1832 m. No large feed zones were identified in the well, but temperature logging after drilling revealed that most of the injected water exited the well at ~700 m depth, with only a small fraction of the water reaching a feed zone at 1250 m depth (Richter et al., 2001). Because of low permeability encountered in the well, hydraulic stimulation tests were performed in the well in October 2019 within the European DESTRESS project (Hofmann et al., 2021). The well was stimulated using packers at four different measured depths; 500 m, 1049-1195 m, 1484 m and 1640 m. The maximum injection rate reached ~60 L/s and the injectivity of the well was increased by a factor of 3.5, to 12.5 L/s/MPa at 2 MPa differential pressure. A dense local seismic network was installed prior to the hydraulic stimulation, consisting of a total of 13 seismic stations, and thus, the seismic sensitivity in the Geldinganes area was very high. Only very minor low magnitude seismicity was recorded during the deepest stimulation stage at 1425 m true vertical depth (1640 m measured depth), with 70 induced events of magnitude Mw between -1.0 and -0.1 occurring in a small cluster at a short distance (100-400 m) from the packer location towards the north, of which only 23 events are identified as stable solutions with magnitude and location determination. Thus, it was concluded that the hydraulic performance of the well was improved without inducing any felt seismicity.

v. **Hofstaðir, W-Iceland**: The low-temperature geothermal field of Hofstaðir is located on the Snæfellsnes Peninsula, W-Iceland, in the Miocene basaltic crust (> 5.3 mill. years). The geothermal field was only discovered by heat flow measurements, as there are no geothermal manifestations at the surface (Axelsson et al., 2005). Utilisation started in 1999, with an average yearly production of ~20 L/s from one well, HO-01, drilled to a depth of 855 m. To counteract a continuous observed pressure drawdown in the geothermal reservoir, injection of ~10 L/s started in 2007 into one well, HO-02, drilled

to a depth of 413 m, with the main feed zone at 319 m depth (Gaoxuan et al., 2010). The seismic sensitivity in this area is low, due to large distances to the next seismic stations of the regional SIL network (> 70 km). However, no seismicity has been located in this area since injection started (Flóvenz et al., 2015).

vi. **Eskifjörður, E-Iceland**: The low-temperature geothermal field of Eskifjörður is in E-Iceland, in the Miocene basaltic crust (Flóvenz et al., 2015). The geothermal field was discovered by resistivity measurements in 1978 (Hersir and Flóvenz, 1978) and shallow gradient wells in the 90's (Stapi - Jarðfræðistofa, 1999), and later confirmed by a production well, drilled to a depth of 1372 m in 2002. Utilisation started in 2005, with an average yearly production of ~20 L/s, and injection of ~8 L/s started in 2008 into three 350-640 m deep wells, with the main feed zones at ~400 m depth (Halldórsdóttir and Gautason, 2013). The seismic sensitivity in this area is low, due to large distances to the next seismic stations of the regional SIL network (>50 km). However, no seismicity has been located in this area since injection started (Flóvenz et al., 2015).

vii. **Laugaland, N-Iceland**: Laugaland is a typical fracture controlled low-temperature geothermal field in central N-Iceland. Production started in 1977 from a reservoir reaching from 500 m depth to at least 2500 m, with temperatures in the range of 90-100°C (Axelsson et al., 2000; Flóvenz et al., 2010). Because of low overall permeability and limited natural recharge, the modest production of ~150 L/s led to a great pressure drawdown. Therefore, injection was considered to improve the productivity of the system, starting with a successful small-scale experiment in 1991 (Axelsson et al., 2000). Production was later decreased to 45 L/s in 1996, and a full-scale injection project was conducted from 1997 to 1999. Injection of 6-22°C water was conducted into a 2820 m deep well, with injection rates varying between 6-21 L/s and maximum wellhead pressure reaching 28 bar. Temperature logs showed that about 50% of the injected water exited the well at the largest feed zone at 320 m depth, 20% at a feed zone at 600 m depth, and the rest at two feed zones at 1335 m (20%) and 1875 m (10%) depth. During the injection project, a local seismic network was designed and installed to locate all microearthquakes of magnitude M_L > -1 which might be induced by the injection (Axelsson et al., 2000; Flóvenz et al., 2015). However, no microearthquakes were recorded during the two-year period, not even during stages of the project when wellhead pressures of up to 30 bar-g were realised. This is believed to result from the fact that 70% of the injected water exits the well above 1000 m depth, where stresses are relatively low (Axelsson et al., 2000).

viii. **Þeistareykir, NE-Iceland**: The Þeistareykir high-temperature geothermal field is located within the Þeistareykir volcanic system, which is one of five active volcanic systems of the Northern Volcanic Zone, NE-Iceland. The volcanic system has a 70-80 km long and 7-8 km wide N-S trending rifting fissure swarm extending through it, intersecting with the WNW-ESE striking Húsavík-Flatey transform fault. The high-temperature geothermal field has been systematically explored over the past 50 years, with around 20 exploration and production wells drilled. Utilisation started in 2017, with an installed capacity of 90 MW_e at present, and future plans for a 45 MW_e expansion already underway. In 2014, three shallow injection wells were drilled to a depth of 400 m in Þeistareykir. Injection into the three wells started in the autumn of 2018, with an average injection rate of ~150-200 L/s since then (e.g., Egilson, 2021).

Seismicity in this area has been closely monitored since 2014, with the local seismic network of the geothermal operator, Landsvirkjun, and ÍSOR, supplemented by nearby seismic stations of the regional SIL network. However, no seismicity has been recorded at shallow depths in Þeistareykir (< 2 km) that could be related to the shallow injection (e.g., Guðnason et al., 2023).

The above-mentioned examples of shallow injection (< 1.5 km) in Iceland are summarised in Table 1. From the available data, it can be concluded that, in general, shallow injection in many areas in Iceland, both within and outside the active plate boundary, has not induced any seismicity, although large volumes of water have been injected (up to 450 L/s) (Guðnason et al., 2022). The Geldinganes area is the only exception, where only very minor (< 0 M_L) seismicity at ~1.5 km depth, not felt by the nearby population, was recorded (Hofmann et al., 2021). However, a dense seismic network was needed to be able to detect these very small events.

Table 1. *Overview of shallow injection (< 1.5 km) sites in Iceland.*

Injection site	Time period	Injection depth (m)	Average injection rate (L/s)	Seismicity
Þrengsli	2016-2018	420-760	~40	None
Nesjavellir	2002-present	300-660	450	None
Hveragerði	2023	250-300	~10	None
Geldinganes	2019	700-1250	60	Very minor
Hofstaðir	2007-present	320	10	None
Eskifjörður	2008-present	400	8	None
Laugaland	1997-1999	320-1875	15	None
Þeistareykir	2017-present	400	150-200	None

5.3 Probability of possible earthquakes

The proposed full-scale injection of the Coda Terminal project of Carbfix in Straumsvík is ~95 ton/s of CO_2 (or 3 Mt CO_2/year) dissolved in ~3,000 L/s of water. The injection will be developed incrementally, with the current plan consisting of four phases, starting at approximately 600 L/s.

The full-scale injection will take place in up to 80 shallow injection wells, ranging in depth from 400 to 800 m, cased 200-350 m below the groundwater table in each well. The wells will be drilled from a maximum of 10 drill pads. For comparison, the proposed volume of injected water is almost an order of magnitude higher than currently injected e.g., into the shallow wells in the Nesjavellir area, SW-Iceland (Guðnason et al., 2022).

The maximum injection rate ever reached during fluid injection in Iceland is at the Húsmúli injection area of the Hellisheiði geothermal power plant, SW-Iceland. Five deep injection wells were drilled in Húsmúli during 2007-2011, ranging in depth from 1950-3000 m. The injection of geothermal wastewater at Húsmúli started in September 2011, with an abrupt start and an

initial injection rate of almost 600 L/s total in all five wells (Bessason et al., 2012). A strong increase in seismicity occurred immediately just north of the injection wells, with the two largest seismic events in the sequence reaching M_L 4 (Bessason et al., 2012; Flóvenz et al., 2015; Juncu et al., 2020; Guðnason et al., 2022). It is argued that the deep fluid injection at Húsmúli caused increase in pore pressure, which resulted in increased seismicity and fault slip, with different faults activated at different times. The seismicity rate was highest at the initial phase of the injection, but with time, the injection rate has been decreased (an average of 2-300 L/s during the last few years), causing a significant reduction in seismicity (Bessason et al., 2012; Hjörleifsdóttir et al., 2021; Guðnason et al., 2022).

The proposed full-scale injection of the Coda Terminal of ~3,000 kg/s of water and dissolved CO_2 is incomparable in volume to any injection operations that have taken place in Iceland before. Therefore, Carbfix, the operators of the Coda Terminal, must be prepared for an increase in seismicity due to the proposed injection. However, the greater Straumsvík area seems to be tectonically inactive, as previously discussed, and injection will take place in shallow wells, which further minimises the risk of induced seismicity, as examples have shown. Therefore, we argue that the probability of felt seismicity is low, further discussed in chapter 7.

5.3.1 Earthquake effects in the greater Straumsvík area

In general, the effects of earthquakes include e.g., ground shaking, surface faulting and ground failure. Possible earthquake effects in the greater Straumsvík area are estimated to be only ground shaking due to possible microearthquakes in the area, a term used to describe the vibration of the ground during an earthquake. Ground shaking is caused by earthquake waves propagating through the Earth, and as a generalisation, the severity of the ground shaking increases as magnitude increases, and vice versa, decreases as distance from the causative fault increases.

The effect of an earthquake on the Earth's surface is called intensity. Numerous intensity scales have been developed that consist of a number of key responses to earthquakes. The one most widely used is the Modified Mercalli (MM) Intensity Scale (Fig. 9), developed in 1931 by seismologists in the USA (https://www.usgs.gov/programs/earthquake-hazards/modified-mercalli-intensity-scale). It is composed of increasing levels of intensity designated by Roman numerals, and the intensity scale does not have a mathematical basis but is instead an arbitrary ranking based on observed effects. For many, the MM intensity value (Fig. 9) has a more meaningful measure of severity than earthquake magnitude, because it refers to the experienced effects.

Intensity	Shaking	Description/Damage
I	Not felt	Not felt except by a very few under especially favorable conditions.
II	Weak	Felt only by a few persons at rest,especially on upper floors of buildings.
III	Weak	Felt quite noticeably by persons indoors, especially on upper floors of buildings. Many people do not recognize it as an earthquake. Standing motor cars may rock slightly. Vibrations similar to the passing of a truck. Duration estimated.
IV	Light	Felt indoors by many, outdoors by few during the day. At night, some awakened. Dishes, windows, doors disturbed; walls make cracking sound. Sensation like heavy truck striking building. Standing motor cars rocked noticeably.
V	Moderate	Felt by nearly everyone; many awakened. Some dishes, windows broken. Unstable objects overturned. Pendulum clocks may stop.
VI	Strong	Felt by all, many frightened. Some heavy furniture moved; a few instances of fallen plaster. Damage slight.
VII	Very strong	Damage negligible in buildings of good design and construction; slight to moderate in well-built ordinary structures; considerable damage in poorly built or badly designed structures; some chimneys broken.
VIII	Severe	Damage slight in specially designed structures; considerable damage in ordinary substantial buildings with partial collapse. Damage great in poorly built structures. Fall of chimneys, factory stacks, columns, monuments, walls. Heavy furniture overturned.
IX	Violent	Damage considerable in specially designed structures; well-designed frame structures thrown out of plumb. Damage great in substantial buildings, with partial collapse. Buildings shifted off foundations.
X	Extreme	Some well-built wooden structures destroyed; most masonry and frame structures destroyed with foundations. Rails bent.

Figure 9. *The Modified Mercalli Intensity Scale (https://www.usgs.gov/programs/earthquake-hazards/modified-mercalli-intensity-scale).*

Although the probability of felt seismicity in Straumsvík is estimated as low (see chapter 7), micro seismicity can be expected due to the proposed large volume of injected water. Based on the MM intensity scale and all available data, the estimated effects of possible micro-earthquakes in the Straumsvík area are in the range of:

- **Intensity levels I-IV**

with estimated ground shaking ranging from "*not felt*", to a worst-case scenario of "*light*". There is no empirical relationship between the Mercalli intensity and earthquake magnitude, however, in the case of Straumsvík, an intensity of IV would most likely represent an earthquake with a magnitude in the range of M_L 2-3.

5.4 Extent of possible earthquake activity

From known cases of induced seismic activity in Iceland, we can try to estimate how far possible earthquake activity at Straumsvík could reach from the research area of the Coda Terminal. A widely observed feature in the spatiotemporal distribution of induced seismicity is a gradual migration from the largest feed zone, where circulation loss starts and the injected fluid escapes the well, to distances farther from the well as fluid injection is progressing. In many cases, as injection proceeds, seismicity continues throughout the volume and moves laterally away from the feed zones with time, often interpreted as an activation of a fault on which the injected fluid moves.

From the known cases of induced seismic activity in Iceland, e.g., Reykjanes (Gudnason et al., 2021), Geldinganes (Hofmann et al., 2021), Hengill (Juncu et al., 2020; Guðnason et al., 2022) and Krafla (Guðnason et al., 2023), experience shows that the maximum distance induced seismicity has migrated from the respective injection well(s) is on the order of 2 km at the Húsmúli injection area of the Hellisheiði geothermal power plant, SW-Iceland, discussed in

chapter 5.3. This is the extreme example, with injection rates at Húsmúli reaching almost 600 L/s, inducing seismic events up to M_L 4 and surface deformation in a tectonically stressed high-temperature geothermal environment (e.g., Bessason et al., 2012; Juncu et al., 2020). In other areas, induced seismicity has migrated to far less distances than in Húsmúli (< 2 km), in most cases laterally away from the injection wells.

In Straumsvík, injected fluid could travel through permeable layers in the subsurface, most likely lithological boundaries of some sort, and reactivate faults not visible on the surface. However, based on the available data, the migration of possible induced seismicity is not expected to reach outside the boundaries of the Coda Terminal research area (e.g., Fig. 5), i.e., to distances less than 2 km from the respective injection well(s). The ability to track details in the spatiotemporal distribution of seismicity in Straumsvík depends primarily on the quality and the configuration of the seismic network, on the quality of the velocity model and on the applied algorithms to invert for event locations.

5.5 Response plan

The maximum allowable seismic magnitude must be determined for each injection site individually, depending on e.g., peak ground velocity (PGV) at the surface, the local geology, and surface fractures (Majer et al., 2012). For Straumsvík, the local geology is well known, and no surface fractures have been mapped in the area, while PGV at the surface has not yet been estimated.

Seismic traffic light systems (TLS) are standard procedures worldwide to manage seismic risks for fluid injection activities. In Iceland, it is currently applied for injection activities at the Hellisheiði high-temperature geothermal field (Thorsteinsson and Gunnarsson, 2014), and was applied for the hydraulic stimulation tests performed in the Geldinganes low-temperature geothermal field in 2019 (Hofmann et al., 2021).

For the Coda Terminal project of Carbfix in Straumsvík, the pre-defined TLS agreed between operator and regulator is shown in Fig. 10, modified from Thorsteinsson and Gunnarsson (2014) and Hofmann et al. (2021). The relevant area for the pre-defined TLS is the research area of the Coda Terminal, shown in green colour in Fig. 5. We use a communication protocol that is similar to the one used in the TLS of the Geldinganes geothermal field due to similar conditions, e.g., proximity to nearby municipalities, while for the Coda Terminal, magnitude levels, seismic protocols and field operations protocols have been specifically designed for this application. Depending on the local magnitude (M_L) of possibly induced seismic events, the flow rates are adapted according to this TLS.

The pre-defined TLS for the Coda Terminal may be summarised as follows: Below M_L 1.5, injection operations may continue as planned if no anomalous seismicity evolution is identified. Above M_L 1.5, flow rates and pressures are decreased until seismicity levels remain below the green alert for at least 4 hours. Above M_L 2.0, injection operations are stopped until seismicity levels remain below the green alert for at least 12 hours. M_L 3.0 is the target magnitude that should be avoided by applying this TLS. If a red traffic light is reached, the injection operations are stopped and injection at the site will not resume without an additional risk study.

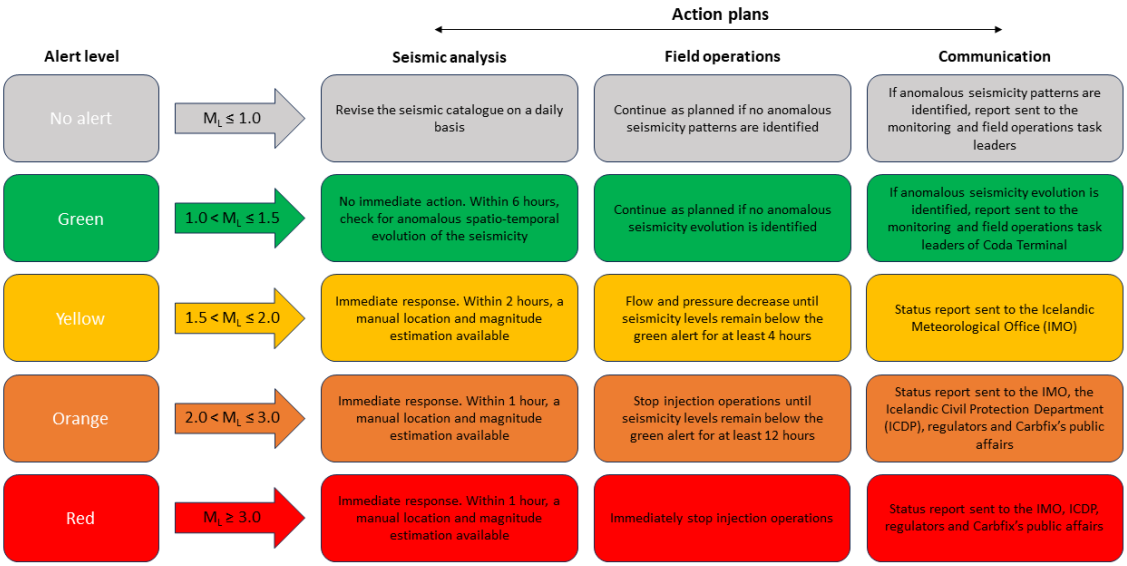

Figure 10. *Pre-defined traffic light system (TLS) for the Coda Terminal project of Carbfix in Straumsvík (modified from Thorsteinsson and Gunnarsson, 2014; Hofmann et al., 2021). The relevant area for the TLS is the research area of the Coda Terminal, shown in green colour in Fig. 5.*

6 Summary

The Coda Terminal project of Carbfix in Straumsvík, SW Iceland, will go through an environmental impact assessment (EIA), before large-scale injection of dissolved CO_2 of up to 2,850 L/s can be initiated. In this report, results of a new seismic assessment in the greater Straumsvík area are presented, taking into account new data on research drilling, initial injection tests and earthquake activity in the area. The main results are summarised here:

- The greater Straumsvík area, located outside the active plate boundary and rift segments of the Reykjanes Peninsula (RP), seems to be tectonically inactive, taking into account all available data, including stress release during the current volcano-tectonic unrest on the Peninsula.
- The first two research wells of the Coda Terminal indicate that permeability in Straumsvík is most likely related to lithological boundaries of some sort, with the main feed points at ~330-375 m depth.
- Fractures or lineaments observed in the two wells do not give evidence of any movement, and there is no evidence of an underlying geothermal system in Straumsvík.
- The extended CODA seismic network in the greater Straumsvík area consists of local seismic stations of Carbfix and ÍSOR, supplemented by data from nearby stations of long-time operating seismic networks on the RP. All data streaming is in real-time for automatic processing.
- Historically, the greater Straumsvík area is seismically quiet, even during the initial injection tests in the two wells of the Coda Terminal. In general, it seems that the uppermost 1-2 km of the crust in Iceland is too weak for brittle failure.
- Shallow injection of fluid (< 1.5 km) in several geothermal areas in Iceland has not induced any felt seismicity, although large volumes of water (up to 450 L/s) have been injected for an extended amount of time.

- For the EIA, the probability and extent of possible earthquake activity in the Straumsvík area is discussed and evaluated, with estimated ground shaking ranging from "*not felt*", to a worst-case scenario of "*light*", and the extent of possible induced seismicity not expected to reach outside the boundaries of the Coda Terminal research area.
- A response plan to any potential earthquake activity is put forward in the form of a seismic traffic light system and discussed with regards to the results of recent research drillings. The relevant area for the pre-defined traffic light system is the research area of the Coda Terminal.

7 Conclusion

Based on the available data, we conclude that the preliminary assessment of potential induced seismicity during fluid injection from the Coda Terminal in Straumsvík would fall under **part 2 of segment 4** in the regulations of the National Energy Authority for preparation and mitigation of earthquake hazard due to fluid injection in injection wells (OS-2016-R01-01): *The probability of felt seismicity is low (in Icelandic: "Hætta á finnanlegri skjálftavirkni er óveruleg").*

Due to the proximity of the injection wells of the Coda Terminal to the nearby municipalities, we recommend that seismicity is closely monitored prior to and during the injection operations, and that the injection rate is increased gradually.

8 Recommendations

i. Although the probability of felt induced seismicity in Straumsvík is considered to be low, it is important that possible seismicity is closely monitored prior to and during the injection operations of Carbfix's Coda Terminal, and that the injection rate is increased gradually. It is also important that the storage site of the Coda Terminal will be developed incrementally, with each increment considering any possible induced seismicity due to previous phases. This approach will minimise the risk for felt seismicity at and near the site.

ii. It is important to follow the risk mitigation measures, including the application of the pre-defined traffic light system (TLS) for the Coda Terminal, based on high resolution real-time seismic monitoring.

iii. In Þeistareykir, NE-Iceland, average injection of ~150-200 L/s into three shallow wells (~400 m) since 2018 has generated subsidence on the order of 10-15 mm/year, localised around the injection wells (e.g., Drouin, 2021). The deformation source is shallow (< 1 km), most likely due to thermal contraction of the host rock by the colder re-injected fluids at around 400 m depth. In Þeistareykir, the deformation takes place seismically. Similarly, shallow fluid injection in Straumsvík might generate localised deformation, due to the possible contraction effect from cooling. We therefore recommend that possible surface deformation within the Coda Terminal research area is monitored using the InSAR (Interferometric Synthetic Aperture Radar) technology, as possible deformation might reveal any effective stress changes in the subsurface.

References

Axelsson, G., Björnsson, G., Egilson, Th., Flóvenz, Ó. G., Gautason, B., Hauksdóttir, S., Ólafsson, M., Smárason, Ó. B. and Sæmundsson, K. (2005). Nature and Properties of Recently Discovered Hidden Low-Temperature Geothermal Reservoirs in Iceland. *Proceedings of the World Geothermal Congress 2005, Antalya, Turkey,* 10 p.

Axelsson, G., Flóvenz, Ó. G., Hjartarson, A., Hauksdóttir, S., Sverrisdóttir, G., Árnason, F., Árnason, Á. and Böðvarsson, R. (2000). Thermal energy extraction by reinjection from the Laugaland geothermal system in N-Iceland. *Proceedings of the World Geothermal Congress 2000, Kyushu-Tohoku, Japan*, 6 p.

Ágústsdóttir, Þ., Horálek, J., Gudnason, E. Á., Doubravová, J., Hersir, G. P., Klicpera, J., Pétursson, F., Magnússon, R. M., Málek, J., Fojtíková, L., Fischer, T., Vlček, J. and Salama, A. (2022). The REYKJANET local seismic network ideally placed for capturing the 2021 Fagradalsfjall pre-eruptive seismicity: in operation since 2013. *EGU General Assembly 2022, Vienna, Austria, EGU22-9802*. https://doi.org/10.5194/egusphere-egu22-9802.

Ágústsdóttir, Þ., Woods, J., Greenfield, T., Green, R. G., White, R. S., Winder, T., Brandsdóttir, B., Steinþórsson, S. and Soosalu, H. (2016). Strike-slip faulting during the 2014 Bárðarbunga-Holuhraun dike intrusion, central Iceland. *Geophys. Res. Lett., 43(4),* 1495-1503. https://doi.org/10.1002/2015GL067423.

Ágústsson, K. and Flóvenz, Ó. G. (2005). The Thickness of the Seismogenic Crust in Iceland and its Implications for Geothermal Systems. *Proceedings of the World Geothermal Congress 2005, Antalya, Turkey*, 9 p.

Ágústsson, K., Rögnvaldsson, S. Th., Bergsson, B. H. and Stefánsson, R. (1998). *Jarðskjálfta-mælanet Veðurstofu Íslands og Hitaveitu Suðurnesja – lýsing á mælaneti og fyrstu niðurstöður*. VÍ-R98002-JA002, 19 p.

Bali, E., Aradi, L. E., Zierenberg, R., Diamond, L. W., Pettke, T., Szabó, Á., Guðfinnsson, G. H., Friðleifsson, G. Ó. and Szabó, C. (2020). Geothermal energy and ore-forming potential of 600°C mid-ocean-ridge hydrothermal fluids. *Geology, 48(12),* 1221-1225. https://doi.org-/10.1130/G47791.1.

Bessason, B., Ólafsson, E. H., Gunnarsson, G., Flóvenz, Ó. G., Jakobsdóttir, S., Björnsson, S. and Árnadóttir, Þ. (2012). *Verklag vegna örvaðrar skjálftavirkni í jarðhitakerfum*. Orkuveita Reykjavíkur, OR-2012-24, 108 p.

Björnsson, S., Einarsson, P., Tulinius, H. and Hjartardóttir, Á. R. (2020). Seismicity of the Reykjanes Peninsula 1971-1976. *J. Volcanol. Geotherm. Res., 391,* 106369. https://doi.org/-10.1016/j.jvolgeores.2018.04.026.

Blanck, H., Jousset, P., Hersir, G. P., Ágústsson, K. and Flóvenz, Ó. G. (2020). Analysis of 2014–2015 on- and off-shore passive seismic data on the Reykjanes Peninsula, SW Iceland. *J. Volcanol. Geotherm. Res., 391*, 106548. https://doi.org/10.1016/j.jvolgeores.2019.02.001.

Caracciolo, A., Bali, E., Halldórsson, S. A., Guðfinnsson, G. H., Kahl, M., Þórðardóttir, I., Pálmadóttir, G. L. and Silvestri, V. (2023). Magma plumbing architectures and timescales of magmatic processes during historical magmatism on the Reykjanes Peninsula, Iceland. *Earth and Planetary Science Letters, 621*, 118378. https://doi.org/10.1016/j.epsl.2023.118378.

Drouin, V. (2021). *InSAR Monitoring of Krafla, Bjarnarflag and Þeistareykir Geothermal Areas. 2021 Update.* Iceland GeoSurvey, ÍSOR-2021/045, LV-2021-050, 19 p.

Ducrocq, C., Árnadóttir, Th., Einarsson, P., Jónsson, S., Drouin, V. Geirsson, H. and Hjartardóttir, Á. R. (2023). Widespread fracture movements during the 2019-2021 volcano-tectonic unrest on the Reykjanes Peninsula from TerraSAR-X interferometry. *EGU General Assembly, Vienna, Austria, EGU23-10732.* https://doi.org/10.5194/egusphere-egu23-10732.

Egilson, Þ. (2021). *Eftirlitsmælingar í Kröflu, Bjarnarflagi og á Þeistareykjum árið 2021*. Iceland GeoSurvey, ÍSOR-2021/040, LV-2021-042, 39 p. + Appendix.

Einarsson, P. (1991). Earthquakes and present-day tectonism in Iceland. *Tectonophysics*, *189* (1-4), 261–279. https://doi.org/10.1016/0040-1951(91)90501-I.

Einarsson, P. and Brandsdóttir, B. (2000). Earthquakes in the Mýrdalsjökull area, Iceland, 1978-1985: seasonal correlation and connection with volcanoes. *Jökull, 49,* 59-73. http://dx.doi.org/10.33799/jokull2000.49.059.

Einarsson, P., Hjartardóttir, Á. R., Hreinsdóttir, S. and Imsland, P. (2020). The structure of seismogenic strike-slip faults in the eastern part of the Reykjanes Peninsula Oblique Rift, SW Iceland. *J. Volcanol. Geotherm. Res., 391,* 106372. https://doi.org/10.1016/j.jvolgeores.2018.04.029.

Erlendsson, P. and Einarsson, P. (1996). The Hvalhnúkur Fault, a strike-slip fault mapped within the Reykjanes Peninsula oblique rift, Iceland. *Seismology in Europe*, 498-504.

Fischer, T., Hrubcová, P., Salama, A., Doubravová, J., Ágústsdóttir, T., Gudnason, E. Á., Horálek, J. and Hersir, G. P. (2022). Swarm seismicity illuminates stress transfer prior to the 2021 Fagradalsfjall eruption in Iceland. *Earth Planet. Sci. Lett., 594,* 117685. https://doi.org/10.1016/j.epsl.2022.117685.

Flóvenz, Ó. G. (1980). Seismic structure of the Icelandic crust above layer three and the relation between body wave velocity and the alteration of the basaltic crust. *J. Geophys. Res., 47,* 211-220.

Flóvenz, Ó. G., Ágústsson, K., Guðnason, E. Á. and Kristjánsdóttir, S. (2015). Reinjection and Induced Seismicity in Geothermal Fields in Iceland. *Proceedings of the World Geothermal Congress 2015, Melbourne, Australia*, 15 p.

Flóvenz, Ó. G., Árnason, F., Gautason, B., Axelsson, G., Egilson, Th., Steindórsson, S. H. and Gunnarsson, H. S. (2010). Geothermal District Heating in Eyjafjördur, N-Iceland; Eighty Years of Problems, Solutions and Success. *Proceedings of the World Geothermal Congress 2010, Bali, Indonesia,* 8 p.

Flóvenz, Ó. G., Wang, R., Hersir, G. P., Dahm, T., Hainzl, S., Vassileva, M., Drouin, V., Heimann, S., Isken, M. P., Gudnason, E. Á., Ágústsson, K., Ágústsdóttir, T., Horálek, J., Motagh, M., Walter, T. R., Rivalta, E., Jousset, P, Krawczyk, C. M. and Milkereit, C. (2022). Cyclical geothermal unrest as a precursor to Iceland's 2021 Fagradalsfjall eruption. *Nat. Geosci., 15*(5), 397–404. https://doi.org/10.1038/s41561-022-00930-5.

Gaoxuan, G., Axelsson, G., Chao, Y. and Baodong, X. (2010). Assessment of the Hofsstadir Geothermal Field, W-Iceland, by Lumped Parameter Modelling, Monte Carlo Simulation and Tracer Test Analysis. *Proceedings of the World Geothermal Congress 2010, Bali, Indonesia,* 10 p.

Gudnason, E. Á., Köpke, R., Gaucher, E., Ágústsson, K., Níelsson, S. and Kohl, T. (2021). Seismic Monitoring During Drilling and Stimulation of Well RN-15/IDDP-2 in Reykjanes, SW-Iceland. *Proceedings of the World Geothermal Congress 2020+1, Reykjavík, Iceland,* 11 p.

Guðnason, E. Á. and Ágústsdóttir, Þ. (2022). *Preliminary Assessment of Potential Induced Seismicity at the Hveragerði Test Site.* GECO, Deliverable 6.7. Iceland GeoSurvey, ÍSOR-2022/050, 17 p.

Guðnason, E. Á., Ágústsdóttir, Þ., Gunnarsdóttir, S. H., Galeczka, I. M., Óladóttir, A. A., Benediktsdóttir, Á. and Einarsson, G. M. (2022). *Sérfræðiskýrsla fyrir umhverfismat fyrir niðurdælingu CO_2 á Hellisheiði. Grunnástand og hugsanlegar breytingar.* Iceland GeoSurvey, ÍSOR-2022/030, 77 p.

Guðnason, E. Á., Ágústsdóttir, Þ., Magnússon, R. L. and Gunnarsson, K. (2023). *Seismic Monitoring in Krafla, Þeistareykir and Námafjall. Reprocessing of the Entire 2006-2022 Catalogue*. Iceland GeoSurvey, ÍSOR-2023/009, LV-2023-021, 56 p.

Gunnarsdóttir, S. H., Leontidis, V., Gainville, M., Kaldal, G. S., Guðnason, E. Á. and Batini, F. (2023). *Report on demonstration campaign and monitoring results.* GECO, Deliverable 6.9, 66 p.

Halldórsdóttir, S. and Gautason, B. (2013). *Eskifjörður. Yfirlit um jarðhitakerfið og vinnslusögu frá 2005-2012 ásamt framtíðarspám.* Iceland GeoSurvey, ÍSOR-2013/023, 47 p.

Heidbach, O., Reiter, K., Ziegler, M. O., and Müller, B. (2023). How to estimate the 3D stress state for a deep geological repository. *Saf. Nucl. Waste Disposal*, *2*, 185–185. https://doi.org/-10.5194/sand-3-185-2023.

Helgadóttir, H. M., Ingólfsson, H. and Pétursson, F. (2023a). *Televiewer Logs from Well CSI-1 in Straumsvík*. Iceland GeoSurvey, ÍSOR-2023/014, 32 p. + Appendix II.

Helgadóttir, H. M., Sigurgeirsson, M. Á. and Gunnarsdóttir, S. H. (2023b). *Geological 3D Model of the Greater Straumsvík Area. Prepared for Carbfix's Coda Terminal Project for the Environmental Impact Assessment*. Iceland GeoSurvey, ÍSOR-2023/018, in prep.

Hersir, G. P. and Flóvenz, Ó. G. (1978). *Viðnámsmælingar á Austurlandi.* Orkustofnun, OS-JHD-7843, 31 p.

Hersir, G. P., Guðnason, E. Á. and Flóvenz, Ó. G. (2022) Geophysical Exploration Techniques. In: *Letcher, Trevor M. (eds.) Comprehensive Renewable Energy, 2nd edition*, vol. *7*, 26–79. Oxford: Elsevier.

Hjörleifsdóttir, V., Ingvarsson, G., Ratouis, T., Gunnarsson, G., Snæbjörnsdóttir, S. Ó. and Sigfússon, B. (2021). Ten years of induced earthquakes in the Húsmúli CO_2 injection site, Hellisheiði, Iceland. *SEG Global Meeting Abstracts,* 96-100. https://doi.org/10.1190/iceg2021-027.1.

Hofmann, H., Zimmermann, G., Huenges, E., Regenspurg, S., Aldaz, S., Milkereit, C., Heimann, S., Dahm, T., Zang, A., Grigoli, F., Karvounis, D., Broccardo, M., Wiemer, S., Hjörleifsdóttir, S., Kristjánsson, B. R., Hersir, G. P., Ásgeirsdóttir, R. S., Magnússon, R. and Árnadóttir, S. (2021). Soft stimulation treatment of geothermal well RV-43 to meet the growing heat demand of Reykjavík. *Geothermics, 96,* 102146. https://doi.org/10.1016-/j.geothermics.2021.102146.

Jakobsdóttir, S. (2008). Seismicity in Iceland: 1994-2007. *Jökull, 58,* 75-100. http://dx.doi.org-/10.33799/jokull2008.58.075.

Jousset, P., Haberland, C., Bauer, K., and Árnason, K. (2011). Hengill geothermal volcanic complex (Iceland) characterized by integrated geophysical observations. *Geothermics, 40*(*1*), 1–24. https://doi.org/10.1016/j.geothermics.2010.12.008.

Jónsdóttir, K., Roberts, R., Pohjola, V., Lund, B., Shomlai, Z. H., Tryggvason, A. and Bödvarsson, R. (2009). Glacial long-period seismic events at Katla volcano, Iceland. *Geophys. Res. Lett., 36,* L11402. https://doi.org/10.1029/2009GL038234.

Jónsson, J. E., Helgadóttir, H. M., Egilson, Þ., Vilhjálmsson, A. M., Árnadóttir, S., Gunnarsdóttir, S. H. and Ingólfsson, H. (2021). *Logging in Well HV-05, Hveragerði, Iceland*. Iceland GeoSurvey, ÍSOR-2021/055, 34 p.

Juncu, D., Árnadóttir, Þ., Geirsson, H., Guðmundsson, G. B., Lund, B., Gunnarsson, G., Hooper, A., Hreinsdóttir, S. and Michalczewska, K. (2020). Injection-induced surface deformation and seismicity at the Hellisheidi geothermal field, Iceland. *J. Volc. Geotherm. Res., 391,* 106337. https://doi.org/10.1016/j.jvolgeores.2018.03.019.

Keiding, M., Árnadóttir, Th., Sturkell, E., Geirsson, H. and Lund, B. (2008). Strain accumulation along an oblique plate boundary: The Reykjanes Peninsula, southwest Iceland. *Geophys. J. Int., 172*(2), 861-872. https://doi.org/10.1111/j.1365-246X.2007.03655.x.

Keiding, M., Lund, B. and Árnadóttir, T. (2009). Earthquakes, stress, and strain along an obliquely divergent plate boundary: Reykjanes peninsula, southwest Iceland. *J. Geophys. Res., 114*, B09306. https://doi.org/10.1029/2008JB006253.

Klaasen, S., Thrastarson, S., Çubuk-Sabuncu, Y., Jónsdóttir, K., Gebraad, L., Paitz, P. and Fichtner, T. (2023). Subglacial volcano monitoring with fibre-optic sensing: Grímsvötn, Iceland. *Volcanica, 6(2),* 301-311. http://dx.doi.org/10.30909/vol.06.02.301311.

Klein, F. W., Einarsson, P. and Wyss, M. (1973). Microearthquakes on the Mid-Atlantic plate boundary on the Reykjanes Peninsula in Iceland, *J. Geophys. Res., 78*, 5084-5099. https://doi.org/10.1029/JB078i023p05084.

Klein, F. W., Einarsson, P. and Wyss, M. (1977). The Reykjanes Peninsula, Iceland, earthquake swarm of September 1972 and its tectonic significance. *J. Geophys. Res., 82*, 865-888. https://doi.org/10.1029/JB082i005p00865.

Kristjánsdóttir, S. (2013). *Microseismicity in the Krýsuvík Geothermal Field, SW Iceland, from May to October 2009*. MSc thesis, University of Iceland, Reykjavík.

Kristjánsdóttir, S. and Ágústsdóttir, Þ. (2020). *Preliminary assessment of induced seismicity due to fluid injection in Straumsvík*. Iceland GeoSurvey, ÍSOR-20035, 13 p.

Majer, E., Nelson, J., Robertson-Tait, A., Savy, J. and Wong, I. (2012). *Protocol For Addressing Induced Seismicity Associated With Enhanced Geothermal Systems*. U.S. Department of Energy, Report, DOE/EE-0662, 52 p.

Obermann, A., Wu, S.-M., Ágústsdóttir, T., Duran, A., Diehl, T., Sánchez-Pastor, P., Kristjánsdóttir, S., Hjörleifsdóttir, V., Wiemer, S. and Hersir, G. P. (2022). Seismicity and 3-D body-wave velocity models across the Hengill geothermal area, SW Iceland. *Front. Earth Sci., Sec. Solid Earth Geophysics, 10*. https://doi.org/10.3389/feart.2022.969836.

Parks, M., Sigmundsson, F., Drouin, V., Hjartardóttir, Á. R., Geirsson, H., Hooper, A., Vogfjörd, K. S., Ófeigsson, B. G., Hreinsdóttir, S., Jensen, E. H., Einarsson, P., Barsotti, S. and Fridriksdóttir, H. M. (2023). Deformation, seismicity, and monitoring response preceding and during the 2022 Fagradalsfjall eruption, Iceland. *Bull. Volcanol., 85*, 60. https://doi.org/10.1007/s00445-023-01671-y.

Richter, B., Jónsson, S. S. and Sigurðsson, Ó. (2001). Geldinganes, rannsóknarhola RV-43. Úrvinnsla og samantekt á borgögnum. *Orkustofnun, BR-SSJo-Omar-2001-01,* 95 p.

Roth, M. P., Verdecchia, A., Harrington, R. and Liu, Y. (2023). Inferring rock strength and fault activation from high-resolution in situ Vp/Vs estimates surrounding induced earthquake clusters. *Seismica*, *2*(2). https://doi.org/10.26443/seismica.v2i2.498.

Scott, S. (2020). Decompression boiling and natural steam cap formation in high-enthalpy geothermal systems. *J. Volcanol. Geotherm. Res., 395,* 106765. https://doi.org/10.1016-/j.jvolgeores.2019.106765.

Sigmundsson, F., Einarsson, P., Hjartardóttir, Á. R., Drouin, V., Jónsdóttir, K., Árnadóttir, T., Geirsson, H., Hreinsdóttir, H., Li, S. and Ófeigsson, B. G. (2020). Geodynamics of Iceland and the signatures of plate spreading. *J. Volcanol. Geotherm. Res., 391*, 106436. https://doi.org/10.1016/j.jvolgeores.2018.08.014.

Sigmundsson, F., Parks, M., Hooper, A., Geirsson, H., Vogfjörd, K. S., Drouin, V., Ófeigsson, B. G., Hreinsdóttir, S., Hjaltadóttir, S., Jónsdóttir, K., Einarsson, P., Barsotti, S., Horálek, J. and Ágústsdóttir, Th. (2022). Deformation and seismicity decline before the 2021 Fagradalsfjall eruption. *Nature, 609*, 523–528. https://doi.org/10.1038/s41586-022-05083-4.

Sigurðsson, F. (1986). Hydrogeology and groundwater on the Reykjanes Peninsula. *Jökull, 36,* 11-29. http://dx.doi.org/10.33799/jokull1986.36.011.

Sigurgeirsson, M. Á., Jónsson, J. E. and Ingólfsson, H. I. (2023a). *Straumsvík – Well CSI-01. Drilling of Well CSI-01 from Surface down to 982 m.* Iceland GeoSurvey, ÍSOR-2023/006, 49 p.

Sigurgeirsson, M. Á., Jónsson, J. E. and Ingólfsson, H. I. (2023b). *Straumsvík – Well CSM-01. Drilling of Well CSM-01 from Surface down to 618 m*. Iceland GeoSurvey, in prep.

Stapi – Jarðfræðistofa (1999). *Jarðhitaleit í Fjarðabyggð árið 1999*. Reykjavík, Stapi – Jarðfræðistofa, 8 p.

Steingrímsson, B. (1991). *Borholur í Ölfusdal: Ástand, hiti og afl*. Orkustofnun, short report, BS-91-01, 16 pp.

Sæmundsson, K. and Sigurgeirsson, M. Á. (2013). Reykjanesskagi. In: Sólnes, Júlíus (Ed.), *Náttúruvá á Íslandi. Eldgos og Jarðskjálftar*. Viðlagatrygging Íslands/Háskólaútgáfan, 379–401.

Sæmundsson, K., Sigurgeirsson, M. Á., Hjartarson, Á., Kaldal, I., Kristinsson, S. G. and Skúlason, V. (2016). *Geological map of Southwest Iceland 1:100 000 (2nd edition)*. Reykjavík: Iceland GeoSurvey.

Sæmundsson, K., Sigurgeirsson, M. Á. and Friðleifsson, G. Ó. (2020). Geology and structure of the Reykjanes volcanic system, Iceland. *J. Volcanol. Geotherm. Res., 391*, 106501. https://doi.org/10.1016/j.jvolgeores.2018.11.022.

Thorsteinsson, H. and Gunnarsson, G. (2014). Induced Seismicity – Stakeholder Engagement in Iceland. *GRC Trans., 38,* 879-881.

Violay, M., Gibert, B., Mainprice, D., Evans, B., Dautria, J.-M., Azais, P. and Pezard, P. (2012). An experimental study of the brittle-ductile transition of basalt at oceanic crust pressure and temperature conditions. *J. Geophys. Res.*, *117*, B03213. http://dx.doi.org/-10.1029-/2011JB008884.

Ward, P. L. and Björnsson, S. (1971). Microearthquakes, swarms and the geothermal areas of Iceland. *J. Geophys. Res., 76*, 3953-3982. https://doi.org/10.1029/JB076i017p03953.

Weir, N. R., White, R. S., Brandsdóttir, B., Einarsson, P., Shimamura, H. and Shiobara, H. (2001). Crustal structure of the northern Reykjanes Ridge and Reykjanes Peninsula, southwest Iceland. *J. Geophys. Res.*, *106*(B4), 6347–6368. https://doi.org/10.1029/2000JB900358.

Zang, A., Oye, V., Jousset, P., Deichmann, N., Gritto, R., McGarr, A., Majer, E. and Bruhn, D. (2014). Analysis of induced seismicity in geothermal reservoirs – An overview. *Geothermics, 52*, 6-21. https://doi.org/10.1016/j.geothermics.2014.06.005.

Appendix A: SIL earthquake locations

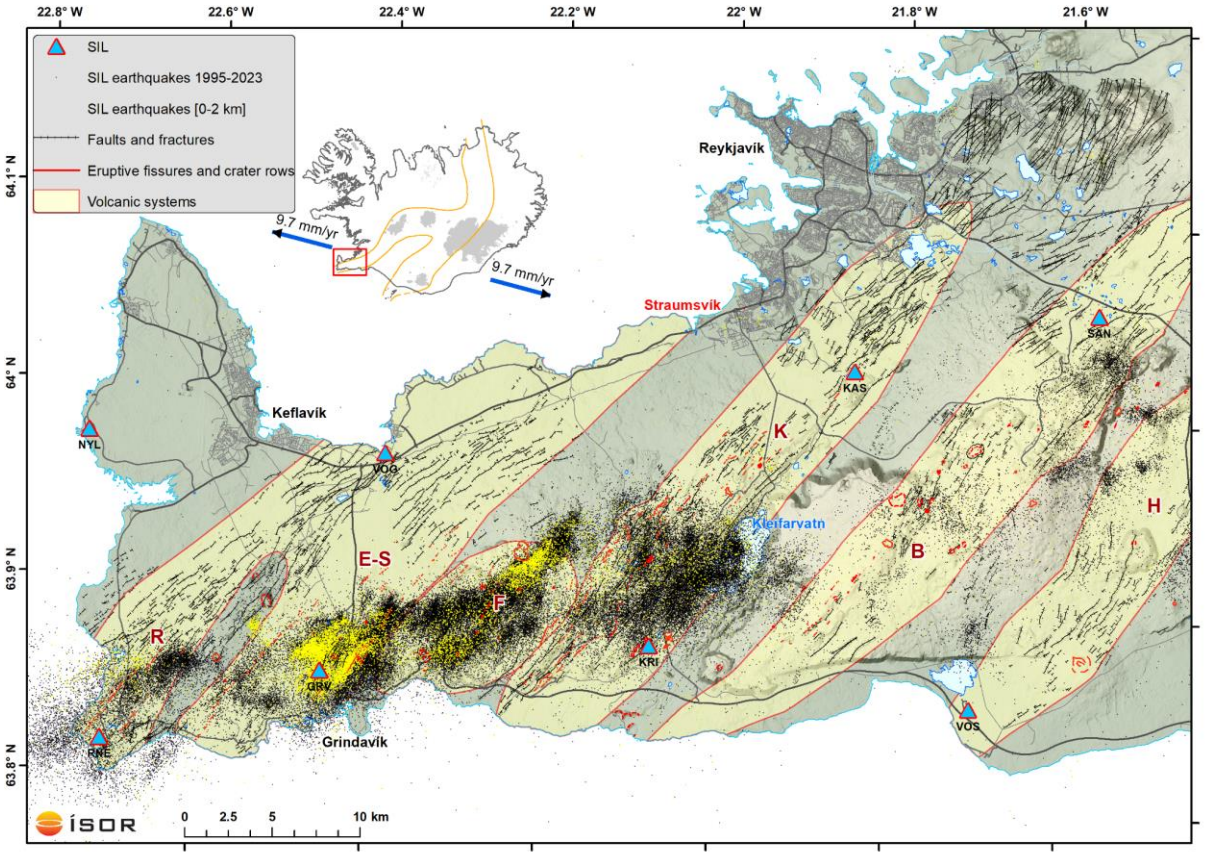

Figure A1. *Earthquake locations of the SIL seismic network on the Reykjanes Peninsula from 1995 to 2023, shown as black dots. Earthquake locations of the uppermost 2 km of the crust are emphasised in yellow. The seismic stations of the SIL network are shown as blue triangles. For further references to the map, please see Fig. 1.*

Appendix B: Injection test in well CSM-01

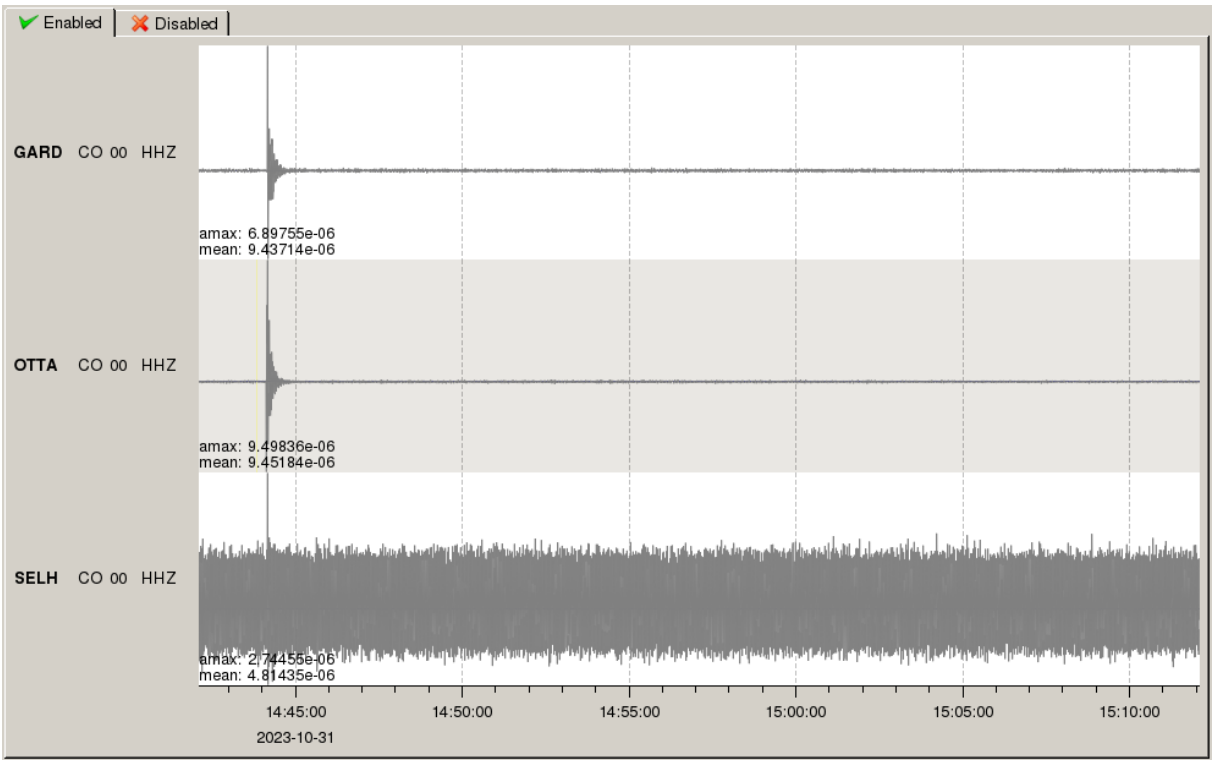

Figure B1. *A 30-minute time window from the 31st of October 2023, showing the horizontal component of the CODA seismic network stations during the injection test in well CSM-01. Vibration from the pumps used for the injection of water is the dominating signal at station SELH, closest to well CSM-01, while a distant earthquake from the volcano-tectonic unrest at Svartsengi is visible at all stations.*

VIÐAUKI V

Report no. 100632-SKI-006-V06

17.05.2024

LCA for Coda Terminal

LCA screening study of CO_2 mineralization in basalt at the Coda Terminal in Iceland

Einföld vistferilsgreining fyrir CO_2 bindingu í basalti í Coda Terminal stöðinni á Íslandi

Sigurður Loftur Thorlacius & Stefán Þór Kristinsson

EFLA Consulting Engineers

Publisher: Carbfix
Supervision and responsibility: Kristinn Heiðar Jakobsson

Report registration

Report no. 100632-SKI-006	Publishing date 17.5.2024	Publishing location Reykjavík
Report name **LCA screening study of CO_2 mineralization in basalt at the Coda Terminal**		
Version 005-IS	Total pages 40	Distribution Carbfix
Author/s Sigurður Loftur Thorlacius & Stefán Þór Kristinsson		Project no. 100632
Client Carbfix		Collaborators
Extract This Life Cycle Assessment (LCA) screening study assesses the environmental impacts and benefits of CO_2 mineralization in basalt at the Coda Terminal in Iceland. The Coda Terminal imports CO_2 that has been captured at industrial sites in Northern Europe. The system boundary of this LCA includes the sea transport to Iceland, offloading liquid CO_2 from a ship, intermediate storage, pumping and gasification, pipeline transport to an injection well, assumed CO_2 leakage during operation (1%) and CO_2 mineralization in basalt. The functional unit is 1 ton of CO_2 mineralized in basalt and the assumed service life of the project is 30 years. The total global warming impacts and benefits assessed over the service life are emissions of 4 100 million kg CO_2 equivalents and mineralization of 76 200 million kg CO_2 eq., i.e. a net reduction of 72 100 million kg CO_2 eq. Most of the emissions are due to maritime CO_2 transport and the assumed 1% leakage. In terms of the functional unit, the emissions are 54 kg CO_2 eq. per ton CO_2 mineralized. This means that there is a net reduction of 946 kg of CO_2 eq. in the atmosphere for every 1000 kg of CO_2 mineralized. It would take 30 days of operation for the plant to fully neutralize the emissions from constructing the plant. Scenario analysis of different locations shows that the CO_2 transportation distance and method, as well as the source of thermal energy do have an impact on the total CO_2 emissions, but when the benefits of CO_2 mineralization are considered, the net reduction of CO_2 in the atmosphere is in the range of 72 000 – 74 000 million kg CO_2 eq. for all three sites.		
Key words CO_2 mineralization, Carbfix, LCA, carbon footprint, basalt, CCS		Reviewed Reynir Sævarsson (EFLA) ERM sustainability consultancy

Samantekt

Skilgreining markmiða og umfangs

Vistferilsgreining var framkvæmd á fyrsta forhönnunarstigi Coda Terminal og gefin út í febrúar 2023. Markmið vistferilsgreiningarinnar er að greina helstu umhverfislegu áhrifaþætti og ávinninga þess að steingera CO_2 í basalt við Straumsvík sem innflutt er í vökvaformi frá iðnaðarstarfsemi í Norður-Evrópu. Greiningin er unnin í samræmi við ISO staðla 14040 og 14044, ásamt staðli EN 15978. Auk þess er stuðst við leiðbeiningar um gerð vistferilsgreininga fyrir umhverfisyfirlýsingar og vöruflokkareglur (e. Product Category Rules, PCR) þegar á við. Greiningin leggur góðan grunn að ýtarlegri lífsferilsgreiningu sem áætlað er að framkvæma á síðari stigum hönnunar og er skipt upp í fjóra meginhluta; skilgreining markmiða og umfangs, gagnaöflun og magngreining (e. Life Cycle Inventory, LCI), áhrifagreining (en. Life Cycle Impact Assessment, LCIA) og túlkun niðurstaðna. Aðgerðareining er 1 tonn af steingerðu CO_2 og líftími verkefnisins er áætlaður 30 ár. Mynd A sýnir virðiskeðju Coda Terminal og kerfismörk greiningarinnar.

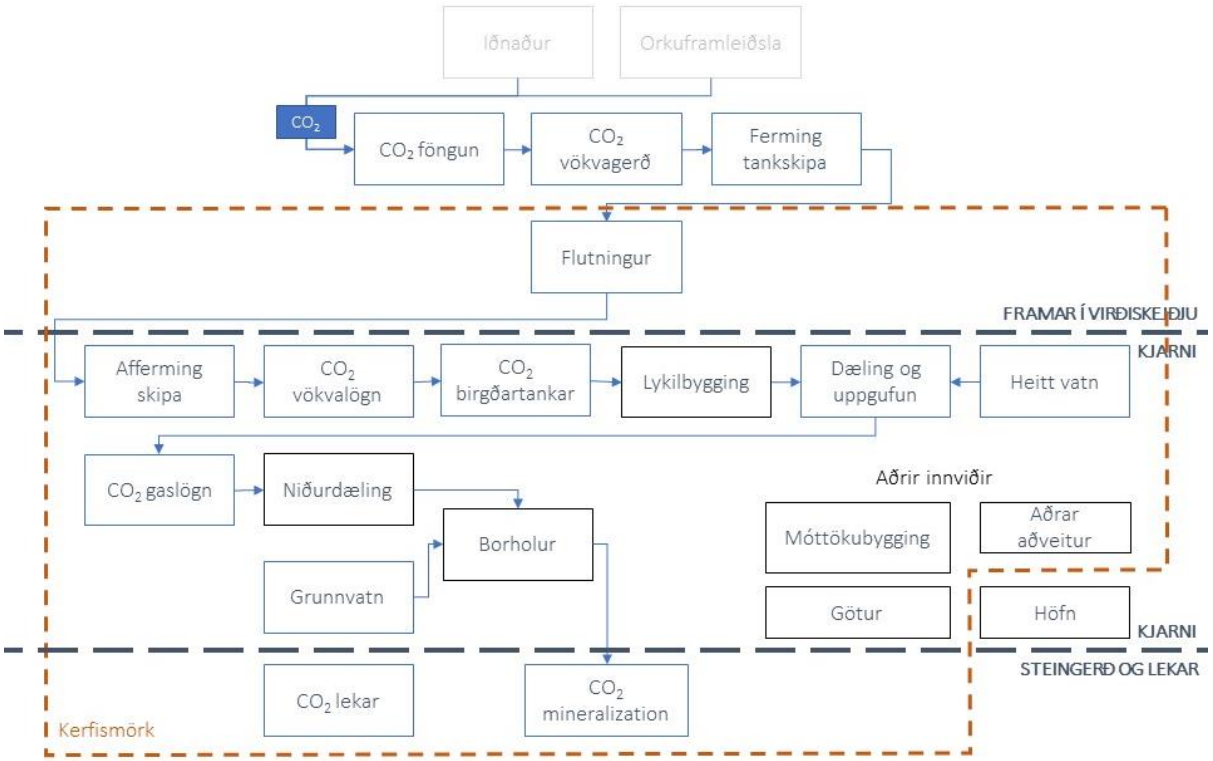

Mynd A **Virðiskeðja föngunar, flutninga og bindingar CO_2 ásamt kerfismörkum vistferils-greiningarinnar.**

Innan kerfismarka eru sjóflutningar CO_2 á vökvaformi til Íslands, afferming, geymsla, gösun, dæling og flutningar með lögnum til niðurdælingar. Mögulegir lekar CO_2 í ferlinu hafa ekki verið metnir en hér er gert ráð fyrir 1% leka samtals frá allri virðiskeðjunni, sem er talið vera nokkuð varfærið mat. Kerfismörkin ná ekki yfir föngun CO_2 í iðnaði erlendis en það orkufrekt ferli og því mögulega mikilvægt ferli í virðiskeðjunni. Sú losun er hins vegar mjög breytileg eftir því hvar föngunin á sér stað en Carbfix mun taka við CO_2 frá ýmsum aðilum.

Undir kjarnastarfsemi falla byggingar, innviðir og starfsemi Coda Terminal stöðvarinnar. Kjarnastarfseminni er skipt í eftirfarandi vistferilsstig:

- Hráefnastig (A1-A3) og flutningar hráefna til byggingarstaðs (A4) - Innifalið

- Byggingar og uppsetning (A5)
    - Innifalið: Byggingar, götur, lagnir, tankar, borholur
    - Ekki innifalið: Höfn, byggingarúrgangur og almenn orkunotkun bygginga
- Notkunarstig (B1-B7) – Innifalið
- Lok líftíma (C) – Ekki innifalið á þessu stigi, er jafnan lítið samanborið við A
- Ávinningur utan vistferils (D) – Ekki innifalið, ávinningur utan virðiskeðju

Gagnaöflun og magngreining

Í töflu 1 eru tekin saman gögn um magn efna, orku og annars sem við kemur vistferilsgreiningunni. Gagnaöfluninni skipt upp í samræmi við kerfismörk greiningar og virðiskeðju ásamt skýringum á öllum nálgunum og forsendum sem gerðar voru í upplýsingasöfnun og reikningum. Alls er reiknað með að flutt verða inn 77.000 milljón kg CO_2 yfir 30 ára rekstrartíma stöðvarinnar sem gerist stigmagnandi eftir rekstrarfösum.

- Fasi 1: Nær yfir 2 ár – 0,5 milljón tonn CO_2 á ári með einu skipi
- Fasi 2: Nær yfir 4 ár – 1,0 milljón tonn CO_2 á ári með tveimur skipum
- Fasi 3: Nær yfir 24 ár – 3,0 milljón tonn CO_2 á ári með fimm skipum

Niðurstöður – Áhrifagreining

Mynd B sýnir niðurstöður vistferilsgreiningarinnar, áhrif á hnattræna hlýnun yfir 30 ára áætlaðan líftíma í heild, sem og áhrif á aðgerðareiningu, tonn CO_2 bundið í basalt.

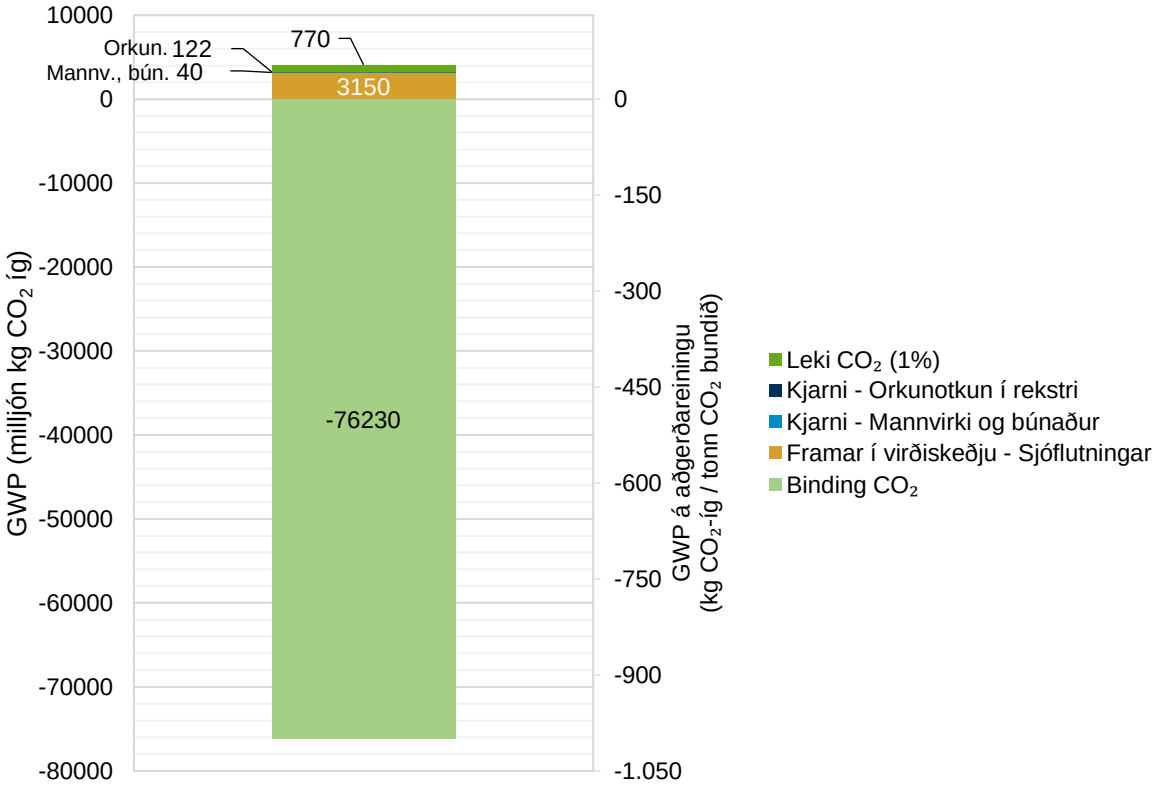

Mynd B **Áhrif á hnattræna hlýnun (e. Global Warming Potential, GWP) og umhverfislegur ávinningur bindingar samkvæmt vistferilsgreiningu. Myndin sýnir bæði heildaráhrif yfir 30 ára líftíma og einnig áhrif á aðgerðareiningu, á hvert tonn CO_2 bundið. Innan kerfismarka greiningarinnar er sjóflutningur CO_2 til Íslands, byggingar, innviðir, tækjabúnaður, orkunotkun í rekstri, lekar CO_2 og binding í basalt.**

Yfir 30 ára líftíma stöðvarinnar er áætluð losun 4.100 milljón kg CO_2 ígildi en binding 76.200 milljón kg CO_2 ígildi, þannig heildarniðurstaða greiningarinnar er nettó binding á 72.100 milljón kg CO_2 ígildi. Reiknað yfir á aðgerðareiningu, þá er losun 54 kg CO_2 ígildi á hver 1000 kg CO_2 sem eru bundin í basalt. Það eru því nettó 946 kg CO_2 ígildi sem eru fjarlægð úr kolefnishringrásinni fyrir hver 1000 kg CO_2 sem eru bundin í basalt.

Sé losunin skoðuð sérstaklega, þá er hún 77% tilkomin vegna skipaflutninga, 19% vegna CO_2 leka, 3% vegna orkunotkunar stöðvar og 1% vegna mannvirkja og búnaðar. Síðustu tveir þættirnir eru kjarnastarfsemi Coda Terminal stöðvarinnar. Gert er ráð fyrir á þessu stigi að nýtt verði heitt vatn til að hita upp CO_2 sem fluttur er til landsins kældur á vökvaformi. Mynd C sýnir niðurbrot áhrifa vegna kjarnastarfsemi stöðvarinnar.

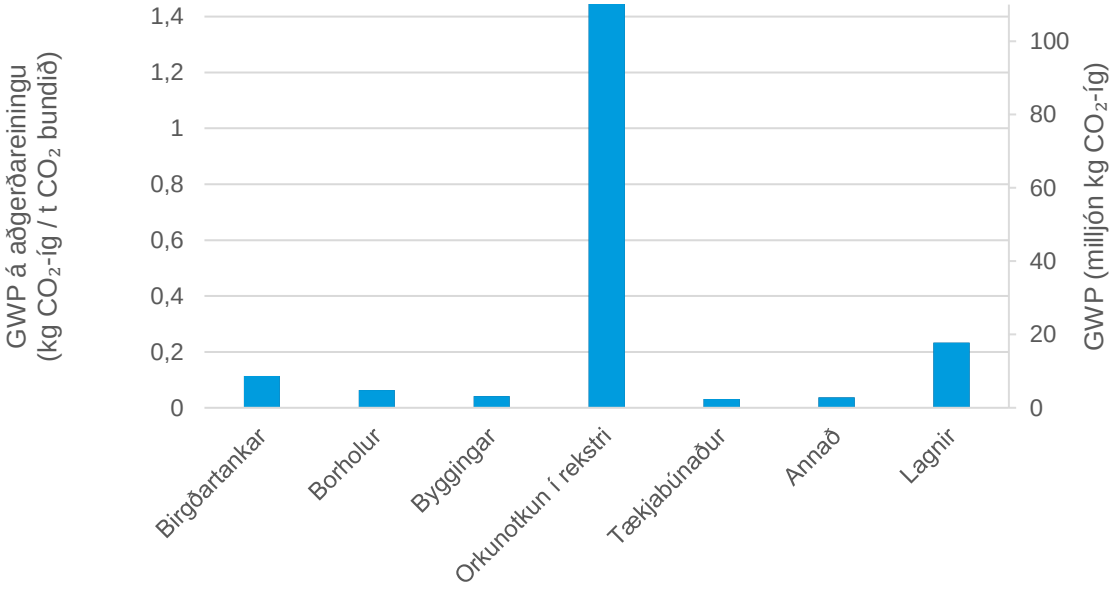

Mynd C **Áhrif á hnattræna hlýnun vegna kjarnastarfsemi Coda Terminal Orkunotkun fellur alfarið undir vistferilsstig B, en aðrir flokkar eru bæði á stigum A og B. Tækjabúnaður er endurnýjaður einu sinni á 30 ára líftíma. Á þessari mynd eru ekki sýnd jákvæð áhrif vegna bindingar CO_2, né heldur losun vegna skipaflutninga og þess CO_2 leka sem gert var ráð fyrir.**

Túlkun

Í vistferilsgreiningunni er greint frá áhrifum á hnattrænnar hlýnun (kolefnisspori) fyrir skipaflutninga CO_2, affermingu, uppgufun, flutning um lagnir, niðurdælingu og bindingu CO_2. Föngun CO_2 er utan kerfismarka en það eru orkukræft ferli sem gæti haft mikil áhrif á niðurstöður greiningarinnar. Vökvagerð og ferming skipa eru líka utan kerfismarka. Áhrif þessara ferla munu fara eftir því hvar föngun er framkvæmd og uppruna orkunnar sem nýtt er í þessa ferla. Við túlkun á niðurstöðum greiningarinnar þarf að hafa þetta í huga, að heildarlosun kann að vera vanmetin vegna þessa ferla utan kerfismarka. Í nánari greiningu á seinni stigum ætti að kanna sviðsmyndir fyrir þessa losun.

Miðað við framangreindar niðurstöður myndi taka Coda Terminal um 30 daga til þess að hlutleysa losun sem hefur átt sér stað á þeim tíma, þar á meðal byggingu stöðvarinnar, skipaflutninga, orkunotkun og mögulegra leka á þessum fyrstu 30 dögum. Þessir útreikningar miðast við fasa 1, þar sem 500.000 tonn CO_2 eru flutt inn á ári til niðurdælingar, og fullan rekstur frá fyrsta degi. Líklega tæki þó aðeins lengri tíma að ná fullum rekstri og hlutleysi. Mynd D sýnir ávinning við bindingu í basalt á fyrstu átta árum reksturs stöðvarinnar.

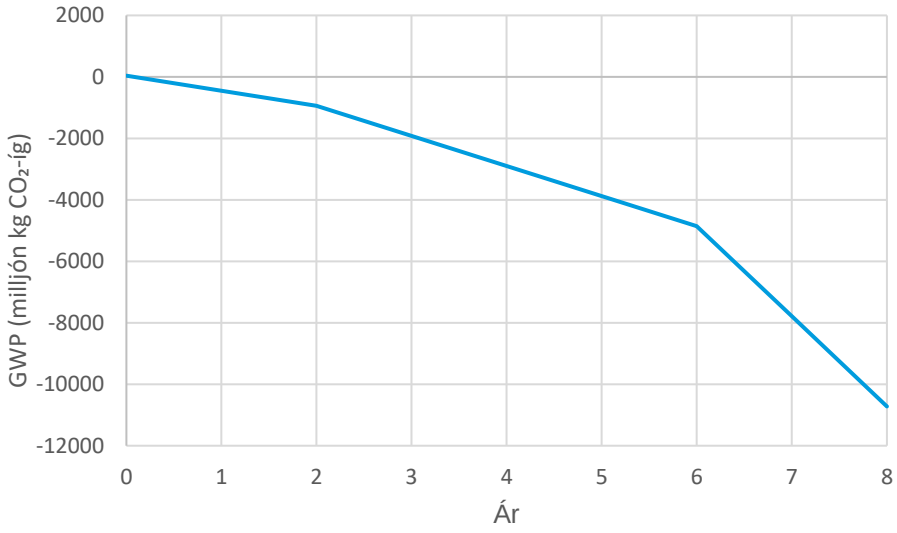

Mynd D Tímalína ávinnings vegna bindingar CO_2 fyrir fyrstu 8 árin frá byggingu stöðvar.

Skipaflutningar eru stór hluti af þessari vistferilsgreiningu og telja 77% af heildarlosun þegar binding er tekin út fyrir sviga, eða um 4-5% af því magni sem tankskipin eru að flytja. Þessir reikningar eru byggðir á þeirri forsendu að um sé að ræða dísil skip sem notar 273 tonn af dísil eða gasolíu fyrir ferð aðra leið frá meginlandi Evrópu (2.173 km). Um er að ræða íhaldsamt mat sem þyrfti að skoða betur á seinni stigum, þar sem skipastærðir, eldsneytistegundir og vegalengdir eru allt breytur sem ekki eru meitlaðar í stein á þessum tímapunkti. Losun gæti minnkað yfir líftíma, þar sem áætlað er að skip munu á einhverju stigi nýta metanól eða aðrar kolefnishlutlausar eldsneytistegundir.

Orkunotkun í rekstri veldur 3% af heildarlosun en sé kjarnastarfsemi Coda Terminal skoðuð sérstaklega þá veldur orkunotkun 76% af losun kjarnastarfseminnar. Losun vegna orkunotkunar gæti mögulega lækkað á síðari hönnunarstigum með lækkun á orkuþörf, öðrum aðferðum til upphitunar og síðast en ekki síst, minni losunar við vinnslu heits vatns þegar föngun og binding CO_2 í jarðhitavirkjunum verður aukin.

CO_2 lekar í virðiskeðjunni allri eru áætlaðir um 1% af öllu sem flutt er til landsins. Þetta er talið varfærið mat en því til rökstuðnings má nefna að áætluð losun vegna CO_2 leka yfir líftíma stöðvarinnar jafnast á við rúmmálið í 22 birgðatönkum. Á síðari stigum er nauðsynlegt öryggisatriði að meta mögulega leka á öllum stigum, t.d. óvæntir lekar vegna gata í lögnum, rofnum lögnum eða jafnvel rofi á birgðatanki, en einnig leka sem tengjast venjulegum rekstri, t.d. við viðhald.

Í greiningunni eru einnig skoðaðar sviðsmyndir fyrir aðrar staðsetningar, Washington í Bandaríkjunum og Nagasaki í Japan, með tilheyrandi breytingum í uppruna hráefna, raforku og flutningaleiðum CO_2. Staðsetningin hefur áhrif á heildarlosun en vegna þess hve mikill ávinningurinn er af bindingunni, þá eru heildaráhrifin í öllum tilfellum nettó binding á bilinu 71.500 – 73.600 milljón kg CO_2 ígildi. Hinar staðsetningarnar gera ráð fyrir varmaorku frá jarðvarma eða lífgasi, en það gæti haft töluverð áhrif á heildarlosun rekstursins ef varmaorkan væri af öðrum uppruna.

Table of contents

Images

Tables

1 Introduction

1.1 Project Background

This is a Life Cycle Assessment (LCA) screening study made for CO_2 mineralization in basalt with the Carbfix method at the Coda Terminal in Iceland. It is a part of a wider project, the first design phase for the Coda Terminal (predesign) and will lay the foundation for a more detailed and in-depth LCA study to be performed in later phases of the overall project.

In the LCA, materials, resources and energy consumed by the project throughout its life cycle are considered in accordance with the ISO standards 14040 and 14044. In line with the standards, the LCA is divided into four phases: *Goal and Scope Definition*, *Inventory Analysis*, *Impact Assessment* and *Interpretation*. The LCA report follows the cycle phasing of standard EN 15978.

In wide terms, The Coda Terminal is a site in Iceland which will receive liquid CO_2 from industry abroad to mineralize the CO_2 in basaltic bedrock and thus ensure permanent removal and of the CO_2 from the atmosphere. The project will contribute to mitigating global warming and climate change by sequestering and permanently mineralize CO_2 that would otherwise have been emitted to the atmosphere. The Coda Terminal plant will offer a disposal option for CO_2 through mineralization that has not been commercially available.

The Coda terminal has been described as follows: 'The Coda Terminal is a cross-border carbon transport and storage hub in Iceland. CO_2 is captured at industrial sites in North Europe and shipped to the Terminal where it is unloaded into onshore tanks for temporary storage. The CO_2 is then pumped into a network of nearby injection wells where it is dissolved in water before being injected into the fresh basaltic bedrock. There the CO_2 remains trapped in the carbonated fluid and transforms into solid minerals in less than two years. Once the process is confirmed, further monitoring is not required.'[1]

1.2 The Carbfix technology

Mineral storage of CO_2 as a method for geological CO_2 storage was first proposed in the 1990's[2]. Within the natural carbon cycle, carbon has thousands to millions of years residence time in rocks, which is by far largest carbon reservoir on Earth hosting over 99% of all carbon.

The process of mineral carbonation proceeds through the interaction of water dissolved CO_2 with the bedrock. The dissolution of the CO_2 into water leads to the production of carbonic acid, which can dissociate to bicarbonate, and carbonate, liberating protons that cause the pH of the water to decrease. The protons promote the dissolution of cation-bearing silicate minerals, which promotes CO_2 mineralisation in two ways: First it consumes protons, which raises the pH of the formation fluids which facilitates carbonate mineral precipitation, and second it provides cations that can react with the dissolved CO_2 to form stable carbonate minerals, such as calcite ($CaCO_3$); magnesite ($MgCO_3$), and siderite ($FeCO_3$), and solid solutions thereof. The degree to which the released cations form minerals depends on the elements, the pH and the temperature, but

[1] Carbfix. Coda Terminal. Accessed on 16.9.2022 at: https://www.carbfix.com/codaterminal
[2] Seifritz, W., 1990. CO_2 disposal by means of silicates. Nature 345, 486-490; Lackner, K., Wendt, C. H., Butt, D. P., Joyce, E. L., Sharp, D. H., 1995. Carbon dioxide disposal in carbonate minerals. Energy 20, 1153-1170.

emphasis on mineral dissolution experiments leads to the commonly accepted view that mineral dissolution is the rate-limiting step in the mineral-carbonation process[3].

The Carbfix technology promotes mineral carbonation via dissolution of CO_2 into water before or during its injection: The CO_2-charged fluid releases metals from the host rock, which combine with the injected CO_2, resulting in the bulk of the CO_2 being permanently transformed to carbonate minerals[4,5]. Risks of leakage is furthermore eradicated since the CO_2-charged water is denser than the surrounding groundwater and does therefore not have the tendency to migrate back to the surface due to buoyancy: Solubility trapping is achieved immediately, and no cap rock is required when injecting the water charged CO_2, as it is denser than CO_2-free water above the storage formations. As such it does not have the tendency to migrate back to the surface. With the injected CO_2 being rapidly transformed into minerals, it is permanently fixed and there is a negligible risk of it ever returning to the atmosphere[2,6]. Furthermore, once mineralisation has been confirmed, no further monitoring of the storage site is required. The Carbfix technology has been applied on an industrial scale since 2014 at the Hellisheiði Power plant with 85 thousand tonnes CO_2 injected to date.

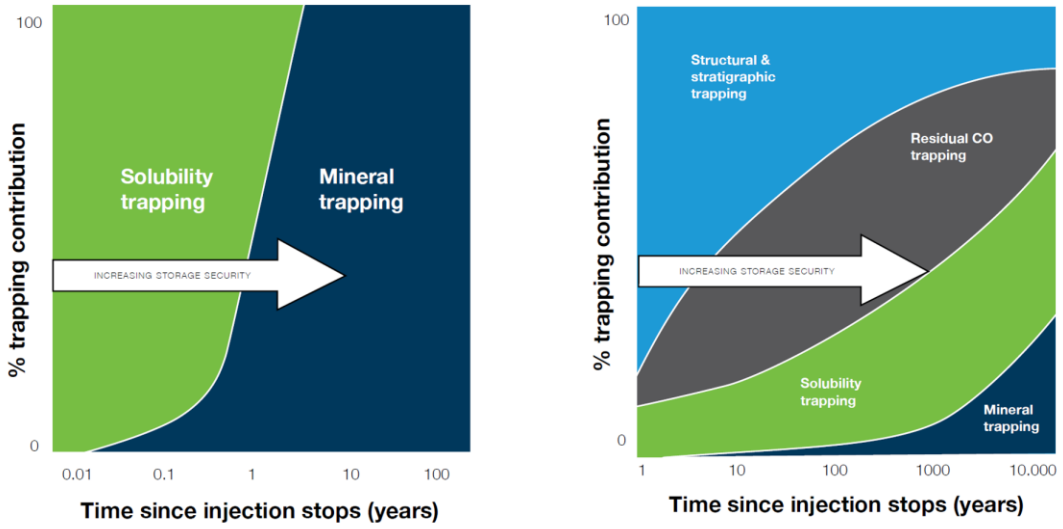

Figure 1 **Comparison of CO_2-trapping mechanisms over time when injecting a) single-phase CO_2 into sedimentary basins, and b) when injecting water- dissolved CO_2 for mineralization based on data from field injection experiments. Modified from (Benson et al., 2005 and Snæbjörnsdóttir et al., 2017)**

[3] Snæbjörnsdóttir, S.Ó., Sigfússon, B., Marieni, C. et al. Carbon dioxide storage through mineral carbonation. Nat Rev Earth Environ 1, 90–102 (2020).
[4] Snæbjörnsdóttir, S.Ó., Oelkers, E.H., Mesfin, K., Aradóttir, E.S., Dideriksen, K., Gunnarsson, I., et al. (2017). The chemistry and saturation states of subsurface fluids during the in situ mineralisation of CO_2 and H_2S at the CarbFix site in SW-Iceland. International Journal of GHG Control, 58, 87-102.
[5] Clark, D.E., Oelkers, E.H., Gunnarsson, I., Sigfússon, B., Snæbjörnsdóttir, S.Ó., Aradóttir, E.A., Gíslason, S.R. (2020). CarbFix2: CO_2 and H_2S mineralization during 3.5 years of continuous injection into basaltic rocks at more than 250 °C. Geochimica et Cosmochimica Acta, 279, 45-66.
[6] Matter J.M., Stute M., Snæbjörnsdottir S.Ó., Oelkers E.H., Gislason S.R., Aradottir E.S., Sigfusson B., Gunnarsson I., Sigurdardottir H., Gunnlaugsson E., Axelsson G., Alfredsson H.A., Wolff-Boenisch D., Mesfin K., Fernandez de la Reguera Taya D., Hall J., Dideriksen K., Broecker W.S.. Rapid carbon mineralization for permanent disposal of anthropogenic carbon dioxide emissions. Science. 2016 Jun 10;352(6291):1312-4. doi: 10.1126/science.aad8132. PMID: 27284192.

1.3 Risk assessment

A preliminary risk assessment was performed at the beginning of the project, covering all phases of the project. A more detailed risk assessment of the Coda terminal has since then been performed for the design stage, covering pre-design for operation, project design for operation, and execution of contractors. The identified risks were split up into 11 categories, covering general issues, occupational health, safety, building elements, organization and administration, project management, technical, construction and commissioning, operation, financial, and external risks. The risks were rated on the scale of 1-25. Out of the 164 risks, five were identified as high risk, rated between 17 and 25. The risk assessment will be updated and monitored throughout the project. The five top risks of the design phase along with their controls are listed in Appendix 1.

1.4 HSE

Safety, health and working environment issues are an integral part of all activities within the Coda Terminal project. The project team endeavours to be exemplary in this field and strives to protect and enhance the lives of its team members by creating an accident-free workplace where the health of employees, contractors and the public is not jeopardised by project activities. No job is important enough to sacrifice the safety of those performing it. Everyone who contributes to the Coda Terminal project is responsible for their own safety and are spokesmen for the increased safety of colleagues, while endeavouring to identify, evaluate and manage risk in the work environment. To this end, all statutory and regulatory requirements will be complied with, and the project team will constantly endeavour to increase the safety of its employees, co-operating parties and customers. The project team is not permitted to take on work without complying with safety regulations and using the appropriate protective equipment. If such safety equipment is not available, work shall be stopped until the appropriate equipment has become available. If a deviation is identified, reform ideas, accidents and incidents will be logged in the project's EHS database (Environment, Health, Safety) with the objective of improving procedures and achieving better results.

Carbfix is certified for the following management systems that will be used in the project:

- ISO 9001 – Quality Management (Dan-Unity CO_2 owner Evergas also certified)
- ISO 14001 – Environmental Management (Dan-Unity CO_2 owner Evergas also certified)
- ISO/IEC 27001 – Information Security Management
- ISO 45001 – Occupational Health and Safety Management
- ÍST 85 – Equal Pay Standard

2 Goal and Scope Definition

2.1 Goal

The purpose of the LCA is to assess the environmental impacts and benefits of the Coda Terminal project, i.e. transport of CO_2 from Europe to the Coda Terminal in Iceland for mineralization in basalt for permanent removal from the atmosphere. The intended application of the LCA is to determine whether the project is environmentally feasible with regards to climate impacts and benefits, as well as to do a quantification of the magnitude of these impacts and benefits. The intended audience is Carbfix and their financers, funds, and associates.

The results are expected to be illustrative of this particular type of CO_2 storage/disposal technology, i.e. mineralization of CO_2 in basalt. The results are not used to make any comparative assertions and the report will not be disclosed to the public.

2.2 Functional Unit and Service Life

The function of the system under study is the service of permanently disposing CO_2 by mineralizing it in basalt bedrock. The functional unit is the service of mineralizing 1 ton of CO_2.

The assumed service life of the project is 30 years.

2.3 System Boundary

The scope of the analysis will include facilities, equipment, and processes, which include ship transport of CO_2, CO_2 liquid offloading, gasification, pipeline transport and injection into basalt with water.

Figure 2 shows how the system boundary is defined within the value chain of CO_2 capture, transport, and mineralization in basalt with a simplified flowchart. The system boundary starts with a loaded liquid CO_2 tanker ship at harbour in Europe. This LCA screening traces the CO_2 flow through ship transport to the Straumsvík port in Iceland, offloading liquid CO_2 from the tanker ship, intermediate storage, pumping and gasification, pipeline transport to injection at an injection well borehole. The LCA includes thermal heat from geothermal hot water for gasification and groundwater for injection, as well as other infrastructure, such as roads, utilities, and a reception building.

CO_2 capture, liquefaction and ship loading activities abroad are outside the scope of the analysis at this stage. The CO_2 capture is potentially an energy intensive step in the value chain and its impacts could be significant, but they are extremely variable depending on a variety of factors, including where the CO_2 is captured, the CO_2 concentration, waste heat availability, electricity sourcing etc. This step is, however, not controlled by Carbfix as the CO_2 mineralization provider. Carbfix could potentially be receiving CO_2 from many sources with very different CO_2 capture impacts.

All essential buildings, equipment, pipelines, and infrastructure are included, except for the construction of the new quay and related land filling (land reclamation), breakwater and infrastructure, such as fuel storage and shore power connections. This harbour will receive the CO_2 transporting ships, but it will also be utilized by nearby industry, so it is a shared infrastructure.

For clarity, the value chain of CO_2 capture, transport and mineralization has been categorized into three modules:

- Upstream module: CO_2-emitting industry or energy (not included), CO_2 capture (not included), pre-treatment (not included), and transport to CO_2 mineralization plant
- Core module: Construction and operation of CO_2 mineralization plant, including buildings, infrastructure, pipelines, and equipment
- Mineralization and leaks: Permanent disposal of CO_2 through in-situ mineralization and leaks occurring throughout the supply chain

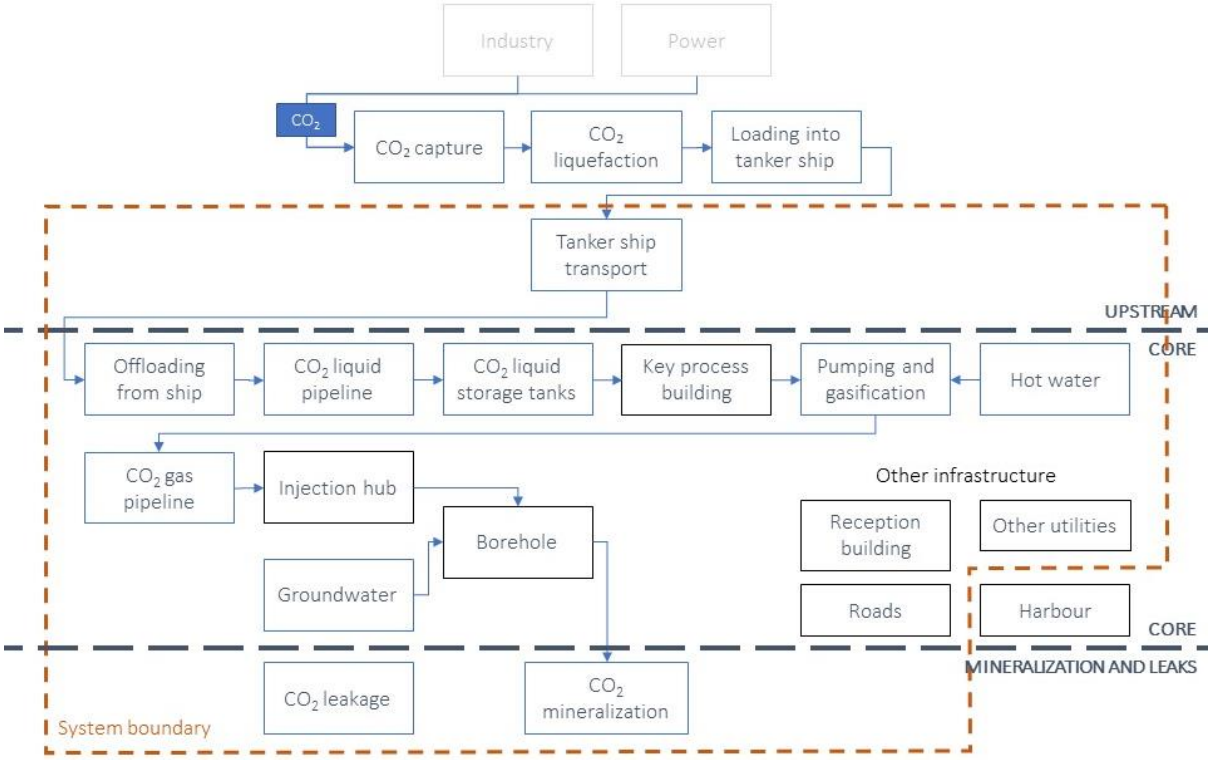

Figure 2 Value chain of CO_2 capture, transport, and mineralization and the LCA system boundary.

2.3.1 Core module: Mineralization plant

The core module (construction and operation of mineralization plant) is further divided into the following building life cycle stages according to standards EN 15804 and EN 15978:

A1-A3 Product Stage

- A1: Raw material supply
- A2: Transport to manufacturing
- A3: Raw material processing and manufacturing

A4-A5 Construction stage

- A4: Transport to construction site
- A5: Construction and installation

B1-B7 Use stage

- B1: Use
- B2: Maintenence
- B3: Repair
- B4: Replacement
- B5: Refurbishment
- B6: Operational energy use
- B7: Operational water

C1-C4 End of life stage

- C1: Demolition and deconstruction
- C2: Transport
- C3: Waste processing
- C4: Disposal

D Benefits beyond the life cycle stage

- Reuse
- Recovery
- Recycling potential

For the core module, the coverage of the building life cycle stages in this LCA is as follows:

- Product stage (A1-A3): Included.
- Transport to construction site (A4): Included.
- Construction and installation (A5):
    - Buildings and roads: Included.
    - Pipelines, tanks, boreholes: Excavation activities and drilling included. Construction waste and other energy use during construction not included.
- Use stage (B1-B7): Included.
- End of life stage (C): Not included at this stage. Its small impact relative to stages A in construction means that it is often excluded in earlier stages.
- Benefits beyond the life cycle stage (D): Stage D includes benefits outside the life cycle, outside the value chain and are therefore omitted here.

2.4 Allocation

The system under study has a single output (disposal of CO_2) and thus requires no allocation.

Some input materials are outputs from multiple product systems or recycling systems. Description of their allocation procedure can be found in documentation for the GaBi Professional database.

Thermal heat from geothermal hot water is one of the inputs into the system under study. High-temperature geothermal power plants produce two products, electricity and hot water. Allocation assumptions for thermal energy from geothermal hot water follow the LCA for the Icelandic Reference Building (ísl. viðmiðunarhús). Usable electricity and usable thermal heat are assumed to be equally sought after, i.e. the environmental impacts of the geothermal power plant are divided between the total usable energy of electricity (GWh) and thermal heat (GWh) over its lifetime. 73% of the impacts are allocated to electricity and 27% of the impacts are allocated to hot water.

2.5 Environmental Impact Categories

This LCA screening study focuses on Global Warming Potential (GWP) impacts [kg CO_2 equivalents], as the main purpose of the wider project is to sequester and permanently mineralize CO_2 to mitigate global warming and climate change. The characterization factors for GWP follow the methodology recommended in standard EN 15804, which corresponds to the CLM 2001 – April 2013 methodology. Interpretation will be made based on the GWP midpoint indicator results only, i.e. no normalization and weighing will be applied. Calculation of endpoint indicators (impact on human health, natural environment and natural resources) is not carried out.

2.6 Cut-off

This LCA screening study is carried out at an early phase of the project the materials have been roughly quantified based on predesign. The aim of the assessment at this stage is to cover the main materials for buildings, largest equipment, pipelines, fuel use of ships and energy use of the plant. A material or impact cut-off threshold has not been determined at this stage.

2.7 Data and uncertainty

2.7.1 Data collection

Material and energy use data was collected from designers (engineers and architects) and the developer (Carbfix) at this stage. As the project is in a relatively early phase, equipment manufacturers are unknown and generic data is therefore used. A more detailed in-depth LCA study will be carried out at later stages when more data will be available.

Data collection, assumptions, and data calculations are described for each process in the Life Cycle Inventory analysis (LCI) in chapter 3.

2.7.2 Uncertainties

The uncertainty range of the results is directly related to uncertainties in design, for example if research boreholes show that fewer boreholes are required than are currently designed, less material and less earthwork is required, which result in lower environmental impacts. The uncertainty range of the design at this stage is assumed to be -20% to +30%. The LCA introduces additional uncertainties through various assumptions, for example by assuming a certain material composition of equipment, which has not yet been thoroughly specified, and by assuming that the equipment assembly has negligible impact in comparison to the production of the equipment's constituents. Another source of uncertainty can be when various small components are overlooked in an LCA due to the small size but when accumulated, they might be important. The uncertainty of this LCA screening study is therefore expected to be greater than that of the design.

2.7.3 Data quality

This Life Cycle Assessment is carried out in the GaBi software by Sphera and utilizes the GaBi Professional 2022 database with the GaBi Construction Materials extension database XIV. These databases are updated annually and the LCA background data is therefore always up to date. The unit process data is subject to validation and review according to the GaBi Modelling Principles.

2.7.4 Data calculation

Most of the material quantity data comes directly from the designers of the Coda Terminal and is therefore the best current estimate of the quantity. This quantity data should be validated in further analysis and as design develops further. However, some of the collected data was reviewed and validated by the LCA conductors, for example the material and energy data for injection wells.

The calculation procedure for relating collected data to unit processes in the LCA databases was in broad terms as follows: Generic processes are favoured over manufacturer specific processes, since no manufacturers are known at this stage. Country-specific unit processes are selected where assumptions were made regarding country of origin, otherwise regional European processes were selected (EU-28).

The calculation procedure for relating data to the reference flow of the functional unit was as follows: The total impacts of the whole life cycle of the Coda Terminal plant were calculated, and then divided by the total amount of mineralized CO_2 over its life cycle.

2.8 Limitations

Limitations of this LCA study regarding value chain coverage are that the CO_2 capture, liquefaction and ship loading activities abroad are outside scope. As outlined in chapter 2.3, the CO_2 capture is potentially an energy intensive step and could be significant. The magnitude of impacts depends on a variety of factors, including where the CO_2 is captured, the CO_2 concentration, waste heat availability, electricity sourcing etc.

Limitations regarding infrastructure coverage are that the construction of the new quay is outside scope, as well as land filling (land reclamation), breakwater and other related infrastructure, such as fuel storage and shore power connections. However, the harbour will be shared with other industry nearby, as outlined in chapter 2.3.

Limitations regarding the early stage at which this LCA is conducted, are that equipment assembly is not considered, generic processes are used, and material and energy amounts could change when the design develops further, as outlined in chapter 2.7.

2.9 Critical review

The LCA report has been reviewed internally at EFLA, by the client (Carbfix) and by ERM, sustainability consultancy. As the report will not be disclosed to the public and there are no comparative assertions made in the report, then a formal critical review by interested parties is not required as per ISO 14040.

2.10 Scenario analysis

Two additional location scenarios are considered to analyse the scalability of the project, as well as a preliminary sensitivity analysis. The scenarios are as follows:

- Main scenario: CO_2 mineralization plant located in Straumsvík, Hafnarfjörður, Iceland
- Location scenario 1: CO_2 mineralization plant in Nagasaki, Japan
- Location scenario 2: CO_2 mineralization plant in Wallula, Washington, United States

2.10.1 Location scenario 1: Nagasaki, Japan

Nagasaki in Japan is selected as one of the alternative location scenarios. The differences in assumptions are as follows:

- Steel emission factor based on producer average (Nippon steel Corporation) from 12 EPDs of various steel products from a single producer and 6 various factories in Japan.
- Steel transport to mineralization plant based on the location of the factories accounted for in the 12 EPDs and their distance from Nagasaki. Road transport assumed.
- 1350 km maritime transport of CO_2 from Tokyo to Nagasaki.
- Thermal energy from biogas and electric energy from Japanese grid (~67% fossil, 10% hydroelectric)[7]

2.10.2 Location scenario 2: Wallula, Washington, United States

Wallula in Washington, United States, is the second alternative location scenarios. The differences in assumptions are as follows:

- Steel emission factor based on industry average from 13 EPDs of various steel products from various producers, producer's associations and factories.
- Steel transport to mineralization plant based on average distance from Wallula to the ten largest steel factories in the United States.
- 1200 km pipeline transport of CO_2, roughly equivalent to the distance to the nearest node in the national CO_2 transportation pipeline network.
- Thermal energy from biogas and electric energy from Washington grid (~30% fossil, 33% hydroelectric)[8]

[7] EnergyTrackerAsia. The Energy Mix review in Japan https://energytracker.asia/the-energy-mix-review-in-japan-a-glimpse-of-the-future
[8] E.I.A. U.S. Energy Atlas with Total Energy Layers https://www.eia.gov/state/?sid=WA

3 Inventory Analysis (LCI)

The inventory analysis and assumptions made are shown in table 1.

Table 1 Inventory analysis of the Coda Terminal project.

W	SW	P	Object	Quantity		Description
			UPSTREAM			
			CO_2 capture			Out of LCA scope
			Maritime transport			
			Amount of CO_2 imported			
			Imported CO_2 over service life	*77 000 000*	tons	Importing over the 30-year period given the completion of each phase. Phase 1: 2 years, 0.5 Mtons/year Phase 2: 4 years, 1 Mtons/year Phase 3: 24 years, 3 Mtons/year LCA assessment performed based on initial Coda Terminal capacity of 3.0 Mtpa, however capacity can potentially be increased to 4.8 Mtpa given planned harbour capacity. The material and energy quantities in the LCA model would have to be altered accordingly.
			Annual imported CO_2	*2 566 667*	tons/y	Average over 30-year assessment period
			Sea transport of CO_2			
			Average number of ships in operation	*4.3*	ships	*The number of ships in operation is assumed to be:* *Phase 1: 2 years, 1 ship* *Phase 2: 4 years, 2 ships* *Phase 3: 24 years, 5 ships*
			Average transport distance (one way)	*2 173*	km	*Based on average maritime transportation distance for Antwerp (Belgium), Dunkirk (France), Stockholm (Sweden), Aalborg (Denmark), Teesport (United Kingdom) and Petershead (United Kingdom).*
			Maritime round trips per year at full utilization	*27.3*	trips	*Assumption from the Coda Terminal Innovation fund application.*
			Fuel use per trip for methanol powered ship			*Methanol is being considered as a fuel for the ships, but the implementation has not been fully planned yet. Methanol fuel is therefore not assumed for maritime transport in this LCA.*
			Methanol use per trip	*503*	tons/ trip	*Assumption from the Coda Terminal Innovation fund application. Methanol fuel required for maritime one-way transportation trip and empty run.*

	Gas oil use per trip	*56*	tons/ trip	*Assumption from the Coda Terminal Innovation fund application. Methanol is burned in combination with LSMGO (low sulphur marine gas oil).*
	Fuel use per trip for diesel powered ship			*As a conservative estimate, gas oil or diesel fuel is assumed for maritime transport in this LCA.*
	Diesel use per trip	*273*	tons/ trip	*The diesel use is derived from the assumed fuel use of methanol ships in the Coda Terminal Innovation fund application. It is assumed that the amount of energy required is the same. Note that methanol and diesel (gas oil) have very different energy densities. These assumptions should be reviewed in further analysis.*

	CORE			
	Materials (A1-A3) and Construction (A5)			
00	***Contractor's temporary works***			
01	***Contractor's site facilities***			
	Contractor's staff	*34*	staff	*Not assessed at this time*
01	***Site facilities and services***			HS Veitur will most likely install transformers in the key building, the pumphouse and the well buildings where needed
02	***Roads and tracks***			
	Paved roads	*1*	km	*Assessed using LCA data for roads in Iceland, not the material in this given road*
	Gravel roads	*5*	km	*Assessed using LCA data for roads in Iceland, not the material in this given road*
03	***Reception building***			
01	*Earthworks*			
	Gravel and sand	*2 674*	m³	*Transported filling material for reception building and parking lot*
	Excavation	*2 674*	m³	*Excavated material for reception building and parking lot*
02	*Structures*			*Estimated based on average emission values per m² for commercial buildings.*
	Floor area net	*2 003*	m²	
	Floor area gross	*2 203*	m²	*Gross area used in accordance with average calculations*
	Concrete	*990*	m³	
	Reinforcement steel	*118 858*	kg	
	All other materials	*-*		*Assessed by assuming average impacts per m² for commercial buildings in Iceland*

04	***Key building (operations building)***			*Building rooms: Control room, storage room, workshop, staff facilities, vaporizing room. Scope of civil contractor excludes control room and vaporizing room.*
01	*Earthworks*			
	Gravel and sand	*3 486*	m³	*Transported filling material for key building and parking lot*
	Excavation	*3 486*	m³	*Excavated material for key building and parking lot*
02	*Structures*			*Estimated based on average emission values per m² for commercial buildings.*
	Floor area net	*2 065*	m²	
	Floor area gross	*2 500*	m²	*Gross area used in accordance with average calculations*
	Concrete	*620*	m³	
	Reinforcement steel	*74 340*	kg	
	Steel	*103 250*	kg	
	All other materials	*-*		*Assessed by assuming average impacts per m² for commercial buildings in Iceland*
05	***Road 41/Reykjanesbraut underpass***			
01	*Earthworks*			*Included in earthwork in other piping*
02	*Structures*			*Reykjanesbraut road is undisturbed, only tunnelling for piping will be required. Included in piping elsewhere.*
06	***Site utilities***			
01	*Electrical power*			
	Electrical cables	*3*	km	*Weight 200kg/km (thereof copper 120kg/km), average cross-section 78,5 mm2 (thereof copper 12,5 mm2 or 16%).*
	Transformer (for key building)	*3 450*	kg	*Total weight 3450 kg; oil 730 kg, copper 450 kg, aluminium 115 kg, core (steel) 1000 kg. The rest is assumed to be carbon steel.*
02	*Thermal power*			
	Thermal piping for buildings		km	*Outside the scope of design (Veitur responsibility) and thus no quantities available.*
03	*Communications*			
04	*Sewerage*			
	Wastewater piping for buildings		km	*Outside the scope of design (Veitur responsibility) and thus no quantities available.*
05	*Potable water*			
	Potable water piping for buildings		km	*Outside the scope of design (Veitur responsibility) and thus no quantities available.*

07		***Site security***			
	01	*Areas fencing and gates*			
		Steel fence	*1.5*	km	*Steel wire for 10 SWG fence with 3" opening assumed; 188 g/sqft = 2,02 kg/m² - Distance unknown - assumed to be 1,500 m*
	02	*Access control*			
02		***Reserve offloading***			
01		***Supporting facilities***			
	01	*Earthworks*			*Included in earthwork for 03 Offloading utilities*
	02	*Structures*			*No structures assigned to 02 Reserve offloading or included elsewhere.*
02		***Piping***			
	01	*Piping*			*Negligible mass. Bypass from ship to reserve offloading pumps and from pumps to main pipe. Any piping included in 03 Offloading utilities*
03		***Power supply***			
		Electrical cables	*3*	km	*Weight 200kg/km (thereof copper 120kg/km), average cross-section 78,5 mm2 (thereof copper 12,5 mm2 or 16%).*
		Transformer	*7 000*	kg	*Total mass 7000 kg; 1460 kg, copper 900 kg, aluminium 240 kg, core (steel) 2000 kg. The rest is assumed carbon steel.*
04		***Communications***			
05		***Reserve offloading pumps***			
		Offloading pumps	*4 245*	kg	*3 pumps, each 1415 kg, assumed carbon and stainless steel.*
06		***Reserve offloading heat exchangers***			*Not included*
03		***Offloading utilities and piping***			
01		***On shore power supply for transport vessel***			*Connecting the ships to electricity and hot water onshore. Outside the scope of this analysis*
02		***Supporting facilities - Jetty building***			
	01	*Earthworks*			
		Gravel and sand	*211*	m³	*Transported filling material for jetty building and vessel offloading arm*
		Excavation	*172*	m³	*Jetty building and vessel offloading arm*
	02	*Structures*			*Estimated based on average emission values per m² for commercial buildings, except concrete and steel modelled separately*
		Floor area net	*65*	m²	

	Floor area gross	*72*	m²	*Gross area used in accordance with average calculations*
	Concrete	*19*	m³	
	Reinforcement steel	*2 328*	kg	
	Steel	*6 500*	kg	
	All other materials			*Assessed by assuming average impacts per m² for commercial buildings in Iceland*
03	***Piping***			
01	*Piping*			
	Piping DN600 - Phase 1	*0.3*	km	*96kg/m, 75% SS316L4, 25% PUR/PE. Above ground.*
	Piping DN200 - Phase 1	*0.3*	km	*33kg/m, 75% SS316L4, 25% PUR/PE. Above ground.*
	Piping DN600 - Phase 2	*0.4*	km	*96kg/m,75% SS316L4, 25% PUR/PE Above ground.*
	Piping DN200 - Phase 2	*0.4*	km	*33kg/m, 75% SS316L4, 25% PUR/PE. Above ground.*
	Valves for piping	*21 000*	kg	*SS316*
02	*Structures - Phase 1*			*The offloading piping is above ground and requires concrete foundations, both in phase 1 for the current harbour site*
	Concrete	*35*	m³	*60 pieces of 0,5 m³ supports plus one larger support of 5 m³.*
	Reinforcement	*4 200*	kg	*Reinforcement 120 kg per m³ of concrete.*
02	*Structures - Phase 2*			
	Concrete	*50*	m³	*90 pieces of 0,5 m³ supports plus one larger support of 5 m³.*
	Reinforcement	*6 000*	kg	*Reinforcement 120 kg per m³ of concrete.*
03	*Earthworks*			
	Gravel and sand	*243*	m³	*Filling for temporary and more permanent underlaying structures*
	Surplus material	*18*	m³	*Transported material off site*
	Excavation	*140*	m³	*Excavation for temporary and more permanent underlaying structures*
04	***Power supply***			
	Electrical cables	*2*	km	*Weight 200kg/km (thereof copper 120kg/km), average cross-section 78,5 mm2 (thereof copper 12,5 mm2 or 16%).*
05	***Communication***			
06	***Heaters***			
	Heaters	*2 600*	kg	*2 pieces, total 2600 kg. Shell side Material Carbon steel / Tube side SS-304.* *Assume 50/50 carbon steel / stainless.*
07	***Vapor compressor***			

	Vapor compressor	*3 600*	kg	*Vapor compression of residual CO_2 vapor, which must be done before the CO_2 enters the tanks. Assumed SS316*
08	***Offloading arms***			
	Offloading arms	*40 000*	kg	*Weight assumed; different types available.*
04	***Storage tanks***			
01	***Supporting facilities***			
01	*Earthworks*			
	Gravel and sand	*12 680*	m³	*Virgin material filling for 6 storage tanks*
	Excess material	*3 600*	m³	*Material transported from site*
	Excavation	*16 280*	m³	*Excavated material for 6 storage tanks*
02	*Structures*			*Structures needed for the tanks*
	Concrete	*2 550*	m³	*425 m³ for each of the 6 tanks.*
	Reinforcement steel	*330 000*	kg	*55.000 kg for each of the 6 tanks.*
	Concrete moulds	*6 000*	m²	*1.000 m² per tank. Assumed to be reused in other projects and wastage assumed to be negligible.*
	Stairs	*14 000*	kg	*Stairs and platforms total weight around tanks, SS304*
02	***Storage tanks***			
	Steel plates	*3 000 000*	kg	*6 tanks, each 500 tons of carbon steel*
03	***Piping***			
	Piping	*24 900*	kg	*One DN600 pipe and two DN200 pipes, total 24,900 kg of SS316.*
	Valves	*14 200*	kg	*Valves are SS316*
04	***Power supply***			
	Electrical cables	*3*	km	*Weight 200kg/km (thereof copper 120kg/km), average cross-section 78,5 mm2 (thereof copper 12,5 mm2 or 16%).*
05	***Communication***			
05	***Pumping and vaporisation***			
01	***Pumps***			
	Injection pumps	*9 600*	kg	*Total of 8 pumps, each 1,200 kg*
	Glycol pumps	*7 200*	kg	*Total of 8 pumps, each 900 kg*
	Recovery compressor	*3 600*	kg	*SS316*
	Bog compressor	*3 000*	kg	*2 identical compressors. Material not confirmed, so SS316 assumed*
02	***Plate & frame exchanger***			
	Plate & frame exchanger	*70 000*	kg	*4 Evaporators, each 17,500 kg, Carbon steel*
03	***Vaporisers (heat exchangers)***			
	Vaporisers (heat exchangers)	*74 000*	kg	*Shell side: CO2 – Material LTCS Tube side: water/glycol – Material CS*

04	***Superheater***			
	Superheater	*16 800*	kg	*Shell side: CO2 – Material LTCS Tube side: water/glycol – Material CS*
05	***Power supply***			
	Electrical cables	*4*	km	*Weight 200kg/km (thereof copper 120kg/km), average cross-section 78,5 mm2 (thereof copper 12,5 mm2 or 16%).*
06	***Communication***			
07	***Other key equipment and materials***			
	Purge tank	*12 000*	kg	*50 m3 SS316 tank*
	Glycol tank	*14 000*	kg	*2 tanks, each 25m³ and 7,000 kg, SS316*
	Glycol heater	*5 200*	kg	*4 heaters, each 1,300 kg, SS316*
	Glycol	*100*	m³	*Material in two 25m³ tanks and flowing through pipes. Could be between 100-200 t. Approximated as ethylene glycol production.*
	Piping	*92 500*	kg	*All piping in key building, SS316L*
	Valves	*55 400*	kg	*Valves inside key building, SS316L*
	Stairs and platforms	*12 000*	kg	*Stairs and platforms in and around the key building, SS304*
06	***Pre-insulated gaseous pipeline***			
01	***Piping***			
01	*Earthworks*			
	Gravel and sand	*57 790*	m³	*Filling material for the pipelines transported to site*
	Material loosening	*132 016*	m³	*Material loosening for excavation*
	Excess material	*57 790*	m³	*Excess material transported from site*
	Excavation	*137 329*	m³	*Excavated material for piping*
02	*Structures*			*Gaseous pipeline is underground and assumed to not require negligible structures.*
03	*Piping*			
	Piping	*8*	km	*DN300 pipe 70kg/m; 81% SS316, 9% PUR insulation and 10% PE plastic. Underground*
	Piping	*7.8*	km	*DN500 pipe 153kg/m; 81% SS316, 9% PUR insulation and 10% PE plastic. Underground.*
04	*Accessories*			
05	*Pig launcher and receiver*			
	Pig launcher and receiver	*-*	kg	*Not assessed separately, included in piping*
02	***Power supply***			
	Electrical cables	*1*	km	*Weight 200kg/km (thereof copper 120kg/km), average cross-section 78,5 mm2 (thereof copper 12,5 mm2 or 16%).*

03		***Communication***			
07		***Groundwater supply***			
	01	***Water wells drilling platform***			
		01 *Earthworks*			*Earthwork for all boreholes included in 08 Injection site*
	02	***Groundwater wells drilling & finalization***			*Same drill is used as for the injection boreholes. Depth is assumed 50 m and diameter around 16" (400 mm). Steel casing is assumed to reach 20 m deep, 400 mm diameter with wall thickness 8 mm. Pumping pipe is assumed to reach to borehole bottom (50 m), 350 mm thickness and wall thickness 8 mm. Material is steel. Pumps are capable of 150 L/s.*
		Groundwater wells	*24*	wells	*Assume 2 per hub. Depth 50 m.*
		Water well volume	*17*	m^3	*26" diameter and 50 m depth*
		Total volume	*411*	m^3	*Total volume of all groundwater wells*
		Emissions per groundwater well	*8*	tCO_2eq	*Same drill is used as for the injection boreholes. Assume the same emissions per m³ of well volume as for injection boreholes, i.e. the emissions are scaled down based on the borehole volume.*
		Transport of drill	*0.3*	tCO_2eq	*Scaled down based on borehole volume.*
		Portland cement	*3.9*	tCO_2eq	*Scaled down based on borehole volume.*
		Silicia flour	*0.5*	tCO_2eq	*Scaled down based on borehole volume.*
		Wyoming bentonite	*0.03*	tCO_2eq	*Scaled down based on borehole volume.*
		Perlite	*0.03*	tCO_2eq	*Scaled down based on borehole volume.*
		Electricity use	*3.4*	tCO_2eq	*Scaled down based on borehole volume.*
		Surface casing	*59 112*	kg	*Assume 20 m depth. Hole diameter 26", casing diameter 20" (500 mm), assumed wall thickness 10 mm and steel density 8000 kg/m³.*
	03	***Piping***			
		01 *Earthworks*			*Earthwork for all boreholes included in 08 Injection site*
		02 *Structures*			*No structures directly related to groundwater wells*
		03 *Piping*			
		Piping	*2*	km	*PE100 plastic pipe, 67kg/m.*
		04 *Accessories*			
	04	***Power supply***			
		Electrical cables	*3*	km	*Weight 200kg/km (thereof copper 120kg/km), average cross-section 78,5 mm2 (thereof copper 12,5 mm2 or 16%).*

05	***Communication***			
06	***Pumps***			
	Pumps	*5 760*	kg	*2 pumps by each of the 12 injection sites, each 240 kg, mostly SS*
08	***Injection site***			
01	***Injection wells drilling platform***			
01	*Earthworks*			
	Gravel and sand	*51 750*	m³	*Filling material transported to site for all injection sites*
	Filling material from cuts - roads	*15 050*	m³	*Filling material for roads by injection sites*
	Filling material from cuts - other	*23 650*	m³	*Filling material for injection sites*
	Filling material from cuts - total	*38 700*	m³	*Filling material for injection sites and roads*
02	***Injection wells drilling & finalization***			
	Injection wells drilling & finalization	*96*	wells	*12 injection sites, each with 8 wells*
	Injection well borehole volume	*57*	m³	*Well depth assumed 800m with a varying diameter with depth as follows:* *0-100m - D=17.5"* *100-350m - D=12.25"* *350-800m - D=9.87"*
	Total volume	*5 449*	m3	*Total volume of all 96 injection wells*
	Casing and gas pipe (per well)			*In the feasibility study, the emissions from steel casings production were assumed to be 157 tonnes CO_2 eq. for a single well, based on a calculation by Jarðboranir. The calculation assumed dimensions of 350 m @ 13 1/2" section; casing thickness 10 mm; assumed steel density 8000 kg/m³. This is deemed to have been an overestimate and is not used in this assessment.*
	Production casing	*20 900*	kg/well	*350 m deep casing with 10 3/4" diameter (273 mm). Assume 273 mm diameter, 9,4 mm wall thickness and steel density 8000 kg/m³*
	Surface casing	*9 538*	kg/well	*Depth 50-100 m and 14" (356 mm) diameter. Assume 100 m, 356 mm diameter, 11 mm wall thickness and steel density 8000 kg/m³*
	Gas pipe	*926*	kg/well	*Assume 4,5" (110 mm) outer diameter. Assume 300 m and wall thickness 10,5 mm. Assume cross-linked polyethylene (PEX).*
	Casing and gas pipe (total)			
	Production casing	*2 006 437*	kg	*Total weight of production casings in injection wells, carbon steel*
	Surface casing	*915 636*	kg	*Total weight of surface casings in injection wells, carbon steel*
	Gas pipe	*88 855*	kg	*Total weight of gas pipe in injection wells, SS316*
	Other emissions per well	*27*	tCO_2eq	*Source: Jarðboranir.*

	Transport of drill	*1.0*	tCO_2eq	*Source: Jarðboranir.*
	Portland cement	*13*	tCO_2eq	*Source: Jarðboranir.*
	Silicia flour	*1.6*	tCO_2eq	*Source: Jarðboranir. For well casing.*
	Wyoming bentonite	*0.1*	tCO_2eq	*Source: Jarðboranir. For well casing.*
	Perlite	*0.1*	tCO_2eq	*Source: Jarðboranir. For well casing.*
	Electricity use	*11*	tCO_2eq	*Source: Jarðboranir. Drilled on electricity which emits ~7% of emissions from diesel driven drill rigs.*
03	***Piping***			
01	*Earthworks*			*Included in drilling platform, 08-01*
02	*Structures*			*No structures directly connected to piping included. Hub buildings in 04 Storage tanks.*
03	*Piping*			
	Piping - plastic	*34 560*	kg	*Water pipeline to key building, PE plastic, 2880 kg for each injection site*
	Piping - CS	*36 000*	kg	*CO_2 pipeline, ~90% CS, 10% PUR/PE insulation, 3000 kg for each injection site*
	Piping and valves inside cellar	*29 472*	kg	*CO_2 pipeline, ~90% CS, 10% PE, no insulation required inside, 2456 kg for each injection site. DN65 and DN200*
	Piping inside cellar	*38 880*	kg	*Water pipeline, 3240 kg for each injection site. SS316*
04	*Accessories*			
04	***Underground injection hub building***			
01	*Earthworks*			
	Gravel and sand	*1 553*	m^3	*Filling material transported to site*
	Surplus material	*2 760*	m^3	*Material transported off site*
	Excavation	*4 313*	m^3	*Total excavation for 2+2+8 well buildings*
02	*Structures*			*Estimated based on average emission values per m^2 for commercial buildings, except concrete and steel modelled separately. No insulation required.*
	Number of hubs	*12*	hubs	
	Floor area net	*128*	m^2	
	Floor area gross	*141*	m^2	
	Concrete (per hub)	*250*	m^3	
	Reinforcement steel (per hub)	*30 000*	kg	
	Steel (per hub)	*2 800*	kg	
	All other materials			*Assessed by assuming average impacts per m^2 for commercial buildings in Iceland*
05	***Power supply***			
	Electrical cables	*2*	km	*Weight 200kg/km (thereof copper 120kg/km), average cross-section 78,5 mm2 (thereof copper 12,5 mm2 or 16%).*

		Transformers (hubs)	*62 000*	kg	*Total weight 62000 kg (for 12 injection hubs); oil 9000 kg, copper 7000 kg, aluminium 1700 kg, core (steel) 13000 kg.*
	06	***Communication***			
09		***Monitoring***			
	01	***Monitoring wells drilling platform***			
	01	*Earthworks*			*Included in 08-01*
	02	***Monitoring wells drilling & finalization***			
		Monitoring wells drilling & finalization	*6*	wells	*6 monitoring wells according to Feasibility study.*
		Hole volume	*25*	m^3	*Well depth assumed 800m with a varying diameter with depth as follows:* *0-100m - D=12.25"* *100-350m - D=8.5"* *350-800m - D=6"*
		Total volume	*150*	m^3	*Total volume of all monitoring wells*
		Casing (per well)	*8 545*	kg/well	*50-100 m, 13,5" (350 mm) diameter. Assume 100m, 10 mm thick casing and steel density 8000 kg/m^3*
		Casing (total)	*51 271*	kg	
		Other emissions per well	*12*	tCO_2eq	*Same drill is used as for the injection boreholes. Assume the same emissions per m^3 of well volume as for injection boreholes, i.e. the emissions are scaled down based on the borehole volume.*
		Transport of drill	*0.4*	tCO_2eq	*Scaled down based on borehole volume.*
		Portland cement	*5.7*	tCO_2eq	*Scaled down based on borehole volume.*
		Silicia flour	*0.7*	tCO_2eq	*Scaled down based on borehole volume.*
		Wyoming bentonite	*0.04*	tCO_2eq	*Scaled down based on borehole volume.*
		Perlite	*0.04*	tCO_2eq	*Scaled down based on borehole volume.*
		Electricity use	*4.9*	tCO_2eq	*Scaled down based on borehole volume.*
	03	***Piping***			*There are no pipes coming to the monitoring wells, this is probably negligible or only around the monitoring wells.*
	01	*Earthworks*			*Included in 08-01*
	02	*Structures*			*No structures directly connected to piping included. Hub buildings in 08-04*
	03	*Piping*			*Assumed negligible.*
	04	*Accessories*			*Assumed negligible*
	05	***Power supply***			
		Electrical cables	*1*	km	*Weight 200kg/km (thereof copper 120kg/km), average cross-section*

				78,5 mm2 (thereof copper 12,5 mm2 or 16%).
06	***Communication***			
10	***Hot water pipeline***			Assumed hot water pipeline from Hafnarfjörður or Garðabær.
01	***Piping***			
01	*Earthworks*			
	Gravel and sand	*5 200*	m³	*Assuming linear correlation from 3000m*
	Material loosening	*8 840*	m³	*Assuming linear correlation from 3000m*
	Excess material	*5 200*	m³	*Material transported from site*
	Excavation	*8 840*	m³	*Assuming linear correlation from 3000m*
02	*Structures*			*Structures for pipeline are not included.*
03	*Piping*			
	Piping	*5 200*	km	*For phase 3 the hot water pipe is DN450. Total length 1500 m within planned area, 1500 m to existing Veitur network and 2200 m enlargement of the existing Veitur network. The hot water pipe is a normal insulated pipe with a plastic sheathing, 93 kg/m DN450; steel 70 kg/m and the rest is 50/50 PUR and PE.*
Transport (A4)				
Transport of materials to site				
	Gravel and sand	*11*	km	*Vatnsskarð mine is assumed.*
	Concrete	*5*	km	*Steinsteypan in Hafnarfjörður is assumed*
	Construction steel, reinforcement steel, steel pipes, PE plastics, pumps, other materials	*3 000*	km	*Mainland Europe assumed (GER/NED/POL)* *Truck 200 km + Ship 2800 km*
	Heat exchangers, superheaters	*5 300*	km	*Mainland Europe assumed (ITA)* *Land 100 km + Sea 5200 km*
	PVC, PP plastics	*8 000*	km	*USA assumed* *Truck 4000 km + Ship 4000 km*
	Electrical cables	*24 000*	km	*SE Asia (South Korea) is assumed* *Truck 400 km + Ship 20000 km*
Transport of waste to disposal or recycling				Transport of waste to disposal, reuse or recycling is only included for buildings, roads and excavated materials.
	Excavated material	*3*	km	*Excess material from excavation is assumed to be utilized in another construction work in the municipality, 3 km transport is assumed.*
Construction (A5)				
Earthworks				

Preparation of material for excavation			*Material is loosened in earlier phases to prepare for excavation. Approximate as 1 excavator movement*
Excavator movements	*1*	movem.	
Excavation, transport and use of material in roads and platforms			*Approximated as 2 excavator movements and 1 km transport on average.*
Transport	*1*	km	
Excavator movements	*2*	movem.	
Excavation			*Trenches for pipelines etc. are dug up and the material is stored on the side. Most of the material is shovelled back into the trench but some excess material is shovelled onto a truck and used in another construction work close by. Approximated as 2 excavator movements in both cases.*
Excavator movements	*2*	movem.	
Virgin material			*Production of material at mine, shovelling onto truck, transport from mine (11 km) and shovelling on site. Shovelling movements approximated as 2 excavator movements.*
Transport	*11*	km	
Excavator movements	*2*	movem.	
Excess material			*Excess material from excavation is assumed to be utilized in another construction work in the municipality, 3 km transport is assumed.*
Transport	*3*	km	

Other fuel use	Only included for buildings and roads.
Hot water use during construction	Only included for buildings and roads.
Electricity use during construction	Only included for buildings, roads and drilling.
Construction waste	Only included for buildings and roads.

Operation and maintenance (B)

Use (B1)

Maintenance (B2)

Glycol	-	kg/y	*No losses can be assumed at this stage*
Other maintenance			*No other maintenance is included in assessment*

Repairs (B3)	Repairs are not included in assessment

Replacement (B4)

Service life	*30*	years	Assessment period taken to be 30-years, can be altered at later stages. Equipment assumed to last around 15 years, meaning renewed once during the assessment period.

Equipment	*15*	years	*Service life of all equipment is assumed to be 15 years and has to be replaced once in the service life of project.*
Water pipes	*100*	years	
Hot water pipes	*50*	years	*At least 50 years, probably closer to 100 years.*
Gas pipes	*30*	years	*More uncertainty, at least 30 years.*
Buildings	*50*	years	*Service life of buildings is assumed to be longer than of the project.*

Refurbishment (B5) — No refurbishment is assumed.

Operational energy use (B6)

Electricity use

Electricity use	*7*	MW	*Assumed to scale linearly with the amount of CO2 mineralized up to 8,5MW in 3rd phase (3M tons CO_2/y). Assessed over the 30-year service life.*

Geothermal hot water use

Geothermal hot water use	*342 222 222*	kWh/y	*In this assessment, the thermal energy required for the key processes is assumed to come from district geothermal hot water in Iceland. Other options for sources of thermal energy should be considered in further studies. Assumed to scale linearly with the amount of CO2 mineralized up to 400 GWh/y in 3rd phase (3M tons CO_2/y). Assessed over the 30-year service life. Assume the average emission factor for Reykjavík, based on a weighted average of high-temperature geothermal (from power plant) and low-temperature geothermal (from borehole). For high-temperature geothermal, Hellisheiði with current carbon capture and mineralization is assumed, throughout the service life.*

On-site fuel use

Diesel oil	*10 000*	L/y	*Rough estimate of employee driving. No other known fuel use in operation.*
Gasoline	*10 000*	L/y	*Rough estimate of employee driving. No other known fuel use in operation.*

Operational water use (B7)

Cold water use	*100 000 000*	m^3/y	*Water collection is on-site, energy use is counted elsewhere.*

End of life (C) — *End of life stage is not taken into account.*

Recycling (D) — *Recycling benefits outside system boundary are not taken into account.*

MINERALIZATION AND LEAKS

CO_2 mineralization

CO_2 mineralization over service life	*76 230 000*	tons	Mineralization after assumed leakage (1%). See description for leakage below.
Annual CO_2 mineralization	*2 541 000*	tons/y	Average over 30-year assessment period

CO_2 leakage

Assumed CO_2 leakage percentage	*1.0*	%	*Potential CO_2 leakage at various stages in the supply chain has not been estimated. A leakage of 1% is arbitrarily assumed in this assessment for illustrative purposes. To put into context, it is equivalent of 22 storage tanks completely emptying over the service life. Must be considered in more detail in further study.*
Assumed CO_2 leakage over service life	*770 000*	tons	*1% of imported CO_2 assumed lost*
Assumed annual CO_2 leakage	*25 667*	tons	*1% of imported CO_2 assumed lost*

4 Impact assessment (LCIA)

4.1 Overall impacts and benefits

As shown in Figure 3, the total global warming impacts and benefits assessed over a service life of 30 years are emissions of 4 100 million kg CO_2 equivalents and mineralization of 76 200 million kg CO_2 eq., i.e. a net reduction of 72 100 million kg CO_2 eq. In terms of the functional unit, the emissions are 54 kg CO_2 eq. per ton CO_2 mineralized, or a net reduction of 946 kg of CO_2 eq. in the atmosphere per CO_2 mineralized. This includes everything within the system boundary, i.e. ship transport of CO_2 to Iceland, buildings, equipment, pipelines and infrastructure at the Coda Terminal, energy use of the plant, assumed CO_2 losses and mineralization of CO_2.

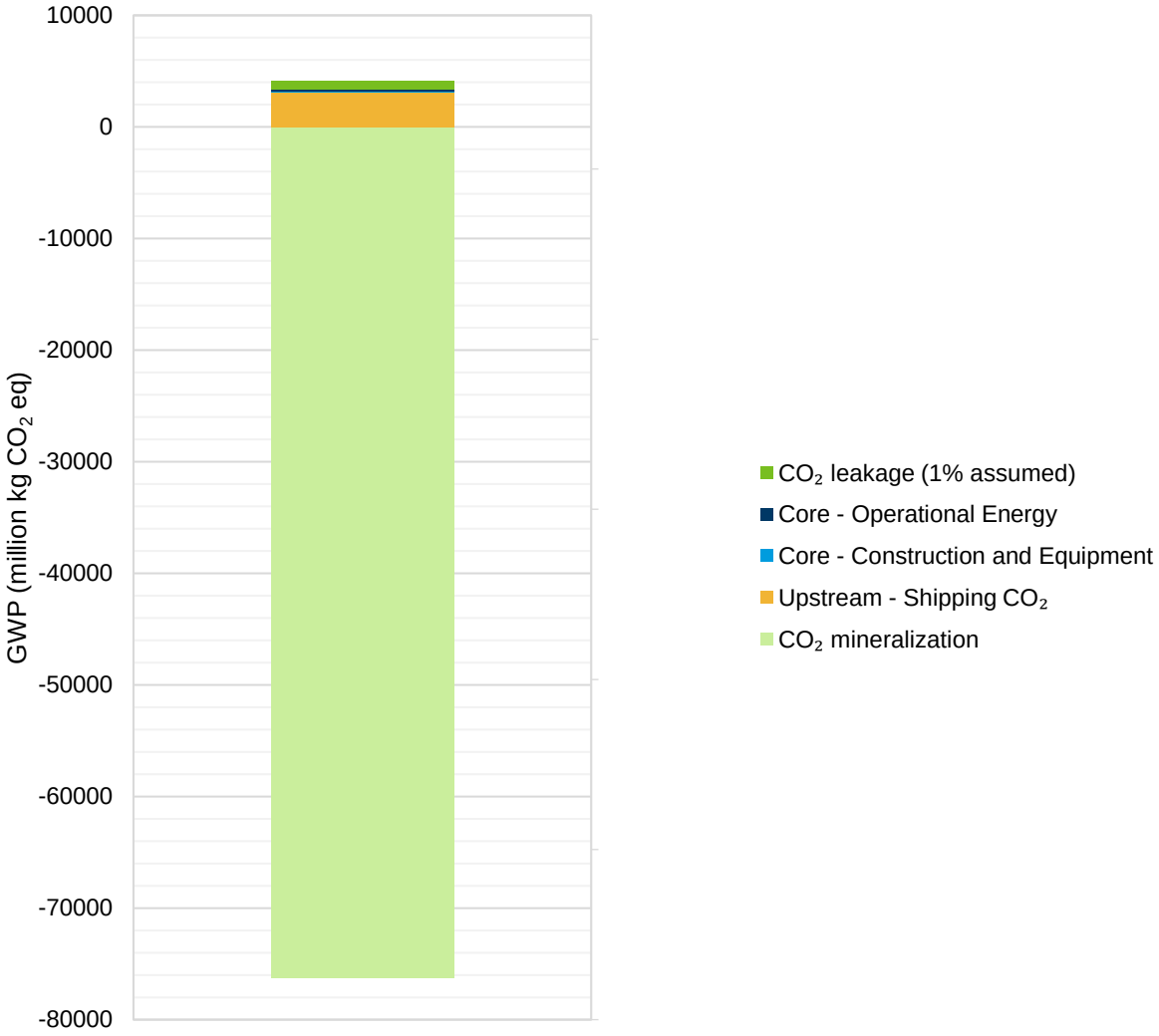

Figure 3 **Total global warming impacts and benefits of assessed life cycle. This includes ship transport of CO_2 to Iceland, buildings, equipment, pipelines and infrastructure at the Coda Terminal, energy use, assumed CO_2 losses and mineralization of CO_2.**

The global warming impacts and benefits are dominated by the CO_2 mineralization, followed by ship transport, and then assumed CO_2 leakage. The global warming impacts of construction and operation of the Coda Terminal plant are much lower.

For better visualization, figure 4 shows the same graph broken into separate columns.

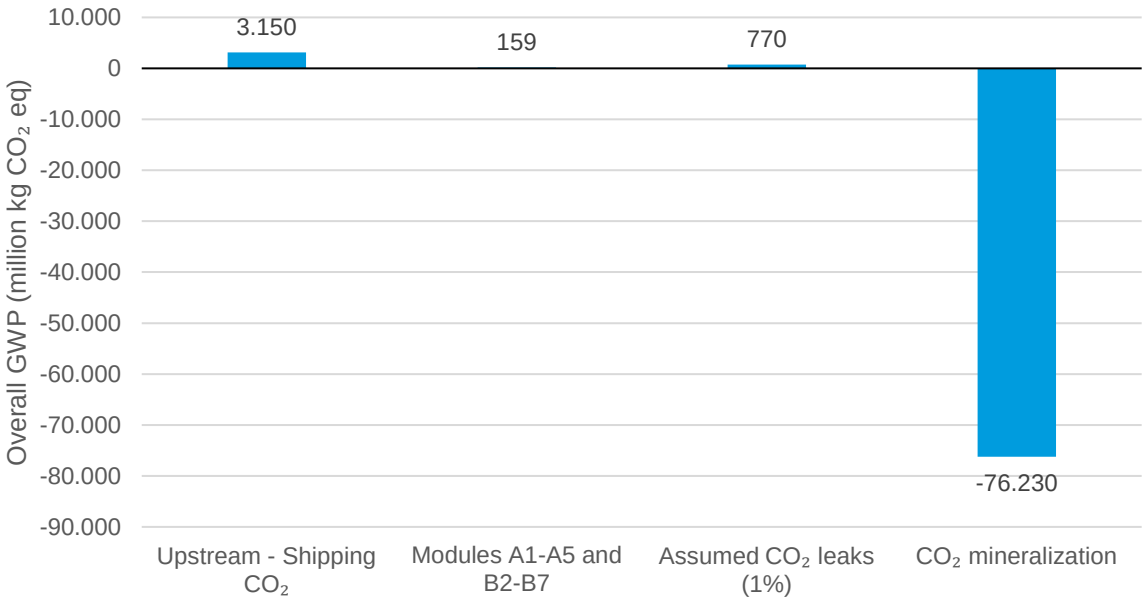

Figure 4 **Total global warming impacts and benefits of assessed life cycle. This includes ship transport of CO_2 to Iceland, buildings, equipment, pipelines and infrastructure at the Coda Terminal, energy use, assumed CO_2 losses and mineralization of CO_2.**

Figure 5 shows the total global warming impacts, excluding the benefits of CO_2 mineralization.

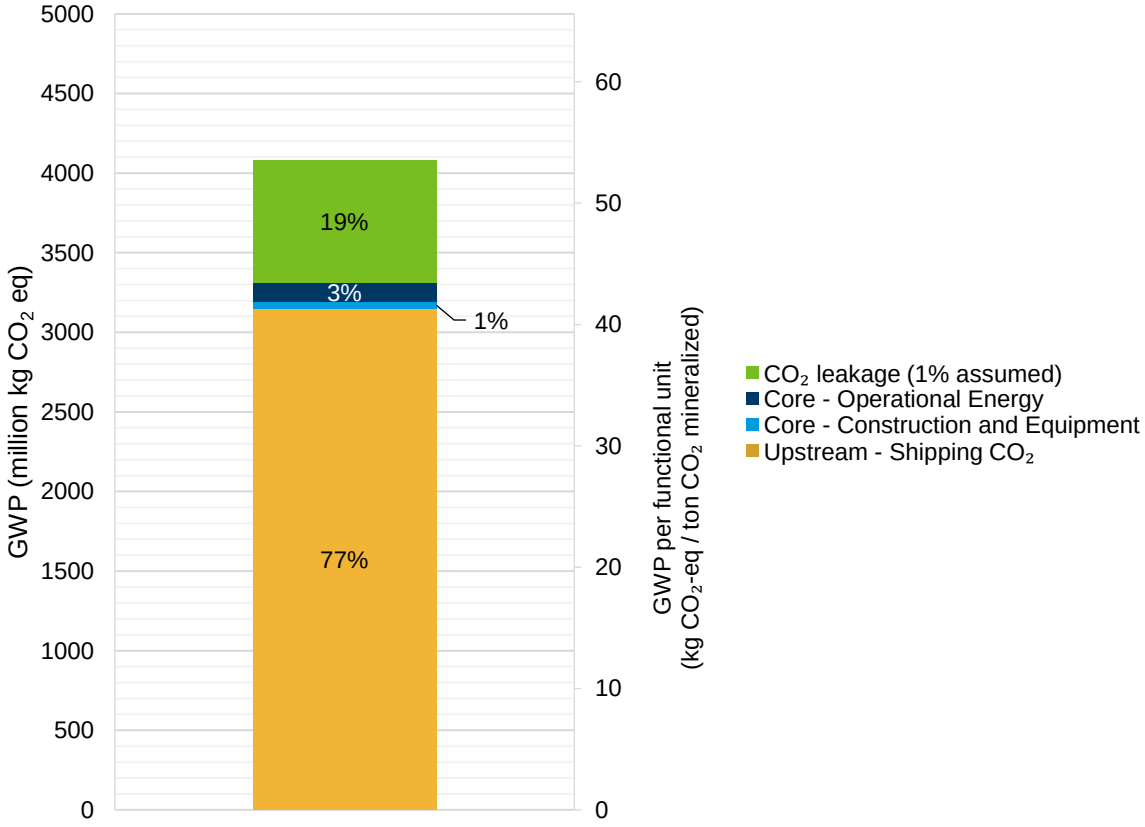

Figure 5 **Total global warming impacts of assessed life cycle, excluding the benefits of mineralizing CO_2. This includes CO_2 ship transport, buildings, equipment, pipelines and infrastructure at the Coda Terminal, energy use and assumed CO_2 losses.**

4.2 Core module impacts (Coda Terminal CO_2 mineralization plant)

4.2.1 Construction (A) and operation (B) of the Coda Terminal plant

The global warming impacts of the core module, i.e. construction and operation of the Coda Terminal CO_2 mineralization plant, are 159 million kg of CO_2 eq. over its service life, or 2.1 kg CO_2 eq. for every ton CO_2 mineralized. This includes the product stage, construction stage and use stage but excludes ship transport of CO_2 to Iceland, assumed CO_2 losses and CO_2 mineralization.

Figure 6 shows how the core module impacts are divided between the building life cycle stages. The majority belongs to the use stage, 121 million kg of CO_2 equivalents or 1.6 kg CO_2 per ton CO_2 mineralized. The global warming impacts of construction (building life cycle stages A1-A5) are 38 million kg CO_2-eq. or 0.5 kg CO_2 eq. per ton CO_2 mineralized.

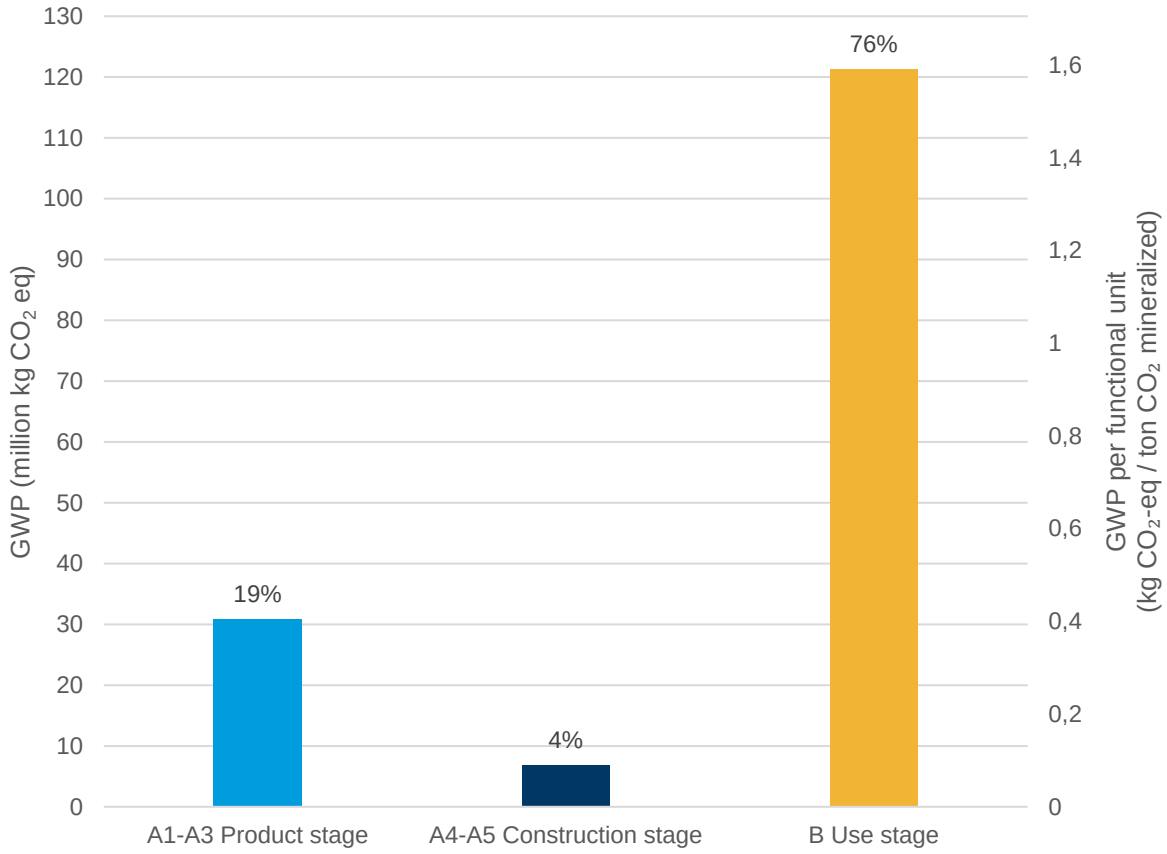

Figure 6 **Global warming impacts of the Coda Terminal CO_2 mineralization plant (core module) categorized into building life cycle stages. Maritime CO_2 transport, assumed CO_2 losses and CO_2 mineralization are not shown in this figure.**

Processes were categorized into categories that they pertain to, that is boreholes, buildings, equipment, piping, storage tanks, energy use and other (such as roads and fencing). Figure 7 shows the global warming impacts of the Coda Terminal plant divided into these categories.

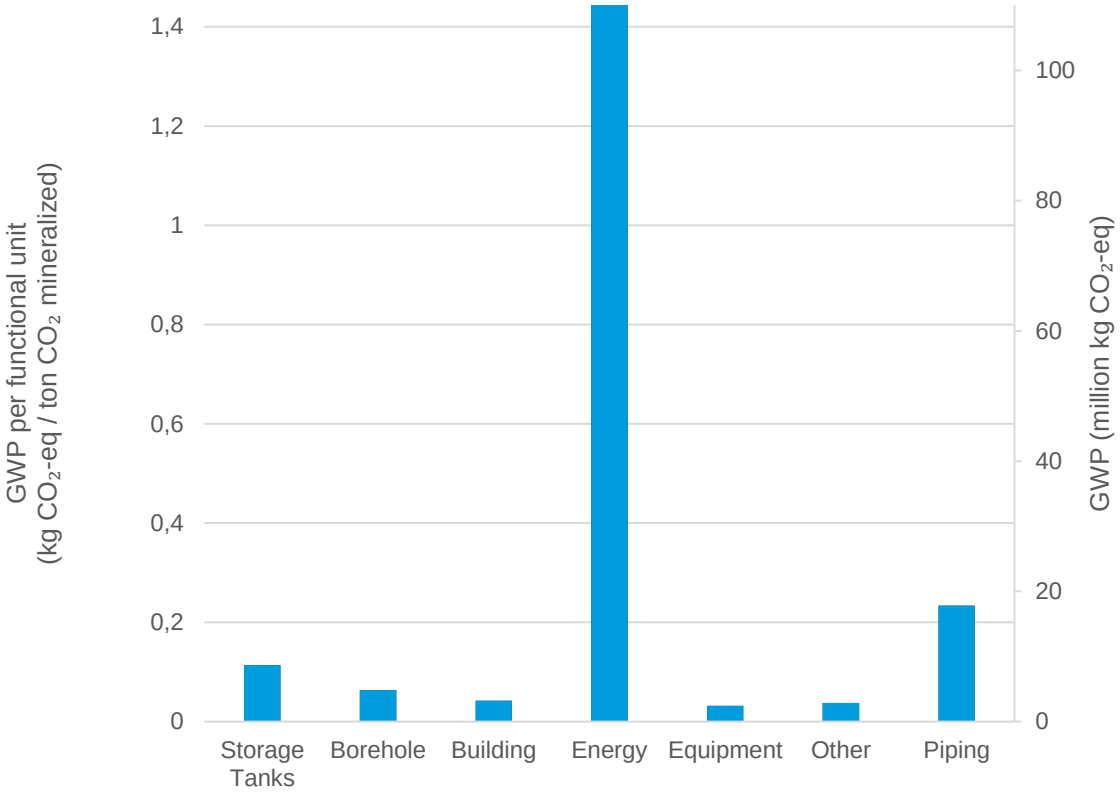

Figure 7 **Global warming impacts of the Coda Terminal CO_2 mineralization plant (core module) divided into categories. The energy category is entirely within life cycle stage B, whereas others are divided between A and B. Everything within equipment is renewed once in the 30-year analysis period. Maritime CO_2 transport, assumed CO_2 losses and CO_2 mineralization are not shown in this figure.**

Figure 8 shows a more detailed categorization where these processes are themselves divided into building life cycle stages A1-A3, A4-A5 and B.

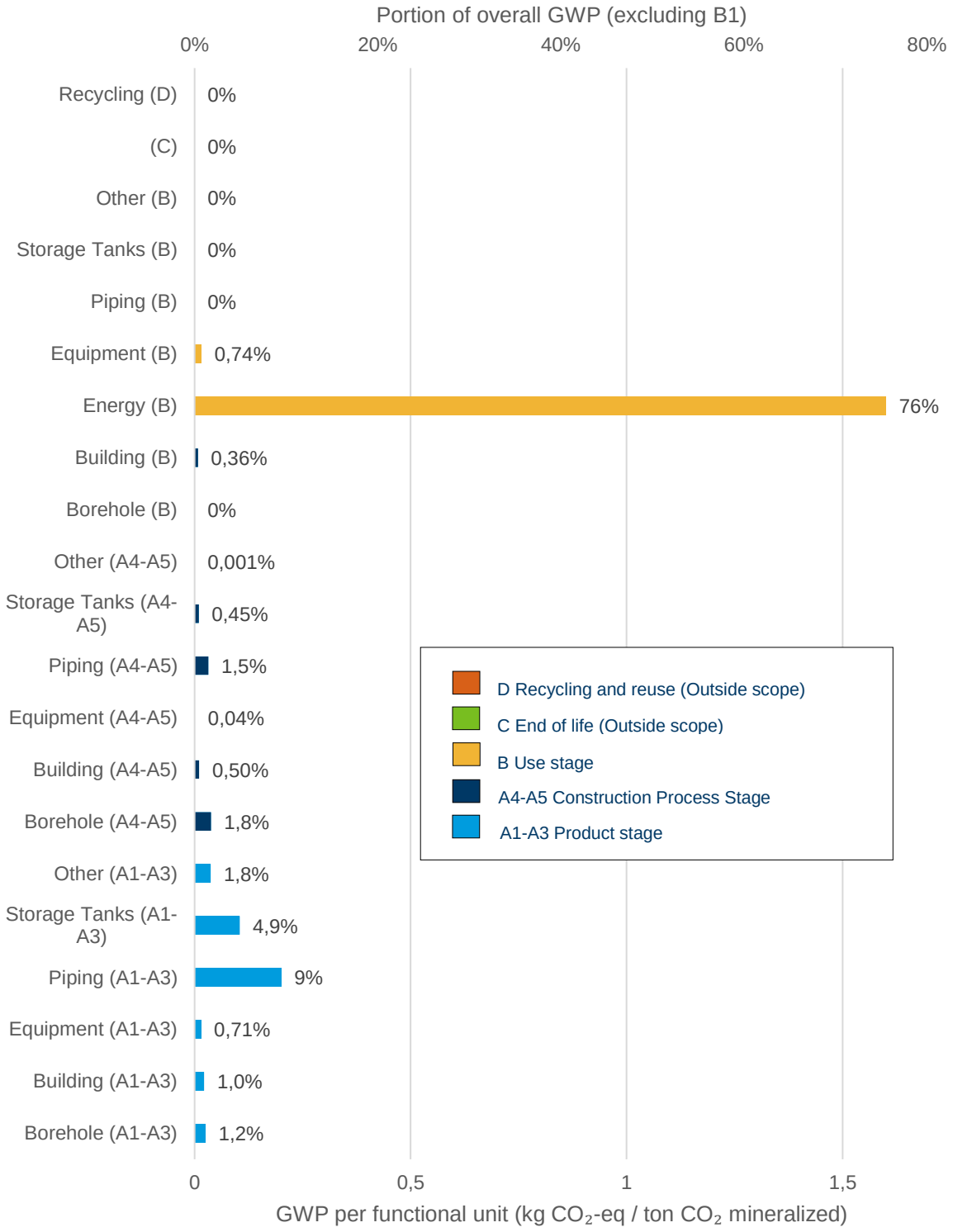

Figure 8 **Detailed categorization of global warming impacts of Coda Terminal CO_2 mineralization plant (core module) by both life cycle stage and the pertaining category. Life cycle stages C and D are outside the scope of this analysis. Maritime CO_2 transport, assumed CO_2 losses and CO_2 mineralization are not shown in this figure.**

4.2.2 Construction (A) of the Coda Terminal plant

As energy use weighs heavily in the impacts of the core module, following are graphs for the construction only, i.e. the material and equipment production (stages A1-A3), transport of materials and the construction itself (A4-A5). Figure 9 shows how the impacts of construction of the Coda Terminal are divided according to the project work breakdown structure, as shown in the LCI in table 1. The plan with the greatest impact is 08 – Injection site, which includes earthwork, drilling and steel for 96 injection wells and 12 injection hub buildings.

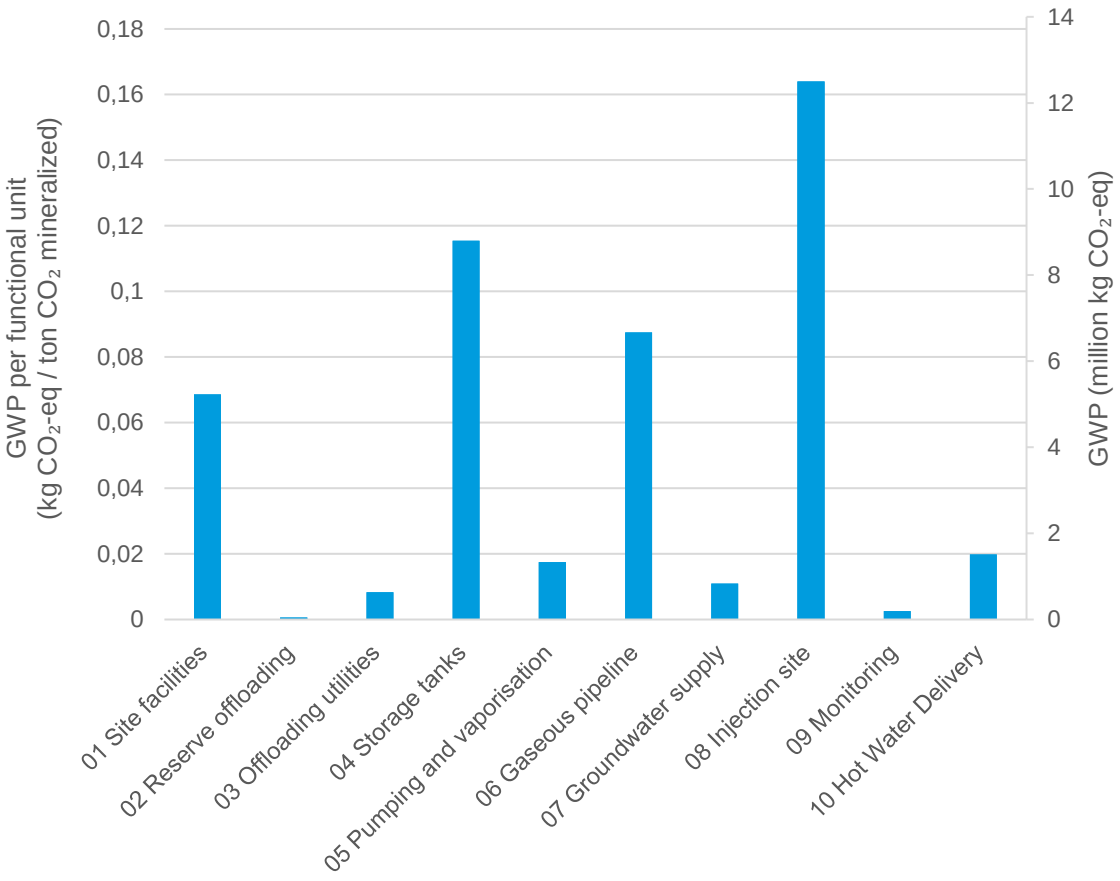

Figure 9 **Global warming impacts of construction of the Coda Terminal (stages A1-A5) categorized by the project work breakdown structure as described in the LCI. Maritime CO_2 transport, operation (life cycle stage B), assumed CO_2 losses and CO_2 mineralization are not shown in this figure.**

Figure 10 shows how the construction of the Coda Terminal plant (A5) is divided by both the life cycle stages (A1-A3 and A4-A5) and the categories that the processes pertain to. Piping within A1-A3 has the highest impact and includes all steel, plastics and insulation material for all piping on site. Boreholes have the highest impact within A4-A5 as impacts of earthwork are more evident.

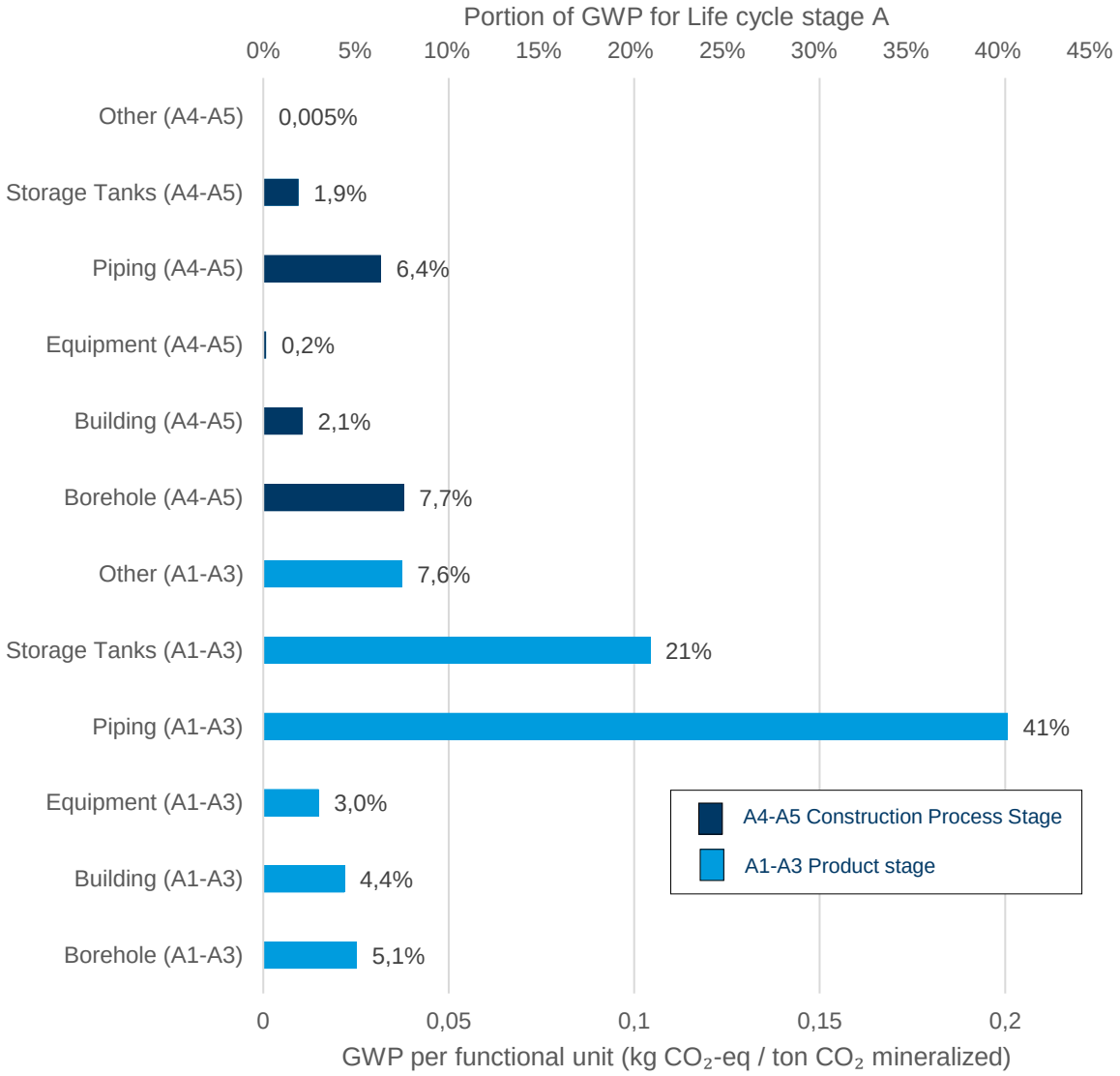

Figure 10 **Detailed categorization of global warming impacts of construction of the Coda Terminal plant (stages A1-A5) by both life cycle stage and the pertaining category. Maritime CO_2 transport, operation (life cycle stage B), assumed CO_2 losses and CO_2 mineralization are not shown in this figure.**

4.3 Scenario analysis: Mineralization plant location

The main LCA model assumes that the CO_2 mineralization plant is located in Straumsvík, Hafnarfjörður, Iceland. In a scenario analysis, two additional location scenarios were considered, that is, Nagasaki, Japan and Wallula, Washington, USA. Figure 11 shows the total global warming impact of each scenario, excluding the benefits of CO_2 mineralization (corresponding to what was shown in figure 5). The modelled scenarios differ in the emission factor and transport of steel for construction, in CO_2 transportation distances and method (maritime or pipeline), and in the source of electric and thermal energy used in the CO_2 mineralization plant (geothermal hot water or biogas). Description of the assumptions behind the scenarios can be found in chapter 2.10.

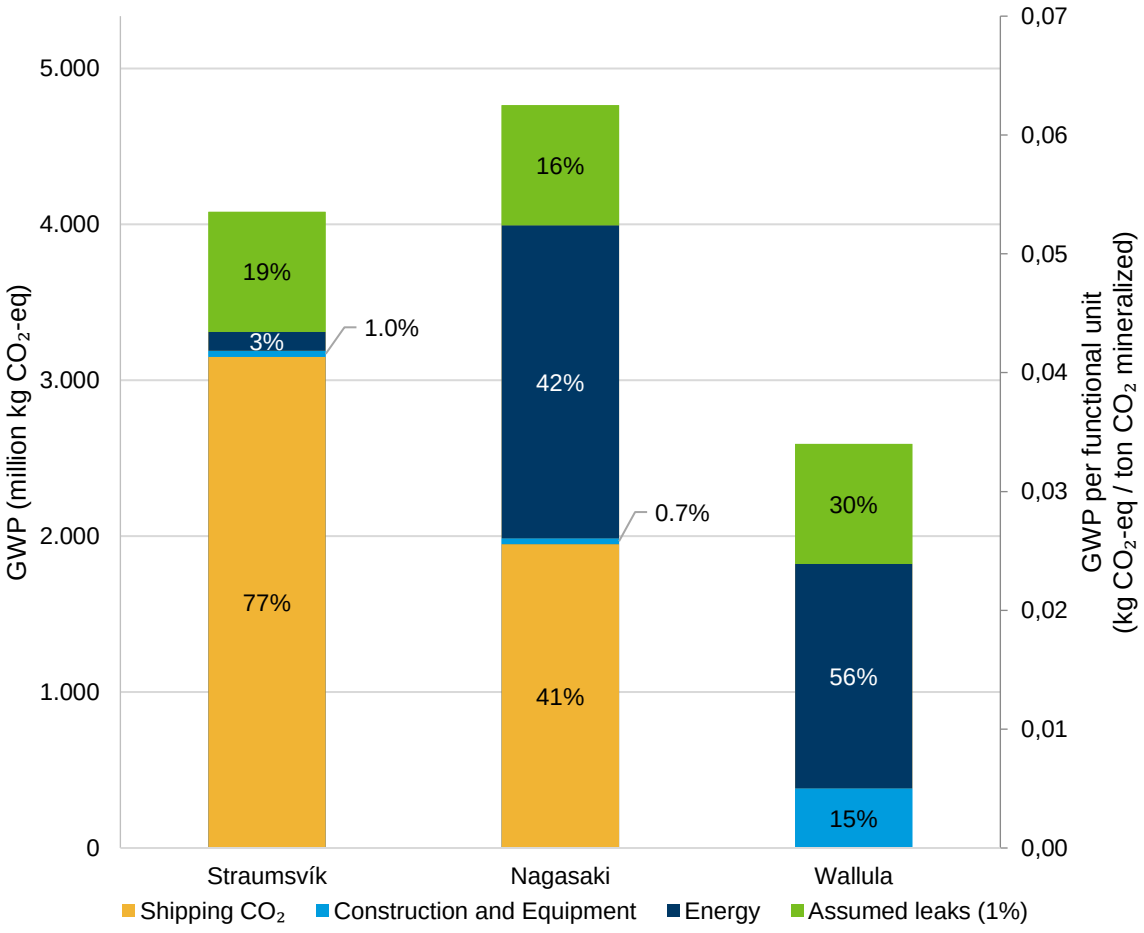

Figure 11 **Total global warming impacts of the assessed life cycle excluding the benefits of mineralizing CO_2, shown for the three location scenarios: Straumsvík (Iceland), Nagasaki (Japan) and Wallula (Washington, USA). This includes CO_2 ship transport, buildings, equipment, pipelines and infrastructure at the Coda Terminal, energy use and assumed CO_2 losses.**

As shown in figure 12, the total GHG emissions (excluding CO_2 mineralization) of each scenario are 4080 million kg CO_2-eq., 4770 million kg CO_2-eq, and 2590 million kg CO_2-eq., respectively, for Straumsvík, Nagasaki and Wallula. When the benefits of CO_2 mineralization (-76 230 million kg CO_2-eq.) are taken into account, there is a net reduction of 72 150 million kg CO_2-eq., 71 460 million kg CO_2-eq., and 73 640 million kg CO_2-eq. in the atmosphere, respectively, for Straumsvík, Nagasaki and Wallula.

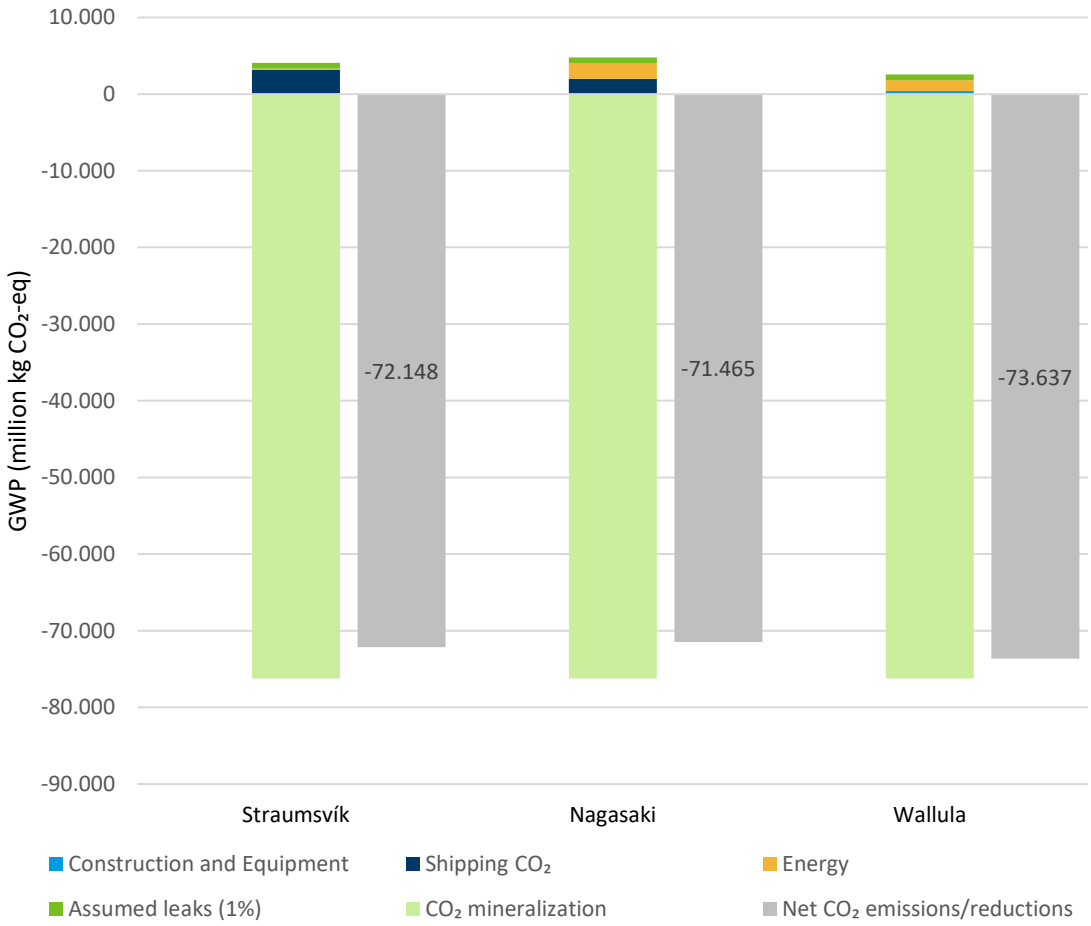

Figure 12 **Net global warming impacts and benefits of the assessed life cycle, shown for the three location scenarios: Straumsvík (Iceland), Nagasaki (Japan) and Wallula (Washington, USA). This includes CO_2 ship transport, buildings, equipment, pipelines and infrastructure at the Coda Terminal, energy use, assumed CO_2 losses and CO_2 mineralization benefits.**

5 Interpretation

This LCA study assesses the GWP impacts of a CO_2 transport and mineralization. More specifically, it considers ship transport of CO_2, CO_2 liquid offloading, gasification, pipeline transport and injection into basalt with water. CO_2 capture, liquefaction and ship loading activities abroad were not considered in this LCA. The CO_2 capture is potentially an energy and emission intensive step and will depend on where the CO_2 is captured, the CO_2 concentration, waste heat availability etc. Interpretation of the results should therefore acknowledge that CO_2 capture, a potentially important step in the value chain, was outside scope of the assessment.

As shown in figure 3 in chapter 4.1, the overall result of the LCA is a net reduction of CO_2 in the atmosphere by 72 100 million kg CO_2 eq. over the assumed service life of the project[9]. The emissions arising from CO_2 transport, construction and operation of the Coda Terminal plant and from an assumed 1% CO_2 leakage, are 54 kg CO_2 eq. per ton CO_2 mineralized. This means that there is a net reduction of 946 kg of CO_2 eq. in the atmosphere for every 1000 kg of CO_2 mineralized[9]. Most of these emissions are due to ship transport and the assumed 1% leakage.

According to this LCA results, it would take 30 days of operation for the plant to fully neutralize the emissions from constructing the plant, including the emissions from maritime CO_2 transport, from the plant's operation and the assumed leakage (for these first 30 days)[9]. This is assuming that in the first year 500.000 tons of CO_2 are imported to be mineralized. If, however, the terminal would operate at full phase 3 capacity from the first day, the emissions would be neutralized within 5 days. Figure 13 shows the impacts of mineralization over the first eight years of operation.

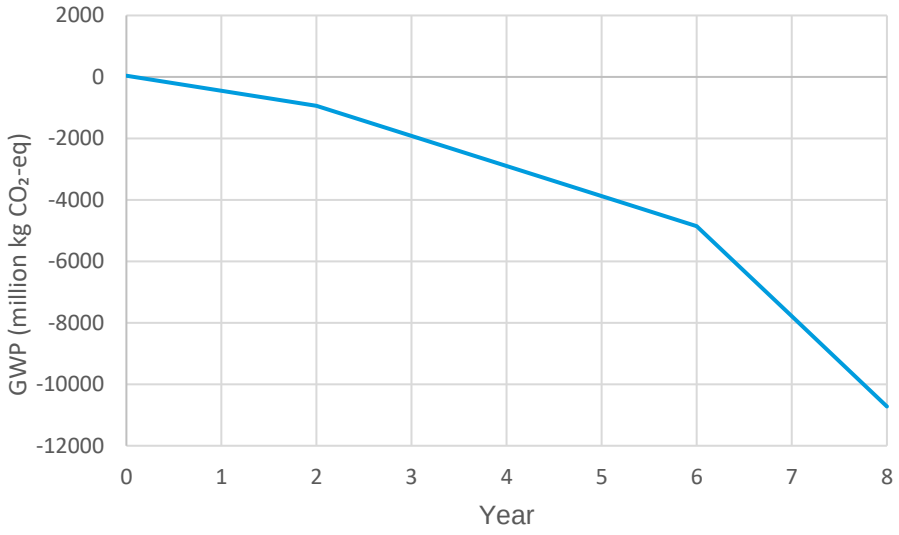

Figure 13 Global warming potential payback time for construction occurring at year 0.[9]

Shipping of carbon dioxide is a key process in this LCA assessment. Shipping emissions constitute 77% of the total global warming impacts when CO_2 mineralization is excluded (figure 5). The CO_2 emissions from operating the tanker ships are in the range of 4-5% of the CO_2 that they are transporting. These emissions are based on the assumption of diesel-powered tanker ships that use 273 tons of diesel / gas oil for a 2173 km long trip (one-way), which is derived from assumptions made in the Coda Terminal Innovation Fund application. This seems like a very conservative

[9] The scope of the study did not include CO_2 capture and liquefaction, which are potentially important steps in the value chain. This should be kept in mind when the results are interpreted.

assumption because generic maritime tanker transport processes in GaBi assume a much lower fuel use. This assumption for fuel use should be reviewed in further assessment. Ship sizes, fuel types and shipping distances are all factors that play a big role in determining the impacts of shipping. The emissions could be reduced in further development of the project by using methanol as fuel or climate neutral fuels.

The construction and operation of the Coda Terminal (core module) was considered specifically in chapter 4.2, where ship CO_2 transport, CO_2 losses and CO_2 mineralization have been excluded. When considering the construction and operation of the plant only, the operational energy use of the Coda terminal has the most global warming impact (76%). This could potentially decrease during the analysis period, as footprint of energy production will decrease over these years, especially with increased use of carbon capture and mineralization at the Hellisheiði geothermal power plant. Utilization of waste heat, for example from nearby heavy industry could also cut down the operation energy use impacts. When considering materials production, transport and construction (A1-A5), then pipelines account for most of the impacts (47%), which include earthwork required for these pipelines, material production and transportation to the site. Storage tanks account for 23% of A1-A5 impacts, requiring a lot of steel, concrete and rebar for the supporting structures. The impact of the buildings is 7% of A1-A5 impacts and include the key building, the reception building, the jetty building and 12 well buildings. The equipment is 3% of the A1-A5 impacts. Most equipment is at this stage approximated as steel and omits the manufacturing process of the equipment. This should be considered in more detail when more information about the equipment will be available at later stages of the project.

Potential CO_2 leakage at various stages in the supply chain has not yet been estimated. But instead of neglecting possible CO_2 leakage in the assessment, a leakage of 1% was arbitrarily assumed. To put into context, that is equivalent of 22 storage tanks completely emptying over the service life of the project. In later phases of this project, an assessment of carbon leakage during key processes must be considered in further detail. This could include accidental releases such as accidents at sea, holes or ruptures on piping and/or tanks as well as releases during regular operation such as boil off of cryogenically stored liquid CO_2 or releases from boreholes.

The scenario analysis in Figure 11 shows that the location and thermal energy source of the mineralization plant does have a large influence on the gross CO_2 emissions. The benefits of CO_2 mineralization (CO_2 emission removal) are, however, an order of magnitude larger than the gross CO_2 emissions. Differences in emissions due to location and thermal energy source therefore become insignificant when the benefits of CO_2 mineralization are considered, that is when the net CO_2 emissions/removals are calculated. Figure 12 shows that when the benefits of CO_2 mineralization are considered, the net reduction of CO_2 in the atmosphere for the scenarios is in the range of 71 500 – 73 600 million kg CO_2 eq[9]. The considered scenarios assume either geothermal hot water or biogas as a source of thermal energy. Other sources of thermal energy could influence the results. Different maritime CO_2 transport distances could also influence the results. Emission factor of steel has a very minor influence.

Appendix 1 – Five top risks

Risk category	Risk identification	Risk item	Control
General - Accident and disaster control	Which major accident can occur? • Terrorism • Hazardous substances (toxic substances) • Fire • Natural hazards, e.g.: eruptions, lightning, weather, storms and cold, lava flows, geothermal hazards, earthquake, gases and volcanic pollution, ash fall. • Other major accidents	Extreme weather or natural hazards. Activities that are optimal in the summer (earthworks, cladding, concrete...) occur in the winter under conditions that further delay the project. Can cause additional cost and/or delays. Ship not able to deliver CO2 due to extreme weather Equipment damaged due to weather, frost. • Performance temporarily reduced. Safety of staff Potential capital cost to fix equipment	1) Operations relying on weather scheduled to not occur over winter period. 2) In the unlikely event of natural hazards, project management team to define an action plan aimed at minimizing delays in timeline while ensuring health and safety of staff and integrity of assets. 3) Assess and plan for some margin in the system (some over dimensioning or some margin in the capacity of equipment) to compensate for variation in CO2 supply 4) Equipment designed to stand extreme weather conditions. Operation procedures to protect equipment when needed. 5) In the unlikely event of natural hazards, operators will define an action plan aimed at minimizing effect on operations while ensuring health and safety of staff. 6) Emergency shutdown system implemented in process design.
Occupational health - Work environment	How is it ensured that indoor air will be comfortable for all users of buildings, adequate ventilation,	Not sufficient ventilation, e.g. in cellars.	Ventilators will be in all cellars and closed areas, shall be used for some time before arrival of personnel.

	without drafts, clean fresh air and location of air intake suitable?	Human mistakes or equipment failure.	Have oxygen masks in those areas as a safety to be able to save injured personnel.
Occupational health - Work environment	Are indoor jobs expected to cause unhealthy circumstances or pollution, treatment of flammable or explosive air mixtures?	Explosive atmospheres can be caused by flammable gases, mists or vapours or by combustible dusts. Air pollution is a major cause of premature death and disease and is the single largest environmental health risk in Europe.	Ventilators will be in all cellars and closed areas, shall be used for some time before arrival of personnel. Have oxygen masks in those areas as a safety to be able to save injured personnel. Spaces should be located only where the air can be cleaned or ventilated and soiled off the air.
Safety - Occupational safety	Will project operation or construction result in inter-relations between construction activities and operation activities? • For example, if a part of a new building is taken into operation even though the building is not finished.	Accident due to electricity	Lockout- Tagout-procedures Work permit procedure. Take into account the possibility for changes and additions.
Project management	Infrastructure not ready in time.	New harbour outside of Carbfix's scope - lack of coordination or project not a priority at the harbour's authorities. • Project delayed until harbour is ready	1) Engage into dialogue with the parties and clearly communicate with them on the importance of having infrastructure ready in time. 2) Ensure close cooperation between the parties (Carbfix, Consultant, transport company, harbour authorities). 3) Monitor progress.

VIÐAUKI VI

Farin var vettvangsferð á áhrifasvæði Coda Terminal í september 2022 og í ágúst 2023 og ljósmyndar teknar af vistgerðum.

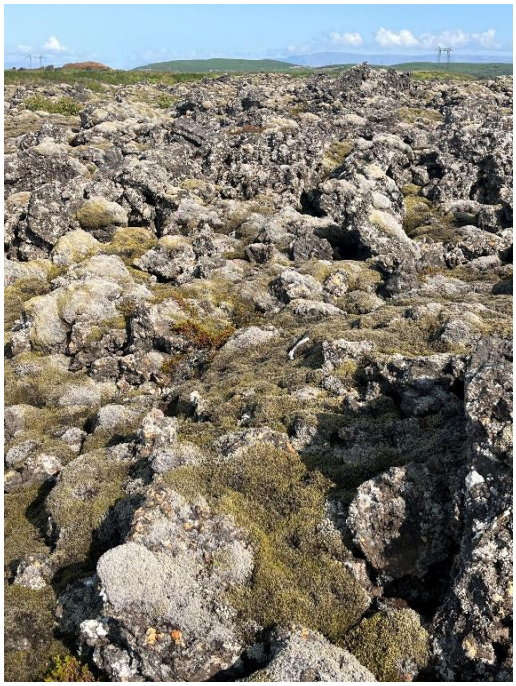

MYND 1 Mosahraunavist.
Hnit: 64°01'16.960" N -21°57'46.400" V

MYND 2 Mosahraunavist.
Hnit: 64°01'16.900" N -21°57'46.329" V

MYND 3 Mosahraunavist.
Hnit: 64°01'16.990" N -21°57'46.479" V

MYND 4 Mosahraunavist.
Hnit: 64°01'17.010" N -21°57'46.440" V

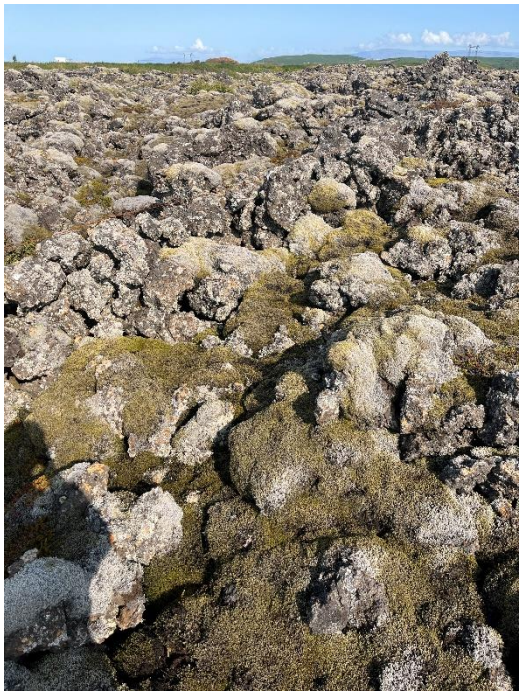

MYND 5 Mosahraunavist.
Hnit: 64°01'17.010" N -21°57'46.440" V

MYND 6 Mosahraunavist.
Hnit: 64°01'17.070" N - 21°57'46.419" V

MYND 7 Mosahraunavist.
Hnit: 64°01'17.040" N -21°57' 46.440" V

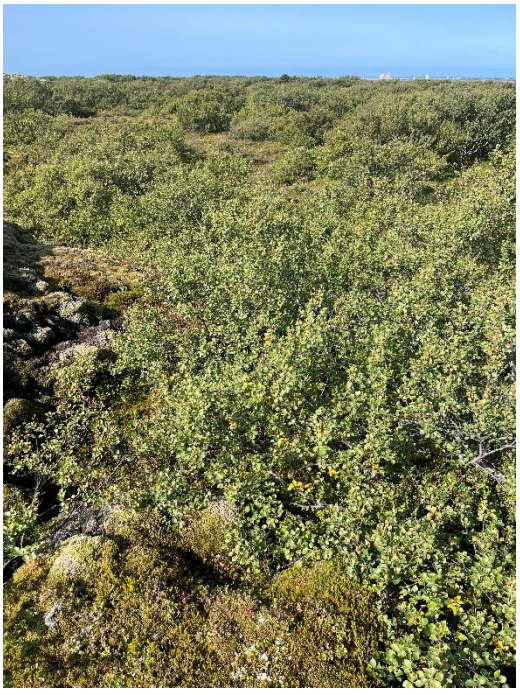

MYND 8 Horft yfir kjarrskógavist.
Hnit: 64°01'11.820" N -21°58'10.620" V

MYND 9 Kjarrskógavist.
Hnit: 64°01'12.100" N -21°58'11.190" V

MYND 10 Kjarrskógavist.
Hnit: 64°01'12.150" N -21°58'11.439" V

MYND 11 Kjarrskógavist
Hnit: 64°01'12.320" N -21°58'12.630" V

MYND 12 Kjarrskógavist.
Hnit: 64°01'12.320" N -21°58'12.630" V

MYND 13 Kjarrskógavist.
Hnit: 64°01'12.340" N -21°58‘12.550" V

MYND 14 Kjarrskógavist.
Hnit: 64°01'12.320" -21°58'12.740" V

MYND 15 Kjarrskógavist.
Hnit: 64°01'12.320" N -21°58'12.889" V

MYND 16 Kjarrskógavist.
Hnit: 64°01'12.290" N -21°58'12.900" V

MYND 17 Kjarrskógavist.
Hnit: 64°01'02.130" N -21°58'07.190" V

MYND 18 Kjarrskógavist.
Hnit: 64°01'02.180" N -21°58'07.150" V

MYND 19 Kjarrskógavist.
Hnit: 64°01'15.420" N -21°59'15.820" V

MYND 20 Kjarrskógavist.
Hnit: 64°01'15.590" N -21°59'15.780" V

MYND 21 Kjarrskógavist.
Hnit: 64°01'15.560" N -21°59'15.749" V

MYND 22 Kjarrskógavist.
Hnit: 64°01'15.450" N -21°59'15.500" V

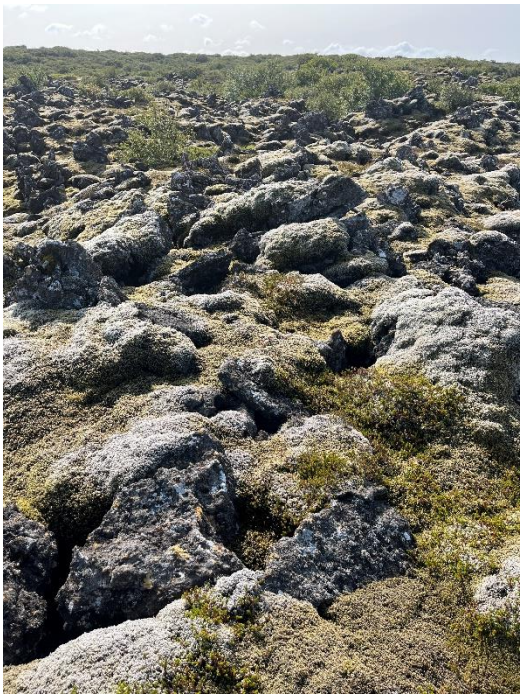

MYND 23 Kjarrskógavist.
Hnit: 64°01'15.530" N -21°59'15.200" V

MYND 24 Kjarrskógavist.
Hnit: 64°01'15.530" N -21°59'15.280" V

MYND 25 Kjarrskógavist.
Hnit: 64°01'15.500" N -21°59'15.309" V

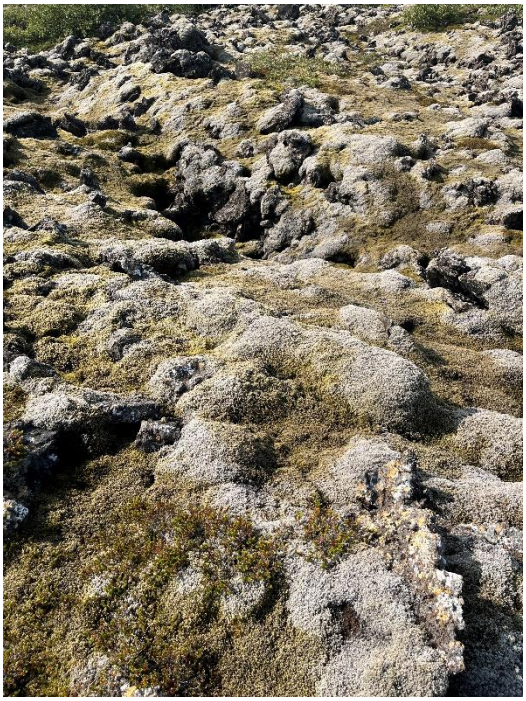

MYND 26 Kjarrskógavist.
Hnit: 64°01'15.500" N -21°59'15.370" V

MYND 27 Lynghraunavist.
Hnit: 64°01'12.840" N -21°59'38.990" V

MYND 28 Lynghraunavist.
Hnit: 64°01'13.310" N -21°59'39.850" V

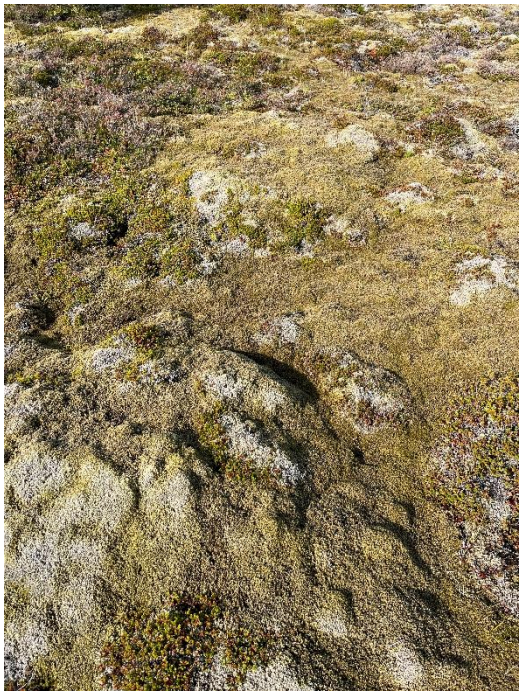

MYND 29 Lynghraunavist.
Hnit: 64°01'13.360" N -21°59'39.999" V

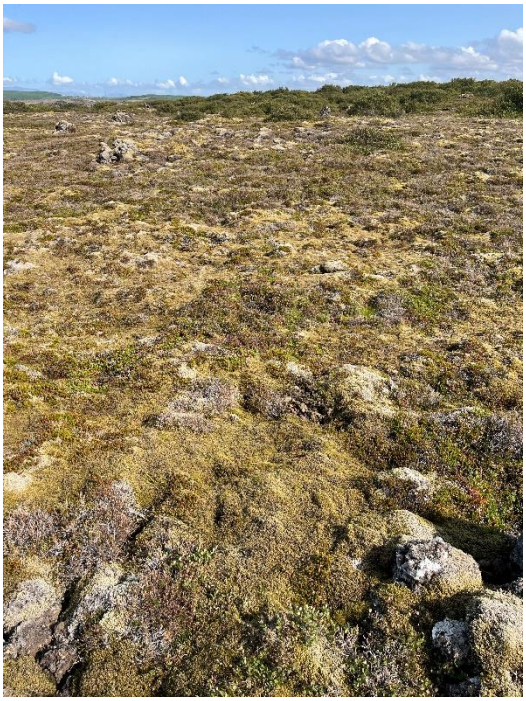

MYND 30 Lynghraunavist.
Hnit: 64°01'13.360" N -21°59'41.439" V

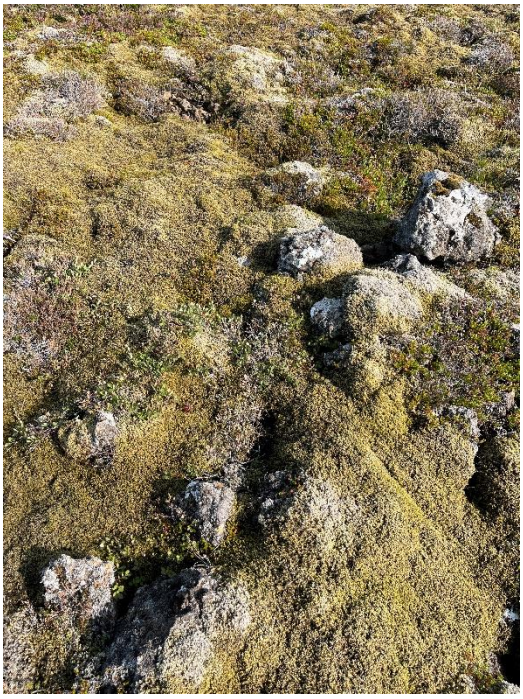

MYND 31 Lynghraunavist.
Hnit: 64°01'13.550" N -21°59'40.819" V

MYND 32 Lynghraunavist.
Hnit: 64°01'13.860" N -21°59'40.419" V

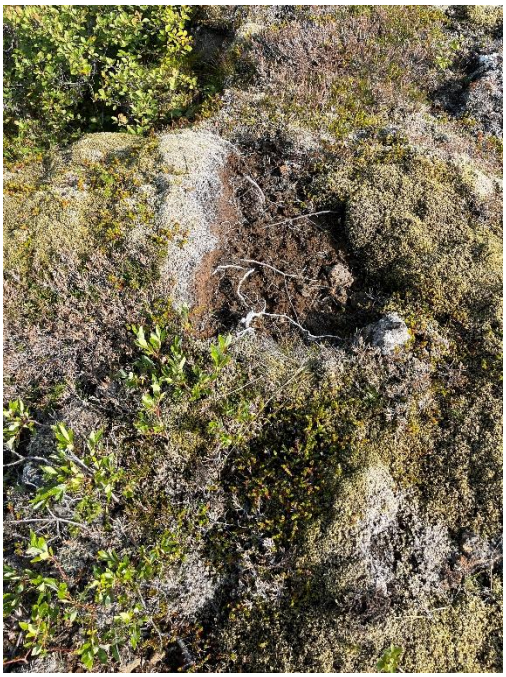

MYND 33 Kjarrskógavist.
Hnit: 64°01'04.050" N -22°00'10.299" V

MYND 34 Kjarrskógavist.
Hnit: 64°01'04.080" N -22°00'10.270" V

MYND 35 Kjarrskógavist.
Hnit: 64°01'04.020" N -22° 00' 10.26000000" W

MYND 36 Kjarrskógavist.
Hnit: 64°01'04.080" N -22°00'10.209" V

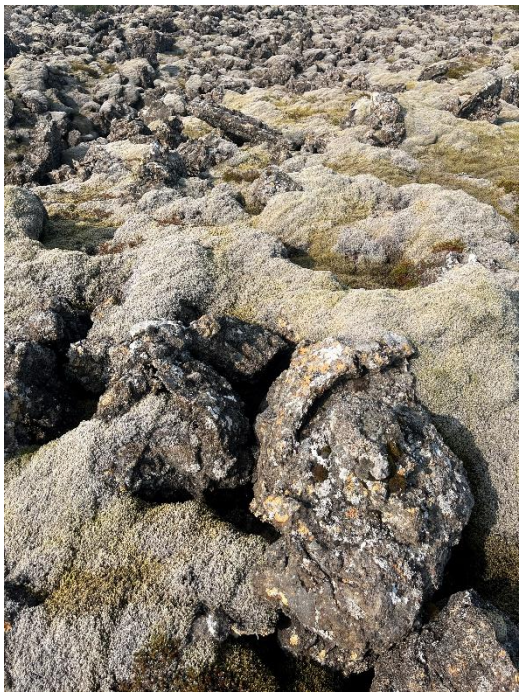

MYND 37 Mosahraunavist.
Hnit: 64°00'51.200" N -22°01'11.619" V

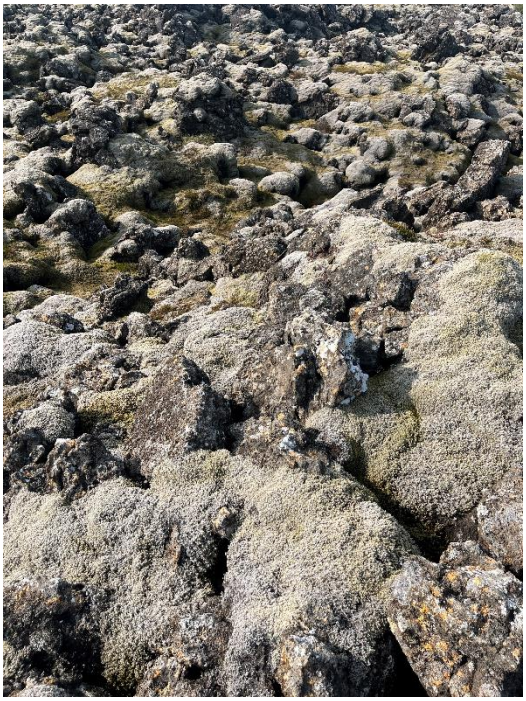

MYND 38 Mosahraunavist.
Hnit: 64°00'51.220" N -22°01'11.269" V

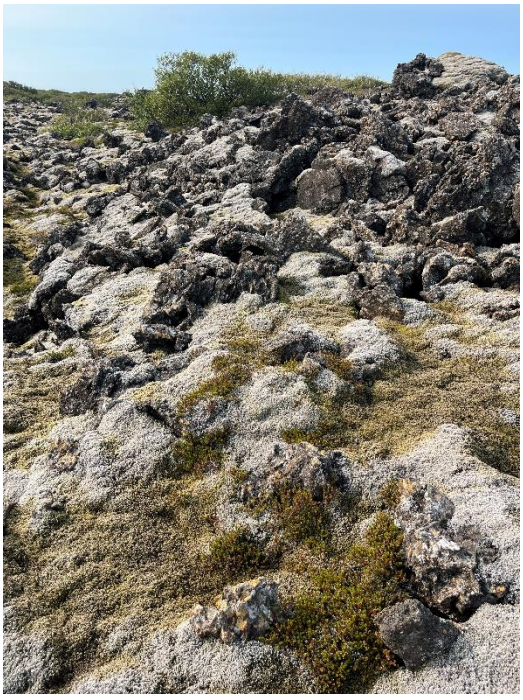

MYND 39 Horft yfir mosahraunavist.
Hnit: 64°01'29.240" N -21°59'29.990" V

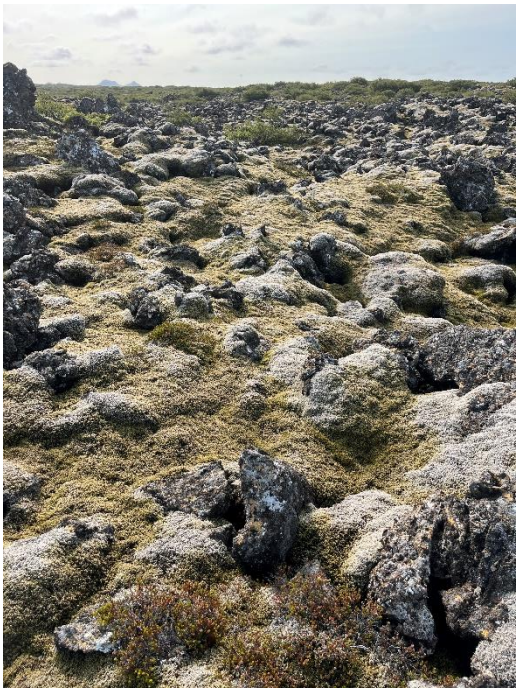

MYND 40 Horft yfir mosahraunavist.
Hnit: 64°01'29.240" N -21°59'29.960" V

MYND 41 Mosahraunavist.
Hnit: 64°01'29.240" N -21°59'29.950" V

MYND 42 Lynghraunavist.
Hnit: 64°02'01.950" N -22°01'55.470" V

MYND 43 Lynghraunavist.
Hnit: 64°02'01.920" N -22°01' 55.549" V

MYND 44 Lynghraunavist.
Hnit: 64°02'01.920" N -22°01'55.639" V

MYND 45 Lynghraunavist.
Hnit: 64°02'01.150" N -22°01'55.819" V

MYND 46 Lynghraunavist.
Hnit: 64°01'52.610" N -22°02'04.629" V

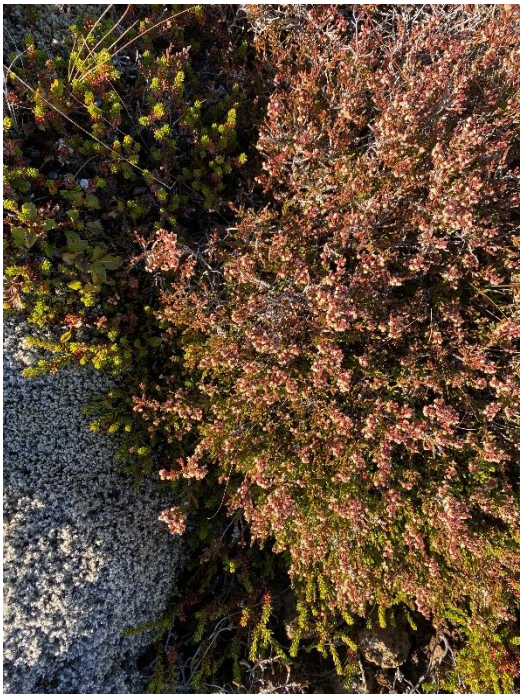

MYND 47 Lynghraunavist.
Hnit: 64°01'52.610" N -22°02'04.629" V

MYND 48 Kjarrskógavist.
Hnit: 64°01'44.479" N -22°02'08.880" V

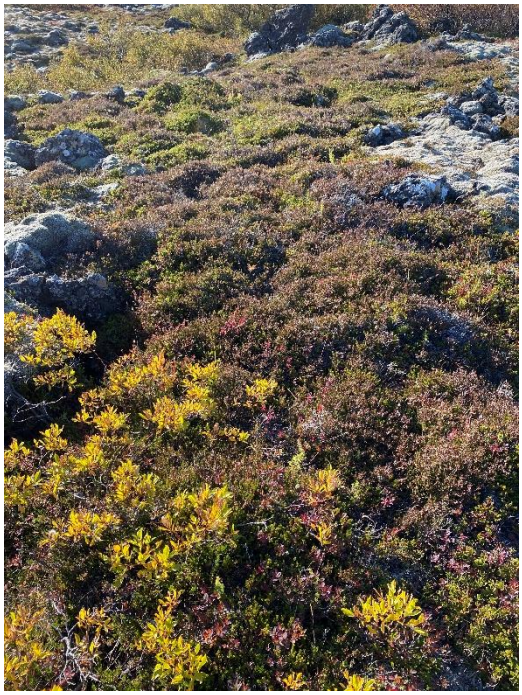

MYND 49 Kjarrskógavist.
Hnit: 64°01'43.460" N-22°02'09.819" V

MYND 50 Kjarrskógavist.
Hnit: 64°01'43.460" N -22°02'09.809" V

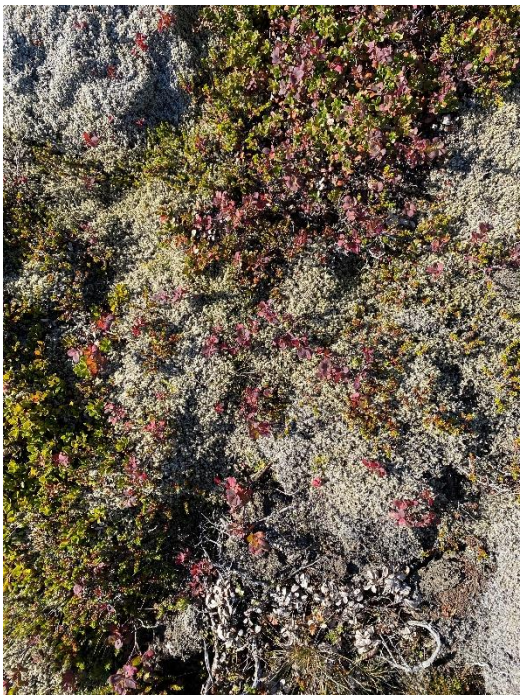

MYND 51 Kjarrskógavist.
Hnit: 64°01'43.84999920" N -22°02'10.939" V

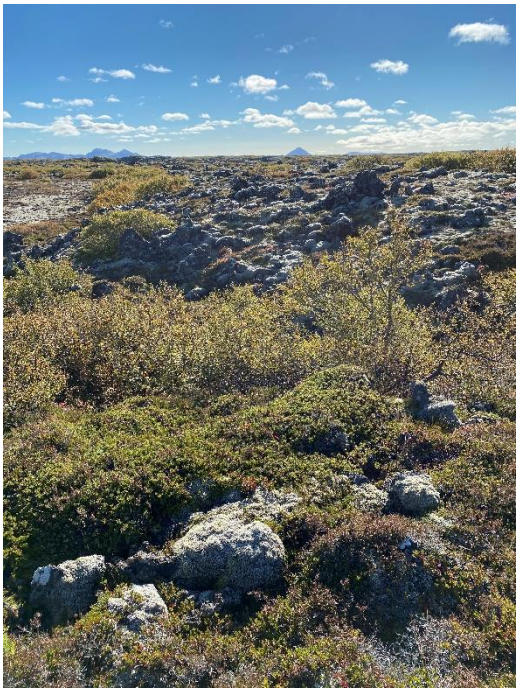

MYND 52 Kjarrskógavist.
Hnit: 64°01'43.439" N -22°02'10.510" V

MYND 53 Kjarrskógavist.
Hnit 64 01'43.460" N -22°02'10.330" V

MYND 54 Kjarrskógavist.
Hnit: 64°01'43.460" N -22°02'10.629" V

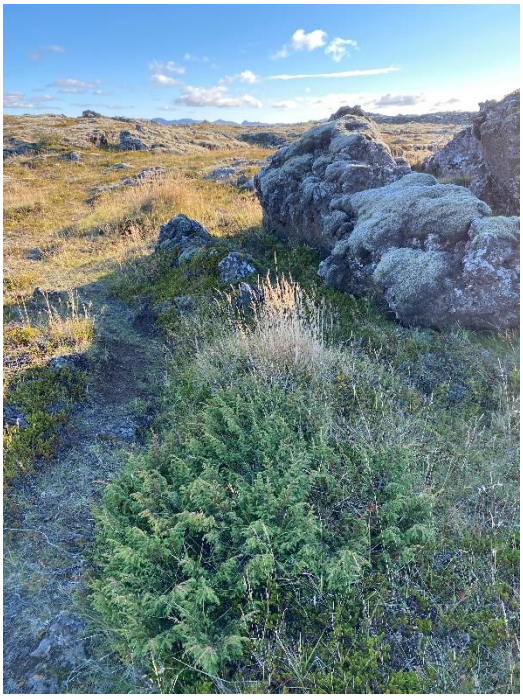

MYND 55 Lynghraunavist.
Hnit: 64°02'17.800" N -22°02'42.200" V

MYND 56 Lynghraunavist.
Hnit: 64°02'17.800" N -22°02'42.209" V

MYND 57 Lynghraunavist.
Hnit: 64°02'07.630" N -22°02'50.240" V

MYND 58 Lynghraunavist.
Hnit: 64°02'07.580" N -22°02'50.730" V

MYND 59 Lynghraunavist.
Hnit: 64°01'52.450" N -22°03'08.750" V

MYND 60 Lynghraunavist.
Hnit: 64°01'52.420" N -22°03'08.700" V

MYND 61 Lynghraunavist.
Hnit: 64°01'52.450" N -22°03'08.750" V

MYND 62 Lynghraunavist.
Hnit: 64°01'50.190" N -22°03'15.300" V

MYND 63 Lynghraunavist.
Hnit: 64°01'51.680" N -22°03'09.479" V

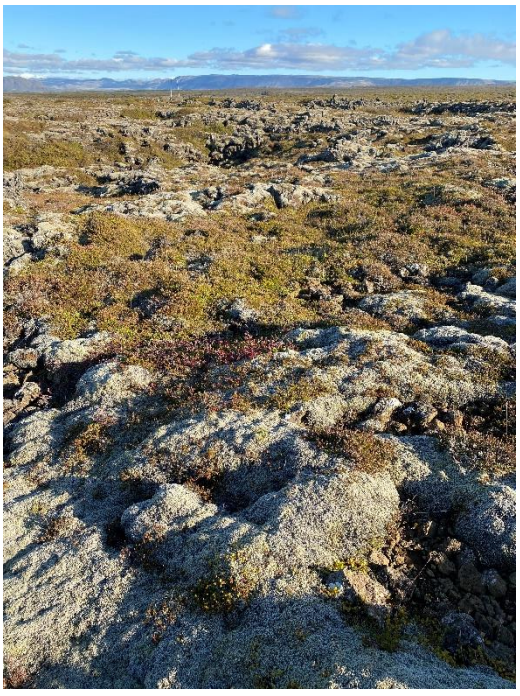

MYND 64 Lynghraunavist.
Hnit: 64°01'43.520" N -22°03'30.290" V

MYND 65 Lynghraunavist.
Hnit: 64°01'43.489" N -22°03'30.089" V

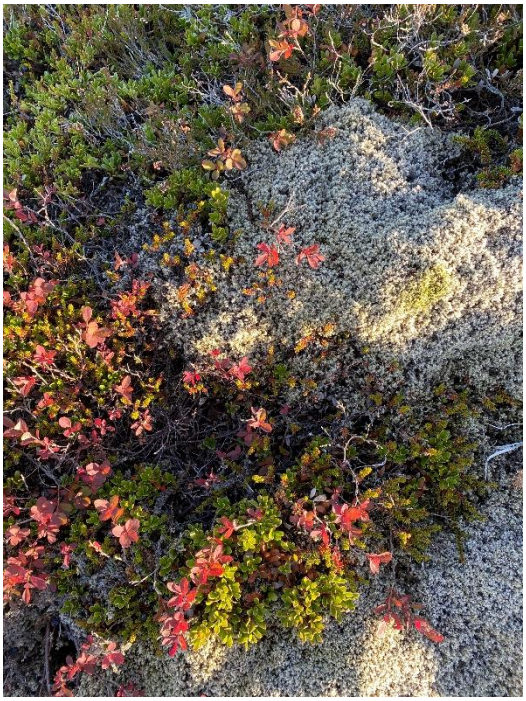

MYND 66 Lynghraunavist.
Hnit: 64°01'43.489" N -22°03'30.070" V

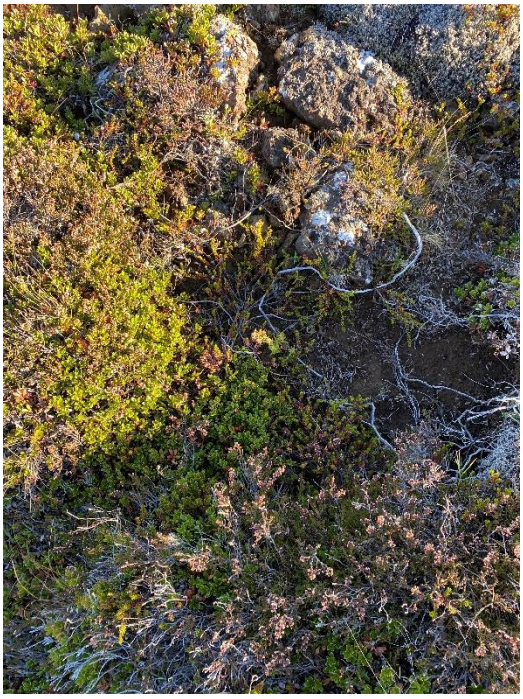

MYND 67 Lynghraunavist.
Hnit: 64°01'43.460" N -22°03'30.049" V

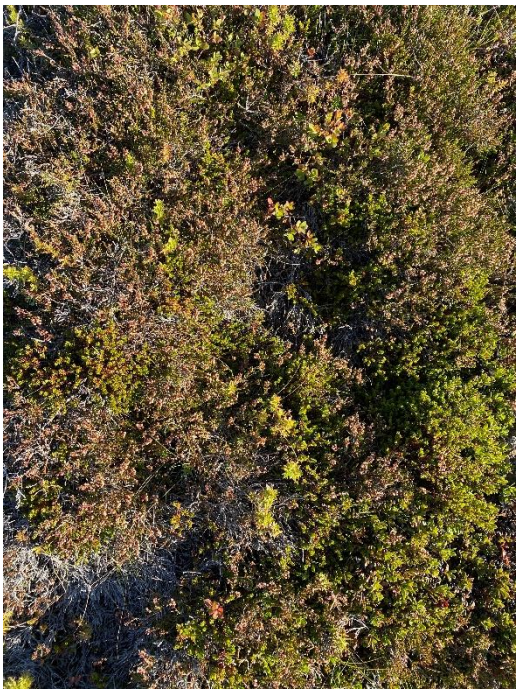

MYND 68 Lynghraunavist.
Hnit: 64°01'43.460" N -22°03'29.919" V

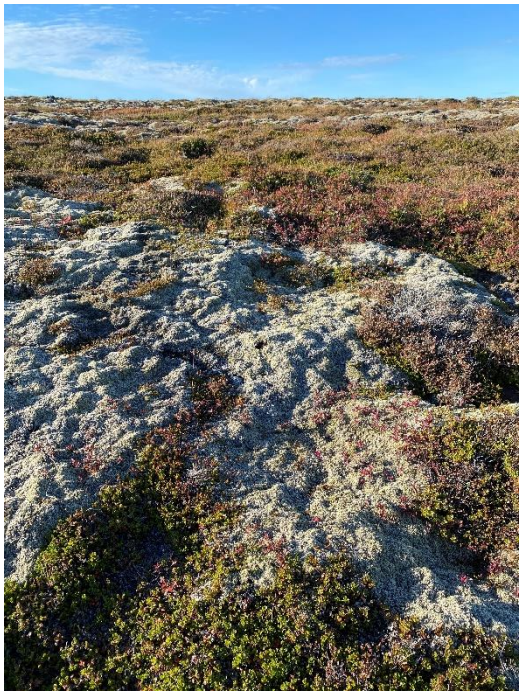

MYND 69 Lynghraunavist.
Hnit: 64°01'49.149" N -22°03'46.509" V

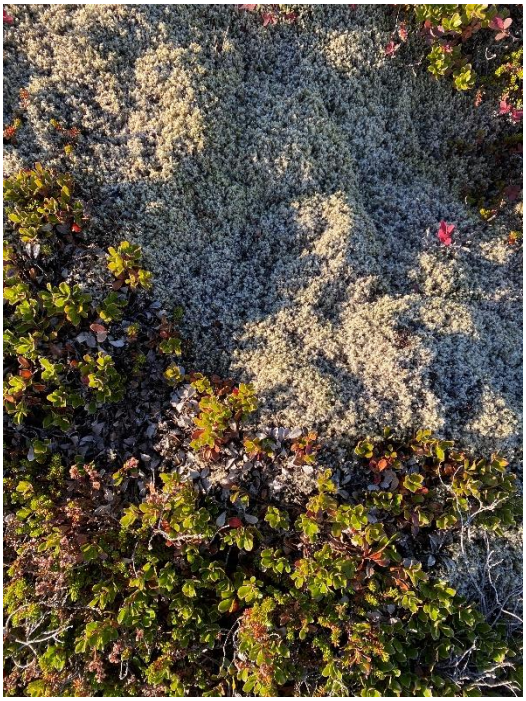

MYND 70 Lynghraunavist.
Hnit: 64°01'49.1800" N -22°03'46.519" V

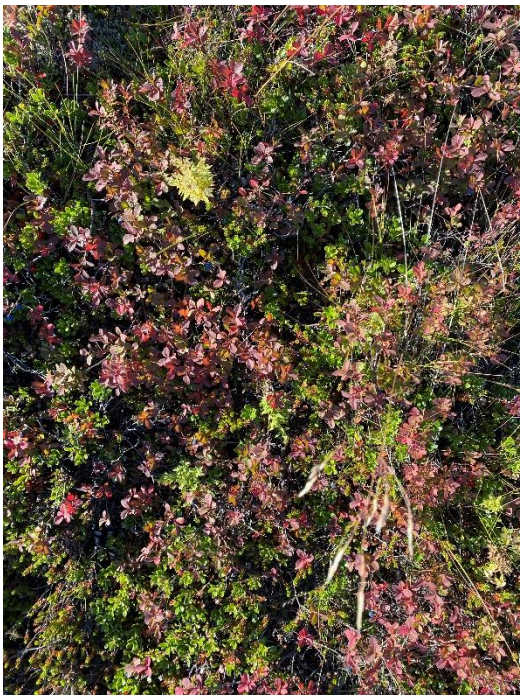

MYND 71 Lynghraunavist.
Hnit: 64°01'49.310" N -22°03'46.540" V

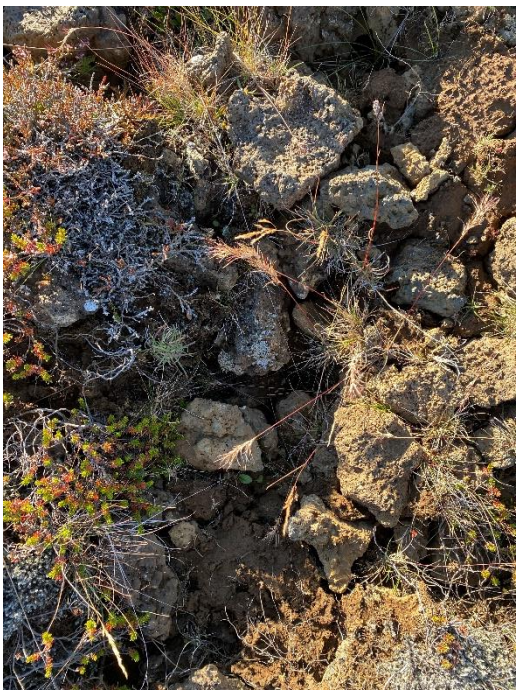

MYND 72 Lynghraunavist.
Hnit: 64°01'49.400" N -22°03'46.869" V

MYND 73 Lynghraunavist.
Hnit: 64°01'48.759" N -22°03'47.859" V

MYND 74 Lynghraunavist.
Hnit: 64°01'49.400" Nn-22°03'46.919" V

MYND 75 Lynghraunavist.
Hnit: 64°01'48.849" N -22°03'47.720" V

MYND 76 Lynghraunavist.
Hnit: 64°02 03.099" N -22°03'27.460" V

MYND 77 Lynghraunavist.
Hnit: 64°02'03.210" N -22°03'27.420" V

MYND 78 Lynghraunavist.
Hnit: 64°02'03.239" N -22°03'27.140" V

MYND 79 Lynghraunavist.
Hnit: 64°02'03.239" N -22°03'27.159" V

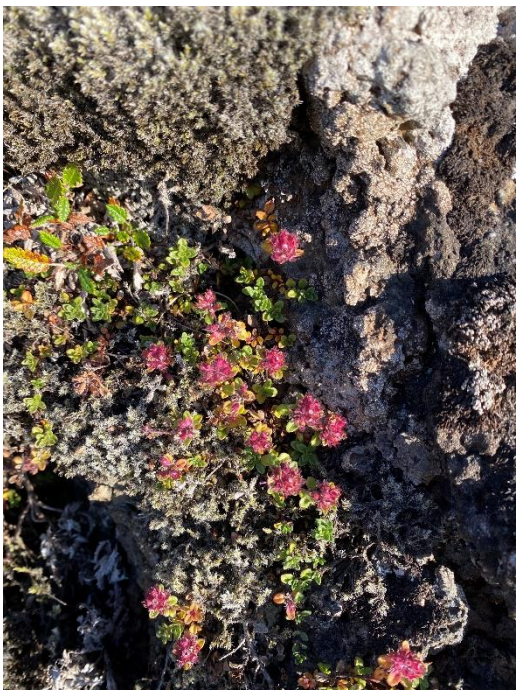

MYND 80 Lynghraunavist.
Hnit: 64°02'03.210" N -22°03'27.090" V

MYND 81 Lynghraunavist.
Hnit: 64°02'11.640" N -22°03'05.760" V

MYND 82 Lynghraunavist.
Hnit: 64°02'11.810" N -22°03'05.870" V

MYND 83 Lynghraunavist.
Hnit: 64°02'11.810" N -22°03'05.870" V

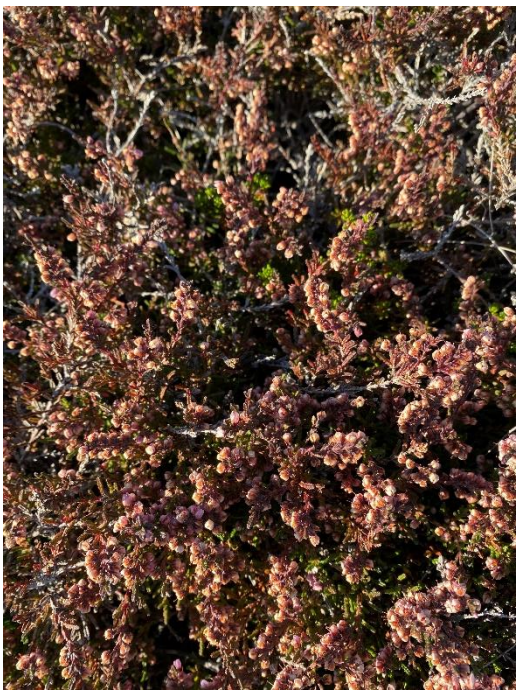

MYND 84 Lynghraunavist.
Hnit: 64°02'12.059" N -22°03'05.810" V

MYND 85 Lynghraunavist.
Hnit: 64°02'12.220" N -22°03'05.150" V

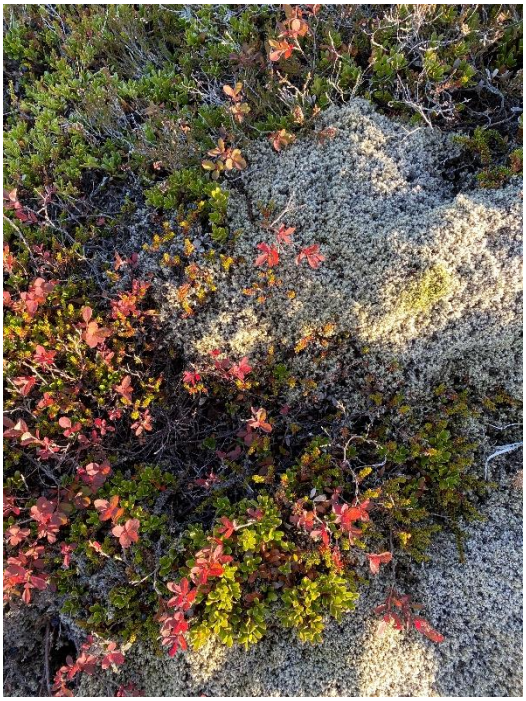

MYND 86 Lynghraunavist.
Hnit: 64°01'43.489" N -22°03'30.070" V

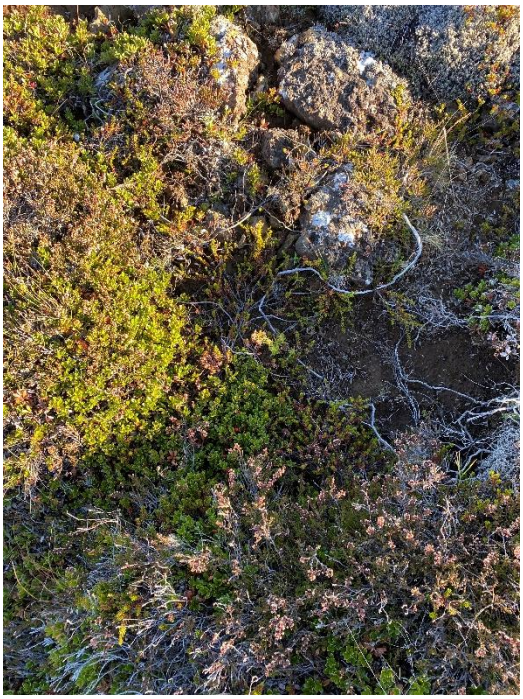

MYND 87 Lynghraunavist.
Hnit: 64°01'43.460" N -22°03'30.049" V

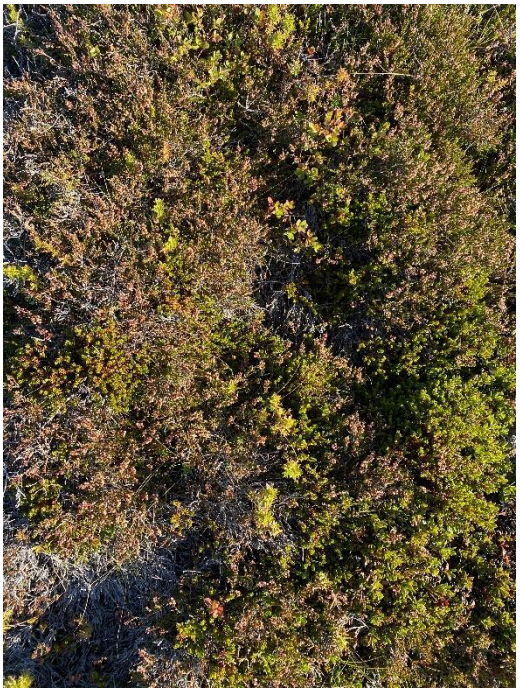

MYND 88 Lynghraunavist.
Hnit: 64°01'43.460" N -22°03'29.91 V